Functional exploration of the Plasmodium tRNA import machinery

Martina Pitolli

Université de Strasbourg

UNIVERSITÉ DE STRASBOUR

École Doctorale des Sciences de la Vie et de la Santé STRASBOURG

ÉCOLE DOCTORALE des Sciences de la Vie et de la Santé

CNRS UPR9002

THÈSE

Présentée par :

Martina Pitolli

Soutenue le : **22 Septembre 2023**

Pour obtenir le grade de : **Docteur de l'Université de Strasbourg**

Discipline : Aspects Moléculaires et Cellulaires de la Biologie

---

Exploration fonctionnelle de la machinerie d'import des ARN de transfert dans *Plasmodium*

THÈSE dirigée par :
FRUGIER Magali DR, CNRS, Université de Strasbourg

CO-ENCADRANT :
RUDINGER-THIRION Joëlle CR, CNRS, Université de Strasbourg

RAPPORTEURS :
RIBAS DE POUPLANA Lluís ICREA Professeur, IRB Barcelona
CERDAN Rachel Professeur, Université Montpellier

EXAMINATEURS :
GIEGÉ Philippe DR CNRS, Université de Strasbourg
FONVIELLE Matthieu CR, INSERM, I2BC Gif-sur-Yvette

Remerciements

Le doctorat est un parcours qui, comme tous les parcours, ne peut être fait seul. C'est pourquoi, je tiens à remercier toutes les personnes qui m'ont accompagnée scientifiquement et humainement dans cette aventure.

Je voudrais tout d'abord exprimer mes remerciements à l'ensemble des membres du jury: Pr Lluís Ribas de Pouplana, Pr Rachel Cerdan, Dr Philippe Giegé and Dr Matthieu Fonvielle, qui ont accepté de juger mon travail de thèse.

Ensuite, je tiens à exprimer ma gratitude pour ma directrice de thèse, Magali Frugier, pour m'avoir accueillie au sein de son laboratoire. Travailler avec une personne aussi rigoureuse et passionnée m'a permis de développer et de croître mes connaissances scientifiques, mais aussi personnelles. Peut-être que je ne finirai pas la thèse avec une totale confiance en moi (ça c'est encore trop), mais j'emporte avec moi tous ces enseignements et je ne les oublierais pas. Alors merci Magali pour ta patience, ton écoute et ta disponibilité malgré les hauts et les bas qui auront animé ces trois années de thèse. Tu as été pour moi un pilier, une référence, avec qui j'ai partagé des moments que je n'oublierais pas.

Joëlle, merci pour ton aide qui m'aura été précieuse au cours de ces années ainsi que lors de la rédaction de la thèse. Je savais que je pouvais compter sur toi, que ce soit pour un soutien scientifique ou un soutien personnel. Ta présence au labo a été essentielle pour moi, merci.

Merci à Anne et Caroline pour m'avoir accueillie dans le laboratoire, pour leurs aides et disponibilité lorsque j'en avais besoin, que ce soit pour les expériences ou les présentations. Merci aux autres membres de l'équipe, Philippe, Claude, Petr, Joanna, pour tous les moments que nous avons partagé en dehors du laboratoire.

Merci à ceux qui m'ont accompagné et aidé avec les petites souris de l'animalerie. Merci à Fabrice, Clarisse et Amandine.
Un gros merci pour toi, Fabrice <3 Tu n'es pas le premier sur la liste, mais le premier dans mon cœur. Je suis vraiment heureuse de t'avoir rencontré et d'avoir travaillé avec toi. Merci pour ton aide et pour toutes les douches que tu as dû prendre pour moi! (Et oui, il fallait que je le dise!) Qui sait, peut-être qu'un jour, nous nous retrouverons à travailler ensemble.

Je voudrais aussi remercier Dr. Eric Marois, pour les conseils, la disponibilité continue et pour m'avoir fait découvrir le monde des moustiques.

Merci au labo 447, mon premier laboratoire à l'IBMC ainsi que toutes les personnes que j'ai pu rencontrer, vous resterez toujours dans mon coeur. Merci aux personnes qui y sont passées, Angelita, Javier et Mattia, je ne vous oublierais pas.

Grazie Angelita e Stefano perché è anche grazie a voi che sono qui, grazie per essermi sempre stati vicino e aiutato. Grazie soprattutto a te Angelita perché sei stata una mamma, un'amica, una confidente, una sorella, una collega e tante altre cose; l'ordine è casuale, sapevi sempre quello di cui avevo bisogno. Grazie perché ci sei stata sempre, pronta ad appoggiami ma anche a farmi vedere le cose da un altro punto di vista quando ce ne era bisogno. Sapere che tu eri lì, dall'altra parte del lab, mi ha aiutato molto, sempre.

Grazie Mattia, perché ormai sei un punto di riferimento importante. Ricorderò sempre con piacere i mesi trascorsi insieme e il supporto che mi hai dato, sia a livello scientifico che personale. Ogni volta che avevo un dubbio, un problema, di qualsiasi genere, mi voltavo verso di te (o correvo nel tuo lab!) perché la tua opinione è sempre stata fondamentale per me.
Grazie perché riesci a gestire (e sopportare) i miei lati piu 'irruenti' e mi aiuti a vedere le cose da un'altra prospettiva.

Merci à tous les doctorants et anciens doctorants de l'IBMC avec qui j'ai partagé de multiples moments, au sein ou en dehors du laboratoire, que je n'oublierai jamais. Je voudrais remercier, en particulier, Javier, Elenia, José, Roberto, Max, Rithu et Riccardo.
Merci Javier, car tu as été la première personne à m'accueillir ici à l'IBMC et à rendre cet endroit si familier pour moi.
Merci Elenia pour nos pauses qui m'ont toujours rechargé et remplie d'énergie positive.
Merci José d'avoir été mon grand frère dans la recherche et de m'avoir donné tous ces précieux conseils, et merci Roberto pour tous ces moments passés ensemble. Je me souviendrai toujours, et avec grand plaisir, de notre congrès aux États-Unis, de la chaleur étouffante de Columbus et de notre petit voyage à New York.

Merci Faustine pour les petites pauses à parler d'histoires italiennes et surtout pour toutes les fois où tu as retrouvé mon téléphone, mon badge et mes écouteurs éparpillés dans l'institut, c'est vrai que j'ai toujours la tête dans les nuages.

Merci à mes amis et collègues du Campus, en particulier de l'INCI.
Merci à Bérangère, Michael et Jason pour le temps que nous avons passé ensemble, le chalet et les soirées. Merci à vous PICCOLI! Un merci tout particulier à Bérangère, l'amie du 'commérage' (ahahah), qui fait souvent du bien.

Grazie Fabiana, semplicemente per esserci, e per esserci sempre stata. Sono felice di aver iniziato e 'finito' questo percorso con te. Quello che c'è stato nel mezzo non si può racchiudere in due righe, ma è così importante da darmi la certezza che la fine del dottorato non sarà altro che l'inizio di un nuovo capitolo.
Grazie Rosanna, volevo dirti quanto apprezzo te e il modo in cui sei entrata nella mia vita. Sei arrivata in punta di piedi, ma il tuo impatto è profondo e duraturo. Grazie per essere diventata così importante per me, per tutti i momenti preziosi che abbiamo condiviso (voglio tornare a mangiare caramelle davanti alla TV!) e, soprattutto, per essere stata sempre disponibile quando avevo bisogno di aiuto o semplicemente di uno sfogo.
Grazie Margherita, perché entri nella vita delle persone come un uragano travolgente e ora non riesco più a fare a meno di te. Sei stata un punto di rifermento importante, sei stata famiglia, sei stata amica e confidente. Ci sei sempre stata quando ne avevo bisogno, perché sei così. So che posso contare su di te.
Grazie Alessia perché la tua allegria è contagiosa. Grazie perché quando ho bisogno di qualche cosa non ti tiri indietro, sei sempre pronta a dare consigli e aiuto. Abbiamo trascorso molti momenti insieme e sono sicura ce ne saranno tanti altri.

Mon expérience n'aurait pas été la même sans mes amis ici à Strasbourg, ma famille italienne, qui m'a accompagné depuis le début. Grazie di nuovo a Fabiana, Alessia, Margherita, Rosanna e ancora Filippo, Fausto, Richi, Sara e Stefan. Ne abbiamo passate tante insieme, ma sapevamo di poter contare sempre gli uni sugli altri. Grazie ancora a Lucrezia, Mattia, Chiara (per la tua contagiosa gioia di vivere), Miriam (per i tuoi piacevolissimi audio) e Marianna (perché mi hai fatto conoscere le origini del Mare ATriatico). Grazie a Luca e Onofrio (il gatto e la volpe) per le risate che mia avete fatto fare. Vi voglio bene, ragazzi!

Grazie a chi dall'Italia mi è rimasto accanto, anche se lontano. Grazie alle mie amiche dell'uni (Fede, Giorgia, Annalaura e Roberta) perché ci allontaniamo, ci avviciniamo, ci rincorriamo ma sempre ci ritroviamo. Quanti anni sono passati dal nostro primo esame? A me sembra ieri!
Grazie a Silvia e Junio, perché siete una presenza costante da molti anni, in ogni esperienza che faccio vi porto con me. Grazie Junio perché so che ti ho stressato molto.

Grazie alla mia famiglia perché mi è sempre stata vicino da lontano. Un grazie particolare a mamma, papà e Mattia. Se tutto questo è stato possibile, è soprattuto grazie a voi.

Grazie Stefano, perché mi hai accudito, aiutato e, soprattutto, migliorato. Sei riuscito ad alleggerire i mesi della scrittura, che quasi sono passati troppo in fretta. Grazie perché 'con te la vita è cosi facile da essere impossibile, e sono cosi libera che posso essere debole'.

Résumé de thèse

Introduction

Le paludisme est causé par un parasite protozoaire, intracellulaire obligatoire, *Plasmodium*. Il existe plus de 200 espèces de *Plasmodia* qui sont transmises par le même moustique du type *Anopheles* mais qui sont spécifiques d'un hôte vertébré (rongeurs, oiseaux, primates…). Il existe cinq espèces différentes de *Plasmodium* qui peuvent infecter les humains, dont *P. falciparum* qui est le plus mortel (plus de 600 000 morts/an), principalement en Afrique sub- saharienne. Les symptômes du paludisme peuvent inclure de la fièvre, des frissons, des maux de tête, des douleurs musculaires et des nausées. Le paludisme est une préoccupation majeure pour la santé mondiale, particulièrement dans les régions tropicales et subtropicales. La maladie est endémique dans de nombreux pays, avec la majorité des cas se produisant en Afrique subsaharienne. Cependant, le paludisme affecte également d'autres régions telles que l'Asie du Sud-Est, la Méditerranée orientale et les Amériques. La transmission du paludisme est liée à des facteurs environnementaux tels que la température, l'humidité et les précipitations, qui affectent la reproduction et la survie des vecteurs de moustiques. L'Organisation mondiale de la santé (OMS) estime qu'il y a eu environ 241 millions de cas de paludisme dans le monde en 2020, dont 95 % en Afrique. On estime que 627 000 personnes sont décédées du paludisme en 2020, principalement des enfants de moins de 5 ans. Ces cas représentent un fardeau considérable pour les systèmes de santé publique et ont un impact significatif sur le développement socio-économique des communautés touchées (OMS, 2020).

Le cycle de *Plasmodium* est complexe et se divise en une phase de reproduction asexuée chez l'hôte vertébré et une phase de reproduction sexuée chez le moustique. Durant son cycle de vie, la morphologie du parasite et les protéines exprimées sont variables, ce qui rend difficile la mise au point de thérapeutiques et de vaccins. Ainsi la connaissance des acteurs moléculaires impliqués au niveau de chaque étape du développement est fondamentale pour la mise en place de traitements efficaces. Dans ce contexte, mon travail de thèse participe à la caractérisation de la protéine tRip (tRNA import protein) de *Plasmodium*. La protéine tRip a été identifiée dans notre laboratoire (Bour et al., 2016). Cette protéine de 402 acides aminés est codée par un gène de 1440 nucléotides situé sur le chromosome 14 et est bien conservée dans toutes les souches de *Plasmodium*. Cette protéine membranaire est présente à la surface de *Plasmodium* et est formée de 2 domaines principaux : le domaine N-terminal de type GST-like interne et le domaine C-terminal qui est présent à la surface du parasite. tRip a été initialement identifiée grâce à une analyse bio-informatique basée sur son homologie avec Arc1p de *S. cerevisiae* car comme elle, tRip contient un domaine N-terminal de type GST-like

et un domaine C-terminal de type EMAPII, capable de se lier aux structures 3D en L des ARNt grâce à deux résidus (Ser312 et Met315) (Cela et al., 2021).

Le domaine N-terminal de type GST-like, en liant des aminoacyl-ARNt synthétases (aaRS), permet la formation de deux complexes multisynthétasiques (MSC). Trois aaRSs, glutamyl-ARNt synthétase (ERS), glutaminyl-ARNt synthétase (QRS) et methionyl-ARNt synthétase (MRS), co-immunoprécipitent spécifiquement avec tRip dans les parasites au stade sanguin de *P. berghei*. Les trois aaRSs contiennent un domaine N-terminal de type GST-like impliqué dans l'assemblage du complexe MSC. Cependant, contrairement à toutes les autres MSC connus à ce jour, il a été démontré que *Plasmodium* contient deux complexes hétérotrimériques exclusifs : le complexe Q (tRip:ERS:QRS) et le complexe M (tRip:ERS:MRS).

tRip reconnait aussi les ARNt via son domaine C-terminal en reconnaissant la coude de la structure à L des ARNt et le domaine est impliquée dans leur import dans le parasite (sporozoïte, forme extracellulaire) (Bour et al., 2016). Cette spécificité a été confirmée par des expériences d'empreinte réalisées sur des ARNt en présence du domaine C-terminal de tRip. En outre, dans l'étude de Cela et al. (2021) utilisant la technique Microarray Identification of Shifted tRNAs (MIST), il a été démontré que les ARNt sont liés avec différentes affinités. La technique MIST a été utilisée pour identifier les ARNt préférentiellement reconnus par le tRip de *P. falciparum* en présence d'un excès d'ARNt humain brut. ARNt humains $ARNt^{Ala}_{hGC}$, $ARNt^{Asn}_{GTT}$, $ARNt^{Ser}_{AGA}$ et $ARNt^{Leu}_{wAG}$ se sont révélés être les meilleurs liants.

Expérience FISH a montré que les sporozoïtes importent l'ARNt dans le parasite. Comme attendu, un parasite tRip-KO ne présente plus cette fonctionnalité d'import, est caractérisé par une synthèse protéique réduite et se développe moins efficacement dans le stade sanguin. Cependant, avant mon arrivée dans le laboratoire le rôle de cet import unique n'avait pas été étudié. Ainsi, au cours de ma thèse j'ai participé à la compréhension de la fonction moléculaire de l'import des ARNt dans le parasite. De plus, dans un deuxième temps, j'ai utilisé tRip comme cible pour le développement de nouvelles approches thérapeutiques. En effet, la présence du domaine C-terminal de tRip à la surface du parasite tout au long de son cycle de développement dans l'hôte vertébré en fait une cible de choix pour, soit sélectionner des ligants/inhibiteurs soit l'utiliser dans une approche vaccinale.

Résultats et discussion

1- Impact de la délétion de tRip sur le protéome du parasite

Il avait été montré par mon équipe que le parasite tRip-KO se développe plus lentement que le parasite sauvage (WT) dans le sang de l'hôte vertébré et que sa synthèse protéique est

aussi réduite. Afin de mieux cerner les mécanismes moléculaires impliqués dans ces phénotypes, nous avons réalisé des analyses protéomiques comparatives.
Des souris ont été infectées par chacun des 2 types de parasite (WT and tRip-KO). Lorsque la parasitémie atteint 10%, le sang des souris a été récupéré par ponction cardiaque et les parasites WT et tRip-KO ont été collectés, purifiés et quantifiés. Après extraction, les protéines, ont été analysées par spectrométrie de masse. Deux échantillons de parasite ont été utilisés : (a) un échantillon contenant essentiellement le stade schizont (n=3) et (b) un échantillon contenant tous les stades sanguins (n=3). Il apparaît que dans les deux échantillons, peu de protéines ont des niveaux d'expression significativement affectés en l'absence de tRip et les protéines dérégulées sont impliquées dans des fonctions totalement différentes. Ces résultats sont attendus car différentes étapes du cycle de vie du parasite nécessitent des processus biologiques et des fonctions distincts, qui sont médiés par des ensembles spécifiques de protéines (Bunnik et al., 2013). Dans l'expérience (a), nous avons principalement identifié des protéines impliquées dans le processus de la traduction, tandis que dans l'expérience (b), nous avons observé une prédominance de protéines liées à la synthèse d'ADN.

Dans ces conditions, plutôt qu'une analyse de functions, j'ai réalisé une analyse de séquence plus poussée en déterminant l'usage des acides aminés dans le parasite KO par rapport au parasite WT. Cette approche m'a permis de montrer que les protéines sous-exprimées dans le parasite tRip-KO sont plus riches en asparagine dans les deux conditions a et b (+35 et +70%, respectivement), suggérant que le parasite tRip-KO est inefficace dans la synthèse des protéines riches en asparagine. En recherchant de telles protéines par analyse bio-informatique des génomes de 6 souches de *Plasmodium*, nous avons identifié deux protéines strictement conservées. Il s'agit des Poly(A) binding protein 3 (PABP3) et du facteur 1 associé à Ccr4 (CAF1), une exonucléase impliquée dans la dégradation des queues poly(A). Les deux protéines reconnaissent le même substrat d'ARN et sont organisées de façon similaire : un domaine N-terminal strictement conservé dans tous les eucaryotes et un domaine C-terminal spécifique à *Plasmodium* et contenant jusqu'à 60% d'asparagins. Parmi ces deux protéines, CAF1 est la seule à avoir été caractérisée. Elle fait partie du complexe Ccr4-Not (carbon catabolite repressor protein 4-N), qui est un régulateur global de l'expression génique, conservé de la levure aux humains. Ce complexe est composé de Ccr4 et de 3 facteurs associés à Ccr4 (CAF1, CAF40 et CAF130) ainsi que de 5 protéines Not, qui régulent ensemble la synthèse des protéines en dégradant les ARNm correspondants (Collart, 2016; Tucker et al., 2001). Récemment, le mécanisme médié par le complexe Ccr4-Not pour réguler la traduction des ARNm contenant des codons non optimaux a été décrypté. Les membres du complexe Ccr4-Not sont bien conservés chez *Plasmodium* (Coulson et al., 2004) et une étude de Balu et al. (Balu et al., 2011) a montré que la délétion du domaine C-terminal de CAF1

stabilise spécifiquement certains ARNm. L'absence du domaine C-terminal de CAF1 riche en asparagines entraîne notamment la surexpression des ARNm codant pour des protéines impliquées directement dans la sortie et l'entrée du parasite dans les globules rouges. Or, ces gènes correspondent également aux protéines qui sont surexprimées dans le parasite tRip-KO, suggérant que l'action du mutant de CAF1 a la même conséquence que la délétion de tRip. En effet, lorsque le domaine C-terminal de la protéine CAF-1 est supprimé chez *Plasmodium*, le phénotype observé est comparable à celui du parasite tRip-KO (Balu et al., 2011; Bour et al., 2016) : les mérozoïtes libérés seraient immatures et donc inefficaces pour infecter les globules rouges de l'hôte. Sur la base de ces observations, nos résultats suggèrent donc que l'import des ARNt de l'hôte, dont l'ARNt^{Asn} dans le parasite WT participe à la synthèse des protéines de *Plasmodium*, et qu'en l'absence d'import dans le parasite tRip-KO, le décodage des régions riches en asparagine par le ribosome devient trop lent et conduit à la fixation du complexe Ccr4-Not et à la dégradation de l'ARNm. Cette hypothèse est soutenue par des études antérieurs montrant que (i) tRip a une préférence pour certains ARNt humains dans *P. falciparum*, en particulier l'ARNt^{Asn} (Cela et al., 2021); (ii) les aminoacyl-ARNt synthétases du parasite sont capables d'aminoacyler efficacement les ARNt humains natifs. Ainsi nous proposons qu'au court du cycle de développement du parasite, le parasite va importer de l'ARNt^{Asn} pour permettre la synthèse de ses protéines et que lorsque cet ARNt^{Asn} vient à manquer le domaine C-terminal de CAF1 ne peut plus être synthétiser, conduisant à la stabilisation spécifique des d'ARNm codants pour les protéines responsables de la libération des mérozoïtes et de l'invasion d'une nouvelle cellule à la recherche de plus d'ARNt.

Certaines expériences sont nécessaires encore pour tester notre hypothèse. Cependant, la concentration de CAF1 n'est pas suffisante dans nos expériences et n'a donc pas permis son identification par spectrométrie de masse. Des recherches supplémentaires pourraient nous aider à tester notre hypothèse en cherchant si effectivement le domaine C-terminal de CAF1 disparait dans le parasite tRip-KO. Pour ce faire, nous pourrions répéter les expériences de spectrométrie de masse soit sur toutes les protéines du parasite (sauvage et tRip-KO), soit sur des échantillons issus d'expériences d'immunoprécipitation pour augmenter nos chances de détecter CAF1. Il faudrait également vérifier si les mérozoïtes tRip-KO sont immatures comme c'est le cas pour le parasite CAF1 mutant. Enfin, *Plasmodium* a une préférence pour les réticulocytes par rapport aux erythrocytes ; bien que les réticulocytes ne représentent que 2% des cellules du sang, il a été démontré que *P. berghei, P. chabaudi, P. yoelii et P. vivax* les infectent préférentiellement (Antia et al., 2008; Cromer et al., 2006; Mons, 1990; Thawani et al., 2014). Les réticulocytes sont des précurseurs des globules rouges très efficaces en traduction et donc riches en ARNt (Smith et McNamara, 1972). Ainsi, nous pourrions tester

l'effet de l'augmentation du nombre de réticulocytes dans le sang de la souris sur l'infectivité et l'efficacité de développement du parasite.

2- tRip comme cible de nouvelles approches thérapeutiques antipaludéennes.

2-1. Sélection d'aptamères d'ARN et caractérisation de leur interaction avec tRip

Nous avons choisi d'utiliser le domaine C-terminal de tRip comme cible pour sélectionner des aptamères capables de se lier spécifiquement à la protéine. Pour ce faire, l'équipe a sélectionné des aptamères d'ARN par la méthode SELEX pour leur capacité à se lier spécifiquement au domaine C-terminal de tRip. 25 nucléotides aléatoires ont été introduits dans une bibliothèque d'ADN construite par PCR et transcrite *in vitro*. Après 5 cycles de sélection, 28 aptamères de séquences différentes ont été obtenus. Étonnamment aucune séquence ne présente de similarités avec celle des ARNt et aucun alignement significatif entre ces séquences n'a pu être effectué.

Cependant, en utilisant RNAfold pour prédire les structures secondaires, les aptamères ont pu être regroupés en trois familles : (i) le groupe A présentait le motif ACCUA dans une boucle apicale, (ii) le groupe B contenait des variants avec des mutations à l'une des cinq positions à l'intérieur du motif ACCUA, et (iii) les aptamères restants, sans motif, formaient le groupe C. Des aptamères représentatifs (Aptamer-15, Aptamer-17, Aptamer-24 et Aptamer-37) du groupe A ont été transcrits de manière radioactive *in vitro* et leur affinité pour tRip a été testée par des expériences de retard sur gel (en présence de concentrations croissantes du domaine C-terminal de tRip). Les résultats ont montré que ces aptamères du groupe A interagissent avec tRip avec une affinité comparable à celle des transcrits d'ARNt (Kd = 74nM). En effet, les aptamères et le transcrit de $ARNt^{Phe}$ (trPhe), que nous avons utilisé comme contrôle, présentent le même profil d'interaction et une affinité comparable. De plus, l'étude de ces différents apatmères a permis de conclure que la taille de la boucle apicale influençe l'efficacité de l'interaction.

Dans une deuxième étape, nous avons porté notre attention sur l'Aptamer-15. La structure de l'aptamère avec une tige et une boucle apicale contenant le motif a été confirmée par des expériences de sondes de structure *in vitro* et la reconnaissance entre tRip et le motif ACCUA a été testée par une expérience d'empreinte. Pour confirmer si effectivement le motif ACCUA est impliqué dans l'interaction avec tRip, différents mutants ont été construits et testés. J'ai introduit plusieurs mutations ponctuelles dans le motif ACCUA à la première, deuxième, troisième, quatrième ou cinquième position du motif, et j'ai construit un mutant global où tout le motif a été muté. J'ai également modifié la taille et la séquence de la tige. Enfin, j'ai montré qu'une protéine tRip mutée qui n'interagissait plus avec les ARNt n'interagit pas non plus avec

l'aptamère et ne protége plus les nucléotides du motif ACCUA dans l'expérience d'empreinte. A partir de ces expériences, nous avons conclu que (i) le motif ACCUA dans la boucle apicale est essentiel pour l'interaction de l'aptamère avec tRip, (ii) le premier nucléotide du motif contribue peu à l'interaction par rapport aux quatre autres, (iii) le motif est reconnu par tRip uniquement lorsqu'il est présent dans une région simple brin et (iv) la taille de la tige peut être raccourcie sans affecter significativement l'affinité de l'aptamère pour tRip.

Ainsi, nous avons identifié un motif, ACCUA, qui a la capacité de lier efficacement la protéine tRip. L'approche thérapeutique qui en découle pourrait inclure les deux hypothèses suivantes : (i) Utiliser l'aptamère pour bloquer l'import des ARNt. En interférant avec l'interaction entre tRip et les ARNt de l'hôte, l'import des ARNt dans le parasite peut être bloqué et/ou réduit. Étant donné l'importance des ARNt de l'hôte dans la synthèse des protéines du parasite, inhiber leur import dans le parasite pourrait affecter significativement la synthèse des protéines du parasite conduisant à un développement altéré. Cette approche est soutenue par le phénotype du parasite tRip-KO, qui présentent un développement réduit dans le sang et une synthèse protéique diminuée (Bour et al., 2016). Bien que tRip lui-même puisse ne pas être essentiel à la survie du parasite, bloquer sa fonction lui confère un désavantage significatif, entravant sa croissance et sa prolifération.

(ii) Utiliser l'aptamère comme transporteur pour convoyer des molécules toxiques spécifiquement à l'intérieur du parasite via tRip. Cette administration ciblée de composés toxiques permettrait d'inhiber des processus biologiques essentiels au sein du parasite. L'avantage de cette approche réside dans la minimisation des effets non spécifiques et la réduction de la toxicité pour l'hôte, étant donné que les composés toxiques sont dirigés vers le parasite.

Cependant, quel que soit l'approche qui sera choisie, plusieurs aspects nécessitent encore des améliorations en particulier en ce qui concerne l'administration *in vivo* de l'aptamère pour éviter toute dégradation ou toxicité potentielle. Des améliorations de sa spécificité envers tRip pourraient également être envisagées. Il convient d'étudier si l'aptamère a la capacité de pénétrer dans le parasite ou s'il bloque l'import des ARNt en restant fixé dessus. Ces questions sont cruciales pour appréhender pleinement le potentiel de l'aptamère et ses applications dans le ciblage de la protéine tRip chez les parasites.

2-2. tRip comme cible pour développer un vaccin contre le paludisme

La présence de tRip à la surface du parasite et la conservation de la séquence de son domaine C-terminal externe dans toutes les souches de *Plasmodium* font de cette protéine une cible intéressante pour immuniser les hôtes vertébrés contre le paludisme. Nous avons choisi comme modèle pour notre expérience des souris BALB/c. Le domaine C-terminal de tRip de *Plasmodium berghei* (le parasite responsable du paludisme chez les rongeurs) correspondant

aux acides aminés 200-402 a été exprimé dans des cellules bactériennes et purifié par chromatographie d'affinité. Pour étudier l'immunogénicité de tRip, nous avons utilisé des souris BALB/c âgées de 4 semaines. Elles ont été réparties en un groupe « expérimental » et un groupe « témoin ». L'immunisation a été réalisée par injection intrapéritonéale de 25 µg de $tRip_{200-402}$ dans du PBS en présence d'un adjuvant pour le premier groupe, ou avec du PBS et de l'adjuvant seulement pour le deuxième groupe. Après 2 doses de rappel (à 3 semaines d'intervalle), toutes les souris ont été infectées par *P. berghei* sauvage (exprimant la GFP), soit (i) par injection intraveineuse de 10^6, 1000 ou 500 globules rouges infectés, (ii) soit par piqûres naturelles en exposant des souris anesthésiées à des moustiques infectés affamés. À chaque immunisation, la production d'anticorps a été déterminée par des tests ELISA et, à la dernière étape, l'évolution de la parasitémie a été suivie par cyrtométrie en flux. Les résultats obtenus indiquent que le domaine C-terminal de tRip est immunogène car il induit efficacement la production d'anticorps spécifiques. En revanche, dans les conditions que nous avons testées, l'immunisation ne confère pas une protection efficace des souris contre l'infection par *P. berghei*. La parasitémie a augmenté de manière similaire dans les 2 groupes de souris et elles sont toutes décédées dans les 2 semaines suivant l'infection.

Étant donné le caractère peu concluant des résultats actuels, plusieurs possibilités de recherche ultérieure s'offrent. Tout d'abord, il serait intéressant de comprendre si le type de réponse immunitaire induit par tRip chez les souris est suffisamment fort pour conférer une protection. Il est important d'étudier si la réponse immunitaire persiste dans le temps, même pendant l'infection par le parasite. De plus, différents types d'adjuvants pourraient également être testés. Les adjuvants sont des substances ajoutées aux vaccins pour renforcer la réponse immunitaire et améliorer l'efficacité du vaccin. Étant donné que différents adjuvants peuvent stimuler différents aspects du système immunitaire, il est essentiel d'identifier l'adjuvant le plus efficace pour chaque candidat vaccin spécifique. Une autre approche pourrait consister à utiliser une protéine recombinante pour renforcer la stimulation de la réponse immunitaire. En effet, il est possible que la protéine seule ne soit pas en mesure de provoquer une réponse immunitaire adéquate. Dans le vaccin RTS,S, la protéine CSP est conjuguée à un antigène de surface du virus de l'hépatite B hautement immunogène pour améliorer son efficacité (Cohen et al., 2010).

Conclusion

L'import des ARNt dans le parasite du paludisme est à ce jour le seul exemple d'un import d'ARNt exogènes et mes travaux montrent que cet import est impliqué dans la régulation de l'expression d'un nombre limité de gènes riches en résidus asparagine. Ce mode de régulation traductionnelle permettrait de contrôler efficacement et rapidement le passage d'un stade à un

autre au cours du développement, et ce en fonction de la disponibilité des ARNt dans la cellule hôte. Ce mécanisme est d'autant plus adapté à *Plasmodium*, que le protéome du parasite est caractérisé par la présence de nombreuses homorépétitions d'asparagines ou longues insertions riches en asparagines (et ou Lysines), dont la ou les fonctions sont encore inconnues. Ainsi, on peut espérer ralentir le développement du parasite ou réduire sa pathogénicité en bloquant tRip ou encore empoisonner spécifiquement le parasite en utilisant tRip comme transporteur spécifique de molécules toxiques.

Références

Antia R, Yates A, De Roode JC. 2008. The dynamics of acute malaria infections. I. Effect of the parasite's red blood cell preference. *Proc Biol Sci* **275**:1449–1458. doi:10.1098/rspb.2008.0198

Balu B, Maher SP, Pance A, Chauhan C, Naumov AV, Andrews RM, Ellis PD, Khan SM, Lin J, Janse CJ, Rayner JC, Adams JH. 2011. CCR4-associated factor 1 coordinates the expression of *Plasmodium falciparum* egress and invasion proteins. *Eukaryot Cell* **10**:1257–1263. doi:10.1128/EC.05099-11

Bour T, Mahmoudi N, Kapps D, Thiberge S, Bargieri D, Ménard R, Frugier M. 2016. *Apicomplexa* -specific tRip facilitates import of exogenous tRNAs into malaria parasites. *Proc Natl Acad Sci USA* **113**:4717–4722. doi:10.1073/pnas.1600476113

Bunnik EM, Chung D-W, Hamilton M, Ponts N, Saraf A, Prudhomme J, Florens L, Le Roch KG. 2013. Polysome profiling reveals translational control of gene expression in the human malaria parasite *Plasmodium falciparum*. *Genome Biol* **14**:R128. doi:10.1186/gb-2013-14-11-r128

Buschauer R, Matsuo Y, Sugiyama T, Chen Y-H, Alhusaini N, Sweet T, Ikeuchi K, Cheng J, Matsuki Y, Nobuta R, Gilmozzi A, Berninghausen O, Tesina P, Becker T, Coller J, Inada T, Beckmann R. 2020. The Ccr4-Not complex monitors the translating ribosome for codon optimality. *Science* **368**:eaay6912. doi:10.1126/science.aay6912

Cela M, Théobald-Dietrich A, Rudinger-Thirion J, Wolff P, Geslain R, Frugier M. 2021. Identification of host tRNAs preferentially recognized by the *Plasmodium* surface protein tRip. *Nucleic Acids Res* **49**:10618–10629. doi:10.1093/nar/gkab769

Cohen J, Nussenzweig V, Vekemans J, Leach A. 2010. From the circumsporozoite protein to the RTS,S/AS candidate vaccine. *Hum Vaccin* **6**:90–96. doi:10.4161/hv.6.1.9677

Collart MA. 2016. The Ccr4-Not complex is a key regulator of eukaryotic gene expression. *WIREs RNA* **7**:438–454. doi:10.1002/wrna.1332

Coulson RMR, Hall N, Ouzounis CA. 2004. Comparative genomics of transcriptional control in the human malaria parasite *Plasmodium falciparum*. *Genome Res* **14**:1548–1554. doi:10.1101/gr.2218604

Cromer D, Evans KJ, Schofield L, Davenport MP. 2006. Preferential invasion of reticulocytes during late-stage *Plasmodium berghei* infection accounts for reduced circulating reticulocyte levels. *Int J Parasitol* **36**:1389–1397. doi:10.1016/j.ijpara.2006.07.009

Mons B. 1990. Preferential invasion of malarial merozoites into young red blood cells. *Blood Cells* **16**:299–312.

Jaramillo Ponce JR, Kapps D, Paulus C, Chicher J, Frugier M. 2022. Discovery of two distinct aminoacyl-tRNA synthetase complexes anchored to the *Plasmodium* surface tRNA import

protein. *J Biol Chem* **298**:101987. doi:10.1016/j.jbc.2022.101987

Jaramillo Ponce JR, Théobald-Dietrich A, Bénas P, Paulus C, Sauter C, Frugier M. 2023. Solution X-ray scattering highlights discrepancies in *Plasmodium* multi-aminoacyl-tRNA synthetase complexes. *Protein Sci* **32**:e4564. doi:10.1002/pro.4564

Smith DWE, McNamara AL. 1972. The transfer RNA content of rabbit reticulocytes. *Biochim Biophys Acta* **269**:67–77. doi:10.1016/0005-2787(72)90075-5

Thawani N, Tam M, Bellemare M-J, Bohle DS, Olivier M, De Souza JB, Stevenson MM. 2014. *Plasmodium* products contribute to severe malarial anemia by inhibiting erythropoietin-induced proliferation of erythroid precursors. *J Infect Dis* **209**:140–149. doi:10.1093/infdis/jit417

Tucker M, Valencia-Sanchez MA, Staples RR, Chen J, Denis CL, Parker R. 2001. The transcription factor associated Ccr4 and Caf1 proteins are components of the major cytoplasmic mRNA deadenylase in *Saccharomyces cerevisiae*. *Cell* **104**:377–386. doi:10.1016/S0092-8674(01)00225-2

TABLE OF CONTENTS

LIST OF FIGURES AND TABLES

Abbreviations

aaRS	aminoacyl-tRNA synthetases
ALBA	acetylation lowers binding
AMA1	apical membrane antigen 1
ART	artemisinin
bp	base pair
cpm	counts per minute
BSA	bovine serum albumin
CDS	coding DNA sequence
CQ	chloroquine
CSP	circumsporozoite protein
DDM	n-dodecyl-β-D-maltoside
dNTP	deoxynucleoside triphosphate
DOZI	development of zygote inhibit
DTE	dithioerythritol
eIF	eukaryotic translation initiation factor
HEPES	4-(2-hydroxyethyl)-1-piperazine ethanesulfonic acid
IDC	intraerythrocytic development cycle
IPTG	isopropyl β- d-1-thiogalactopyranoside
iRBCs	infected red blood cells
LB	Luria Bertani
LCR	low complexity region
MSP	merozoite surface protein
Min	minutes
mRNP	messenger ribonucleoproteins
Ni-NTA	nickel- nitriloacetic acid
OD	optical denisty
PABP	poly(A)-binding protein
PAGE	polyacrylamide gel electrophoresis
PBS	phosphate buffered saline
RBC	red blood cell
PI3K	phosphoinositide 3-kinase
PI3P	phosphatidylinositol 3-monophosphate
Rpm	revolutions per minute
RPMI	Roswell Park Memorial Institute medium
TBE	tris-borate-EDTA
tr	transcript
tRNA	RNA transfer
UPR	unfolded protein response
UTR	untranslated region
SDS	sodium dodecyl sulfate
Sec	seconds
V	volt
VLP	virus-like particles
WT	wild-type

INTRODUCTION

I. The Malaria

Malaria is caused by an unicellular protozoan parasites belonging to the *Plasmodium* genus, transmitted to humans by female mosquitoes of the *Anopheles* genus. In humans, five species of *Plasmodium* are infectious: *P. falciparum*, *P. vivax*, *P. ovale*, *P. malariae* and *P. knowlesi*. However, most of the mortality is attributed to *P. falciparum* (WHO, 2018).

1. The history of malaria

The history of malaria is as old as that of humankind itself (reviewed in Dobson, 1999; Fantini, 1999; Sallares et al., 2004). It has plagued human populations throughout history, leaving a devastating impact and shaping civilizations. The origins of malaria date back to ancient times. In the ancient world, the disease was prevalent in regions with warm climates and stagnant water, providing ideal breeding grounds for mosquitoes carrying the malaria parasite. Various civilizations, including ancient Greece, Rome, India, and China, were significantly affected by malaria. In ancient Greece the disease was known as "marsh fever" or "swamp fever" due to its association with marshy areas. The Greek physician Hippocrates (460-377 BC) recognized and described malaria symptoms, such as recurring fevers and chills. However, the exact cause of the disease remained unknown at that time. In ancient Rome malaria represented a significant threat to the expanding empire and may have played a role in its decline and fall. The disease was commonly referred to as "Roman fever." Ancient eastern civilizations, such as China and India, faced similar challenges. Throughout the middle age, malaria continued to afflict populations across Europe, Africa, and Asia, affecting both rural and urban areas. The disease hindered agricultural productivity and impeded economic development.

Originally, malaria was believed to be caused by foul air emanating from swamps and marshes, hence its name "malaria," derived from the Italian words for "bad" (mal) and "air" (aria). Although descriptions of malaria symptoms can be traced back to antiquity, it took a long time to identify the vector and causative agent of this major human parasitic disease. It was not until the 19th century that significant advancements were made in understanding the cause and transmission of malaria. In 1880, French army surgeon Charles Louis Alphonse Laveran identified the malaria parasite in infected individuals' blood, revealing that the disease was caused by parasitic protozoans. As early as 1882, further breakthroughs came with the understanding of mosquitoes' role in transmitting malaria. This hypothesis was later confirmed in 1897 when Ronald Ross discovered the importance of mosquitoes in the avian malaria life cycle and described malaria cysts in the stomach walls of *Anopheles* mosquitoes. In 1898, Giovanni Battista Grassi described the complete transmission cycle of the parasite and demonstrated that malaria observed in humans is transmitted by mosquitoes of the *Anopheles* genus.

2. Endemic regions and clinical aspects

Malaria is a significant global health concern, particularly in tropical and subtropical regions (Figure 1A). The disease is endemic in many countries, with the majority of cases occurring in sub-Saharan Africa. However, malaria also affects other regions such as Southeast Asia, the Eastern Mediterranean, and the Americas. The transmission of malaria is closely linked to environmental factors, such as temperature, humidity, and rainfall, which affect the breeding and survival of mosquito vectors. The World Health Organization (WHO) estimates that there were approximately 241 million cases of malaria worldwide in 2020, with 95% of them occurring in Africa. It is estimated that 627,000 people died from malaria in 2020, mostly children under the age of 5. These cases pose a considerable burden on public health systems and have a significant impact on the socioeconomic development of affected communities (WHO, 2020).

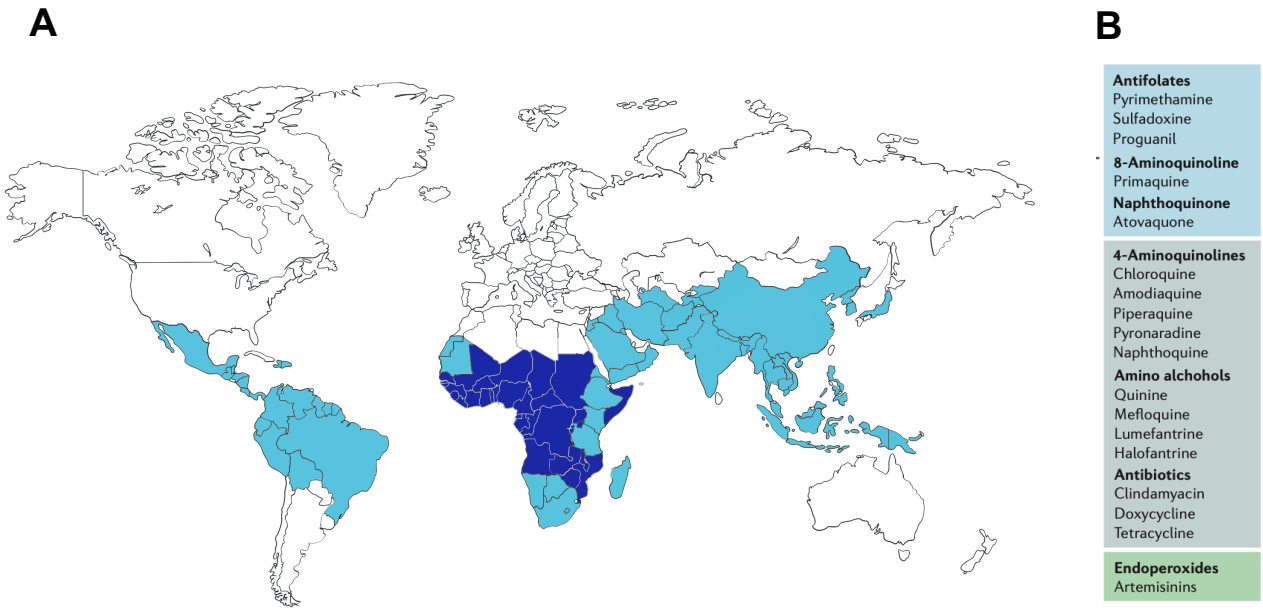

Figure 1: Regions of the world where malaria transmission is endemic.
(A) The map is adapted from the Centers for Diseases Control and Prevention site (CDC, 2020). Dark blue: malaria is present everywhere. The highest transmission is observed in Africa (south of the Sahara) and in certain parts of Oceania, such as Papua New Guinea. Light blue: malaria is only present in certain areas. In such regions, transmission is less intense and more seasonal. Finally, in temperate regions, such as Western Europe and the USA, economic development and public health measures have eliminated malaria. However, in most of these regions, *Anopheles* mosquitoes can transmit malaria, and reintroduction of the disease is a constant risk. **(B)** Classification of the different drugs active against the development of the malaria parasite.

Malarial episodes typically present as fever attacks accompanied by multiple symptoms such as flu-like illness, including chills, headache, muscle aches, and tiredness. Nausea, vomiting, and diarrhea may also occur. Malaria may cause anemia and jaundice (yellow coloring of the

skin and eyes) because of the loss of red blood cells. If not promptly treated, the infection can become severe and may cause kidney failure, seizures, mental confusion, coma, and death (White, 1996).

These clinical manifestations result from the infection of human erythrocytes by the parasite and its rapid development. The frequency of fever episodes depends on the *Plasmodium* species involved: three days for *P. falciparum*, *P. vivax*, and *P. ovale*, and four days for *P. malariae*. In the case of *P. falciparum*, there are three major complications that can occur concurrently and have a fatal prognosis: severe anemia, acute respiratory distress syndrome, and cerebral malaria. The mortality rate for this complication is about 20% in adults and 15% in children. Furthermore, 5% of adults and 10% of surviving children experience persistent neurological sequelae such as deafness, blindness, hemiplegia, psychosis, mental retardation, and behavioral disorders (Dugbartey et al., 1998).

Efforts to control and eliminate malaria involve various strategies, including vector control measures, early diagnosis, prompt treatment, and the development of malaria vaccines.

II. Therapeutic approaches against malaria

1. Advancements in antimalarial medications

Malaria is a global health problem that can lead to death if not treated in time. The use of drugs is the oldest way to treating malaria. A drug is a substance, natural or synthetic, used to prevent and treat the disease (Mathur and Hoskins, 2017). Many antimalarial drugs are known (Alam et al., 2009); they are classified into 7 chemical classes (Figure 1B) (Nqoro et al., 2017). All of them target the asexual stages of the parasite, either in the blood (artemisinins) or in the liver (antifolates, primaquine and atovaquone). Primaquine is the only drug that targets latency form in the liver to prevent the recurrent infections characteristic of *P. vivax* (the development cycle of *Plasmodium* is explained in the chapter III of this introduction). However, each group of drug corresponds to a precise mode of action against the malaria parasite.

Important antimalarial drugs belonging to the 4-aminoquinoline class, such as chloroquine (CQ) and amodiaquine (AQ), have been used to prevent and treat malaria for many years (Parhizgar and Tahghighi, 2017). They inhibit the action of heme polymerase (Sullivan et al., 1996). However, the resistance to CQ and its analogues have reduced their consumption in many geographical areas such as Papua New Guinea, Indonesia and India (Parhizgar and Tahghighi, 2017). The rise in resistance to chloroquine and sulfadoxine-pyrimethamine has led to the use of artemisinin and its related treatments (ARTs) especially in Africa. They are strongly recommended for the treatment of malaria by the World Health Organization (WHO, 2018). Because artemisinin is poorly soluble in oil and water, it is its derivatives (dihydroartemisinin, artesunate and artemether) that are most often used (Yang et al., 2020). Artemisinin and derivatives are active against asexual blood stages and male gametocyte by alkylating plasmodial key proteins and thus by hindering the transmission of the parasite to the mosquito (Rosenthal and Ng, 2020).

1.1. Artemisinin-Related Treatments (ARTs) as antimalarial therapy

Artemisinin is a sesquiterpene-lactone, a secondary metabolite isolated from the Chinese herb Qing Hao, also known as *Artemisia annua* (Tu, 2011). This compound is characterized by the presence of a peroxide bridge, that is supposed to be involved in its antimalarial activity (Ma et al., 2020). However, the exact mode of action of artemisinin and its derivatives is not yet fully understood (Tandoh et al., 2021) especially because it is radically different from that of other antimalarial drugs, which target specific enzymes or pathways. Indeed, it has been established that ARTs must be activated by reduced Fe^{2+} released by the enzymatic digestion of hemoglobin resulting from the infection of red blood cells by *Plasmodium* (Ma et al., 2021) (Figure 2A).

These drugs (i) damage DNA (Gopalakrishnan and Kumar, 2015); (ii) trigger ubiquitination of phosphatidylinositol-3-kinase (PI3K) leading to accumulation of reduced lipid phosphatidylinositol 3-phosphate (PI3P) (Tawk et al., 2010); (iii) disrupt proteasome function (Bridgford et al., 2018) as well as the unfolded protein response (UPR) pathway of the parasite (Talman et al., 2019), leading to an accumulation of non-functional proteins in the parasite; (iv) induces endoplasmic reticulum stress; (v) inhibits hematin crystallisation and hence heme detoxification (Ma et al., 2021); and (vi) leads to the production of radical oxygen species (ROS) (following cleavage of the endoperoxide bridge in artemisinin). Together, these actions ultimately lead to the death of the parasite. Ring forms and trophozoites (blood stage) of the parasite are particularly affected by this process (Yang et al., 2020).

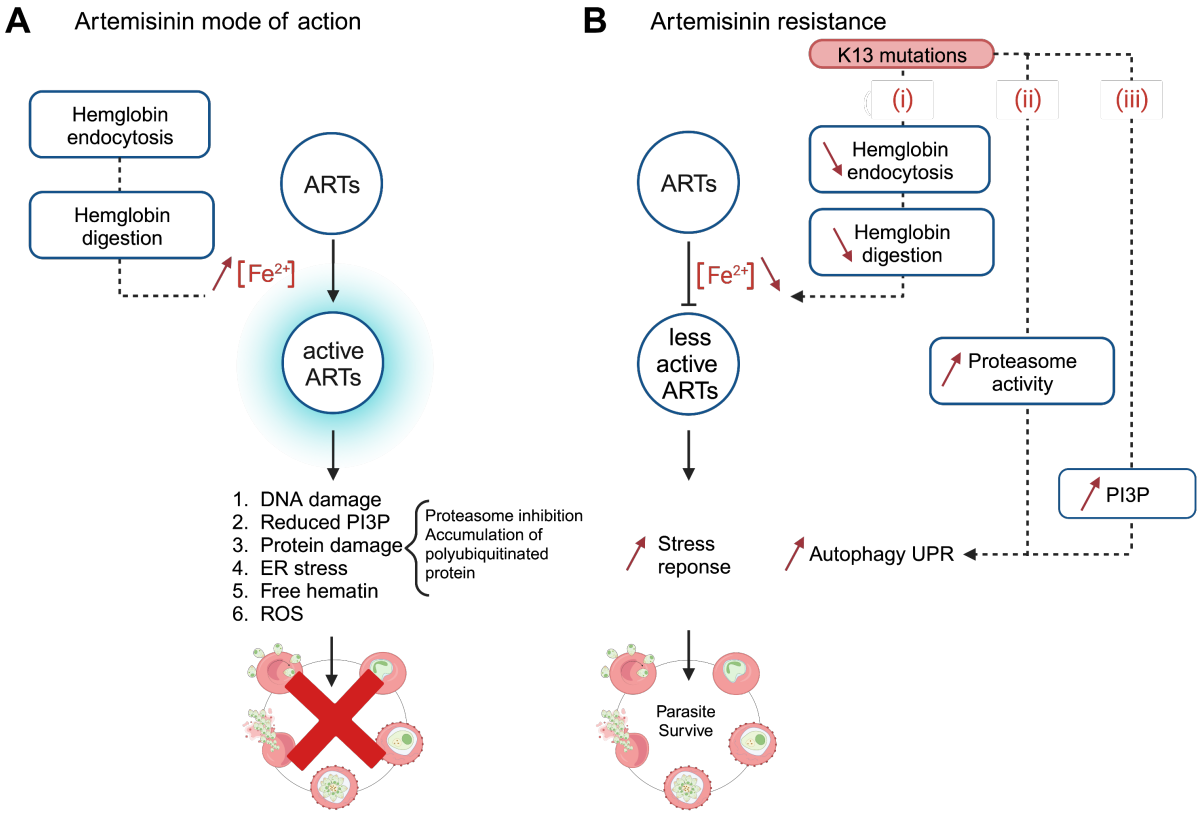

Figure 2: Possible mechanisms of artemisinin mode of action (A) and resistance (B) in *P. falciparum*.
(A) During red blood cell invasion, hemoglobin endocytosis occurs, digestion of hemoglobin releases Fe^{2+}, which in turn is able to activate artemisinin and derivatives (ARTs). These drugs alter different cellular functions of the parasite, such as unfolded protein response, protein polyubiquitination, proteasome and phosphatidylinositol-3-kinase (PI3K). The accumulation of polyubiquitinated proteins, damaged DNA and reactive oxygen species lead the parasite to death. **(B)** Resistance is associated with mutations in the K13 protein, which reduces hemoglobin digestion and lowers free Fe^{2+} required for ARTs activation. Reduction of the damages listed above results in parasite survival (mechanism proposed by Azmi et al., 2023).

1.2. Artemisinin resistance

Plasmodium drug resistance is a growing problem, and now also affects artemisinin alone and ARTs. Resistance is characterized by decreased medication efficacy and a prolonged parasite elimination period during therapy (Tilley et al., 2016). In South-East Asia, particularly in Cambodia, Thailand, Laos, and Vietnam, as well as in Africa, cases of resistance have been documented (WHO, 2020; Rogers et al., 2009; Balikagala et al., 2021). Mutations in the kelch13 (k13) gene is the primary indicator of artemisinin resistance (Azmi et al., 2023). In *P. falciparum* k13 gene encodes the protein K13, crucial for the parasite's intraerythrocytic stage (Coppée et al., 2019). The hypothesized mechanism of artemisinin resistance associated to the K13 mutations in *P. falciparum* (Figure 2B) involves (i) a reduction in hemoglobin endocytosis and thus in hemoglobin digestion. The reduction of free Fe^{2+} in turn inhibits artemisinin activation (Xie et al., 2020); (ii) improved proteasome activity (Bridgford et al., 2018) and (iii) reduced proteolysis of PI3K and therefore increased levels of PI3P which stimulate autophagy, engaging UPR that initiate a stress response (Mbengue et al., 2015), thereby promoting parasite survival.

1.3. Artemisinin-based combination treatments (ACTs) as antimalarial therapy

Although artemisinin and its derivatives have been extensively used worldwide as first-line drugs for the treatment of malaria, the emergence of parasite resistance to these drugs is a major cause of concern. To prevent the recrudescence and development of resistance, the use of ART in combination with other drugs, or artemisinin-based combination therapy (ACT), are the main treatment for both severe and uncomplicated *P. falciparum* malaria infections (Talman et al., 2019). It consists in artemisinin administration with a partner drug with a longer half-life (Rosenthal and Ng, 2020) to reduce the emergence of medication resistance. The WHO provides precise recommendations for six partner medication combinations that are utilized in ARTs (WHO, 2020) (Table 1). In this strategy, artemisinin confers rapid and strong efficacy, while its very short half-life (<1h00) is compensated for by a second, longer-lasting antimalarial partner drug, such as lumefantrine, mefloquine, piperaquine, amodiaquine or sulfadoxine-pyrimethamine (Table 1). Thus, parasites resistant to artemisinin will be eliminated by the partner drug.

Table 1: List of antimalarial drugs used as partner of artemisinin in the Artemisinin-based combinations therapy.

Associated drug	Target and mechanism
Amodiaquine	The mechanism is unknown, although it is assumed that it prevents the activity of heme polymerase. The toxic amodiaquine-heme complex interferes with the parasite's ability to maintain its membrane integrity.
Lumefantrine	Unknown the exact mechanism, maybe it interferes with protein and nucleic acid synthesis. Additionally, it acts against the erythrocytic stages of *Plasmodium* sp.
Mefloquine	It's unclear exactly how the mechanism works. It directly binds to the *P.falciparum* 80S-ribosome in the cytoplasm, inhibiting the synthesis of parasite proteins. It disrupts the membrane of the parasite.
Piperaquine	Chloroquine's mechanism is comparable to this one. It prevents heme detoxification pathway.
Pyrimethamine	Dihydro-folate reductase (DHFR) is inhibited by pyrimethamine.
Pyronaridine	It attaches to DNA and interferes with the metabolism of nucleic acids.
Sulfadoxine	Sulfadoxine specifically targets the dihydropteroate synthase (DHPS) and dihydrofolate reductase (DHFR) proteins of *Plasmodium*. DHPS transforms para-aminobenzoic acid into folic acid, which aids in the nucleic acids synthesis.

Adapted from (Tripathi et al., 2023).

2. Malaria vaccines: the state of art

Vaccines remain one of the most effective strategies in the fight against malaria. Research on this subject began several decades ago. Early studies showed that by infecting mice with irradiated *P. berghei* (rodent specific parasite) sporozoites and then exposing the immunised mice to infected sporozoites, the mice were protected against the infection. However, when the immunised mice were infected with infected red blood cells (iRBCs), they developed parasitaemia (Nussenzweig et al., 1967). This experiment provides a clear indication of the variability of the parasite proteome. Indeed, *Plasmodium* expresses a variety of proteins throughout its life cycle, specific to different stages (Florens et al., 2002). This complexity represents a major challenge in the search for an effective vaccine. Thus, current research is focusing on studying the different proteomes that characterize each stage of the parasite (summarized in Figure 3A), in order to identify proteins with the aim of developing candidate vaccines specific to each stage. Malaria vaccines have thus been designed to act at (i) the pre-erythrocytic stage, (ii) the erythrocytic stage, or (iii) the sexually differentiated stage in order to block transmission (Figure 3B) (Arora et al., 2021).

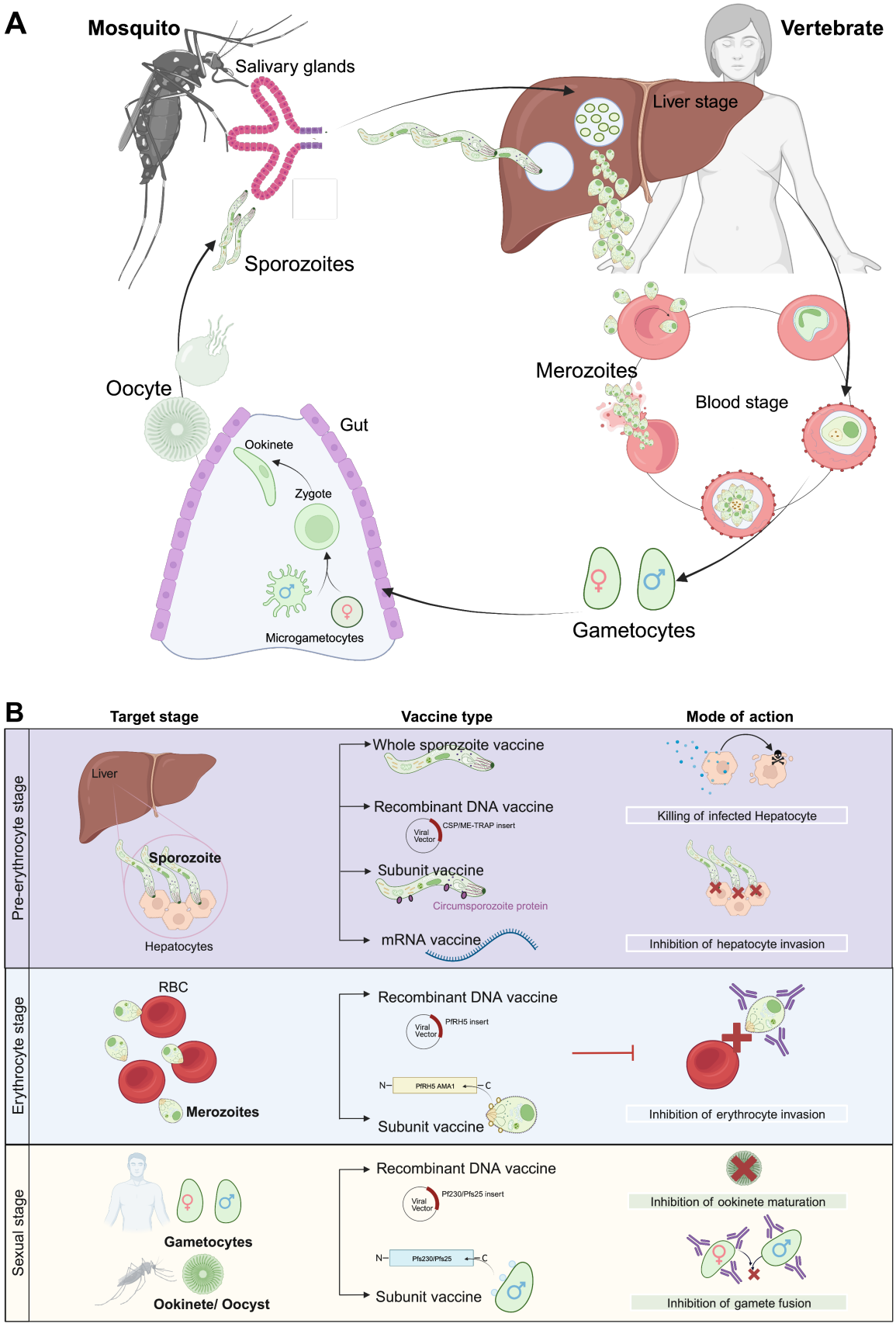

Figure 3: *Plasmodium* life cycle and summary of the major malarial vaccine types as well as their mode of action.

Legend continues on next page.

(A) Simplified *Plasmodium* life cycle: when a mosquito infected with *Plasmodium* bites a human, the parasite, present in the salivary glands, is injected into the bloodstream of the vertebrate host and travels to the liver. During the liver stage, the parasite reproduces intensively in the hepatocytes. The parasites are then released into the bloodstream to complete the erythrocytic stages (rings, trophozoites and merozoites) and differentiate into gametocytes. Any mosquito that feeds on infected blood can suck up the gametocytes, which transform into ookinetes and oocysts in the mosquito, then finally migrate to the salivary glands, where they are stored in the form of sporozoites.
(B) Vaccinal strategies developed against the different parasites development stages (adapted from Tripathi et al., 2023).

These vaccines often target surface proteins such as the circumsporozoite protein (CSP) abundantly expressed on the surface of sporozoites (Young et al., 1985), cell-traversal protein for ookinetes and sporozoites (CelTOS), merozoite surface proteins (MSPs or AMA1) (Miura et al., 2009), as well as Pfs230 and Pfs25 on the surface of gametocytes and ookinetes, respectively (Tripathi et al., 2023). To date, the most effective type of vaccine is the pre- erythrocytic vaccine, which directly targets the sporozoites as soon as they are injected by the mosquito, thus preventing infection of the hepatocytes.
In the following paragraphs, I will summarise the main types of vaccine developed against malaria: the whole parasite vaccine, the “subunit” vaccine and the recombinant DNA or viral vector vaccines (Figure 3B).

2.1. Whole organism approaches

Numerous studies have been carried out to create a malaria vaccine using infected mosquitoes. These approaches use sporozoites attenuated either by radiation or by the modification of the genome. In the first approach, a natural infection is simulated; the whole parasite is extracted from the salivary glands of mosquitoes irradiated with gamma rays (Nussenzweig et al., 1967). This method was used to create the Sanaria *P. falciparum* sporozoite vaccine (PfSPZ, phase II in completion) (Epstein et al., 2017; Mordmüller et al., 2022), which provides complete protection for weeks and controlled infection for the following months. The second approach uses genetically attenuated parasites (GAP) either by overexpressing immunogenic proteins or toxins (known as suicide parasites) or by deleting critical genes (single, double or triple knock-out) (Roestenberg et al., 2020). One example is the PfSPZ-GAP1 vaccine (phase I/IIa completed). In this case, the sporozoites are deleted of the two genes encoding the Slarp and b9 proteins, both proteins being essential for the liver stage development. The modified parasites are then no longer infectious but still immunogenic (Roestenberg et al., 2020).
However, there are limits to the use of whole parasites as vaccines, in particular concerning the risk of causing disease if parasite inactivation is not complete. In addition, the cost,

logistical considerations and potentially limited duration of the protection must be taken into account. However, ongoing research is aimed at overcoming these limitations and optimising the efficacy and safety of these vaccines.

2.2. Subunit vaccines

Subunit vaccine is considered the safest method of immunization, as it carries a low chance of toxicity and reactogenicity (Cid and Bolívar, 2021). In the context of malaria, various subunit vaccines have been developed, each targeting specific proteins of the parasite. Among the many subunit vaccines under development and/or in clinical trials, some examples targeting the pre-erythrocytic or erythrocytic stage will be given.

2.2.1. Pre-erythrocyte stage subunit vaccines target the circumsporozoite protein (CSP)

Pre-erythrocytic vaccines target *Plasmodium* sporozoite and hepatic stage antigens (Duffy and Patrick Gorres, 2020). The RTS,S/AS01 pre-erythrocytic vaccine is the first vaccine to be approved by the World Health Organization (WHO, 2021), while the R21/Matrix M vaccine has passed phase II clinical trials and is now in phase III (Datoo et al., 2022). In both examples, the target protein used is the circumsporozoite protein (CSP), a surface protein that completely covers the sporozoites and induces a strong immune response (Coppi et al., 2005). The CSP plays an essential role in sporozoite maturation and migration through the cells of the mosquito and host dermis. These different roles depend on the structural folding of CSP: in its adhesive conformation (with region II exposed) CSP is involved in the transformation of oocysts into sporozoites and the invasion of hepatocytes whereas it adopts a non-adhesive conformation (region II hidden) during the migration stages through the different host cells that the sporozoite passes across. Once in the liver, the CSP binds specifically to the heparan sulphate proteoglycans that coat the hepatocytes, allowing the sporozoite to invade the cell and initiate the liver stage.

In *P. falciparum* (strain NF54), CSP is made up of 397 amino acids. Apart from the N-terminal signal peptide and the C-terminal glycosylphosphatidylinositol (GPI) anchor sequence, the protein is divided into three well-defined structural domains (Figure 4A).

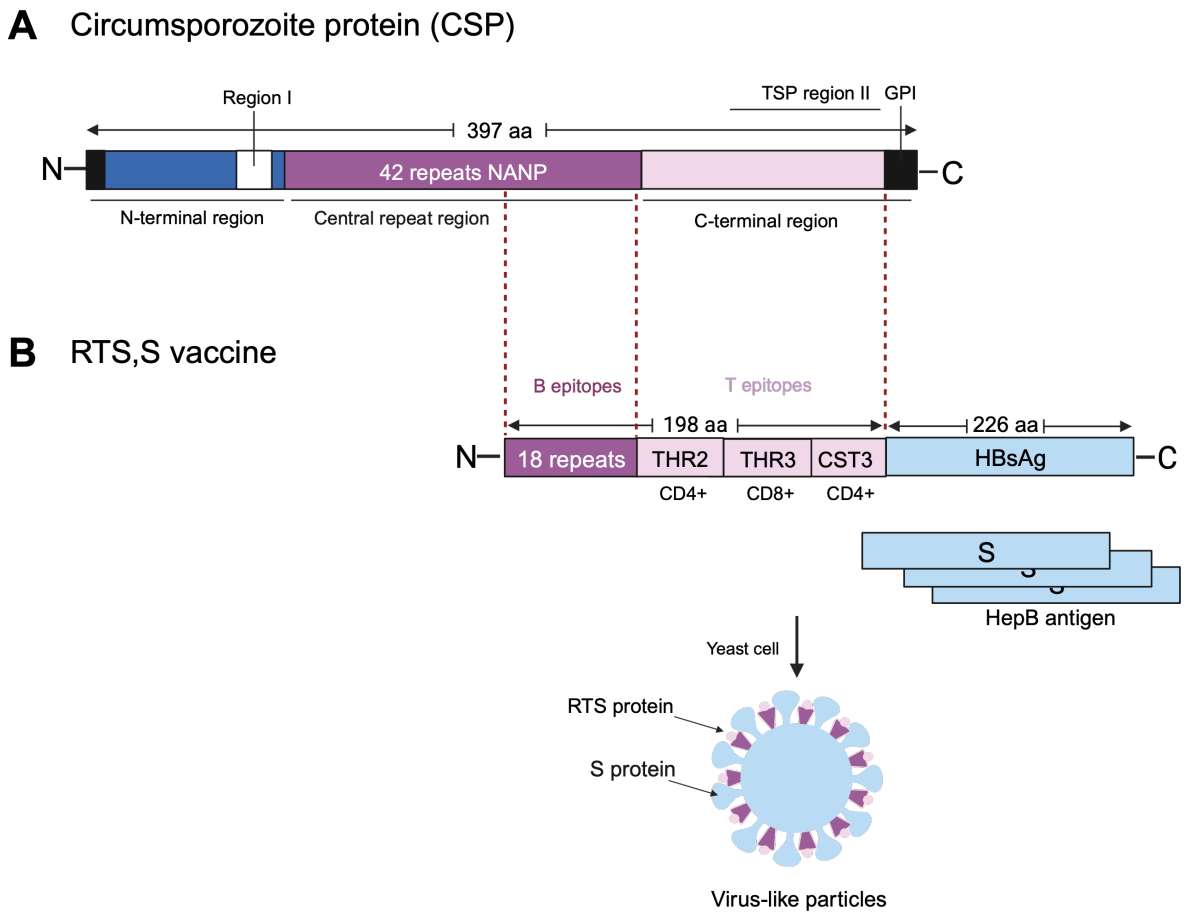

Figure 4: Schematic representation of the CSP-based vaccines strategy.
(A) Modular organization of the *P. falciparum* CSP. The N-terminal signal peptide and the C-terminal GPI anchor sequence are shown in black. The N-terminal domain is in blue with Region I shown in white, while the C-terminal region is in light pink and encompasses Region II. The central region in purple contains 42 NANP repeats. **(B)** RTS,S vaccine construct: B cell epitopes are present amongst 18 NANP repeats from the central domain and the 3 CD4+ and CD8+ T-cell epitopes present in the C-terminal domain of CSP are fused to the Hepatitis B virus surface antigen (HBsAg). When expressed in yeast, these fusion proteins and additional copies of HBsAg (in light blue) self-assemble into virus-like particles (VLP) and serve as protein carriers.

(1) The N-terminal domain contains Region I that not only binds to heparan sulphate proteoglycans located on liver tissues and plays thus a crucial role in hepatocyte invasion (Doolan et al., 1997) but also that displays a conserved five amino acids proteolytic cleavage site (KLKQP) that is associated with productive invasion of cells (Coppi et al., 2005) and occurs when sporozoites contact hepatocytes.
(2) The C-terminal domain contains a conserved sequence similar to the thrombospondin (TSP)-like domain, referred to as Region II (Goundis and Reid, 1988) and displays also three known T-cell epitopes (TH2R, TH3R and CS.T3) recognized either by CD4+ or CD8+ T-cells (Almeida et al., 2021).

(3) The central region is composed of 42 four amino acid repeats (NANP/NVDP), which constitutes immunodominant B-cell epitopes (Gordon et al., 1995).
The different domains of the CSP are conserved among *Plasmodium* species infecting rodents, primates and humans, although the central repeat region varies from one *Plasmodium* species to another.

2.2.1.1. RTS,S/AS01 vaccine

The RTS,S/AS01 vaccine was initiated in 1987 by Walter Reed Army Institute of Research (WRAIR) and GlaxoSmithKline (GSK). It was further developed in 2001 by GSK, PATH's Malaria Vaccine Initiative and the Bill and Melinda Gates foundation. It was first used in 2019 on infants and young children in malaria-endemic areas. The overall strategy was based on an early observation in which the National Institute of Health (NIH) and WRAIR demonstrated that irradiated sporozoites triggered an immune response directed against the CSP. The CSP was cloned and sequenced (Zavala et al., 1985) and GSK researchers used the hepatitis B surface antigen (HBsAg) as a carrier matrix for the CSP central repeat (18 NANP) and C-terminal regions that contain B- and T-cell epitopes, respectively (Cohen et al., 2010) (Figure 4B). The RTS,S construct therefore contains 189 amino acids from the CSP and 226 amino acids from the HBsAg. Although this first-generation malaria vaccine has demonstrated modest efficacy, it remains promising as a public health tool, particularly for children in areas where the mortality is high.

2.2.1.2. R21/Matrix M vaccine

The R21 vaccine is similar to the RTS,S vaccine, except that the R21 VLPs are formed from a single CSP-HBsAg fusion protein, increasing the proportion of CSP on the antigen surface and therefore inducing a stronger anti-CSP antibody response. This vaccine is a new-generation vaccine characterized by an enhanced immune response, and preclinical trials (phase II) have demonstrated increased protection. R21 is a promising contender for malaria vaccination in the near future (Datoo et al., 2021). It shows high efficiency following a fourth booster dose since it reduced clinical malaria cases by 39% and severe malaria by 30%. However, as R21 is still in the early stages of development, questions remain as to its efficacy in people infected in a controlled manner (deliberate infection with malaria parasites, either by mosquito bite or direct injection of sporozoites) or naturally in people living in endemic areas.

2.2.1.3. Self-assembling protein nanoparticle (SAPN)

This technology uses the ability of proteins and peptides to self-assemble into mechanically and chemically stable particles. SAPNs are designed to increase immunogenicity by exposing

multiple copies of the antigen to their surface and solve the problems that arise with linear peptide antigens, which are unstable and rapidly degraded (Burkhard and Lanar, 2015). Such a strategy has been developed for a pre-erythrocytic stage subunit malaria vaccine that targets the *P. falciparum* CSP: the particle consists of 60 copies of the protein region that includes the CD4+ and CD8+ epitopes and 6 repeats of the NANP motifs (Seth et al., 2017). The nanoparticles are highly immunogenic and protect mice against infection. This vaccine is currently being tested in clinical trials.

2.2.2. Erythrocyte stage vaccines

Vaccines targeting the erythrocyte stage that undergoes repeated multiplicative cycles in erythrocytes and causes disease and death. These vaccines are designed to prevent or block invasion of red blood cells by the parasite. The glycoproteins MSP1, MSP2, MSP3, MSP4, MSP8, MSP10 are well-known merozoite surface proteins and are the most widely used target in the development of erythrocyte stage vaccines (Perraut et al., 2017).

This strategy is based on the observation that MSP1 is the main target of the antibody response of naturally acquired immunity during the blood stage of the parasite. MSP1 is a 185 kDa protein, and only the 42 kDa C-terminal fragment has been shown to be immunogenic (Shen et al., 2021). Clinical trials have therefore mainly focused on this area, alone or in combination with other merozoite antigens such as AMA1 in *P. falciparum* (Elias et al., 2014; Mehrizi et al., 2021) or MSP8 in *P. vivax* (Shen et al., 2021), for example. While immunization trials with these antigens in animals have been promising, those carried out in humans have not been convincing and have therefore failed to demonstrate protection against malaria.

Other candidate vaccines have been developed based on other merozoite surface proteins such as MSP3, AMA1 (apical membrane antigen 1), SERA5 (serine-repeat antigen protein 5) and PvDBP (*P. vivax* duffy binding protein) or the erythrocyte-binding antigen RH5 (reticulocyte binding-like protein 5) (reviewed in Miura, 2016). These vaccines prevent erythrocyte invasion and symptom progression, but ultimately the results showed little evidence of protection against controlled human infection or natural infection. Future studies will therefore need to further improve the quality of immunity developed by the vaccinated host.

2.2.3. Transmission blocking vaccine

Transmission blocking vaccines aim to reduce the transmission of the parasite from an infected vertebrate host (human) to the mosquito. To do this, they target the surface antigens of the sexual stages of mosquitoes (gametocytes in the vertebrate host and gametes, zygotes or ookinetes in the mosquito) in order to induce antibodies that kill the parasites in the mosquito's blood meal and interrupt transmission of the parasite by the vector (Gwadz, 1976; Sauerwein

and Bousema, 2015; Schorderet-Weber et al., 2017). The two main antigens used are surface proteins expressed by (i) gametocytes in human blood, Pfs230, and (ii) the zygote in the mosquito, Pfs25. Pfs25 has been the focus of the majority of trials published to date, as it is not only the first TBV candidate prepared as a recombinant protein, but also effectively blocks transmission of the parasite (Barr et al., 1991; Radtke et al., 2017).

However, recombinant Pfs25 antigens have shown poor immunogenicity as a monomer. To improve its immunogenicity, it was coupled to carriers to generate nanoparticles, which are well tolerated and functional antibodies in humans that block transmission of *P. falciparum* to mosquitoes in membrane feeding assays (Talaat et al., 2016). However, functional activity in most vaccinees required 4 doses and antibody titres declined rapidly.

The same approaches were used to test the activity of candidate vaccines against Pfs230 (Read et al., 1994) and studies are underway combining Pfs25 and Pfs230 vaccine antigens. The major challenge in the development of transmission blocking vaccines is obtaining sufficient responses to maintain high antibody levels over time. In addition, these vaccines must have an exceptional safety profile as they do not confer any direct benefit to the individual.

2.3. Nucleic acid vaccines

Nucleic acid-based vaccines represent a new approach involving the synthesis of immunogenic proteins or peptides *in situ* (Restifo et al., 2000).

The DNA vaccine approach represents one of these promising platforms for malaria vaccine development, due to its ease of production, low cost, stability and ability to induce cellular and humoral responses (Ferraro et al., 2013; Molina-Franky et al., 2020; Yusuf et al., 2019). DNA vaccines have been developed for pre-erythrocytic stages, targeting CSP or TRAP (thrombospondin-related adhesion protein fused to a chain of multiple CD4+ and CD8+ malaria epitopes) and for erythrocytic stages, targeting PfRH5, as well as for transmission, targeting Pfs230 and Pfs25, and have been tested alone or in combination. For example, DNA vaccines encoding PfCSP have already been shown to induce specific T-cell responses and anti-CSP antibodies that can provide substantial protection against malaria infection in mice, monkeys and humans and have since been significantly improved.

Technological advances continue to offer unique opportunities for the development of nucleic acid-based vaccines, such as the use of mRNA-LPN vaccines. Indeed, the transient nature of RNA and its localisation in the cytoplasm make it a safe candidate. Unlike DNA, RNA does not need to be transported into the nucleus, so there is no risk of insertional mutagenesis. In addition, mRNA undergoes degradation by normal cellular processes, and its *in vivo* half-life can be controlled by different modifications and delivery methods (Guan and Rosenecker, 2017; Kauffman et al., 2016). Two *P. falciparum* vaccine candidates, Pfs25 and PfCSP,

administered as mRNA- LPN vaccines, induced extremely potent immune responses, superior to the corresponding DNA vaccine formulations (Hayashi et al., 2022). A combination of these two vaccines, targeting both the infectious and sexual stages, will produce a very effective vaccine and interrupt malaria transmission.

The same technology has been used for a slightly different approach by blocking macrophage migration factor (PMIF), a cytokine secreted by the parasite to reduce and control the host immune response to infection. In this case, control of *Plasmodium* infection in liver and blood was possible and complete protection against reinfection was observed (Baeza Garcia et al., 2018). These experiments were carried out in the mouse model and have not yet been extended to humans.

To conclude this first part, the various malaria vaccines, whatever their advantages and disadvantages (Figure 5), are progressing through clinical trials and the first of them, RTS,S, has reached the implementation stage. In addition to questions about the efficacy of these malaria vaccines and the number of boosters needed to achieve sufficient efficacy, there are also questions about how these vaccines can best be deployed to benefit communities devastated by malaria. Researchers are currently continuing to focus on the discovery of new antigens in order to develop and improve these powerful approaches.

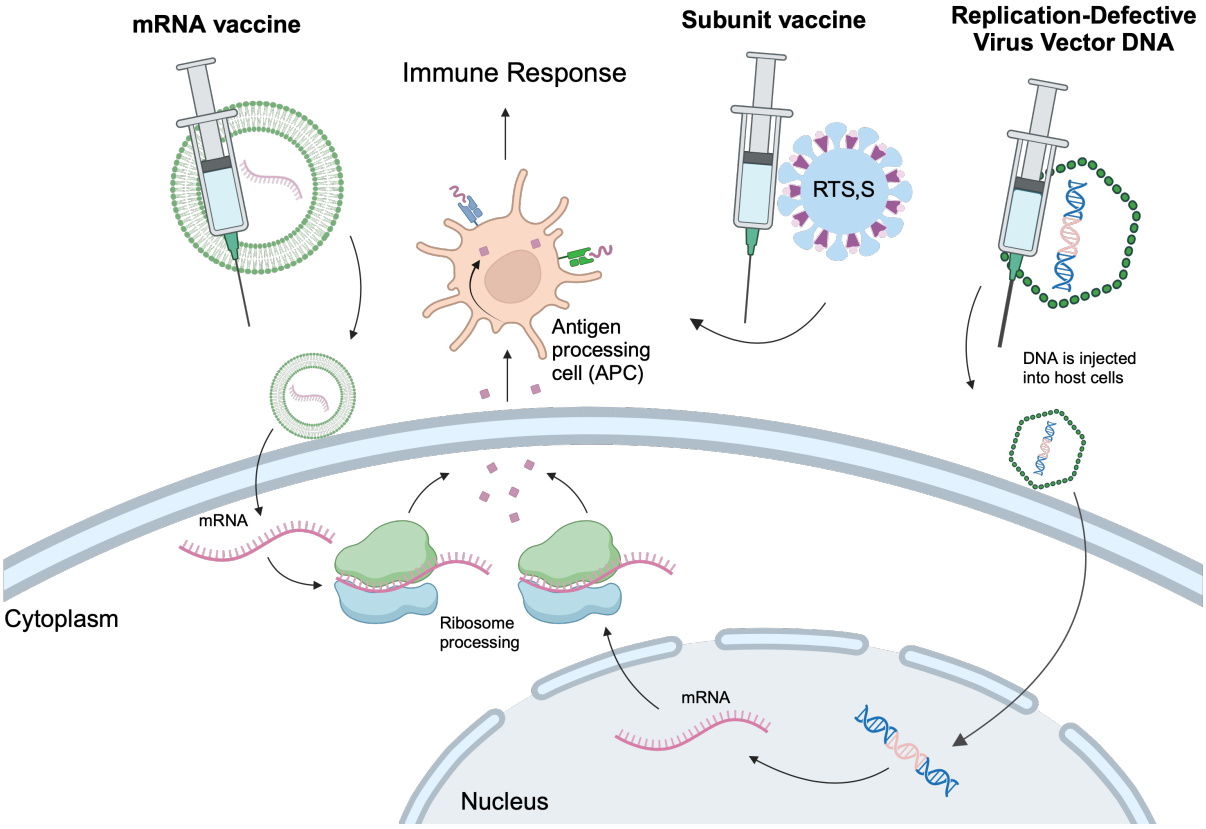

Figure 5: Different vaccine mechanisms.
Legend continues on the next page.

We summarise three main vaccine types. The mRNA vaccine directly injects the RNA sequence coding for the protein, which is directly translated by the ribosomes. In the DNA vaccine, the DNA molecule is introduced and transcribed into the nucleus and then translated into protein. The advantage of the mRNA vaccine over the DNA vaccine is that it is safer, does not reach the nucleus and there is no risk of insertion or mutation. The half-life of RNA is short and can be regulated by processes such as post-transcriptional modifications. Being less stable than DNA, it requires storage at lower temperatures (Pardi et al., 2018). The third type of vaccine is the subunit vaccine, among the most widely used. The RTS,S vaccine that has been approved by the WHO is a subunit vaccine. Subunit vaccine is considered the safest method of immunization, as it carries a low chance of toxicity and reactogenicity (Cid and Bolívar, 2021). All of the proposed vaccines lead to the production of the antigen that must be recognised by Antigen Processing Cells (APC) that expose the antigen to the immune system to activate the immune response.

III. How is *Plasmodium* parasite life cycle regulated?

The life cycle of the *Plasmodium* parasite is complex and involves two hosts: the female *Anopheles* mosquito and a vertebrate, here human (Figure 6).

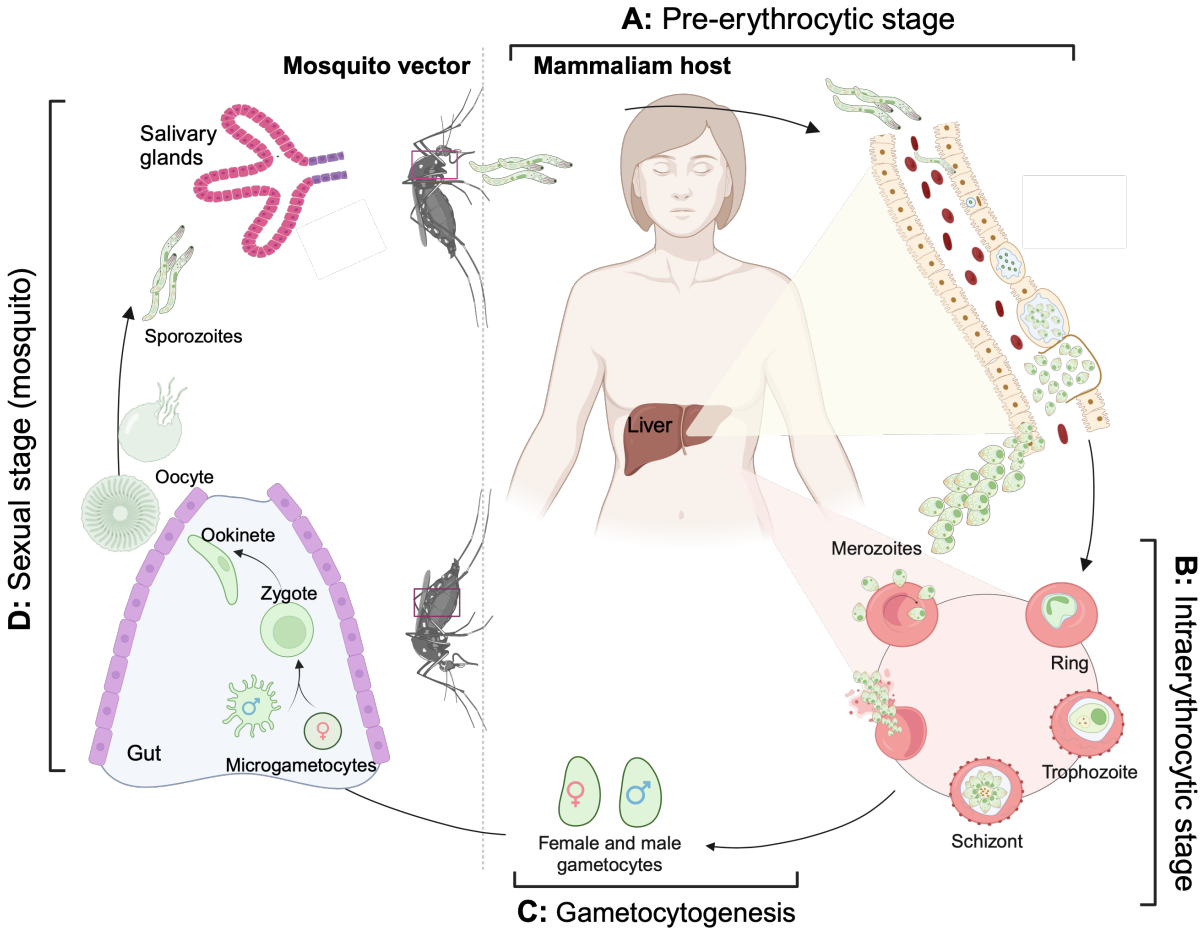

Figure 6: Life cycle of the parasite *Plasmodium*.
In the vertebrate host (human), the parasite develops through three well-known stages: **(A)** the pre-erythrocytic stage, from sporozoite injection to release of hepatic merozoites into the bloodstream, **(B)** the erythrocytic stage and **(C)** gametogenesis. More detailed explanations are given in the text.

During its life cycle, the parasite passes through various developmental stages, each characterized by specific morphological and physiological features dependent on its specific transcriptomic and proteomic profiles (Florens et al., 2002). To ensure dynamic gene expression, a tight coordinated regulation at every stage is necessary for optimal parasite development. A complete understanding of the mechanisms regulating gene expression is still lacking. Studying these mechanisms is essential to find new ways of specifically hindering parasite proliferation. The contribution of epigenetics and chromatin-associated proteins, the

role of chromatin organization and some transcriptional regulatory mechanisms in *Plasmodium* were reviewed by (Hollin and Le Roch, 2020). Only few transcription factors encoded by the parasite's genomic DNA have been identified. To date, DNA-binding proteins of the Apicomplexan AP2 (ApiAP2) family are the main identified proteins as transcription factors in *Plasmodium* (Painter et al., 2011). It suggests that most regulatory processes take place post-transcriptionally. For this reason, in the following pages, I will focus on some key post-transcriptional processes that regulate the development of the parasite and its progression through the different stages of its life cycle (Vembar et al., 2016) (Figure 6).

1. The *Plasmodium* life cycle

1.1. Pre-erythrocyte stage (Figure 6A)

In humans, infection is initiated during the blood meal of an infected mosquito, when sporozoites present in its saliva are injected subcutaneously. The sporozoite stage is a period of quiescence for the parasite, which can remain infectious for up to fifteen days in the mosquito's salivary glands (Lindner et al., 2013). The passage of the parasite from mosquito to vertebrate host is a critical bottleneck in its life cycle. Only a few dozen of the sporozoites injected during the mosquito bite will eventually develop in the liver (Frischknecht et al., 2004). Thus, immediately after injection, the sporozoites leave the skin to reach the liver; some of them cross the dermis, enter the bloodstream, and migrate towards the liver cells, while others are lost in the lymphatic vessels (Amino et al., 2007, 2006). Sporozoites' entry into the liver is a sequential process involving migration through several cell types (Frevert, 2004): after interacting with liver epithelial cells, sporozoites migrate along the endothelium, and traverse Kupffer macrophage cells, without damaging them, to reach the hepatocytes (Frevert, 2004). Sporozoites do not settle inside this initial hepatocyte but migrate through several cells by forming a function with the surface of the cells; they glide through this junstion inside a parasitophosphorous vacuola (Mota et al., 2001), or only a transient vacuole (Risco-Castillo et al., 2015) before settling and beginning development in the host hepatocyte (reviewed in Ménard et al., 2008). Within 24 hours, the sporozoite transforms into a hepatic trophozoite (Frevert, 2004). Some hepatic trophozoites of *P. ovale* and *P. vivax* stop their development in the hepatocyte and form hypnozoites, which may be the cause of reported relapses (Markus, 2020). The parasite then begins the process of cell division, which lasts six to seven days and leads to the development of a hepatic schizont, containing thousands of merozoites. Following the rupture of the parasitophorous membrane of the schizont and the plasma membrane of the hepatocyte, merozoites are released into the bloodstream (Prudêncio et al., 2006).

1.2. Intraerythrocytic development cycle (IDC) (Figure 6B)

The asexual blood cycle can be divided into four phases: erythrocyte invasion, ring, trophozoite and schizont formation.

1.2.1. Merozoites and erythrocyte invasion

The erythrocytic cycle of *P. falciparum* lasts approximately 48 hours (Haldar and Mohandas, 2009); it begins with the invasion of an erythrocyte by a merozoite. In addition to its nucleus, its single mitochondrion and the apicoplast, the merozoite has organelles specific to the invasion process and the formation of the parasitophorous vacuole inside the red blood cells. These organelles are secretory vesicles located at the apical pole of the parasite called rhoptries, micronemes and dense granules (Figure 7A). These vesicles release their contents sequentially during erythrocyte invasion, inducing changes in the erythrocyte plasma membrane and playing a crucial role in the formation of the parasitophorous vacuole (Bannister et al., 2000; Chitnis and Blackman, 2000).

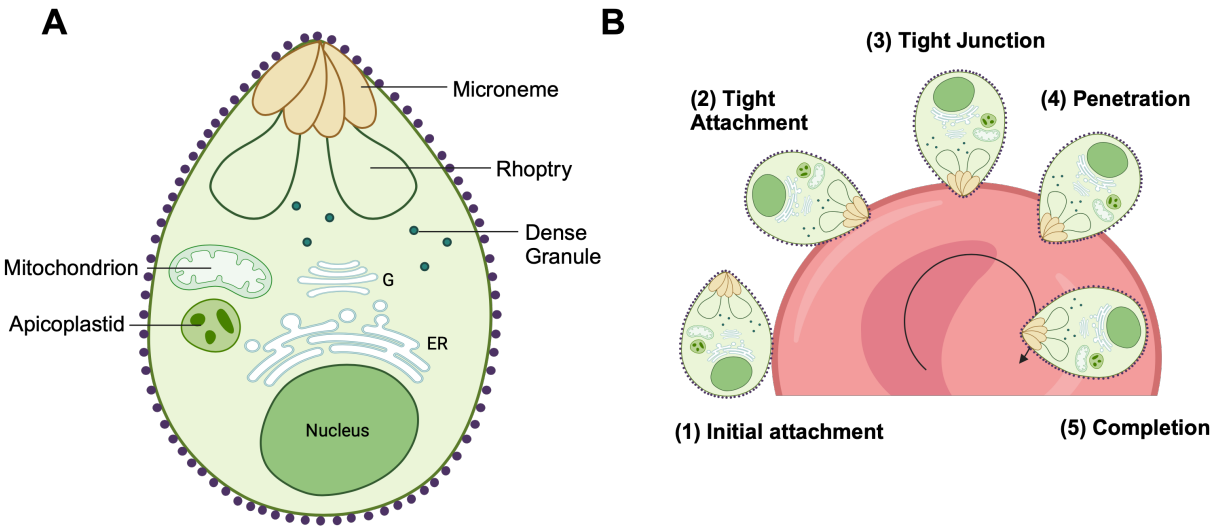

Figure 7: Merozoite structure and red blood cell invasion process.
(A) Structure of the merozoite with micronemes, rhoptry and dense granules located in the apical part; the nucleus, the mitochondrion, the apicoplast and the endoplasmic reticulum are located in the basal part of the parasite. **(B)** The five steps of the invasion of erythrocytes by the parasite. (1) During the initial attachment, the merozoite binds to the red blood cell (RBC) by probably involving the merozoite surface protein (MSP1) and its receptor on the erythrocyte surface. This process induces a reorientation of the parasite on the surface of the RBC, whose membrane begins to invaginate. (2) Tight attachment happens when the parasite and the RBC establish new interactions. (3) Tight junction involves the release of rhoptries' content and the interaction between the merozoite surface and the host membrane. (4) During the penetration process, the parasite enter the RBC, forming the parasitophorous vacuole. (5) Completion is obtained when the merozoite is surrounded by the parasitophorous vacuole inside the red blood cell.

The different stages of the red blood cells (RBC) invasion are explained in Figure 7B. The initial stage involves a low-affinity interaction between the merozoite and the host cell, facilitated by merozoite surface proteins (MSPs) (Chitnis and Blackman, 2000; Das et al., 2015). The erythrocyte membrane begins to invaginate, and the parasite and RBC establish new interactions (Cowman et al., 2017). This step is mediated by two families of adhesins released by (i) micronemes: DBL (Duffy binding-like protein) and Rh (reticulocyte-binding like protein homolog) (Lopaticki et al., 2011), or by (ii) rhoptries such as AMA1 (apical membrane antigen-1) and RON2 (Rhoptry Neck protein 2) which interact to form a tight junction between the parasite and the infected red blood cell (iRBC); finally, dense granules migrate towards the parasite surface and release their contents into the parasitophorous vacuole, inducing an expansion of the parasite membrane (Culvenor et al., 1991), marking the beginning of the rest of the blood stage (Figure 8).

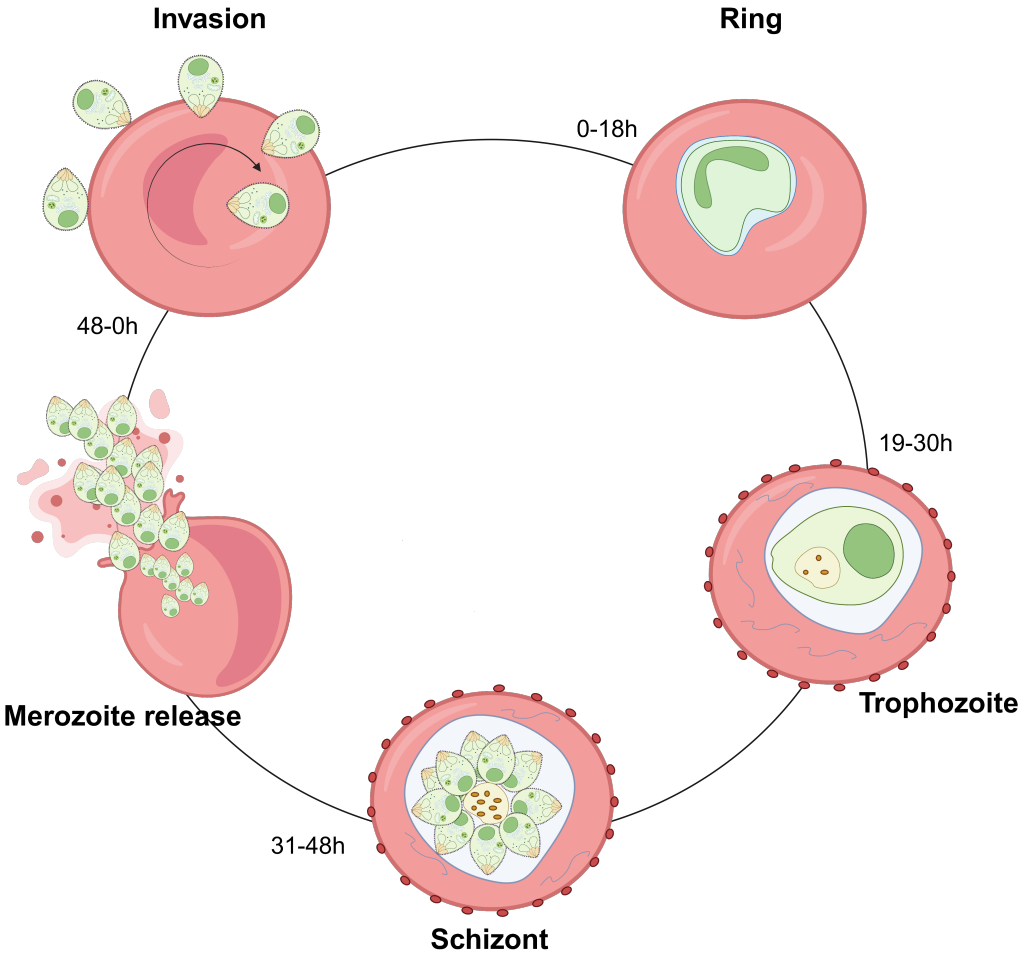

Figure 8: Asexual blood stage, also known as the intraerythrocytic development cycle (IDC).
The parasite infects RBC, following the steps detailed in Figure 7B. Once the parasite is embedded in the parasitophorous vacuole inside the iRBC, the ring phase, so called because of its shape, begins. The parasite continues its development into a trophozoite. At this stage,

hemoglobin from RBC is digested, toxic heme is released, but detoxification occur by its crystallization into hemozoin (indicated by orange dots in the yellow vesicle). The parasite divides, entering the schizont phase containing 16 to 32 merozoites. After 48 hours, the mature schizont cell releases merozoites that can infect other cells and continue the blood cycle.

1.2.2. The ring stage

The ring stage (Figure 8) occurs between 1 hour and 18 hours after invasion (Lazarus et al., 2008). During this phase, the parasite begins to consume the hemoglobin in the erythrocyte, releasing toxic heme which is transformed into non-toxic hemozoin crystals by the parasite known as malarial brown pigments (Pandey and Tekwani, 1996).

1.2.3. The trophozoite stage

This phase occurs between 19 and 30 hours after invasion and is characterised by increased export of parasite proteins to the erythrocyte surface. In the cytosol of the erythrocyte, a network of membranes (Maurer's clefts) develops, establishing connections between the parasitophorous vacuole and the erythrocyte membrane (Haldar, 1998) and allowing the expression of parasite proteins on the surface of the iRBC. Those proteins aggregate to form protuberances called "knobs" (Cooke et al., 2004). These knobs play a role in the ability of parasitized erythrocytes to adhere to epithelial cells and are therefore responsible for severe *P. falciparum* malaria (Wiser, 2023). At the same time, ingestion of the erythrocyte cytosol continues, producing even more hemozoin, and the trophozoite progressively enlarges as its digestive vacuole increases.

1.2.4. The schizont stage

The schizont stage (31 to 48 hours after invasion) represents the final phase of parasite development in the erythrocyte, culminating in the production of 16 to 32 merozoites in the case of *P. falciparum* (Lazarus et al., 2008). At the same time, hemoglobin depletion from the cytosol continues. During the last nuclear division, apical organelles are synthesized for merozoite formation. As the schizont matures, individual mitochondria and plastids migrate to the central region of the cytoplasm. Then, each merozoite undergoes physical separation by the formation of membranes, marking the final stage of schizogony (Voß et al., 2023). Finally, an active mechanism involving multiple proteases leads to the rupture of the parasitophorous vacuole membrane and the erythrocyte membrane (Wickham et al., 2003). This process releases the merozoites, initiating a new erythrocytic cycle.

1.3. Gametocytogenesis (Figure 6C)

Gametocytogenesis is a process that leads a small proportion of parasites to cease asexual proliferation and begin sexual differentiation, becoming gametocytes, the infectious form for the mosquito. In the case of *P. falciparum* infection, gametocytes are not observed until 7 to 15 days after the asexual stages (Eichner et al., 2001). The influence of various environmental factors has been described in the initiation of this sexual cycle, like the host immune response and "stress" factors (Dyer and Day, 2000). This process of merozoite-to-gametocyte differentiation is only partially understood. It has been established that all merozoites emerging from the same schizont share the same fate towards asexual proliferation or sexual differentiation (Bruce et al., 1990) and that all merozoites from the same schizont become either male or female gametocytes (Silvestrini et al., 2000). These transformations result in significant changes in the parasite's metabolism, protein expression and morphology, and enable the adaptation of the parasite to the drastic environmental changes (temperature and pH) represented by its entry into the mosquito (Bennink and Gabriele Pradel, 2019). Numerous variations in RNA and protein content have been identified in gametocytes compared to other stages, illustrated by, among other things, the expression of a different type of ribosomal RNA in gametocytes and during parasite development in the mosquito (Waters et al., 1989).

1.4. Sexual cycle in the mosquito (Figure 6D)

During a blood meal from an infected vertebrate, the mosquito ingests male and female gametocytes. Upon arrival in the mosquito's gut, gametocytes rapidly differentiate into microgametes (male) and macrogametes (female) (Beri et al., 2018) that initiate the sexual development by their fusion. The resulting zygote differentiates into an ookinete; the ookinete passes through the mosquito's intestinal epithelium and differentiates into an oocyst, which in turn replicates abundantly to form invasive sporozoites. Sporozoites are then released from the oocyst into the hemocoel cavity and migrate to the salivary glands of the mosquito for transmission to a new host.

2. An overview of regulatory mechanisms in *Plasmodium* life cycle (Figure 9)

In the following paragraphs, I will focus only on vertebrate stages of the *Plasmodium* life cycle, which I have divided into three main events: pre-erythrocytic stage (mosquito-to-vertebrate), asexual blood stage and gametocytogenesis (vertebrate-to-mosquito). Figure 9 shades light on the main post-transcriptional regulatory events that take place during these specific stages, and that will be detailed below.

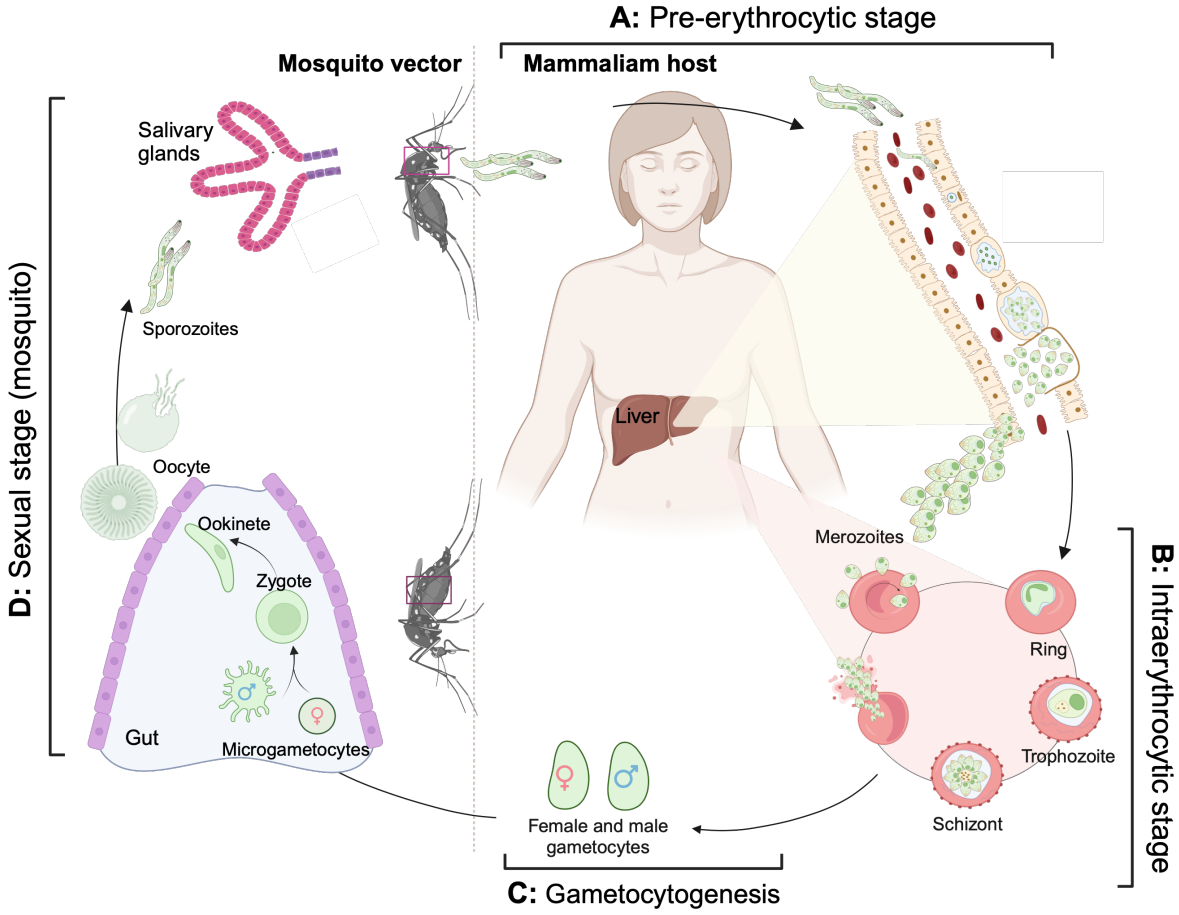

Figure 9: Main post-transcriptional events in the vertebrate development cycle.
See the legend of Figure 6. Post-transcriptional regulations occur at each stage of the parasite development.

2.1. The concept of just-in-time expression

A particular feature of the *Plasmodium* parasite is the temporal dynamics of gene transcription/translation, which follows a "just-in-time" model. During the intraerythrocytic development cycle (IDC), the parasite undergoes a series of changes and replications. Studies of mRNA expression have revealed that around 70% of parasite genes show synchronized

mRNA and protein peaks at a specific time in the cycle (Foth et al., 2011; Le Roch et al., 2004). This means that mRNA and corresponding protein production occur simultaneously, indicating close coordination between both transcription and translation processes. Thus, the mRNAs translated into proteins at any given time belong to the same biological process, such as DNA replication, protein translation, protein degradation, etc. These proteins are expressed precisely at the point in the life cycle when they are needed. Bunnik et al. (2013) have shown the differential expression of proteins during the IDC: (i) genes associated with heme synthesis are enriched at the ring stage; (ii) at the trophozoite stage, there is a peak in transcription for genes linked to DNA replication, corresponding to the daughter cell division stage; (iii) in the mature stages of schizonts and merozoites, there is an abundant expression of genes involved in the translation process, in particular ribosomal proteins. Transcripts of genes involved in the invasion of a new host cell also show the highest levels in the stationary and polysomal fractions.

However, for around 30% of genes, there is a noticeable delay between the peak of mRNA expression and the corresponding peak of protein levels (Le Roch et al., 2004). In this case, there is therefore a time lag where protein production is delayed relative to mRNA production (Caro et al., 2014). This phenomenon is particularly important at all stages of the parasite's life, especially at the mosquito-to-vertebrate and vertebrate-to-mosquito transition stages (Cui et al., 2015).

2.2. Translational control in the mosquito-to-vertebrate transition stage (pre-erythrocytic stage)

Translational regulations are particularly important in the transitional phases between mosquito and vertebrate; such mechanisms enable the parasite to respond rapidly to external stimuli (Cui et al., 2015) either by sequestering/releasing mRNAs in/from mRNP (messenger ribonucleoprotein) granules or by inhibiting/activating translation initiation.

Plasmodium sporozoites, which are the infectious form of the parasite transmitted by mosquitoes to vertebrates, can remain infectious in mosquito salivary glands for up to 2 weeks (Lindner et al., 2013). During this period, the sporozoite transcriptome remains stable and untranslated (Cui et al., 2015). The regulation of protein synthesis is crucial in this process: it concerns a group of upregulated transcripts in infectious sporozoites (UIS) that are only translated when the parasite infects a hepatocyte (Silvie et al., 2014).

The sporozoite latency is controlled by inhibition of translation initiation (Figure 10A) mediated by phosphorylation of the α subunit of the translation initiation factor eIF2 (Zhang et al., 2013). There are three serine/threonine eIF2α kinases encoded by the *Plasmodium* genome: the eIF2α kinases eIK1 and eIK2 (UIS1), and the protein kinase PK4, which are expressed at

different stages of the parasite life cycle (Vembar et al., 2016). The UIS1 (eIk2) protein is expressed specifically during the sporozoite stage and maintains eIF2α under its inactive phosphorylated form (Matuschewski et al., 2002; Zhang et al., 2010) (Figure 10B). However, once the sporozoite enters the vertebrate host, eIF2α dephosphorylation is reversed by the phosphatase UIS2 (Zhang et al., 2016), reactivating protein translation to allow parasite transformation and development in the liver (Briquet et al., 2021).

It has been hypothesized that Puf2 represses the synthesis of UIS2 in sporozoites, by sequestering its mRNA in mRNP granules (Zhang et al., 2016). Indeed, Puf2-KO sporozoites show an increase in UIS2 protein, leading to premature sporozoite transformation while still in the mosquito's salivary glands (Gomes-Santos et al., 2011).

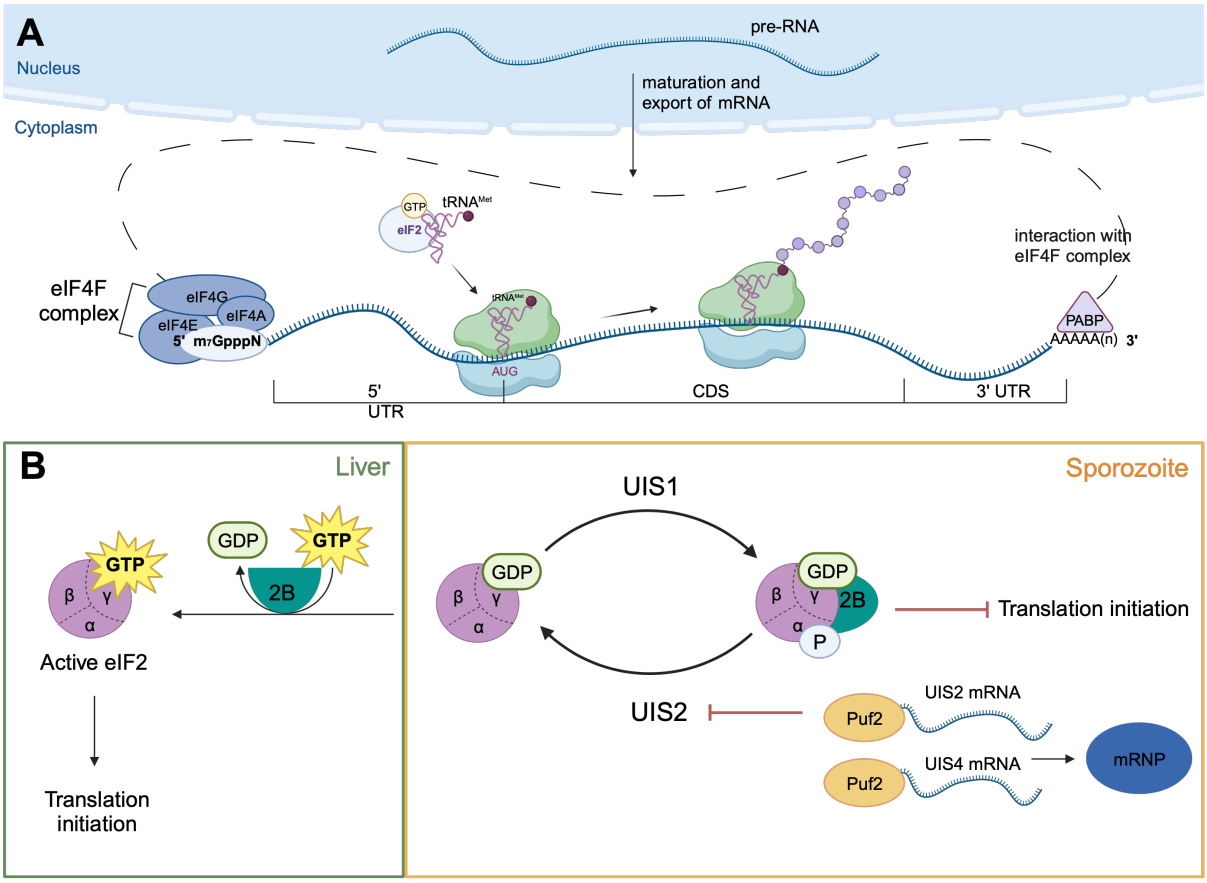

Figure 10: Overview of translation initiation and its control in the pre-erythrocytic stage. **(A)** After maturation (splicing, m7GpppN cap structure and poly(A) tail), the mRNA (5'UTR-CDS-3'UTR) is transported to the cytoplasm, where it is translated into proteins. The components of the translation machinery are well conserved in *Plasmodium* (Jackson et al., 2011). The main difference concerns ribosomal RNA. The *Plasmodium* genome has only 4-8 single copies of rRNA genes classified as type A (specific to asexual stages in liver and blood), type O (specific to ookinetes) and type S (specific to sporozoites) (Gunderson et al., 1987; Waters et al., 1989). Translation initiation begins with the formation of the eIF4F complex, which results from the association of eIF4A, eIF4G and eIF4E (Gebauer and Hentze, 2004). Poly(A)-binding protein (PABP) ensures mRNA circularisation, which makes translation more

efficient and prevents mRNA degradation (Vembar et al., 2016). Protein synthesis then starts with the assembly of 80S ribosomes on mRNA. This step is controlled especially by the eukaryotic initiation factor 2 (eIF2); it interacts with GTP and the aminoacylated initiator $tRNA^{Met}$ to form a ternary complex that in turn associates with the small subunit of the ribosome and other initiation factors to form the 43S pre-initiation complex (Bennink and Gabriele Pradel, 2019). Any mechanism that hinders the 43S pre-initiation complex formation inhibits the translation initiation. **(B)** In the mosquito-to-vertebrate transition stage, translation initiation is regulated by the phosphorylation/dephosphorylation cycle of eIF2α catalyzed by UIS1 and UIS2, respectively.

A regulatory mechanism is the phosphorylation of α subunit of eIF2 by eIF2α kinases. eIF2α forms, together with eIF2β and eIF2γ, the eIF2 translational initiation factor (Wek, 2018). This complex binds GTP and then interacts with initiator $tRNA^{Met}$ to form a ternary complex. Then it associates with the small ribosomal subunit and some eIFs (1, 1A, 3, 5) to form the 43S pre-initiation complex (Bennink and Gabriele Pradel, 2019). During the process in which the 43S pre-initiation complex is loaded on the AUG start codon, eIF2 hydrolyzes GTP into GDP, lowering thus its affinity for initiator $tRNA^{Met}$ and translation starts. Finally, for eIF2 reactivation, GDP is replaced by GTP by eIF2B, the guanine nucleotide exchange factor. In sporozoites, this exchange is blocked by the phosphorylation of eIF2α on Ser59 catalyzed by UIS1 (or eIK2) (Bennink and Gabriele Pradel, 2019); in this case, the eIF2B factor remains bound to the eIF2 complex and translation initiation is blocked (reviewed in Gebauer and Hentze, 2004) (Figure 10B). Dephosphorylation of eIF2α is mediated by USI2 and is possible once the parasite develops in the liver, where Puf2 is repressed and UIS2 mRNA is released from mRNP granules. Puf2 is also involved in UIS4 mRNA repression.

Puf2 is involved in other regulatory mechanisms in sporozoites amongst which the translational repression of mRNA UIS4 (Silvie et al., 2014) (Figure 10B); translation of UIS4 mRNA is repressed in the mature sporozoite while the UIS4 protein belongs to the early transcribed membrane protein family expressed only during the blood stage (Lindner et al., 2019; Silva et al., 2016; Silvie et al., 2014). The Puf protein family is conserved across all eukaryotes (Quenault et al., 2011), the proteins possess a conserved RNA-binding domain that specifically recognize an 8-9 nucleotide target sequence called PBE (Puf binding element). Most of these proteins bind either to the 3' UTR of mRNA, repressing its translation or inducing its degradation (Quenault et al., 2011; Wickens et al., 2002), or to the 5' UTR region (Miao et al., 2013) with the same molecular mechanism. Puf2 inhibits UIS4 mRNA translation by binding (Lindner et al., 2013a) and stabilizing it in cytoplasmic granules. Puf2 is not essential for the development of the liver stage, but it is crucial for maintaining sporozoite infectivity in mosquito salivary glands. Depletion of Puf2 leads also to premature transformation of sporozoites and thus their loss of infectivity (Müller et al., 2011a).

In addition to Puf proteins, sporozoites express another family of ALBA1-4 (acetylation lowers binding affinity 1-4) proteins (Goyal et al., 2016). Although initially described as a DNA-binding protein, numerous studies have shown that these ALBA proteins are involved in the regulation of mRNA translation in protozoan parasites such as *Trypanosoma*, *Toxoplasma* and *Leishmania* (Dupé et al., 2014; Gissot et al., 2013; Mani et al., 2011). It has been shown in *P. yoelii* that ALBA4 (like Puf2) contributes to mRNA homeostasis as it is also found in cytoplasmic granules at the sporozoite stage, allows sporozoites to grow semi-synchronously (Briquet et al., 2021) and its deletion alters the level of many proteins in sporozoites (Muñoz et al., 2017).

2.3. Regulation of translation during blood stage

2.3.1. Translation initiation

In the erythrocyte cycle, phosphorylation of the α-subunit of eIF2 is also one of the main patterns of translation inhibition. The mechanism is the same as that already described in sporozoites, but in this case it is the protein kinases eIK1 and PK4 that are involved. eIK1 is translated specifically during the blood stage and is not essential (Fennell et al., 2009), but it is central to the melatonin signaling pathways involved in parasite cell cycle synchronization (Dias et al., 2020). As for the PK4 kinase, it leads to the arrest of global protein synthesis in schizonts, where merozoite formation occurs, and in gametocytes that infect *Anopheles* mosquitoes (Zhang et al., 2012).

Another global mechanism of translational regulation has been demonstrated in *P. falciparum*. It involves PfDZ50 (or DOZI), which is a DDX6/DHH1-type cytosolic RNA helicase (Tarique et al., 2013). By binding to eIF4E, PfDZ50 prevents the interaction between eIF4E and eIF4G and thus the binding of PABP (Figure 11). The formation of the translation initiation eIF4F complex is thus impeded, inhibiting the association of the large ribosome subunit with the 43S pre-initiation complex. Nonetheless, PfDZ50's mRNA targets are not known.

ALBA family proteins are also important for parasite development at the blood stage (Chêne et al., 2012). In *P. falciparum*, these proteins have been shown to bind and consequently control the translation of numerous mRNAs, playing thus a role in maintaining mRNA homeostasis. For example, ALBA1 binds to around 1,000 transcripts in the trophozoite phase (Vembar et al., 2015). This is also true at the merozoite stage, where ALBA family proteins bind in particular to mRNAs encoding proteins involved in RBCs invasion such as RAP1 (Rhoptry associated protein 1), AMA1 (Apical membrane antigen 1), RhopH3 (Rhoptry protein RhopH3) and CDPK1 (Calcium dependent proteinkinase 1) and modulate the protein translation events necessary for merozoite invasion.

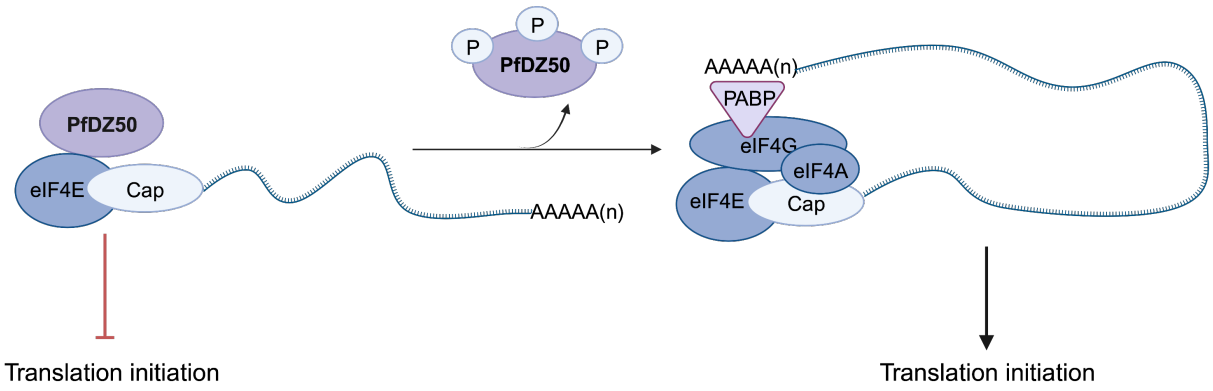

Figure 11: Repression of translation by PfDZ50 (DOZI) during the intraerythrocytic stage.
PfDZ50 blocks the interaction between eIF4E and eIF4G, and consequently between PABP and the eIF4F complex, which in turn inhibits cap-dependent protein synthesis (Vembar et al., 2016). When PfDZ50 is hyperphosphorylated, it is released and translation can start. The parasite has lost many of the components of the mTOR complex, including mTOR kinase (Serfontein et al., 2010), consequently such kinases have not yet been identified in *Plasmodium* (Bennink and Gabriele Pradel, 2019).

2.3.2. mRNA degradation

The process of mRNA degradation is particularly important for the regulation of gene expression during IDC. mRNA decay has been studied for around 4,000 genes during IDC in *P. falciparum* (Shock et al., 2007). The abundance of a particular mRNA species is determined by the balance between its transcriptional production and its degradation rate. Degradation rates of mRNA molecules have been shown to change throughout the IDC. Initially, during the ring stage, mRNA molecules have relatively short half-lives, but as the cycle progresses towards the schizont stage, half-lives become significantly longer (Martin et al., 2005).
Poly (A) nucleases Pan2-Pan3, PARN and the Ccr4/Not complex are involved in this crucial step (Wahle and Winkler, 2013). Particularly, the Ccr4-Not complex (carbon catabolite repressor protein 4-N) is a global regulator of gene expression, conserved from yeast to man. It consists of Ccr4 and 3 Ccr4-associated factors (CAF1, CAF40 and CAF130), and the 5 Not proteins, which together regulate protein translation via mRNA degradation (Collart, 2016; Tucker et al., 2001) (Figure 12A). Although this Ccr4-Not complex has been associated with transcriptional regulation by influencing the positioning of TBPs on TATA boxes (Badarinarayana et al., 2000), its role in RNA degradation is essential as it is the main complex involved in mRNA deadenylation in eukaryotes. Members of the Ccr4-Not complex are well conserved in *Plasmodium* (Coulson et al., 2004) and a study by Balu et al. (2011) showed that depletion of CAF1 alters mRNA stability during IDC. Especially, since CAF1 is essential for the

parasite survival, it is the deletion of the C-terminal domain of CAF1 that leads to deregulation of mRNAs encoding proteins involved in the parasite invasion and exit of the erythrocyte. Recently, the mechanism that target the Ccr4-Not complex *via* Not 5 subunit towards the ribosomal E site was proposed. It occurs when decoding is not optimal (empty A-site) and explains the cotranslational degradation of mRNA enriched in non-optimal codons by Ccr4 and CAF1 (Buschauer et al., 2020) (Figure 12B).

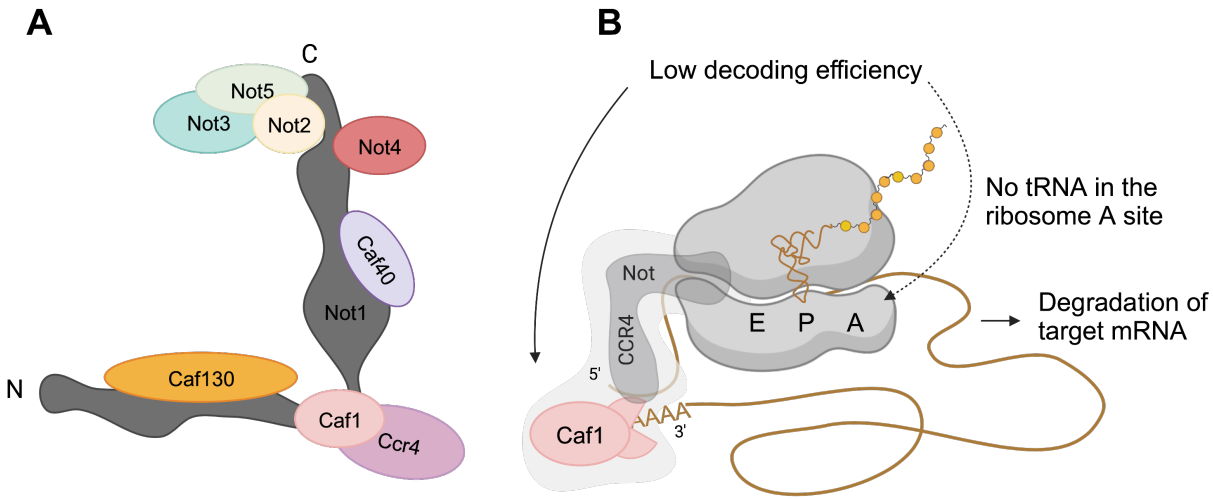

Figure 12: Degradation of mRNA via Ccr4-Not complex.
Degradation of mRNA results from non-reversible termination of translation. This process is initiated by shortening of the poly(A) tail, known as deadenylation. Following deadenylation, mRNA can be degraded in either the 5′ to 3′ direction or the 3′ to 5′ direction (reviewed in Garneau et al., 2007). Here we will focus on Ccr/Not complex. **(A)** Cartoon representation of the Ccr4/Not complex, both Ccr4 and CAF1 have 3' to 5' deanylase activity. **(B)** Targeting of mRNA degradation by the Ccr4-Not complex.

2.4. Translational regulation during vertebrate-mosquito transition

Several genes have been identified as early markers of gametocyte differentiation. Amongst them, p25 and p28 are highly transcribed in gametocytes, but their translation only begins when the parasite arrives in the mosquito, at the zygote and ookinete stages (Hall et al., 2005; Paton et al., 1993). In *P. berghei*, DOZI (development of zygote inhibit) is the homolog of the *P. falciparum* inhibitor of translation initiation PfDZ50. With its partner CITH (CAR-I (in worms) and Trailer Hitch (in flies) homolog), DOZI has been identified as regulators of p25 and p28 mRNAs (Mair et al., 2010) that associate both mRNAs with mRNP granules. Especially, DOZI-knockout is characterized by a significant reduction in p25 and p28 mRNAs in female gametocytes (Mair et al., 2010), suggesting their exposition to cellular degradation.

Moreover, p25 and p28 mRNA expression is also regulated by the Puf family proteins: Puf1 and Puf2 are both expressed in gametocytes (Cui, 2002; Fan et al., 2004). In *P. falciparum*, Puf1 and Puf2, by repressing pf25 and pf28 mRNAs, control gametocytogenesis. Puf1 is

expressed at all gametocyte stages, but at higher levels in female gametocytes. Depletion of Puf1 does not disrupt the parasite's asexual cycle, but results in a sharp drop in the number of mature gametocytes, particularly female gametocytes (Shrestha et al., 2016). Similarly, inhibition of Puf2 results in increased translation of p25 and p28 proteins and consequently leads to accelerated differentiation of the sexual stages and specific increased production of male gametocytes (Miao et al., 2013, 2010; Müller et al., 2011b).
In addition, mutant parasites, which have lost the C-terminal part of CAF1, also have difficulties with the gametocyte development and male gametogenesis (Hart et al., 2019), indicating that this step is also regulated at the level of mRNA degradation.

In conclusion, *Plasmodium* controls the expression profile of its genes depending not only on the host but also on its stage of development. An increasing number of studies are identifying post-transcriptional and translational control mechanisms at different stages of the parasite's life cycle. These regulatory mechanisms coexist with 'just-in-time' transcription and translation strategies to coordinate protein expression, synchronize the parasite development, and allow the timely development of mature/infectious parasites.

IV. The impact of the genetic code on gene expression

1. Background

The genetic code exerts diverse effects on translation and protein expression. During translation, codons specify specific amino acids, guiding the ribosomal complex to select the corresponding aminoacylated tRNAs. The precise recognition of mRNA codons by tRNA molecules directs the correct sequence of amino acids, ultimately determining the protein's structure and function.

Among the 64 codons known, 61 encode the 20 amino acids, while the remaining three (UAA, UAG, and UGA) serve as termination signals for translation. The genetic code is considered as degenerated because multiple codons can represent the same amino acid (Figure 13). Thus, the presence of isoacceptor tRNAs (tRNAs with the same amino acid specificity but with different anticodons) is required for decoding. With the exception of tryptophan and methionine, all other amino acids are encoded by multiple synonymous codons (Quax et al., 2015).

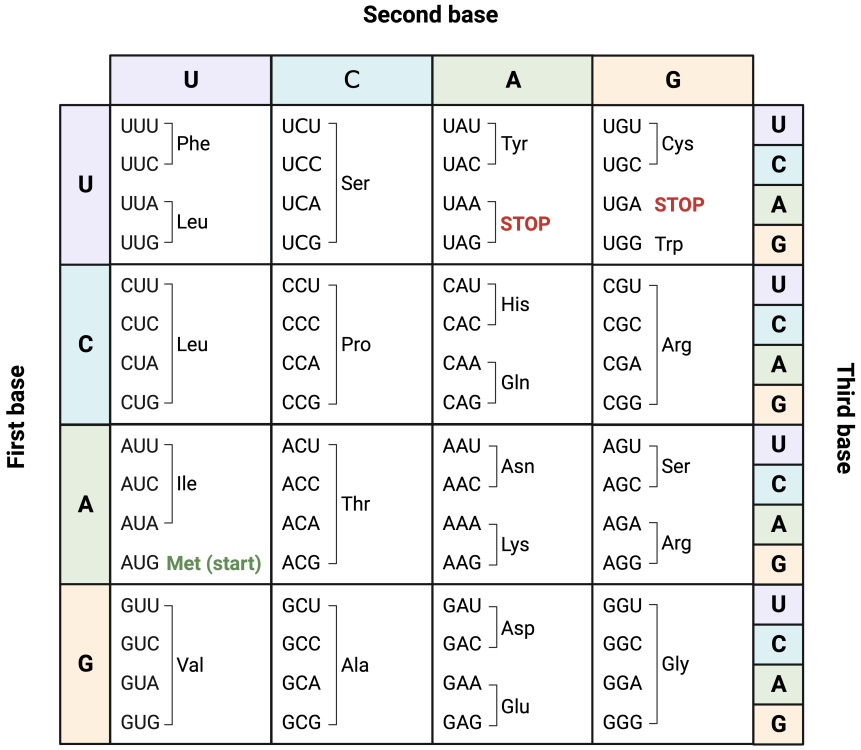

Figure 13: Diagram of the 64 codons and corresponding amino acids that are used in the universal genetic code.

Most of the amino acids are encoded by synonymous codons that differ only in the third codon position (Yu and Li, 2011), named the wobble position of the codon, which is less specific in determining the amino acid than the other two positions. The genetic code's degeneracy is

thought to minimize the risk of dangerous mutations (Radványi and Kun, 2021). However, most of all, synonymous codons are not used randomly or equally; there is often a preference for one codon over others. This preference in codon usage among synonymous codons is known as codon usage bias. This codon usage bias is considered as a secondary genetic code, since it influences the translation efficiency and accuracy of protein synthesis (Liu, 2020; Ma et al., 2015). However, it is more accurate to speak of optimal or preferred codons than codon usage. Codon optimality depends on the translation elongation rate of the mRNA; non-optimal codons elongate slowly, while optimal codons elongate rapidly. Preferred codons are used more frequently to encode a particular amino acid within an organism. For example, for the amino acid leucine, the codon CUG is the preferred codon in *Escherichia coli* and *Drosophila melanogaster*, but it is UUA in *Bacillus subtilis*, and UUG in *Saccharomyces cerevisiae* (Sharp et al., 1988). Most importantly, the preference for certain codons can have functional implications, like influencing the speed or the accuracy of translating ribosomes (Tuller et al., 2010) and thus regulating protein folding (Spencer et al., 2012). Optimal codons allow for rapid ribosome translocation, (Figure 14A) (Hanson and Coller, 2018). On the contrary, several non-optimal codons cause the ribosome to move more slowly while it waits for a rare cognate tRNA. According to Hanson and Coller (2018), elongation of non-optimal codons may even cause ribosome congestion, eventually generating a queue that, if long enough, might prevent translation elongation but also translation initiation (Figure 14B).

The speed of translational elongation is also determined by the GC content of the genome, the quantity of corresponding tRNAs, the level of aminoacylation of these tRNAs and the state of post-transcriptional modification of the tRNAs.

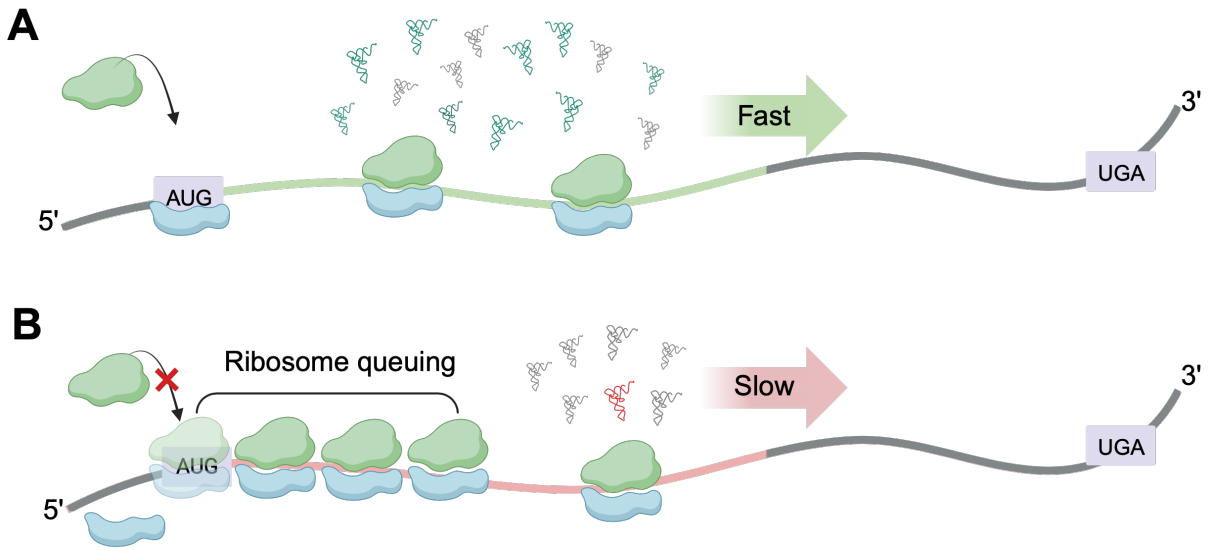

Figure 14: Modulation of translational rate.
(A) Optimal translation efficiency is due to high availability of cognate tRNAs that read optimal codons. **(B)** Slow translation and ribosome queuing are due to the presence of non-optimal

codons read by rare tRNAs (in red). The crowding of ribosomes can also inhibit the initiation process.

2. Codon optimality and genomic GC content

Analysis of a genome's GC composition can be performed at the global or local level (Gajbhiye et al., 2017). As a rule, it can be observed that the GC content of Coding DNA Sequences (CDS) is higher than the GC content of the genome, and that variations in GC composition influence the selection of synonymous codons (Mondal et al., 2016). The preference for codons with a wobble G or C position (GC3) increases with genomic GC bias. And finally, GC3 codons can be designated as optimal codons compared to codons with A or T at the wobble position since, in human, they are recognized by ILF2-ILF3 heterodimers that increase translation and thus mRNA stability (Hia et al., 2019).

The AT contents *of Homo sapiens (58.9%), D. melanogaster (57.9%), Arabidopsis thaliana* (63.4%) and the eukaryotic pathogens *Toxoplasma gondii* (47.7%) and *Trypanosoma bruceii* (53.2%) genomes are all in the average range (Hamilton et al., 2016). This is not the case for *Plasmodium* parasites. Table 2 summarizes the GC content of six *Plasmodium* species. *P. knowlesi* and *P. vivax* show GC compositions broadly comparable to other eukaryotes, between 40% and 45%, respectively in the CDS (Yadav and Swati, 2012). In *P. falciparum*, on the other hand, GC content is extremely low, at around 20% for the whole genome, and barely reaches 24% in CDS, resulting in a very high use of AT-rich codons (Rao et al., 2011). Similar trends are observed in *P. yoelii*, *P. chabaudi* and *P. berghei* (Yadav and Swati, 2012) (Table 2), suggesting that the GC3-dependent mRNA stability observed in human is not preponderant in these parasites.

Table 2: Comparison of GC-contents in genomes and CDSs for six different *Plasmodium* species.

Species	Chromosomes	Genome Size (Mb)	Genomic GC%	CDS GC%	CDS GC3%
P.falciparum	14	23.3	19.41	23.78	17.4
P.vivax	14	27.01	42.3	46.21	56.49
P.knowlesi	14	23.46	37.5	40.19	45.39
P.yoelii	14	23.12	24.69	24.22	16.56
P.chabaudi	14	18.83	24.33	26.42	18.91
P.berghei	14	18.52	23.71	23.73	16.97

CDS, coding sequence; GC3, third site of codon in CDS.

However, logically, the GC content of the genome determines the amino acid content of the proteome. Whereas GC-rich genomes code for proteins enriched in glycine (G), alanine (A), arginine (R) and proline (P) (Foster et al., 1997), AT-rich genomes show an increase in specific amino acids, such as phenylalanine (F), tyrosine (Y), methionine (M), isoleucine (I), asparagine (N) and lysine (K). This is observed in *P. falciparum*, where the most used amino acids are N, K, I and L (Figure 15) (Bastien et al., 2004) and in *P. vivax* and *P. knowlesi*, which use A, G, P and valine (V) more than other *Plasmodium* species (Yadav and Swati, 2012). The high AT content of the genome and the correlated amino acid usage that characterize *Plasmodia* proteomes are further intriguing when considering the existence of the numerous Low Complexity Regions (LCR) that colonize the parasite proteins (see chapter III, paragraphe 4.2, below).

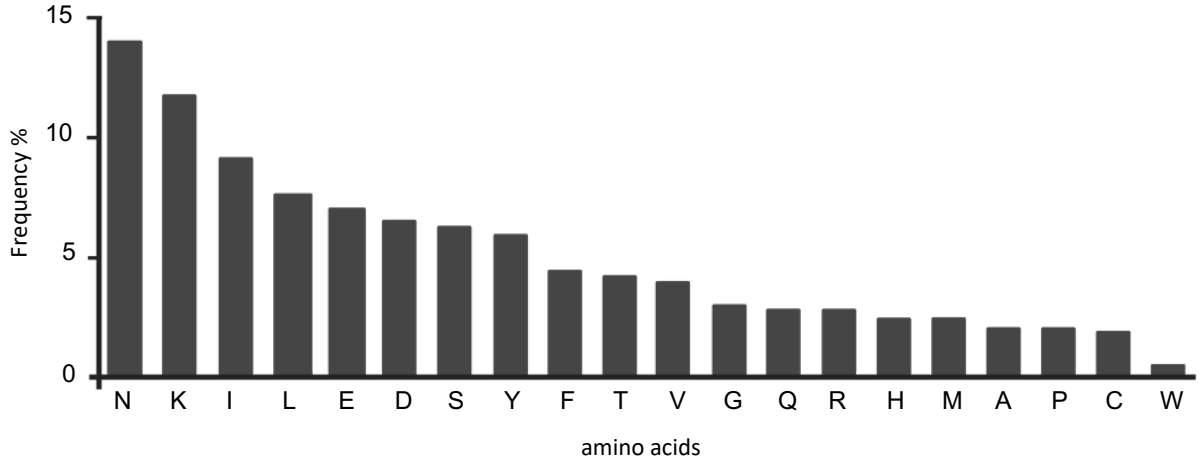

Figure 15: Amino acid distribution in *P. falciparum* proteomes.
The results were taken from Bastien et al., 2004.

3. Codon optimality and tRNA abundance

All the tRNA genes of hundreds of species have now been characterized (Chan and Lowe, 2016). tRNA genes with certain types of anticodons (isoacceptor) are represented dozens of times in a genome, while others are represented only once or are even absent. However, the availability of different molecules of mature tRNA do not only depends on the number of tRNA genes in the genome but is also controlled by several transcriptional regulatory processes: the efficiency of transcription can be regulated by the sequences of the internal promoters of the tRNA genes (located in their D and T loops) but also by epigenetic modifications of the chromatin in the vicinity of the tRNA genes (reviewed in Wagh et al., 2021). The tRNA repertoire has a profound impact on many aspects of cellular life, including the efficiency of protein expression, the accuracy of protein translation and folding and even the stability of mRNA. This regulation shapes the proteome according to cellular state.

3.1. tRNA, an intermediary molecule

tRNA is an essential RNA molecule, 75 to 96 nucleotide long, that plays a crucial role in protein synthesis and influence codon usage based on their availability in the cell during translation. Indeed, tRNA acts as an intermediary between the genetic code contained in DNA/mRNA and the assembly of amino acids during translation. Its importance in the translation process is underscored by the presence of a highly conserved three-dimensional structure that allows its recognition by the ribosome to decode specific mRNA codons. tRNAs are charged by their corresponding aminoacyl-tRNA synthetases (aaRSs) to form an aminoacyl-tRNA that will be delivered to the ribosome (reviewed in Giegé and Eriani, 2023 and the references herein).

The aminoacylation reaction is made in two-steps (Figure 16): (i) the activation of the amino acid by the aaRS with the formation of an aminoacyl-adenylate and the release of an inorganic pyrophosphate, and (ii) the transfer of activated amino acid to either the 2'-OH or 3'-OH of the terminal adenosine present at the 3' end of the accepting tRNA (Rajendran et al., 2018). Specific recognition (positive and negative) of tRNAs by aaRS depends on the subtle balance between sequence, structure and post-transcriptional modifications of the tRNAs (reviewed in Giegé et al., 1986).

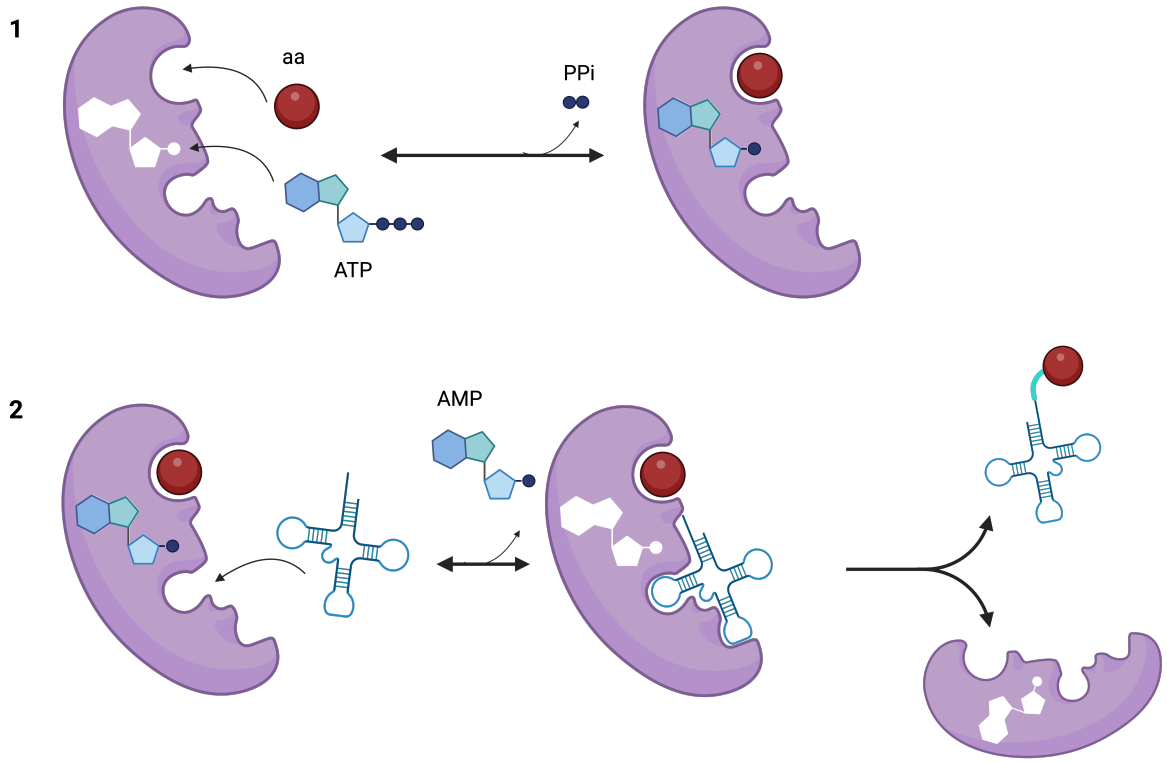

Figure 16: The aminoacylation reaction.
(1) Activation of the amino acid (aa) in the active site of the aaRS (in purple) in the presence of ATP, leading to the formation of an aminoacyl-adenylate and pyrophosphate (PPi). (Legend continues on next page).

(2) Transfer of the activated amino acid on the 3’ end of the tRNA. Figure adapted from Rajendran et al., 2018.

3.2. tRNA structure

tRNA exhibits a hierarchical structure comprising a primary, a secondary and a tertiary structure. The primary structure of tRNA represents the linear nucleotidic sequence arranged from 5' to 3' as firstly described by Robert W. Holley in 1969. The secondary structure of tRNA is commonly referred to as a "cloverleaf structure" due to its characteristic configuration (Figure 17A). This structure arises from specific base-pairing interactions within the tRNA molecule. It consists of five main domains: the acceptor domain, the D domain, the anticodon domain, the variable region and the T domain. The acceptor domain is formed by the base pairing of the 5' and 3' ends of the tRNA molecule. The 3' end terminates with a conserved CCA sequence. The last adenosine at the 3' end is where the amino acid is attached during the process of aminoacylation. Both the T and anticodon domains consist of a 5-base pair arm and a 7-nucleotide loop. The T loop contains several conserved residues, including G53, T54, Ψ55, C56, A58, C61, and two semi-conserved residues, R57 and Y60. In the anticodon domain, the conserved residues are Y32, U33 and R38, while amino acids 34-36 form the anticodon and play a critical role in recognizing the codon on the mRNA. The D domain exhibits the most variability among tRNA molecules, with an arm containing 3 to 4 base pairs and a loop containing 7 to 11 residues. Conserved residues within the D loop include A14, G18, G19, and A21. The variable region, ranging from 4 to 21 nucleotides, always contains the residue Y48. It is through the variable region that tRNA molecules can be categorized into two families: tRNA-class 1, which have 4 or 5 nucleotides in this region, and tRNA-class 2, which possess 13 to 21 nucleotides.

The three-dimensional conformation of tRNA is L-shaped (Figure 17B, C) and arises mainly from interactions between the conserved residues of the D and T loops that form an elbow. The first tertiary structure was determined by X-ray crystallography on the *S. cerevisiae* $tRNA^{Phe}$ (Kim et al., 1974; Robertus et al., 1974). In Figure 17B we can see the interactions that lead to the 3D structure. The intramolecular interactions are as follows: U8-A14, A14-A21, R15-Y48, G18- Ψ55, G19-C56, T54-A58 (reviewed in Giegé et al., 2012).

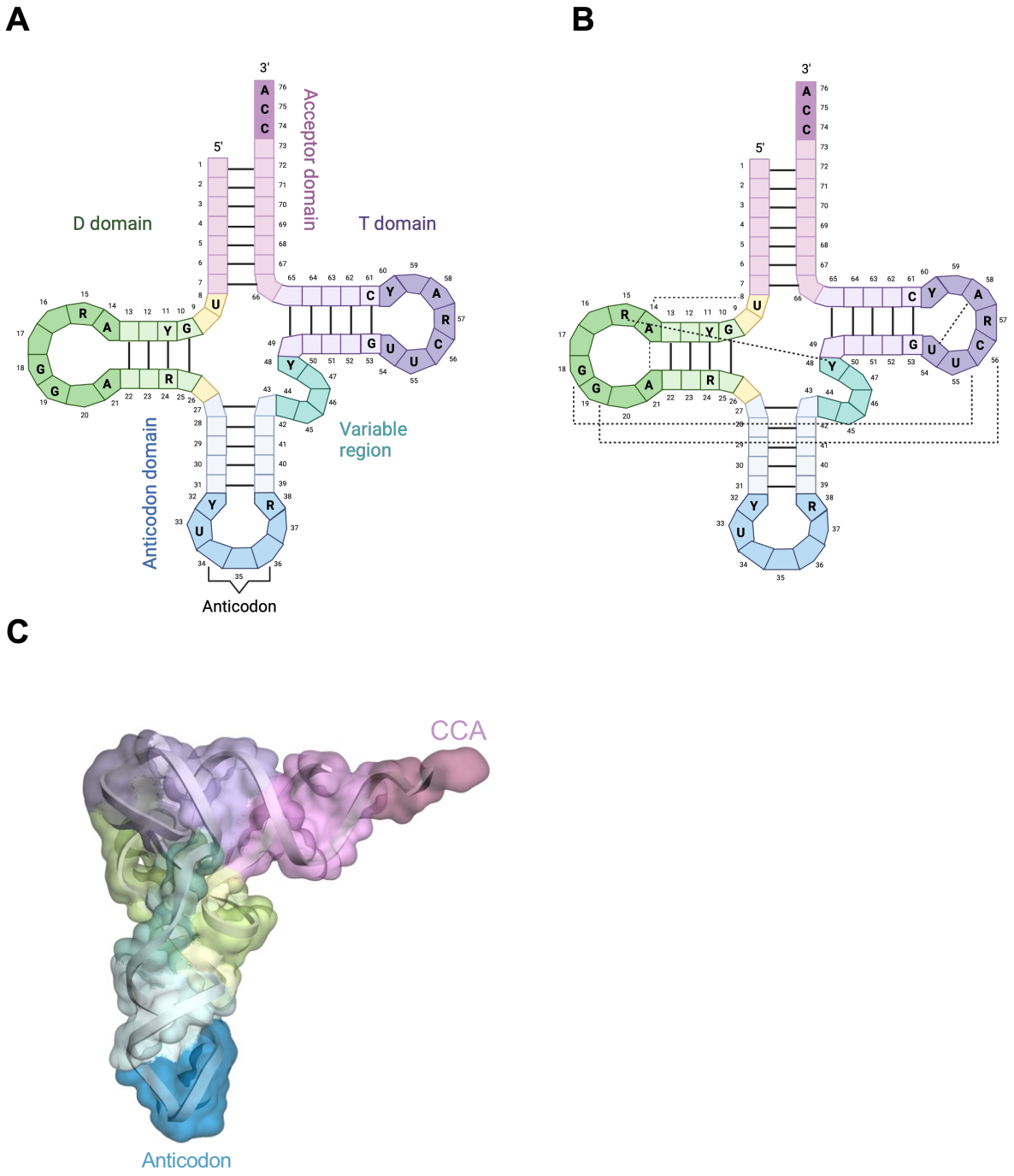

Figure 17: tRNA cloverleaf secondary structure leading to a L-shaped tertiary structure. **(A)** Secondary structure: base pairings in the acceptor, D, anticodon and T arms enable the tRNA sequence to be folded into its typical cloverleaf shape. Each domain is represented by a specific color: the acceptor arm in pink, the D domain (D arm and loop) in green, the anticodon domain (arm and loop) in blue and the T domain (T arm and loop) in purple. Conserved residues are indicated explicitly. **(B)** Interactions between conserved residues that enable formation of the tertiary structure are indicated by dotted lines. **(C)** L-shaped tertiary structure: the colors indicating domain location are the same as in (A). The anticodon and CCA sequence where the amino acid attaches are indicated.

3.3. Effect of tRNA post-transcriptional modifications on protein synthesis

In all organisms, tRNAs are extensively modified at the post-transcriptional level. Some modifications are strictly conserved in all tRNAs (T54, Ψ55, D18-19), while others are unique and specific to certain tRNAs. These modifications not only contribute to thermodynamic stability, tRNA folding and aaRS recognition, but also ensure optimal tRNA interactions with mRNA and the ribosome. Indeed, post-transcriptional modifications in the anticodon loop are particularly important for regulating translational efficiency and fidelity. Particularly, modifications at position 34 of the anticodon (wobble interaction with mRNA codons) are essential for codon recognition and hence protein expression (Ranjan and Rodnina, 2016). It has been shown by quantitative mass spectrometry that certain protein families are down-regulated in cells deficient in tRNA modification, such as ribosomal proteins, proteins involved for example in the synthesis and processing of tRNA and rRNA and, translation regulation (Alings et al., 2015). Indeed, in yeast, thiolation of U34 (s2U34) is required for efficient translation of mRNAs rich in AAA, CAA and GAA codons, the slowing of decoding in the absence of the modification being responsible for differential translation (Rezgui et al., 2013).

3.4. Effect of tRNA abundance on protein synthesis

Some studies have shown variations in aminoacylated tRNA levels (Evans et al., 2017), and suggest that tRNA abundance and availability is a step that controls translation efficiency. The cell tRNA repertoire (level of specific isoacceptors, post-transcriptional modifications, etc…) can change in response to different stimuli. By limiting the rate of translation of an mRNA, the low concentration of one or more specific tRNAs leads to the slowing down or even stopping of peptide synthesis and consequently controls the dynamics of mRNA codon-mediated stability. Thus, the regulatory properties of a given codon may vary according to the availability of tRNA in response to external stimuli and the tissue of interest (Dittmar et al., 2006; Kirchner and Ignatova, 2015; Rak et al., 2018). Therefore, these differences in ribosome elongation rates, influenced by the availability and demand for tRNAs, also allow to classify decoded codons into optimal and non-optimal categories.

Moreover, the availability of aminoacylated tRNA dictates the translation rate of the ribosome, which in turn controls the co-translational folding of the translated protein. Indeed, nascent proteins start to fold as soon as they exit the ribosome tunnel (Kim et al., 2015), and for multi-domain proteins, the rate of ribosome elongation is generally slowed down between two domains. This means that the domain that has already been synthesized can fold independently of the next domain. Alterations to this rhythm, by changing either the local use

of codons or the availability of certain tRNAs, can lead to co-translational misfolding, resulting in inactivity of the protein.

4. Codon optimality and mRNA translation in *Plasmodium*

4.1. Translational compartments

In addition to its nuclear genome, *Plasmodium* possesses two other organellar genomes that are expressed and essential for the survival of the parasite: the mitochondrion and the apicoplast ones (Sato, 2011). In *Plasmodium*, both the nuclear and apicoplast genomes encode tRNA molecules, with no evidence of tRNA-encoding genes in the mitochondrial genome (Jackson et al., 2011). The apicoplast genome codes for its own tRNAs, ribosomal RNAs and proteins, as well as for the translation elongation factor EF-Tu. The apicoplast genome carries 26 tRNA genes that are, *a priori*, used locally. As for the mitochondrial genome, it is the smallest, spanning 6 kb and encoding only three proteins: cytochrome subunits I and II (Cox1 and Cox3) and cytochrome b, but no tRNAs or other component of the translational machinery (reviewed in Jackson et al., 2011). Most of the proteins required for organelle function are encoded by the nuclear genome and transported to their respective organelles (Waller et al., 1998). Among these, 550 nuclear-encoded proteins have been identified to target the apicoplast (Gardner et al., 2002), and 300 to target the mitochondrion (Ke and Mather, 2017). While, the apicoplast is known to be translationally active (Chaubey et al., 2005), there is no definitive evidence of translation occurring within the mitochondrion. However, the presence of genes encoding essential proteins, implies that they have to be translated locally. The *Plasmodium* nuclear genome (23 kb) encodes 5385 genes amongst which genes encoding 7 rRNA and 36 aaRSs could be identified. It contains also 46 tRNA genes, encoding 45 different unique tRNA isoacceptors. The only exception being 2 distinct genes for the initiator and elongator $tRNA^{Met}$ molecules. Based on this statement, *Plasmodium* encodes all the molecules necessary and sufficient to express its proteome. However, *Plasmodium* genomes, have the smallest set of tRNA genes among eukaryotic cells, with only one gene copy per tRNA isoacceptor in the nuclear genome (Gardner et al., 2002). Despite this limited number, they are sufficient to decode all 61 codons. Cytosolic tRNAs bear resemblance to eukaryotic tRNAs and their tertiary structures seem L-shaped as they possess the conserved nucleotides (Pütz et al., 2010).

4.2. Amino acid usage and LCRs in *Plasmodium* proteins

The number of proteins encoded by the *Plasmodium* genome is around 5300, which is comparable to that of *Saccharomyces cerevisiae*, although *Plasmodium* has a genome around 50% larger (Gardner et al., 2002). This is due to the presence of insertions in plasmodial

proteins, known as Low Complexity Regions or LCRs. Almost 90% of *P. falciparum* proteins possess at least one LCR. These LCRs are thought to encode non-globular regions that extend from the protein core without compromising correct functional folding (Pizzi and Frontali, 2001). The length of these insertions varies from small insertions of less than 10 amino acids to long insertions of over several hundreds of amino acids (Aravind et al., 2003). The composition of these LCRs is strongly influenced by the high AT content of the *Plasmodium* genome. In *P. falciparum*, *P. yoelii*, *P. berghei* and *P. chabaudi*, LCRs are mainly composed of asparagine (N) and lysine (K), which are encoded by A- and U-rich codons. Glutamic acid (E) and aspartic acid (D) are also enriched in LCR, but to a lesser extent. In *P. vivax* and *P. knowlesi*, whose genomes are relatively GC-rich, LCRs are composed of alanine (A) repeats (Dalby, 2009).
Interestingly, while proteins with large N homorepeats (runs of asparagine residue), tend to form insoluble aggregates in other organisms (Halfmann et al., 2011), *Plasmodium* possesses efficient chaperones that prevent this aggregation (Muralidharan et al., 2012), especially at high temperatures, since fever is one of the characteristic responses induced by the parasite. These repetitive regions promote significant variations during DNA replication, resulting in size polymorphisms within the parasite population. Not only LCRs are observed in surface antigens, such as CSP on the sporozoite surface or MSP1 on the merozoite surface but they are also highly immunogenic, therefore they are suspected of being involved in antigenic variations of the parasite to evade the host immune response (MacRaild et al., 2016).

4.3. LCR and co-transcriptional folding of proteins in *Plasmodium*

Most of the parasite proteins contain LCRs, including many highly conserved housekeeping genes that are not expressed at the surface the parasite. This is in contradiction with a unique role played by LCRs in antigenic variation on the parasite surface.
With a minimal pool of tRNA genes and a unique use of amino acids over-utilizing asparagine and lysine residues, it was proposed that LCRs would be positioned between the structural domains of *Plasmodium* proteins, thereby able to locally slowing ribosome translation and thus controlling protein co-translational folding. This process is supported by the fact that (i) these LCRs vary in size and sequence in the different *Plasmodia*, but their position in the protein is highly conserved (Dickson and Golding, 2022), suggesting that it is indeed the positioning that is important for their function and (ii) the high AT content in the parasite genome does not, *a priori*, allow the formation of stable structures in the mRNA, responsible for ribosome slowing in other organisms. Interestingly, in the particular case of *Plasmodium*, it was proposed by Frugier et al., (2010), that it is not the abundance of tRNAs that controls translation, but rather the local accumulation of codons that act as tRNA sponges (Figure 18).

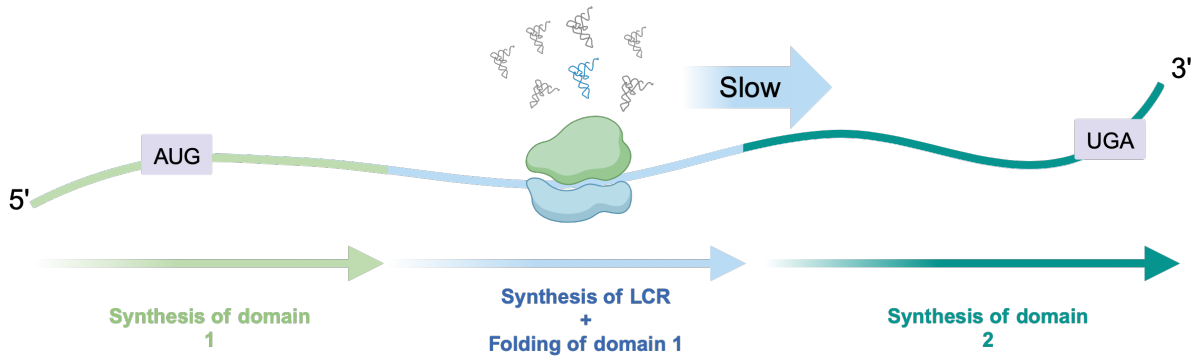

Figure 18: Translational control of the ribosome speed by the presence of LCR in *Plasmodium*.
In light blue, an asparagine-rich LCR is translated. Due to the imbalance between the low amount of $tRNA^{Asn}$ and the high concentration of Asn codons in the mRNA encoding LCRs, translation slows down locally, allowing domain 1 (light green) of the protein to fold correctly and independently of domain 2 (dark green).

A key question is how so many long repetitive sequences can be synthesized and whether endogenous *Plasmodium* tRNAs are sufficient to support the translation of all these sequences.

Understanding the underlying mechanisms and functional implications of codon optimality in malaria parasite provides valuable insights into the intricate relationship between the genotype and the phenotype at the level of protein synthesis. In the following pages, I will recall the factors correlated to codon optimality and the peculiarities in *Plasmodium* genome that could affect the parasite translation.

V. tRip-mediated tRNA import: a process found exclusively in *Plasmodium*

1. tRip is an AIMP: aminoacyl-tRNA synthetase-interacting multifunctional protein

1.1. Multi-aminoacyl-tRNA synthetase complexes (MSCs)

In eukaryotes, cytosolic aaRSs form complexes called multi-aminoacyl-tRNA synthetase complexes (MSCs). Depending on the organism, MSCs are composed of certain aaRSs and accessory proteins that enable the different components to interact.

1.1.1. Aminoacyl-tRNA synthetases (aaRSs)

The aaRSs are a family of 20 enzymes that play a key role in the translation process. They are divided into two classes based on the structure of their catalytic site (Eriani et al., 1990) and in eukaryotes, some of them are organized into MSC (Figure 19). In the yeast *S. cerevisiae*, the MSC consists of glutamyl-tRNA synthetase (ERS) and methionyl-tRNA synthetase (MRS) (Simos et al., 1996). In *Toxoplasma gondii*, ERS and MRS are also found, as well as tyrosyl-tRNA synthetase (YRS) and glutaminyl- tRNA synthetase (QRS) (Van Rooyen et al., 2014). *Trypanosoma brucei* MSC comprises six aaRSs: MRS, QRS, alanyl tRNA synthetase (ARS), tryptophanyl tRNA synthetase (WRS), prolyl tRNA synthetase (PRS), aspartyl tRNA synthetase (DRS) (Cestari et al., 2013). Finally, in mammals, the MSC comprises 9 aaRS activities: QRS, MRS, glutamyl-prolyl tRNA synthetase (EPRS), isoleucyl-tRNA synthetase (IRS), leucyl-tRNA synthetase (LRS), lysyl-tRNA synthetase (KRS), arginyl tRNA synthetase (RRS) and DRS (Khan et al., 2020). It has been proposed that, by binding to translating ribosomes, MSCs allow charged tRNAs to reach more efficiently the A site of the ribosome and increase protein synthesis (Kyriacou and Deutscher, 2008).

However, some of the aaRS associated with MSC perform non-canonical functions beyond their essential role in tRNA aminoacylation. These non-canonical activities include regulating gene transcription, mediating glucose and amino acid metabolism, controlling mRNA translation, triggering or inhibiting inflammatory responses, amplifying or inhibiting the immune response, angiogenesis, apoptosis, amino acid sensing and cell signaling, among others; and it has been proposed that the switch between canonical and non-canonical functions is regulated by the association of aaRSs to the MSC and their dissociation, respectively (Guo and Schimmel, 2013). In all cases, MSCs are formed thanks to the presence of essential accessory proteins named AIMPs for aaRS-interacting multifunctional proteins.

1.1.2. AIMPs

Among these accessory proteins, there is a multifunctional protein common to all known MSCs: Arc1p in *S. cerevisiae* (Simos et al., 1996), Tgp43 in *Toxoplasma gondii* (Van Rooyen et al., 2014), MCP1 in *Trypanosoma brucei* (Cestari et al., 2013), AIMP1/AIMP2 complex in mammals (Kim et al., 2013) (Figure 19). This AIMP is a polypeptide composed of an N-terminal domain similar to glutathione-S-transferase (GST) fused to a C-terminal domain similar to endothelial monocyte activating polypeptide II (EMAPII). The AIMP-GST-like domain interacts with other GST-like domains fused to aaRSs that are part of the MSC (Karanasios and Simos, 2010), while the C-terminal domain recognizes the conserved 3D structure of tRNAs (Kapps et al., 2016). These two functional domains are linked via a poly-lysine linker that participates in the non-specific binding of tRNA (Mirande, 2017).

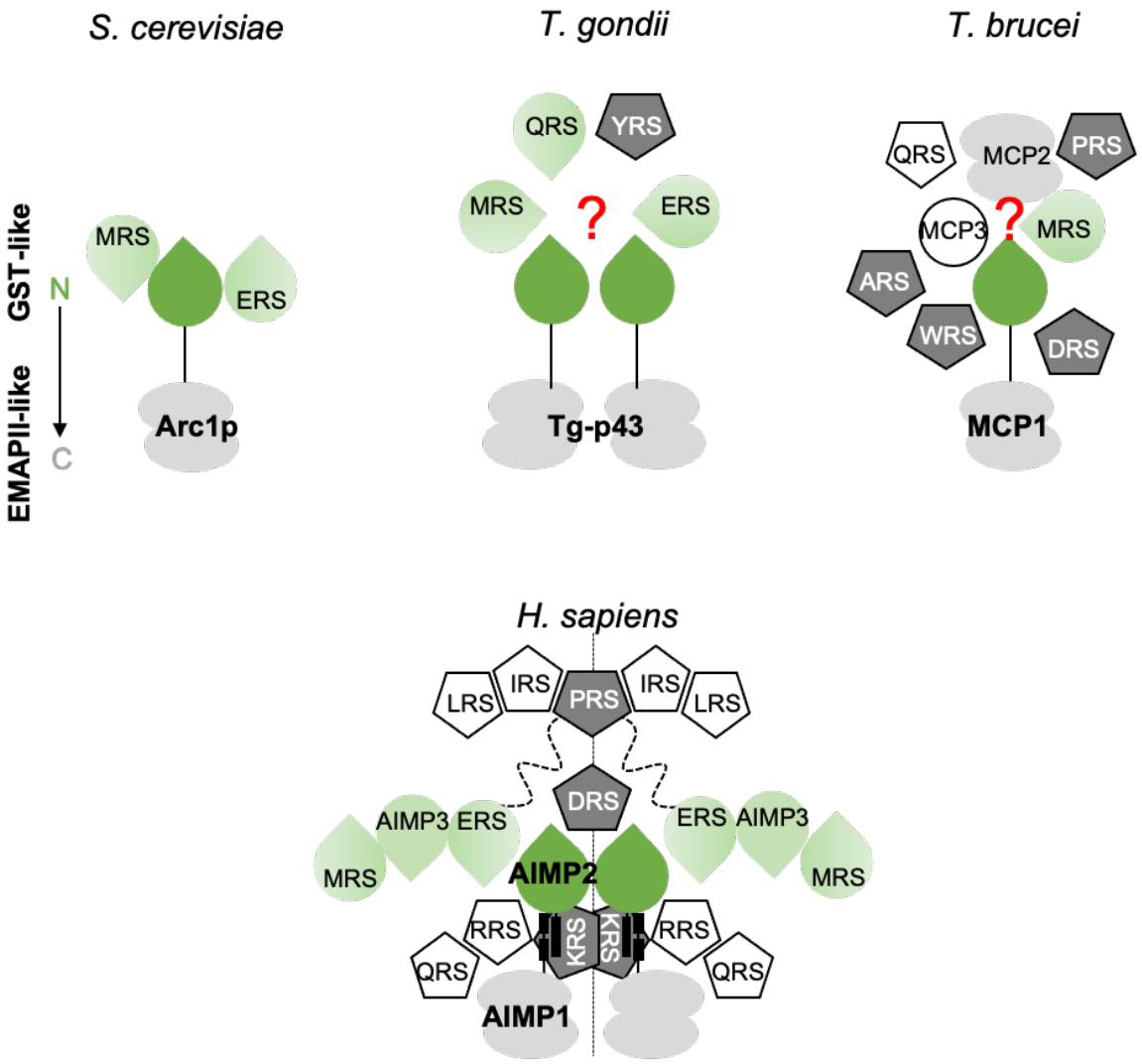

Figure 19: MSC architectures around AIMPs.
Known AIMPs containing N-terminal GST and C-terminal EMAPII-like domains. In *S. cerevisiae*, Arc1p is monomeric, Tgp43 is dimeric and the interactions between the two leucine-zippers of human AIMP1 and AIMP2 reconstitute a split protein that homodimerize *via* the GST

domain of AIMP2. Nothing is known about the oligomerization *of T. brucei* MCP1. In *S. cerevisiae*, Arc1p binds to ERS and MRS, the *T. gondii* MSC is composed of Tg-p43 and ERS, QRS, MRS, and YRS, *T. brucei* MSC contains 3 AIMPs (MCP1, MCP2 and MCP3) and at least 6 aaRSs. How the proteins associate in these two parasite MSCs is still unknown (indicated by red question mark). In the human MSC, AIMP2 is the component with the largest number of binding partners and is essential for complex assembly. Human MSC components are organized into two subcomplexes based on their association with AIMP2. Sub-complex I contains MRS, AIMP3, EPRS, IRS, LRS, KRS and DRS and sub-complex II is composed of AIMP1, QRS and RRS. AaRSs without GST-like domain are represented by pentagons, which are colored in dark grey when the enzyme is homodimeric. The figure is adapted from Jaramillo Ponce et al., 2022.

1.2. tRip act as an AIMP in Plasmodium

The protein tRip (tRNA import protein) was identified in our laboratory (Bour et al., 2016). This 402-amino acids protein is encoded by a 1440-nucleotide gene located on chromosome 14 and is well conserved in all *Plasmodium* strains. tRip was initially identified through bioinformatics analysis based on its homology to *S. cerevisiae* Arc1p since it contains a N-terminal GST-like domain and a C-terminal EMAPII OB-fold domain, capable of binding tRNA structures thanks to two residues (Ser_{312} and Met_{315}) (Cela et al., 2021). Three aaRS, ERS, QRS, and MRS were shown to specifically co-immunoprecipitated with tRip in blood stage parasites of *P. berghei*. All three aaRSs contain an N-terminal GST-like domain involved in MSC assembly. However, unlike all other MSCs known to date, *Plasmodium* has been shown to contain two exclusive dimeric heterotrimeric complexes: Q-complex (tRip:ERS:QRS) and M-complex (tRip:ERS:MRS). Gel filtration, light scattering and SEC-MALS suggest a stoichiometry of 2:2:2 in which the association of the GST-like domains of tRip and ERS (tRip-N:ERS-N) is central (Jaramillo Ponce et al., 2022). Thanks to the crystal structure of the GST-like domains of tRip and ERS, the study of the solution architecture of the Q- and M-complexes by small-angle X-ray scattering (SAXS) made it possible to propose different organizations of the GST-like domains in the two *Plasmodium* MSCs (Jaramillo Ponce et al., 2023) (Figure 20). Whereas the Q-complex is organized around the tRip dimer which binds ERS, the M-complex is organized around an ERS homodimer which binds tRip. The functional roles of the two MSCs and their different structures are not yet understood. However, these two complexes are also different from the others because of their membrane localization.

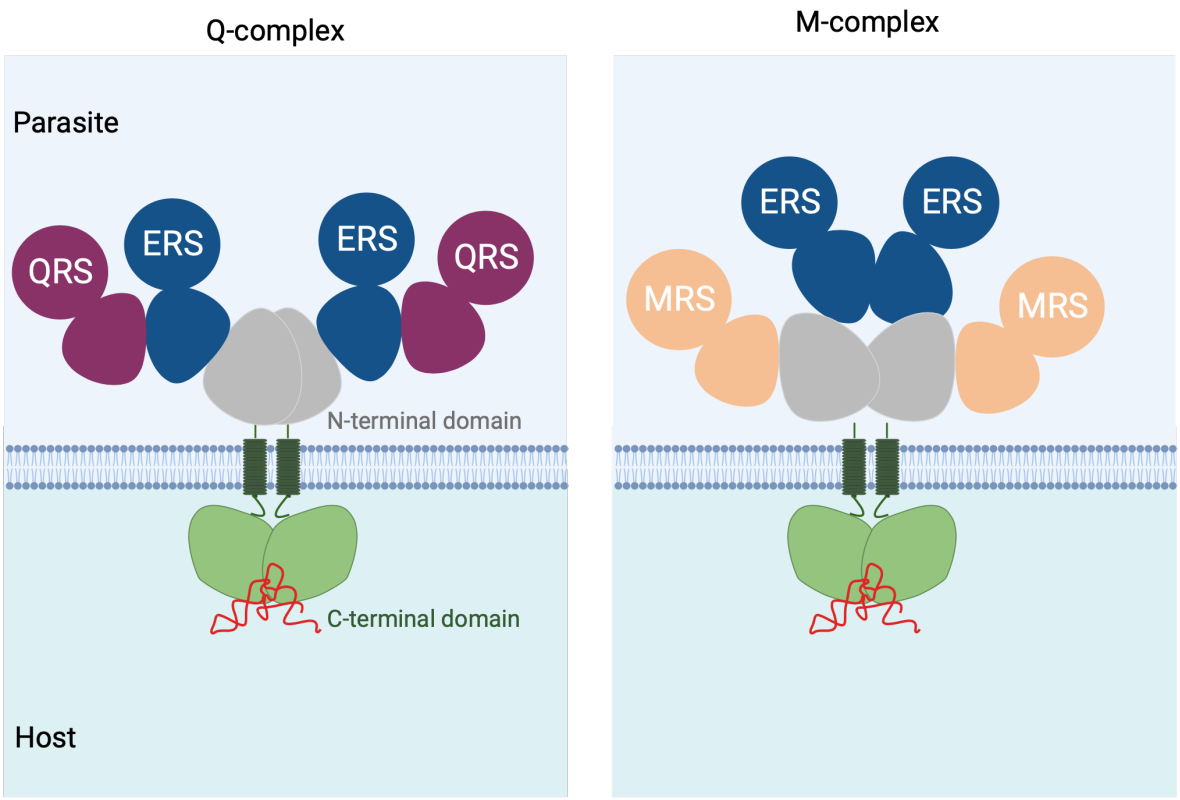

Figure 20: Existence of two MSCs in *Plasmodium*.
In *Plasmodium* two MSCs called Q-complex and M-complex have been identified. Both complexes have the same 2:2:2 stoichiometry, but the GST-like domains are organized differently. The C-terminal domain of tRip (green) is able to bind exogenous tRNAs.

2. Identification and characterization of tRip, an AIMP like no other

Like in other AIMPs, it has been shown *in vitro* that tRip is a homodimer that binds specifically tRNAs via its C-terminal domain. However, tRip is a unique AIMP, because it is localized on the parasite's surface and it mediates the import of exogenous tRNA into sporozoites. It has been also shown that tRip is expressed in all stages of the *Plasmodium* life cycle, and although it is not an essential protein, it is important for the parasite development in the blood stage.

2.1. tRip binds the elbow of tRNAs via the C-terminal domain

Electrophoretic mobility shift analysis (EMSA) showed that the dimeric tRip binds one molecule of tRNA (Cela et al., 2021) and is able to bind all tRNAs via its C-terminal domain with a Kd of 5-10 nM; by comparison, the Kd of bacterial Trbp111, *S. cerevisaie* ARC1p and human AIMP2 for tRNAs are 32 nM, 5-10 nM and 200 nM, respectively (Morales, 1999; Shalak et al., 2001; Simos et al., 1998). Competition experiments revealed that tRip specifically recognizes only tRNAs since 5S ribosomal RNA (rRNA), 18S rRNA and 28S rRNA cannot dissociate a tRip/tRNA complex whereas only total RNA (including tRNA) and crude tRNA can compete

and efficiently dissociate this tRip/tRNA complex. This specificity was further confirmed by footprinting experiments performed on tRNAs in the presence of the C-terminal domain of tRip, demonstrating that tRip recognizes the three-dimensional structure of the tRNA by binding the corner of the L-shaped structure formed between the T and D loops as well as the upper region of the anticodon stem of the molecule (Bour et al., 2016; Cela et al., 2021).

Further, in the study by Cela et al. (2021) using the Microarray Identification of Shifted tRNAs (MIST) technique, it was shown that tRNAs are bound with different affinities. The MIST technique was used to identify the tRNAs preferentially recognized by *P. falciparum* tRip in the presence of an excess of crude human tRNAs. Human $tRNA^{Ala}_{hGC}$, $tRNA^{Asn}_{GTT}$, $tRNA^{Ser}_{AGA}$ and $tRNA^{Leu}_{wAG}$ were shown to be the best binders. In contrast, other tRNAs, such as $tRNA^{Ala}_{IGC}$, $tRNA^{Ser}_{CGA}$, $tRNA^{Thr}_{CGT-2}$, $tRNA^{Asp}_{GTC}$, $tRNA^{Arg}_{ICG}$ and $tRNA^{Pro}_{hGC}$ proved to be poor binders. On the one hand, sequence analysis between the two groups did not reveal any obvious signal that might be responsible for this discrimination. On the other hand, screening of the Modomics database (https://genesilico.pl/modomics/modifications) identified potential modifications involved in tRip-tRNA binding. Indeed, some modifications appear to be absent in tRNAs that bind with low affinity to tRip, such as ac4C (N4-acetyl-2′-O-methylcytidine) at position 12, Ψ (pseudouridine) in the anticodon arm and m7G (7-methylguanosine). In contrast, Ψ at position 13 in the D arm, two consecutive 5-methylcytidines (m5C) in the variable region, or 5,2′-O-dimethyluridine (m5Um) in the T loop are absent among the tRNAs that bind most strongly to tRip ($tRNA^{Arg}_{TCT}$, $tRNA^{Ser}_{wGA}$, $tRNA^{Asn}_{GTT}$ and $tRNA^{Leu}_{wAG}$). Importantly, these post-transcriptional modifications are present in the tRNA domains recognized by tRip in the footprinting experiments (Bour et al., 2016; Cela et al., 2021), strongly suggesting that these modifications modulate the interaction with tRip (Figure 21).

Notably, one of the preferred tRNA species by tRip is the human $tRNA^{Asn}_{GTT}$, while, asparagine is one of the most frequently used amino acid in *Plasmodium* (see Introduction, chapter IV, paragraph 2).

Figure 21: Post-transcriptional modifications and tRNA recognition by tRip.
Legend continues on next page.

Location of modifications potentially involved in tRNA:tRip complex formation. The modifications identified were placed on the crystallographic structure of *S. cerevisiae* $tRNA^{Phe}_{GAA}$ (PDB1EHZ). The structure in the middle summarizes the regions of $tRNA^{Phe}_{GAA}$ that are in contact with tRip as shown by footprinting experiments (Cela et al., 2021). Nucleotides strongly protected by tRip from lead cleavage are indicated in green and those moderately protected are in yellow.

2.2. tRip is expressed at all stages of the Plasmodium life cycle

Transcriptomic and proteomic analyses provided by *P. falciparum* and *P. yoelii* indicate that tRip is expressed throughout the parasite's life cycle, including both sexual and asexual stages in the blood, during mosquito stages, and in the pre-erythrocytic stage (plasmodb.org/plasmo/). Immunofluorescence experiments using a specific anti-tRip$_{214-402}$ antibody have confirmed the presence of tRip in mosquitoe's salivary gland sporozoites and gut ookinetes, as well as at the blood and liver stages of vertebrate (Figure 22).

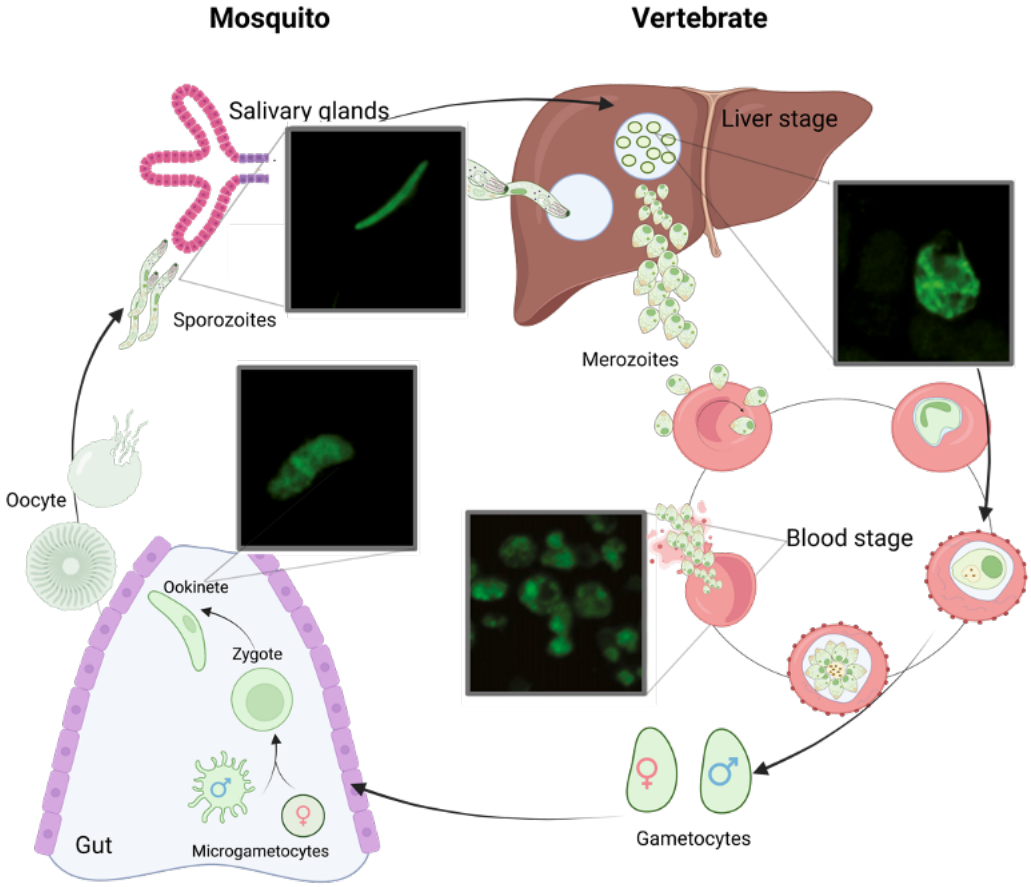

Figure 22: Immunodetection of tRip.
Immunofluorescence assay with anti-tRip$_{214-402}$ antibodies that recognize specifically the C-terminal tRNA binding domain. tRip is expressed throughout the life cycle (green fluorescence) - in ookinetes, sporozoites, blood stage, and liver stage (Bour et al., 2016). Immunodetection results are from Bour et al. (2016).

2.3. tRip is localized at the surface of sporozoites

Immunofluorescence experiments revealed that tRip colocalizes with circumsporozoite protein (CSP), the major surface protein of the sporozoite (Figure 23A). Since sporozoites possess a complex of two inner membranes in addition to the external plasma membrane, the precise localization of tRip was made possible by utilizing Triton X-100. Typically, the inner membrane complex remains resistant to Triton X-100, in contrast to the external plasma membrane.

Immunofluorescence images of sporozoites with anti-tRip$_{214-402}$ and anti-CSP antibodies show a peripheral signal in the absence of Triton X-100 treatment, but following the disruption of the plasma membrane with Triton X-100 detergent, no distinct signal for tRip and CSP is observed (Figure 23B). Such behavior of the two proteins confirmed that tRip is a membrane protein, anchored to the plasma membrane. Immunolocalization in native conditions and using the C-terminal domain directed antibody showed that the GST-like domain is localized inside the parasite, while the C-terminal domain is exposed on the external side of the membrane (Figure 23C).

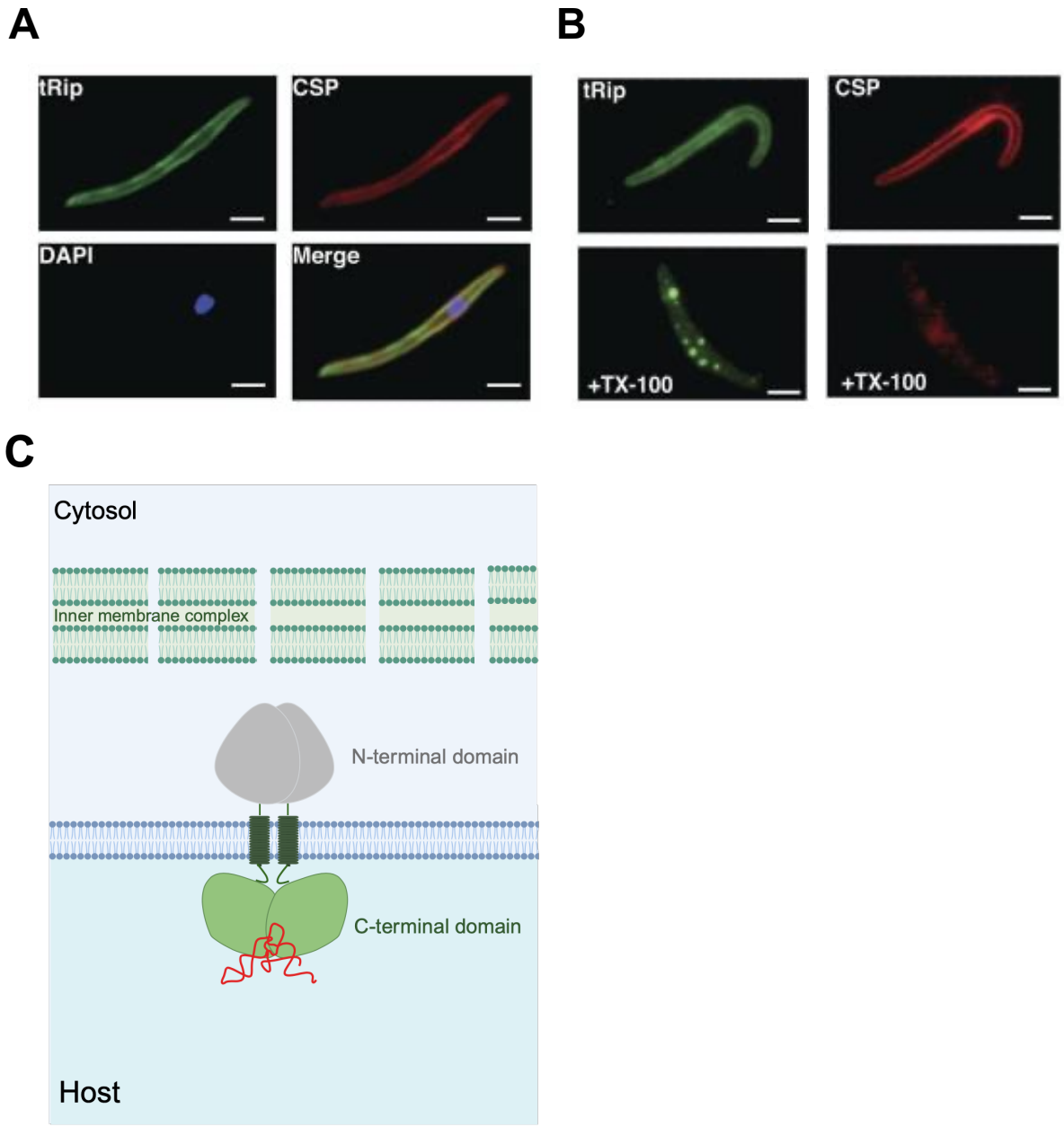

Figure 23: tRip localization.
(A) Coimmunolocalization assay on purified sporozoites from the salivary glands of *P. berghei*. tRip (green signal) was detected using anti-tRip$_{214-402}$ antibodies, while CSP (red signal) was detected using anti-CSP antibodies. Nuclei were stained with DAPI (blue). **(B)** Triton X-100

extraction. In the upper panel, untreated sporozoites show a peripheral green signal for tRip and a red signal for CSP. In the lower panel, Triton X-100 treatment disrupts the external membrane only and lead to the disappearance of both signals. (Scale bars 2 µm). **(C)** Based on these immunolocalization experiments, tRip is a membrane protein anchored to the plasma membrane through a transmembrane helix (dark green). The N-terminal GST-like domain (grey) is localized within the parasite, while the C-terminal tRNA binding domain (light green) is external. Immunodetection results are from (Bour et al., 2016).

2.4. tRip mediates the import of exogenous tRNA into sporozoites

Sporozoites, along with ookinetes, are the only extracellular forms of the parasite that lack a parasitophorous vacuole and can be manipulated *in vitro*. This is why sporozoites were chosen to study the parasite's ability to import exogenous tRNA molecules. Fluorescent *in situ* hybridisation (FISH) experiments provided convincing evidence for the import of exogenous tRNA into the parasite. Experiments were carried out on *P. berghei* sporozoites incubated with and without *E. coli* tRNA. tRNA import is visible exclusively in live wild-type sporozoites incubated with $tRNA^{Val}$ (Figure 24), whereas live sporozoites cannot import human 5S rRNA (not shown). The experiment gave the same results with *P. falciparum* and *P. yoelii* sporozoites. Further confirmation that tRNA import is mediated by tRip was supported by two substantial lines of evidence:

(i) By performing FISH experiments in the presence of increasing concentrations of anti-$tRip_{214-402}$ antibodies: under these conditions, tRNA import is significantly reduced, indicating that tRNA competes with antibodies for binding to the C-terminal domain of tRip.

(ii) By using a tRip-KO parasite where the gene encoding tRip has been replaced by the gene encoding mCherry: no longer import of tRNA was observed (Figure 24).

These data provide strong evidence that tRip plays a crucial role in facilitating the import of exogenous tRNA molecules into sporozoites (Bour et al., 2016).

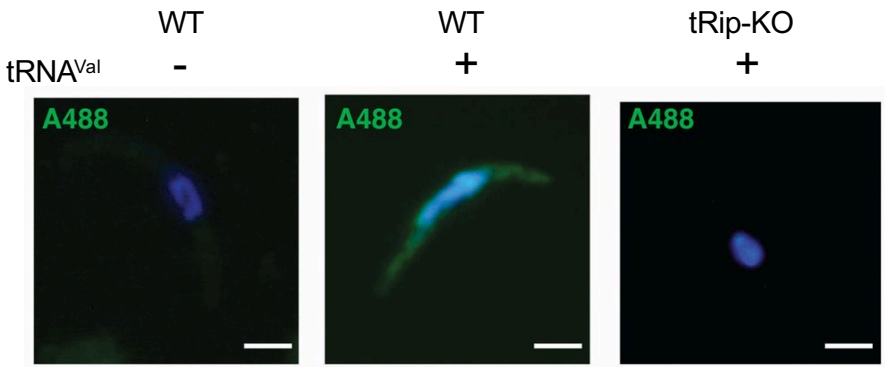

Figure 24: Comparison of tRNA import in *P. berghei* sporozoites WT and tRip-KO.
P. berghei WT and tRip-KO sporozoites were incubated with (+) and without (-) $tRNA^{Val}$. The probe used for the FISH experiment was labelled with Alexa Fluor 488 (green). tRNA import (green fluorescence) was observed in the WT parasite, but not in the KO parasites or in the control without tRNA.

2.5. tRip is important for parasite development in the blood stage

The tRip-KO parasite was generated by deleting the tRip gene and replacing it with the mCherry gene and with a pyrimethamine resistance gene through double homologous recombination. The non-lethality of the tRip-KO parasite indicates that tRip is not essential for the parasite's survival. However, its absence leads to reduced development of the parasite during the blood stage (Bour et al., 2016). A group of mice was infected with an intravenous injection of infected red blood cells, containing both *P. berghei* WT and tRip-KO parasites. The WT parasite expresses green fluorescent protein (GFP), whereas the tRip-KO parasite expresses mCherry. Parasitemia and the KO/WT parasite ratio were evaluated for 4 consecutive days (Figure 25, orange line). Blood was then collected from the first group of mice and injected into another group of mice, three times, and the KO/WT ratio was calculated (Figure 25, blue line). Over the course of the passages, the population of tRip-KO parasites disappeared and only WT parasites were detected in the last round, indicating that the tRip-KO parasites were unable to sustain their population in successive infections.

This correlates with a reduced translational activity in the tRip-KO parasite compared to the WT, suggesting that tRip plays a significant role in facilitating the translation process within the parasite (Bour et al., 2016).

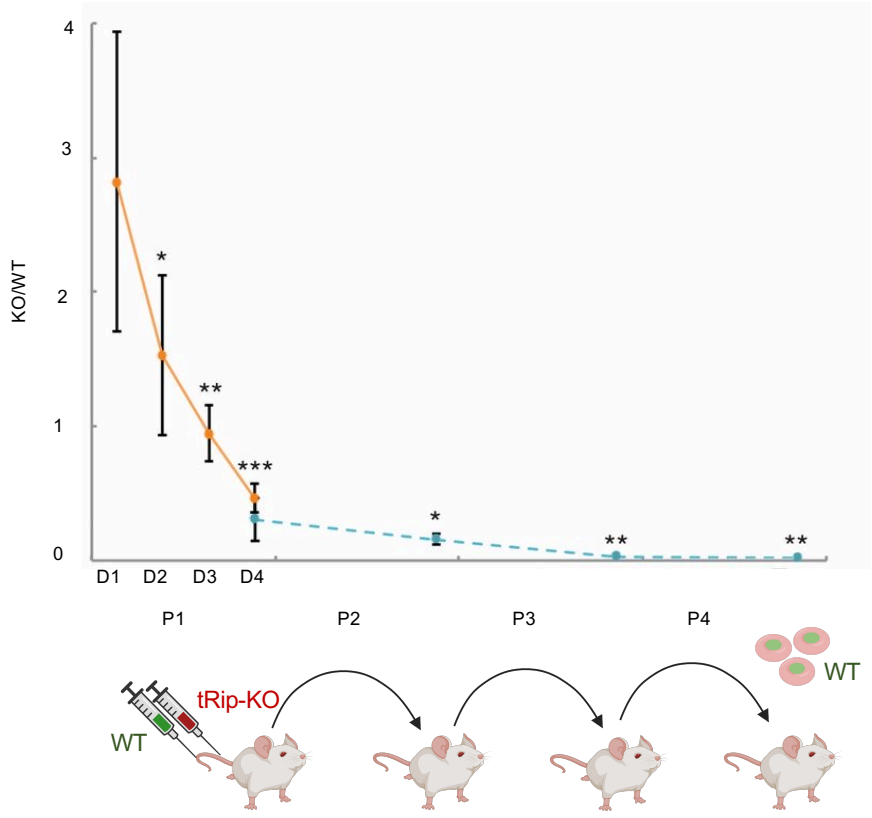

Figure 25: Development of the blood stage tRip-KO parasite.
Measurement of KO/WT ratio across passages between mouse groups. At time zero, a group of mice was co-infected with tRip-KO and WT parasites. After four passages, no KO parasites were detected, only WT parasites remained in the blood of infected mice (Bour et al., 2016).

2.6. Localization of tRip in the blood stage parasites

tRip was also localized at the surface of the parasite in the blood stage (merozoite). The localization of tRip was performed on schizonts by immunolocalization compared to MSP1 (Figure 26A) and by differential dissociation experiments (carbonate *versus* Triton X-100 dissociation) compared to AMA1 (Figure 26B and C). Each time, tRip behaves like the two well characterized membrane bound surface proteins, further supporting that tRip is localized on the external membrane of the parasite during the blood stage (Figure 26D).

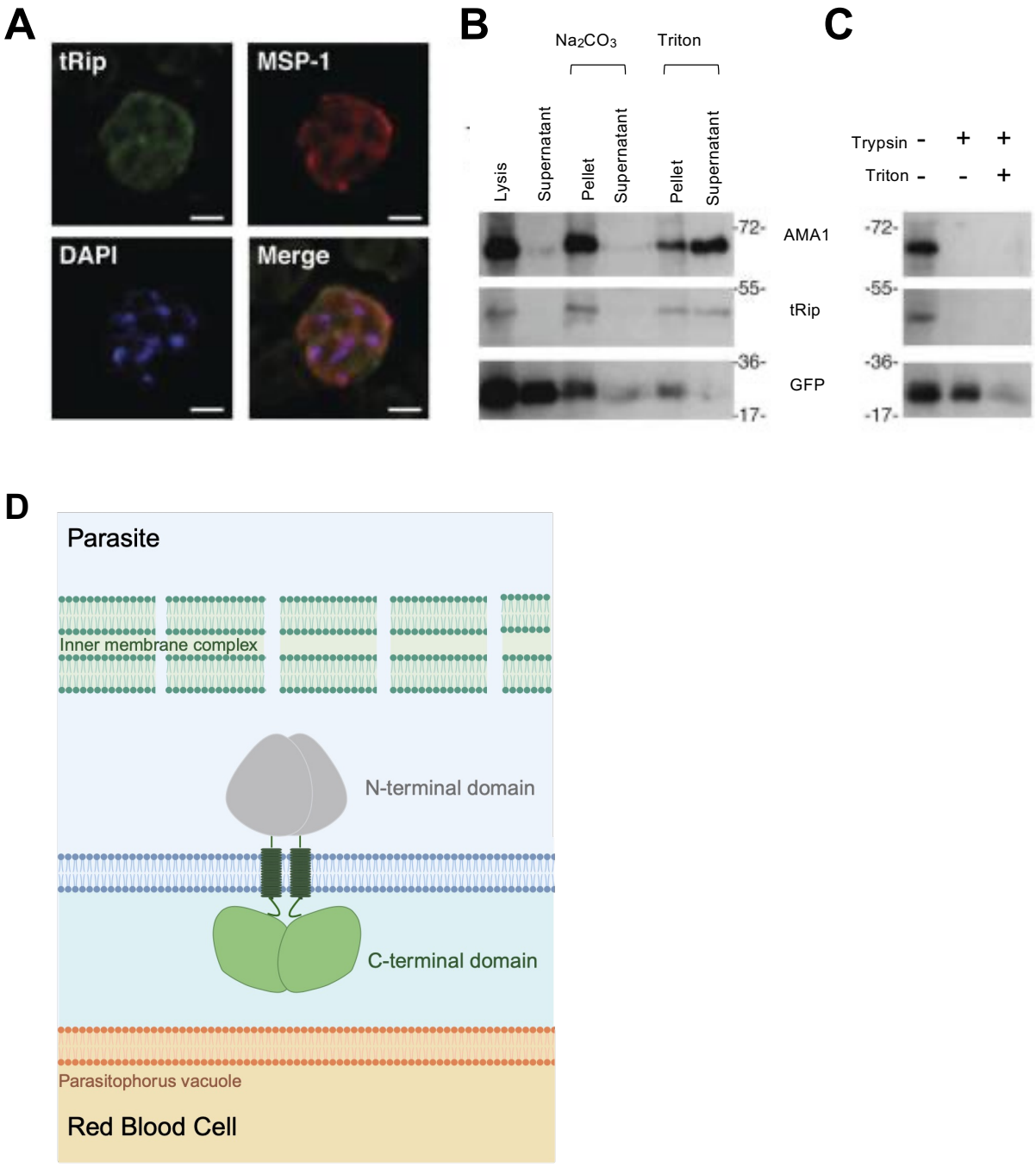

Figure 26: Localization of tRip in blood stage parasites.
(A) Immunolocalization assays on schizonts purified from the blood stage of *P. berghei*. tRip (green signal) was detected using anti-tRip$_{214-402}$ antibodies, while MSP1 (red signal) was

detected using anti-MSP1 antibodies. Nuclei were stained with DAPI (blue). **(B)** Differential extraction Na_2CO_3 versus Triton X-100 on *P. berghei* blood stage. Both tRip and AMA1 are found in the pellet after lysis and after carbonate treatment, indicating that they are both integral membrane proteins. They are released from the membrane only after treatment with Triton X-100. As a control, GFP (Green Fluorescent Protein), which is not membrane-associated, is localized in the supernatant immediately after lysis. **(C)** Protease-protection assay during blood stage parasite. The signals of AMA1 and tRip disappear when the blood stage parasite is incubated with trypsin, while the cytosolic GFP is still visible, indicating that AMA1 and tRip are located at the surface of the parasite. **(D)** tRip is a membrane protein anchored to the plasma membrane of the blood stage of the parasite through its transmembrane helix (dark green). The N-terminal domain (grey) is localized within the parasite, while the C-terminal domain (light green) is external. The only difference observed between the sporozoite and merozoite stages is the presence of the parasitophorous vacuole (orange) that encloses the parasite.

VI. My contribution

At the functional level, several observations have been made in the host laboratory. The import of exogenous tRNAs has been demonstrated in the infectious stage of the parasite, the sporozoite (Bour et al., 2016), but the phenotype of the tRip-KO parasite was observed during the blood stage, by developing much more slowly than the wild-type parasite. However, the availability of tRNA in the erythrocyte and the presence of a parasitophorous vacuole are strong indications against tRNA import at this stage of parasite development. Indeed, mature red blood cells are highly specialized cells that contain little RNA and therefore little tRNA. This paradox could explain *P. berghei*'s strong preference for reticulocytes (with a 150-fold higher affinity than mature erythocytes (Cromer et al., 2006). In mice, the number of reticulocytes varies between 1 and 5% of total blood cells (Chatterjee et al., 2016) and are cells characterized by very active translation, and therefore rich in tRNAs.

Once imported, the function of host tRNAs in the parasite cytoplasm is still unknown. Characterization of the tRip-KO parasite has shown that protein synthesis is reduced in the blood stage (Bour et al., 2016), suggesting that at least some of the imported tRNAs are involved in gene expression, either by acting directly on translation or by acting on the production or stability of messenger RNAs. The function of imported tRNAs will depend essentially on whether or not they can be aminoacylated by the parasite's aminoacyl-tRNA synthetases. On the one hand, it has been shown that tRNAs are imported as full-length tRNAs and are not degraded on arrival in the parasite (Bour et al., 2016). If the host tRNA is a substrate for the parasite's homologous aaRSs, they will participate in parasite protein synthesis. On the other hand, if the host tRNAs are not aminoacylated, they will be available to perform other functions. Indeed, tRNAs are also involved in a wide variety of signalling pathways (Kirchner and Ignatova, 2015; Schimmel, 2018), most of which are related to the stress response. Host tRNAs imported into the parasite, if not aminoacylated, will not be taken up by the parasite's translation machinery; it is therefore conceivable that these tRNAs could then enter a signaling pathway.

A particular feature of the *Plasmodium* proteome is the translation of long asparagine repeats, which certainly requires a large quantity of Asn-tRNA^{Asn} in the parasite. However, previous results indicate that tRNA^{Asn} is not at all overexpressed in the parasite compared with other tRNAs that are less used for protein synthesis (Filisetti et al., 2013). On the other hand, vertebrate tRNA^{Asn} is one of the 4 tRNAs best recognized by tRip *in vitro*, and would therefore be among the tRNAs preferentially imported into the parasite.

During my thesis, I studied and compared the proteomes of tRip-KO and wild-type parasites to determine the consequences of the absence of exogenous tRNA import on the synthesis of parasite proteins. This study, combined with the detection of host tRNA only in wild-type

parasites (compared to the tRip-KO parasites), confirms that tRNA import is important to support efficient translation in the blood stage of the parasite. These observations led us to propose a host tRNA-dependent post-transcriptional regulatory mechanism involving the Ccr4-Not complex.

Secondly, given the localization of tRip on the parasite surface, the expression of tRip at all developmental stages and the high sequence conservation of its C-terminal domain in all *Plasmodium* species, we used the C-terminal domain of tRip as a target for the selection of tRNA binding inhibitors and as an antigen to initiate an immune response, potentially capable of protecting mice from infection.

RESULTS

I. Comparative proteomic analysis of tRip-KO and wild-type parasites

The tRip-KO parasite exhibits slower growth compared to the wild-type parasite and reduced translation efficiency in the bloodstream of the vertebrate host (Bour et al., 2016). To better understand the molecular mechanisms involved in these phenotypes, we conducted comparative proteomic analyses between the wild-type and the tRip-KO parasite.

To perform the experiments, mice CD1 were infected with either the tRip-KO (n=3) or the wild-type (n=3) parasite. Blood samples were collected from the mice through cardiac puncture once the parasitemia reached 5-10% parasites were purified and quantified. After protein extraction, proteomic analysis was performed by mass spectrometry. Our findings indicate that only a small set of proteins show significantly altered expression levels in the tRip-KO parasite compared to the wild-type. The results obtained from the all-blood stages sample were compared with those previously obtained by Delphine Kapps, who had analyzed the proteome of the tRip-KO and wild-type parasites synchronized at the schizont stage. The deregulated proteins are involved in different functions in the two independent experiments. However, sequence analysis show that the proteins that are under-expressed in the tRip-KO parasite have a higher content of asparagine, with an increase of 35% to 70% compared to the proteins which expression is not affected. This suggests that the tRip-KO parasite may encounter difficulties in efficiently synthesizing proteins that are rich in asparagine.

A bioinformatics analysis of 6 *Plasmodium* genomes, searching for asparagine-rich proteins, revealed two proteins conserved in all *Plasmodium* strains: Poly(A) binding protein 3 (PABP3) and Ccr4-associated factor 1 (CAF-1), an exonuclease involved in the degradation of poly(A) tails. Both proteins recognize the same RNA substrate and are characterized by the same organization: an N-terminal domain strictly conserved in all eukaryotes and a C-terminal domain specific to *Plasmodium* and particularly rich in asparagine. Of the two proteins, CAF-1 is the best-characterized protein. It is part of the Ccr4-Not (carbon catabolite repressor protein 4-N) complex, that is a global regulator of gene expression, conserved from yeast to humans. It consists of Ccr4 and 3 Ccr4-associated factors (CAF1, CAF40 and CAF130) and 5 Not proteins, which together regulate protein translation through mRNA degradation (Collart, 2016; Tucker et al., 2001). Recently, the Ccr4-Not complex-mediated mechanism that regulate translation of non-optimal codons containing mRNAs, has been deciphered (Figure 27). It has been shown that the association between the ribosome and the Ccr4-Not complex occurs when a segment of mRNA rich in non-optimal codons is translated. In this case, the dissociation of the tRNA from the E-site occurs before that an aminoacyl-tRNA positions itself

in the A-site. This causes the E site to adopt a specific conformation that is recognized by the N-terminal of the Not5 subunitof the Ccr4-Not complex (Figure 27). The recruited Ccr4 complex can then initiate mRNA degradation catalyzed by the CAF-1 subunit (Buschauer et al., 2020). Members of the Ccr4-Not complex are well conserved in *Plasmodium* (Coulson et al., 2004) and a study by Balu et al. (Balu et al., 2011) showed that depletion of the C-terminal domain of CAF1 alters the stability of specific mRNAs at the parasite blood stage. When the C-terminal domain of the CAF-1 protein is deleted in *Plasmodium*, the phenotype observed is comparable to that of the tRip-KO parasite (Balu et al., 2011). This deletion, in particular, causes the upregulation of mRNAs encoding proteins involved in parasite invasion, which correspond to proteins overexpressed in the tRip-KO parasite proteome (all blood stages).

Based on all of these observations, our results suggest that the tRip-KO parasite has difficulty translating asparagine-rich proteins that characterize the parasite proteome and that the import of $tRNA^{Asn}$ into the WT parasite could help in the synthesis of these proteins. This hypothesis is supported by previous work showing that *P. falciparum* tRip has a preference for certain human tRNAs, including $tRNA^{Asn}$ (Cela et al., 2021) and by the fact that parasite aminoacyl-tRNA synthetases are capable of efficiently aminoacylating native human tRNAs.

We propose that in the absence of import of of $tRNA^{Asn}$, the C-terminal of CAF-1 would not be translated, leading to the specific and too early expression of mRNAs encoding the proteins responsible for the release and infectivity of merozoites. As a result, the released merozoites are immature and therefore ineffective in infecting the host's red blood cells.

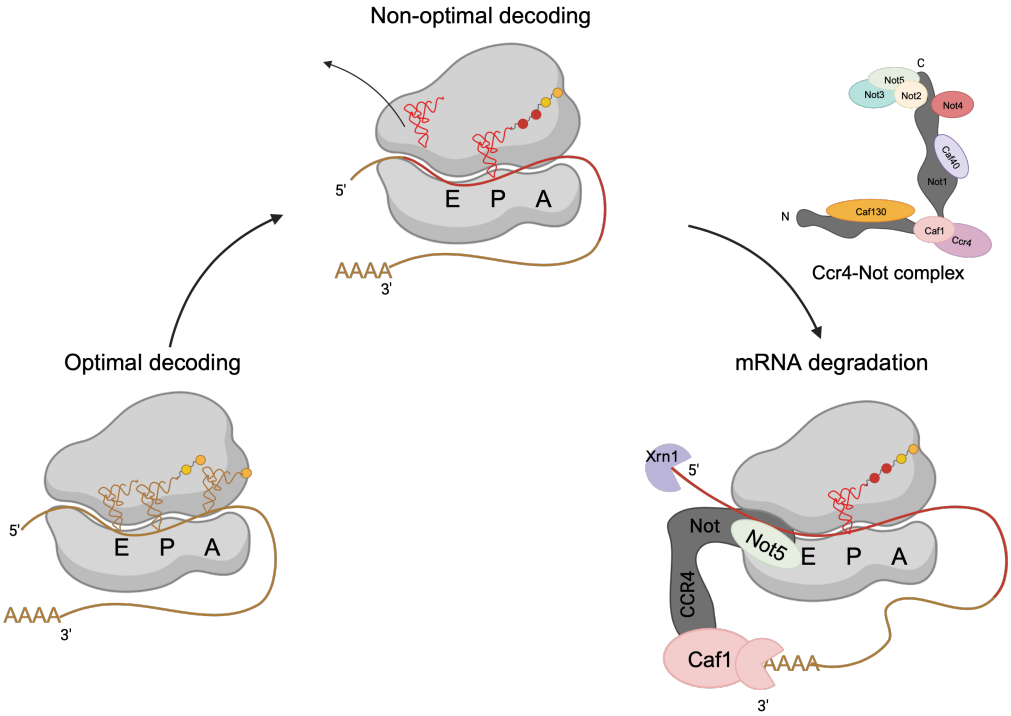

Figure 27: Ccr4-Not complex regulates the translation of mRNA containing non-optimal codons.

Legend continues on next page.

When translation is optimal (in yellow), the three ribosome sites are simultaneously occupied by tRNAs. The new aminoacyl-tRNA enter the A site before the deacylated tRNA has left the E site, while the tRNA with the forming polypeptide chain is located on the P site. When non-optimal codons are translated (red), there is a good chance that the tRNA will leave the E site before a new aminoacyl-tRNA settles in the A site. In this case, the A and E sites of the ribosome remain empty. In the proposed mechanism, the E-site takes on a conformation that would be recognized by the N-terminal domain of Not5, leading to the recruitment of the Ccr4-Not complex. In turn the Caf-1 subunit, would mediate mRNA degradation from the poly(A) tail of the mRNA. This induce activation of RNA degradation pathway that induces mRNA decapping and 3'-RNA degradation mediated by Ccr4-Not complex and 5'-RNA degradation mediated by Xrn1 (Buschauer et al., 2020).

Comparative proteomics uncovers correlation between tRip-mediated host tRNA import and asparagine insertion in *Plasmodium* proteins.

Martina Pitolli[a], Marta Cela[a1], Delphine Kapps[a], Johana Chicher[b], Laurence Despons[a] and Magali Frugier[a*]

[a]Université de Strasbourg, CNRS, Architecture et Réactivité de l'ARN, UPR 9002, F-67084 Strasbourg, France

[b]Strasbourg-Esplanade Proteomics facility, Université de Strasbourg, F-67084 Strasbourg, France.

[1]present address: Molecular Microbiology and Structural Biochemistry, CNRS UMR 5086, Université Claude Bernard Lyon 1, Lyon, France

*to whom correspondence should be addressed: Email: m.frugier@ibmc-cnrs.unistra.fr

Authors Contributions: MP, DK and MC performed experiments, data acquisition, and analysis, JC performed mass spectrometry analysis and LD provided computer programming. MF managed the conception, design, interpretation of data and funding acquisition and wrote, reviewed, and edited the manuscript.

Competing Interest Statement: The authors declare no conflict of interest.

Classification: Biochemistry

Key words: tRNA, translational control, proteomics, amino acid usage

This PDF file includes:

Main Text, Figures 1 to 4, and supporting information.

Abstract

tRNAs are not only essential for decoding the genetic code, but their abundance also has a strong impact on the rate of protein production, folding, and on the stability of their encoding messenger RNAs. *Plasmodium* expresses a unique surface protein called tRip, involved in the import of exogenous tRNAs into the parasite. Comparative proteomic analysis of the blood stage of wild-type and tRip-KO variant of *P. berghei* parasites revealed that down-regulated proteins in the mutant parasite are distinguished by a bias in their asparagine content. We therefore propose a model in which a dynamic import of host $tRNA^{Asn}$ allows the synthesis of asparagine-rich regulatory proteins that efficiently and selectively control the parasite infectivity. These results suggest a novel mechanism of translational control where import of host tRNAs emerge as critical regulator of gene expression in the *Plasmodium* developmental cycle and pathogenesis.

Significance Statement

tRip is a surface protein involved in the import of exogenous tRNAs into the malaria parasite, *Plasmodium*. To better understand tRNA import and protein synthesis in *Plasmodium*, the proteomes of wild-type and tRip-KO parasites were compared. Most of the proteins deregulated in the tRip-KO parasite were under expressed compared to the wild-type. Asparagine usage was greatly increased in the proteins that were down-regulated in the tRip-KO, suggesting that the mutated parasite is impaired in inserting asparagine into proteins. Moreover, the presence of host tRNAs inside the blood stage parasite and the possibility of charging these imported tRNAs with endogenous aminoacyl-tRNA synthetases, led us to propose that, imported host tRNAs participate in parasite protein synthesis and control its development.

Introduction

We have discovered the only example to date of an exogenous tRNA import pathway, summarized in Figure 1 (1–4). In *Plasmodium*, the malaria parasite, *P. berghei* sporozoites (the extracellular infective form of the parasite, Figure S1) isolated from the salivary glands of infected mosquitoes import exogenous tRNAs *via* a surface protein, named tRip (tRNA import protein). However, the absence of homologous mechanisms in other organisms raises the question of the role of this unique tRNA import and its mode of action. It has been established that (i) tRip is a homodimeric protein made of an N-terminal GST-like domain and a C-terminal EMAPII-like tRNA binding domain; (ii) tRip binds human tRNAs with high affinity *in vitro* and with a stoichiometry of one tRNA per tRip dimer; (iii) tRip is located on the parasite surface with its tRNA binding domain exposed to the host system; (iv) immunolocalization experiments found tRip expressed both in the liver and blood stages in the vertebrate host, as well as in the intestine and salivary glands of the mosquito; (v) *in vitro*, exogenous tRNAs enter living sporozoites; (vi) the knockout parasite, tRip-KO, does not import tRNAs, its protein biosynthesis is significantly reduced, and its growth is decreased in vertebrate blood compared to the wild-type parasite.

Recently, the crystal structure of the dimeric N-terminal GST-like domain of *P. vivax* tRip was solved and revealed a unique homodimerization interface (5). We confirmed by SAXS that this unusual interface exists in solution and that it allows Multi-Synthetase Complex (MSC) formation (3, 4). Indeed, three aminoacyl-tRNA synthetases (aaRS), namely glutamyl- (ERS), glutaminyl- (QRS) and methionyl- (MRS) tRNA synthetases, specifically co-immunoprecipitate with tRip; These enzymes all contain an N-terminal GST-like domain involved in MSC assembly. Unexpectedly, these proteins form two exclusive heterotrimeric MSCs with a 2:2:2 stoichiometry: a Q-complex (tRip:ERS:QRS) and an M-complex (tRip:ERS:MRS) characterized by different biophysical properties and interaction networks (Figure 1). We could also identify a set of host tRNAs preferentially bound by tRip and potentially best imported into the parasite. Interestingly, tRip does not bind to tRNAs in a sequence-dependent manner, but rather recognizes post-transcriptional modifications that modulate this interaction (2). In contrast to what was found with the cytosolic yeast Arc1p (6), the tRNAs that best bind tRip do not correspond to the aaRSs that compose the two MSCs, suggesting that, although tRip is an aminoacyl-tRNA synthetase interacting multifunctional protein (AIMP), it is not dedicated to the aminoacylation of specific tRNAs (2), thereby

leading us to search for a novel function for this unique membrane protein and the tRNA import with which it is associated.

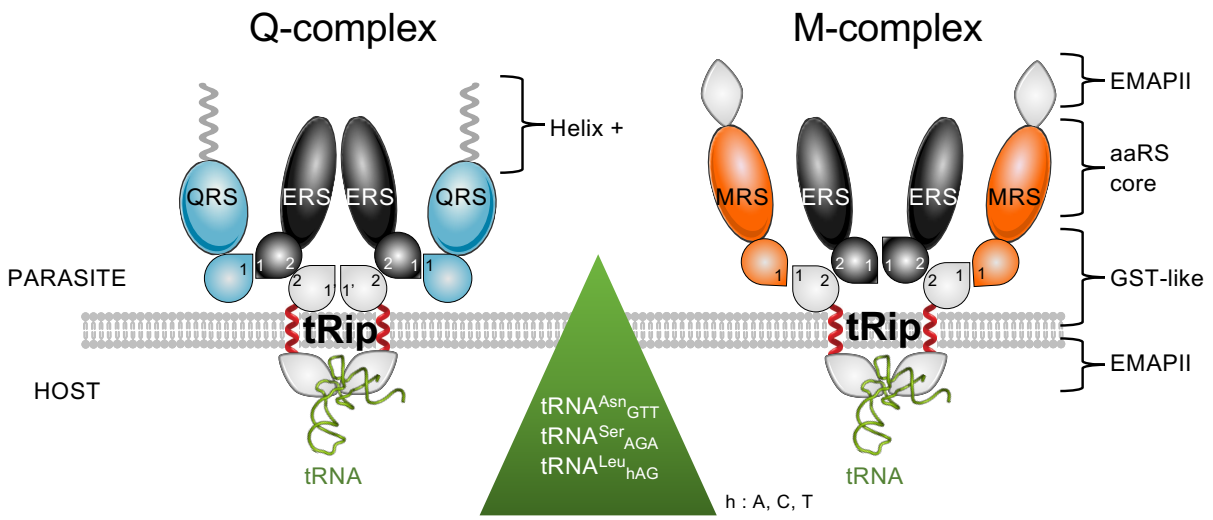

Figure 1: *P. berghei* membrane-bound multi-synthetase complexes. *Plasmodium* is characterized by the presence of two multisynthetase complexes (MSC) named Q-complex and M-complex. The Q-complex is composed of glutamyl- (ERS) and glutaminyl- (QRS) tRNA synthetases linked to a dimer of tRip whereas the M-complex is composed of tRip and Methionyl-tRNA synthetase (MRS) organized around a dimer of ERS. tRip is therefore an AIMP (Aminoacyl-tRNA synthetase Interacting Multifunctional Protein). tRip, ERS, QRS, and MRS are schematized and colored in grey, black, cyan, and orange, respectively. the GST-like domains are shown as a drop and the C-terminal domains of tRip, QRS and MRS involved in tRNA binding are either EMAPII-like domains (tRip and MRS, grey diamonds) or a positively-charged α-helix (QRS, shown as a grey helix). The characteristic feature of *Plasmodium* MSCs is that tRip is a membrane protein (the transmembrane helix is shown in red) with the GST-like domain required for MSC formation localized inside the parasite and the tRNA binding domain exposed outside the parasite to host tRNAs. This unique organization justifies that only the EMAPII-like domain of tRip ($tRip_{200-402}$) is fused at the C-terminal domain of a GST domain and used as a target for the selection of aptamers capable of inhibiting tRip tRNA binding. Interfaces 1, 1' or 2, involved in protein-protein interactions, are indicated in the corresponding GST-like domains.

Interestingly, tRip is not the only protein that has been characterized as cytosolic in other organisms and is actually localized on the surface of *Plasmodium*. This is also the case for other RNA-binding proteins such as the poly-A binding protein-1 (PABP-1) (7) and the glyceraldehyde-3 phosphate dehydrogenase (GAPDH) (8), which are both found on the surface of the sporozoite. The presence of different RNA-binding proteins at the parasite-host interface is another indication that RNA

exchange might control unsuspected host-parasite interactions that take place during the parasite life cycle. In the present study, we compared the proteomes of the wild-type (WT) and the tRip-KO blood stage parasites with the objective of understanding the fate of imported tRNAs in *Plasmodium* protein synthesis and its infectious process.

Results

Quantitative proteomics of tRip-KO *versus* wild-type (WT) schizonts. We investigated the relative protein abundance of tRip-KO *versus* WT in the schizont stage of synchronized parasites (Figure S1) using liquid chromatography coupled to tandem mass spectrometry (LC-MS/MS) and a label-free quantification method. Three biological replicates for tRip-KO and WT were defined for the schizonts samples (Table S1). The proteomic data sets (KO and WT) were considered comparable as most proteins were stable. This is notably the case for four constitutively expressed proteins: EF1-α (PBANKA_1133300), Hsp70 (PBANKA_0914400), enolase (PBANKA_1214300) and histone H4 (PBANKA_941900) (Table S1). Protein abundance was calculated using the intensity of *P. berghei* peptides, which identified between 347 and 469 proteins. Metric multidimensional scaling (MDS) (included in Table S1) indicated clustering of the tRip-KO and WT parasites, suggesting there are distinct groups of differentially abundant proteins between the two genotypes. Among these proteins, only 8 were significantly up-regulated and 49 were down-regulated in the tRip-KO parasites compared to the WT (*p-value* < 0.05) with a at least a 2-fold change in abundance; they are highlighted in the volcano plots in orange and green, respectively (Figure 2A). Most of down-regulated proteins are involved in translation (31% ribosomal proteins, initiation, and elongation factors); the two other abundant categories were surface proteins involved in transport and invasion (16%) and proteins with unknown functions (14%) (Table S1).

Amino acid compositions of tRip-KO down-regulated proteins. Amino acid utilization in the 100 most expressed stable proteins was compared with that of the significantly down-regulated proteins in the tRip-KO parasite (Figure 2B). There is a 70% increase in asparagine in the proteins down-regulated in the tRip-KO parasite compared to the wild-type (Table S2, 11.6% in tRip-KO *versus* 6.8% in WT), thus, suggesting that the tRip-KO parasite has difficulty translating asparagine-rich proteins.

Quantitative proteomics of tRip-KO *versus* WT in "Blood stages" samples. Three biological replicates for tRip-KO and WT containing all blood stages (rings, trophozoites, and schizonts) were used

for comparative proteomics (Figure S1, Table S3). Triplicate proteomic data sets (KO and WT) were compared and identified between 617 and 1017 proteins each time. Sixty-nine proteins were significantly deregulated (at least a 2-fold change in abundance), 8 were up-regulated and 61 were down-regulated in the tRip-KO parasites compared to the WT (*p-value* < 0.05) (Figure 2C). The few up-regulated proteins are especially rhoptry associated proteins (a specialized organelle in *Plasmodia*) and proteins involved

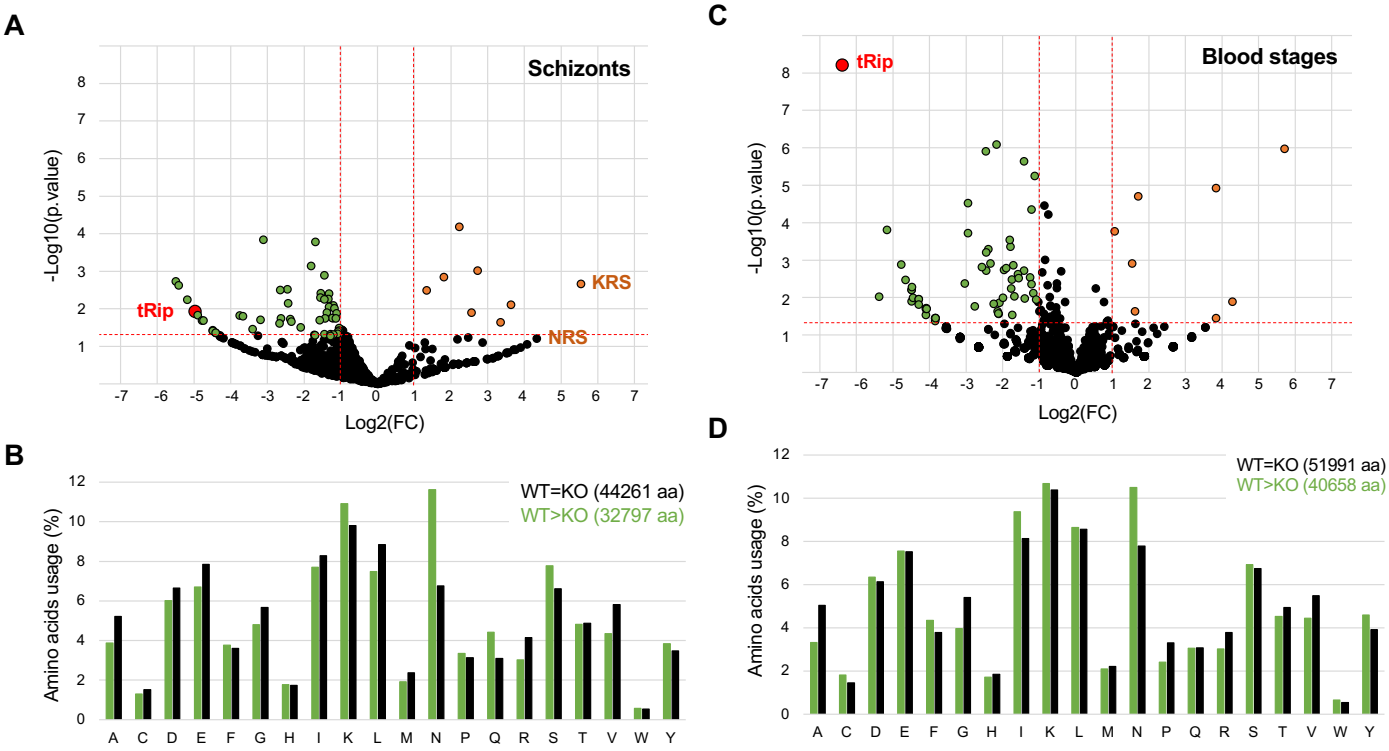

Figure 2: Comparative proteomic analysis and amino acid usage of proteins identified in WT and tRip-KO samples containing schizonts (A and B) or all blood stages (C and D). (**A**) Volcano plot of all quantified proteins from WT and tRip-KO parasites displaying the relationship between statistical significance (−log10(*p-value*), y-axis) and log fold change (FC) of each protein (log2(FC), x-axis). Statistics are based on three independent experiments (Table S1). Deregulated proteins in tRip-KO parasite compared to the WT parasite are shown in orange (up-regulated, FC≥2 and *p-value* ≤ 0.05) and green (down-regulated, FC≤-1 and *p-value* ≤ 0.05). tRip is shown in red and black dots represent proteins with no significant change. KRS and NRS correspond to Lysyl- and asparaginyl-tRNA synthetases. (**B**) Comparison of amino acid usage (%) of proteins whose expression is stable in the tRip-KO parasite (the 150 most expressed proteins, black) and all proteins that are down-regulated in the tRip-KO parasite (green). Amino acids are designated by their one letter symbol and the total number of amino acids used in the analyses is specified. (**C**) Volcano plot of all quantified proteins from WT and tRip-KO parasites. Statistics are based on three independent experiments (Table S3). (**D**) Comparison of amino acid usage (%) between proteins whose expression is stable in the tRip-KO parasite (the 100 most expressed proteins, black) and proteins down-regulated in the tRip-KO parasite (green).

in mobility and invasion (Table S3), while down-regulated proteins were distributed across different functional families: Apart from the 20% of proteins with unknown function, most are involved in DNA replication (41%). Yet, none were common to the schizonts samples (compare Tables S1 and S3). Amino acid usage in the tRip-KO down-regulated proteins shows also that these proteins contain more asparagine residues (10.5% in tRip-KO *versus* 7.8% in WT) than the 150 most expressed stable proteins (Figures 2D, Table S2), leading to the same conclusion as above: in the absence of tRip, asparagine-rich proteins are less efficiently translated.

The mRNAs encoding 3 up- and 3 down-regulated proteins were quantified by qRT-PCR. While the mRNAs for the up-regulated proteins were not significantly affected, the mRNAs of the down-regulated proteins all showed a strong decrease in the tRip-KO parasite compared with the WT parasite (Figure S2, Table S4). Decreased translation of these mRNAs likely favors their rapid degradation, suggesting that down-regulated proteins are controlled at the level of mRNA stability.

Identification of asparagine-rich proteins in *Plasmodia* strains. Since both "schizonts" and blood stages samples strongly suggest that the tRip-KO parasite is hindered in inserting asparagine into proteins, the complete proteomes of six *Plasmodium* lineages (*P. falciparum*-5476 proteins, *P. berghei*-5076 proteins, *P. yoelii*-6097 proteins, *P. chabaudi*-5222 proteins, *P. knowlesi*-5340 proteins and *P. vivax*-6708 proteins) as well as *Toxoplasma gondii* (control, 8322 proteins) were retrieved from ApiDB (9) and analyzed for their asparagine content (Figure S3A). *Plasmodium* proteins contain more asparagine residues than *Toxoplasma*. Yet, the *P. knowlesi* and *P. vivax* proteomes contain fewer asparagine residues (an average of about 8 %) than the 4 other *Plasmodia* strains (average of about 12%) (Figure S3A, Table S2). Proteins were then ranked from highest to lowest asparagine contents to identify those that might be impacted by decreased asparagine decoding efficiency. For all proteomes, only the top 0.5% proteins were considered to identify conserved proteins containing the highest asparagine content. Depending on the strain, 25 to 30 proteins were selected (Table S5). This list includes 2 proteins that are strictly concerved in all strains and different members of AP2 domain transcription factors in all strains except *P. vivax*; The two ubiquitous proteins correspond to the CCR4-associated factor-1 (CAF-1) and the poly-A binding protein-3 (PABP-3). They share a particular modular organization with an N-terminal domain of high complexity and a low complexity C-terminal domain with a very high asparagine content (Figure S3B, C). The proportion of asparagine varies locally between 35 and 60% in *P. falciparum*, *P. yoelii*, *P. chabaudi* and *P. berghei* and between 20 and 25% in *P. knowlesi*

and *P. vivax*. But these two proteins are only detected by a few spectral counts in the proteomic data (Tables S1 and S3) which are therefore not usable.

Comparison of tRip-KO and ΔC-CAF-1 phenotypes. The *Plasmodium* CAF1 N-terminal domain is highly conserved in eukaryotes while the additional asparagine-rich C-terminal domain is found only in *Plasmodia.* The deletion of this *Plasmodium*-specific C-terminal domain results in overexpression of mRNAs encoding proteins involved in parasite egress and invasion (10): of the 19 *P. falciparum* mRNAs up-regulated in this ΔC-CAF-1 mutant (10), 8 of the corresponding proteins can be detected in the present study (all blood stages) (Figure 3): proteins essential for merozoite formation and entry into and exit from erythrocytes, such as the rhoptry proteins, RAP1, RAP2/3 and the major surface proteins AMA-1 and MSP1 (LogFC = 1.26, *p-value* = 0.078) are up-regulated in the tRip-KO proteome and their mRNA levels vary similarly in the ΔC-CAF-1 mutant (10). Another protein associated with merozoite invasion of erythrocytes (RON2) is up-regulated only in the tRip-KO parasite. However, the 3 other proteins GAP50, RhopH2 and RhopH3, encoded by up-regulated mRNAs in ΔC-CAF-1 (10) show no variation between the tRip-KO and the WT proteomes.

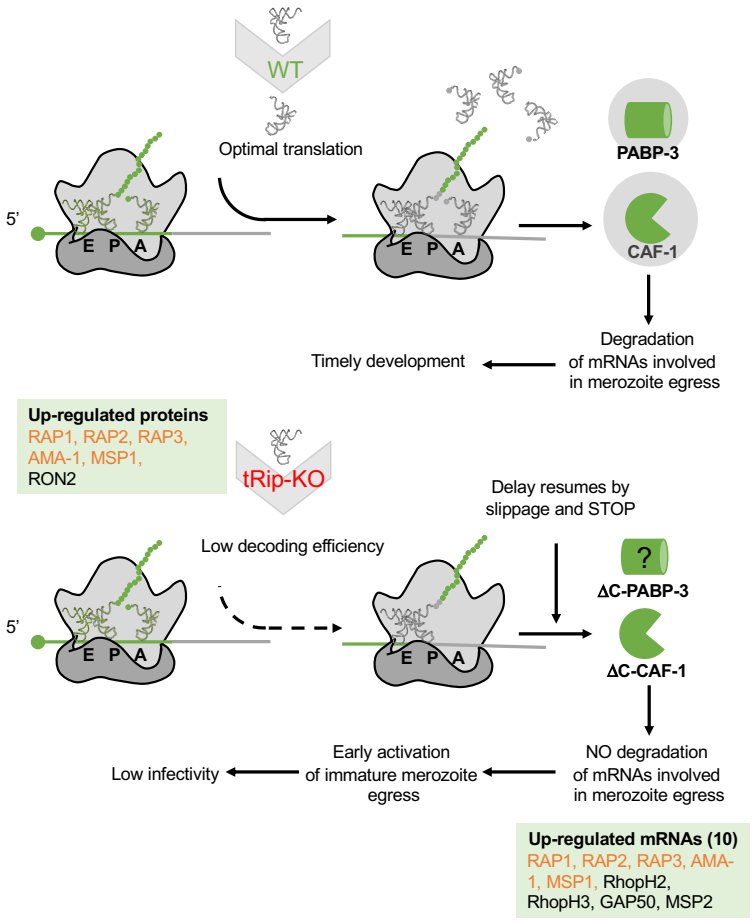

Figure legend on next page

Figure 3: Model of the mechanism of inhibition of protein synthesis in the tRip-KO parasite and consequences for timely egress of merozoites at the blood stage. In WT parasites, the asparagine-rich C-terminal domains of *Plasmodium* CAF-1 and PABP-3 are efficiently translated by additional $tRNA^{Asn}$ provided by tRip-mediated tRNA import from the host. Full-length CAF-1 can thus down-regulate specific mRNAs including those involved in egress and invasion that adequately control parasite development. On the contrary, in the tRip-KO parasite, translation of the C-terminal domains of CAF-1 and PABP-3 is hindered by the absence of host $tRNA^{Asn}$. The delay in translation can lead to frameshifting and the occurrence of stop codons. Such a mismatch may help the stalled ribosome population to be released from the mRNA, since in the *Plasmodium* AT-rich mRNAs non-decoded asparagine codons will be shortly followed by a stop codon in the new reading frame. The resulting ΔC-CAF-1 protein can no longer regulate the translation of genes involved in parasite egress/invasion leading to early release of infectivity-deficient immature merozoites. Genes up-regulated in both mutants are highlighted in orange, they correspond to roptry-associated proteins 1, 2 and 3 (RAP1, PF3D7_1410400/PBANKA_1032100; RAP2/3, PF3D7_0501600/0501500, PBANKA_1101400), apical membrane antigen (AMA1, PF3D7_1133400/PBANKA_0915000) and merozoite surface protein 1 (MSP1, PF3D7_0930300/PBANKA_0831000).Up-regulated genes involved in merozoite's egress either in *P. falciparum* ΔC-CAF1 mutant or *P. berghei* tRip-KO parasite are listed inside green boxes: genes not in common between both strains are indicated in black: merozoite surface protein 2 (MSP2, PF3D7_0206800), glidosome associated protein 50 (GAP50, PF3D7_0918000/PBANKA_0819000), high molecular weight rhoptry proteins 2 and 3 (RhopH2, PF3D7_0929400/PBANKA_0830200 and RhopH3, PF3D7_0905400/PBANKA0416000) and Rhoptry neck protein 2 (RON2, PBANKA_1315700); Ten genes were up-regulated in the ΔC-CAF-1 mutant but were not detectable in blood stages proteomes. They are not shown on the figure; they correspond to: erythrocyte binding antigens 140, 175 and 181 (EBA140, PF3D7_1301600; EBA175, PF3D7_0731500; EBA181, PF3D7_0102500), 6-cysteine proteins P12 and P38 (PF3D7_0612700 and PF3D7_0508000), glideosome-associated protein 45 (GAP45, PF3D7_1222700), myosin A-tail interaction protein (MTIP, PF3D7_1246400/PBANKA_1459500), myosin A (MyoA, PF3D7_1342600), subtilisin-like protease 1 (SUB1, PF3D7_0507500) and calcium-dependent protein kinase 5 (CDPK5, PF3D7_1337800).

Can host tRNAs be detected inside WT parasites and be aminoacylated by the parasite aaRSs? To date, the import of exogenous tRNA has been demonstrated at the sporozoite stage *in vitro*, only. In blood, both reticulocytes (about 2%) and mature red blood cells (RBC) can be infected by *Plasmodia*. While reticulocytes are characterized by a dynamic protein synthesis, RBC are hyper-specialized anucleate cells taht retain about 10 % of the protein synthesis observed in reticulocytes (11). RNAs purified from mouse blood and liver have the same profile, however, the purification yield indicates that RBCs contain about 100 times less RNA than liver cells do (Figure S4A). Several human tRNAs were specifically detected by Northern Blots (Figure S4B and S5A). In a second part of the study,

Northern Blots were performed on RNA samples purified from infected blood. The profiles of the RNA samples from blood cells infected by WT *versus* tRip-KO parasites are similar, but different from that of

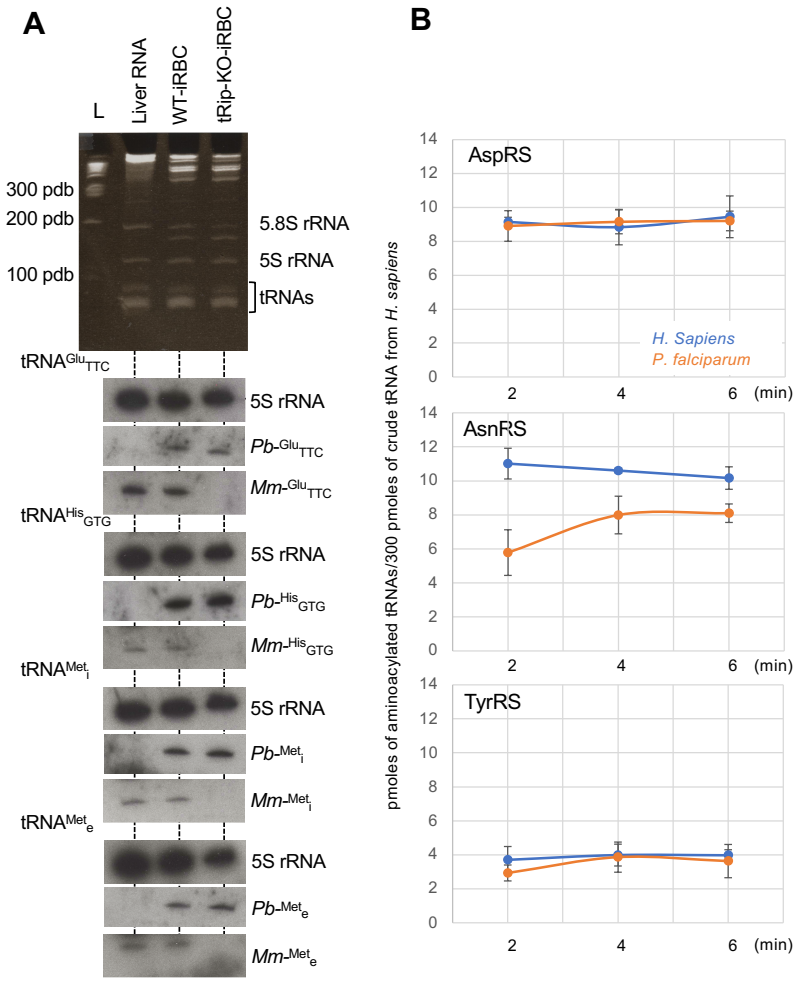

Figure 4: Detection of host tRNAs in WT parasites and cross aminoacylation of host tRNAs by the parasite aminoacyl-tRNA synthetases. (**A**) One µg of total RNA from the liver of non-infected (mice and 1 µg of total RNA from WT and KO parasites were analyzed on a ethidium bromide-stained 12% denaturing analytical gel. L corresponds to a DNA ladder. Northern blots experiments were completed with either probes designed to detect *P. berghei* tRNAs (*Pb*-$^{Glu}_{TTC}$, *Pb*-^{His}, *Pb*-$^{Met}_{i}$ and *Pb*-$^{Met}_{e}$) or *M. musculus* tRNAs (*Mm*-$^{Glu}_{TTC}$, *Mm*-^{His}, *Mm*-$^{Met}_{i}$ and *Mm*-$^{Met}_{e}$) (Figure S5). The four tRNAs belong to the category of tRNAs that interact most strongly with tRip *in vitro* (Cela et al., 2021). Detection of *Mm* tRNAs by Western blots necessitated extensive washing and long exposure of the films. (**B**) Comparative aminoacylation plateaus. Six aaRSs, aspartyl-, asparaginyl- and tyrosyl-tRNA synthetases from *H. sapiens* (in blue) or *P. falciparum* (in orange) were tested with crude human tRNAs under the same experimental conditions (6 µM crude tRNA and 0.2 µM aaRSs). Aminoacylation plateaus were measured at 2, 4, 6 min of incubation. Human crude tRNAs are potentially transcribed from 420 genes, amongst which 19 genes encode $tRNA^{Asp}$, 34 genes encoding $tRNA^{Asn}$ and 15 genes encoding $tRNA^{Tyr}$ (Chan and Lowe 2016). Error bars represent the standard deviation (SEM) of three independent experiments.

mouse RNA (Figure 4A). Four membranes were prepared with mouse liver RNA (positive control) and RNA from blood infected with the WT or the tRip-KO parasites. These samples were tested with probes designed to specifically discriminate mouse from parasite for the $tRNA^{Glu}_{TTC}$, $tRNA^{His}_{GTG}$, $tRNA^{Met}_{i}$, and $tRNA^{Met}_{e}$ isoacceptors (Figure S5B). Probes directed specifically against *P. berghei* tRNAs indicate that both parasite forms (WT and tRip-KO) contain equivalent amounts of endogenous tRNAs, as expected. In contrast, the probes designed specifically against mouse tRNAs (Figure S5A) demonstrate the presence of mouse tRNAs in liver (positive control) and in the WT parasite, indicating that the wild-type parasite imports host tRNAs. Despite the loading controls (5S rRNA) showing that the RNA deposits are comparable, mouse tRNAs were not detected in the tRip-KO parasite (Figure 5A), indicating that, tRip is essential for tRNA import

Finally, cross-aminoacylation reactions were tested using the aspartyl-, tyrosyl-, and asparaginyl-tRNA synthetases from *H. sapiens* and *P. falciparum in vitro* to determine their ability to aminoacylate human $tRNA^{Asp}$, $tRNA^{Tyr}$, and $tRNA^{Asn}$, respectively using crude human crude tRNA (Figure 4B). All three *Plasmodium* aaRSs can aminoacylate nearly the same level of tRNA as their human counterparts, although asparaginylation by the parasite enzyme is effective on about 80% of human $tRNA^{Asn}$ isodecoders. It indicates that host tRNAs, when imported into parasites by tRip can be aminoacylated by parasite aaRSs to be used in protein translation.

Discussion

To achieve efficient and specific protein synthesis, codon usage of mRNA must be balanced with the availability of corresponding aminoacylated tRNAs in the cell (i.e.(12–15). Any discrepancy can affect the rate of protein elongation in ribosomes and result in pauses in translation that lead to mRNA degradation (16). Here, by comparing the proteomes of wild-type and tRip-KO *P. berghei*, we observe in two independent experiments that down-regulated proteins in the tRip-KO parasite are asparagine-rich proteins. Asparagine is the most used amino acid in the *P. berghei* proteome and is often found in long homorepeats (17, 18). This asparagine abundance is also found in *P. falciparum*, *P. chabaudi*, *P. yoelii* and to a lesser extent in *P.knowlesi* and *P. vivax* (Figure S3A), however proteins in the latter two parasites do not contain long asparagine repeats.

Based on our results, we propose that the absence of tRNA import in the tRip-KO parasite would prevent the accumulation of host $tRNA^{Asn}$ in the parasite and would thus explain why asparagine-rich

proteins are poorly translated. This hypothesis is strongly supported by several observations: (i) asparaginyl- and lysyl-tRNA synthetases (NRS: *p-value* = 0.063 and KRS) are overexpressed in the proteomes of tRip-KO schizonts (Figure 2A, Table S1). Both aaRSs aminoacylate tRNAs that are most used to synthesize *P. berghei* proteins. In general, increased expression of aminoacyl-tRNA synthetase is the result of a decrease in cognate aminoacyl-tRNA (19, 20). This observation suggests, that $tRNA^{Asn}$ and $tRNA^{Lys}$ levels are not high enough for efficient translation in tRip-KO schizonts. The distribution of lysines in parasite proteins is more homogeneous than that of asparagines such that the depletion of $tRNA^{Lys}$ should not affect translation as much as that of $tRNA^{Asn}$. (ii) Furthermore, mammalian (human) $tRNA^{Asn}$ is among the tRNAs with the highest affinity for *P. falciparum* tRip, along with $tRNA^{Ser}_{AGA}$ and $tRNA^{Leu}_{hGA}$ ((2), Figure 1); It is reasonable to assume that the tRNAs with the highest affinity for tRip are also those that are most efficiently imported into the parasite. (iii) Finally, compensation for low $tRNA^{Asn}$ by tRip-mediated tRNA import is only possible if the host $tRNA^{Asn}$ is a substrate for the parasite AsnRS. This is indeed the case (Figure 4B) indicating that once in the parasite, at least some host tRNA isoacceptors can be efficiently aminoacylated and used in parasite mRNA translation. Thus, some proteins down-regulated in the tRip-KO parasite would be the consequence of low $tRNA^{Asn}$ concentration that impedes their synthesis; in wild-type parasite, the selective import of $tRNA^{Asn}$ would increase its abundance in the WT parasite and play an essential role in the decoding of asparagine-rich proteins.

In the present study, despite several attempts, we were unable to design specific probes that could efficiently differentiate human from parasite $tRNA^{Asn}$ (Figure S5B). However, a non-specific Northern Blot probe hybridizing both endogenous parasite tRNAs and imported host tRNAs showed that, despite their excessive use in protein translation, *P. falciparum* $tRNA^{Asn}$ does not accumulate more than other tRNAs in the blood stages of the parasite (21). This observation is in line with our hypothesis that insertions, and especially asparagine-rich insertions, could regulate ribosome translation rates and influence protein co-translational folding (22, 23). Here, we propose that the import of host $tRNA^{Asn}$ enables the decoding of such asparagine-rich sequences. These two scenarios can coexist, if $tRNA^{Asn}$ import remains moderate. Both mechanisms of translational regulation depend on how much $tRNA^{Asn}$ is available to decode asparagine-rich sequences, as long as the $tRNA^{Asn}$ concentration remains limited to slow down ribosomal translation locally to facilitate protein folding.

Two asparagine-rich proteins stand out and are conserved in the six *Plasmodium* species analyzed (Table S5): the CCr4-associated factor 1 (CAF-1), involved in the poly-(A) decay of mRNAs

(24), and to the poly-(A) binding protein-3 (PABP3), which has not yet been characterized in *Plasmodium*. Not only are both proteins involved in poly-(A) recognition, but they also adopt a common global structure with highly conserved N-terminal domain sequences and a C-terminal domain found only in *Plasmodia* with very high asparagine content. The conserved N-terminal domain of CAF-1 is essential for the decay of mRNAs enriched in non-optimally decoded codons; it belongs to the eukaryotic CCr4-Not complex, which binds to the empty E-site of the ribosome and properly positions CAF-1 to initiate the decay of the 3′-poly(A)-tails of stalled mRNAs (25). Interestingly, the deletion of the C-terminal sequence of *Plasmodium* CAF-1 is not essential and leads to the premature release of non-infectious merozoites *in vitro* (10) and the inappropriate development of gametocytes involved in transmission from host to vector *in vivo* (26). Here, in the absence of tRip-mediated tRNA import, the asparagine-rich C-terminal domain of CAF-1 (and of PABP-3) would remain untranslated, leading to parasites with low invasion capacities. Indeed, disruption of tRip and of the C-terminal domain of CAF-1 not only lead to the same phenotype: parasites have reduced infectivity and multiplication in the blood stage (1, 10), but also results in overexpression of the same gene products involved in invasion (Table S3, Figure 3).

In conclusion, the complex life cycle of *Plasmodium* is highly regulated and involves tight transcriptional and especially post-transcriptional controls (27, 28). In this study, host tRNAs imported by tRip would ensure correct translation of asparagine-rich protein domains, including the C-terminal domains of CAF-1. This domain tightly controls the expression of mRNAs encoding proteins responsible for the release of mature merozoites and thus ensures efficient infection and parasite development in the blood (Figure 3). The amount of tRNA in RBC is small and yet sufficient to be imported inside the wild-type parasite (Figure 4A). It is interesting to note that blood also contains reticulocytes, which are precursors of RBCs very active in translation and therefore rich in tRNAs (Smith and McNamara, 1972). Despite the rarity of these reticulocytes in blood (about 2% of blood cells), *P. berghei* (29), *P.chabaudi* (30), *P. yoelii* (31) and *P. vivax* (32) preferentially invade these cells compared to mature RBCs. In addition, variations in tRNA isodecoder expression and post-transcriptional modifications between tissues (33, 34), represent diverse sources of exogenous tRNAs that may differentially control parasite translation profiles and enable efficient stage transitions not only in the vertebrate blood or liver but also in mosquitoes. In such model, variations in tRNA, and especially $tRNA^{Asn}$, supply could play a major role in parasite development by modulating the translational efficiency of certain mRNAs, further supporting the of “just-in-time” translation model (27).

Material and Methods

Parasite production: Four- to six-week-old female mice (C57BL/6), weighing approximately 20 g, were injected intraperitoneally with 200 µL of frozen infected red blood cells (10-15% parasitemia diluted in phosphate-buffered saline (PBS)) either with wild-type (WT, *Pb* gfpGOMO14) or with tRip-KO (*Pb* tRip-KO mCherry) malaria parasites derived from the *P. berghei* (ANKA strain). Parasitemia was monitored daily by cytometry (BD Accuri C6). Mice with parasitemia between 5 and 10% were selected for testing. Therefore, in this study, only mice without or low symptoms were used. These parasitemia levels were reached 3-6 days after parasite injection. Mice were put to sleep and blood was collected by intracardiac puncture (about 1 to 1.5 mL) and parasites were directly purified (all blood stages) or cultured for 24 hours in RPMI at 37°C under 5% CO2 (only schizonts).

infected blood was filtered through a Plasmodipur filter (Europroxima) to remove mouse leukocytes, centrifuged for 10 min at 450 g and recovered in 4 mL of RPMI. A 7.2 mL cushion of 60% isotonic Percoll was gently pipetted under the red blood cells and the tube was centrifuged for 20 min at 1450 g (swinging buckets), to separate infected red blood cells (iRBC) at the Percoll/RPMI interface from non-infected RBC at the bottom of the tube. Parasitized RBCs were recovered in 2 tubes, washed 3 times in 1 mL of PBS and combined with 200 µL each of PBS. Infected RBCs were then lysed with 0.02% saponin for 5 min in ice (in 400 µL). Free parasites were recovered by centrifugation for 5 min at 2000 g and washed in 500 µL of PBS. The two pellets were resuspended either in 50 µL of protein loading buffer and stored at -80°C until mass spectrometry analysis, or as is and placed at -80°C for RNA preparation. All experiments were performed in accordance with relevant guidelines and regulations under the project license for animal experimentation #11124-2018010312571506.

Mass spectrometry (MS) and data analyses. Approximately 10 µg of protein was obtained from the half of the blood (~0.75 mL of a 5-10% infected mouse). Protein concentrations were determined by Bradford assay using bovine serum albumin as the standard. Proteins were precipitated, reduced, and alkylated as described in (3). After digestion overnight with sequencing grade porcine trypsin (300 ng, w/w, Promega, Fitchburg, MA, USA), the generated peptides were analyzed either using Easy-nanoLC-1000 system coupled to a Q-Exactive Plus mass spectrometer (Thermo Fisher Scientific, Germany) with 160-minutes gradients (blood stages) or a NanoLC-2DPlus system (nanoFlexChiP module; Eksigent, ABSciex, Concord, Ontario, Canada) coupled to a TripleTOF 5600 mass spectrometer (ABSciex) operating in positive mode with 120-minutes gradients (schizonts). Data were searched using the

Mascot algorithm (version 2.6.2, Matrix Science) against the Uniprot database with *P.Berghei* taxonomy (release 2021_03, 4 927 sequences) with a decoy strategy. The resulting .dat Mascot files were then imported into Proline version 2.0 software (35) to align the identified proteins. Proteins were then validated with Mascot pretty rank equal to 1, and 1% false discovery rate (FDR) on both peptide spectrum matches (PSM) and protein sets (based on Mascot score).

For statistical analyses, raw Spectral Count values were imported into R (v. 3.5.0) where the number of spectra were first normalized using the DESeq2 median of ratio normalization method. A negative-binomial test using an edgeR GLM regression generated for each identified protein a p-value and a protein fold-change (FC). The R script used to process the dataset is published on Github (36). Proteins were statistically enriched or decreased with a p-value < 0.05 and a minimum fold change (FC) of 2 or 0.5, respectively. Mass spectrometry proteomic data will be deposited within the ProteomeXchange Consortium via the PRIDE partner repository (37) with the dataset ID PXD043916.

Northern blots. Infected red blood cell (iRBC) pellets were incubated in 2 mL of cold lysis buffer (10 mM $KHCO_3$, 150 mM NH_4Cl and 0.1 mM EDTA) for 15 min on ice. Cellular debris was removed by centrifugation for 5 min at 100 g and parasites were recovered by centrifugation of the supernatant for 5 min at 6000 g. Parasites were then washed three times in 2 mL of PBS. Northern blots were performed, using ^{32}P-labeled DNA probes designed to detect *Mus musculus* (*Mm*) tRNAs in RBCs or differentiate *P. berghei* (*Pb*) from *Mm* tRNAs in iRBCs (Figure S5). One µg or 5 µg of total RNA (from *Mm* Liver, RBCs or iRBCs) were separated on a 12% acrylamide/bisacrylamide (19 :1), 8 M urea, 1 x TBE denaturing gel. RNAs were transferred to a positively charged nylon membrane (BrightStarTM Plus, Ambion) at 200 mA for 30 min and crosslinked for 2 min at 120 mJ (Stratagen). Membranes were pre-incubated for 2 h at 60ºC and hybridized overnight at 60ºC in hybridization buffer (UltraSensitive Buffer, Ambion) with 3.10^6 cpm of radioactive probe. Membranes were rinsed and washed twice for 20 min at 60ºC with 5 mL of 2X SSC (300 mM sodium chloride and 34 mM sodium citrate, 0.1% SDS). This protocol was conducted twice in a row first with the tRNA probes and second with the common 5S rRNA probe before being exposed to a high-resolution film (Carestream).

Aknowledgments

We are grateful to Philippe Hammann, Lauriane Kuhn, and Béatrice Chane Woon Ming for LC-MS/MS analysis, Fabrice Auge and Eric Marois for animal experiments, and to Dr Alain Lescure and

Prof Tamara Hendrickson for providing comments on this manuscript. This work was performed under the framework of the Interdisciplinary Thematic Institute IMCBio, as part of the ITI 2021-2028 program of the University of Strasbourg, CNRS and Inserm. It was supported by IdEx Unistra (ANR-10-IDEX-0002), by SFRI-STRAT'US project (ANR 20-SFRI-0012), and EUR IMCBio (IMCBio ANR-17-EURE-0023) under the framework of the French Investments for the Future Program, by previous Labex NetRNA (ANR-10-LABX-0036), by the CNRS and the Université de Strasbourg, IdEx "Equipement mi-lourd" (2015) and Equipement d'Excellence (EquipEx) I2MC (ANR-11-EQPX-0022), and by the Fondation pour la Recherche Médicale (FRM) (grant number FDT201704337050) to Marta Cela.

References

1. T. Bour, *et al.*, *Apicomplexa*-specific tRip facilitates import of exogenous tRNAs into malaria parasites. *Proc Natl Acad Sci USA* **113**, 4717–4722 (2016).

2. M. Cela, *et al.*, Identification of host tRNAs preferentially recognized by the *Plasmodium* surface protein tRip. *Nucleic Acids Research*, gkab769 (2021).

3. J. R. Jaramillo Ponce, D. Kapps, C. Paulus, J. Chicher, M. Frugier, Discovery of two distinct aminoacyl-tRNA synthetase complexes anchored to the Plasmodium surface tRNA import protein. *Journal of Biological Chemistry* **298**, 101987 (2022).

4. J. R. Jaramillo Ponce, *et al.*, Solution X-ray scattering highlights discrepancies in *Plasmodium* multi-aminoacyl-tRNA synthetase complexes. *Protein Science* **32** (2023).

5. S. Gupta, *et al.*, Crystal structures of the two domains that constitute the *Plasmodium vivax* p43 protein. *Acta Crystallogr D Struct Biol* **76**, 135–146 (2020).

6. K. Deinert, F. Fasiolo, E. C. Hurt, G. Simos, Arc1p organizes the yeast aminoacyl-tRNA aynthetase complex and stabilizes its interaction with the cognate tRNAs. *Journal of Biological Chemistry* **276**, 6000–6008 (2001).

7. A. M. Minns, K. J. Hart, S. Subramanian, S. Hafenstein, S. E. Lindner, Nuclear, cytosolic, and surface-localized Poly(A)-binding proteins of *Plasmodium yoelii*. *mSphere* **3** (2018).

8. S.-J. Cha, M.-S. Kim, A. Pandey, M. Jacobs-Lorena, Identification of GAPDH on the surface of *Plasmodium* sporozoites as a new candidate for targeting malaria liver invasion. *Journal of Experimental Medicine* **213**, 2099–2112 (2016).

9. C. Aurrecoechea, *et al.*, ApiDB: integrated resources for the apicomplexan bioinformatics resource center. *Nucleic Acids Research* **35**, D427–D430 (2007).

10. B. Balu, *et al.*, CCR4-Associated Factor 1 Coordinates the Expression of *Plasmodium falciparum* egress and invasion proteins. *Eukaryot Cell* **10**, 1257–1263 (2011).

11. S. D. Kumar, *et al.*, Evidence for low-level translation in human erythrocytes. *MBoC* **33**, br21 (2022).

12. E. M. Novoa, L. Ribas de Pouplana, Speeding with control: codon usage, tRNAs, and ribosomes. *Trends in Genetics* **28**, 574–581 (2012).

13. J. D. Richter, J. Coller, Pausing on polyribosomes: Make way for elongation in translational control. *Cell* **163**, 292–300 (2015).

14. M. Torrent, G. Chalancon, N. S. de Groot, A. Wuster, M. Madan Babu, Cells alter their tRNA abundance to selectively regulate protein synthesis during stress conditions. *Sci. Signal.* **11**, eaat6409 (2018).

15. P. C. Dedon, T. J. Begley, Dysfunctional tRNA reprogramming and codon-biased translation in cancer. *Trends in Molecular Medicine* **28**, 964–978 (2022).

16. Q. Wu, *et al.*, Translation affects mRNA stability in a codon-dependent manner in human cells. *eLife* **8**, e45396 (2019).

17. S. R. Chaudhry, N. Lwin, D. Phelan, A. A. Escalante, F. U. Battistuzzi, Comparative analysis of low complexity regions in *Plasmodia*. *Sci Rep* **8**, 335 (2018).

18. F. U. Battistuzzi, *et al.*, Profiles of low complexity regions in *Apicomplexa*. *BMC Evol Biol* **16**, 47 (2016).

19. Harald Putzer, Laalami Soumaya, "Regulation of the expression of aminoacyl-tRNA synthetases and translation factors" in *Madame Curie Bioscience Database*, (Landes Bioscience, 2000).

20. O. Levi, S. Garin, Y. Arava, RNA mimicry in post-transcriptional regulation by aminoacyl tRNA synthetases. *WIREs RNA* **11** (2020).

21. D. Filisetti, *et al.*, Aminoacylation of *Plasmodium falciparum* $tRNA^{Asn}$ and Insights in the synthesis of asparagine repeats. *Journal of Biological Chemistry* **288**, 36361–36371 (2013).

22. M. Frugier, *et al.*, Low Complexity Regions behave as tRNA sponges to help co-translational folding of plasmodial proteins. *FEBS Lett* **584**, 448–54 (2010).

23. Y. Wang, H. J. Yang, P. M. Harrison, The relationship between protein domains and homopeptides in the *Plasmodium falciparum* proteome. *PeerJ* **8**, e9940 (2020).

24. M. A. Collart, The Ccr4-Not complex is a key regulator of eukaryotic gene expression. *WIREs RNA* **7**, 438–454 (2016).

25. R. Buschauer, *et al.*, The Ccr4-Not complex monitors the translating ribosome for codon optimality. *Science* **368**, eaay6912 (2020).

26. K. J. Hart, *et al.*, *Plasmodium* male gametocyte development and transmission are critically regulated by the two putative deadenylases of the CAF1/CCR4/NOT complex. *PLoS Pathog* **15**, e1007164 (2019).

27. S. S. Vembar, D. Droll, A. Scherf, Translational regulation in blood stages of the malaria parasite *Plasmodium spp.* : systems-wide studies pave the way: Translational regulation in blood stages of the malaria parasite. *WIREs RNA* **7**, 772–792 (2016).

28. S. Bennink, G. Pradel, The molecular machinery of translational control in malaria parasites. *Mol Microbiol* **112**, 1658–1673 (2019).

29. D. Cromer, K. J. Evans, L. Schofield, M. P. Davenport, Preferential invasion of reticulocytes during late-stage *Plasmodium berghei* infection accounts for reduced circulating reticulocyte levels. *International Journal for Parasitology* **36**, 1389–1397 (2006).

30. R. Antia, A. Yates, J. C. De Roode, The dynamics of acute malaria infections. I. Effect of the parasite's red blood cell preference. *Proc. R. Soc. B.* **275**, 1449–1458 (2008).

31. B. Mons, Preferential invasion of malarial merozoites into young red blood cells. *Blood Cells* **16**, 299–312 (1990).

32. N. Thawani, *et al.*, Plasmodium Products Contribute to Severe Malarial Anemia by Inhibiting Erythropoietin-Induced Proliferation of Erythroid Precursors. *The Journal of Infectious Diseases* **209**, 140–149 (2014).

33. K. A. Dittmar, J. M. Goodenbour, T. Pan, Tissue-specific differences in Human transfer RNA expression. *PLoS Genet* **2**, e221 (2006).

34. O. Pinkard, S. McFarland, T. Sweet, J. Coller, Quantitative tRNA-sequencing uncovers metazoan tissue-specific tRNA regulation. *Nat Commun* **11**, 4104 (2020).

35. D. Bouyssié, *et al.*, Proline: an efficient and user-friendly software suite for large-scale proteomics. *Bioinformatics* **36**, 3148–3155 (2020).

36. L. Kuhn, T. Vincent, P. Hammann, H. Zuber, “Exploring Protein Interactome Data with IPinquiry: Statistical Analysis and Data Visualization by Spectral Counts” in *Statistical Analysis of Proteomic Data*, Methods in Molecular Biology., T. Burger, Ed. (Springer US, 2023), pp. 243–265.

37. Y. Perez-Riverol, *et al.*, The PRIDE database resources in 2022: a hub for mass spectrometry-based proteomics evidences. *Nucleic Acids Research* **50**, D543–D552 (2022).

Supporting Information

SI Materials and Methods

Bioinformatics. Protein sequences as well as proteomes from all *Plasmodium* strains were retrieved from PlasmoDB. A home-made Python 2.7 script was used to calculate the asparagine content for each protein sequence. *Toxoplasma gondii* was the outgroup species.

RNA purification and QRT-PCR. Total RNA was extracted from parasites using the RNeasy Mini Kit (Qiagen) according to the manufacturer's protocol and was subjected to DNAse treatment with the Rapid OUT DNA removal kit (Thermo Scientific). Total RNA was analyzed and quantified on Bioanalyser (puce PICO). Each sample was reverse transcribed in a 20 µL reaction volume containing 10 µL (0.16 to 0.5 µg) of RNA, using the SuperScript II reverse transcriptase (Invitrogen) according to the manufacturer's protocol. The mRNAs levels were measured by RT-PCR (25 µL containing 4 µL of cDNA) on a CFx94 (Bio-Rad) using the Syber Green kit (Thermo Scientific). Oligonucleotides used for qRT-PCR are listed in Table S4. qRT-PCR reactions were designed according MIQE guidelines (Bustin et al. 2009), the specificity of the oligonucleotides was validated, and the amplification efficiencies of the primer sets are all between 90 and 110% and r^2 values greater than 0.96. The mRNAs levels were calculated according to the ΔCq method and normalized by the mRNA level of both the EF1-α and Hsp70 in each sample. Raw data are indicated as mean of three measurements, and results were expressed as the average of 3 biological samples ± standard error of the mean (SEM).

Purification of aminoacyl-tRNA synthetases and aminoacylation assays. Recombinant *P. falciparum* and *H. sapiens* NRS and DRS were cloned, expressed and purified as described in references (Filisetti et al. 2013; T. Bour et al. 2009) respectively. The gene encoding the *P. falciparum* TyrRS was amplified by PCR from *P. falciparum* cDNA and cloned into pQE30 (Qiagen) and the plasmid encoding the *H. sapiens* YRS was a gift from P. Schimmel. Both *P. falciparum* and *H. sapiens* YRS were expressed and purified as described for NRS (Filisetti et al. 2013). Purified enzymes are shown in Fig S4C. *H. sapiens* crude tRNAs was prepared as described in (Cela et al. 2021).

Aminoacylation assays were performed under the same conditions: at 37 °C for 2, 4 and 6 min in 50 mM HEPES-KOH (pH 7.5), 20 mM KCl, 10 mM $MgCl_2$, 2 mM ATP, 6 µM total tRNA from HeLa cells, in the presence of 20 µM of the corresponding L-[^{14}C]-amino acid (Perkin Elmer). AaRSs were diluted in 100 mM HEPES-KOH pH 7.5, 1 mM DTT, 5 mg/mL BSA, and 10% glycerol and used at a final concentration of 200 nM in the aminoacylation assay. The aminoacylation plateaus are the mean of 3 independent experiments ± standard deviation (SD).

SI Figures

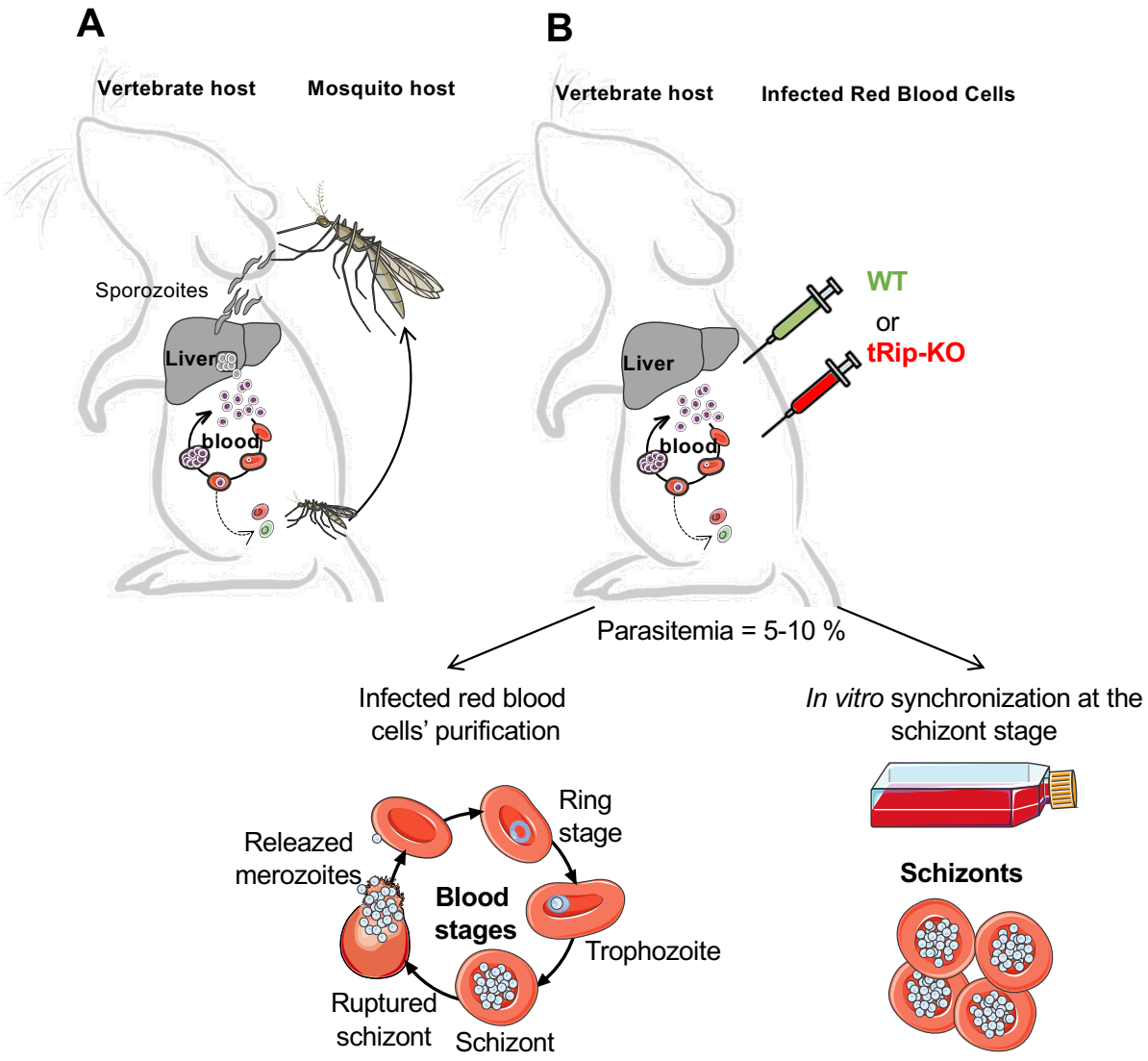

Figure S1: Mice infections and sample preparation. (**A**) *Plasmodium* life cycle. The cycle of vertebrate infection starts when a mosquito injects sporozoites into the host. Sporozoites invade hepatocytes (liver stage), multiply, and produce tens of thousands of merozoites per infected hepatocyte (Rankin et al. 2010). Merozoites exit the liver and develop in red blood cells (blood stages) to produce 10 to 30 new merozoites per intra-erythrocytic cycle (Cowman and Crabb 2006). Some of the erythrocytic merozoites differentiate into gametocytes (sexual forms, dashed lines) (Talman et al. 2004). Fertilization takes place in mosquitoes where gametocytes are ingested during a blood meal. In 8-15 days, sporozoites invade the mosquito salivary glands, completing the cycle. (**B**) Alternatively, mice are infected with frozen stocks of red blood cells infected with wild-type (GFP) or tRip-KO (mCherry) *P. berghei* parasites. Three to six days later (5-10% parasitemia), infected blood is collected and used as is for analysis (all blood stages) or synchronized *in vitro* to the schizont stage. "All blood stages" samples contain rings, trophozoites and merozoites.

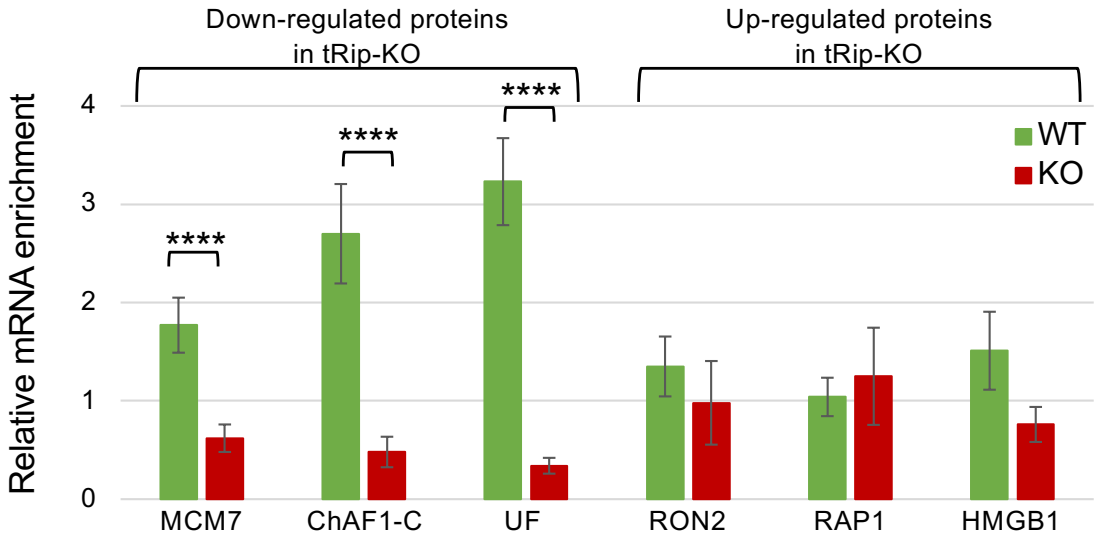

Figure S2. qRT-PCR analysis of the mRNAs coding for deregulated proteins in the tRip-KO parasite. The relative enrichment of mRNA was measured by qRT-PCR and determined by the $\Delta\Delta Ct$ method using both EF1-α (PBANKA_1133300) and Hsp70 (PBANKA_0914400) as normalizers. mRNAs are coding either for (i) down-regulated proteins: the DNA replication licensing factor MCM7 (MCM7, FC = 5.7, *p-value* =1.3 x 10^{-6}), chromatin assembly factor 1-subunit C (ChAF1-C, FC = 2.2, *p-value* = 5.7 x 10^{-6}) and a protein with unknown function (UF, FC = 3.6, *p-value* = 2.9 x 10^{-4}) or (ii) up-regulated protein: rhoptry neck protein 2 (RON2, FC = 57.6, *p-value* = 1.2 x 10^{-5}), rhoptry-associated protein 1 (RAP1, FC = 3.2, *p-value* = 2 x 10^{-5}) and high mobility group protein B1 (HMGB1, FC = 2.1, *p-value* = 1.7 x 10^{-4}). Error bars represent the standard errors of the means (SEM) of three independent experiments performed on "All blood stages" samples, each corresponding to triplicate qRT-PCR measurements (Table S4). Asterisks indicate statistically significant differences with the WT control mRNA: **** *p-value* < 0.0001 based on Student's *t* test.

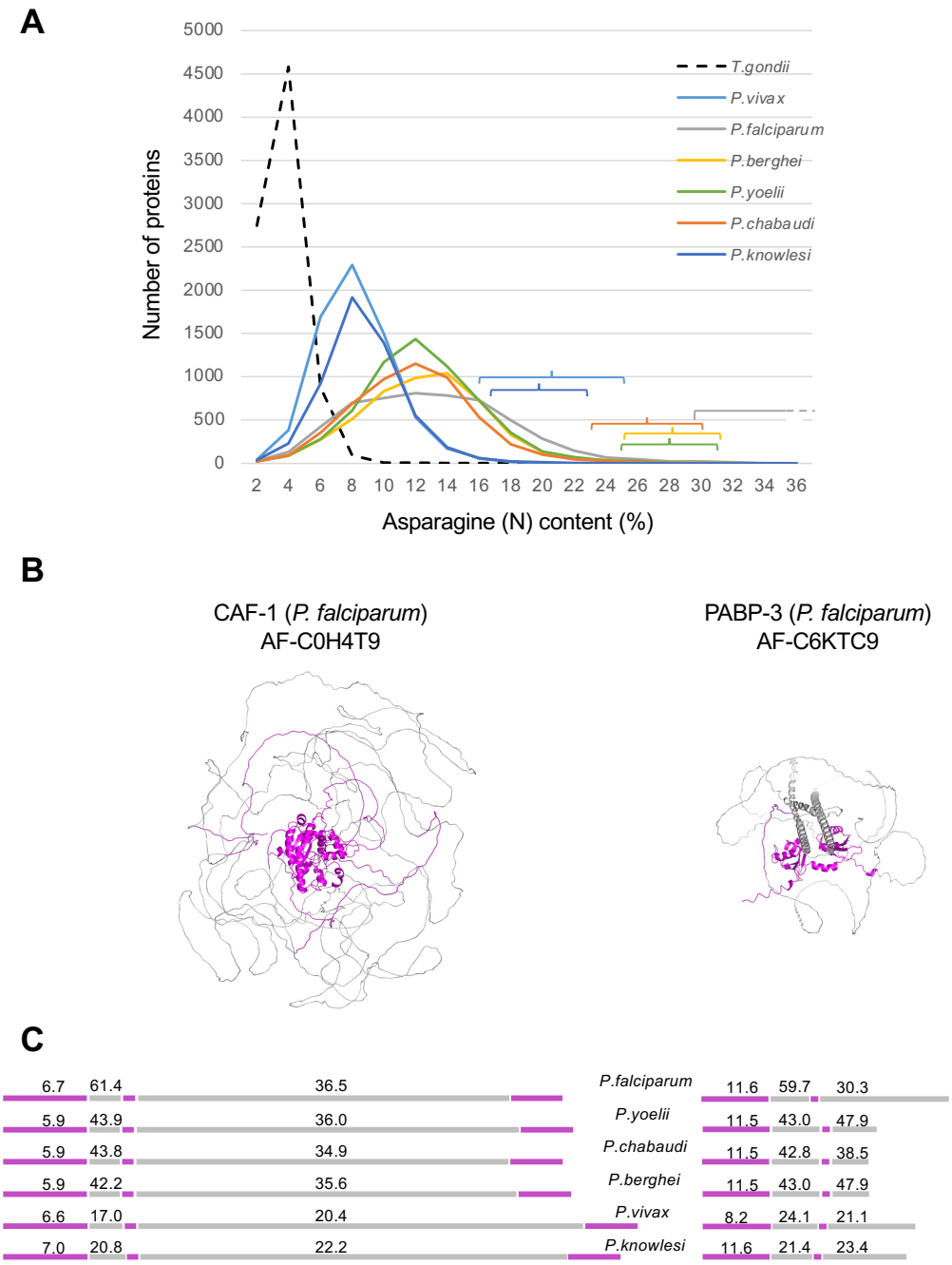

Figure S3: Asparagine frequency in *Plasmodium* proteins. (**A**) Proteomes of *P. falciparum, P. yoelii, P. berghei, P. chabaudi*, *P. knowlesi* and *P. vivax* were compared and the proteome of *Toxoplasma gondii* was used as a negative control (Aurrecoechea et al. 2007). For each species, the number of proteins is indicated for a given asparagine content. Brackets show the top 0.5 % proteins containing the highest percentage of asparagine residues. (**B**) AlphaFold models of *P. falciparum* CAF-1 and PABP-3 (Aurrecoechea et al. 2007). Both models show conserved domains (pink) and an unfolded asparagine-rich *Plasmodium* specific C-terminal extensions (grey). (**C**) Domain alignments of CAF-1 and PABP-3. The corresponding domains are shown with the same color code and the corresponding percentage of asparagine.

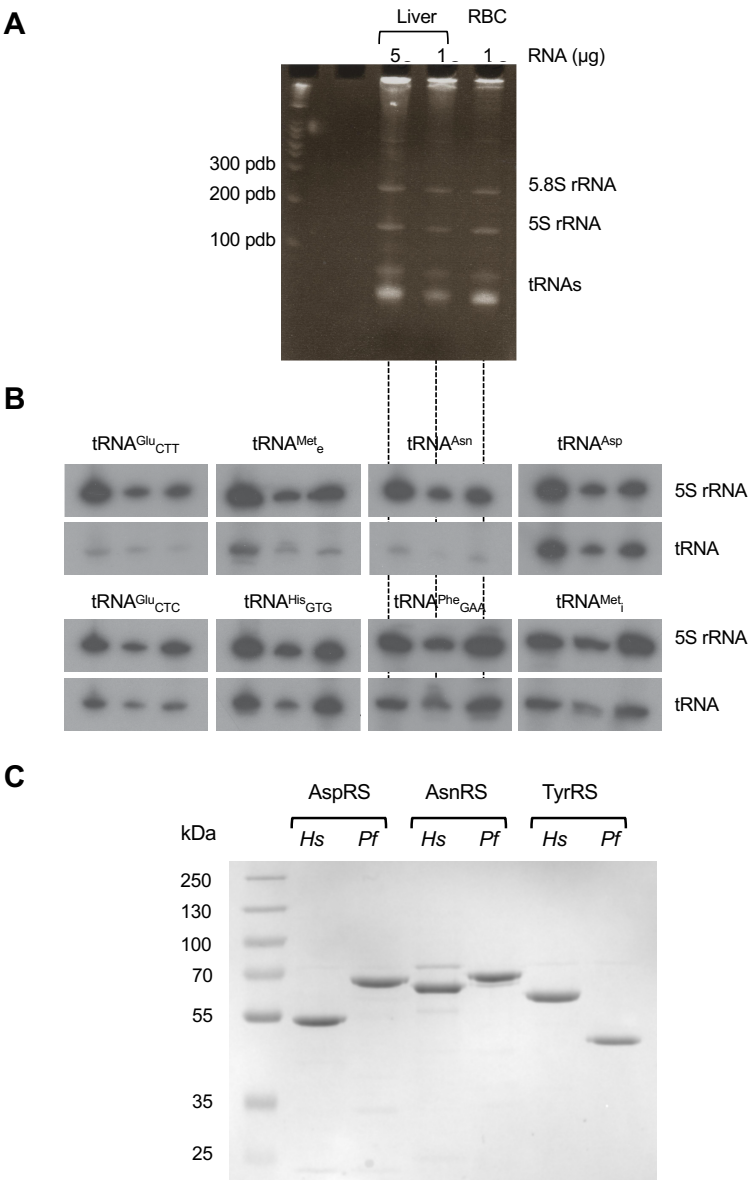

Figure S4. Specific detection of mouse tRNAs in blood (**A**) BET-stained 12% denaturing analytical gel. Five and 1 µg of liver RNA and 1 µg of RBC RNA are compared. Adult naïve mice were sacrificed, white blood cells were removed (plasmodipur filter) from the blood. Only 8 µg of total RNA was retrieved from 2.5 mL of blood, a low yield compared to 1250 µg of total RNA obtained from about 400 mg of liver. However, both total RNAs have the same profile. (**B**) Northern blot with probes designed to specifically detect mouse tRNAs (*Mm*-$^{Glu}_{TTC}$, *Mm*-$^{Glu}_{CTC}$, *Mm*-^{Asn}, *Mm*-^{Asp}, *Mm*-$^{His}_{GTG}$, *Mm*-^{Phe}, *Mm*-$^{Met}_{i}$ and *Mm*-$^{Met}_{e}$) and 5S ribosomal RNA (5S rRNA) (Figure S2). Based on the intensity of the bands corresponding to either 5S rRNA or tRNAs, it can be concluded that RBC RNA contains overall the same proportion of tRNA as liver cell. Unfortunately, the probes against *Mm*-tRNA^{Asn} (2 different probes were tested, Figure S2) and *Mm*-tRNA$^{Glu}_{CTT}$ do not detect efficiently the corresponding tRNAs. Furthermore, the variations in tRNA detection between liver and RBC are consistent with the different tRNA expression profiles already observed in different tissues. (**C**) Gel analysis of aminoacyl-tRNA synthetases. Oneµg of each enzyme aspartyl- (DRS), asparaginyl- (NRS) and tyrosyl-(YRS) tRNA synthetases from *H. sapiens* (*Hs*) or *P. falciparum* (*Pf*) was run on a 10 % SDS PAGE.

A Probes only for mouse tRNAs

tRNA^{Asp}: 5′-GCGGGGATACTCACCACTATACTAACGAGGA-3′

```
>berghei ARNtAspGTC                 TCCGAGATAGTATAGTGGCAAGTATTTCCGCCTGTCACGCGGAAGACCCGGGTTCAATTCCCGGTCTCGGAG
Mus_musculus_chr2.trna211-AspGTC    TCCTCGTTAGTATAGTGGTGAGTATCCCTGCCTGTCACGCAGGACACCAGGGTTCGATTTCCTGACGGGGAG
Mus_musculus_chr5.trna719-AspGTC    TCCTCGTTAGTATAGTGGTGAGTATCCCCGCCTGTCACACAGGAGACCGGGGTTCGATTCCCCGATGGGGAG
Mus_musculus_chr1.trna450-AspGTC    TCCTCGTTAGTATAGTGGTGAGTATCCCCGCCTGTCACGCGGGAGACCGGGGTTCGATTCCCCGACGGGGAG
Mus_musculus_chr13.trna48-AspGTC    TCCTCGTTAGTATAGTGGTGAGTATCCCCGCCTGTCACGCGGGAGACCGGGGTTCGATTCCCCGACGGGGAG
Mus_musculus_chr1.trna443-AspGTC    TCCTCGTTAGTATAGTGGTGAGTATCCCCGCCTGTCACGCGGGAGACCGGGGTTCGATTCCCCGACGGGGAG
Mus_musculus_chr1.trna440-AspGTC    TCCTCGTTAGTATAGTGGTGAGTATCCCCGCCTGTCACGCGGGAGACCGGGGTTCGATTCCCCGACGGGGAG
Mus_musculus_chr1.trna297-AspGTC    TCCTCGTTAGTATAGTGGTGAGTATCCCCGCCTGTCACGCGGGAGACCGGGGTTCGATTCCCCGACGGGGAG
Mus_musculus_chr5.trna588-AspGTC    TCCTCGTTAGTATAGTGGTGAGTATCCCCGCCTGTCACGCGGGAGACCGGGGTTCGATTCCCCGACGGGGAG
Mus_musculus_chr10.trna379-AspTC    TCCTCGTTAGTATAGTGGTGAGTATCCCCGCCTGTCACGCGGGAGACCGGGGTTCGATTCCCCGACGGGGAG
Mus_musculus_chr11.trna29-AspGTC    TCCTCGTTAGTATAGTGGTGAGTATCCCCGCCTGTCACGCGGGAGACCGGGGTTCGATTCCCCGACGGGGAG
Mus_musculus_chr5.trna586-AspGTC    TCCTCGTTAGTATAGTGGTGAGTATCCCCGCCTGTCACGCGGGAGACCGGGGTTCGATTCCCCGACGGGGAG
Mus_musculus_chr1.trna446-AspGTC    TCCTCGTTAGTATAGTGGTGAGTATCCCCGCCTGTCACGCGGGAGACCGGGGTTCGATTCCCCGACGGGGAG
Mus_musculus_chr13.trna472-AspGTC   TCCTCGTTAGTATAGTGGTGAGTATCCCCGCCTGTCACGCGGGAGACCGGGGTTCGATTCCCCGACGGGGAG
Mus_musculus_chr13.trna474-AspGTC   TCCTCGTTAGTATAGTGGTGAGTATCCCCGCCTGTCACGCGGGAGACCGGGGTTCGATTCCCCGACGGGGAG
Mus_musculus_chr11.trna189-AspGTC   TCCTCGTTAGTATAGTGGTGAGTATCCCCGCCTGTCACGCGGGAGACCGGGGTTCGATTCCCCGACGGGGAG
Mus_musculus_chr10.trna383-AspGTC   TCCTCGTTAGTATAGTGGTTAGTATCCCCGCCTGTCACGCGGGAGACCGGGGTTCAATTCCCCGACGGGGAG
```

tRNA^{Asn} #1: 5′-CAACCTTTCGGTTAACAGCCGAACGCGC-3′

tRNA^{Asn} #2: 5′-CGCGCTAACCGATTGCGCCACAGAGAC-3′

```
>PbergheiAsnGTT                     GGTTCCGTAGCTCAGTTGGTTAGAGCGTGCGGCTGTTAACCGCAAGGTCGTTGGTTCGATCCCAGCCGGTACCG
Mus_musculus_chr3.trna350-AsnGTT    GTCTCTGTGGCGCAATCGGTTAGCGCGTTCGGCTGTTAACCGAAAGGTTGGTGGTTCGAGCCCACCCAGGGACG
Mus_musculus_chr3.trna128-AsnGTT    GTCTCTGTGGCGCAATCGGTTAGCGCGTTCGGCTGTTAACCGAAAGGTTGGTGGTTCGAGCCCACCCAGGGACG
Mus_musculus_chr1.trna451-AsnGTT    GTCTCTGTGGCGCAATCGGTTAGCGCGTTCGGCTGTTAACCGAAAGGTTGGTGGTTCGAGCCCACCCAGGGACG
Mus_musculus_chr2.trna819-AsnGTT    GTCTCTGTGGCGCAATCGGTTAGCGCGTTCGGCTGTTAACCGAAAGGTTGGTGGTTCGAGCCCACCCAGGGACG
Mus_musculus_chr3.trna134-AsnGTT    GTCTCTGTGGCGCAATCGGTTAGCGCGTTCGGCTGTTAACCGAAAGGTTGGTGGTTCGAGCCCACCCAGGGACG
Mus_musculus_chr3.trna138-AsnGTT    GTCTCTGTGGCGCAATCGGTTAGCGCGTTCGGCTGTTAACCGAAAGGTTGGTGGTTCGAGCCCACCCAGGGACG
Mus_musculus_chr3.trna343-AsnGTT    GTCTCTGTGGCGCAATCGGTTAGCGCGTTCGGCTGTTAACCGAAAGGTTGGTGGTTCGAGCCCACCCAGGGACG
Mus_musculus_chr3.trna141-AsnGTT    GTCTCTGTGGCGCAATCGGTTAGCGCGTTCGGCTGTTAACCGAAAGGTTGGTGGTTCGAGCCCACCCAGGGACG
Mus_musculus_chr5.trna472-AsnGTT    GTCTCTGTGGCGCAATCGGTTAGCGCGTTCGGCTGTTAACCGAAAGGTTGGTGGTTCGAGCCCACCCAGGGACG
Mus_musculus_chr10.trna167-AsnGTT   GTCTCTGTGGCGCAATTGGTTAGCGCGTTCGGCTGTTAACCGAAAGGTTGGTGGTTCAAGCCCACCCAGGGACG
Mus_musculus_chr11.trna632-AsnGTT   GTCTCTGTGGCGCGATCGGTTAGTGCGTTTGGCTGTTAACCGAAAGGTTGGTGGTTCAAACCCACCCGGGGACG
Mus_musculus_chr15.trna437-AsnGTT   GTCTCCGTGGCGCAATCGGTCAGCGCGTTCGGCTGTTAACCGAAAGGTTGGTGGTTCGAGCCCACCCGGGGACG
```

tRNA$^{Phe}_{GAA}$: 5′-CAGTCTAACGCTCTCCCAACTGAGCTATTTC-3′

```
>berghei ARNtPheGAA                 GCCGTGATAGCTCAGTTGGGAGAGCGTCAGACTGAAGATCTGAAGGTCCCTGGTTCGATCCCTGGTCACGGCA
Mus_musculus_chr5.trna587-PheG      GCCGAAATAGCTCAGTTGGGAGAGCGTTAGACTGAAGATCTAAAGGTCCCTGGTTCGATCCCGGGTTTCGGCA
Mus_musculus_chr19.trna48-PheG      GCTGAAATAGCTCAGTTGGGAGAGCGTTAGACTGAAGATCTAAAGGTCCCTGGTTCGATCCCGGGTTTCAGCA
Mus_musculus_chr19.trna46-PheG      GCCGAAATAGCTCAGTTGGGAGAGCGTTAGACTGAAGATCTAAAGGTCCCTGGTTCGATCCCGGGTTTCGGCA
Mus_musculus_chr14.trna204-Phe      GCCGAAATAGCTCAGTTGGGAGAGCGTTAGACTGAAGATCTAAAGGTCCCTGGTTCGATCCCGGGTTTCGGCA
Mus_musculus_chr13.trna25-PheG      GCCGAAATAGCTCAGTTGGGAGAGCGTTAGACTGAAGATCTAAAGGTCCCTGGTTCGATCCCGGGTTTCGGCA
Mus_musculus_chr10.trna427-Phe      GCCGAAATAGCTCAGTTGGGAGAGCGTTAGACTGAAGATCTAAAGGTCCCTGGTTCGATCCCGGGTTTCGGCA
Mus_musculus_chr13.trna480-Phe      GCCGAAATAGCTCAGTTGGGAGAGCGTTAGACTGAAGATCTAAAGGTCCCTGGTTCAATCCCGGGTTTCGGCA
```

tRNA$^{Glu}_{CTC}$: 5′-CCGCGGCGGTGAGAGCGCCGAATCC-3′

```
>berghei ARNtGluCTC                 TCCCACGTGGTCTAGTGGCTAGGATATTCGGCTCTCACCCGAAAGGCCCGGGTTCAATTCCCGGCGTGGGAA
Mus_musculus_chr3.trna622-GluCTC    TCCCTGATGGTATAGTGGTTAGGACTCGGTGGTCTCACCAGCGCTGCCCGGGTTCAATTCCTGGTTAGGGAA
Mus_musculus_chr12.trna892-GluCTC   TCCCTGGTGGTCTAGTGGTTAGGAGTCATTGCTCTCACCACCGCGTCCCGGGTTCGATTCCCGGTCAGGGAA
Mus_musculus_chr7.trna969-GluCTC    TCCCTGGTGGTCTAGTGGTTAGGCTTTGGTGCTCTCACCTCCATGGCCCAGGTTTGATTCCTGGTCAGGGAA
Mus_musculus_chr17.trna719-GluCTC   TCCCTGGTGGTCTAGTGGTTAGGATTTGGCGCTCTCACCGCCGCGGCCTGGGTTCGATTCCCGGTCAGGGAA
Mus_musculus_chr10.trna90-GluCTC    TCCCTGGTGGTCTAGTGGTTAGGATTCGGCGCTCTCACCGCCGCGGCCCGGGTTCGATTCCCGGTCAGGGAA
Mus_musculus_chr1.trna1004-GluCTC   TCCCTGGTGGTCTAGTGGTTAGGATTCGGCGCTCTCACCGCCGCGGCCCGGGTTCGATTCCCGGTCAGGGAA
Mus_musculus_chr1.trna1007-GluCTC   TCCCTGGTGGTCTAGTGGTTAGGATTCGGCGCTCTCACCGCCGCGGCCCGGGTTCGATTCCCGGTCAGGGAA
Mus_musculus_chr1.trna1010-GluCTC   TCCCTGGTGGTCTAGTGGTTAGGATTCGGCGCTCTCACCGCCGCGGCCCGGGTTCGATTCCCGGTCAGGGAA
Mus_musculus_chr11.trna1912-GluCTC  TCCCTGGTGGTCTAGTGGTTAGGATTCGGCGCTCTCACCGCCGCGGCCCGGGTTCGATTCCCGGTCAGGGAA
Mus_musculus_chr13.trna1013-GluCTC  TCCCTGGTGGTCTAGTGGTTAGGATTCGGCGCTCTCACCGCCGCGGCCCGGGTTCGATTCCCGGTCAGGGAA
Mus_musculus_chr1.trna709-GluCTC    TCCCTGGTGGTCTAGTGGTTAGGATTCGGCGCTCTCACCGCCGCGGCCCGGGTTCGATTCCCGGTCAGGGAA
Mus_musculus_chr3.trna303-GluCTC    TCCCTGGTGGTCTAGTGGTTAGGATTCGGCGCTCTCACCGCCGCGGCCCGGGTTCGATTCCCGGTCAGGGAA
Mus_musculus_chr3.trna745-GluCTC    TCCCTGGTGGTCTAGTGGTTAGGATTCGGCGCTCTCACCGCCGCGGCCCGGGTTCGATTCCCGGTCAGGGAA
Mus_musculus_chr3.trna286-GluTTC    TCCCTGGTGGTCTAGTGGCTAGGATTCGGCGCTTTCACCGCCGCGGCCCGGGTTCGATTCCCGGTCAGGGAA
Mus_musculus_chr3.trna754-GluTTC    TCCCTGGTGGTCTAGTGGCTAGGATTCGGCGCTTTCACCGCCGCGGCCCGGGTTCGATTCCCGGTCAGGGAA
```

B

Probes to distinguish M. musculus from P. berghei tRNAs

5S rRNA *M.musculus/P.berghei* : 5′-gtgttcccgagcggtctcccacctc-3′

```
>berghei5SrRNA          TGACTCGTTCATACTACAGTGGCCACACCAGATCCCATCAGAACTCTGAAGTTAAGCACTGTAAGGC-
TTGGCTAGTACTGAGGTGGGAGACCGCTCGGGAACACTAAGTGATG-AGTCAT-
mus_musculus_5SrRNA     -
TCTACGGCCATACCACCCTGAACGCGCCCGATCTCGTGTGATGTCGGAAGCTAAGCAGGGTCGGGCCTTGGTTAGTACTTGGATGGGAGACCGCCTGGGAATACCGGGTGCT
GTAGGCTTT
```

tRNA$^{Glu}_{TTC}$ *M.musculus*: 5′-GCCGCCTGGGTGAAAACCAGGAA-3′

tRNA$^{Glu}_{TTC}$ *P.berghei*: 5′-GTCGTTCGGGTGAAAGCCGAATATCC-3′

```
>berghei ARNtGluTTC                 TCCCACGTAGTCTAGACGGTTAGGATATTCGGCTTTCACCCGAACGACCCGGGTTCGAGTCCCGGCGTGGGAA
Mus_musculus_chr1.trna1555-GluTTC   TCCCATATGGTCTAG-CGGTTAGGATTCCTGGTTTTCACCCAGGCGGCCCGGGTTCGACTCCCGGTATGGGAA
Mus_musculus_chr14.trna364-GluTTC   TCCCATATGGTCTAG-CGGTTAGGATTCCTGGTTTTCACCCAGGCGGCCCGGGTTCGACTCCCGGTATGGGAA
Mus_musculus_chr13.trna105-GluTTC   TCCCACATGGTCTAG-CGGTTAGGATTCCTGGTTTTCACCCAGGCGGCCCGGGTTCGACTCCCGGTGTGGGAA
Mus_musculus_chr14.trna352-GluTTC   TCCCACATGGTCTAG-CGGTTAGGATTCCTGGTTTTCACCCAGGCGGCCCGGGTTCGACTCCCGGTGTGGGAA
Mus_musculus_chr7.trna339-GluTTC    TCCCACATGGTCTAG-CGGTTAGGATTCCTGGTTTTCACCCAGGCGGCCCGGGTTCGACTCCCGGTGTGGGAA
Mus_musculus_chr9.trna961-GluTTC    TCCCACATGGTCTAG-CGGTTAGGATTCCTGGTTTTCACCCAGGCGGCCCGGGTTCGACTCCCGGTGTGGGAA
```

tRNA$^{His}_{GTG}$ *M.musculus*: 5′-ACGCAGAGTACTAACCACTATACGATCACGG-3′

tRNA$^{His}_{GTG}$ *P.berghei*: 5′-GTGTGGAGTCCTAACCACTAGACGATTTGGA-3′

```
>berghei ARNtHisGTG                 GTCCAAATCGTCTAGTGGTTAGGACTCCACACTGTGGATGTGGCAACGCAGGTTCGAATCCTGCTTTGGACA
Mus_musculus_chr3.trna293-HisGTG    GCCGTGATCGTATAGGGGTTAGTACTCTGCGTTGTGGCCGCAGCAACCTCGGTTCGAATCCGAGTCACGGCA
Mus_musculus_chr2.trna1431-HisGTG   GCCGTGATCGTATAGTGGTTAGTACTCTGCGTTGTGGCCGCAGCAACCTCGGTTCGAATCCGAGTCACGGCA
Mus_musculus_chr2.trna1432-HisGTG   GCCGTGATCGTATAGTGGTTAGTACTCTGCGTTGTGGCCGCAGCAACCTCGGTTCGAATCCGAGTCACGGCA
Mus_musculus_chr2.trna587-HisGTG    GCCGTGATCGTATAGTGGTTAGTACTCTGCGTTGTGGCCGCAGCAACCTCGGTTCGAATCCGAGTCACGGCA
Mus_musculus_chr3.trna291-HisGTG    GCCGTGATCGTATAGTGGTTAGTACTCTGCGTTGTGGCCGCAGCAACCTCGGTTCGAATCCGAGTCACGGCA
Mus_musculus_chr3.trna295-HisGYG    GCCGTGATCGTATAGTGGTTAGTACTCTGCGTTGTGGCCGCAGCAACCTCGGTTCGAATCCGAGTCACGGCA
Mus_musculus_chr3.trna747-HisGTG    GCCGTGATCGTATAGTGGTTAGTACTCTGCGTTGTGGCCGCAGCAACCTCGGTTCGAATCCGAGTCACGGCA
Mus_musculus_chr3.trna751-HisGTG    GCCGTGATCGTATAGTGGTTAGTACTCTGCGTTGTGGCCGCAGCAACCTCGGTTCGAATCCGAGTCACGGCA
Mus_musculus_chr4.trna1691-HisGTG   GCCGTGATCGTATAGTGGTTAGTACTCTGCGTTGTGGCCGCAGCAACCTCGGTTCGAATCCGAGTCACGGCA
Mus_musculus_chr3.trna749-HisGTG    GCCGAGATCGTATAGTGGTTAGTACTCTGCATTGTGGCTGCAGCAACCTCGGTTCGAATCCGAGTCTCGGCA
```

tRNA$^{Met}_{i}$ *M.musculus*: 5′-AGGATGGTTTCGATCCATCGACCTCT-3′

tRNA$^{Met}_{i}$ *P.berghei*: 5′-CGCGTGGTTTCGATCCACGGTCCTGG-3′

```
>berghei ARNtMeti                   AGCAGCGTAGCTCAGAGGAAGAGTGGGGGGCTCATAACCCCCAGGACCGTGGATCGAAACCACGCGCTGCTA
Mus_musculus_chr13.trna82-MetC      AGCAGAGTGGCGCAGCGGAAGCGTGCTGGGCCCATAACCCAGAGGTCGATAGATCGAAACCATCCTCTGCTA
Mus_musculus_chr15.trna876-Met      AGCAGAGTGGCGCAGCGGAAGCATGCTGGGCCCATAACCCAGAGGTCGATGGATCGAAACCATCCTCTGCTA
Mus_musculus_chr13.trna108-Met      AGCAGAGTGGCGCAGCGGAAGCGTGCTGGGCCCATAACCCAGAGGTCGATGGATCGAAACCATCCTCTGCTA
Mus_musculus_chr13.trna111-Met      AGCAGAGTGGCGCAGCGGAAGCGTGCTGGGCCCATAACCCAGAGGTCGATGGATCGAAACCATCCTCTGCTA
Mus_musculus_chr13.trna78-MetC      AGCAGAGTGGCGCAGCGGAAGCGTGCTGGGCCCATAACCCAGAGGTCGATGGATCGAAACCATCCTCTGCTA
Mus_musculus_chr13.trna90-MetC      AGCAGAGTGGCGCAGCGGAAGCGTGCTGGGCCCATAACCCAGAGGTCGATGGATCGAAACCATCCTCTGCTA
Mus_musculus_chr13.trna959-Met      AGCAGAGTGGCGCAGCGGAAGCGTGCTGGGCCCATAACCCAGAGGTCGATGGATCGAAACCATCCTCTGCTA
Mus_musculus_chr13.trna995-Met      AGCAGAGTGGCGCAGCGGAAGCGTGCTGGGCCCATAACCCAGAGGTCGATGGATCGAAACCATCCTCTGCTA
Mus_musculus_chr3.trna792-MetC      AGCAGAGTGGCGCAGCGGAAGCGTGCTGGGCCCATAACCCAGAGGTCGATGGATCGAAACCATCCTCTGCTA
```

tRNA$^{Met}_{e}$ *M.musculus*: 5′-ACGCGCTGCCTACTGCGCTAAGAAGGC-3′

tRNA$^{Met}_{e}$ *P.berghei*: 5′-GCGCGCTAACCGACTGCGCCAATTACCC-3′

```
>berghei ARNTMete                   GGGTAATTGGCGCAGTCGGTTAGCGCGCGGGTCTCATAATCCCGAGGTCGTGAGTTCGAGCCTCACATTACCCA
Mus_musculus_chr13.trna99-MetC      GCCTTCTTAGCGCAGTAGGC-AGCGCGTCAGTCTCATAATCTGAAGGTCCTGAGTTCGAGCCTCAGAGAAGGCA
Mus_musculus_chr13.trna1006-Me      GCCTTCTTAGCGCAGTAGGC-AGCGCGTCAGTCTCATAATCTGAAGGTCCTGAGTTCGAACCTCAGAGAGGGCA
Mus_musculus_chr13.trna1011-Me      GCCTCCTTAGCGCAGTAGGC-AGCGCGTCAGTCTCATAATCTGAAGGTCCTGAGTTCGAACCTCAGAGGGGGCA
Mus_musculus_chr13.trna61-MetC      GCCTCCTTAGCGCAGTAGGC-AGCGCGTCAGTCTCATAATCTGAAGGTCCTGAGTTCGAACCTCAGAGGGGGCA
Mus_musculus_chr15.trna913-Met      GCCTCGTTAGCGCAGTAGGT-AGCGCGTCAGTCTCATAATCTGAAGGTCGTGAGTTCGATCCTCACACGGGGCA
Mus_musculus_chr8.trna788-MetC      GCCTCGTTAGCGCAGTAGGT-AGCGCGTCAGTCTCATAATCTGAAGGTCGTGAGTTCGATCCTCACACGGGGCA
Mus_musculus_chr11.trna1132-Me      GCCTCCTTAGTGTAGTAGGC-ATTGCGTCAGTCTCATAATCTGAAGGTCCTGAGTTCAAGCCTCAGAGTGGGCA
Mus_musculus_chr19.trna371-Met      GCCTCCTTAGTGTAGTAGGC-ATTGCGTCAGTCTCATAATCTGAAGGTCCTGAGTTCAAGCCTCAGAGTGGGCA
Mus_musculus_chr15.trna355-Met      GCCTCCTTAGCGCAGTAGGC-AGCCCGTCAGTCTCATAATCTGAAGGTCCTGAGTTCAAACCTCAGAGGGGGCA
```

Figure S5. Probes designed to specifically recognize *M. musculus* and *P. berghei* tRNAs. *M. musculus* tRNA sequences recognized by the probes are highlighted in yellow while *P. berghei* tRNA sequences recognized by the probes are highlighted in grey. The sequences of parasite tRNAs are very similar to vertebrate tRNA sequences, making it difficult to design specific probes capable of differentiating mouse from *Plasmodium* tRNAs. However, it was possible to design such probes against tRNA$^{Glu}_{TTC}$, tRNA$^{His}_{GTG}$, tRNA$^{Met}_{i}$ and tRNA$^{Met}_{e}$.

Table S1: LCMSMS analyses of “Only Schizonts” parasites (raw data). Legends are indicated as well as the overall variability between samples (WT-B3, WT-B6, WT-B8, KO-N, KO-R1 and KO-R4 is visualized using MDS plot.

SCHIZONTS

Spectral count legend:

# spectra (BASIC Spectral Count)	= 1 spectrum
# spectra (BASIC Spectral Count)	= 2-5 spectra
# spectra (BASIC Spectral Count)	= 6-10 spectra
# spectra (BASIC Spectral Count)	= 11-30 spectra
# spectra (BASIC Spectral Count)	>= 31 spectra

Statistics legend:

8 proteins overexpressed in KO	FC>2
49 proteins underexpressed in KO	FC<0,5
	p.value<0,05

GO Terms/EupathDB function prediction

- DNA Replication/metabolism/synthesis
- Motion & transport
- Chaperones
- Unknown functions
- Translation
- The most expressed stable proteins (100)
- Aminoacyl-tRNA synthetases
- Others

MultiDimentionnal Scaling plot (R)

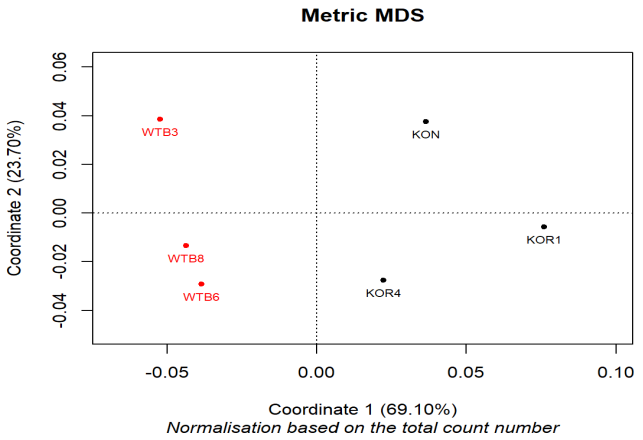

Normalisation based on the total count number

Total number of identified proteins:

accession	WT-B3	WT-B6	WT-B8	KO-N	KO-R1	KO-R4
Total number of proteins identified by Mascot and validated at FDR<1% by Proline (ProFI consortium)	425	441	469	347	423	456

Proteins validated at FDR<1% in the UniProtKB-P.berghei database

	BASIC Spectral Count						Statistics with R		moy Nb SpC		Annotations	
Accession	WT-B3	WT-B6	WT-B8	KO-N	KO-R1	KO-R4	LogFC	p.value	WT	KO	gene	gene_product
PBANKA_1125600	2	6	4	26	36	25	2,23	6,58E-05	4,00	29,00	PBANKA_1125600	pyruvate kinase, putative
PBANKA_0407700	1	1	2	19	23	1	2,73	9,65E-04	1,33	14,33	PBANKA_0407700	cytoplasmic translational elongation [GO:0002182]
PBANKA_1235600	1	5	7	11	29	31	1,81	1,45E-03	4,33	23,67	PBANKA_1235600	one-carbon metabolic process [GO:0006730]
PBANKA_1362900				4	8	8	5,55	2,20E-03		6,67	PBANKA_1362900	Lysyl-tRNA aminoacylation [GO:0006430]
PBANKA_1326400	21	13	10	58	51	44	1,34	3,28E-03	14,67	51,00	PBANKA_1326400	glucose metabolic process [GO:0006006]; glycolytic process [GO:0006096]
PBANKA_1008500	1			4	11	8	3,64	7,84E-03	1,00	7,67	PBANKA_1008500	translocon component
PBANKA_0603200		1	2	14	8	5	2,56	1,28E-02	1,50	9,00	PBANKA_0603200	Eukaryotic translation initiation factor 5A
PBANKA_1218900	1			6	10	3	3,36	2,33E-02	1,00	6,33	PBANKA_1218900	Elongation factor 1-delta, putative
PBANKA_1224200			2	1	12	7	2,48	5,88E-02	2,00	6,67	PBANKA_1224200	DNA J protein
PBANKA_0308600				1	5	3	4,34	6,27E-02		3,00	PBANKA_0308600	Asparaginyl-tRNA aminoacylation [GO:0006421]
PBANKA_0304900	2		1	2	10	9	2,18	6,58E-02	1,50	7,00	PBANKA_0304900	Serine repeat antigen 3 OS=Plasmodium berghei (strain Anka) OX=5823 GN=PBANKA_0304900 PE=3 SV=1
PBANKA_0109100			1	1	7	6	2,87	7,91E-02	1,00	4,67	PBANKA_0109100	Transketolase OS=Plasmodium berghei (strain Anka) OX=5823 GN=PBANKA_0109100 PE=3 SV=1
PBANKA_0943600	5	1	4	17	13	4	1,29	8,03E-02	3,33	11,33	PBANKA_0943600	60S acidic ribosomal protein P1, putative OS=Plasmodium berghei (strain Anka) OX=5823 GN=PBANKA_0943600 PE=3 SV=1
PBANKA_1137900				2	3	2	4,08	8,88E-02		2,33	PBANKA_1137900	Proliferating cell nuclear antigen OS=Plasmodium berghei (strain Anka) OX=5823 GN=PBANKA_1137900 PE=3 SV=1
PBANKA_0105300					2	4	3,90	1,09E-01		3,00	PBANKA_0105300	Uncharacterized protein OS=Plasmodium berghei (strain Anka) OX=5823 GN=PBANKA_0105300 PE=4 SV=1
PBANKA_1401300	6	2	6	8	17	16	1,03	1,11E-01	4,67	13,67	PBANKA_1401300	40S ribosomal protein S7 OS=Plasmodium berghei (strain Anka) OX=5823 GN=PBANKA_1401300 PE=3 SV=1
PBANKA_1010000	4	1	1	14	7	2	1,50	1,18E-01	2,00	7,67	PBANKA_1010000	Mitochondrial acidic protein MAM33, putative OS=Plasmodium berghei (strain Anka) OX=5823 GN=PBANKA_1010000 PE=4 SV=1
PBANKA_1309900	4	2	2	10	10	8	1,31	1,18E-01	2,67	9,33	PBANKA_1309900	M17 leucyl aminopeptidase, putative OS=Plasmodium berghei (strain Anka) OX=5823 GN=PBANKA_1309900 PE=3 SV=1
LSM3 PBANKA_0710900				4	1		3,77	1,23E-01		2,50	LSM3 PBANKA_0710900	U6 snRNA-associated Sm-like protein LSm3 OS=Plasmodium berghei (strain Anka) OX=5823 GN=LSM3 PE=3 SV=1
PBANKA_1117700					4	2	3,72	1,24E-01		3,00	PBANKA_1117700	L-lactate dehydrogenase OS=Plasmodium berghei (strain Anka) OX=5823 GN=PBANKA_1117700 PE=3 SV=1
PBANKA_0517500					4	2	3,72	1,24E-01		3,00	PBANKA_0517500	Bromodomain protein 1, putative OS=Plasmodium berghei (strain Anka) OX=5823 GN=PBANKA_0517500 PE=4 SV=1
PBANKA_1210100				4			3,57	1,48E-01		4,00	PBANKA_1210100	UV excision repair protein RAD23 OS=Plasmodium berghei (strain Anka) OX=5823 GN=PBANKA_1210100 PE=3 SV=1
PBANKA_0816400					3	2	3,52	1,49E-01		2,50	PBANKA_0816400	Probable ATP-dependent 6-phosphofructokinase OS=Plasmodium berghei (strain Anka) OX=5823 GN=PBANKA_0816400 PE=3 SV=1
PBANKA_1240600						4	3,52	1,54E-01		4,00	PBANKA_1240600	Inner membrane complex protein 1g, putative OS=Plasmodium berghei (strain Anka) OX=5823 GN=PBANKA_1240600 PE=4 SV=1
PBANKA_1409200				2	2		3,31	1,79E-01		2,00	PBANKA_1409200	RNA-binding protein, putative OS=Plasmodium berghei (strain Anka) OX=5823 GN=PBANKA_1409200 PE=4 SV=1
PBANKA_1145400					2	2	3,28	1,83E-01		2,00	PBANKA_1145400	Uncharacterized protein OS=Plasmodium berghei (strain Anka) OX=5823 GN=PBANKA_1145400 PE=4 SV=1
PBANKA_1028300					2	2	3,28	1,83E-01		2,00	PBANKA_1028300	Serine/threonine-protein phosphatase OS=Plasmodium berghei (strain Anka) OX=5823 GN=PBANKA_1028300 PE=3 SV=1
PBANKA_0619900	1	3	3	4	11	10	1,18	1,90E-01	2,33	8,33	PBANKA_0619900	Obg-like ATPase 1 OS=Plasmodium berghei (strain Anka) OX=5823 GN=PBANKA_0619900 PE=3 SV=1
PBANKA_1450200				1		2	3,16	2,06E-01		1,50	PBANKA_1450200	Glycine hydroxymethyltransferase OS=Plasmodium berghei (strain Anka) OX=5823 GN=PBANKA_1450200 PE=3 SV=1
PBANKA_1211000						3	3,14	2,08E-01		3,00	PBANKA_1211000	Glutamine amidotransferase OS=Plasmodium berghei (strain Anka) OX=5823 GN=PBANKA_1211000 PE=4 SV=1
PBANKA_1326800					4		3,00	2,19E-01		4,00	PBANKA_1326800	Replication factor C subunit 3, putative OS=Plasmodium berghei (strain Anka) OX=5823 GN=PBANKA_1326800 PE=3 SV=1
PBANKA_0306900					4		3,00	2,19E-01		4,00	PBANKA_0306900	Sec61-gamma subunit of protein translocation complex, putative OS=Plasmodium berghei (strain Anka) OX=5823 GN=PBANKA_0306900 PE=3 SV=1
PBANKA_0922800					1	2	2,99	2,22E-01		1,50	PBANKA_0922800	Small nuclear ribonucleoprotein Sm D1 OS=Plasmodium berghei (strain Anka) OX=5823 GN=PBANKA_0922800 PE=3 SV=1
PBANKA_0905600		1	1	4	5	3	1,84	2,24E-01	1,00	4,00	PBANKA_0905600	Eukaryotic translation initiation factor 4C OS=Plasmodium berghei (strain Anka) OX=5823 GN=PBANKA_0905600 PE=3 SV=1

Table S1: LCMSMS analyses of “Only Schizonts” parasites (raw data). Legends are indicated as well as the overall variability between samples (WT-B3, WT-B6, WT-B8, KO-N, KO-R1 and KO-R4 is visualized using MDS plot.

PBANKA_0915000		3	1		4	4	7	1,45	2,40E-01	2,00	5,00	PBANKA_0915000	Apical membrane antigen 1 OS=Plasmodium berghei (strain Anka) OX=5823 GN=PBANKA_0915000 PE=3 SV=1
PBANKA_0906200					2			2,67	2,54E-01		2,00	PBANKA_0906200	ATP synthase-associated protein, putative OS=Plasmodium berghei (strain Anka) OX=5823 GN=PBANKA_0906200 PE=4 SV=1
PBANKA_1222800					1		1	2,65	2,56E-01		1,00	PBANKA_1222800	Tyrosine--tRNA ligase
PBANKA_0517200							2	2,63	2,58E-01		2,00	PBANKA_0517200	Haloacid dehalogenase-like hydrolase, putative OS=Plasmodium berghei (strain Anka) OX=5823 GN=PBANKA_0517200 PE=4 SV=1
PBANKA_0208600							2	2,63	2,58E-01		2,00	PBANKA_0208600	Uncharacterized protein OS=Plasmodium berghei (strain Anka) OX=5823 GN=PBANKA_0208600 PE=4 SV=1
PBANKA_1341500							2	2,63	2,58E-01		2,00	PBANKA_1341500	RNA-binding protein, putative OS=Plasmodium berghei (strain Anka) OX=5823 GN=PBANKA_1341500 PE=4 SV=1
PBANKA_1348100							2	2,63	2,58E-01		2,00	PBANKA_1348100	AMMECR1 domain-containing protein OS=Plasmodium berghei (strain Anka) OX=5823 GN=PBANKA_1348100 PE=4 SV=1
PBANKA_0100400							2	2,63	2,58E-01		2,00	PBANKA_0100400	Reticulocyte binding protein, putative OS=Plasmodium berghei (strain Anka) OX=5823 GN=PBANKA_0100400 PE=4 SV=1
PBANKA_0112200							2	2,63	2,58E-01		2,00	PBANKA_0112200	Myosin E, putative OS=Plasmodium berghei (strain Anka) OX=5823 GN=PBANKA_0112200 PE=3 SV=1
PBANKA_1437600							2	2,63	2,58E-01		2,00	PBANKA_1437600	Gliadesome-associated protein 45, putative OS=Plasmodium berghei (strain Anka) OX=5823 GN=PBANKA_1437600 PE=4 SV=1
PBANKA_1142800					1	1		2,45	2,76E-01		1,00	PBANKA_1142800	Uncharacterized protein OS=Plasmodium berghei (strain Anka) OX=5823 GN=PBANKA_1142800 PE=4 SV=1
PBANKA_1111400					1	1		2,45	2,76E-01		1,00	PBANKA_1111400	Inositol-3-phosphate synthase OS=Plasmodium berghei (strain Anka) OX=5823 GN=PBANKA_1111400 PE=3 SV=1
PBANKA_1426700						1	1	2,43	2,78E-01		1,00	PBANKA_1426700	6-hydroxymethyl-7,8-dihydropterin pyrophosphokinase OS=Plasmodium berghei (strain Anka) OX=5823 GN=PBANKA_1426700 PE=4 SV=1
PBANKA_1458000						1	1	2,43	2,78E-01		1,00	PBANKA_1458000	Translation machinery-associated protein 46, putative OS=Plasmodium berghei (strain Anka) OX=5823 GN=PBANKA_1458000 PE=4 SV=1
PBANKA_1454200						1	1	2,43	2,78E-01		1,00	PBANKA_1454200	Uncharacterized protein OS=Plasmodium berghei (strain Anka) OX=5823 GN=PBANKA_1454200 PE=4 SV=1
PBANKA_1103100				1		4	4	2,08	2,92E-01	1,00	4,00	PBANKA_1103100	Actin-depolymerizing factor 1 OS=Plasmodium berghei (strain Anka) OX=5823 GN=PBANKA_1103100 PE=3 SV=1
PBANKA_1310400		2		0	5	5		1,73	2,93E-01	1,00	5,00	PBANKA_1310400	Centrin-2, putative OS=Plasmodium berghei (strain Anka) OX=5823 GN=PBANKA_1310400 PE=3 SV=1
PBANKA_0201500						2		2,21	2,99E-01		2,00	PBANKA_0201500	Uncharacterized protein OS=Plasmodium berghei (strain Anka) OX=5823 GN=PBANKA_0201500 PE=4 SV=1
PBANKA_1404700						2		2,21	2,99E-01		2,00	PBANKA_1404700	Uncharacterized protein OS=Plasmodium berghei (strain Anka) OX=5823 GN=PBANKA_1404700 PE=4 SV=1
PBANKA_0704500						2		2,21	2,99E-01		2,00	PBANKA_0704500	HECT-like E3 ubiquitin ligase, putative OS=Plasmodium berghei (strain Anka) OX=5823 GN=PBANKA_0704500 PE=4 SV=1
PBANKA_0505800						2		2,21	2,99E-01		2,00	PBANKA_0505800	2-deoxy-D-ribose 5-phosphate aldolase OS=Plasmodium berghei (strain Anka) OX=5823 GN=PBANKA_0505800 PE=4 SV=1
PBANKA_1223800						2		2,21	2,99E-01		2,00	PBANKA_1223800	V-type proton ATPase subunit a OS=Plasmodium berghei (strain Anka) OX=5823 GN=PBANKA_1223800 PE=3 SV=1
PBANKA_1113400						2		2,21	2,99E-01		2,00	PBANKA_1113400	Secreted ookinete protein OS=Plasmodium berghei (strain Anka) OX=5823 GN=PBANKA_1113400 PE=4 SV=1
PBANKA_1201900		1			2	3	2	2,06	3,10E-01	1,00	2,33	PBANKA_1201900	40S ribosomal protein S20e, putative OS=Plasmodium berghei (strain Anka) OX=5823 GN=PBANKA_1201900 PE=3 SV=1
PBANKA_0807400					1			1,85	3,64E-01		1,00	PBANKA_0807400	26S proteasome non-ATPase regulatory subunit 9, putative OS=Plasmodium berghei (strain Anka) OX=5823 GN=PBANKA_0807400 PE=4 SV=1
PBANKA_0932500					1			1,85	3,64E-01		1,00	PBANKA_0932500	Histone-lysine N-methyltransferase SET7, putative OS=Plasmodium berghei (strain Anka) OX=5823 GN=PBANKA_0932500 PE=4 SV=1
PBANKA_1439400					1			1,85	3,64E-01		1,00	PBANKA_1439400	Histone chaperone ASF1, putative OS=Plasmodium berghei (strain Anka) OX=5823 GN=PBANKA_1439400 PE=3 SV=1
PBANKA_0501800					1			1,85	3,64E-01		1,00	PBANKA_0501800	Myosin essential light chain ELC, putative OS=Plasmodium berghei (strain Anka) OX=5823 GN=PBANKA_0501800 PE=4 SV=1
PBANKA_1009500					1			1,85	3,64E-01		1,00	PBANKA_1009500	Glutamate synthase [NADH], putative OS=Plasmodium berghei (strain Anka) OX=5823 GN=PBANKA_1009500 PE=3 SV=1
PBANKA_1002600							1	1,82	3,67E-01		1,00	PBANKA_1002600	6-cysteine protein P41, putative OS=Plasmodium berghei (strain Anka) OX=5823 GN=PBANKA_1002600 PE=4 SV=1
PBANKA_0611800							1	1,82	3,67E-01		1,00	PBANKA_0611800	N-acetyltransferase, GNAT family, putative OS=Plasmodium berghei (strain Anka) OX=5823 GN=PBANKA_0611800 PE=4 SV=1
PBANKA_1130500							1	1,82	3,67E-01		1,00	PBANKA_1130500	Proteasome subunit alpha type OS=Plasmodium berghei (strain Anka) OX=5823 GN=PBANKA_1130500 PE=3 SV=1
PBANKA_0716900							1	1,82	3,67E-01		1,00	PBANKA_0716900	Armadillo-domain containing rhoptry protein, putative OS=Plasmodium berghei (strain Anka) OX=5823 GN=PBANKA_0716900 PE=4 SV=1
PBANKA_0411300							1	1,82	3,67E-01		1,00	PBANKA_0411300	Uncharacterized protein OS=Plasmodium berghei (strain Anka) OX=5823 GN=PBANKA_0411300 PE=4 SV=1
PBANKA_1312200							1	1,82	3,67E-01		1,00	PBANKA_1312200	Ubiquitin-protein ligase, putative OS=Plasmodium berghei (strain Anka) OX=5823 GN=PBANKA_1312200 PE=4 SV=1
PBANKA_1220800							1	1,82	3,67E-01		1,00	PBANKA_1220800	Uncharacterized protein OS=Plasmodium berghei (strain Anka) OX=5823 GN=PBANKA_1220800 PE=4 SV=1
PBANKA_0931600							1	1,82	3,67E-01		1,00	PBANKA_0931600	Guanine nucleotide-exchange factor SEC12, putative OS=Plasmodium berghei (strain Anka) OX=5823 GN=PBANKA_0931600 PE=4 SV=1
PBANKA_0501400							1	1,82	3,67E-01		1,00	PBANKA_0501400	Rhoptry neck protein 12 OS=Plasmodium berghei (strain Anka) OX=5823 GN=PBANKA_0501400 PE=4 SV=1
PBANKA_1108600							1	1,82	3,67E-01		1,00	PBANKA_1108600	Alpha-soluble NSF attachment protein, putative OS=Plasmodium berghei (strain Anka) OX=5823 GN=PBANKA_1108600 PE=3 SV=1
PBANKA_1353700							1	1,82	3,67E-01		1,00	PBANKA_1353700	Nucleolar complex protein 2, putative OS=Plasmodium berghei (strain Anka) OX=5823 GN=PBANKA_1353700 PE=3 SV=1
PBANKA_1416900							1	1,82	3,67E-01		1,00	PBANKA_1416900	Structural maintenance of chromosomes protein OS=Plasmodium berghei (strain Anka) OX=5823 GN=PBANKA_1416900 PE=3 SV=1
PBANKA_1244500							1	1,82	3,67E-01		1,00	PBANKA_1244500	SNARE protein, putative OS=Plasmodium berghei (strain Anka) OX=5823 GN=PBANKA_1244500 PE=4 SV=1
PBANKA_1355700							1	1,82	3,67E-01		1,00	PBANKA_1355700	Myosin A OS=Plasmodium berghei (strain Anka) OX=5823 GN=PBANKA_1355700 PE=3 SV=1
PBANKA_1037300		1	1		6	2		1,44	4,01E-01	1,00	4,00	PBANKA_1037300	Uncharacterized protein OS=Plasmodium berghei (strain Anka) OX=5823 GN=PBANKA_1037300 PE=4 SV=1
PBANKA_0500600	PBANKA_1000041					1		1,53	4,03E-01		1,00	PBANKA_0500600	PBANKA_1000041 Fam-b protein OS=Plasmodium berghei (strain Anka) OX=5823 GN=PBANKA_0500600 PE=4 SV=1
PBANKA_1023500						1		1,53	4,03E-01		1,00	PBANKA_1023500	Uncharacterized protein OS=Plasmodium berghei (strain Anka) OX=5823 GN=PBANKA_1023500 PE=4 SV=1
PBANKA_0819300						1		1,53	4,03E-01		1,00	PBANKA_0819300	Eukaryotic translation initiation factor 3 subunit F, putative OS=Plasmodium berghei (strain Anka) OX=5823 GN=PBANKA_0819300 PE=4 SV=1
PBANKA_0928800						1		1,53	4,03E-01		1,00	PBANKA_0928800	Splicing factor U2AF small subunit, putative OS=Plasmodium berghei (strain Anka) OX=5823 GN=PBANKA_0928800 PE=4 SV=1
PBANKA_1305700						1		1,53	4,03E-01		1,00	PBANKA_1305700	Vacuolar protein sorting-associated protein 60, putative OS=Plasmodium berghei (strain Anka) OX=5823 GN=PBANKA_1305700 PE=4 SV=1
PBANKA_0925200						1		1,53	4,03E-01		1,00	PBANKA_0925200	Calcium-dependent protein kinase 7 OS=Plasmodium berghei (strain Anka) OX=5823 GN=PBANKA_0925200 PE=4 SV=1
PBANKA_0510200						1		1,53	4,03E-01		1,00	PBANKA_0510200	Uncharacterized protein OS=Plasmodium berghei (strain Anka) OX=5823 GN=PBANKA_0510200 PE=4 SV=1
PBANKA_1117400						1		1,53	4,03E-01		1,00	PBANKA_1117400	Uncharacterized protein OS=Plasmodium berghei (strain Anka) OX=5823 GN=PBANKA_1117400 PE=4 SV=1
PBANKA_1220200						1		1,53	4,03E-01		1,00	PBANKA_1220200	Lysophospholipase, putative OS=Plasmodium berghei (strain Anka) OX=5823 GN=PBANKA_1220200 PE=4 SV=1
PBANKA_0314600						1		1,53	4,03E-01		1,00	PBANKA_0314600	Uncharacterized protein OS=Plasmodium berghei (strain Anka) OX=5823 GN=PBANKA_0314600 PE=4 SV=1
PBANKA_0922300						1		1,53	4,03E-01		1,00	PBANKA_0922300	Threonyl-tRNA synthetase
PBANKA_1205900			1		2		3	1,62	4,41E-01	1,00	2,50	PBANKA_1205900	AP2 domain transcription factor AP2-I, putative OS=Plasmodium berghei (strain Anka) OX=5823 GN=PBANKA_1205900 PE=4 SV=1
PBANKA_1348900				2		6	3	1,32	4,43E-01	2,00	4,50	PBANKA_1348900	Chaperone binding protein, putative OS=Plasmodium berghei (strain Anka) OX=5823 GN=PBANKA_1348900 PE=4 SV=1
PBANKA_0202300				1		4	2	1,60	4,46E-01	1,00	3,00	PBANKA_0202300	UMP-CMP kinase, putative OS=Plasmodium berghei (strain Anka) OX=5823 GN=PBANKA_0202300 PE=3 SV=1
PBANKA_0100700			1	2	4	4	2	1,07	4,66E-01	1,50	3,33	PBANKA_0100700	Uncharacterized protein OS=Plasmodium berghei (strain Anka) OX=5823 GN=PBANKA_0100700 PE=4 SV=1
PBANKA_0920800				1		2	3	1,50	4,87E-01	1,00	2,50	PBANKA_0920800	CRAL/TRIO domain-containing protein, putative OS=Plasmodium berghei (strain Anka) OX=5823 GN=PBANKA_0920800 PE=4 SV=1
PBANKA_0813000				1		3	2	1,39	5,18E-01	1,00	2,50	PBANKA_0813000	Inhibitor of cysteine proteases OS=Plasmodium berghei (strain Anka) OX=5823 GN=PBANKA_0813000 PE=4 SV=1
PBANKA_1225700		1				2	2	1,29	5,61E-01	1,00	2,00	PBANKA_1225700	GTPase-activating protein, putative OS=Plasmodium berghei (strain Anka) OX=5823 GN=PBANKA_1225700 PE=4 SV=1
PBANKA_1246161				2	1	1	4	1,03	5,81E-01	2,00	2,00	PBANKA_1246161	Fam-a protein OS=Plasmodium berghei (strain Anka) OX=5823 GN=PBANKA_1246161 PE=4 SV=1
PBANKA_1411300		10	10	10		3	2	-3,11	1,47E-04	10,00	2,50	PBANKA_1411300	Eukaryotic translation initation factor 4 gamma, putative
PBANKA_0831000		101	64	43	34	21	30	-1,69	1,68E-04	69,33	28,33	PBANKA_0831000	Merozoite surface antigens
PBANKA_0305100		24	18	14	6	13	5	-1,81	7,36E-04	18,67	8,00	PBANKA_0305100	serine repeat antigen 1
PBANKA_1439200		37	38	53	19	30	21	-1,44	1,31E-03	42,67	23,33	PBANKA_1439200	Polyadenylate-binding protein
PBANKA_0519900			6	6				-5,49	1,87E-03	6,00		PBANKA_0519900	conserved Plasmodium protein, unknown function
PBANKA_0403800		2	4	6				-5,41	2,43E-03	4,00		PBANKA_0403800	transporter, putative
PBANKA_0300600		9	8	9		4	3	-2,45	3,04E-03	8,67	3,50	PBANKA_0300600	conserved Plasmodium protein, unknown function
PBANKA_0914300		8	7	9	3	1	1	-2,65	3,20E-03	8,00	1,67	PBANKA_0914300	Protein disulfide isomerase, putative
PBANKA_1231800		15	18	18	10	8	7	-1,54	3,91E-03	17,00	8,33	PBANKA_1231800	60S ribosomal protein L12, putative
PBANKA_0416000		35	35	29	17	17	22	-1,32	4,00E-03	33,00	18,67	PBANKA_0416000	High molecular weight rhoptry protein 3, putative
PBANKA_1200600		16	12	18	2	10	11	-1,55	5,10E-03	15,33	7,67	PBANKA_1200600	conserved Plasmodium protein, unknown function
PBANKA_1237800		17	26	28	5	13	23	-1,34	5,54E-03	23,67	13,67	PBANKA_1237800	multidrug resistance protein 1, putative
PBANKA_0610900		22	14	19	5	15	10	-1,44	5,73E-03	18,33	10,00	PBANKA_0610900	HSP40, subfamily A, putative
PBANKA_1309500		2	5	3				-5,18	5,84E-03	3,33		PBANKA_1309500	conserved Plasmodium protein, unknown function
PBANKA_1209000		5	8	9	1	3	2	-2,43	7,17E-03	7,33	2,00	PBANKA_1209000	Eukaryotic translation initiation factor 2 subunit beta, putative
PBANKA_1106700		23	33	39	15	22	24	-1,20	8,33E-03	31,67	20,33	PBANKA_1106700	60S ribosomal protein L4, putative
PBANKA_1231700		19	18	23	12	8	13	-1,32	8,92E-03	20,00	11,00	PBANKA_1231700	60S ribosomal protein L2, putative
PBANKA_1229000		30	29	39	9	28	28	-1,17	9,78E-03	32,67	21,67	PBANKA_1229000	conserved Plasmodium protein, unknown function
PBANKA_1306200		2	2	5				-4,97	1,17E-02	3,00		PBANKA_1306200	tRip

Table S1: LCMSMS analyses of “Only Schizonts” parasites (raw data). Legends are indicated as well as the overall variability between samples (WT-B3, WT-B6, WT-B8, KO-N, KO-R1 and KO-R4 is visualized using MDS plot.

PBANKA_1019400	16	14	13	5	10	9	-1,38	1,29E-02	14,33	8,00	PBANKA_1019400	60S ribosomal protein L7a
PBANKA_0702800	50	33	26	22	27	22	-1,11	1,34E-02	36,33	23,67	PBANKA_0702800	protein disulfide-isomerase, putative
PBANKA_1349000	5	2	2				-4,89	1,49E-02	3,00		PBANKA_1349000	MSP7-like protein
PBANKA_1242800	4	4	4		1		-3,75	1,51E-02	4,00	1,00	PBANKA_1242800	Eukaryotic translation initiation factor 3 subunit E
PBANKA_0103300	1	3	8			1	-3,66	1,59E-02	4,00	1,00	PBANKA_0103300	conserved Plasmodium protein, unknown function
PBANKA_0826700	17	22	17	12	11	12	-1,20	1,77E-02	18,67	11,67	PBANKA_0826700	parasitophorous vacuolar protein 5
PBANKA_1450300	26	13	15	16	7	7	-1,23	1,80E-02	18,00	10,00	PBANKA_1450300	ATP synthase subunit beta, mitochonfrial
PBANKA_1305300	6	5	6		3	1	-2,63	1,82E-02	5,67	2,00	PBANKA_1305300	FACT complex subunit SSRP1
PBANKA_0604800	8	13	14	4	6	9	-1,42	1,83E-02	11,67	6,33	PBANKA_0604800	Eukaryotic translation initiation factor 3 subunit C
PBANKA_1352000	17	26	25	12	14	19	-1,13	1,84E-02	22,67	15,00	PBANKA_1352000	elongation factor 1-gamma, putative
PBANKA_1202400	7	5	7	1	2	2	-2,37	1,90E-02	6,33	1,67	PBANKA_1202400	60S ribosomal protein L13
PBANKA_1302200	3	5	5		2		-3,18	2,01E-02	4,33	2,00	PBANKA_1302200	translocon protein Sec62
PBANKA_0942500	14	9	7	3	5	6	-1,57	2,05E-02	10,00	4,67	PBANKA_0942500	Thioredxin lke mero protein, putative
PBANKA_0205200	2	1	5				-4,78	2,09E-02	2,67		PBANKA_0205200	conserved Plasmodium protein, unknown function
PBANKA_0615200	8		1				-4,74	2,09E-02	4,50		PBANKA_0615200	Ca-dependent protein kinase 4
PBANKA_1232500	5	7	6	2	2	1	-2,34	2,22E-02	6,00	1,67	PBANKA_1232500	Eukaryotic translation initiation factor 3 subunit B, putative
PBANKA_0924800	3	6	6			3	-2,67	2,46E-02	5,00	3,00	PBANKA_0924800	golgi protein 2
PBANKA_1308600	13	4	3	1	2	3	-2,09	3,18E-02	6,67	2,00	PBANKA_1308600	Fructose-bisphosphate aldolase
PBANKA_1210200	17	22	23	11	18	16	-1,04	3,32E-02	20,67	15,00	PBANKA_1210200	PRE-binding protein, putative
PBANKA_0918300	2	4	4			1	-3,40	3,52E-02	3,33	1,00	PBANKA_0918300	major facilitator superfamily-related transporter, putative
PBANKA_0932200	5	1	1				-4,48	3,75E-02	2,33	#DIV/0!	PBANKA_0932200	Peptidyl-prolyl cis-trans isomerase
PBANKA_0619100	11	23	18	10	17	12	-1,04	3,85E-02	17,33	13,00	PBANKA_0619100	40S ribosomal protein S5
PBANKA_1123500	1	3	2				-4,48	3,98E-02	2,00	#DIV/0!	PBANKA_1123500	SNF2 helicase, transcription, putative
PBANKA_0906400	11	15	20	6	11	15	-1,07	4,16E-02	15,33	10,67	PBANKA_0906400	60S ribosomal protein L35ae
PBANKA_0414500	2	2	2				-4,41	4,39E-02	2,00	#DIV/0!	PBANKA_0414500	Protein YOP1, putative
PBANKA_1349200	2	2	2				-4,41	4,39E-02	2,00	#DIV/0!	PBANKA_1349200	MSP7-like protein
PBANKA_1365500	13	13	16	5	11	13	-1,08	4,65E-02	14,00	9,67	PBANKA_1365500	Exported protein IBIS1
PBANKA_1324400	6	6	13	4	4	5	-1,44	4,82E-02	8,33	4,33	PBANKA_1324400	60S ribosomal protein L27
PBANKA_1207200	7	9	13	5	5	7	-1,28	4,86E-02	9,67	5,67	PBANKA_1207200	Adenylate kinase, putative
PBANKA_1032700	9	13	10	5	6	9	-1,20	4,91E-02	10,67	6,67	PBANKA_1032700	CUGBP Elav-like family member 2, putative
PBANKA_1003800	7	6	7	1	5	3	-1,72	5,02E-02	6,67	3,00	PBANKA_1003800	Vacuolar proton pump subunit B OS=Plasmodium berghei (strain Anka) OX= 5823 GN= PBANKA_1003800 PE=3 SV=1
PBANKA_0519400	4	1	1				-4,29	5,11E-02	2,00	#DIV/0!	PBANKA_0519400	Uncharacterized protein OS=Plasmodium berghei (strain Anka) OX=5823 GN=PBANKA_0519400 PE=4 SV=1
PBANKA_1144000	7	8	5	2	4	3	-1,70	5,14E-02	6,67	3,00	PBANKA_1144000	26S proteasome regulatory subunit RPN11 OS= Plasmodium berghei (strain Anka) OX= 5823 GN= PBANKA_1144000 PE=4 SV=1
PBANKA_1417300	3	5	1			1	-3,25	5,27E-02	3,00	1,00	PBANKA_1417300	Translocation protein SEC63, putative OS= Plasmodium berghei (strain Anka) OX= 5823 GN= PBANKA_1417300 PE=4 SV=1
PBANKA_0707400	8	9	11	5	4	7	-1,28	5,31E-02	9,33	5,33	PBANKA_0707400	RNA-binding protein, putative OS=Plasmodium berghei (strain Anka) OX= 5823 GN=PBANKA_0707400 PE=4 SV=1
PBANKA_1202200		3	2				-4,29	5,45E-02	2,50	#DIV/0!	PBANKA_1202200	U5 small nuclear ribonucleoprotein component, putative OS=Plasmodium berghei (strain Anka) OX=5823 GN =PBANKA_1202200 PE=3 SV=1
PBANKA_1101300		2	3				-4,25	5,69E-02	2,50	#DIV/0!	PBANKA_1101300	Skeleton-binding protein 1 OS=Plasmodium berghei (strain Anka) OX= 5823 GN=PBANKA_1101300 PE=4 SV=1
PBANKA_1309700	2	3				0	-4,19	6,11E-02	2,50	0,00	PBANKA_1309700	ATP-dependent RNA helicase DDX5, putative OS=Plasmodium berghei (strain Anka) OX=5823 GN=PBANKA_1309700 PE=3 SV=1
PBANKA_1460400	3	11	20	7	5	11	-1,08	6,38E-02	11,33	7,67	PBANKA_1460400	Peptidylprolyl isomerase OS= Plasmodium berghei (strain Anka) OX=5823 GN= PBANKA_1460400 PE=4 SV=1
PBANKA_1217700	8	7	10	5	8	2	-1,32	6,48E-02	8,33	5,00	PBANKA_1217700	ATP-dependent RNA helicase DDX6 OS=Plasmodium berghei (strain Anka) OX=5823 GN=PBANKA_1217700 PE=3 SV=1
PBANKA_1206100	9	8	11	4	5	8	-1,20	6,78E-02	9,33	5,67	PBANKA_1206100	Eukaryotic translation initiation factor 3 subunit D OS=Plasmodium berghei (strain Anka) OX=5823 GN=PBANKA_1206100 PE=3 SV=1
PBANKA_1030100	13	5	5	3	3	5	-1,45	6,87E-02	7,67	3,67	PBANKA_1030100	Actin II OS=Plasmodium berghei (strain Anka) OX=5823 GN=PBANKA_1030100 PE=3 SV=1
PBANKA_1362000	5	6	6	1	2	4	-1,76	7,23E-02	5,67	2,33	PBANKA_1362000	Glutamyl-tRNA synthetase
PBANKA_0801200	2	4	4			2	-2,60	7,75E-02	3,33	2,00	PBANKA_0801200	Erythrocyte membrane-associated antigen, putative OS=Plasmodium berghei (strain Anka) OX=5823 GN=PBANKA_0801200 PE=3 SV=1
PBANKA_0913700	2	4	4			2	-2,60	7,75E-02	3,33	2,00	PBANKA_0913700	Coatomer subunit delta OS=Plasmodium berghei (strain Anka) OX=5823 GN=PBANKA_0913700 PE=3 SV=1
PBANKA_0520200	9	11	6	7	5	4	-1,20	7,76E-02	8,67	5,33	PBANKA_0520200	ADP/ATP translocase OS=Plasmodium berghei (strain Anka) OX=5823 GN=PBANKA_0520200 PE=3 SV=1
PBANKA_0820000		2	2				-3,96	7,97E-02	2,00		PBANKA_0820000	DnaJ protein, putative OS=Plasmodium berghei (strain Anka) OX=5823 GN=PBANKA_0820000 PE=4 SV=1
PBANKA_0706800		2	2				-3,96	7,97E-02	2,00		PBANKA_0706800	DnaJ protein, putative OS=Plasmodium berghei (strain Anka) OX=5823 GN=PBANKA_0706800 PE=4 SV=1
PBANKA_0520900		2	2				-3,96	7,97E-02	2,00		PBANKA_0520900	Antigen UB05, putative OS=Plasmodium berghei (strain Anka) OX=5823 GN=PBANKA_0520900 PE=4 SV=1
PBANKA_1018600	8	10	12	8	9	4	-1,08	8,12E-02	10,00	7,00	PBANKA_1018600	60S ribosomal protein L21, putative OS=Plasmodium berghei (strain Anka) OX=5823 GN=PBANKA_1018600 PE=3 SV=1
PBANKA_1025200		1	3				-3,92	8,29E-02	2,00		PBANKA_1025200	HACA ribonucleoprotein complex subunit 4,putative OS=Plasmodium berghei (strain Anka) OX=5823 GN=PBANKA_1025200 PE=3 SV=1
PBANKA_1103000		1	3				-3,92	8,29E-02	2,00		PBANKA_1103000	Serine/arginine-rich splicing factor 12, putative OS=Plasmodium berghei (strain Anka) OX=5823 GN=PBANKA_1103000 PE=4 SV=1
PBANKA_0830000	3	3	4			2	-2,56	8,48E-02	3,33	2,00	PBANKA_0830000	RNA-binding protein, putative OS=Plasmodium berghei (strain Anka) OX= 5823 GN=PBANKA_0830000 PE=4 SV=1
PBANKA_1208700	1	1	2				-3,86	8,74E-02	1,33		PBANKA_1208700	Succinate dehydrogenase subunit 4, putative OS=Plasmodium berghei (strain Anka) OX=5823 GN=PBANKA_1208700 PE=4 SV=1
PBANKA_0408400	2	2					-3,85	8,85E-02	2,00		PBANKA_0408400	Phosphoglycerate mutase, putative OS=Plasmodium berghei (strain Anka) OX=5823 GN=PBANKA_0408400 PE=4 SV=1
PBANKA_0918100	5	6	7	4		4	-1,53	9,23E-02	6,00	4,00	PBANKA_0918100	60S ribosomal protein L38, putative OS=Plasmodium berghei (strain Anka) OX=5823 GN=PBANKA_0918100 PE=3 SV=1
PBANKA_0302500	5	10	12	5	4	9	-1,09	9,37E-02	9,00	6,00	PBANKA_0302500	Hexose transporter OS=Plasmodium berghei (strain Anka) OX=5823 GN=PBANKA_0302500 PE=3 SV=1
PBANKA_1214700	3	1	0				-3,73	9,74E-02	1,33		PBANKA_1214700	Uncharacterized protein OS=Plasmodium berghei (strain Anka) OX=5823 GN=PBANKA_1214700 PE=4 SV=1
PBANKA_1455100	3	1					-3,73	9,74E-02	2,00		PBANKA_1455100	Replication factor C subunit 4, putative OS=Plasmodium berghei (strain Anka) OX=5823 GN=PBANKA_1455100 PE=3 SV=1
PBANKA_1354400	7	13	9	6	7	8	-1,02	9,91E-02	9,67	7,00	PBANKA_1354400	60S ribosomal protein L18a OS=Plasmodium berghei (strain Anka) OX=5823 GN=PBANKA_1354400 PE=3 SV=1
PBANKA_0414600	6	9	11	8	4	5	-1,09	1,01E-01	8,67	5,67	PBANKA_0414600	40S ribosomal protein S15A, putative OS=Plasmodium berghei (strain Anka) OX=5823 GN=PBANKA_0414600 PE=3 SV=1
PBANKA_1302800	5	5	4	0	4	2	-1,82	1,02E-01	4,67	2,00	PBANKA_1302800	Thioredoxin peroxidase 1 OS=Plasmodium berghei (strain Anka) OX= 5823 GN=PBANKA_1302800 PE=3 SV=1
PBANKA_1226600	5	7	6	4	2	3	-1,46	1,02E-01	6,00	3,00	PBANKA_1226600	Tubulin gamma chain OS=Plasmodium berghei (strain Anka) OX=5823 GN=PBANKA_1226600 PE=3 SV=1
PBANKA_0709000	6	4	5	2	2	2	-1,75	1,02E-01	5,00	2,00	PBANKA_0709000	Protein transport protein Sec61 subunit beta OS=Plasmodium berghei (strain Anka) OX= 5823 GN=PBANKA_0709000 PE=3 SV=1
PBANKA_0718800	2	5	5	1	0	3	-1,97	1,09E-01	4,00	1,33	PBANKA_0718800	Small GTP-binding protein sar1, putative OS=Plasmodium berghei (strain Anka) OX= 5823 GN=PBANKA_0718800 PE=3 SV=1
PBANKA_0939600	4	4	4		1	3	-2,00	1,11E-01	4,00	2,00	PBANKA_0939600	Polyadenylate-binding protein-interacting protein 1, putative OS=Plasmodium berghei (strain Anka) OX=5823 GN=PBANKA_0939600 PE=4 SV=1
PBANKA_1027900	2	1	4		1		-3,00	1,16E-01	2,33	1,00	PBANKA_1027900	Small nuclear ribonucleoprotein-associated protein B, putative OS=Plasmodium berghei (strain Anka) OX=5823 GN=PBANKA_1027900 PE=4 SV=1
PBANKA_1023900		2	1				-3,61	1,17E-01	1,50		PBANKA_1023900	Glutathione S-transferase, putative OS=Plasmodium berghei (strain Anka) OX= 5823 GN=PBANKA_1023900 PE=4 SV=1
PBANKA_0109600		2	1				-3,61	1,17E-01	1,50		PBANKA_0109600	ATP synthase-associated protein, putative OS= Plasmodium berghei (strain Anka) OX= 5823 GN= PBANKA_0109600 PE=4 SV=1
PBANKA_1234800	5	8	10	5	10	2	-1,10	1,25E-01	7,67	5,67	PBANKA_1234800	40S ribosomal protein S9, putative OS= Plasmodium berghei (strain Anka) OX= 5823 GN= PBANKA_1234800 PE=3 SV=1
PBANKA_0824800	1	4	5	1		2	-2,10	1,27E-01	3,33	1,50	PBANKA_0824800	Polyadenylate-binding protein 2, putative OS=Plasmodium berghei (strain Anka) OX=5823 GN=PBANKA_0824800 PE=4 SV=1
PBANKA_1239200	3	4	5		3	2	-1,84	1,29E-01	4,00	2,50	PBANKA_1239200	Ribosome-interacting GTPase 1, putative OS= Plasmodium berghei (strain Anka) OX= 5823 GN= PBANKA_1239200 PE=4 SV=1
PBANKA_0928200			3				-3,49	1,29E-01	3,00		PBANKA_0928200	Uncharacterized protein OS=Plasmodium berghei (strain Anka) OX=5823 GN=PBANKA_0928200 PE=4 SV=1
PBANKA_1217800	5	4	3	2		2	-1,88	1,31E-01	4,00	2,00	PBANKA_1217800	Signal peptidase complex subunit 2, putative OS=Plasmodium berghei (strain Anka) OX=5823 GN=PBANKA_1217800 PE=3 SV=1
PBANKA_1019700	3	5	6	1	4	2	-1,61	1,31E-01	4,67	2,33	PBANKA_1019700	NTF2 domain-containing protein OS=Plasmodium berghei (strain Anka) OX= 5823 GN=PBANKA_1019700 PE=4 SV=1
PBANKA_1013100	5	5	9	2	3	6	-1,27	1,32E-01	6,33	3,67	PBANKA_1013100	60S ribosomal protein L14, putative OS=Plasmodium berghei (strain Anka) OX= 5823 GN=PBANKA_1013100 PE=3 SV=1
PBANKA_1320500	3	11	7		6	9	-1,12	1,33E-01	7,00	7,50	PBANKA_1320500	H(+)-exporting diphosphatase OS=Plasmodium berghei (strain Anka) OX=5823 GN=PBANKA_1320500 PE=3 SV=1
PBANKA_1438000	1		2				-3,41	1,37E-01	1,50		PBANKA_1438000	cAMP-dependent protein kinase regulatory subunit,putative OS=Plasmodium berghei (strain Anka) OX=5823 GN =PBANKA_1438000 PE=3 SV=1
PBANKA_1322700	1	5	5	1		3	-1,86	1,39E-01	3,67	2,00	PBANKA_1322700	ATP-dependent RNA helicase DBP5, putative OS=Plasmodium berghei (strain Anka) OX=5823 GN=PBANKA_1322700 PE=4 SV=1
PBANKA_1303700	5	3	3		2	2	-1,91	1,45E-01	3,67	2,00	PBANKA_1303700	Vesicle-associated membrane protein, putative OS=Plasmodium berghei (strain Anka) OX=5823 GN=PBANKA_1303700 PE=4 SV=1
PBANKA_1346600	5	5	8	2	5	4	-1,27	1,45E-01	6,00	3,67	PBANKA_1346600	Glutamine--tRNA ligase
PBANKA_1013200	2		1				-3,33	1,46E-01	1,50	#DIV/0!	PBANKA_1013200	Succinate--CoA ligase [ADP-forming] subunit beta, mitochondrial OS=Plasmodium berghei (strain Anka) OX=5823 GN=PBANKA_1013200 PE=3 SV=1

Table S1: LCMSMS analyses of “Only Schizonts” parasites (raw data). Legends are indicated as well as the overall variability between samples (WT-B3, WT-B6, WT-B8, KO-N, KO-R1 and KO-R4 is visualized using MDS plot.

PBANKA_1223300	3	3	5	1	1	2	-1,87	1,48E-01	3,67	1,33	PBANKA_1223300	Ras-related protein Rab-18, putative OS=Plasmodium berghei (strain Anka) OX=5823 GN=PBANKA_1223300 PE=4 SV=1
PBANKA_0412800	4	4	4	1	2	2	-1,74	1,48E-01	4,00	1,67	PBANKA_0412800	Eukaryotic translation initiation factor 4E, putative OS= Plasmodium berghei (strain Anka) OX= 5823 GN= PBANKA_0412800 PE=3 SV=1
PBANKA_0310000	5	4	5	1		5	-1,56	1,50E-01	4,67	3,00	PBANKA_0310000	Protein SIS1, putative OS=Plasmodium berghei (strain Anka) OX=5823 GN=PBANKA_0310000 PE=4 SV=1
PBANKA_1431050	7	5	1	5			-1,65	1,54E-01	4,33	5,00	PBANKA_1431050	10 kDa chaperonin, putative OS=Plasmodium berghei (strain Anka) OX= 5823 GN=PBANKA_1431050 PE= 3 SV=1
PBANKA_1428500		2					-3,13	1,67E-01	2,00		PBANKA_1428500	Glycerol-3-phosphate 1-O-acyltransferase, putative OS=Plasmodium berghei (strain Anka) OX=5823 GN=PBANKA_1428500 PE=4 SV=1
PBANKA_1451600		2					-3,13	1,67E-01	2,00		PBANKA_1451600	SUMO-activating enzyme subunit OS=Plasmodium berghei (strain Anka) OX=5823 GN=PBANKA_1451600 PE= 3 SV=1
PBANKA_1321000		2					-3,13	1,67E-01	2,00		PBANKA_1321000	MA3 domain-containing protein, putative OS=Plasmodium berghei (strain Anka) OX=5823 GN=PBANKA_1321000 PE=3 SV= 1
PBANKA_1035500		2					-3,13	1,67E-01	2,00		PBANKA_1035500	Vacuolar protein sorting-associated protein 29 OS=Plasmodium berghei (strain Anka) OX=5823 GN=PBANKA_1035500 PE= 3 SV=1
PBANKA_1457800	6	5	6	3		6	-1,26	1,67E-01	5,67	4,50	PBANKA_1457800	ADP-ribosylation factor GTPase-activating protein, putative OS=Plasmodium berghei (strain Anka) OX=5823 GN=PBANKA_1457800 PE=4 SV=1
PBANKA_0611600	10	2	2	2	2	2	-1,55	1,68E-01	4,67	2,00	PBANKA_0611600	Ribonucleoside-diphosphate reductase OS=Plasmodium berghei (strain Anka) OX=5823 GN=PBANKA_0611600 PE=3 SV=1
PBANKA_0414400	6	6	6	4	3	4	-1,18	1,70E-01	6,00	3,67	PBANKA_0414400	Formate-nitrite transporter, putative OS=Plasmodium berghei (strain Anka) OX=5823 GN=PBANKA_0414400 PE= 3 SV=1
PBANKA_0919200		1	1				-3,05	1,72E-01	1,00		PBANKA_0919200	Fam-d protein OS=Plasmodium berghei (strain Anka) OX=5823 GN=PBANKA_0919200 PE=4 SV=1
PBANKA_1415100		1	1				-3,05	1,72E-01	1,00		PBANKA_1415100	Choline-phosphate cytidylyltransferase OS= Plasmodium berghei (strain Anka) OX= 5823 GN= PBANKA_1415100 PE=3 SV=1
PBANKA_1228600		1	1				-3,05	1,72E-01	1,00		PBANKA_1228600	Uncharacterized protein OS=Plasmodium berghei (strain Anka) OX=5823 GN=PBANKA_1228600 PE=4 SV=1
PBANKA_1410400	5	7	9	1	8	7	-1,01	1,75E-01	7,00	5,33	PBANKA_1410400	H(+)-transporting two-sector ATPase OS=Plasmodium berghei (strain Anka) OX=5823 GN=PBANKA_1410400 PE=3 SV=1
PBANKA_1351900	4	6	7	2	8	2	-1,19	1,77E-01	5,67	4,00	PBANKA_1351900	60S ribosomal protein L6, putative OS=Plasmodium berghei (strain Anka) OX=5823 GN=PBANKA_1351900 PE=3 SV=1
PBANKA_1320700			2				-2,96	1,78E-01	2,00		PBANKA_1320700	Signal peptide peptidase, putative OS= Plasmodium berghei (strain Anka) OX= 5823 GN= PBANKA_1320700 PE=3 SV=1
PBANKA_0911400			2				-2,96	1,78E-01	2,00		PBANKA_0911400	CLPTM1 domain-containing protein, putative OS=Plasmodium berghei (strain Anka) OX=5823 GN=PBANKA_0911400 PE=3 SV=1
PBANKA_1036600			2				-2,96	1,78E-01	2,00		PBANKA_1036600	Ribonucleoside-diphosphate reductase small chain, putative OS=Plasmodium berghei (strain Anka) OX=5823 GN=PBANKA_1036600 PE=3 SV=1
PBANKA_0707500			2				-2,96	1,78E-01	2,00		PBANKA_0707500	RWD domain-containing protein, putative OS=Plasmodium berghei (strain Anka) OX=5823 GN=PBANKA_0707500 PE=4 SV=1
PBANKA_1334300	2	6	5		6	2	-1,44	1,78E-01	4,33	4,00	PBANKA_1334300	Exported protein 2 OS=Plasmodium berghei (strain Anka) OX=5823 GN=PBANKA_1334300 PE=4 SV=1
PBANKA_1320400	1	1					-2,94	1,79E-01	1,00		PBANKA_1320400	Uncharacterized protein OS=Plasmodium berghei (strain Anka) OX=5823 GN=PBANKA_1320400 PE=4 SV=1
PBANKA_0609900	2	4	7		3	4	-1,46	1,80E-01	4,33	3,50	PBANKA_0609900	Heat shock protein DNAJ homologue Pfj4, putative OS= Plasmodium berghei (strain Anka) OX= 5823 GN= PBANKA_0609900 PE=4 SV=1
PBANKA_1331400	4	5	5	0	4	4	-1,39	1,80E-01	4,67	2,67	PBANKA_1331400	Kelch domain-containing protein, putative OS=Plasmodium berghei (strain Anka) OX=5823 GN=PBANKA_1331400 PE=4 SV=1
PBANKA_1318100	2	2	2			1	-2,62	1,81E-01	2,00	1,00	PBANKA_1318100	Aminopeptidase P, putative OS= Plasmodium berghei (strain Anka) OX=5823 GN= PBANKA_1318100 PE=3 SV=1
PBANKA_0524200	2	2	2			1	-2,62	1,81E-01	2,00	1,00	PBANKA_0524200	Small exported protein OS=Plasmodium berghei (strain Anka) OX=5823 GN=PBANKA_0524200 PE=4 SV=1
PBANKA_1140600	2	2	2			1	-2,62	1,81E-01	2,00	1,00	PBANKA_1140600	DNA-directed RNApolymerases I, II, and III subunit RPABC1, putative OS=Plasmodium berghei (strain Anka) OX=5823 GN=PBANKA_1140600 PE=3 SV=1
PBANKA_0623100	2	2	3		2		-2,33	1,83E-01	2,33	2,00	PBANKA_0623100	Tryptophan-rich protein OS=Plasmodium berghei (strain Anka) OX=5823 GN=PBANKA_0623100 PE=4 SV=1
PBANKA_0717800	6	5	4	5	2	1	-1,33	1,84E-01	5,00	2,67	PBANKA_0717800	Ribosomal protein L15 OS=Plasmodium berghei (strain Anka) OX=5823 GN=PBANKA_0717800 PE=3 SV=1
PBANKA_1331100	1		1				-2,86	1,85E-01	1,00		PBANKA_1331100	Uncharacterized protein OS=Plasmodium berghei (strain Anka) OX=5823 GN=PBANKA_1331100 PE=4 SV=1
PBANKA_0315600	1		1				-2,86	1,85E-01	1,00		PBANKA_0315600	40S ribosomal protein S30 OS= Plasmodium berghei (strain Anka) OX= 5823 GN= PBANKA_0315600 PE=3 SV=1
PBANKA_0720300	1		1				-2,86	1,85E-01	1,00		PBANKA_0720300	Eukaryotic translation initiation factor 3 subunit M OS=Plasmodium berghei (strain Anka) OX=5823 GN=PBANKA_0720300 PE=3 SV=1
PBANKA_1237900	4	5	4		3	4	-1,44	1,88E-01	4,33	3,50	PBANKA_1237900	Mitochondrial-processing peptidase subunit alpha, putative OS=Plasmodium berghei (strain Anka) OX=5823 GN=PBANKA_1237900 PE=4 SV=1
PBANKA_1445800	2	6	4	1	1	4	-1,48	1,91E-01	4,00	2,00	PBANKA_1445800	Ras-related protein Rab-2, putative OS=Plasmodium berghei (strain Anka) OX=5823 GN=PBANKA_1445800 PE=4 SV=1
PBANKA_0931100	2						-2,75	1,93E-01	2,00		PBANKA_0931100	Uncharacterized protein OS=Plasmodium berghei (strain Anka) OX=5823 GN=PBANKA_0931100 PE=4 SV=1
PBANKA_0621300	2						-2,75	1,93E-01	2,00		PBANKA_0621300	Uncharacterized protein OS=Plasmodium berghei (strain Anka) OX=5823 GN=PBANKA_0621300 PE=4 SV=1
PBANKA_0601900	2						-2,75	1,93E-01	2,00		PBANKA_0601900	High mobility group protein B1, putative OS= Plasmodium berghei (strain Anka) OX= 5823 GN= PBANKA_0601900 PE=4 SV=1
PBANKA_0417500	4	4	7	3	4	2	-1,27	1,94E-01	5,00	3,00	PBANKA_0417500	60S ribosomal protein L32, putative OS=Plasmodium berghei (strain Anka) OX=5823 GN=PBANKA_0417500 PE=3 SV=1
PBANKA_0524800	6	7	5	4	4	4	-1,09	1,94E-01	6,00	4,00	PBANKA_0524800	Small exported protein OS=Plasmodium berghei (strain Anka) OX=5823 GN=PBANKA_0524800 PE=4 SV=1
PBANKA_1317400	6	6	5	3	4	4	-1,14	1,98E-01	5,67	3,67	PBANKA_1317400	HSP90 co-chaperone p23, putative OS=Plasmodium berghei (strain Anka) OX=5823 GN=PBANKA_1317400 PE=4 SV=1
PBANKA_0803400	3	1	2	1			-2,52	2,00E-01	2,00	1,00	PBANKA_0803400	40S ribosomal protein S29, putative OS= Plasmodium berghei (strain Anka) OX= 5823 GN= PBANKA_0803400 PE=3 SV=1
PBANKA_1409100	3	1	2	1			-2,52	2,00E-01	2,00	1,00	PBANKA_1409100	Ras-related protein Rab-5B, putative OS=Plasmodium berghei (strain Anka) OX=5823 GN=PBANKA_1409100 PE=4 SV=1
PBANKA_1351800	2	3	3	1	2		-1,94	2,00E-01	2,67	1,50	PBANKA_1351800	26S proteasome regulatory subunit RPN3, putative OS= Plasmodium berghei (strain Anka) OX= 5823 GN= PBANKA_1351800 PE=3 SV=1
PBANKA_0937700	4	2	2		3		-1,98	2,04E-01	2,67	3,00	PBANKA_0937700	60S ribosomal protein L36 OS=Plasmodium berghei (strain Anka) OX=5823 GN=PBANKA_0937700 PE=3 SV=1
PBANKA_0711200	4	2	3			3	-1,84	2,05E-01	3,00	3,00	PBANKA_0711200	Ubiquitin-like domain-containing protein OS= Plasmodium berghei (strain Anka) OX= 5823 GN= PBANKA_0711200 PE=4 SV=1
PBANKA_1012800	2	1	5		2	1	-1,91	2,13E-01	2,67	1,50	PBANKA_1012800	Voltage-dependentanion-selective channel protein, putative OS=Plasmodium berghei (strain Anka) OX=5823 GN=PBANKA_1012800 PE=4 SV=1
PBANKA_0210200	1	3	5	1	2	1	-1,71	2,14E-01	3,00	1,33	PBANKA_0210200	Aspartyl-tRNA synthetase
PBANKA_1116500		3	2			1	-2,49	2,16E-01	2,50	1,00	PBANKA_1116500	Mitochondrial import receptor subunit TOM40, putative OS=Plasmodium berghei (strain Anka) OX=5823 GN=PBANKA_1116500 PE=3 SV=1
PBANKA_0107300	2	5	4	1	3	2	-1,47	2,17E-01	3,67	2,00	PBANKA_0107300	T-complex protein 1 subunit zeta, putative OS=Plasmodium berghei (strain Anka) OX=5823 GN=PBANKA_0107300 PE=3 SV=1
PBANKA_1360100	4	4	6	2	2	4	-1,26	2,17E-01	4,67	2,67	PBANKA_1360100	Nucleoside transporter 1 OS=Plasmodium berghei (strain Anka) OX=5823 GN=PBANKA_1360100 PE=3 SV=1
PBANKA_1101400	10	5	3	2	5	5	-1,06	2,19E-01	6,00	4,00	PBANKA_1101400	Rhoptry-associated protein 2/3 OS=Plasmodium berghei (strain Anka) OX=5823 GN=PBANKA_1101400 PE=4 SV=1
PBANKA_1234200	4	6	6	3	4	4	-1,08	2,30E-01	5,33	3,67	PBANKA_1234200	40S ribosomal protein S24 OS=Plasmodium berghei (strain Anka) OX=5823 GN= PBANKA_1234200 PE=3 SV=1
PBANKA_0309100	1	3	4			3	-1,78	2,30E-01	2,67	3,00	PBANKA_0309100	Eukaryotic peptide chain release factor subunit 1 OS= Plasmodium berghei (strain Anka) OX= 5823 GN= PBANKA_0309100 PE=3 SV=1
PBANKA_1115300	5	2			1	1	-2,08	2,36E-01	3,50	1,00	PBANKA_1115300	Glideosome-associated protein 40, putative OS=Plasmodium berghei (strain Anka) OX=5823 GN=PBANKA_1115300 PE=4 SV=1
PBANKA_0416600	6	2			2	1	-1,81	2,46E-01	4,00	1,50	PBANKA_0416600	Replication protein A1, small OS=Plasmodium berghei (strain Anka) OX=5823 GN=PBANKA_0416600 PE=3 SV=1
PBANKA_0804100	1	1	3	1			-2,35	2,47E-01	1,67	1,00	PBANKA_0804100	Uncharacterized protein OS=Plasmodium berghei (strain Anka) OX=5823 GN=PBANKA_0804100 PE=4 SV=1
PBANKA_1452500	3	6	4		5	4	-1,18	2,54E-01	4,33	4,50	PBANKA_1452500	Uncharacterized protein OS=Plasmodium berghei (strain Anka) OX=5823 GN=PBANKA_1452500 PE=4 SV=1
PBANKA_0209200	5		2		1	1	-2,02	2,55E-01	3,50	1,00	PBANKA_0209200	Parasite-infected erythrocyte surface protein OS=Plasmodium berghei (strain Anka) OX=5823 GN=PBANKA_0209200 PE=4 SV=1
PBANKA_1202000	2	1	2			1	-2,32	2,55E-01	1,67	1,00	PBANKA_1202000	Inner membrane complex protein 1c OS=Plasmodium berghei (strain Anka) OX=5823 GN=PBANKA_1202000 PE=4 SV=1
PBANKA_1223000		1					-2,25	2,56E-01	1,00		PBANKA_1223000	Uncharacterized protein OS=Plasmodium berghei (strain Anka) OX=5823 GN=PBANKA_1223000 PE=4 SV=1
PBANKA_1218400		1					-2,25	2,56E-01	1,00		PBANKA_1218400	Protein transport protein SEC22, putative OS= Plasmodium berghei (strain Anka) OX= 5823 GN= PBANKA_1218400 PE=3 SV=1
PBANKA_1325600		1					-2,25	2,56E-01	1,00		PBANKA_1325600	Valyl-tRNA synthetase
PBANKA_1231500	3	3	5	1	2	3	-1,35	2,57E-01	3,67	2,00	PBANKA_1231500	Ubiquitin carboxyl-terminal hydrolase 2, putative OS= Plasmodium berghei (strain Anka) OX= 5823 GN= PBANKA_1231500 PE=4 SV=1
PBANKA_1445400	4	6	4	1	2	6	-1,12	2,57E-01	4,67	3,00	PBANKA_1445400	Protein transport protein SEC13 OS= Plasmodium berghei (strain Anka) OX= 5823 GN= PBANKA_1445400 PE=3 SV=1
PBANKA_1222900	3	4	3		1	4	-1,44	2,57E-01	3,33	2,50	PBANKA_1222900	26S proteasome regulatory subunit RPN10, putative OS=Plasmodium berghei (strain Anka) OX=5823 GN=PBANKA_1222900 PE=4 SV=1
PBANKA_0601100	2	1	2	1			-2,30	2,59E-01	1,67	1,00	PBANKA_0601100	Mitochondrial phosphate carrier protein, putative OS=Plasmodium berghei (strain Anka) OX=5823 GN=PBANKA_0601100 PE=3 SV=1
PBANKA_1355500			1				-2,13	2,67E-01	1,00		PBANKA_1355500	Casein kinase II subunit beta OS=Plasmodium berghei (strain Anka) OX= 5823 GN=PBANKA_1355500 PE= 3 SV=1
PBANKA_0307000			1				-2,13	2,67E-01	1,00		PBANKA_0307000	60S ribosomal protein L37ae, putative OS=Plasmodium berghei (strain Anka) OX=5823 GN=PBANKA_0307000 PE=3 SV=1
PBANKA_0500741 PBANKA_1000071			1				-2,13	2,67E-01	1,00		PBANKA_0500741 PBANK	Fam-b protein OS=Plasmodium berghei (strain Anka) OX=5823 GN=PBANKA_0500741 PE=4 SV=1
PBANKA_1402000			1				-2,13	2,67E-01	1,00		PBANKA_1402000	Sodium/hydrogen exchanger, putative OS=Plasmodium berghei (strain Anka) OX=5823 GN=PBANKA_1402000 PE=3 SV=1
PBANKA_1132600			1				-2,13	2,67E-01	1,00		PBANKA_1132600	E2 ubiquitin-conjugating enzyme OS=Plasmodium berghei (strain Anka) OX=5823 GN=PBANKA_1132600 PE=3 SV=1
PBANKA_0807000			1				-2,13	2,67E-01	1,00		PBANKA_0807000	DNA-directed RNA polymerase subunit OS=Plasmodium berghei (strain Anka) OX=5823 GN=PBANKA_0807000 PE=3 SV=1
PBANKA_0921400			1				-2,13	2,67E-01	1,00		PBANKA_0921400	Protein phosphatase, putative OS= Plasmodium berghei (strain Anka) OX=5823 GN= PBANKA_0921400 PE=4 SV=1
PBANKA_1409000			1				-2,13	2,67E-01	1,00		PBANKA_1409000	ER membrane protein complex subunit 7, putative OS=Plasmodium berghei (strain Anka) OX=5823 GN=PBANKA_1409000 PE=4 SV=1
PBANKA_0923700			1				-2,13	2,67E-01	1,00		PBANKA_0923700	Ethanolamine kinase, putative OS= Plasmodium berghei (strain Anka) OX=5823 GN= PBANKA_0923700 PE=4 SV=1
PBANKA_1015100			1				-2,13	2,67E-01	1,00		PBANKA_1015100	Uncharacterized protein OS=Plasmodium berghei (strain Anka) OX=5823 GN=PBANKA_1015100 PE=4 SV=1
PBANKA_0804000			1				-2,13	2,67E-01	1,00		PBANKA_0804000	Ribosomal protein L37 OS=Plasmodium berghei (strain Anka) OX=5823 GN=PBANKA_0804000 PE=3 SV=1
PBANKA_0717900			1				-2,13	2,67E-01	1,00		PBANKA_0717900	RNA-binding protein, putative OS=Plasmodium berghei (strain Anka) OX= 5823 GN= PBANKA_0717900 PE=4 SV=1
PBANKA_1301400			1				-2,13	2,67E-01	1,00		PBANKA_1301400	Proteasome subunit alpha type-1, putative OS= Plasmodium berghei (strain Anka) OX= 5823 GN= PBANKA_1301400 PE=3 SV= 1
PBANKA_1131600	2	5	1		2	2	-1,58	2,69E-01	2,67	2,00	PBANKA_1131600	DNA helicase OS=Plasmodium berghei (strain Anka) OX=5823 GN=PBANKA_1131600 PE=3 SV=1
PBANKA_0311000		4	5		2	3	-1,44	2,72E-01	4,50	2,50	PBANKA_0311000	Protein transport protein SEC31, putative OS= Plasmodium berghei (strain Anka) OX= 5823 GN= PBANKA_0311000 PE=3 SV=1
PBANKA_0803600	3	5	4		4	4	-1,19	2,76E-01	4,00	4,00	PBANKA_0803600	Importin-7, putative OS=Plasmodium berghei (strain Anka) OX=5823 GN=PBANKA_0803600 PE=4 SV=1

Table S1: LCMSMS analyses of “Only Schizonts” parasites (raw data). Legends are indicated as well as the overall variability between samples (WT-B3, WT-B6, WT-B8, KO-N, KO-R1 and KO-R4 is visualized using MDS plot.

PBANKA_1358800	1						-1,98	2,82E-01	1,00		PBANKA_1358800	Kinetochore protein SPC25 OS=Plasmodium berghei (strain Anka) OX=5823 GN=PBANKA_1358800 PE=3 SV=1
PBANKA_1425000	2	1	4		2	1	-1,72	2,86E-01	2,33	1,50	PBANKA_1425000	Peptidylprolyl isomerase OS=Plasmodium berghei (strain Anka) OX=5823 GN=PBANKA_1425000 PE=4 SV=1
PBANKA_1126500	2	5	2	1	2	2	-1,40	2,87E-01	3,00	1,67	PBANKA_1126500	Acetyl-CoA synthetase, putative OS=Plasmodium berghei (strain Anka) OX=5823 GN=PBANKA_1126500 PE=3 SV=1
PBANKA_0506100	3	4	1		2	2	-1,53	2,88E-01	2,67	2,00	PBANKA_0506100	PHAX domain-containing protein, putative OS=Plasmodium berghei (strain Anka) OX=5823 GN=PBANKA_0506100 PE=4 SV=1
PBANKA_0105400	3	4	3		3	3	-1,31	2,92E-01	3,33	3,00	PBANKA_0105400	Coatomer alpha subunit, putative OS=Plasmodium berghei (strain Anka) OX=5823 GN=PBANKA_0105400 PE=4 SV=1
PBANKA_1138200		3	2		2		-2,01	2,93E-01	2,50	2,00	PBANKA_1138200	RuvB-like helicase OS=Plasmodium berghei (strain Anka) OX=5823 GN=PBANKA_1138200 PE=3 SV=1
PBANKA_1315500	1	2	3			2	-1,86	2,97E-01	2,00	2,00	PBANKA_1315500	Sortilin, putative OS=Plasmodium berghei (strain Anka) OX=5823 GN=PBANKA_1315500 PE=4 SV=1
PBANKA_0501100	2	1	1		1		-2,24	2,97E-01	1,33	1,00	PBANKA_0501100	Early transcribed membrane protein OS=Plasmodium berghei (strain Anka) OX=5823 GN=PBANKA_0501100 PE=4 SV=1
PBANKA_0617200	1	3	4	1	1	2	-1,47	3,00E-01	2,67	1,33	PBANKA_0617200	40S ribosomal protein S10, putative OS=Plasmodium berghei (strain Anka) OX=5823 GN=PBANKA_0617200 PE=4 SV=1
PBANKA_1417500		2	2			1	-2,16	3,07E-01	2,00	1,00	PBANKA_1417500	Uncharacterized protein OS=Plasmodium berghei (strain Anka) OX=5823 GN=PBANKA_1417500 PE=4 SV=1
PBANKA_0823900		2	2			1	-2,16	3,07E-01	2,00	1,00	PBANKA_0823900	DNA-directed RNApolymerase II subunit RPB3, putative OS=Plasmodium berghei (strain Anka) OX=5823 GN=PBANKA_0823900 PE=3 SV=1
PBANKA_1413200		2	2			1	-2,16	3,07E-01	2,00	1,00	PBANKA_1413200	PINHSDKMetMAdomain-containing protein, putative OS=Plasmodium berghei (strain Anka) OX=5823 GN=PBANKA_1413200 PE=4 SV=1
PBANKA_1406800	4	5	3	2	3	3	-1,11	3,08E-01	4,00	2,67	PBANKA_1406800	40S ribosomal protein S27, putative OS=Plasmodium berghei (strain Anka) OX=5823 GN=PBANKA_1406800 PE=3 SV=1
PBANKA_1340400	5			1			-2,10	3,09E-01	5,00	1,00	PBANKA_1340400	L-lactate dehydrogenase OS=Plasmodium berghei (strain Anka) OX=5823 GN=PBANKA_1340400 PE=3 SV=1
PBANKA_1449000	5			1			-2,10	3,09E-01	5,00	1,00	PBANKA_1449000	Microgamete surface protein MiGS, putative OS=Plasmodium berghei (strain Anka) OX=5823 GN=PBANKA_1449000 PE=4 SV=1
PBANKA_0708000	3	4	3	1	2	3	-1,23	3,15E-01	3,33	2,00	PBANKA_0708000	Protein transport protein SEC23 OS=Plasmodium berghei (strain Anka) OX=5823 GN=PBANKA_0708000 PE=3 SV=1
PBANKA_0924900	3	3	4		2	4	-1,22	3,22E-01	3,33	3,00	PBANKA_0924900	Translation elongation factor EF-1, subunit alpha, putative OS=Plasmodium berghei (strain Anka) OX=5823 GN=PBANKA_0924900 PE=4 SV=1
PBANKA_1323700	1	1	2			1	-2,06	3,34E-01	1,33	1,00	PBANKA_1323700	FYVE and coiled-coil domain-containing protein, putative OS=Plasmodium berghei (strain Anka) OX=5823 GN=PBANKA_1323700 PE=4 SV=1
PBANKA_1216500	9	2	2	1	2	5	-1,04	3,36E-01	4,33	2,67	PBANKA_1216500	Peptidyl-prolyl cis-trans isomerase OS=Plasmodium berghei (strain Anka) OX=5823 GN=PBANKA_1216500 PE=3 SV=1
PBANKA_1446500	1	4	6	1		6	-1,07	3,39E-01	3,67	3,50	PBANKA_1446500	Asparagine-rich protein, putative OS=Plasmodium berghei (strain Anka) OX=5823 GN=PBANKA_1446500 PE=4 SV=1
PBANKA_0518700	2	3	3		3	2	-1,28	3,54E-01	2,67	2,50	PBANKA_0518700	Methionine--tRNA ligase
PBANKA_0103900		2	1		1		-2,05	3,56E-01	1,50	1,00	PBANKA_0103900	RNA-binding protein, putative OS=Plasmodium berghei (strain Anka) OX=5823 GN=PBANKA_0103900 PE=4 SV=1
PBANKA_1225800	2		2	1			-1,92	3,66E-01	2,00	1,00	PBANKA_1225800	Peptidyl-prolyl cis-trans isomerase OS=Plasmodium berghei (strain Anka) OX=5823 GN=PBANKA_1225800 PE=3 SV=1
PBANKA_0610400		4	2		4		-1,44	3,69E-01	3,00	4,00	PBANKA_0610400	Non-SERCA-type Ca2+-transporting P-ATPase, putative OS=Plasmodium berghei (strain Anka) OX=5823 GN=PBANKA_0610400 PE=4 SV=1
PBANKA_1345800		1	2		1		-1,99	3,69E-01	1,50	1,00	PBANKA_1345800	RNA-binding protein, putative OS=Plasmodium berghei (strain Anka) OX=5823 GN=PBANKA_1345800 PE=4 SV=1
PBANKA_0934200	2	2	2	1	2		-1,53	3,72E-01	2,00	1,50	PBANKA_0934200	Ubiquitin domain-containing protein DSK2, putative OS=Plasmodium berghei (strain Anka) OX=5823 GN=PBANKA_0934200 PE=4 SV=1
PBANKA_0942800	1	1	1		1		-1,92	3,88E-01	1,00	1,00	PBANKA_0942800	Syntaxin, putative OS=Plasmodium berghei (strain Anka) OX=5823 GN=PBANKA_0942800 PE=4 SV=1
PBANKA_0404600	2	3	4		2	4	-1,10	3,88E-01	3,00	3,00	PBANKA_0404600	Activator of Hsp90 ATPase, putative OS=Plasmodium berghei (strain Anka) OX=5823 GN=PBANKA_0404600 PE=3 SV=1
PBANKA_0401600	2	3	0		0	2	-1,60	3,95E-01	1,67	1,00	PBANKA_0401600	Vesicle-fusing ATPase OS=Plasmodium berghei (strain Anka) OX=5823 GN=PBANKA_0401600 PE=3 SV=1
PBANKA_1014900	1	4	2			4	-1,23	3,98E-01	2,33	4,00	PBANKA_1014900	Coatomer subunit beta, putative OS=Plasmodium berghei (strain Anka) OX=5823 GN=PBANKA_1014900 PE=4 SV=1
PBANKA_1026600	1	3	2			3	-1,37	4,01E-01	2,00	3,00	PBANKA_1026600	Protein SEY1 homolog OS=Plasmodium berghei (strain Anka) OX=5823 GN=PBANKA_1026600 PE=3 SV=1
PBANKA_0408600		2	1			1	-1,79	4,13E-01	1,50	1,00	PBANKA_0408600	Eukaryotic translation initiation factor 3 subunit K OS=Plasmodium berghei (strain Anka) OX=5823 GN=PBANKA_0408600 PE=3 SV=1
PBANKA_0311800	1		4			2	-1,53	4,16E-01	2,50	2,00	PBANKA_0311800	Acyl-CoA synthetase, putative OS=Plasmodium berghei (strain Anka) OX=5823 GN=PBANKA_0311800 PE=4 SV=1
PBANKA_1222300	1	2				1	-1,72	4,32E-01	1,50	1,00	PBANKA_1222300	Coatomer subunit epsilon, putative OS=Plasmodium berghei (strain Anka) OX=5823 GN=PBANKA_1222300 PE=3 SV=1
PBANKA_1312700	3				1		-1,71	4,44E-01	3,00	1,00	PBANKA_1312700	Gamete egress and sporozoite traversal protein OS=Plasmodium berghei (strain Anka) OX=5823 GN=PBANKA_1312700 PE=4 SV=1
PBANKA_1433500	1		2			1	-1,60	4,64E-01	1,50	1,00	PBANKA_1433500	PPPDEpeptidase domain-containing protein, putative OS=Plasmodium berghei (strain Anka) OX=5823 GN=PBANKA_1433500 PE=3 SV=1
PBANKA_1028700	1	3	3	2	2	1	-1,03	4,66E-01	2,33	1,67	PBANKA_1028700	26S proteasome regulatory subunit RPN13, putative OS=Plasmodium berghei (strain Anka) OX=5823 GN=PBANKA_1028700 PE=4 SV=1
PBANKA_0405500	1	2	4	1	2	2	-1,02	4,75E-01	2,33	1,67	PBANKA_0405500	60S ribosomal protein L7, putative OS=Plasmodium berghei (strain Anka) OX=5823 GN=PBANKA_0405500 PE=3 SV=1
PBANKA_0811300	1	3	1		1	2	-1,25	4,84E-01	1,67	1,50	PBANKA_0811300	Exportin-7, putative OS=Plasmodium berghei (strain Anka) OX=5823 GN=PBANKA_0811300 PE=4 SV=1
PBANKA_1337100	2		1			1	-1,52	4,86E-01	1,50	1,00	PBANKA_1337100	Splicing factor 1, putative OS=Plasmodium berghei (strain Anka) OX=5823 GN=PBANKA_1337100 PE=4 SV=1
PBANKA_0715500	2	2	2	1	2	1	-1,10	4,89E-01	2,00	1,33	PBANKA_0715500	Phosphoglucomutase-2 OS=Plasmodium berghei (strain Anka) OX=5823 GN=PBANKA_0715500 PE=4 SV=1
PBANKA_0709100	2		1	1			-1,50	4,93E-01	1,50	1,00	PBANKA_0709100	60S ribosomal protein L22, putative OS=Plasmodium berghei (strain Anka) OX=5823 GN=PBANKA_0709100 PE=3 SV=1
PBANKA_1425900	1	2	1			2	-1,30	5,07E-01	1,33	2,00	PBANKA_1425900	Uncharacterized protein OS=Plasmodium berghei (strain Anka) OX=5823 GN=PBANKA_1425900 PE=4 SV=1
PKG PBANKA_1008200		3			2		-1,41	5,07E-01	3,00	2,00	PKG PBANKA_1008200	cGMP-dependent protein kinase OS=Plasmodium berghei (strain Anka) OX=5823 GN=PKG PE=1 SV=1
PBANKA_1315700	3					1	-1,44	5,09E-01	3,00	1,00	PBANKA_1315700	Rhoptry neck protein 2 OS=Plasmodium berghei (strain Anka) OX=5823 GN=PBANKA_1315700 PE=4 SV=1
PBANKA_1137000	3	1			1	1	-1,31	5,15E-01	2,00	1,00	PBANKA_1137000	Bergheilysin OS=Plasmodium berghei (strain Anka) OX=5823 GN=PBANKA_1137000 PE=3 SV=1
PBANKA_0406200		2	1		2		-1,35	5,23E-01	1,50	2,00	PBANKA_0406200	Uncharacterized protein OS=Plasmodium berghei (strain Anka) OX=5823 GN=PBANKA_0406200 PE=4 SV=1
PBANKA_1450700		1	1		1		-1,51	5,25E-01	1,00	1,00	PBANKA_1450700	Clustered-asparagine-rich protein, putative OS=Plasmodium berghei (strain Anka) OX=5823 GN=PBANKA_1450700 PE=4 SV=1
PBANKA_0916100	2	2				2	-1,25	5,27E-01	2,00	2,00	PBANKA_0916100	Nucleic acid binding protein, putative OS=Plasmodium berghei (strain Anka) OX=5823 GN=PBANKA_0916100 PE=4 SV=1
PBANKA_1328100	2	1	2	1	1	1	-1,11	5,35E-01	1,67	1,00	PBANKA_1328100	V-type proton ATPase subunit OS=Plasmodium berghei (strain Anka) OX=5823 GN=PBANKA_1328100 PE=3 SV=1
PBANKA_1241800	3		1	1	1		-1,24	5,36E-01	2,00	1,00	PBANKA_1241800	DNA replication licensing factor MCM3, putative OS=Plasmodium berghei (strain Anka) OX=5823 GN=PBANKA_1241800 PE=3 SV=1
PBANKA_0713100	2	2	1			3	-1,04	5,55E-01	1,67	3,00	PBANKA_0713100	Rhoptry neck protein 5, putative OS=Plasmodium berghei (strain Anka) OX=5823 GN=PBANKA_0713100 PE=4 SV=1
PBANKA_1317500	1	2	2		3	1	-1,01	5,58E-01	1,67	2,00	PBANKA_1317500	Glucose-6-phosphate dehydrogenase 6-phosphogluconolactonase, putative OS=Plasmodium berghei (strain Anka) OX=5823 GN=PBANKA_0713100 PE=4 SV=1
PBANKA_1347800	2	2	1	1		2	-1,03	5,59E-01	1,67	1,50	PBANKA_1347800	20 kDa chaperonin, putative OS=Plasmodium berghei (strain Anka) OX=5823 GN=PBANKA_1347800 PE=3 SV=1
PBANKA_0105200	1		1		1		-1,33	5,73E-01	1,00	1,00	PBANKA_0105200	Polypyrimidine tract-binding protein, putative OS=Plasmodium berghei (strain Anka) OX=5823 GN=PBANKA_0105200 PE=4 SV=1
PBANKA_1308200		1	1			1	-1,23	5,98E-01	1,00	1,00	PBANKA_1308200	1-acyl-sn-glycerol-3-phosphate acyltransferase, putative OS=Plasmodium berghei (strain Anka) OX=5823 GN=PBANKA_1308200 PE=4 SV=1
PBANKA_1345400	2				1		-1,22	6,00E-01	2,00	1,00	PBANKA_1345400	ER lumen protein retaining receptor 1, putative OS=Plasmodium berghei (strain Anka) OX=5823 GN=PBANKA_1345400 PE=3 SV=1
PBANKA_0312400		1	2	1	1		-1,09	6,03E-01	1,50	1,00	PBANKA_0312400	DNA-directed RNA polymerase subunit beta OS=Plasmodium berghei (strain Anka) OX=5823 GN=PBANKA_0312400 PE=3 SV=1
PBANKA_0405300	1	1				1	-1,12	6,29E-01	1,00	1,00	PBANKA_0405300	40S ribosomal protein S23, putative OS=Plasmodium berghei (strain Anka) OX=5823 GN=PBANKA_0405300 PE=3 SV=1
PBANKA_1127800	1	1		1			-1,09	6,37E-01	1,00	1,00	PBANKA_1127800	DnaJ protein, putative OS=Plasmodium berghei (strain Anka) OX=5823 GN=PBANKA_1127800 PE=4 SV=1
PBANKA_0830200	34	26	18	9	28	22	-0,98	3,58E-02	26,00	19,67	PBANKA_0830200	High molecular weight rhoptry protein 2 OS=Plasmodium berghei (strain Anka) OX=5823 GN=PBANKA_0830200 PE=4 SV=1
PBANKA_0711900	222	228	291	157	217	242	-0,80	5,65E-02	247,00	205,33	PBANKA_0711900	Heat shock protein 70 OS=Plasmodium berghei (strain Anka) OX=5823 GN=PBANKA_0711900 PE=3 SV=1
PBANKA_0805700	156	189	193	131	196	233	-0,49	2,43E-01	179,33	186,67	PBANKA_0805700	Heat shock protein 90, putative OS=Plasmodium berghei (strain Anka) OX=5823 GN=PBANKA_0805700 PE=3 SV=1
PBANKA_1133300 PBANKA_1133400	**111**	**146**	**154**	**85**	**135**	**159**	**-0,68**	**1,11E-01**	**137,00**	**126,33**	**PBANKA_1133300 PBANK**	**Elongation factor 1-alpha**
PBANKA_0818900	110	100	102	95	92	100	-0,61	1,53E-01	104,00	95,67	PBANKA_0818900	Endoplasmic reticulum chaperone BiP, putative OS=Plasmodium berghei (strain Anka) OX=5823 GN=PBANKA_0818900 PE=3 SV=1
PBANKA_1459300	**105**	**107**	**106**	**63**	**99**	**110**	**-0,76**	**7,48E-02**	**106,00**	**90,67**	**PBANKA_1459300**	**Actin I**
PBANKA_0823400	79	91	105	60	84	85	-0,81	5,94E-02	91,67	76,33	PBANKA_0823400	Phosphoglycerate kinase OS=Plasmodium berghei (strain Anka) OX=5823 GN=PBANKA_0823400 PE=3 SV=1
PBANKA_1206900	54	38	38	71	71	49	0,06	8,86E-01	43,33	63,67	PBANKA_1206900	Tubulin beta chain OS=Plasmodium berghei (strain Anka) OX=5823 GN=PBANKA_1206900 PE=3 SV=1
PBANKA_0914400	44	61	68	44	60	61	-0,63	1,48E-01	57,67	55,00	PBANKA_0914400	Heat shock protein 70
PBANKA_0712600	36	34	39	47	63	46	-0,03	9,39E-01	36,33	52,00	PBANKA_0712600	14-3-3 protein OS=Plasmodium berghei (strain Anka) OX=5823 GN=PBANKA_0712600 PE=3 SV=1
PBANKA_1314800	41	42	47	39	49	54	-0,40	3,65E-01	43,33	47,33	PBANKA_1314800	Elongation factor 2, putative OS=Plasmodium berghei (strain Anka) OX=5823 GN=PBANKA_1314800 PE=3 SV=1
PBANKA_1219300	14	27	34	27	40	67	0,29	5,12E-01	25,00	44,67	PBANKA_1219300	Heat shock protein 110, putative OS=Plasmodium berghei (strain Anka) OX=5823 GN=PBANKA_1219300 PE=4 SV=1
PBANKA_1437300	53	33	46	41	44	44	-0,50	2,50E-01	44,00	43,00	PBANKA_1437300	Endoplasmin, putative OS=Plasmodium berghei (strain Anka) OX=5823 GN=PBANKA_1437300 PE=3 SV=1
PBANKA_1214000	53	54	49	38	34	49	-0,85	5,40E-02	52,00	40,33	PBANKA_1214000	Heat shock protein 60, putative OS=Plasmodium berghei (strain Anka) OX=5823 GN=PBANKA_1214000 PE=3 SV=1
PBANKA_1331900	35	34	43	28	46	41	-0,52	2,39E-01	37,33	38,33	PBANKA_1331900	Eukaryotic initiation factor 4a, putative OS=Plasmodium berghei (strain Anka) OX=5823 GN=PBANKA_1331900 PE=3 SV=1
PBANKA_1137800	30	54	39	11	51	52	-0,76	8,33E-02	41,00	38,00	PBANKA_1137800	Glideosome-associated connector OS=Plasmodium berghei (strain Anka) OX=5823 GN=PBANKA_1137800 PE=4 SV=1
PBANKA_0930300	32	39	48	29	46	38	-0,65	1,38E-01	39,67	37,67	PBANKA_0930300	GTP-binding nuclear protein OS=Plasmodium berghei (strain Anka) OX=5823 GN=PBANKA_0930300 PE=3 SV=1
PBANKA_0938400	45	22	34	49	41	18	-0,37	4,07E-01	33,67	36,00	PBANKA_0938400	Endoplasmic reticulum-resident calcium binding protein, putative OS=Plasmodium berghei (strain Anka) OX=5823 GN=PBANKA_0938400 PE=4 SV=1
PBANKA_1423300	39	35	38	32	41	32	-0,63	1,53E-01	37,33	35,00	PBANKA_1423300	DNA/RNA-binding protein Alba 1, putative OS=Plasmodium berghei (strain Anka) OX=5823 GN=PBANKA_1423300 PE=4 SV=1
PBANKA_0405200	18	20	26	27	38	40	0,17	7,03E-01	21,33	35,00	PBANKA_0405200	CCT-beta OS=Plasmodium berghei (strain Anka) OX=5823 GN=PBANKA_0405200 PE=3 SV=1
PBANKA_0610300	33	27	23	27	39	35	-0,24	5,86E-01	27,67	33,67	PBANKA_0610300	Polyubiquitin, putative OS=Plasmodium berghei (strain Anka) OX=5823 GN=PBANKA_0610300 PE=4 SV=1
PBANKA_0941800	31	24	31	25	29	35	-0,44	3,27E-01	28,67	29,67	PBANKA_0941800	Histone H2B OS=Plasmodium berghei (strain Anka) OX=5823 GN=PBANKA_0941800 PE=3 SV=1

Table S1: LCMSMS analyses of “Only Schizonts” parasites (raw data). Legends are indicated as well as the overall variability between samples (WT-B3, WT-B6, WT-B8, KO-N, KO-R1 and KO-R4 is visualized using MDS plot.

PBANKA_1444100	13	23	22	19	31	36	-0,01	9,79E-01	19,33	28,67	PBANKA_1444100	T-complex protein 1 subunit gamma OS=Plasmodium berghei (strain Anka) OX=5823 GN=PBANKA_1444100 PE=3 SV=1
PBANKA_0928100	23	34	40	21	29	35	-0,74	9,46E-02	32,33	28,33	PBANKA_0928100	Phosphoglycerate mutase OS=Plasmodium berghei (strain Anka) OX=5823 GN=PBANKA_0928100 PE=3 SV=1
PBANKA_1238800	20	26	22	14	33	36	-0,30	5,15E-01	22,67	27,67	PBANKA_1238800	Karyopherin beta, putative OS=Plasmodium berghei (strain Anka) OX=5823 GN=PBANKA_1238800 PE=4 SV=1
PBANKA_1217600	29	20	29	27	29	26	-0,42	3,54E-01	26,00	27,33	PBANKA_1217600	Histone H2A
PBANKA_1118600	22	20	14	16	31	33	-0,03	9,55E-01	18,67	26,67	PBANKA_1118600	Cell division cycle protein 48 homologue, putative OS=Plasmodium berghei (strain Anka) OX=5823 GN=PBANKA_1118600 PE=4 SV=1
PBANKA_1214300	**22**	**12**	**6**	**17**	**35**	**24**	**0,40**	**4,14E-01**	**13,33**	**25,33**	**PBANKA_1214300**	**Enolase**
PBANKA_0918000	22	27	25	20	31	23	-0,58	2,02E-01	24,67	24,67	PBANKA_0918000	60S acidic ribosomal protein P0 OS=Plasmodium berghei (strain Anka) OX=5823 GN=PBANKA_0918000 PE=3 SV=1
PBANKA_0916200	19	15	20	15	26	32	-0,08	8,66E-01	18,00	24,33	PBANKA_0916200	CCT-alpha OS=Plasmodium berghei (strain Anka) OX=5823 GN=PBANKA_0916200 PE=3 SV=1
PBANKA_1443300	11	9	6	20	34	17	0,87	9,49E-02	8,67	23,67	PBANKA_1443300	Merozoite surface protein 9, putative OS=Plasmodium berghei (strain Anka) OX=5823 GN=PBANKA_1443300 PE=4 SV=1
PBANKA_1360300	33	30	28	12	26	31	-0,94	3,86E-02	30,33	23,00	PBANKA_1360300	DNA/RNA-binding protein Alba 4, putative OS=Plasmodium berghei (strain Anka) OX=5823 GN=PBANKA_1360300 PE=4 SV=1
PBANKA_1117000	9	8	14	19	31	19	0,57	2,57E-01	10,33	23,00	PBANKA_1117000	Histone H2A OS=Plasmodium berghei (strain Anka) OX=5823 GN=PBANKA_1117000 PE=3 SV=1
PBANKA_0903600	19	22	24	13	22	32	-0,49	2,96E-01	21,67	22,33	PBANKA_0903600	Dynamin-like protein, putative OS=Plasmodium berghei (strain Anka) OX=5823 GN=PBANKA_0903600 PE=3 SV=1
PBANKA_1016700	8	7	14	27	25	15	0,68	1,82E-01	9,67	22,33	PBANKA_1016700	Leucine-rich repeat protein OS=Plasmodium berghei (strain Anka) OX=5823 GN=PBANKA_1016700 PE=4 SV=1
PBANKA_1102200	16	15	18	16	24	25	-0,13	7,95E-01	16,33	21,67	PBANKA_1102200	Merozoite surface protein 8 OS=Plasmodium berghei (strain Anka) OX=5823 GN=PBANKA_1102200 PE=4 SV=1
PBANKA_0819900	7	9	13	27	22	16	0,64	2,13E-01	9,67	21,67	PBANKA_0819900	Nucleosome assembly protein OS=Plasmodium berghei (strain Anka) OX=5823 GN=PBANKA_0819900 PE=3 SV=1
PBANKA_1206600	4	12	10	6	32	26	0,60	2,52E-01	8,67	21,33	PBANKA_1206600	26S protease regulatory subunit 4, putative OS=Plasmodium berghei (strain Anka) OX=5823 GN=PBANKA_1206600 PE=3 SV=1
PBANKA_0522800	26	26	34	20	20	23	-0,95	3,72E-02	28,67	21,00	PBANKA_0522800	40S ribosomal protein S19, putative OS=Plasmodium berghei (strain Anka) OX=5823 GN=PBANKA_0522800 PE=3 SV=1
PBANKA_1034400	24	22	24	18	23	20	-0,73	1,19E-01	23,33	20,33	PBANKA_1034400	Plasmepsin IV OS=Plasmodium berghei (strain Anka) OX=5823 GN=PBANKA_1034400 PE=3 SV=1
PBANKA_0703900	9	14	18	11	24	26	-0,02	9,75E-01	13,67	20,33	PBANKA_0703900	Receptor for activated c kinase, putative OS=Plasmodium berghei (strain Anka) OX=5823 GN=PBANKA_0703900 PE=4 SV=1
PBANKA_1329300	14	21	25	16	19	24	-0,56	2,34E-01	20,00	19,67	PBANKA_1329300	40S ribosomal protein S3, putative OS=Plasmodium berghei (strain Anka) OX=5823 GN=PBANKA_1329300 PE=3 SV=1
PBANKA_1410000	14	20	21	13	25	20	-0,53	2,73E-01	18,33	19,33	PBANKA_1410000	26S protease regulatory subunit 7, putative OS=Plasmodium berghei (strain Anka) OX=5823 GN=PBANKA_1410000 PE=3 SV=1
PBANKA_1446800	16	15	21	12	24	22	-0,40	4,04E-01	17,33	19,33	PBANKA_1446800	60 kDa chaperonin, putative OS=Plasmodium berghei (strain Anka) OX=5823 GN=PBANKA_1446800 PE=3 SV=1
PBANKA_0833000	13	9	17	22	19	17	0,09	8,55E-01	13,00	19,33	PBANKA_0833000	Profilin OS=Plasmodium berghei (strain Anka) OX=5823 GN=PBANKA_0833000 PE=3 SV=1
PBANKA_1116800	15	19	16	16	16	25	-0,32	5,15E-01	16,67	19,00	PBANKA_1116800	Uncharacterized protein OS=Plasmodium berghei (strain Anka) OX=5823 GN=PBANKA_1116800 PE=4 SV=1
PBANKA_0203000	19	14	16	18	29	8	-0,43	3,84E-01	16,33	18,33	PBANKA_0203000	Chromatin assembly factor 1 protein WD40 domain, putative OS=Plasmodium berghei (strain Anka) OX=5823 GN=PBANKA_0203000 PE=4 SV=1
PBANKA_0522700	32	15	11	15	25	13	-0,64	1,88E-01	19,33	17,67	PBANKA_0522700	Tubulin alpha chain OS=Plasmodium berghei (strain Anka) OX=5823 GN=PBANKA_0522700 PE=3 SV=1
PBANKA_1145800	17	17	15	13	20	20	-0,43	3,85E-01	16,33	17,67	PBANKA_1145800	Membrane associated histidine-rich protein 1a OS=Plasmodium berghei (strain Anka) OX=5823 GN=PBANKA_1145800 PE=4 SV=1
PBANKA_0941900	**14**	**15**	**17**	**15**	**15**	**22**	**-0,32**	**5,21E-01**	**15,33**	**17,33**	**PBANKA_0941900**	**Histone H4**
PBANKA_1424300	11	16	14	17	19	16	-0,22	6,67E-01	13,67	17,33	PBANKA_1424300	NPL domain-containing protein OS=Plasmodium berghei (strain Anka) OX=5823 GN=PBANKA_1424300 PE=4 SV=1
PBANKA_0310900	13	13	12	12	15	23	-0,10	8,41E-01	12,67	16,67	PBANKA_0310900	T-complex protein 1 subunit theta, putative OS=Plasmodium berghei (strain Anka) OX=5823 GN=PBANKA_0310900 PE=3 SV=1
PBANKA_1340100	13	13	2	16	17	16	0,29	5,84E-01	9,33	16,33	PBANKA_1340100	L-lactate dehydrogenase OS=Plasmodium berghei (strain Anka) OX=5823 GN=PBANKA_1340100 PE=3 SV=1
PBANKA_1215600	15	21	18	8	23	17	-0,80	1,03E-01	18,00	16,00	PBANKA_1215600	40S ribosomal protein S3a OS=Plasmodium berghei (strain Anka) OX=5823 GN=PBANKA_1215600 PE=3 SV=1
PBANKA_0814200	5	10	7	14	17	17	0,55	3,26E-01	7,33	16,00	PBANKA_0814200	Elongation factor 1-beta, putative OS=Plasmodium berghei (strain Anka) OX=5823 GN=PBANKA_0814200 PE=3 SV=1
PBANKA_1423500	13	16	16	13	19	15	-0,51	3,14E-01	15,00	15,67	PBANKA_1423500	60S ribosomal protein L13-2, putative OS=Plasmodium berghei (strain Anka) OX=5823 GN=PBANKA_1423500 PE=3 SV=1
PBANKA_0922100	16	17	22	17	14	15	-0,75	1,24E-01	18,33	15,33	PBANKA_0922100	40S ribosomal protein S18, putative OS=Plasmodium berghei (strain Anka) OX=5823 GN=PBANKA_0922100 PE=3 SV=1
PBANKA_1400600	16	22	16	6	21	19	-0,85	8,48E-02	18,00	15,33	PBANKA_1400600	Cytoadherence linked asexual protein, putative OS=Plasmodium berghei (strain Anka) OX=5823 GN=PBANKA_1400600 PE=4 SV=1
PBANKA_1135700	15	18	19	12	16	18	-0,71	1,49E-01	17,33	15,33	PBANKA_1135700	CUGBP Elav-like family member 1, putative OS=Plasmodium berghei (strain Anka) OX=5823 GN=PBANKA_1135700 PE=4 SV=1
PBANKA_1033900	13	16	21	12	18	16	-0,68	1,70E-01	16,67	15,33	PBANKA_1033900	40S ribosomal protein S8 OS=Plasmodium berghei (strain Anka) OX=5823 GN=PBANKA_1033900 PE=3 SV=1
PBANKA_1355100	18	18	24	17	13	15	-0,90	6,53E-02	20,00	15,00	PBANKA_1355100	40S ribosomal protein S6, putative OS=Plasmodium berghei (strain Anka) OX=5823 GN=PBANKA_1355100 PE=3 SV=1
PBANKA_0941500	14	11	8	9	20	16	-0,11	8,35E-01	11,00	15,00	PBANKA_0941500	40S ribosomal protein S4 OS=Plasmodium berghei (strain Anka) OX=5823 GN=PBANKA_0941500 PE=3 SV=1
PBANKA_1204400	16	16	16	13	15	15	-0,68	1,79E-01	16,00	14,33	PBANKA_1204400	DNA/RNA-binding protein Alba 3, putative OS=Plasmodium berghei (strain Anka) OX=5823 GN=PBANKA_1204400 PE=4 SV=1
PBANKA_0604300	13	12	19	17	15	11	-0,54	2,87E-01	14,67	14,33	PBANKA_0604300	Tetratricopeptide repeat protein, putative OS=Plasmodium berghei (strain Anka) OX=5823 GN=PBANKA_0604300 PE=3 SV=1
PBANKA_1231000	14	15	15	12	13	18	-0,54	2,93E-01	14,67	14,33	PBANKA_1231000	40S ribosomal protein S11, putative OS=Plasmodium berghei (strain Anka) OX=5823 GN=PBANKA_1231000 PE=3 SV=1
PBANKA_1303800	9	14	11	8	16	19	-0,24	6,53E-01	11,33	14,33	PBANKA_1303800	Triosephosphate isomerase OS=Plasmodium berghei (strain Anka) OX=5823 GN=PBANKA_1303800 PE=3 SV=1
PBANKA_0417700	19	9	10	11	19	12	-0,37	4,84E-01	12,67	14,00	PBANKA_0417700	Tubulin alpha chain OS=Plasmodium berghei (strain Anka) OX=5823 GN=PBANKA_0417700 PE=3 SV=1
PBANKA_0406500	12	10	10	8	15	18	-0,17	7,60E-01	10,67	13,67	PBANKA_0406500	T-complex protein 1 subunit eta OS=Plasmodium berghei (strain Anka) OX=5823 GN=PBANKA_0406500 PE=3 SV=1
PBANKA_1404900	10	8	8	8	17	16	0,11	8,47E-01	8,67	13,67	PBANKA_1404900	26S protease regulatory subunit 10B, putative OS=Plasmodium berghei (strain Anka) OX=5823 GN=PBANKA_1404900 PE=3 SV=1
PBANKA_0511900	10	11	14	13	16	11	-0,36	4,96E-01	11,67	13,33	PBANKA_0511900	60S ribosomal protein L3, putative OS=Plasmodium berghei (strain Anka) OX=5823 GN=PBANKA_0511900 PE=3 SV=1
PBANKA_1000600	12	6	15	6	20	14	-0,30	5,86E-01	11,00	13,33	PBANKA_1000600	Erythrocyte membrane antigen 1 OS=Plasmodium berghei (strain Anka) OX=5823 GN=PBANKA_1000600 PE=4 SV=1
PBANKA_1218200	8	4	7	7	17	16	0,54	3,75E-01	6,33	13,33	PBANKA_1218200	CCT-epsilon OS=Plasmodium berghei (strain Anka) OX=5823 GN=PBANKA_1218200 PE=3 SV=1
PBANKA_0306800	15	14	16	8	16	15	-0,76	1,41E-01	15,00	13,00	PBANKA_0306800	ATP-dependent RNA helicase UAP56, putative OS=Plasmodium berghei (strain Anka) OX=5823 GN=PBANKA_0306800 PE=4 SV=1
PBANKA_0917900	6	5	6	8	15	14	0,57	3,67E-01	5,67	12,33	PBANKA_0917900	26S protease regulatory subunit 6A, putative OS=Plasmodium berghei (strain Anka) OX=5823 GN=PBANKA_0917900 PE=3 SV=1
PBANKA_1019500	12	11	16	13	15	8	-0,66	2,13E-01	13,00	12,00	PBANKA_1019500	60S ribosomal protein L5, putative OS=Plasmodium berghei (strain Anka) OX=5823 GN=PBANKA_1019500 PE=3 SV=1
PBANKA_0108800	16	16	15	12	8	15	-0,88	8,90E-02	15,67	11,67	PBANKA_0108800	Histone H3 OS=Plasmodium berghei (strain Anka) OX=5823 GN=PBANKA_0108800 PE=3 SV=1
PBANKA_0505100	8	10	11	8	15	12	-0,31	5,80E-01	9,67	11,67	PBANKA_0505100	ADP-ribosylation factor, putative OS=Plasmodium berghei (strain Anka) OX=5823 GN=PBANKA_0505100 PE=3 SV=1
PBANKA_1032100	13	9	6	7	14	13	-0,24	6,72E-01	9,33	11,33	PBANKA_1032100	Rhoptry-associated protein 1 OS=Plasmodium berghei (strain Anka) OX=5823 GN=PBANKA_1032100 PE=4 SV=1
PBANKA_1134100	8	10	8	4	14	16	-0,20	7,36E-01	8,67	11,33	PBANKA_1134100	T-complex protein 1 subunit delta OS=Plasmodium berghei (strain Anka) OX=5823 GN=PBANKA_1134100 PE=3 SV=1
PBANKA_0201600	19	10	17	13	11	9	-0,93	7,55E-02	15,33	11,00	PBANKA_0201600	Early transcribed membrane protein OS=Plasmodium berghei (strain Anka) OX=5823 GN=PBANKA_0201600 PE=4 SV=1
PBANKA_1423600	13	15	17	10	8	15	-0,92	7,78E-02	15,00	11,00	PBANKA_1423600	40S ribosomal protein S16, putative OS=Plasmodium berghei (strain Anka) OX=5823 GN=PBANKA_1423600 PE=3 SV=1
PBANKA_0623300	12	15	12	4	13	15	-0,86	1,10E-01	13,00	10,67	PBANKA_0623300	Tryptophan-rich protein OS=Plasmodium berghei (strain Anka) OX=5823 GN=PBANKA_0623300 PE=4 SV=1
PBANKA_0807600	14	10	14	10	11	11	-0,74	1,74E-01	12,67	10,67	PBANKA_0807600	40S ribosomal protein S11, putative OS=Plasmodium berghei (strain Anka) OX=5823 GN=PBANKA_0807600 PE=3 SV=1
PBANKA_1461800	5	10	8	6	14	12	-0,15	8,07E-01	7,67	10,67	PBANKA_1461800	26S protease regulatory subunit 8, putative OS=Plasmodium berghei (strain Anka) OX=5823 GN=PBANKA_1461800 PE=3 SV=1
PBANKA_1242300	7	5	9	9	12	11	0,09	8,88E-01	7,00	10,67	PBANKA_1242300	Hsc70-interacting protein, putative OS=Plasmodium berghei (strain Anka) OX=5823 GN=PBANKA_1242300 PE=4 SV=1
PBANKA_1031900	11	12	10	7	15	9	-0,69	2,22E-01	11,00	10,33	PBANKA_1031900	Protein-synthesizing GTPase OS=Plasmodium berghei (strain Anka) OX=5823 GN=PBANKA_1031900 PE=4 SV=1
PBANKA_1359200	8	11	11	6	11	14	-0,51	3,77E-01	10,00	10,33	PBANKA_1359200	DNA/RNA-binding protein Alba 2, putative OS=Plasmodium berghei (strain Anka) OX=5823 GN=PBANKA_1359200 PE=4 SV=1
PBANKA_1338300	7	3	6	10	12	8	0,41	5,54E-01	5,33	10,00	PBANKA_1338300	60S ribosomal protein L6, putative OS=Plasmodium berghei (strain Anka) OX=5823 GN=PBANKA_1338300 PE=3 SV=1
PBANKA_1122900	4	5	3	10	12	8	0,75	3,05E-01	4,00	10,00	PBANKA_1122900	Phosphotransferase OS=Plasmodium berghei (strain Anka) OX=5823 GN=PBANKA_1122900 PE=3 SV=1
PBANKA_1135100	11	12	11	6	13	10	-0,81	1,53E-01	11,33	9,67	PBANKA_1135100	40S ribosomal protein S15, putative OS=Plasmodium berghei (strain Anka) OX=5823 GN=PBANKA_1135100 PE=3 SV=1
PBANKA_1105400	7	11	11	10	7	12	-0,50	3,93E-01	9,67	9,67	PBANKA_1105400	Small ubiquitin-related modifier, putative OS=Plasmodium berghei (strain Anka) OX=5823 GN=PBANKA_1105400 PE=4 SV=1
PBANKA_1028400	8	5	5	11	5	13	0,30	6,52E-01	6,00	9,67	PBANKA_1028400	60S ribosomal protein L10, putative OS=Plasmodium berghei (strain Anka) OX=5823 GN=PBANKA_1028400 PE=4 SV=1
PBANKA_1428700	11	13	14	3	9	16	-0,97	7,97E-02	12,67	9,33	PBANKA_1428700	Eukaryotic translation initiation factor 3 subunit A OS=Plasmodium berghei (strain Anka) OX=5823 GN=PBANKA_1428700 PE=3 SV=1
PBANKA_0836800	8	11	11	6	13	9	-0,71	2,29E-01	10,00	9,33	PBANKA_0836800	Erythrocyte membrane associated protein 1 OS=Plasmodium berghei (strain Anka) OX=5823 GN=PBANKA_0836800 PE=4 SV=1
PBANKA_1112300	12	7	8	11	7	10	-0,37	5,40E-01	9,00	9,33	PBANKA_1112300	Ras-related protein Rab-1B, putative OS=Plasmodium berghei (strain Anka) OX=5823 GN=PBANKA_1112300 PE=4 SV=1
PBANKA_1329700	6	7	10	6	11	11	-0,28	6,57E-01	7,67	9,33	PBANKA_1329700	26S proteasome regulatory subunit RPN2, putative OS=Plasmodium berghei (strain Anka) OX=5823 GN=PBANKA_1329700 PE=3 SV=1
PBANKA_0404800	16	10	7	8	9	9	-0,81	1,65E-01	11,00	8,67	PBANKA_0404800	Glycerol-3-phosphate dehydrogenase OS=Plasmodium berghei (strain Anka) OX=5823 GN=PBANKA_0404800 PE=3 SV=1
PBANKA_1117100	12	10	9	8	11	7	-0,79	1,82E-01	10,33	8,67	PBANKA_1117100	Histone H3 OS=Plasmodium berghei (strain Anka) OX=5823 GN=PBANKA_1117100 PE=3 SV=1
PBANKA_1022000	7	12	9	9	7	10	-0,62	2,97E-01	9,33	8,67	PBANKA_1022000	40S ribosomal protein S25 OS=Plasmodium berghei (strain Anka) OX=5823 GN=PBANKA_1022000 PE=3 SV=1
PBANKA_0405400	8	9	10	10	11	5	-0,62	3,14E-01	9,00	8,67	PBANKA_0405400	40S ribosomal protein S12 OS=Plasmodium berghei (strain Anka) OX=5823 GN=PBANKA_0405400 PE=3 SV=1
PBANKA_1310800	8	7	11	3	12	10	-0,65	3,03E-01	8,67	8,33	PBANKA_1310800	40S ribosomal protein S5, putative OS=Plasmodium berghei (strain Anka) OX=5823 GN=PBANKA_1310800 PE=3 SV=1
PBANKA_1452600	7	7	10	5	9	11	-0,47	4,55E-01	8,00	8,33	PBANKA_1452600	Calcyclin binding protein, putative OS=Plasmodium berghei (strain Anka) OX=5823 GN=PBANKA_1452600 PE=4 SV=1
PBANKA_0817700	6	9	11	6	10	8	-0,70	2,64E-01	8,67	8,00	PBANKA_0817700	RNA-binding protein musashi, putative OS=Plasmodium berghei (strain Anka) OX=5823 GN=PBANKA_0817700 PE=4 SV=1
PBANKA_1420600	8	6	8	6	12	6	-0,45	4,96E-01	7,33	8,00	PBANKA_1420600	Histone H2B OS=Plasmodium berghei (strain Anka) OX=5823 GN=PBANKA_1420600 PE=3 SV=1

Table S1: LCMSMS analyses of “Only Schizonts” parasites (raw data). Legends are indicated as well as the overall variability between samples (WT-B3, WT-B6, WT-B8, KO-N, KO-R1 and KO-R4 is visualized using MDS plot.

PBANKA_0821700	1	4	3	5	9	10	0,96	2,73E-01	2,67	8,00	PBANKA_0821700	Inosine-5'-monophosphate dehydrogenase OS=Plasmodium berghei (strain Anka) OX=5823 GN=PBANKA_0821700 PE=3 SV=1
PBANKA_1346700	7	10	10	6	8	9	-0,78	2,12E-01	9,00	7,67	PBANKA_1346700	60S ribosomal protein L23, putative OS=Plasmodium berghei (strain Anka) OX=5823 GN=PBANKA_1346700 PE=3 SV=1
PBANKA_1010500	12	7	8	4	10	9	-0,75	2,33E-01	9,00	7,67	PBANKA_1010500	Hsp70/Hsp90 organizing protein, putative OS=Plasmodium berghei (strain Anka) OX=5823 GN=PBANKA_1010500 PE=4 SV=1
PBANKA_1117500	5	8	9	8	9	6	-0,51	4,46E-01	7,33	7,67	PBANKA_1117500	Ribosomal protein L27a, putative OS=Plasmodium berghei (strain Anka) OX=5823 GN=PBANKA_1117500 PE=3 SV=1
PBANKA_0929900	9	5	8	6	7	10	-0,40	5,53E-01	7,33	7,67	PBANKA_0929900	Heat shock protein 90, putative OS=Plasmodium berghei (strain Anka) OX=5823 GN=PBANKA_0929900 PE=3 SV=1
PBANKA_1416300	6	9	12	9	5	8	-0,78	2,13E-01	9,00	7,33	PBANKA_1416300	40S ribosomal protein S19, putative OS=Plasmodium berghei (strain Anka) OX=5823 GN=PBANKA_1416300 PE=3 SV=1
PBANKA_0926700	10	9	8	7	6	9	-0,77	2,24E-01	9,00	7,33	PBANKA_0926700	Exported protein 1 OS=Plasmodium berghei (strain Anka) OX=5823 GN=PBANKA_0926700 PE=4 SV=1
PBANKA_0800400	9	7	8	6	9	7	-0,66	3,20E-01	8,00	7,33	PBANKA_0800400	Uncharacterized protein OS=Plasmodium berghei (strain Anka) OX=5823 GN=PBANKA_0800400 PE=4 SV=1
PBANKA_1239900	7	10	5		11	11	-0,64	3,47E-01	7,33	11,00	PBANKA_1239900	Acyl-CoA synthetase, putative OS=Plasmodium berghei (strain Anka) OX=5823 GN=PBANKA_1239900 PE=4 SV=1
PBANKA_0305000	7	4	1		16	6	0,18	8,36E-01	4,00	11,00	PBANKA_0305000	Serine repeat antigen 2 OS=Plasmodium berghei (strain Anka) OX=5823 GN=PBANKA_0305000 PE=3 SV=1
PBANKA_0906500	7	9	8	7	8	6	-0,74	2,61E-01	8,00	7,00	PBANKA_0906500	60S ribosomal protein L28, putative OS=Plasmodium berghei (strain Anka) OX=5823 GN=PBANKA_0906500 PE=3 SV=1
PBANKA_1456100	9	7	7	7	8	6	-0,64	3,41E-01	7,67	7,00	PBANKA_1456100	40S ribosomal protein S17, putative OS=Plasmodium berghei (strain Anka) OX=5823 GN=PBANKA_1456100 PE=3 SV=1
PBANKA_1305100	7	5	9	6	9	6	-0,54	4,39E-01	7,00	7,00	PBANKA_1305100	60S ribosomal protein L1, putative OS=Plasmodium berghei (strain Anka) OX=5823 GN=PBANKA_1305100 PE=3 SV=1
PBANKA_0316800	6	3	9	6	12	3	-0,38	6,11E-01	6,00	7,00	PBANKA_0316800	Erythrocyte membrane associated protein 2 OS=Plasmodium berghei (strain Anka) OX=5823 GN=PBANKA_0316800 PE=4 SV=1
PBANKA_0510900	7	10	9	6	7	7	-0,92	1,55E-01	8,67	6,67	PBANKA_0510900	40S ribosomal protein SA OS=Plasmodium berghei (strain Anka) OX=5823 GN=PBANKA_0510900 PE=3 SV=1
PBANKA_0912300	6	8	10	3	5	12	-0,76	2,50E-01	8,00	6,67	PBANKA_0912300	Tudor staphylococcal nuclease, putative OS=Plasmodium berghei (strain Anka) OX=5823 GN=PBANKA_0912300 PE=4 SV=1
PBANKA_0402800	1	5	6	1	9	10	0,07	9,29E-01	4,00	6,67	PBANKA_0402800	EH domain-containing protein, putative OS=Plasmodium berghei (strain Anka) OX=5823 GN=PBANKA_0402800 PE=4 SV=1
PBANKA_0715600	4	4	2	3	8	9	0,44	6,25E-01	3,33	6,67	PBANKA_0715600	26S protease regulatory subunit 6B, putative OS=Plasmodium berghei (strain Anka) OX=5823 GN=PBANKA_0715600 PE=3 SV=1
PBANKA_0517000	6	6	15	3	5	11	-0,99	1,25E-01	9,00	6,33	PBANKA_0517000	Early transcribed membrane protein OS=Plasmodium berghei (strain Anka) OX=5823 GN=PBANKA_0517000 PE=4 SV=1
PBANKA_1127700	2	6	12	3	11	5	-0,76	2,94E-01	6,67	6,33	PBANKA_1127700	Nicotinate phosphoribosyltransferase OS=Plasmodium berghei (strain Anka) OX=5823 GN=PBANKA_1127700 PE=3 SV=1
PBANKA_0823100	4	10	6	3	6	10	-0,65	3,62E-01	6,67	6,33	PBANKA_0823100	S-adenosylmethionine synthase OS=Plasmodium berghei (strain Anka) OX=5823 GN=PBANKA_0823100 PE=3 SV=1
PBANKA_0418200	7	7	6	7	8	4	-0,62	3,91E-01	6,67	6,33	PBANKA_0418200	Ras-related protein RAB7, putative OS=Plasmodium berghei (strain Anka) OX=5823 GN=PBANKA_0418200 PE=4 SV=1
PBANKA_1135000	6	8	6	6	6	7	-0,60	4,05E-01	6,67	6,33	PBANKA_1135000	YOP1-like protein, putative OS=Plasmodium berghei (strain Anka) OX=5823 GN=PBANKA_1135000 PE=3 SV=1
PBANKA_1010800	4	6	7	3	4	12	-0,33	6,62E-01	5,67	6,33	PBANKA_1010800	CCR4-associated factor 16, putative OS=Plasmodium berghei (strain Anka) OX=5823 GN=PBANKA_1010800 PE=4 SV=1
PBANKA_1400700	5	5	5	2	11	6	-0,31	7,05E-01	5,00	6,33	PBANKA_1400700	Uncharacterized protein OS=Plasmodium berghei (strain Anka) OX=5823 GN=PBANKA_1400700 PE=4 SV=1
PBANKA_1357200	6	4	2	2	6	11	0,18	8,34E-01	4,00	6,33	PBANKA_1357200	Heat shock protein 110, putative OS=Plasmodium berghei (strain Anka) OX=5823 GN=PBANKA_1357200 PE=4 SV=1
PBANKA_0924400	4	3	4	6	7	6	0,27	7,60E-01	3,67	6,33	PBANKA_0924400	Ribonucloprotein OS=Plasmodium berghei (strain Anka) OX=5823 GN=PBANKA_0924400 PE=3 SV=1
PBANKA_0511400	7	8	4	5	6	7	-0,60	4,21E-01	6,33	6,00	PBANKA_0511400	Peroxiredoxin, putative OS=Plasmodium berghei (strain Anka) OX=5823 GN=PBANKA_0511400 PE=4 SV=1
PBANKA_1113500	9	4	4	9	4	5	-0,30	7,00E-01	5,67	6,00	PBANKA_1113500	Ras-related protein Rab-1A, putative OS=Plasmodium berghei (strain Anka) OX=5823 GN=PBANKA_1113500 PE=4 SV=1
PBANKA_1232100	5	4	6	3	9	6	-0,33	6,90E-01	5,00	6,00	PBANKA_1232100	Serine/arginine-rich splicing factor 1, putative OS=Plasmodium berghei (strain Anka) OX=5823 GN=PBANKA_1232100 PE=4 SV=1
PBANKA_0919100	2	2	3	6	10	2	0,71	4,93E-01	2,33	6,00	PBANKA_0919100	Parasitophorous vacuolar protein 1 OS=Plasmodium berghei (strain Anka) OX=5823 GN=PBANKA_0919100 PE=4 SV=1
PBANKA_1418900	7	4	7	5	3	9	-0,48	5,28E-01	6,00	5,67	PBANKA_1418900	Ras-related protein Rab-11A OS=Plasmodium berghei (strain Anka) OX=5823 GN=PBANKA_1418900 PE=4 SV=1
PBANKA_0614500	3	8	6	6	3	8	-0,50	5,16E-01	5,67	5,67	PBANKA_0614500	Eukaryotic translation initiation factor 3 subunit I OS=Plasmodium berghei (strain Anka) OX=5823 GN=PBANKA_0614500 PE=3 SV=1
PBANKA_0313800	7	6	4	6	5	6	-0,47	5,47E-01	5,67	5,67	PBANKA_0313800	ATP synthase subunit alpha OS=Plasmodium berghei (strain Anka) OX=5823 GN=PBANKA_0313800 PE=3 SV=1
PBANKA_1145900	5	6	7	2	8	6	-0,78	3,25E-01	6,00	5,33	PBANKA_1145900	Membrane associated histidine-rich protein 1b OS=Plasmodium berghei (strain Anka) OX=5823 GN=PBANKA_1145900 PE=4 SV=1
PBANKA_0207000	5	7	5	3	7	6	-0,68	4,00E-01	5,67	5,33	PBANKA_0207000	Calcium-transporting ATPase, putative OS=Plasmodium berghei (strain Anka) OX=5823 GN=PBANKA_0207000 PE=4 SV=1
PBANKA_0823000	3	4	6	4	6	6	-0,25	7,72E-01	4,33	5,33	PBANKA_0823000	Ubiquitin-like protein, putative OS=Plasmodium berghei (strain Anka) OX=5823 GN=PBANKA_0823000 PE=4 SV=1
PBANKA_1205000	3	3	5	5	6	5	0,00	9,99E-01	3,67	5,33	PBANKA_1205000	Single-strand telomeric DNA-binding protein GBP2,putative OS=Plasmodium berghei (strain Anka) OX=5823 GN=PBANKA_1205000 PE=4 SV=1
PBANKA_0107400		3	4		12	4	0,34	7,53E-01	3,50	8,00	PBANKA_0107400	Ornithine aminotransferase OS=Plasmodium berghei (strain Anka) OX=5823 GN=PBANKA_0107400 PE=3 SV=1
PBANKA_1425100	6	7	8	3	4	8	-0,98	1,91E-01	7,00	5,00	PBANKA_1425100	Importin subunit alpha OS=Plasmodium berghei (strain Anka) OX=5823 GN=PBANKA_1425100 PE=3 SV=1
PBANKA_1340300	3	7	8	3	5	7	-0,83	2,95E-01	6,00	5,00	PBANKA_1340300	Phosphoribosylpyrophosphate synthetase, putative OS=Plasmodium berghei (strain Anka) OX=5823 GN=PBANKA_1340300 PE=3 SV=1
PBANKA_1407600	5	7	6	5	4	6	-0,76	3,34E-01	6,00	5,00	PBANKA_1407600	60S ribosomal protein L24, putative OS=Plasmodium berghei (strain Anka) OX=5823 GN=PBANKA_1407600 PE=3 SV=1
PBANKA_0931200	1	6	8		4	11	-0,57	4,98E-01	5,00	7,50	PBANKA_0931200	Heat shock protein 101 OS=Plasmodium berghei (strain Anka) OX=5823 GN=PBANKA_0931200 PE=3 SV=1
PBANKA_1429600		5	8	3	4	8	-0,36	6,78E-01	6,50	5,00	PBANKA_1429600	Prolyl-tRNA synthetase
PBANKA_1349100	6	2	3	7	5	3	0,02	9,87E-01	3,67	5,00	PBANKA_1349100	MSP7-like protein OS=Plasmodium berghei (strain Anka) OX=5823 GN=PBANKA_1349100 PE=4 SV=1
PBANKA_0836200		1	4	4	6	5	0,96	4,13E-01	2,50	5,00	PBANKA_0836200	Uncharacterized protein OS=Plasmodium berghei (strain Anka) OX=5823 GN=PBANKA_0836200 PE=4 SV=1
PBANKA_0617100	6	6	6	5	5	4	-0,87	2,82E-01	6,00	4,67	PBANKA_0617100	60S ribosomal protein L11a, putative OS=Plasmodium berghei (strain Anka) OX=5823 GN=PBANKA_0617100 PE=3 SV=1
PBANKA_1365200	8	5	2	4	4	6	-0,54	5,38E-01	5,00	4,67	PBANKA_1365200	Thioredoxin-related protein, putative OS=Plasmodium berghei (strain Anka) OX=5823 GN=PBANKA_1365200 PE=4 SV=1
PBANKA_0303600	2	5	6	3	5	6	-0,47	6,05E-01	4,33	4,67	PBANKA_0303600	26S proteasome regulatory subunit RPN1, putative OS=Plasmodium berghei (strain Anka) OX=5823 GN=PBANKA_0303600 PE=3 SV=1
PBANKA_1016300		3	4	2	6	6	0,33	7,60E-01	3,50	4,67	PBANKA_1016300	Proliferation-associated protein 2g4, putative OS=Plasmodium berghei (strain Anka) OX=5823 GN=PBANKA_1016300 PE=3 SV=1
PBANKA_0707700	2	1	2	1	4	9	0,98	4,15E-01	1,67	4,67	PBANKA_0707700	Uncharacterized protein OS=Plasmodium berghei (strain Anka) OX=5823 GN=PBANKA_0707700 PE=4 SV=1
PBANKA_1434700	7	5	7	3	2	8	-0,95	2,37E-01	6,33	4,33	PBANKA_1434700	Clathrin heavy chain OS=Plasmodium berghei (strain Anka) OX=5823 GN=PBANKA_1434700 PE=3 SV=1
PBANKA_1229200	3	3	10	4	4	5	-0,80	3,54E-01	5,33	4,33	PBANKA_1229200	60S ribosomal protein L19, putative OS=Plasmodium berghei (strain Anka) OX=5823 GN=PBANKA_1229200 PE=3 SV=1
PBANKA_1301300	8		7	7	4	2	-0,57	5,25E-01	7,50	4,33	PBANKA_1301300	Tailer hitch homolog OS=Plasmodium berghei (strain Anka) OX=5823 GN=PBANKA_1301300 PE=4 SV=1
PBANKA_0922500	4	7	4	1	6	6	-0,82	3,55E-01	5,00	4,33	PBANKA_0922500	Kelch domain-containing protein, putative OS=Plasmodium berghei (strain Anka) OX=5823 GN=PBANKA_0922500 PE=4 SV=1
PBANKA_0919300	4	7	4	4	4	5	-0,74	3,98E-01	5,00	4,33	PBANKA_0919300	Spermidine synthase, putative OS=Plasmodium berghei (strain Anka) OX=5823 GN=PBANKA_0919300 PE=3 SV=1
PBANKA_1110500	3	3	4	3	7	3	-0,24	8,17E-01	3,33	4,33	PBANKA_1110500	Histamine-releasing factor OS=Plasmodium berghei (strain Anka) OX=5823 GN=PBANKA_1110500 PE=3 SV=1
PBANKA_1121700	2	4	2	2	6	5	0,06	9,52E-01	2,67	4,33	PBANKA_1121700	Leucyl-tRNA synthetase
PBANKA_0519100	4		2	5	6	2	0,64	5,97E-01	3,00	4,33	PBANKA_0519100	Uncharacterized protein OS=Plasmodium berghei (strain Anka) OX=5823 GN=PBANKA_0519100 PE=4 SV=1
PBANKA_0410300	5	6	3	4	3	5	-0,70	4,48E-01	4,67	4,00	PBANKA_0410300	26S proteasome regulatory subunit RPN12, putative OS=Plasmodium berghei (strain Anka) OX=5823 GN=PBANKA_0410300 PE=3 SV=1
PBANKA_0404200	6	4	4	2	3	7	-0,66	4,76E-01	4,67	4,00	PBANKA_0404200	Ubiquitin-conjugating enzyme E2, putative OS=Plasmodium berghei (strain Anka) OX=5823 GN=PBANKA_0404200 PE=4 SV=1
PBANKA_0819000	8	3	1	2	4	6	-0,42	6,75E-01	4,00	4,00	PBANKA_0819000	Secreted acid phosphatase, putative OS=Plasmodium berghei (strain Anka) OX=5823 GN=PBANKA_0819000 PE=4 SV=1
PBANKA_1440700	3	4	3		5	7	-0,32	7,58E-01	3,33	6,00	PBANKA_1440700	Ubiquitin-activating enzyme E1, putative OS=Plasmodium berghei (strain Anka) OX=5823 GN=PBANKA_1440700 PE=3 SV=1
PBANKA_1406700		2	2		7	5	0,80	5,49E-01	2,00	6,00	PBANKA_1406700	Carbamoyl phosphate synthetase, putative OS=Plasmodium berghei (strain Anka) OX=5823 GN=PBANKA_1406700 PE=4 SV=1
PBANKA_1426900	4	2	8		5	6	-0,89	3,56E-01	4,67	5,50	PBANKA_1426900	ATP-dependent RNA helicase DBP1, putative OS=Plasmodium berghei (strain Anka) OX=5823 GN=PBANKA_1426900 PE=4 SV=1
PBANKA_1232200	4	4	2	2	3	6	-0,35	7,45E-01	3,33	3,67	PBANKA_1232200	FACT complex subunit OS=Plasmodium berghei (strain Anka) OX=5823 GN=PBANKA_1232200 PE=3 SV=1
PBANKA_0910200		1	7	3	3	5	-0,07	9,53E-01	4,00	3,67	PBANKA_0910200	Protein phosphatase PPM2 OS=Plasmodium berghei (strain Anka) OX=5823 GN=PBANKA_0910200 PE=3 SV=1
PBANKA_1103400	3	1	4	3	4	4	-0,03	9,80E-01	2,67	3,67	PBANKA_1103400	60S ribosomal protein L31, putative OS=Plasmodium berghei (strain Anka) OX=5823 GN=PBANKA_1103400 PE=3 SV=1
PBANKA_0721700			4		5	6	0,81	5,54E-01	4,00	5,50	PBANKA_0721700	Ran-specific GTPase-activating protein 1, putative OS=Plasmodium berghei (strain Anka) OX=5823 GN=PBANKA_0721700 PE=4 SV=1
PBANKA_0401500	3	5	4	1	4	5	-0,84	4,17E-01	4,00	3,33	PBANKA_0401500	Exportin-1, putative OS=Plasmodium berghei (strain Anka) OX=5823 GN=PBANKA_0401500 PE=3 SV=1
PBANKA_1453300	4	2	3	1	4	5	-0,35	7,58E-01	3,00	3,33	PBANKA_1453300	Acyl-CoA synthetase, putative OS=Plasmodium berghei (strain Anka) OX=5823 GN=PBANKA_1453300 PE=4 SV=1
PBANKA_0834400	4	3	3	1	4	4	-0,69	5,45E-01	3,33	3,00	PBANKA_0834400	Mitochondrial-processing peptidase subunit beta, putative OS=Plasmodium berghei (strain Anka) OX=5823 GN=PBANKA_0834400 PE=3 SV=1
PBANKA_0618900		3	5	1	2	6	-0,37	7,51E-01	4,00	3,00	PBANKA_0618900	Rhoptry protein, putative OS=Plasmodium berghei (strain Anka) OX=5823 GN=PBANKA_0618900 PE=4 SV=1
PBANKA_0919000	2	3	3	2	2	5	-0,32	7,90E-01	2,67	3,00	PBANKA_0919000	26S proteasome regulatory subunit RPN7, putative OS=Plasmodium berghei (strain Anka) OX=5823 GN=PBANKA_0919000 PE=4 SV=1
PBANKA_0602700	3	2	2	4	2	3	-0,06	9,58E-01	2,33	3,00	PBANKA_0602700	Nucleosome assembly protein, putative OS=Plasmodium berghei (strain Anka) OX=5823 GN=PBANKA_0602700 PE=3 SV=1
PBANKA_1210800	3	2	1		1	8	0,18	8,88E-01	2,00	4,50	PBANKA_1210800	Hypoxanthine phosphoribosyltransferase OS=Plasmodium berghei (strain Anka) OX=5823 GN=PBANKA_1210800 PE=3 SV=1
PBANKA_0905000	3		2	3	4	2	0,37	7,91E-01	2,50	3,00	PBANKA_0905000	40S ribosomal protein S21 OS=Plasmodium berghei (strain Anka) OX=5823 GN=PBANKA_0905000 PE=3 SV=1
PBANKA_0316000	4			3	2	4	0,84	5,61E-01	4,00	3,00	PBANKA_0316000	Replication factor C subunit 1 OS=Plasmodium berghei (strain Anka) OX=5823 GN=PBANKA_0316000 PE=3 SV=1
PBANKA_0904100	4	4	3	3	3	2	-0,96	3,91E-01	3,67	2,67	PBANKA_0904100	Ras-related protein Rab-6 OS=Plasmodium berghei (strain Anka) OX=5823 GN=PBANKA_0904100 PE=4 SV=1
PBANKA_0101000	2	4	3	1	4	3	-0,79	5,11E-01	3,00	2,67	PBANKA_0101000	MYND-type zinc finger protein, putative OS=Plasmodium berghei (strain Anka) OX=5823 GN=PBANKA_0101000 PE=4 SV=1
PBANKA_0714200	2	2	5	1	3	4	-0,70	5,60E-01	3,00	2,67	PBANKA_0714200	Chaperone protein ClpB1, putative OS=Plasmodium berghei (strain Anka) OX=5823 GN=PBANKA_0714200 PE=4 SV=1
PBANKA_1364200	2	4	2	1	4	3	-0,63	6,14E-01	2,67	2,67	PBANKA_1364200	60S ribosomal protein L17, putative OS=Plasmodium berghei (strain Anka) OX=5823 GN=PBANKA_1364200 PE=3 SV=1

Table S1: LCMSMS analyses of “Only Schizonts” parasites (raw data). Legends are indicated as well as the overall variability between samples (WT-B3, WT-B6, WT-B8, KO-N, KO-R1 and KO-R4 is visualized using MDS plot.

PBANKA_1221600	3	2	2	2	3	3	-0,31	8,13E-01	2,33	2,67	PBANKA_1221600	Cell division cycle ATPase, putative OS=Plasmodium berghei (strain Anka) OX=5823 GN=PBANKA_1221600 PE=4 SV=1
PBANKA_0923600	2	1	3	4	2	2	-0,02	9,84E-01	2,00	2,67	PBANKA_0923600	GrpE protein homolog OS=Plasmodium berghei (strain Anka) OX=5823 GN=PBANKA_0923600 PE=3 SV=1
PBANKA_0212100		1	4		2	6	0,13	9,25E-01	2,50	4,00	PBANKA_0212100	Eukaryotic translation initiation factor 2 subunit alpha OS=Plasmodium berghei (strain Anka) OX=5823 GN=PBANKA_0212100 PE=3 SV=1
PBANKA_0314500	1	2	2	1	3	4	0,09	9,49E-01	1,67	2,67	PBANKA_0314500	40S ribosomal protein S26 OS=Plasmodium berghei (strain Anka) OX=5823 GN=PBANKA_0314500 PE=3 SV=1
PBANKA_0105600		2	2		2	6	0,40	7,84E-01	2,00	4,00	PBANKA_0105600	Translation initiation factor IF-2, putative OS=Plasmodium berghei (strain Anka) OX=5823 GN=PBANKA_0105600 PE=4 SV=1
PBANKA_1463000	4	2	2	2	5		-0,80	5,45E-01	2,67	3,50	PBANKA_1463000	Osmiophilic body protein G377 OS=Plasmodium berghei (strain Anka) OX=5823 GN=PBANKA_1463000 PE=4 SV=1
PBANKA_1359000	3	1	4	2	4	1	-0,74	5,70E-01	2,67	2,33	PBANKA_1359000	Protein transport protein SEC61 subunit alpha, putative OS=Plasmodium berghei (strain Anka) OX=5823 GN=PBANKA_1359000 PE=3 SV=1
PBANKA_0502200	2	2	2		5	2	-0,47	7,41E-01	2,00	3,50	PBANKA_0502200	26S proteasome regulatory subunit p55, putative OS=Plasmodium berghei (strain Anka) OX=5823 GN=PBANKA_0502200 PE=3 SV=1
PBANKA_0404700	2	2	2	2	4	1	-0,39	7,82E-01	2,00	2,33	PBANKA_0404700	Glutaredoxin 1, putative OS=Plasmodium berghei (strain Anka) OX=5823 GN=PBANKA_0404700 PE=4 SV=1
PBANKA_1143600	1	2	2	1	6		-0,32	8,31E-01	1,67	3,50	PBANKA_1143600	Alanine--tRNA ligase
PBANKA_0407600	1		3		2	5	0,31	8,40E-01	2,00	3,50	PBANKA_0407600	Asparagine synthase (glutamine-hydrolyzing) OS=Plasmodium berghei (strain Anka) OX=5823 GN=PBANKA_0407600 PE=4 SV=1
PBANKA_1422400	1		3		5	2	0,11	9,46E-01	2,00	3,50	PBANKA_1422400	Importin subunit beta, putative OS=Plasmodium berghei (strain Anka) OX=5823 GN=PBANKA_1422400 PE=4 SV=1
PBANKA_1221200	2	2	3	1	2	3	-0,72	6,02E-01	2,33	2,00	PBANKA_1221200	60S ribosomal protein L34, putative OS=Plasmodium berghei (strain Anka) OX=5823 GN=PBANKA_1221200 PE=3 SV=1
PBANKA_1364300	3	2	2		2	4	-0,69	6,16E-01	2,33	3,00	PBANKA_1364300	Glycerol kinase OS=Plasmodium berghei (strain Anka) OX=5823 GN=PBANKA_1364300 PE=3 SV=1
PBANKA_1018500	4	1	2	2	2	2	-0,62	6,54E-01	2,33	2,00	PBANKA_1018500	Nascent polypeptide-associated complex subunit beta OS=Plasmodium berghei (strain Anka) OX=5823 GN=PBANKA_1018500 PE=3 SV=1
PBANKA_1452300	2	3	1	2	2	2	-0,52	7,16E-01	2,00	2,00	PBANKA_1452300	DUF4149 domain-containing protein OS=Plasmodium berghei (strain Anka) OX=5823 GN=PBANKA_1452300 PE=4 SV=1
PBANKA_1039600	2		2	1	3	2	0,07	9,69E-01	2,00	2,00	PBANKA_1039600	26S proteasome regulatory subunit RPN6, putative OS=Plasmodium berghei (strain Anka) OX=5823 GN=PBANKA_1039600 PE=3 SV=1
PBANKA_1326300	1	1	2	4	2		0,08	9,61E-01	1,33	3,00	PBANKA_1326300	Cytochrome c1, putative OS=Plasmodium berghei (strain Anka) OX=5823 GN=PBANKA_1326300 PE=4 SV=1
PBANKA_1008800	1	2			4	2	0,22	8,99E-01	1,50	3,00	PBANKA_1008800	Glucose-6-phosphate isomerase OS=Plasmodium berghei (strain Anka) OX=5823 GN=PBANKA_1008800 PE=3 SV=1
PBANKA_1325000	3	3	1	2	2	1	-0,97	4,97E-01	2,33	1,67	PBANKA_1325000	40S ribosomal protein S28e, putative OS=Plasmodium berghei (strain Anka) OX=5823 GN=PBANKA_1325000 PE=3 SV=1
PBANKA_0715200		3	2	2	1	2	-0,54	7,27E-01	2,50	1,67	PBANKA_0715200	Eukaryotic translation initiation factor 3 subunit G OS=Plasmodium berghei (strain Anka) OX=5823 GN=PBANKA_0715200 PE=3 SV=1
PBANKA_1338600		3	2	1		4	-0,47	7,58E-01	2,50	2,50	PBANKA_1338600	60S ribosomal protein L23, putative OS=Plasmodium berghei (strain Anka) OX=5823 GN=PBANKA_1338600 PE=3 SV=1
PBANKA_0605300	2	1	2		2	3	-0,49	7,59E-01	1,67	2,50	PBANKA_0605300	Eukaryotic translation initiation factor 5, putative OS=Plasmodium berghei (strain Anka) OX=5823 GN=PBANKA_0605300 PE=3 SV=1
PBANKA_1356700	1	1	3			5	-0,37	8,09E-01	1,67	5,00	PBANKA_1356700	Kelch protein K13, putative OS=Plasmodium berghei (strain Anka) OX=5823 GN=PBANKA_1356700 PE=4 SV=1
PBANKA_1303300		1	2	2	2	1	0,11	9,49E-01	1,50	1,67	PBANKA_1303300	Cytochrome b-c1 complex subunit Rieske, putative OS=Plasmodium berghei (strain Anka) OX=5823 GN=PBANKA_1303300 PE=3 SV=1
PBANKA_0503600		1	1		4	1	0,40	8,36E-01	1,00	2,50	PBANKA_0503600	60S ribosomal protein L30e, putative OS=Plasmodium berghei (strain Anka) OX=5823 GN=PBANKA_0503600 PE=3 SV=1
PBANKA_1432200	2	2	2	3	1		-0,99	5,28E-01	2,00	2,00	PBANKA_1432200	Male development gene 1 OS=Plasmodium berghei (strain Anka) OX=5823 GN=PBANKA_1432200 PE=4 SV=1
PBANKA_1419100	3	2		1	2	1	-0,81	6,39E-01	2,50	1,33	PBANKA_1419100	Dihydrolipoyllysine-residue succinyltransferase OS=Plasmodium berghei (strain Anka) OX=5823 GN=PBANKA_1419100 PE=3 SV=1
PBANKA_0912700	2	2	1		2	2	-0,86	6,14E-01	1,67	2,00	PBANKA_0912700	3-oxo-5-alpha-steroid 4-dehydrogenase, putative OS=Plasmodium berghei (strain Anka) OX=5823 GN=PBANKA_0912700 PE=3 SV=1
PBANKA_1354500		2	2		4		-0,89	6,31E-01	2,00	4,00	PBANKA_1354500	60S ribosomal protein L18-2, putative OS=Plasmodium berghei (strain Anka) OX=5823 GN=PBANKA_1354500 PE=3 SV=1
PBANKA_1306000	2		2	4			-0,22	8,99E-01	2,00	4,00	PBANKA_1306000	Replication factor A protein 3, putative OS=Plasmodium berghei (strain Anka) OX=5823 GN=PBANKA_1306000 PE=3 SV=1
PBANKA_0937200.2			3		4		-0,43	8,27E-01	3,00	4,00	PBANKA_0937200.2	RNA-binding protein, putative OS=Plasmodium berghei (strain Anka) OX=5823 GN=PBANKA_0937200.2 PE=4 SV=1
PBANKA_1241900			3		2	2	-0,20	9,18E-01	3,00	2,00	PBANKA_1241900	Ubiquitin-conjugating enzyme E2 N, putative OS=Plasmodium berghei (strain Anka) OX=5823 GN=PBANKA_1241900 PE=3 SV=1
CDPK1 PBANKA_0314200	3			1	2	1	0,02	9,93E-01	3,00	1,33	CDPK1 PBANKA_0314200	Calcium-dependent protein kinase 1 OS=Plasmodium berghei (strain Anka) OX=5823 GN=CDPK1 PE=2 SV=1
PBANKA_1029800		2	1		2	2	-0,30	8,78E-01	1,50	2,00	PBANKA_1029800	Glycylpeptide N-tetradecanoyltransferase OS=Plasmodium berghei (strain Anka) OX=5823 GN=PBANKA_1029800 PE=3 SV=1
PBANKA_1228400		1	1		2	2	0,26	8,97E-01	1,00	2,00	PBANKA_1228400	Mannose-6-phosphate isomerase OS=Plasmodium berghei (strain Anka) OX=5823 GN=PBANKA_1228400 PE=3 SV=1
PBANKA_0912100		2	1		2	1	-0,74	7,13E-01	1,50	1,50	PBANKA_0912100	Casein kinase I OS=Plasmodium berghei (strain Anka) OX=5823 GN=PBANKA_0912100 PE=3 SV=1
PBANKA_0316200		1	2	1	1	1	-0,53	7,88E-01	1,50	1,00	PBANKA_0316200	Uncharacterized protein OS=Plasmodium berghei (strain Anka) OX=5823 GN=PBANKA_0316200 PE=4 SV=1
PBANKA_1126400		2	1			3	-0,47	8,10E-01	1,50	3,00	PBANKA_1126400	Transportin, putative OS=Plasmodium berghei (strain Anka) OX=5823 GN=PBANKA_1126400 PE=4 SV=1
PBANKA_0524300	1	1	1		3		-0,77	7,09E-01	1,00	3,00	PBANKA_0524300	Tryptophan-rich protein OS=Plasmodium berghei (strain Anka) OX=5823 GN=PBANKA_0524300 PE=4 SV=1
PBANKA_1306300			2		1	2	0,03	9,88E-01	2,00	1,50	PBANKA_1306300	Uncharacterized protein OS=Plasmodium berghei (strain Anka) OX=5823 GN=PBANKA_1306300 PE=4 SV=1
PBANKA_1434200		1	1		2	1	-0,19	9,34E-01	1,00	1,50	PBANKA_1434200	Arginyl-tRNA synthetase
PBANKA_0940900		1	1			3	0,10	9,63E-01	1,00	3,00	PBANKA_0940900	RuvB-like helicase OS=Plasmodium berghei (strain Anka) OX=5823 GN=PBANKA_0940900 PE=3 SV=1
PBANKA_1200800	1	1		1	1	1	0,07	9,74E-01	1,00	1,00	PBANKA_1200800	Transformer-2 protein homolog beta, putative OS=Plasmodium berghei (strain Anka) OX=5823 GN=PBANKA_1200800 PE=4 SV=1
PBANKA_1456200			1		1	2	0,86	7,04E-01	1,00	1,50	PBANKA_1456200	Rab GDP dissociation inhibitor OS=Plasmodium berghei (strain Anka) OX=5823 GN=PBANKA_1456200 PE=3 SV=1
PBANKA_1347300		1			2	1	0,60	7,85E-01	1,00	1,50	PBANKA_1347300	SAM-dependent RNA methyltransferase, putative OS=Plasmodium berghei (strain Anka) OX=5823 GN=PBANKA_1347300 PE=4 SV=1
PBANKA_1430800	3					2	-0,65	7,49E-01	3,00	2,00	PBANKA_1430800	Thioredoxin peroxidase 2, putative OS=Plasmodium berghei (strain Anka) OX=5823 GN=PBANKA_1430800 PE=3 SV=1
PBANKA_0700561			2		2		-0,73	7,45E-01	2,00	2,00	PBANKA_0700561	Fam-a protein OS=Plasmodium berghei (strain Anka) OX=5823 GN=PBANKA_0700561 PE=4 SV=1
PBANKA_0809100		2				2	-0,49	8,21E-01	2,00	2,00	PBANKA_0809100	Proteasome activator 28 subunit beta, putative OS=Plasmodium berghei (strain Anka) OX=5823 GN=PBANKA_0809100 PE=3 SV=1
PBANKA_0932000	2					2	-0,15	9,40E-01	2,00	2,00	PBANKA_0932000	Rhoptry neck protein 4 OS=Plasmodium berghei (strain Anka) OX=5823 GN=PBANKA_0932000 PE=4 SV=1
PBANKA_1211700	1	1		1		1	-0,31	8,86E-01	1,00	1,00	PBANKA_1211700	Uncharacterized protein OS=Plasmodium berghei (strain Anka) OX=5823 GN=PBANKA_1211700 PE=4 SV=1
PBANKA_1444000	1			1		1	0,67	7,85E-01	1,00	1,00	PBANKA_1444000	Macrophage migration inhibitory factor OS=Plasmodium berghei (strain Anka) OX=5823 GN=PBANKA_1444000 PE=3 SV=1
PBANKA_1459500	1					2	0,65	7,92E-01	1,00	2,00	PBANKA_1459500	Myosin light chain 1, putative OS=Plasmodium berghei (strain Anka) OX=5823 GN=PBANKA_1459500 PE=4 SV=1
PBANKA_0804500			1	2			0,54	8,24E-01	1,00	2,00	PBANKA_0804500	Rhoptry-associated membrane antigen, putative OS=Plasmodium berghei (strain Anka) OX=5823 GN=PBANKA_0804500 PE=4 SV=1
PBANKA_1020100			1	1		1	0,51	8,31E-01	1,00	1,00	PBANKA_1020100	Serine/threonine-protein phosphatase OS=Plasmodium berghei (strain Anka) OX=5823 GN=PBANKA_1020100 PE=3 SV=1
PBANKA_1220300			1	1		1	0,51	8,31E-01	1,00	1,00	PBANKA_1220300	Prodrug activation and resistance esterase, putative OS=Plasmodium berghei (strain Anka) OX=5823 GN=PBANKA_1220300 PE=4 SV=1
PBANKA_1360500			1			2	0,49	8,38E-01	1,00	2,00	PBANKA_1360500	CTP:phosphoethanolamine cytidylyltransferase OS=Plasmodium berghei (strain Anka) OX=5823 GN=PBANKA_1360500 PE=3 SV=1
PBANKA_0834000		1			1	1	0,18	9,36E-01	1,00	1,00	PBANKA_0834000	Calcyclin-binding protein, putative OS=Plasmodium berghei (strain Anka) OX=5823 GN=PBANKA_0834000 PE=4 SV=1
PBANKA_1407800			1		2		0,08	9,66E-01	1,00	1,00	PBANKA_1407800	U4/U6 small nuclear ribonucleoprotein PRP3, putative OS=Plasmodium berghei (strain Anka) OX=5823 GN=PBANKA_1407800 PE=4 SV=1
PBANKA_1338900	2					1	-0,93	6,87E-01	2,00	1,00	PBANKA_1338900	Gliding associated protein with multiple membrane spans 1, putative OS=Plasmodium berghei (strain Anka) OX=5823 GN=PBANKA_1338900 PE=4 SV=1
PBANKA_1033100	2					1	-0,93	6,87E-01	2,00	1,00	PBANKA_1033100	Uncharacterized protein OS=Plasmodium berghei (strain Anka) OX=5823 GN=PBANKA_1033100 PE=4 SV=1
PBANKA_1035400	2					1	-0,93	6,87E-01	2,00	1,00	PBANKA_1035400	Gliding associated protein with multiple membrane spans 3, putative OS=Plasmodium berghei (strain Anka) OX=5823 GN=PBANKA_1035400 PE=4 SV=1
PBANKA_1410300	2			1			-0,89	6,95E-01	2,00	1,00	PBANKA_1410300	M1-family alanyl aminopeptidase, putative OS=Plasmodium berghei (strain Anka) OX=5823 GN=PBANKA_1410300 PE=3 SV=1
PBANKA_1357700		1				1	-0,43	8,57E-01	1,00	1,00	PBANKA_1357700	Aspartate carbamoyltransferase OS=Plasmodium berghei (strain Anka) OX=5823 GN=PBANKA_1357700 PE=3 SV=1
PBANKA_0501051 PBANKA_0524821 PBANKA_10002	1					1	-0,43	8,57E-01	1,00	1,00	PBANKA_0501051 PBANK	Fam-a protein OS=Plasmodium berghei (strain Anka) OX=5823 GN=PBANKA_0501051 PE=4 SV=1
PBANKA_1119300		1		1			-0,40	8,67E-01	1,00	1,00	PBANKA_1119300	ATP synthase-associated protein, putative OS=Plasmodium berghei (strain Anka) OX=5823 GN=PBANKA_1119300 PE=4 SV=1
PBANKA_1128200	1					1	-0,15	9,35E-01	1,00	1,00	PBANKA_1128200	Polyadenylate-binding protein 3, putative OS=Plasmodium berghei (strain Anka) OX=5823 GN=PBANKA_1128200 PE=4 SV=1
PBANKA_0402300	1					1	-0,15	9,35E-01	1,00	1,00	PBANKA_0402300	Dihydrolipoamide acetyltransferase component of pyruvate dehydrogenase complex OS=Plasmodium berghei (strain Anka) OX=5823 GN=PBANKA_0402300 PE=3 SV=1
PBANKA_0206500	1					1	-0,15	9,35E-01	1,00	1,00	PBANKA_0206500	Ras-related protein Rab-5C, putative OS=Plasmodium berghei (strain Anka) OX=5823 GN=PBANKA_0206500 PE=4 SV=1
PBANKA_1458300	1			1			-0,12	9,45E-01	1,00	1,00	PBANKA_1458300	Kinesin-13, putative OS=Plasmodium berghei (strain Anka) OX=5823 GN=PBANKA_1458300 PE=3 SV=1

Table S2: Comparison of amino acid usage in down-regulated proteins (raw data).

Schizonts

	number of aa			%	
	WT>KO	WT=KO		WT>KO	WT=KO
A	1269	2309	A	3,8692563	5,216782
C	426	668	C	1,2988993	1,509229
D	1971	2942	D	6,009696	6,646935
E	2197	3473	E	6,6987834	7,846637
F	1234	1598	F	3,7625393	3,610402
G	1574	2512	G	4,7992194	5,675425
H	581	769	H	1,7715035	1,737421
I	2525	3667	I	7,6988749	8,284946
K	3578	4338	K	10,909534	9,800953
L	2454	3918	L	7,4823917	8,852037
M	631	1048	M	1,9239565	2,367773
N	**3811**	**2994**	**N**	**11,619965**	**6,76442**
P	1096	1386	P	3,3417691	3,131425
Q	1451	1366	Q	4,4241851	3,086238
R	989	1836	R	3,0155197	4,148121
S	2551	2930	S	7,7781504	6,619823
T	1581	2158	T	4,8205629	4,875624
V	1428	2575	V	4,3540568	5,817763
W	190	239	W	0,5793213	0,539979
Y	1260	1535	Y	3,8418148	3,468064
Total aa	**32797**	**44261**			

Blood stages

	number of aa			%	
	WT>KO	KO=WT		WT>KO	KO=WT
A	1350	2624	A	3,3203798	5,047027
C	738	754	C	1,8151409	1,450251
D	2582	3187	D	6,3505337	6,129907
E	3071	3907	E	7,5532491	7,514762
F	1769	1971	F	4,3509273	3,791041
G	1613	2808	G	3,9672389	5,400935
H	696	957	H	1,7118402	1,840703
I	3814	4227	I	9,3806877	8,130253
K	4342	5395	K	10,679325	10,3768
L	3512	4455	L	8,6379064	8,568791
M	855	1148	M	2,1029072	2,208074
N	**4268**	**4048**	**N**	**10,497319**	**7,785963**
P	983	1716	P	2,4177284	3,300571
Q	1239	1594	Q	3,0473708	3,065915
R	1227	1963	R	3,0178563	3,775653
S	2815	3503	S	6,9236067	6,737705
T	1844	2567	T	4,5353928	4,937393
V	1805	2852	V	4,4394707	5,485565
W	265	283	W	0,6517783	0,544325
Y	1870	2032	Y	4,5993408	3,908369
Total aa	**40658**	**51991**			

Table S2: Comparison of amino acid usage in down-regulated proteins (raw data).

Proteome analysis for their content in asparagine							
% of Asn	**number of proteins**						
	T. gondii	***P.vivax***	***P.falciparum***	***P.berghei***	***P.yoelii***	***P.chabaudi***	***P.knowlesi***
2	2747	42	26	27	23	22	40
4	4581	385	133	86	91	93	232
6	876	1695	423	273	278	355	923
8	91	2292	701	514	612	691	1917
10	10	1498	754	833	1169	970	1391
12	9	532	811	985	1436	1152	554
14	3	172	786	1041	1121	994	184
16	3	63	731	727	726	530	56
18	1	16	498	330	355	221	25
20	1	9	287	132	138	100	13
22	0	2	147	57	73	45	4
24	0	1	67	37	34	29	1
26	0	1	49	20	28	12	0
28	0	0	21	11	9	5	0
30	0	0	22	2	2	3	0
32	0	0	14	1	2	0	0
34	0	0	4	0	0	0	0
36	0	0	1	0	0	0	0
38	0	0	0	0	0	0	0
40	0	0	0	0	0	0	0
42	0	0	0	0	0	0	0
44	0	0	1	0	0	0	0
46	0	0	0	0	0	0	0
48	0	0	0	0	0	0	0
50	0	0	0	0	0	0	0

Table S3: LCMSMS analyses of "all blood stages" parasites (raw data). Legends are indicated as well as the overall variability between samples (WT-2, WT-3, WT-4, KO-1, KO-2 and KO-4) is visualized using MDS plot.

Blood stages

Spectral count legend:

# spectra (BASIC Spectral Count)	= 1 spectrum
# spectra (BASIC Spectral Count)	= 2-5 spectra
# spectra (BASIC Spectral Count)	= 6-10 spectra
# spectra (BASIC Spectral Count)	= 11-30 spectra
# spectra (BASIC Spectral Count)	>= 31 spectra

Statistics legend:

8 proteins overexpressed in KO	FC>2
49 proteins underexpressed in KO	FC<0,5
	p.value<0,05

GO Terms/EupathDB function prediction

- DNA Replication/metabolism/synthesis
- Motion & transport
- Chaperones
- Unknown functions
- Translation
- The most expressed stable proteins (100)
- Aminoacyl-tRNA synthetases
- Others

MultiDimentionnal Scaling plot (R)

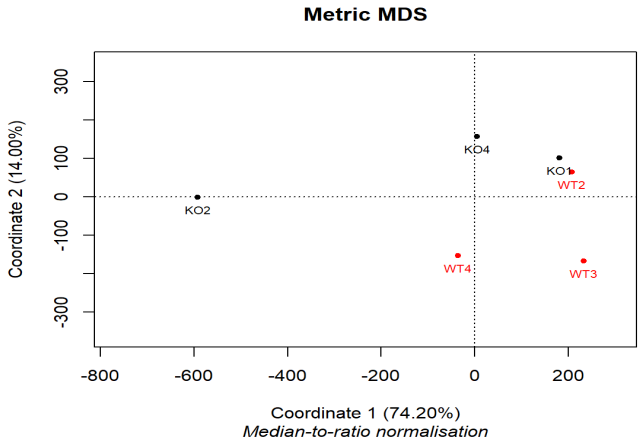

Total number of identified proteins:

accession	WT-2	WT-3	WT-4	KO-1	KO-2	KO-4
Total number of proteins identified by Mascot and validated at FDR<1% by Proline (ProFI consortium)	988	840	1017	617	613	602

Proteins validated at FDR<1% in the UniProtKB-P.berghei database

	Samples						Statistics with R		moy Nb SpC		Annotations	
Accession	KO1	KO2	KO4	WT2	WT3	WT4	LogFC	p.value	KO	WT	gene	gene_product
PBANKA_0915000.1-p1	**9**	**4**	**6**	**0**	**0**	**0**	**5,71**	**1,07E-06**	**6,3**	**0,0**	**PBANKA_0915000**	**apical membrane antigen 1**
PBANKA_1315700.1-p1	7	5	7	1	0	0	3,84	1,21E-05	6,3	0,3	PBANKA_1315700	rhoptry neck protein 2
PBANKA_1032100.1-p1	**25**	**17**	**16**	**7**	**6**	**5**	**1,71**	**1,98E-05**	**19,3**	**6,0**	**PBANKA_1032100**	**rhoptry-associated protein 1**
PBANKA_0601900.1-p1	28	25	35	15	12	15	1,07	1,72E-04	29,3	14,0	PBANKA_0601900	high mobility group protein B1, putative (pathogenesis)
PBANKA_1101400.1-p1	**16**	**9**	**10**	**5**	**4**	**3**	**1,55**	**1,24E-03**	**11,7**	**4,0**	**PBANKA_1101400**	**rhoptry-associated protein 2/3**
PBANKA_1023800.1-p1	3	0	4	0	0	0	4,29	1,29E-02	2,3	0,0	PBANKA_1023800	conserved Plasmodium protein, unknown function
PBANKA_0205200.1-p1	3	5	5	2	1	1	1,63	2,34E-02	4,3	1,3	PBANKA_0205200	conserved Plasmodium protein, unknown function
PBANKA_0941200.1-p1	1	1	3	0	0	0	3,84	3,55E-02	1,7	0,0	PBANKA_0941200	tRNA-splicing ligase RtcB, putative
PBANKA_1010600.1-p1	3	3	4	1	2	0	1,64	5,14E-02	3,3	1,0	PBANKA_1010600	calmodulin, putative
PBANKA_0813500.1-p1	9	5	6	6	2	2	1,02	6,00E-02	6,7	3,3	PBANKA_0813500	SAP domain-containing protein, putative
PBANKA_0510200.1-p1	1	1	5	1	0	0	2,43	6,08E-02	2,3	0,3	PBANKA_0510200	conserved Plasmodium protein, unknown function
PBANKA_1144100.1-p1	8	7	5	6	3	1	1,03	6,17E-02	6,7	3,3	PBANKA_1144100	ABC transporter E family member 1, putative
PBANKA_1337100.1-p1	2	0	2	0	0	0	3,55	6,40E-02	1,3	0,0	PBANKA_1337100	splicing factor 1, putative
PBANKA_1432000.1-p1	2	0	2	0	0	0	3,55	6,40E-02	1,3	0,0	PBANKA_1432000	signal recognition particle subunit SRP19, putative
PBANKA_0939200.1-p1	2	0	2	0	0	0	3,55	6,40E-02	1,3	0,0	PBANKA_0939200	pescadillo homolog, putative
PBANKA_1443300.1-p1	1	11	2	2	0	1	2,13	6,48E-02	4,7	1,0	PBANKA_1443300	merozoite surface protein 9, putative
PBANKA_0831000.1-p1	**36**	**78**	**26**	**26**	**22**	**13**	**1,26**	**7,81E-02**	**46,7**	**20,3**	**PBANKA_0831000**	**merozoite surface protein 1**
PBANKA_1412100.1-p1	2	1	5	1	1	0	1,82	8,26E-02	2,7	0,7	PBANKA_1412100	Maf-like protein, putative
PBANKA_0404000.1-p1	2	2	2	0	0	1	2,23	9,35E-02	2,0	0,3	PBANKA_0404000	conserved Plasmodium protein, unknown function
PBANKA_0519000.1-p1	1	1	1	0	0	0	3,18	1,11E-01	1,0	0,0	PBANKA_0519000	S-antigen, putative
PBANKA_1403800.1-p1	1	1	1	0	0	0	3,18	1,11E-01	1,0	0,0	PBANKA_1403800	translational activator GCN1, putative
PBANKA_0707700.1-p1	1	2	0	0	0	0	3,19	1,17E-01	1,0	0,0	PBANKA_0707700	conserved Plasmodium protein, unknown function
PBANKA_1140400.1-p1	2	0	1	0	0	0	3,18	1,17E-01	1,0	0,0	PBANKA_1140400	exosome complex component RRP45, putative
PBANKA_0102600.1-p1	2	0	1	0	0	0	3,18	1,17E-01	1,0	0,0	PBANKA_0102600	centrosomal protein CEP76, putative
PBANKA_1452100.1-p1	1	0	2	0	0	0	3,17	1,18E-01	1,0	0,0	PBANKA_1452100	conserved Plasmodium protein, unknown function
PBANKA_1130900.1-p1	1	0	2	0	0	0	3,17	1,18E-01	1,0	0,0	PBANKA_1130900	large subunit rRNA methyltransferase, putative
PBANKA_0921400.1-p1	0	1	2	0	0	0	3,17	1,18E-01	1,0	0,0	PBANKA_0921400	protein phosphatase, putative
PBANKA_1207000.1-p1	7	2	8	5	3	0	1,08	1,20E-01	5,7	2,7	PBANKA_1207000	nucleolar protein 5, putative
PBANKA_0943500.1-p1	1	5	1	0	0	2	1,66	1,50E-01	2,3	0,7	PBANKA_0943500	iron-sulfur cluster assembly protein SufD
PBANKA_1347600.1-p1	2	2	1	0	0	1	1,99	1,58E-01	1,7	0,3	PBANKA_1347600	eukaryotic translation initiation factor 6, putative
PBANKA_0939100.1-p1	2	0	3	1	0	0	1,98	1,68E-01	1,7	0,3	PBANKA_0939100	AP2 domain transcription factor, putative
PBANKA_1202000.1-p1	1	1	0	0	0	0	2,68	2,03E-01	0,7	0,0	PBANKA_1202000	inner membrane complex protein 1c
PBANKA_1441500.1-p1	1	1	0	0	0	0	2,68	2,03E-01	0,7	0,0	PBANKA_1441500	U3 small nucleolar RNA-interacting protein 2, putative

Table S3: LCMSMS analyses of “all blood stages” parasites (raw data). Legends are indicated as well as the overall variability between samples (WT-2, WT-3, WT-4, KO-1, KO-2 and KO-4) is visualized using MDS plot.

PBANKA_1220800.1-p1	1	1	0	0	0	0	2,68	2,03E-01	0,7	0,0	PBANKA_1220800	conserved Plasmodium protein, unknown function
PBANKA_0311200.1-p1	1	0	1	0	0	0	2,67	2,04E-01	0,7	0,0	PBANKA_0311200	conserved protein, unknown function
PBANKA_1449900.1-p1	1	0	1	0	0	0	2,67	2,04E-01	0,7	0,0	PBANKA_1449900	CCR4-NOT transcription complex subunit 4, putative
PBANKA_1325300.1-p1	1	0	1	0	0	0	2,67	2,04E-01	0,7	0,0	PBANKA_1325300	splicing factor 3B subunit 2, putative
PBANKA_0905700.1-p1	1	0	1	0	0	0	2,67	2,04E-01	0,7	0,0	PBANKA_0905700	DNA-directed RNA polymerases I and III subunit RPAC1, putative
PBANKA_0100200.1-p1	1	0	1	0	0	0	2,67	2,04E-01	0,7	0,0	PBANKA_0100200	Plasmodium exported protein, unknown function
PBANKA_1002600.1-p1	0	1	1	0	0	0	2,67	2,04E-01	0,7	0,0	PBANKA_1002600	6-cysteine protein P41, putative
PBANKA_1409100.1-p1	0	1	1	0	0	0	2,67	2,04E-01	0,7	0,0	PBANKA_1409100	ras-related protein Rab-5B, putative
PBANKA_1114600.1-p1	0	1	1	0	0	0	2,67	2,04E-01	0,7	0,0	PBANKA_1114600	pre-mRNA-splicing factor CWC2, putative
PBANKA_1345300.1-p1	0	1	1	0	0	0	2,67	2,04E-01	0,7	0,0	PBANKA_1345300	DnaJ protein, putative
PBANKA_1461600.1-p1	3	1	2	1	1	0	1,45	2,09E-01	2,0	0,7	PBANKA_1461600	conserved Plasmodium protein, unknown function
PBANKA_1134800.1-p1	2	0	0	0	0	0	2,68	2,11E-01	0,7	0,0	PBANKA_1134800	zinc finger protein, putative
PBANKA_0804500.1-p1	0	2	0	0	0	0	2,68	2,11E-01	0,7	0,0	PBANKA_0804500	rhoptry-associated membrane antigen, putative
PBANKA_0501400.1-p1	0	2	0	0	0	0	2,68	2,11E-01	0,7	0,0	PBANKA_0501400	rhoptry neck protein 12
PBANKA_1020400.1-p1	0	0	2	0	0	0	2,66	2,12E-01	0,7	0,0	PBANKA_1020400	nucleolar GTP-binding protein 2, putative
PBANKA_1034000.1-p1	0	0	2	0	0	0	2,66	2,12E-01	0,7	0,0	PBANKA_1034000	conserved Plasmodium protein, unknown function
PBANKA_1143000.1-p1	0	0	2	0	0	0	2,66	2,12E-01	0,7	0,0	PBANKA_1143000	U1 small nuclear ribonucleoprotein 70 kDa homolog, putative
PBANKA_1461100.1-p1	0	0	2	0	0	0	2,66	2,12E-01	0,7	0,0	PBANKA_1461100	pre-mRNA-splicing factor RBM22, putative
PBANKA_1004900.1-p1	0	0	2	0	0	0	2,66	2,12E-01	0,7	0,0	PBANKA_1004900	transcription factor, putative
PBANKA_0213500.1-p1	0	0	2	0	0	0	2,66	2,12E-01	0,7	0,0	PBANKA_0213500	ribosome biogenesis protein BRX1, putative
PBANKA_1349000.1-p1	1	5	0	0	1	1	1,45	2,34E-01	2,0	0,7	PBANKA_1349000	MSP7-like protein
PBANKA_1349100.1-p1	2	4	1	1	1	1	1,16	2,36E-01	2,3	1,0	PBANKA_1349100	MSP7-like protein
PBANKA_1303500.1-p1	3	3	0	0	0	2	1,45	2,36E-01	2,0	0,7	PBANKA_1303500	cytochrome c oxidase subunit ApiCOX26, putative
PBANKA_1003300.1-p1	3	2	2	2	1	0	1,16	2,38E-01	2,3	1,0	PBANKA_1003300	TMEM33 domain-containing protein, putative
PBANKA_0714800.1-p1	1	2	1	1	0	0	1,70	2,53E-01	1,3	0,3	PBANKA_0714800	ribosome assembly protein RRB1, putative
PBANKA_1352700.1-p1	1	0	3	1	0	0	1,68	2,69E-01	1,3	0,3	PBANKA_1352700	conserved protein, unknown function
PBANKA_0923500.1-p1	0	0	4	1	0	0	1,67	2,84E-01	1,3	0,3	PBANKA_0923500	ribosome biogenesis regulatory protein, putative
PBANKA_1208700.1-p1	0	0	4	0	0	1	1,66	2,89E-01	1,3	0,3	PBANKA_1208700	succinate dehydrogenase subunit 4, putative
PBANKA_0810600.1-p1	2	1	2	1	1	0	1,20	3,23E-01	1,7	0,7	PBANKA_0810600	exoribonuclease, putative
PBANKA_1404700.1-p1	2	1	2	1	0	1	1,20	3,23E-01	1,7	0,7	PBANKA_1404700	conserved protein, unknown function
PBANKA_1445500.1-p1	2	1	2	1	0	1	1,20	3,23E-01	1,7	0,7	PBANKA_1445500	pre-mRNA-splicing regulator WTAP, putative
PBANKA_0607600.1-p1	3	1	1	2	0	0	1,22	3,29E-01	1,7	0,7	PBANKA_0607600	U6 snRNA-associated Sm-like protein LSm7, putative
PBANKA_0707300.1-p1	2	0	3	1	1	0	1,19	3,40E-01	1,7	0,7	PBANKA_0707300	histone acetyltransferase GCN5, putative
PBANKA_1136300.1-p1	1	0	4	1	1	0	1,18	3,48E-01	1,7	0,7	PBANKA_1136300	RNA-binding protein, putative
PBANKA_0921900.1-p1	1	0	0	0	0	0	1,89	3,74E-01	0,3	0,0	PBANKA_0921900	WD repeat-containing protein, putative
PBANKA_1132000.1-p1	1	0	0	0	0	0	1,89	3,74E-01	0,3	0,0	PBANKA_1132000	NLI interacting factor-like phosphatase
PBANKA_1360200.1-p1	1	0	0	0	0	0	1,89	3,74E-01	0,3	0,0	PBANKA_1360200	conserved Plasmodium protein, unknown function
PBANKA_0933400.1-p1	1	0	0	0	0	0	1,89	3,74E-01	0,3	0,0	PBANKA_0933400	GTPase-activating protein, putative
PBANKA_1040100.1-p1	1	0	0	0	0	0	1,89	3,74E-01	0,3	0,0	PBANKA_1040100	choline kinase
PBANKA_0912200.1-p1	1	0	0	0	0	0	1,89	3,74E-01	0,3	0,0	PBANKA_0912200	signal recognition particle subunit SRP72, putative
PBANKA_1207300.1-p1	1	0	0	0	0	0	1,89	3,74E-01	0,3	0,0	PBANKA_1207300	diphthine methyl ester synthase, putative
PBANKA_1126700.1-p1	1	0	0	0	0	0	1,89	3,74E-01	0,3	0,0	PBANKA_1126700	6-pyruvoyltetrahydropterin synthase, putative
PBANKA_0915600.1-p1	1	0	0	0	0	0	1,89	3,74E-01	0,3	0,0	PBANKA_0915600	aquaglyceroporin
PBANKA_0710300.1-p1	1	0	0	0	0	0	1,89	3,74E-01	0,3	0,0	PBANKA_0710300	protein transport protein YIF1, putative
PBANKA_1031600.1-p1	1	0	0	0	0	0	1,89	3,74E-01	0,3	0,0	PBANKA_1031600	ribosome maturation protein SBDS, putative
PBANKA_1452800.1-p1	1	0	0	0	0	0	1,89	3,74E-01	0,3	0,0	PBANKA_1452800	pre-mRNA-splicing factor CWC22, putative
PBANKA_1134500.1-p1	1	0	0	0	0	0	1,89	3,74E-01	0,3	0,0	PBANKA_1134500	conserved Plasmodium protein, unknown function
PBANKA_0414900.1-p1	1	0	0	0	0	0	1,89	3,74E-01	0,3	0,0	PBANKA_0414900	dynein intermediate light chain, putative
PBANKA_1419200.1-p1	1	0	0	0	0	0	1,89	3,74E-01	0,3	0,0	PBANKA_1419200	RNA-binding protein, putative
PBANKA_0803200.1-p1	1	0	0	0	0	0	1,89	3,74E-01	0,3	0,0	PBANKA_0803200	inositol-phosphate phosphatase, putative
PBANKA_0312800.1-p1	1	0	0	0	0	0	1,89	3,74E-01	0,3	0,0	PBANKA_0312800	conserved Plasmodium protein, unknown function
PBANKA_1031800.1-p1	1	0	0	0	0	0	1,89	3,74E-01	0,3	0,0	PBANKA_1031800	conserved protein, unknown function
PBANKA_1443500.1-p1	1	0	0	0	0	0	1,89	3,74E-01	0,3	0,0	PBANKA_1443500	WD repeat-containing protein, putative
PBANKA_1228600.1-p1	1	0	0	0	0	0	1,89	3,74E-01	0,3	0,0	PBANKA_1228600	conserved protein, unknown function
PBANKA_1223000.1-p1	0	1	0	0	0	0	1,89	3,74E-01	0,3	0,0	PBANKA_1223000	conserved Plasmodium protein, unknown function
PBANKA_0519400.1-p1	0	1	0	0	0	0	1,89	3,74E-01	0,3	0,0	PBANKA_0519400	conserved Plasmodium protein, unknown function
PBANKA_0506300.1-p1	0	1	0	0	0	0	1,89	3,74E-01	0,3	0,0	PBANKA_0506300	methyltransferase, putative
PBANKA_0519100.1-p1	0	1	0	0	0	0	1,89	3,74E-01	0,3	0,0	PBANKA_0519100	conserved Plasmodium protein, unknown function
PBANKA_1007700.1-p1	0	1	0	0	0	0	1,89	3,74E-01	0,3	0,0	PBANKA_1007700	protein phosphatase PPM1
PBANKA_0519200.1-p1	0	1	0	0	0	0	1,89	3,74E-01	0,3	0,0	PBANKA_0519200	conserved Plasmodium protein, unknown function
PBANKA_0713100.1-p1	0	1	0	0	0	0	1,89	3,74E-01	0,3	0,0	PBANKA_0713100	rhoptry neck protein 5
PBANKA_0100600.1-p1	0	1	0	0	0	0	1,89	3,74E-01	0,3	0,0	PBANKA_0100600	schizont membrane associated cytoadherence protein
PBANKA_1306800.1-p1	0	1	0	0	0	0	1,89	3,74E-01	0,3	0,0	PBANKA_1306800	Sec7 domain-containing protein ARFGEF, putative
PBANKA_0814400.1-p1	0	1	0	0	0	0	1,89	3,74E-01	0,3	0,0	PBANKA_0814400	conserved Plasmodium protein, unknown function
PBANKA_0930700.1-p1	0	0	1	0	0	0	1,87	3,75E-01	0,3	0,0	PBANKA_0930700	conserved protein, unknown function
PBANKA_0511200.1-p1	0	0	1	0	0	0	1,87	3,75E-01	0,3	0,0	PBANKA_0511200	U3 small nucleolar ribonucleoprotein protein MPP10, putative
PBANKA_1343000.1-p1	0	0	1	0	0	0	1,87	3,75E-01	0,3	0,0	PBANKA_1343000	ribose-phosphate pyrophosphokinase, putative
PBANKA_1324100.1-p1	0	0	1	0	0	0	1,87	3,75E-01	0,3	0,0	PBANKA_1324100	ubiquitin carboxyl-terminal hydrolase isozyme L3, putative
PBANKA_0814300.1-p1	0	0	1	0	0	0	1,87	3,75E-01	0,3	0,0	PBANKA_0814300	conserved protein, unknown function
PBANKA_1120300.1-p1	0	0	1	0	0	0	1,87	3,75E-01	0,3	0,0	PBANKA_1120300	mRNA-binding protein PUF3, putative
PBANKA_0914200.1-p1	0	0	1	0	0	0	1,87	3,75E-01	0,3	0,0	PBANKA_0914200	conserved Plasmodium protein, unknown function
PBANKA_1424000.1-p1	0	0	1	0	0	0	1,87	3,75E-01	0,3	0,0	PBANKA_1424000	PUB domain-containing protein, putative
PBANKA_1234600.1-p1	0	0	1	0	0	0	1,87	3,75E-01	0,3	0,0	PBANKA_1234600	EELM2 domain-containing protein, putative
PBANKA_0522500.1-p1	0	0	1	0	0	0	1,87	3,75E-01	0,3	0,0	PBANKA_0522500	transmembrane emp24 domain-containing protein, putative
PBANKA_1440400.1-p1	0	0	1	0	0	0	1,87	3,75E-01	0,3	0,0	PBANKA_1440400	small subunit rRNA processing factor, putative
PBANKA_0607700.1-p1	0	0	1	0	0	0	1,87	3,75E-01	0,3	0,0	PBANKA_0607700	telomere repeat-binding zinc finger protein, putative
PBANKA_0717300.1-p1	0	0	1	0	0	0	1,87	3,75E-01	0,3	0,0	PBANKA_0717300	cdc2-related protein kinase 3
PBANKA_0807400.1-p1	0	0	1	0	0	0	1,87	3,75E-01	0,3	0,0	PBANKA_0807400	26S proteasome non-ATPase regulatory subunit 9, putative
PBANKA_0601700.1-p1	0	0	1	0	0	0	1,87	3,75E-01	0,3	0,0	PBANKA_0601700	conserved Plasmodium protein, unknown function
PBANKA_1118200.1-p1	0	0	1	0	0	0	1,87	3,75E-01	0,3	0,0	PBANKA_1118200	conserved protein, unknown function
PBANKA_1324000.1-p1	0	0	1	0	0	0	1,87	3,75E-01	0,3	0,0	PBANKA_1324000	60S ribosomal protein L29, putative
PBANKA_0516900.1-p1	0	0	1	0	0	0	1,87	3,75E-01	0,3	0,0	PBANKA_0516900	S-adenosylmethionine decarboxylase/ornithine decarboxylase, putative

Table S3: LCMSMS analyses of "all blood stages" parasites (raw data). Legends are indicated as well as the overall variability between samples (WT-2, WT-3, WT-4, KO-1, KO-2 and KO-4) is visualized using MDS plot.

PBANKA_1236300.1-p1	0	0	1	0	0	0	1,87	3,75E-01	0,3	0,0	PBANKA_1236300	ATP-dependent RNA helicase DDX1, putative
PBANKA_1131200.1-p1	0	0	1	0	0	0	1,87	3,75E-01	0,3	0,0	PBANKA_1131200	60S ribosomal protein L7-2, putative
PBANKA_1137100.1-p1	0	0	1	0	0	0	1,87	3,75E-01	0,3	0,0	PBANKA_1137100	protein arginine N-methyltransferase 5, putative
PBANKA_0312300.1-p1	0	0	1	0	0	0	1,87	3,75E-01	0,3	0,0	PBANKA_0312300	conserved Plasmodium protein, unknown function
PBANKA_0805100.1-p1	0	0	1	0	0	0	1,87	3,75E-01	0,3	0,0	PBANKA_0805100	ribosomal protein S8e, putative
PBANKA_1315600.1-p1	0	0	1	0	0	0	1,87	3,75E-01	0,3	0,0	PBANKA_1315600	ribosome biogenesis protein TSR1, putative
PBANKA_0823600.1-p1	0	0	1	0	0	0	1,87	3,75E-01	0,3	0,0	PBANKA_0823600	pre-mRNA-splicing factor 18, putative
PBANKA_0701600.1-p1	0	0	1	0	0	0	1,87	3,75E-01	0,3	0,0	PBANKA_0701600	coiled-coil domain-containing protein 124, putative
PBANKA_1313400.1-p1	0	0	1	0	0	0	1,87	3,75E-01	0,3	0,0	PBANKA_1313400	exosome complex exonuclease RRP6, putative
PBANKA_1455200.1-p1	0	0	1	0	0	0	1,87	3,75E-01	0,3	0,0	PBANKA_1455200	ATP-dependent RNA helicase DBP9, putative
PBANKA_0417900.1-p1	0	0	1	0	0	0	1,87	3,75E-01	0,3	0,0	PBANKA_0417900	nucleoporin NUP138
PBANKA_1403400.1-p1	0	0	1	0	0	0	1,87	3,75E-01	0,3	0,0	PBANKA_1403400	DNA-directed RNA polymerase II subunit RPB11, putative
PBANKA_0920400.1-p1	0	0	1	0	0	0	1,87	3,75E-01	0,3	0,0	PBANKA_0920400	conserved Plasmodium protein, unknown function
PBANKA_1405300.1-p1	0	0	1	0	0	0	1,87	3,75E-01	0,3	0,0	PBANKA_1405300	RED-like protein, putative
PBANKA_0605700.1-p1	0	0	1	0	0	0	1,87	3,75E-01	0,3	0,0	PBANKA_0605700	pre-rRNA-processing protein ESF1, putative
PBANKA_0512400.1-p1	0	0	1	0	0	0	1,87	3,75E-01	0,3	0,0	PBANKA_0512400	rRNA-processing protein EBP2, putative
PBANKA_1014600.1-p1	0	0	1	0	0	0	1,87	3,75E-01	0,3	0,0	PBANKA_1014600	serine/threonine protein phosphatase 2A activator, putative
PBANKA_0933000.1-p1	0	0	1	0	0	0	1,87	3,75E-01	0,3	0,0	PBANKA_0933000	cyclin-dependent-like kinase CLK3, putative
PBANKA_0617700.1-p1	0	0	1	0	0	0	1,87	3,75E-01	0,3	0,0	PBANKA_0617700	conserved protein, unknown function
PBANKA_0101900.1-p1	0	0	1	0	0	0	1,87	3,75E-01	0,3	0,0	PBANKA_0101900	RNA-binding protein, putative
PBANKA_1034900.1-p1	0	0	1	0	0	0	1,87	3,75E-01	0,3	0,0	PBANKA_1034900	pre-mRNA-splicing factor 38B, putative
PBANKA_1347500.1-p1	0	0	1	0	0	0	1,87	3,75E-01	0,3	0,0	PBANKA_1347500	ATP-dependent RNA helicase DBP8, putative
PBANKA_1436100.1-p1	0	0	1	0	0	0	1,87	3,75E-01	0,3	0,0	PBANKA_1436100	heterochromatin protein 1
PBANKA_0915300.1-p1	0	0	1	0	0	0	1,87	3,75E-01	0,3	0,0	PBANKA_0915300	conserved Plasmodium protein, unknown function
PBANKA_1233300.1-p1	0	0	1	0	0	0	1,87	3,75E-01	0,3	0,0	PBANKA_1233300	ATP-dependent RNA helicase DDX23, putative
PBANKA_1363000.1-p1	1	1	1	1	0	0	1,32	3,98E-01	1,0	0,3	PBANKA_1363000	small nuclear ribonucleoprotein E, putative
PBANKA_0512500.1-p1	1	1	1	1	0	0	1,32	3,98E-01	1,0	0,3	PBANKA_0512500	ribosome biogenesis protein RPF2, putative
PBANKA_0517400.1-p1	1	1	1	0	1	0	1,31	4,03E-01	1,0	0,3	PBANKA_0517400	pre-mRNA-splicing factor CEF1, putative
PBANKA_1243900.1-p1	1	1	1	0	1	0	1,31	4,03E-01	1,0	0,3	PBANKA_1243900	conserved Plasmodium protein, unknown function
PBANKA_0504900.1-p1	1	1	1	0	0	1	1,31	4,03E-01	1,0	0,3	PBANKA_0504900	N-acetyltransferase, GNAT family, putative
PBANKA_0806100.1-p1	2	0	1	1	0	0	1,32	4,07E-01	1,0	0,3	PBANKA_0806100	CCR4 domain-containing protein 4, putative
PBANKA_0618300.1-p1	2	0	1	1	0	0	1,32	4,07E-01	1,0	0,3	PBANKA_0618300	Ham1-like protein, putative
PBANKA_1036000.1-p1	1	0	2	1	0	0	1,31	4,10E-01	1,0	0,3	PBANKA_1036000	transcription elongation factor SPT6, putative
PBANKA_0811600.1-p1	1	0	2	1	0	0	1,31	4,10E-01	1,0	0,3	PBANKA_0811600	selenide water dikinase, putative
PBANKA_1225000.1-p1	0	2	1	0	1	0	1,31	4,13E-01	1,0	0,3	PBANKA_1225000	serine/threonine protein kinase, FIKK family
PBANKA_1348500.1-p1	1	0	2	0	1	0	1,30	4,15E-01	1,0	0,3	PBANKA_1348500	Voldacs domain-containing protein, putative
PBANKA_0912900.1-p1	0	0	3	1	0	0	1,30	4,24E-01	1,0	0,3	PBANKA_0912900	conserved Plasmodium protein, unknown function
PBANKA_1306200.1-p1	**0**	**0**	**0**	**10**	**11**	**10**	**-6,39**	**6,18E-09**	**0,0**	**10,3**	**PBANKA_1306200**	**tRNA import protein tRIP**
PBANKA_1449000.1-p1	4	9	5	29	37	17	-2,16	8,22E-07	6,0	27,7	PBANKA_1449000	microgamete surface protein MiGS, putative
PBANKA_0803100.1-p1	3	2	4	17	24	10	-2,45	1,26E-06	3,0	17,0	PBANKA_0803100	DNA replication licensing factor MCM7, putative
PBANKA_1340400.1-p1	14	20	11	44	44	35	-1,41	2,31E-06	15,0	41,0	PBANKA_1340400	lactate dehydrogenase, putative
PBANKA_0203000.1-p1	25	28	34	62	79	49	-1,12	5,70E-06	29,0	63,3	PBANKA_0203000	chromatin assembly factor 1 subunit C, putative
PBANKA_1214200.1-p1	2	0	1	10	10	6	-2,94	3,06E-05	1,0	8,7	PBANKA_1214200	ribonucleoside-diphosphate reductase small chain, putative
PBANKA_1032700.1-p1	15	14	11	32	31	31	-1,20	4,47E-05	13,3	31,3	PBANKA_1032700	CUGBP Elav-like family member 2, putative
PBANKA_0314700.1-p1	0	0	0	3	8	2	-5,16	1,57E-04	0,0	4,3	PBANKA_0314700	replication factor C subunit 2, putative
PBANKA_1326800.1-p1	1	1	0	4	9	5	-2,94	1,93E-04	0,7	6,0	PBANKA_1326800	replication factor C subunit 3, putative
PBANKA_1029400.1-p1	4	5	4	17	24	6	-1,80	2,88E-04	4,3	15,7	PBANKA_1029400	conserved Plasmodium protein, unknown function
PBANKA_1131600.1-p1	4	4	2	13	15	8	-1,78	4,43E-04	3,3	12,0	PBANKA_1131600	DNA replication licensing factor MCM6, putative
PBANKA_0610200.1-p1	3	3	0	12	15	7	-2,39	5,21E-04	2,0	11,3	PBANKA_0610200	DNA replication licensing factor MCM5, putative
PBANKA_1026600.1-p1	1	1	1	5	8	5	-2,44	6,32E-04	1,0	6,0	PBANKA_1026600	protein SEY1, putative
PBANKA_0936500.1-p1	1	2	0	7	6	4	-2,33	1,26E-03	1,0	5,7	PBANKA_0936500	replication factor C subunit 5, putative
PBANKA_1427700.1-p1	0	0	0	5	2	3	-4,77	1,33E-03	0,0	3,3	PBANKA_1427700	RuvB-like helicase 1, putative
PBANKA_0615200.1-p1	5	6	1	14	18	9	-1,70	1,40E-03	4,0	13,7	PBANKA_0615200	calcium-dependent protein kinase 4
PBANKA_1355200.1-p1	3	0	0	9	6	5	-2,56	1,54E-03	1,0	6,7	PBANKA_1355200	aconitate hydratase, putative
PBANKA_0828000.1-p1	4	1	1	9	6	9	-1,90	1,65E-03	2,0	8,0	PBANKA_0828000	zinc finger protein, putative
PBANKA_1415600.1-p1	1	3	1	8	9	4	-1,96	1,83E-03	1,7	7,0	PBANKA_1415600	DNA replication licensing factor MCM4, putative
PBANKA_1024900.1-p1	9	6	5	20	27	8	-1,41	1,93E-03	6,7	18,3	PBANKA_1024900	DNA replication licensing factor MCM2, putative
PBANKA_1455100.1-p1	3	1	0	10	11	3	-2,44	1,95E-03	1,3	8,0	PBANKA_1455100	replication factor C subunit 4, putative
PBANKA_1328100.1-p1	5	3	2	17	9	6	-1,58	2,41E-03	3,3	10,7	PBANKA_1328100	ATP synthase (C/AC39) subunit, putative
PBANKA_1241800.1-p1	7	10	4	15	24	12	-1,24	2,95E-03	7,0	17,0	PBANKA_1241800	DNA replication licensing factor MCM3, putative
PBANKA_0836800.1-p1	2	3	4	14	8	6	-1,56	3,08E-03	3,0	9,3	PBANKA_0836800	erythrocyte membrane associated protein 1
PBANKA_0923600.1-p1	2	2	2	6	8	7	-1,74	3,33E-03	2,0	7,0	PBANKA_0923600	GrpE protein homolog, mitochondrial, putative
PBANKA_0925400.1-p1	0	0	0	1	6	2	-4,65	3,39E-03	0,0	3,0	PBANKA_0925400	dynein heavy chain, putative
PBANKA_1034100.1-p1	1	0	0	4	5	2	-3,03	4,28E-03	0,3	3,7	PBANKA_1034100	FANCJ-like helicase, putative
PBANKA_1312700.1-p1	12	8	3	18	20	17	-1,20	4,40E-03	7,7	18,3	PBANKA_1312700	gamete egress and sporozoite traversal protein
PBANKA_1108000.1-p1	0	0	0	3	3	2	-4,47	5,34E-03	0,0	2,7	PBANKA_1108000	conserved protein, unknown function
PBANKA_0916100.1-p1	2	1	2	6	8	4	-1,76	5,77E-03	1,7	6,0	PBANKA_0916100	nucleic acid binding protein, putative
PBANKA_1129100.1-p1	0	0	0	2	5	1	-4,48	6,25E-03	0,0	2,7	PBANKA_1129100	DNA polymerase epsilon catalytic subunit A, putative
PBANKA_1037900.1-p1	0	0	0	2	5	1	-4,48	6,25E-03	0,0	2,7	PBANKA_1037900	conserved Plasmodium protein, unknown function
PBANKA_0416600.1-p1	4	7	7	13	21	7	-1,16	7,70E-03	6,0	13,7	PBANKA_0416600	replication protein A1, small fragment
PBANKA_1011400.1-p1	1	1	4	8	10	2	-1,67	9,35E-03	2,0	6,7	PBANKA_1011400	DNA topoisomerase 2, putative
PBANKA_0416100.1-p1	0	0	0	2	11	2	-5,37	9,53E-03	0,0	5,0	PBANKA_0416100	dynein heavy chain, putative
PBANKA_1006100.1-p1	0	1	2	3	5	5	-1,99	1,02E-02	1,0	4,3	PBANKA_1006100	flap endonuclease 1, putative
PBANKA_0920100.1-p1	0	0	0	6	2	0	-4,44	1,03E-02	0,0	2,7	PBANKA_0920100	prefoldin subunit 5, putative
PBANKA_1317500.1-p1	2	3	3	9	7	6	-1,39	1,06E-02	2,7	7,3	PBANKA_1317500	glucose-6-phosphate dehydrogenase-6-phosphogluconolactonase,
PBANKA_0924300.1-p1	0	0	0	2	4	1	-4,29	1,12E-02	0,0	2,3	PBANKA_0924300	endoplasmic reticulum oxidoreductin, putative
PBANKA_0812000.1-p1	0	0	0	2	4	1	-4,29	1,12E-02	0,0	2,3	PBANKA_0812000	DNA primase large subunit, putative
PBANKA_0824700.1-p1	5	7	5	13	14	10	-1,08	1,14E-02	5,7	12,3	PBANKA_0824700	thioredoxin reductase, putative
PBANKA_1320100.1-p1	0	0	0	2	6	0	-4,48	1,26E-02	0,0	2,7	PBANKA_1320100	conserved Plasmodium protein, unknown function
PBANKA_0313800.1-p1	11	4	6	16	19	9	-1,02	1,32E-02	7,0	14,7	PBANKA_0313800	ATP synthase subunit alpha, mitochondrial, putative
PBANKA_1402600.1-p1	2	1	0	3	9	2	-2,08	1,40E-02	1,0	4,7	PBANKA_1402600	DNA ligase I, putative
PBANKA_1447000.1-p1	2	0	0	4	4	3	-2,24	1,49E-02	0,7	3,7	PBANKA_1447000	cytochrome b5, putative

Table S3: LCMSMS analyses of “all blood stages” parasites (raw data). Legends are indicated as well as the overall variability between samples (WT-2, WT-3, WT-4, KO-1, KO-2 and KO-4) is visualized using MDS plot.

PBANKA_1101600.1-p1	0	0	0	2	5	0	-4,29	1,56E-02	0,0	2,3	PBANKA_1101600	chromatin assembly factor 1 subunit A, putative
PBANKA_1429300.1-p1	1	0	0	2	4	3	-2,76	1,73E-02	0,3	3,0	PBANKA_1429300	integral membrane protein GPR180, putative
PBANKA_0200600.1-p1	0	0	0	2	2	2	-4,08	1,94E-02	0,0	2,0	PBANKA_0200600	fam-a protein
PBANKA_0917400.1-p1	0	0	0	1	3	2	-4,09	2,01E-02	0,0	2,0	PBANKA_0917400	armadillo repeat protein PF16
PBANKA_1417900.1-p1	0	0	0	2	3	1	-4,08	2,03E-02	0,0	2,0	PBANKA_1417900	conserved Plasmodium protein, unknown function
PBANKA_1125300.1-p1	0	0	0	3	2	1	-4,07	2,04E-02	0,0	2,0	PBANKA_1125300	conserved Plasmodium protein, unknown function
PBANKA_1226600.1-p1	0	1	1	2	4	4	-2,13	2,34E-02	0,7	3,3	PBANKA_1226600	tubulin gamma chain, putative
PBANKA_0923200.1-p1	1	0	1	4	5	1	-2,11	2,70E-02	0,7	3,3	PBANKA_0923200	ATP synthase F0 subunit b-like protein, putative
PBANKA_1030500.1-p1	0	1	1	5	4	1	-2,10	2,75E-02	0,7	3,3	PBANKA_1030500	mini-chromosome maintenance complex-binding protein, putative
PBANKA_0507300.1-p1	0	0	0	1	5	0	-4,09	2,91E-02	0,0	2,0	PBANKA_0507300	dynein heavy chain, putative
PBANKA_1411100.1-p1	1	1	1	5	4	2	-1,73	2,93E-02	1,0	3,7	PBANKA_1411100	2-oxoisovalerate dehydrogenase subunit alpha, mitochondrial
PBANKA_1330000.1-p1	0	0	0	1	2	2	-3,84	3,56E-02	0,0	1,7	PBANKA_1330000	enkurin domain-containing protein, putative
PBANKA_1358800.1-p1	0	0	0	2	2	1	-3,83	3,58E-02	0,0	1,7	PBANKA_1358800	kinetochore protein SPC25, putative
PBANKA_1302600.1-p1	0	0	0	2	2	1	-3,83	3,58E-02	0,0	1,7	PBANKA_1302600	DNA primase small subunit, putative
PBANKA_0816200.1-p1	0	0	0	1	3	1	-3,84	3,68E-02	0,0	1,7	PBANKA_0816200	ribonuclease H2 subunit C, putative
PBANKA_1361600.1-p1	0	0	0	1	4	0	-3,84	4,29E-02	0,0	1,7	PBANKA_1361600	E1-E2 ATPase, putative
PBANKA_0713900.1-p1	0	1	1	5	3	1	-1,95	5,07E-02	0,7	3,0	PBANKA_0713900	adenylate kinase 2, putative
PBANKA_0834300.1-p1	0	0	0	1	2	1	-3,54	6,12E-02	0,0	1,3	PBANKA_0834300	gamma-tubulin complex component, putative
PBANKA_1326900.1-p1	0	0	0	1	2	1	-3,54	6,12E-02	0,0	1,3	PBANKA_1326900	DNA polymerase alpha subunit B, putative
PBANKA_0818500.1-p1	0	0	0	1	2	1	-3,54	6,12E-02	0,0	1,3	PBANKA_0818500	conserved protein, unknown function
PBANKA_0706400.1-p1	0	0	0	1	2	1	-3,54	6,12E-02	0,0	1,3	PBANKA_0706400	conserved Plasmodium protein, unknown function
PBANKA_0906900.1-p1	0	0	0	2	1	1	-3,53	6,15E-02	0,0	1,3	PBANKA_0906900	conserved Plasmodium protein, unknown function
PBANKA_0828600.1-p1	2	0	1	6	2	2	-1,58	6,43E-02	1,0	3,3	PBANKA_0828600	cytochrome c oxidase subunit 5B, putative
PBANKA_0707800.1-p1	0	0	0	0	2	2	-3,55	6,60E-02	0,0	1,3	PBANKA_0707800	U5 small nuclear ribonucleoprotein 40 kDa protein, putative
PBANKA_0921600.1-p1	0	0	0	2	2	0	-3,53	6,68E-02	0,0	1,3	PBANKA_0921600	alternative splicing factor SR-MG
PBANKA_1009700.1-p1	0	0	0	0	3	1	-3,55	6,77E-02	0,0	1,3	PBANKA_1009700	ribonuclease H2 subunit B, putative
PBANKA_1122800.1-p1	0	0	0	1	3	0	-3,54	6,81E-02	0,0	1,3	PBANKA_1122800	ribonuclease H2 subunit A, putative
PBANKA_1427200.1-p1	0	0	0	1	3	0	-3,54	6,81E-02	0,0	1,3	PBANKA_1427200	protein phosphatase PPM5
PBANKA_1105500.1-p1	0	0	0	3	0	1	-3,52	6,88E-02	0,0	1,3	PBANKA_1105500	mediator of RNA polymerase II transcription subunit 11, putative
PBANKA_0211300.1-p1	1	0	0	4	3	0	-2,39	7,06E-02	0,3	2,3	PBANKA_0211300	cysteine desulfurase IscS, putative
PBANKA_1326000.1-p1	0	0	1	5	2	0	-2,39	7,16E-02	0,3	2,3	PBANKA_1326000	GTP-binding protein, putative
PBANKA_0506900.1-p1	5	3	0	6	6	7	-1,17	7,49E-02	2,7	6,3	PBANKA_0506900	phospholipid scramblase, putative
PBANKA_0512800.1-p1	6	2	0	8	6	6	-1,23	8,05E-02	2,7	6,7	PBANKA_0512800	merozoite TRAP-like protein
PBANKA_0614000.1-p1	1	0	1	5	2	1	-1,78	8,96E-02	0,7	2,7	PBANKA_0614000	conserved protein, unknown function
PBANKA_0209300.1-p1	2	0	0	4	3	1	-1,78	9,64E-02	0,7	2,7	PBANKA_0209300	actin-related protein
PBANKA_1431500.1-p1	0	1	0	1	3	2	-2,21	1,00E-01	0,3	2,0	PBANKA_1431500	radial spoke head protein 9, putative
PBANKA_0940900.1-p1	2	3	1	5	4	4	-1,04	1,11E-01	2,0	4,3	PBANKA_0940900	RuvB-like helicase 2, putative
PBANKA_1439400.1-p1	2	2	2	3	6	4	-1,06	1,11E-01	2,0	4,3	PBANKA_1439400	histone chaperone ASF1, putative
PBANKA_1217800.1-p1	2	1	3	2	7	4	-1,07	1,11E-01	2,0	4,3	PBANKA_1217800	signal peptidase complex subunit 2, putative
PBANKA_0410400.1-p1	0	0	0	1	1	1	-3,16	1,14E-01	0,0	1,0	PBANKA_0410400	glycogen synthase kinase 3, putative
PBANKA_0942300.1-p1	0	0	0	1	1	1	-3,16	1,14E-01	0,0	1,0	PBANKA_0942300	radial spoke head protein, putative
PBANKA_0104700.1-p1	0	0	0	1	1	1	-3,16	1,14E-01	0,0	1,0	PBANKA_0104700	elongation of fatty acids protein, putative
PBANKA_0708100.1-p1	0	0	0	1	1	1	-3,16	1,14E-01	0,0	1,0	PBANKA_0708100	dynein light chain 1
PBANKA_1411400.1-p1	0	0	0	1	1	1	-3,16	1,14E-01	0,0	1,0	PBANKA_1411400	ubiquitin-like protein nedd8 homologue, putative
PBANKA_1243300.1-p1	0	0	0	1	1	1	-3,16	1,14E-01	0,0	1,0	PBANKA_1243300	peptidyl-prolyl cis-trans isomerase, putative
PBANKA_0520000.1-p1	0	0	0	1	1	1	-3,16	1,14E-01	0,0	1,0	PBANKA_0520000	pyruvate kinase 2, putative
PBANKA_0312400.1-p1	0	2	2	3	5	2	-1,24	1,15E-01	1,3	3,3	PBANKA_0312400	DNA-directed RNA polymerase II subunit RPB2, putative
PBANKA_0515000.1-p1	0	0	0	0	2	1	-3,17	1,20E-01	0,0	1,0	PBANKA_0515000	ookinete surface protein P25
PBANKA_1219200.1-p1	0	0	0	1	0	2	-3,16	1,21E-01	0,0	1,0	PBANKA_1219200	Cg8 protein, putative
PBANKA_0801500.1-p1	0	0	0	1	2	0	-3,16	1,21E-01	0,0	1,0	PBANKA_0801500	conserved Plasmodium protein, unknown function
PBANKA_1033700.1-p1	0	0	0	1	2	0	-3,16	1,21E-01	0,0	1,0	PBANKA_1033700	conserved Plasmodium protein, unknown function
PBANKA_1223400.1-p1	0	0	0	1	2	0	-3,16	1,21E-01	0,0	1,0	PBANKA_1223400	conserved Plasmodium protein, unknown function
PBANKA_0612300.1-p1	0	0	0	1	2	0	-3,16	1,21E-01	0,0	1,0	PBANKA_0612300	conserved Plasmodium protein, unknown function
PBANKA_1356300.1-p1	0	0	0	1	2	0	-3,16	1,21E-01	0,0	1,0	PBANKA_1356300	CDT1-like protein, putative
PBANKA_0310400.1-p1	0	0	0	1	2	0	-3,16	1,21E-01	0,0	1,0	PBANKA_0310400	tetratricopeptide repeat protein, putative
PBANKA_1344300.1-p1	0	0	0	1	2	0	-3,16	1,21E-01	0,0	1,0	PBANKA_1344300	chromatin assembly factor 1 subunit B, putative
PBANKA_0621400.1-p1	0	0	0	2	0	1	-3,15	1,22E-01	0,0	1,0	PBANKA_0621400	RNA-binding protein, putative
PBANKA_1243600.1-p1	3	0	1	5	3	2	-1,21	1,24E-01	1,3	3,3	PBANKA_1243600	conserved Plasmodium protein, unknown function
PBANKA_1336900.1-p1	0	0	0	0	3	0	-3,17	1,29E-01	0,0	1,0	PBANKA_1336900	conserved Plasmodium protein, unknown function
PBANKA_1013200.1-p1	8	4	0	12	9	9	-1,24	1,32E-01	4,0	10,0	PBANKA_1013200	succinyl-CoA ligase [ADP-forming] subunit beta, putative
PBANKA_1438300.1-p1	1	0	1	2	3	2	-1,63	1,35E-01	0,7	2,3	PBANKA_1438300	phospholipid-transporting ATPase, putative
PBANKA_1039600.1-p1	1	0	1	2	3	2	-1,63	1,35E-01	0,7	2,3	PBANKA_1039600	26S proteasome regulatory subunit RPN6, putative
PBANKA_0105400.1-p1	3	1	1	5	4	2	-1,05	1,36E-01	1,7	3,7	PBANKA_0105400	coatomer alpha subunit, putative
PBANKA_1202200.1-p1	2	0	3	5	4	2	-1,06	1,36E-01	1,7	3,7	PBANKA_1202200	U5 small nuclear ribonucleoprotein component, putative
PBANKA_1033100.1-p1	1	1	0	2	3	2	-1,62	1,38E-01	0,7	2,3	PBANKA_1033100	conserved protein, unknown function
PBANKA_0415000.1-p1	0	1	1	3	3	1	-1,62	1,40E-01	0,7	2,3	PBANKA_0415000	Maf-like protein, putative
PBANKA_0819300.1-p1	6	0	2	9	6	3	-1,09	1,42E-01	2,7	6,0	PBANKA_0819300	eukaryotic translation initiation factor 3 subunit F, putative
PBANKA_0820300.1-p1	1	0	1	4	1	2	-1,61	1,43E-01	0,7	2,3	PBANKA_0820300	protein disulfide-isomerase PDI-Trans
PBANKA_1107100.1-p1	0	2	0	3	2	2	-1,61	1,50E-01	0,7	2,3	PBANKA_1107100	subtilisin-like protease 1
PBANKA_1246600.1-p1	1	1	1	3	3	2	-1,29	1,52E-01	1,0	2,7	PBANKA_1246600	cleft-like protein 1
PBANKA_0930900.1-p1	0	0	1	2	2	1	-1,96	1,64E-01	0,3	1,7	PBANKA_0930900	ubiquitin carboxyl-terminal hydrolase UCH54, putative
PBANKA_1008200.1-p1	1	1	0	5	2	0	-1,59	1,65E-01	0,7	2,3	PBANKA_1008200	cGMP-dependent protein kinase
PBANKA_0520900.1-p1	1	0	0	1	1	3	-1,96	1,67E-01	0,3	1,7	PBANKA_0520900	antigen UB05, putative
PBANKA_1432400.1-p1	2	0	1	4	3	1	-1,28	1,73E-01	1,0	2,7	PBANKA_1432400	perforin-like protein 2
PBANKA_0931600.1-p1	2	0	1	4	3	1	-1,28	1,73E-01	1,0	2,7	PBANKA_0931600	guanine nucleotide-exchange factor SEC12, putative
PBANKA_1131100.1-p1	4	0	2	7	5	1	-1,03	1,74E-01	2,0	4,3	PBANKA_1131100	adenylosuccinate synthetase, putative
PBANKA_0710100.1-p1	2	0	2	2	4	3	-1,10	1,77E-01	1,3	3,0	PBANKA_0710100	2-oxoglutarate dehydrogenase E1 component, putative
PBANKA_0416400.1-p1	2	1	1	5	2	2	-1,06	1,78E-01	1,3	3,0	PBANKA_0416400	conserved Plasmodium protein, unknown function
PBANKA_1238200.1-p1	0	0	1	1	4	0	-1,97	1,78E-01	0,3	1,7	PBANKA_1238200	DnaJ protein, putative
PBANKA_1209400.1-p1	1	0	0	2	3	0	-1,94	1,79E-01	0,3	1,7	PBANKA_1209400	inner membrane complex sub-compartment protein 1
PBANKA_0607400.1-p1	0	1	0	0	4	1	-1,97	1,80E-01	0,3	1,7	PBANKA_0607400	protein phosphatase PPM11, putative
PBANKA_0304300.1-p1	2	0	2	5	3	1	-1,07	1,93E-01	1,3	3,0	PBANKA_0304300	adenylosuccinate lyase, putative

Table S3: LCMSMS analyses of “all blood stages” parasites (raw data). Legends are indicated as well as the overall variability between samples (WT-2, WT-3, WT-4, KO-1, KO-2 and KO-4) is visualized using MDS plot.

PBANKA_0501300.1-p1	2	0	1	4	4	0	-1,28	1,95E-01	1,0	2,7	PBANKA_0501300	DNA polymerase delta catalytic subunit, putative
PBANKA_1013800.1-p1	0	0	0	0	1	1	-2,66	2,08E-01	0,0	0,7	PBANKA_1013800	cytochrome c oxidase subunit 2B, putative
PBANKA_1138000.1-p1	0	0	0	0	1	1	-2,66	2,08E-01	0,0	0,7	PBANKA_1138000	cytochrome c oxidase subunit ApiCOX24, putative
PBANKA_1132600.1-p1	0	0	0	0	1	1	-2,66	2,08E-01	0,0	0,7	PBANKA_1132600	ubiquitin-conjugating enzyme E2, putative
PBANKA_1033300.1-p1	0	0	0	0	1	1	-2,66	2,08E-01	0,0	0,7	PBANKA_1033300	conserved Plasmodium protein, unknown function
PBANKA_1462700.1-p1	0	0	0	0	1	1	-2,66	2,08E-01	0,0	0,7	PBANKA_1462700	THO complex subunit 2, putative
PBANKA_0702700.1-p1	0	0	0	0	1	1	-2,66	2,08E-01	0,0	0,7	PBANKA_0702700	rhomboid protease ROM3
PBANKA_0206500.1-p1	0	0	0	0	1	1	-2,66	2,08E-01	0,0	0,7	PBANKA_0206500	ras-related protein Rab-5C, putative
PBANKA_0818800.1-p1	0	0	0	1	0	1	-2,65	2,08E-01	0,0	0,7	PBANKA_0818800	conserved Plasmodium protein, unknown function
PBANKA_0510000.1-p1	0	0	0	1	1	0	-2,65	2,08E-01	0,0	0,7	PBANKA_0510000	conserved protein, unknown function
PBANKA_0912700.1-p1	0	0	0	1	1	0	-2,65	2,08E-01	0,0	0,7	PBANKA_0912700	3-oxo-5-alpha-steroid 4-dehydrogenase, putative
PBANKA_0309400.1-p1	0	0	0	1	1	0	-2,65	2,08E-01	0,0	0,7	PBANKA_0309400	conserved Plasmodium protein, unknown function
PBANKA_1124300.1-p1	0	0	0	1	1	0	-2,65	2,08E-01	0,0	0,7	PBANKA_1124300	conserved Plasmodium protein, unknown function
PBANKA_1351300.1-p1	0	0	0	1	1	0	-2,65	2,08E-01	0,0	0,7	PBANKA_1351300	conserved Plasmodium protein, unknown function
PBANKA_0907400.1-p1	0	0	0	1	1	0	-2,65	2,08E-01	0,0	0,7	PBANKA_0907400	dolichol-phosphate mannosyltransferase, putative
PBANKA_1204200.1-p1	0	0	0	1	1	0	-2,65	2,08E-01	0,0	0,7	PBANKA_1204200	IMP1-like protein, putative
PBANKA_1214500.1-p1	0	0	0	1	1	0	-2,65	2,08E-01	0,0	0,7	PBANKA_1214500	conserved Plasmodium protein, unknown function
PBANKA_0925200.1-p1	0	0	0	1	1	0	-2,65	2,08E-01	0,0	0,7	PBANKA_0925200	calcium-dependent protein kinase 7
PBANKA_1034300.1-p1	0	0	0	1	1	0	-2,65	2,08E-01	0,0	0,7	PBANKA_1034300	AP2 domain transcription factor AP2-G2
PBANKA_1311700.1-p1	0	0	0	1	1	0	-2,65	2,08E-01	0,0	0,7	PBANKA_1311700	multidrug resistance protein 2, putative
PBANKA_0623200.1-p1	0	0	0	1	1	0	-2,65	2,08E-01	0,0	0,7	PBANKA_0623200	lysophospholipase, putative
PBANKA_1237600.1-p1	0	0	0	0	0	2	-2,66	2,15E-01	0,0	0,7	PBANKA_1237600	zinc finger protein, putative
PBANKA_0520600.1-p1	0	0	0	0	0	2	-2,66	2,15E-01	0,0	0,7	PBANKA_0520600	enhancer of rudimentary homolog, putative
PBANKA_1442300.1-p1	0	0	0	0	2	0	-2,66	2,15E-01	0,0	0,7	PBANKA_1442300	conserved Plasmodium protein, unknown function
PBANKA_1458800.1-p1	0	0	0	0	2	0	-2,66	2,15E-01	0,0	0,7	PBANKA_1458800	kinesin-15, putative
PBANKA_0927700.1-p1	0	0	0	0	2	0	-2,66	2,15E-01	0,0	0,7	PBANKA_0927700	DDRGK domain-containing protein, putative
PBANKA_0507900.1-p1	0	0	0	0	2	0	-2,66	2,15E-01	0,0	0,7	PBANKA_0507900	conserved Plasmodium protein, unknown function
PBANKA_1329200.1-p1	0	0	0	0	2	0	-2,66	2,15E-01	0,0	0,7	PBANKA_1329200	dynein beta chain, putative
PBANKA_1361500.1-p1	0	0	0	0	2	0	-2,66	2,15E-01	0,0	0,7	PBANKA_1361500	WD repeat-containing protein 16, putative
PBANKA_1443000.1-p1	0	0	0	0	2	0	-2,66	2,15E-01	0,0	0,7	PBANKA_1443000	NIMA related kinase 1, putative
PBANKA_1308000.1-p1	0	0	0	0	2	0	-2,66	2,15E-01	0,0	0,7	PBANKA_1308000	conserved Plasmodium protein, unknown function
PBANKA_0721900.1-p1	0	0	0	0	2	0	-2,66	2,15E-01	0,0	0,7	PBANKA_0721900	60S ribosomal protein L7ae/L30e, putative
PBANKA_1454800.1-p1	0	0	0	2	0	0	-2,64	2,17E-01	0,0	0,7	PBANKA_1454800	RNA-binding protein, putative
PBANKA_1205400.1-p1	0	0	0	2	0	0	-2,64	2,17E-01	0,0	0,7	PBANKA_1205400	rho GTPase-activating protein, putative
PBANKA_1103600.1-p1	0	0	0	2	0	0	-2,64	2,17E-01	0,0	0,7	PBANKA_1103600	cation transporting P-ATPase, putative
PBANKA_0712300.1-p1	0	0	0	2	0	0	-2,64	2,17E-01	0,0	0,7	PBANKA_0712300	zinc finger protein, putative
PBANKA_0507100.1-p1	0	0	0	2	0	0	-2,64	2,17E-01	0,0	0,7	PBANKA_0507100	CDGSH iron-sulfur domain-containing protein, putative
PBANKA_1244600.1-p1	1	0	1	2	1	3	-1,41	2,20E-01	0,7	2,0	PBANKA_1244600	phosphoenolpyruvate/phosphate translocator
PBANKA_1142400.1-p1	5	0	1	11	5	1	-1,39	2,20E-01	2,0	5,7	PBANKA_1142400	nucleoside diphosphate kinase b, putative
PBANKA_0911800.1-p1	1	0	1	1	4	1	-1,42	2,24E-01	0,7	2,0	PBANKA_0911800	DnaJ protein, putative
PBANKA_1434200.1-p1	1	1	0	3	1	2	-1,39	2,27E-01	0,7	2,0	PBANKA_1434200	arginine--tRNA ligase, putative
PBANKA_1204900.1-p1	1	0	1	4	1	1	-1,39	2,31E-01	0,7	2,0	PBANKA_1204900	conserved Plasmodium protein, unknown function
PBANKA_1409800.1-p1	2	0	0	2	2	2	-1,40	2,32E-01	0,7	2,0	PBANKA_1409800	ATP synthase subunit gamma, mitochondrial, putative
PBANKA_1341100.1-p1	1	1	1	3	2	2	-1,11	2,48E-01	1,0	2,3	PBANKA_1341100	conserved Plasmodium protein, unknown function
PBANKA_1009100.1-p1	2	0	1	2	2	3	-1,11	2,58E-01	1,0	2,3	PBANKA_1009100	ataxin-2 like protein, putative
PBANKA_0204200.1-p1	2	0	1	3	2	2	-1,11	2,61E-01	1,0	2,3	PBANKA_0204200	tubulin-specific chaperone a, putative
PBANKA_1139400.1-p1	0	0	1	1	2	1	-1,67	2,63E-01	0,3	1,3	PBANKA_1139400	polyubiquitin binding protein, putative
PBANKA_0306500.1-p1	0	0	1	2	1	1	-1,66	2,65E-01	0,3	1,3	PBANKA_0306500	conserved protein, unknown function
PBANKA_0613200.1-p1	1	0	0	1	2	1	-1,65	2,66E-01	0,3	1,3	PBANKA_0613200	DNA polymerase alpha catalytic subunit A, putative
PBANKA_1124900.1-p1	1	0	0	1	2	1	-1,65	2,66E-01	0,3	1,3	PBANKA_1124900	oxidoreductase, putative
PBANKA_0204800.1-p1	3	0	1	6	3	0	-1,06	2,72E-01	1,3	3,0	PBANKA_0204800	secreted ookinete protein, putative
PBANKA_1304500.1-p1	0	1	0	0	3	1	-1,67	2,77E-01	0,3	1,3	PBANKA_1304500	protein SOC3
PBANKA_0205900.1-p1	0	1	0	2	2	0	-1,64	2,79E-01	0,3	1,3	PBANKA_0205900	Niemann-Pick type C1-related protein, putative
PBANKA_0100800.1-p1	1	0	0	3	0	1	-1,63	2,83E-01	0,3	1,3	PBANKA_0100800	zinc finger protein, putative
PBANKA_1228200.1-p1	2	0	1	5	0	2	-1,09	2,94E-01	1,0	2,3	PBANKA_1228200	glutamate dehydrogenase, putative
PBANKA_1449400.1-p1	0	0	1	4	0	0	-1,63	2,96E-01	0,3	1,3	PBANKA_1449400	splicing factor 3B subunit 3, putative
PBANKA_0917500.1-p1	1	0	1	1	1	3	-1,17	3,37E-01	0,7	1,7	PBANKA_0917500	structural maintenance of chromosomes protein 1, putative
PBANKA_1434800.1-p1	1	0	1	2	2	1	-1,16	3,38E-01	0,7	1,7	PBANKA_1434800	aminophospholipid-transporting P-ATPase, putative
PBANKA_1314100.1-p1	1	0	1	3	1	1	-1,15	3,45E-01	0,7	1,7	PBANKA_1314100	E3 ubiquitin-protein ligase ZNF598, putative
PBANKA_0915500.1-p1	1	0	1	3	1	1	-1,15	3,45E-01	0,7	1,7	PBANKA_0915500	glycine cleavage system H protein, putative
PBANKA_0509300.1-p1	1	1	0	3	1	1	-1,14	3,50E-01	0,7	1,7	PBANKA_0509300	glutamine--fructose-6-phosphate aminotransferase [isomerizing], putative
PBANKA_1244500.1-p1	0	0	0	0	0	1	-1,87	3,79E-01	0,0	0,3	PBANKA_1244500	SNARE protein, putative
PBANKA_1230800.1-p1	0	0	0	0	0	1	-1,87	3,79E-01	0,0	0,3	PBANKA_1230800	pyridoxal kinase, putative
PBANKA_0211900.1-p1	0	0	0	0	0	1	-1,87	3,79E-01	0,0	0,3	PBANKA_0211900	cation transporting ATPase, putative
PBANKA_1343200.1-p1	0	0	0	0	1	0	-1,87	3,79E-01	0,0	0,3	PBANKA_1343200	conserved Plasmodium protein, unknown function
PBANKA_1322600.1-p1	0	0	0	0	1	0	-1,87	3,79E-01	0,0	0,3	PBANKA_1322600	golgi apparatus membrane protein TVP23, putative
PBANKA_1038600.1-p1	0	0	0	0	1	0	-1,87	3,79E-01	0,0	0,3	PBANKA_1038600	conserved Plasmodium protein, unknown function
PBANKA_0720000.1-p1	0	0	0	0	1	0	-1,87	3,79E-01	0,0	0,3	PBANKA_0720000	conserved Plasmodium protein, unknown function
PBANKA_1304000.1-p1	0	0	0	0	1	0	-1,87	3,79E-01	0,0	0,3	PBANKA_1304000	cohesin complex subunit, putative
PBANKA_1013900.1-p1	0	0	0	0	1	0	-1,87	3,79E-01	0,0	0,3	PBANKA_1013900	PhIL1 interacting protein PIP3, putative
PBANKA_0907800.1-p1	0	0	0	0	1	0	-1,87	3,79E-01	0,0	0,3	PBANKA_0907800	ATP synthase-associated protein, putative
PBANKA_1003400.1-p1	0	0	0	0	1	0	-1,87	3,79E-01	0,0	0,3	PBANKA_1003400	lysine decarboxylase, putative
PBANKA_0514900.1-p1	0	0	0	0	1	0	-1,87	3,79E-01	0,0	0,3	PBANKA_0514900	ookinete surface protein P28
PBANKA_1426000.1-p1	0	0	0	0	1	0	-1,87	3,79E-01	0,0	0,3	PBANKA_1426000	histone-arginine methyltransferase CARM1, putative
PBANKA_1432100.1-p1	0	0	0	0	1	0	-1,87	3,79E-01	0,0	0,3	PBANKA_1432100	conserved Plasmodium protein, unknown function
PBANKA_0307100.1-p1	0	0	0	0	1	0	-1,87	3,79E-01	0,0	0,3	PBANKA_0307100	conserved Plasmodium protein, unknown function
PBANKA_0406000.1-p1	0	0	0	0	1	0	-1,87	3,79E-01	0,0	0,3	PBANKA_0406000	conserved Plasmodium protein, unknown function
PBANKA_0202700.1-p1	0	0	0	0	1	0	-1,87	3,79E-01	0,0	0,3	PBANKA_0202700	kinesin-8B
PBANKA_0202500.1-p1	0	0	0	0	1	0	-1,87	3,79E-01	0,0	0,3	PBANKA_0202500	P-loop containing nucleoside triphosphate hydrolase, putative
PBANKA_0908500.1-p1	0	0	0	0	1	0	-1,87	3,79E-01	0,0	0,3	PBANKA_0908500	myosin K
PBANKA_0809000.1-p1	0	0	0	0	1	0	-1,87	3,79E-01	0,0	0,3	PBANKA_0809000	translation initiation factor SUI1, putative
PBANKA_1417700.1-p1	0	0	0	0	1	0	-1,87	3,79E-01	0,0	0,3	PBANKA_1417700	conserved Plasmodium protein, unknown function

Table S3: LCMSMS analyses of “all blood stages” parasites (raw data). Legends are indicated as well as the overall variability between samples (WT-2, WT-3, WT-4, KO-1, KO-2 and KO-4) is visualized using MDS plot.

PBANKA_0919200.1-p1	0	0	0	0	1	0	-1,87	3,79E-01	0,0	0,3	PBANKA_0919200	fam-d protein
PBANKA_1420700.1-p1	0	0	0	0	1	0	-1,87	3,79E-01	0,0	0,3	PBANKA_1420700	MAATS1 domain-containing protein, putative
PBANKA_0504800.1-p1	0	0	0	0	1	0	-1,87	3,79E-01	0,0	0,3	PBANKA_0504800	conserved Plasmodium protein, unknown function
PBANKA_1450600.1-p1	0	0	0	0	1	0	-1,87	3,79E-01	0,0	0,3	PBANKA_1450600	vesicle transport v-SNARE protein VTI1, putative
PBANKA_0522100.1-p1	0	0	0	0	1	0	-1,87	3,79E-01	0,0	0,3	PBANKA_0522100	conserved Plasmodium protein, unknown function
PBANKA_1109700.1-p1	0	0	0	0	1	0	-1,87	3,79E-01	0,0	0,3	PBANKA_1109700	conserved protein, unknown function
PBANKA_1236600.1-p1	0	0	0	0	1	0	-1,87	3,79E-01	0,0	0,3	PBANKA_1236600	conserved Plasmodium protein, unknown function
PBANKA_1109600.1-p1	0	0	0	0	1	0	-1,87	3,79E-01	0,0	0,3	PBANKA_1109600	conserved Plasmodium protein, unknown function
PBANKA_1100441.1-p1	0	0	0	0	1	0	-1,87	3,79E-01	0,0	0,3	PBANKA_1100441	fam-b protein
PBANKA_1358200.1-p1	0	0	0	0	1	0	-1,87	3,79E-01	0,0	0,3	PBANKA_1358200	conserved Plasmodium protein, unknown function
PBANKA_0828700.1-p1	0	0	0	0	1	0	-1,87	3,79E-01	0,0	0,3	PBANKA_0828700	phosphatidylserine decarboxylase, putative
PBANKA_0601200.1-p1	0	0	0	0	1	0	-1,87	3,79E-01	0,0	0,3	PBANKA_0601200	dynein heavy chain, putative
PBANKA_1355000.1-p1	0	0	0	0	1	0	-1,87	3,79E-01	0,0	0,3	PBANKA_1355000	V-type proton ATPase subunit D, putative
PBANKA_1440100.1-p1	0	0	0	0	1	0	-1,87	3,79E-01	0,0	0,3	PBANKA_1440100	DNA-binding protein, putative
PBANKA_0824600.1-p1	0	0	0	1	0	0	-1,86	3,80E-01	0,0	0,3	PBANKA_0824600	conserved protein, unknown function
PBANKA_0807100.1-p1	0	0	0	1	0	0	-1,86	3,80E-01	0,0	0,3	PBANKA_0807100	stomatin-like protein
PBANKA_1137500.1-p1	0	0	0	1	0	0	-1,86	3,80E-01	0,0	0,3	PBANKA_1137500	actin-depolymerizing factor 2
PBANKA_0909100.1-p1	0	0	0	1	0	0	-1,86	3,80E-01	0,0	0,3	PBANKA_0909100	ER membrane protein complex subunit 8, putative
PBANKA_1328300.1-p1	0	0	0	1	0	0	-1,86	3,80E-01	0,0	0,3	PBANKA_1328300	ATP-dependent zinc metalloprotease FTSH, putative
PBANKA_0608100.1-p1	0	0	0	1	0	0	-1,86	3,80E-01	0,0	0,3	PBANKA_0608100	conserved protein, unknown function
PBANKA_0416300.1-p1	0	0	0	1	0	0	-1,86	3,80E-01	0,0	0,3	PBANKA_0416300	nucleoporin NUP221
PBANKA_0620900.1-p1	0	0	0	1	0	0	-1,86	3,80E-01	0,0	0,3	PBANKA_0620900	conserved Plasmodium protein, unknown function
PBANKA_1124800.1-p1	0	0	0	1	0	0	-1,86	3,80E-01	0,0	0,3	PBANKA_1124800	conserved Plasmodium protein, unknown function
PBANKA_1233500.1-p1	0	0	0	1	0	0	-1,86	3,80E-01	0,0	0,3	PBANKA_1233500	mRNA-binding protein PUF1
PBANKA_1209100.1-p1	0	0	0	1	0	0	-1,86	3,80E-01	0,0	0,3	PBANKA_1209100	dolichyl-phosphate-mannose–protein mannosyltransferase, putative
PBANKA_1031300.1-p1	0	0	0	1	0	0	-1,86	3,80E-01	0,0	0,3	PBANKA_1031300	rhomboid protease ROM8
PBANKA_0716500.1-p1	0	0	0	1	0	0	-1,86	3,80E-01	0,0	0,3	PBANKA_0716500	RNA-binding protein, putative
PBANKA_0201800.1-p1	0	0	0	1	0	0	-1,86	3,80E-01	0,0	0,3	PBANKA_0201800	TatD-like deoxyribonuclease
PBANKA_1021800.1-p1	0	0	0	1	0	0	-1,86	3,80E-01	0,0	0,3	PBANKA_1021800	mitochondrial import inner membrane translocase subunit TIM8, putative
PBANKA_1459900.1-p1	0	0	0	1	0	0	-1,86	3,80E-01	0,0	0,3	PBANKA_1459900	signal recognition particle receptor subunit beta, putative
PBANKA_0101800.1-p1	0	0	0	1	0	0	-1,86	3,80E-01	0,0	0,3	PBANKA_0101800	SDE2 domain-containing protein, putative
PBANKA_1020700.1-p1	0	0	0	1	0	0	-1,86	3,80E-01	0,0	0,3	PBANKA_1020700	conserved Plasmodium protein, unknown function
PBANKA_0309000.1-p1	0	0	0	1	0	0	-1,86	3,80E-01	0,0	0,3	PBANKA_0309000	ribosomal protein L12, mitochondrial, putative
PBANKA_1408200.1-p1	0	0	0	1	0	0	-1,86	3,80E-01	0,0	0,3	PBANKA_1408200	vacuolar protein sorting-associated protein 18, putative
PBANKA_0619700.1-p1	0	0	0	1	0	0	-1,86	3,80E-01	0,0	0,3	PBANKA_0619700	rhoptry-associated leucine zipper-like protein 1, putative
PBANKA_0404300.1-p1	0	0	0	1	0	0	-1,86	3,80E-01	0,0	0,3	PBANKA_0404300	P-loop containing nucleoside triphosphate hydrolase, putative
PBANKA_1128600.1-p1	0	0	0	1	0	0	-1,86	3,80E-01	0,0	0,3	PBANKA_1128600	cullin-like protein, putative
PBANKA_1242000.1-p1	0	0	0	1	0	0	-1,86	3,80E-01	0,0	0,3	PBANKA_1242000	ubiquitin carboxyl-terminal hydrolase 14, putative
PBANKA_1328400.1-p1	0	0	0	1	0	0	-1,86	3,80E-01	0,0	0,3	PBANKA_1328400	cytochrome c oxidase subunit ApiCOX25, putative
PBANKA_0105700.1-p1	0	0	0	1	0	0	-1,86	3,80E-01	0,0	0,3	PBANKA_0105700	MYND-type zinc finger protein, putative
PBANKA_0505600.1-p1	0	0	0	1	0	0	-1,86	3,80E-01	0,0	0,3	PBANKA_0505600	endomembrane protein 70, putative
PBANKA_0710900.1-p1	0	0	1	1	1	1	-1,29	4,11E-01	0,3	1,0	PBANKA_0710900	U6 snRNA-associated Sm-like protein LSm3, putative
PBANKA_0709800.1-p1	0	0	1	1	1	1	-1,29	4,11E-01	0,3	1,0	PBANKA_0709800	conserved Plasmodium protein, unknown function
PBANKA_0821900.1-p1	1	0	0	1	1	1	-1,28	4,15E-01	0,3	1,0	PBANKA_0821900	ubiquitin-conjugating enzyme E2, putative
PBANKA_0313300.1-p1	1	0	0	1	1	1	-1,28	4,15E-01	0,3	1,0	PBANKA_0313300	sugar transporter, putative
PBANKA_0516600.1-p1	1	0	0	1	1	1	-1,28	4,15E-01	0,3	1,0	PBANKA_0516600	leucine-rich repeat protein, putative
PBANKA_1408900.1-p1	0	0	1	1	2	0	-1,29	4,20E-01	0,3	1,0	PBANKA_1408900	conserved Plasmodium protein, unknown function
PBANKA_1348800.1-p1	0	1	0	0	2	1	-1,29	4,21E-01	0,3	1,0	PBANKA_1348800	conserved protein, unknown function
PBANKA_0109700.1-p1	0	0	1	2	0	1	-1,28	4,23E-01	0,3	1,0	PBANKA_0109700	SWI/SNF-related matrix-associated actin-dependent regulator of chromatin, putativ
PBANKA_0906300.1-p1	0	0	1	2	1	0	-1,28	4,23E-01	0,3	1,0	PBANKA_0906300	methyltransferase, putative
PBANKA_0604700.1-p1	1	0	0	2	1	0	-1,26	4,27E-01	0,3	1,0	PBANKA_0604700	shewanella-like protein phosphatase 2, putative
PBANKA_0800600.1-p1	1	0	0	2	1	0	-1,26	4,27E-01	0,3	1,0	PBANKA_0800600	centrin, putative
PBANKA_1363900.1-p1	0	1	0	2	0	1	-1,26	4,28E-01	0,3	1,0	PBANKA_1363900	conserved protein, unknown function
PBANKA_1239100.1-p1	0	0	1	3	0	0	-1,26	4,38E-01	0,3	1,0	PBANKA_1239100	conserved Plasmodium protein, unknown function
PBANKA_0719600.1-p1	0	0	1	3	0	0	-1,26	4,38E-01	0,3	1,0	PBANKA_0719600	memo-like protein
PBANKA_1320400.1-p1	1	0	0	3	0	0	-1,25	4,42E-01	0,3	1,0	PBANKA_1320400	conserved Plasmodium protein, unknown function
PBANKA_0711900.1-p1	481	425	526	553	624	579	-0,29	1,33E-02	477,3	585,3	PBANKA_0711900	heat shock protein 70
PBANKA_0805700.1-p1	324	267	406	492	446	379	-0,39	2,00E-03	332,3	439,0	PBANKA_0805700	heat shock protein 90, putative
PBANKA_1326400.1-p1	355	279	379	405	329	294	0,00	9,81E-01	337,7	342,7	PBANKA_1326400	glyceraldehyde-3-phosphate dehydrogenase
PBANKA_1133300.1-p1	**323**	**307**	**378**	**326**	**301**	**301**	**0,13**	**2,77E-01**	**336,0**	**309,3**	**PBANKA_1133300**	**elongation factor 1-alpha**
PBANKA_0818900.1-p1	262	244	216	270	292	251	-0,15	3,03E-01	240,7	271,0	PBANKA_0818900	endoplasmic reticulum chaperone BiP, putative
PBANKA_1214300.1-p1	**207**	**187**	**243**	**248**	**220**	**204**	**-0,06**	**6,45E-01**	**212,3**	**224,0**	**PBANKA_1214300**	**enolase, putative**
PBANKA_1125600.1-p1	169	133	177	185	176	189	-0,19	1,99E-01	159,7	183,3	PBANKA_1125600	pyruvate kinase, putative
PBANKA_1308600.1-p1	131	136	145	170	175	160	-0,28	6,45E-02	137,3	168,3	PBANKA_1308600	fructose-bisphosphate aldolase 2
PBANKA_1314800.1-p1	144	127	157	181	162	161	-0,22	1,37E-01	142,7	168,0	PBANKA_1314800	elongation factor 2, putative
PBANKA_0823400.1-p1	140	122	158	173	158	152	-0,19	2,07E-01	140,0	161,0	PBANKA_0823400	phosphoglycerate kinase, putative
PBANKA_0702800.1-p1	168	126	102	172	147	154	-0,21	2,78E-01	132,0	157,7	PBANKA_0702800	protein disulfide-isomerase, putative
PBANKA_0712600.1-p1	109	113	109	107	134	121	-0,12	4,74E-01	110,3	120,7	PBANKA_0712600	14-3-3 protein
PBANKA_1437300.1-p1	105	90	85	128	128	101	-0,32	6,52E-02	93,3	119,0	PBANKA_1437300	endoplasmin, putative
PBANKA_0914400.1-p1	85	69	95	120	132	104	-0,51	4,26E-03	83,0	118,7	PBANKA_0914400	heat shock protein 70, putative
PBANKA_1340100.1-p1	91	87	111	108	106	95	-0,09	6,02E-01	96,3	103,0	PBANKA_1340100	L-lactate dehydrogenase
PBANKA_1459300.1-p1	**98**	**93**	**79**	**97**	**80**	**86**	**0,07**	**6,79E-01**	**90,0**	**87,7**	**PBANKA_1459300**	**actin I**
PBANKA_1214000.1-p1	83	56	77	112	104	96	-0,51	5,69E-03	72,0	104,0	PBANKA_1214000	heat shock protein 60, putative
PBANKA_1210200.1-p1	97	46	122	166	81	51	-0,12	8,27E-01	88,3	99,3	PBANKA_1210200	PRE-binding protein, putative
PBANKA_1439200.1-p1	86	80	91	92	83	92	-0,04	8,18E-01	85,7	89,0	PBANKA_1439200	polyadenylate-binding protein 1, putative
PBANKA_1355100.1-p1	77	68	118	123	79	64	0,01	9,64E-01	87,7	88,7	PBANKA_1355100	40S ribosomal protein S6, putative
PBANKA_1215600.1-p1	87	68	123	110	95	72	0,01	9,33E-01	92,7	92,3	PBANKA_1215600	40S ribosomal protein S3A, putative
PBANKA_1106700.1-p1	95	81	109	79	88	79	0,22	2,19E-01	95,0	82,0	PBANKA_1106700	60S ribosomal protein L4, putative
PBANKA_1360300.1-p1	83	78	77	76	87	83	-0,03	8,51E-01	79,3	82,0	PBANKA_1360300	DNA/RNA-binding protein Alba 4, putative
PBANKA_1463000.1-p1	106	70	14	97	76	79	-0,32	7,06E-01	63,3	84,0	PBANKA_1463000	osmiophilic body protein G377
PBANKA_0511900.1-p1	81	66	98	89	83	67	0,05	7,84E-01	81,7	79,7	PBANKA_0511900	60S ribosomal protein L3, putative
PBANKA_1219300.1-p1	83	61	92	96	87	63	-0,04	8,27E-01	78,7	82,0	PBANKA_1219300	heat shock protein 110, putative

Table S3: LCMSMS analyses of “all blood stages” parasites (raw data). Legends are indicated as well as the overall variability between samples (WT-2, WT-3, WT-4, KO-1, KO-2 and KO-4) is visualized using MDS plot.

PBANKA_1145800.1-p1	51	48	56	61	78	69	-0,42	3,64E-02	51,7	69,3	PBANKA_1145800	membrane associated histidine-rich protein 1a
PBANKA_1432200.1-p1	80	71	27	61	54	82	-0,10	8,69E-01	59,3	65,7	PBANKA_1432200	male development gene 1
PBANKA_1034400.1-p1	81	54	67	82	70	62	-0,05	7,81E-01	67,3	71,3	PBANKA_1034400	plasmepsin IV
PBANKA_1113000.1-p1	97	75	95	86	78	62	0,26	1,41E-01	89,0	75,3	PBANKA_1113000	purine nucleoside phosphorylase, putative
PBANKA_1410300.1-p1	82	56	77	104	79	62	-0,15	4,15E-01	71,7	81,7	PBANKA_1410300	M1-family alanyl aminopeptidase, putative
PBANKA_1423300.1-p1	68	69	73	67	66	73	0,04	8,29E-01	70,0	68,7	PBANKA_1423300	DNA/RNA-binding protein Alba 1, putative
PBANKA_1019400.1-p1	74	58	99	97	62	57	0,12	5,19E-01	77,0	72,0	PBANKA_1019400	60S ribosomal protein L7-3, putative
PBANKA_1331900.1-p1	56	48	61	74	59	45	-0,08	6,88E-01	55,0	59,3	PBANKA_1331900	eukaryotic initiation factor 4a, putative
PBANKA_0405200.1-p1	63	42	56	81	70	60	-0,36	6,82E-02	53,7	70,3	PBANKA_0405200	T-complex protein 1 subunit beta, putative
PBANKA_0610300.1-p1	48	41	54	52	56	53	-0,16	4,17E-01	47,7	53,7	PBANKA_0610300	polyubiquitin, putative
PBANKA_1237800.1-p1	42	24	52	86	69	41	-0,71	9,79E-03	39,3	65,3	PBANKA_1237800	multidrug resistance protein 1, putative
PBANKA_1235600.1-p1	66	61	82	71	59	58	0,17	3,64E-01	69,7	62,7	PBANKA_1235600	adenosylhomocysteinase, putative
PBANKA_1016700.1-p1	59	46	53	77	67	47	-0,24	2,36E-01	52,7	63,7	PBANKA_1016700	leucine-rich repeat protein
PBANKA_0417700.1-p1	48	56	32	49	57	67	-0,32	2,27E-01	45,3	57,7	PBANKA_0417700	alpha tubulin 1
PBANKA_1019500.1-p1	70	52	79	75	58	50	0,16	4,08E-01	67,0	61,0	PBANKA_1019500	60S ribosomal protein L5, putative
PBANKA_1210800.1-p1	77	54	83	83	58	39	0,29	1,64E-01	71,3	60,0	PBANKA_1210800	hypoxanthine-guanine phosphoribosyltransferase, putative
PBANKA_1303800.1-p1	55	45	52	66	56	56	-0,20	3,04E-01	50,7	59,3	PBANKA_1303800	triosephosphate isomerase, putative
PBANKA_1102200.1-p1	59	38	56	51	47	43	0,14	5,17E-01	51,0	47,0	PBANKA_1102200	merozoite surface protein 8
PBANKA_1118600.1-p1	50	45	59	61	70	48	-0,21	3,04E-01	51,3	59,7	PBANKA_1118600	cell division cycle protein 48 homologue, putative
PBANKA_0928100.1-p1	47	51	66	58	63	49	-0,05	8,14E-01	54,7	56,7	PBANKA_0928100	phosphoglycerate mutase, putative
PBANKA_0938400.1-p1	54	33	60	72	55	39	-0,15	4,89E-01	49,0	55,3	PBANKA_0938400	endoplasmic reticulum-resident calcium binding protein, putative
PBANKA_0930300.1-p1	56	52	60	67	55	50	-0,01	9,68E-01	56,0	57,3	PBANKA_0930300	GTP-binding nuclear protein RAN/TC4, putative
PBANKA_0416000.1-p1	54	55	78	70	51	35	0,29	1,60E-01	62,3	52,0	PBANKA_0416000	high molecular weight rhoptry protein 3, putative
PBANKA_1444100.1-p1	50	37	49	63	53	45	-0,22	2,92E-01	45,3	53,7	PBANKA_1444100	T-complex protein 1 subunit gamma, putative
PBANKA_0819900.1-p1	38	43	46	57	58	44	-0,31	1,43E-01	42,3	53,0	PBANKA_0819900	nucleosome assembly protein
PBANKA_1301300.1-p1	56	45	25	51	47	51	-0,19	5,15E-01	42,0	49,7	PBANKA_1301300	trailer hitch homolog
PBANKA_1423500.1-p1	48	44	75	48	54	51	0,11	5,77E-01	55,7	51,0	PBANKA_1423500	60S ribosomal protein L13-2, putative
PBANKA_1352000.1-p1	59	51	60	49	56	52	0,12	5,38E-01	56,7	52,3	PBANKA_1352000	elongation factor 1-gamma, putative
PBANKA_1122900.1-p1	53	32	49	61	61	39	-0,24	2,68E-01	44,7	53,7	PBANKA_1122900	hexokinase, putative
PBANKA_1216500.1-p1	39	45	56	50	46	54	-0,10	6,41E-01	46,7	50,0	PBANKA_1216500	peptidyl-prolyl cis-trans isomerase, putative
PBANKA_0517000.1-p1	42	32	46	45	45	41	-0,12	5,88E-01	40,0	43,7	PBANKA_0517000	early transcribed membrane protein
PBANKA_1231000.1-p1	48	34	61	59	46	40	0,00	9,84E-01	47,7	48,3	PBANKA_1231000	40S ribosomal protein S11, putative
PBANKA_1238800.1-p1	45	31	55	63	53	45	-0,28	1,80E-01	43,7	53,7	PBANKA_1238800	karyopherin beta, putative
PBANKA_1310800.1-p1	36	31	54	51	47	41	-0,20	3,61E-01	40,3	46,3	PBANKA_1310800	40S ribosomal protein S5, putative
PBANKA_1229000.1-p1	42	35	43	45	41	47	-0,13	5,29E-01	40,0	44,3	PBANKA_1229000	Plasmodium exported protein (PHIST), unknown function
PBANKA_0918000.1-p1	44	34	58	57	47	41	-0,08	7,04E-01	45,3	48,3	PBANKA_0918000	60S acidic ribosomal protein P0, putative
PBANKA_1242300.1-p1	37	31	48	56	43	45	-0,30	1,64E-01	38,7	48,0	PBANKA_1242300	Hsc70-interacting protein, putative
PBANKA_1354400.1-p1	46	40	56	56	49	42	-0,03	8,70E-01	47,3	49,0	PBANKA_1354400	60S ribosomal protein L18, putative
PBANKA_0830200.1-p1	79	49	68	74	42	27	0,51	8,74E-02	65,3	47,7	PBANKA_0830200	high molecular weight rhoptry protein 2
PBANKA_0703900.1-p1	42	30	40	52	51	38	-0,31	1,58E-01	37,3	47,0	PBANKA_0703900	receptor for activated c kinase, putative
PBANKA_0942500.1-p1	51	36	46	57	47	37	-0,05	8,07E-01	44,3	47,0	PBANKA_0942500	thioredoxin-like mero protein, putative
PBANKA_0610900.1-p1	32	27	34	56	48	32	-0,52	2,55E-02	31,0	45,3	PBANKA_0610900	HSP40, subfamily A, putative
PBANKA_1018600.1-p1	35	39	55	48	44	40	-0,03	8,97E-01	43,0	44,0	PBANKA_1018600	60S ribosomal protein L21, putative
PBANKA_1033900.1-p1	42	35	48	45	38	39	0,05	8,13E-01	41,7	40,7	PBANKA_1033900	40S ribosomal protein S8e, putative
PBANKA_1428700.1-p1	43	23	47	63	37	30	-0,17	5,07E-01	37,7	43,3	PBANKA_1428700	eukaryotic translation initiation factor 3 subunit A, putative
PBANKA_1202400.1-p1	44	35	55	44	47	37	0,07	7,41E-01	44,7	42,7	PBANKA_1202400	60S ribosomal protein L13, putative
PBANKA_0522800.1-p1	44	37	47	40	39	42	0,09	6,72E-01	42,7	40,3	PBANKA_0522800	40S ribosomal protein S19, putative
PBANKA_0916200.1-p1	38	30	41	54	44	33	-0,24	2,84E-01	36,3	43,7	PBANKA_0916200	T-complex protein 1 subunit alpha, putative
PBANKA_1137800.1-p1	54	38	41	61	44	31	0,02	9,35E-01	44,3	45,3	PBANKA_1137800	glideosome-associated connector
PBANKA_1329300.1-p1	35	35	43	39	46	35	-0,08	7,18E-01	37,7	40,0	PBANKA_1329300	40S ribosomal protein S3, putative
PBANKA_0941800.1-p1	38	35	46	37	39	34	0,12	5,81E-01	39,7	36,7	PBANKA_0941800	histone H2B, putative
PBANKA_0914300.1-p1	35	26	26	52	41	31	-0,47	5,14E-02	29,0	41,3	PBANKA_0914300	protein disulfide-isomerase, putative
PBANKA_1204400.1-p1	37	33	38	42	37	34	-0,04	8,47E-01	36,0	37,7	PBANKA_1204400	DNA/RNA-binding protein Alba 3, putative
PBANKA_0941900.1-p1	**46**	**34**	**42**	**47**	**40**	**27**	**0,13**	**5,58E-01**	**40,7**	**38,0**	**PBANKA_0941900**	**histone H4, putative**
PBANKA_0941500.1-p1	37	37	54	46	40	34	0,10	6,27E-01	42,7	40,0	PBANKA_0941500	40S ribosomal protein S4, putative
PBANKA_0619100.1-p1	40	38	42	40	39	37	0,07	7,61E-01	40,0	38,7	PBANKA_0619100	40S ribosomal protein S5, putative
PBANKA_0524800.1-p1	42	29	42	39	36	27	0,17	4,60E-01	37,7	34,0	PBANKA_0524800	early transcribed membrane protein
PBANKA_1010500.1-p1	48	29	47	49	42	32	0,04	8,74E-01	41,3	41,0	PBANKA_1010500	Hsp70/Hsp90 organizing protein, putative
PBANKA_0610400.1-p1	47	21	44	47	35	23	0,13	6,48E-01	37,3	35,0	PBANKA_0610400	non-SERCA-type Ca2+ -transporting P-ATPase, putative
PBANKA_1231700.1-p1	31	33	46	35	35	41	-0,02	9,41E-01	36,7	37,0	PBANKA_1231700	60S ribosomal protein L2, putative
PBANKA_0816400.1-p1	37	28	39	49	37	31	-0,14	5,32E-01	34,7	39,0	PBANKA_0816400	ATP-dependent 6-phosphofructokinase, putative
PBANKA_0109100.1-p1	35	18	32	50	39	32	-0,48	5,02E-02	28,3	40,3	PBANKA_0109100	transketolase, putative
PBANKA_1218200.1-p1	33	21	33	44	38	29	-0,33	1,69E-01	29,0	37,0	PBANKA_1218200	T-complex protein 1 subunit epsilon, putative
PBANKA_1030600.1-p1	31	19	24	45	32	32	-0,52	3,63E-02	24,7	36,3	PBANKA_1030600	p1/s1 nuclease, putative
PBANKA_1401300.1-p1	35	30	49	40	34	35	0,07	7,52E-01	38,0	36,3	PBANKA_1401300	40S ribosomal protein S7, putative
PBANKA_0519900.1-p1	36	23	47	45	35	27	0,00	9,92E-01	35,3	35,7	PBANKA_0519900	conserved Plasmodium protein, unknown function
PBANKA_1362900.1-p1	46	36	63	48	29	35	0,39	7,97E-02	48,3	37,3	PBANKA_1362900	lysine--tRNA ligase, putative
PBANKA_0912300.1-p1	34	28	45	44	32	32	0,00	9,87E-01	35,7	36,0	PBANKA_0912300	tudor staphylococcal nuclease, putative
PBANKA_0513600.1-p1	37	38	36	42	32	27	0,17	4,42E-01	37,0	33,7	PBANKA_0513600	adenosine deaminase, putative
PBANKA_1135100.1-p1	36	32	41	39	31	31	0,13	5,58E-01	36,3	33,7	PBANKA_1135100	40S ribosomal protein S15, putative
PBANKA_1318100.1-p1	31	14	27	43	31	23	-0,39	1,43E-01	24,0	32,3	PBANKA_1318100	aminopeptidase P, putative
PBANKA_0814200.1-p1	40	29	50	45	29	26	0,28	2,32E-01	39,7	33,3	PBANKA_0814200	elongation factor 1-beta, putative
PBANKA_0826700.1-p1	25	19	28	34	33	28	-0,39	1,15E-01	24,0	31,7	PBANKA_0826700	parasitophorous vacuolar protein 5
PBANKA_1305100.1-p1	32	29	43	35	31	34	0,06	7,85E-01	34,7	33,3	PBANKA_1305100	60S ribosomal protein L1, putative
PBANKA_0932200.1-p1	30	22	20	43	32	30	-0,50	4,72E-02	24,0	35,0	PBANKA_0932200	peptidyl-prolyl cis-trans isomerase, putative
PBANKA_1426900.1-p1	24	15	21	36	28	27	-0,57	2,79E-02	20,0	30,3	PBANKA_1426900	ATP-dependent RNA helicase DBP1, putative
PBANKA_1400600.1-p1	47	26	54	43	28	23	0,46	6,18E-02	42,3	31,3	PBANKA_1400600	cytoadherence linked asexual protein, putative
PBANKA_1302800.1-p1	31	24	28	35	25	25	0,00	9,99E-01	27,7	28,3	PBANKA_1302800	thioredoxin peroxidase 1
PBANKA_0807600.1-p1	35	32	38	32	31	29	0,21	3,69E-01	35,0	30,7	PBANKA_0807600	40S ribosomal protein S11, putative
PBANKA_0405500.1-p1	22	22	32	28	25	26	-0,05	8,39E-01	25,3	26,3	PBANKA_0405500	60S ribosomal protein L7, putative
PBANKA_1357200.1-p1	40	14	18	42	35	20	-0,37	4,59E-01	24,0	32,3	PBANKA_1357200	endoplasmic reticulum chaperone GRP170, putative
PBANKA_1231800.1-p1	34	23	35	31	27	24	0,18	4,45E-01	30,7	27,3	PBANKA_1231800	60S ribosomal protein L12, putative

Table S3: LCMSMS analyses of “all blood stages” parasites (raw data). Legends are indicated as well as the overall variability between samples (WT-2, WT-3, WT-4, KO-1, KO-2 and KO-4) is visualized using MDS plot.

PBANKA_1229200.1-p1	30	25	34	32	27	25	0,10	6,66E-01	29,7	28,0	PBANKA_1229200	60S ribosomal protein L19, putative
PBANKA_1424300.1-p1	30	33	52	28	33	30	0,33	1,68E-01	38,3	30,3	PBANKA_1424300	conserved protein, unknown function
PBANKA_1324400.1-p1	35	28	42	41	26	25	0,22	3,48E-01	35,0	30,7	PBANKA_1324400	60S ribosomal protein L27, putative
PBANKA_1113400.1-p1	40	22	3	33	26	34	-0,44	6,46E-01	21,7	31,0	PBANKA_1113400	secreted ookinete protein
PBANKA_0310900.1-p1	22	17	25	37	25	28	-0,47	6,47E-02	21,3	30,0	PBANKA_0310900	T-complex protein 1 subunit theta, putative
PBANKA_0603200.1-p1	36	34	49	39	29	25	0,38	1,01E-01	39,7	31,0	PBANKA_0603200	eukaryotic translation initiation factor 5A, putative
PBANKA_1137000.1-p1	25	11	23	47	32	19	-0,69	3,26E-02	19,7	32,7	PBANKA_1137000	bergheilysin
PBANKA_1309900.1-p1	28	22	31	42	28	24	-0,18	4,55E-01	27,0	31,3	PBANKA_1309900	M17 leucyl aminopeptidase, putative
PBANKA_1450200.1-p1	31	15	13	37	34	25	-0,65	5,39E-02	19,7	32,0	PBANKA_1450200	serine hydroxymethyltransferase, putative
PBANKA_0417500.1-p1	32	25	42	37	22	22	0,31	1,96E-01	33,0	27,0	PBANKA_0417500	60S ribosomal protein L32, putative
PBANKA_1022000.1-p1	32	28	39	31	26	27	0,25	2,86E-01	33,0	28,0	PBANKA_1022000	40S ribosomal protein S25, putative
PBANKA_1134100.1-p1	24	16	26	40	28	21	-0,40	1,24E-01	22,0	29,7	PBANKA_1134100	T-complex protein 1 subunit delta, putative
PBANKA_1441100.1-p1	28	18	30	47	26	22	-0,28	2,75E-01	25,3	31,7	PBANKA_1441100	haloacid dehalogenase-like hydrolase, putative
PBANKA_0406500.1-p1	16	20	26	36	28	25	-0,50	4,92E-02	20,7	29,7	PBANKA_0406500	T-complex protein 1 subunit eta, putative
PBANKA_1205000.1-p1	32	29	41	27	31	29	0,23	3,32E-01	34,0	29,0	PBANKA_1205000	G-strand-binding protein 2
PBANKA_0510900.1-p1	23	18	32	36	28	21	-0,20	4,25E-01	24,3	28,3	PBANKA_0510900	40S ribosomal protein S2, putative
PBANKA_1446800.1-p1	33	23	28	31	30	21	0,06	8,00E-01	28,0	27,3	PBANKA_1446800	60 kDa chaperonin, putative
PBANKA_0717800.1-p1	29	28	27	34	28	21	0,05	8,24E-01	28,0	27,7	PBANKA_0717800	60S ribosomal protein L15, putative
PBANKA_0306800.1-p1	25	16	31	30	27	25	-0,18	4,76E-01	24,0	27,3	PBANKA_0306800	ATP-dependent RNA helicase UAP56, putative
PBANKA_1207200.1-p1	30	22	32	27	31	25	0,02	9,19E-01	28,0	27,7	PBANKA_1207200	adenylate kinase, putative
PBANKA_1117500.1-p1	28	23	37	39	20	25	0,10	6,97E-01	29,3	28,0	PBANKA_1117500	ribosomal protein L27a, putative
PBANKA_1234800.1-p1	19	19	29	31	26	24	-0,26	2,95E-01	22,3	27,0	PBANKA_1234800	40S ribosomal protein S9, putative
PBANKA_1456100.1-p1	26	16	36	32	24	25	-0,05	8,52E-01	26,0	27,0	PBANKA_1456100	40S ribosomal protein S17, putative
PBANKA_0524200.1-p1	34	13	21	27	28	24	-0,19	5,12E-01	22,7	26,3	PBANKA_0524200	early transcribed membrane protein
PBANKA_1206100.1-p1	22	17	22	31	27	25	-0,42	9,81E-02	20,3	27,7	PBANKA_1206100	eukaryotic translation initiation factor 3 subunit D, putative
PBANKA_0201600.1-p1	17	19	23	25	21	20	-0,14	5,83E-01	19,7	22,0	PBANKA_0201600	early transcribed membrane protein
PBANKA_0404800.1-p1	24	20	14	24	30	25	-0,42	1,30E-01	19,3	26,3	PBANKA_0404800	FAD-dependent glycerol-3-phosphate dehydrogenase, putative
PBANKA_1217700.1-p1	27	24	9	29	15	32	-0,28	6,11E-01	20,0	25,3	PBANKA_1217700	ATP-dependent RNA helicase DDX6
PBANKA_0906400.1-p1	24	18	31	35	23	18	-0,03	9,08E-01	24,3	25,3	PBANKA_0906400	60S ribosomal protein L35ae, putative
PBANKA_1239900.1-p1	26	24	36	37	25	15	0,19	4,54E-01	28,7	25,7	PBANKA_1239900	acyl-CoA synthetase, putative
PBANKA_0308600.1-p1	37	26	49	32	27	25	0,42	7,81E-02	37,3	28,0	PBANKA_0308600	asparagine--tRNA ligase, putative
PBANKA_0931300.1-p1	26	20	28	35	21	25	-0,10	6,88E-01	24,7	27,0	PBANKA_0931300	dipeptidyl aminopeptidase 1, putative
PBANKA_0922100.1-p1	22	16	27	25	26	16	-0,03	9,06E-01	21,7	22,3	PBANKA_0922100	40S ribosomal protein S18, putative
PBANKA_0903600.1-p1	28	26	36	35	25	19	0,22	3,76E-01	30,0	26,3	PBANKA_0903600	dynamin-like protein, putative
PBANKA_1232200.1-p1	22	15	22	32	37	12	-0,43	2,05E-01	19,7	27,0	PBANKA_1232200	FACT complex subunit SPT16
PBANKA_1135700.1-p1	23	18	26	24	24	21	-0,03	9,03E-01	22,3	23,0	PBANKA_1135700	CUGBP Elav-like family member 1, putative
PBANKA_1016300.1-p1	26	17	31	33	27	16	-0,01	9,56E-01	24,7	25,3	PBANKA_1016300	proliferation-associated protein 2g4, putative
PBANKA_1434700.1-p1	28	11	18	38	23	15	-0,36	3,10E-01	19,0	25,3	PBANKA_1434700	clathrin heavy chain, putative
PBANKA_0407700.1-p1	33	27	28	32	20	24	0,25	3,11E-01	29,3	25,3	PBANKA_0407700	60S acidic ribosomal protein P2, putative
PBANKA_1354500.1-p1	35	22	31	32	21	21	0,28	2,57E-01	29,3	24,7	PBANKA_1354500	60S ribosomal protein L18-2, putative
PBANKA_1026200.1-p1	24	17	22	30	28	17	-0,22	4,02E-01	21,0	25,0	PBANKA_1026200	NADP-specific glutamate dehydrogenase, putative
PBANKA_1450300.1-p1	21	18	15	24	23	18	-0,23	3,97E-01	18,0	21,7	PBANKA_1450300	ATP synthase subunit beta, mitochondrial
PBANKA_1019700.1-p1	18	10	27	29	21	20	-0,34	2,28E-01	18,3	23,3	PBANKA_1019700	conserved Plasmodium protein, unknown function
PBANKA_0604300.1-p1	45	51	54	93	100	80	-0,85	3,52E-05	50,0	91,0	PBANKA_0604300	tetratricopeptide repeat protein, putative
PBANKA_1206900.1-p1	86	86	80	130	166	132	-0,75	6,08E-05	84,0	142,7	PBANKA_1206900	tubulin beta chain, putative
PBANKA_1145900.1-p1	23	21	27	36	47	43	-0,83	1,00E-03	23,7	42,0	PBANKA_1145900	membrane associated histidine-rich protein 1b
PBANKA_1116800.1-p1	71	63	116	66	52	53	0,55	5,82E-03	83,3	57,0	PBANKA_1116800	BFR1 domain-containing protein, putative
PBANKA_0205000.1-p1	25	11	31	16	13	10	0,78	1,32E-02	22,3	13,0	PBANKA_0205000	EELM2 domain-containing protein, putative
PBANKA_1300700.1-p1	22	14	1	21	25	16	-0,68	5,07E-01	12,3	20,7	PBANKA_1300700	LCCL domain-containing protein
PBANKA_1035200.1-p1	21	17	1	29	25	24	-0,92	3,59E-01	13,0	26,0	PBANKA_1035200	LCCL domain-containing protein
PBANKA_0611600.1-p1	12	15	3	21	17	15	-0,75	1,21E-01	11,0	16,8	PBANKA_0611600	ribonucleoside-diphosphate reductase large subunit, putative
PBANKA_0408400.1-p1	14	12	4	12	18	19	-0,67	1,31E-01	11,0	14,8	PBANKA_0408400	phosphoglycerate mutase, putative
PBANKA_1115200.1-p1	10	8	0	7	5	15	-0,53	6,55E-01	6,0	9,0	PBANKA_1115200	gamete egress protein GEP
PBANKA_1305300.1-p1	8	9	6	13	19	9	-0,80	4,35E-02	7,7	13,8	PBANKA_1305300	FACT complex subunit SSRP1, putative
PBANKA_1031900.1-p1	25	14	29	32	21	20	-0,08	7,64E-01	22,7	24,3	PBANKA_1031900	eukaryotic translation initiation factor 2 subunit gamma, putative
PBANKA_1137900.1-p1	11	12	15	23	29	20	-0,91	2,15E-03	12,7	24,0	PBANKA_1137900	proliferating cell nuclear antigen 1, putative
PBANKA_1365500.1-p1	19	20	18	25	42	31	-0,77	4,77E-03	19,0	32,7	PBANKA_1365500	exported protein IBIS1
PBANKA_0522700.1-p1	54	66	40	75	82	79	-0,53	1,86E-02	53,3	78,7	PBANKA_0522700	alpha tubulin 2
PBANKA_1010000.1-p1	21	14	26	28	23	17	-0,14	6,05E-01	20,3	22,7	PBANKA_1010000	mitochondrial acidic protein MAM33, putative
PBANKA_0520200.1-p1	17	16	16	28	20	19	-0,41	1,30E-01	16,3	22,3	PBANKA_0520200	ADP/ATP transporter on adenylate translocase, putative
PBANKA_0937200.2-p1	23	15	40	31	21	15	0,23	4,18E-01	26,0	22,3	PBANKA_0937200	RNA-binding protein, putative
PBANKA_1013100.1-p1	18	19	30	25	23	22	-0,06	8,13E-01	22,3	23,3	PBANKA_1013100	60S ribosomal protein L14, putative
PBANKA_0929900.1-p1	23	12	17	20	20	22	-0,24	4,04E-01	17,3	20,7	PBANKA_0929900	heat shock protein 90, putative
PBANKA_1318400.1-p1	13	10	19	24	24	20	-0,69	1,72E-02	14,0	22,7	PBANKA_1318400	6-phosphogluconate dehydrogenase, decarboxylating, putative
PBANKA_0107300.1-p1	13	12	16	25	24	18	-0,69	1,65E-02	13,7	22,3	PBANKA_0107300	T-complex protein 1 subunit zeta, putative
PBANKA_0301300.1-p1	15	20	20	19	23	24	-0,26	3,55E-01	18,3	22,0	PBANKA_0301300	conserved Plasmodium protein, unknown function
PBANKA_0604800.1-p1	19	8	19	31	20	15	-0,49	1,11E-01	15,3	22,0	PBANKA_0604800	eukaryotic translation initiation factor 3 subunit C, putative
PBANKA_0821700.1-p1	24	14	23	21	22	20	-0,04	8,94E-01	20,3	21,0	PBANKA_0821700	inosine-5'-monophosphate dehydrogenase, putative
PBANKA_1364200.1-p1	21	21	24	18	23	22	0,07	7,90E-01	22,0	21,0	PBANKA_1364200	60S ribosomal protein L17, putative
PBANKA_0804000.1-p1	18	13	27	20	21	14	0,08	7,81E-01	19,3	18,3	PBANKA_0804000	60S ribosomal protein L37, putative
PBANKA_1410400.1-p1	17	10	18	26	20	19	-0,51	7,47E-02	15,0	21,7	PBANKA_1410400	V-type proton ATPase catalytic subunit A, putative
PBANKA_1410000.1-p1	22	20	20	29	20	17	-0,05	8,53E-01	20,7	22,0	PBANKA_1410000	26S protease regulatory subunit 7, putative
PBANKA_1338600.1-p1	21	21	32	24	19	18	0,29	2,62E-01	24,7	20,3	PBANKA_1338600	60S ribosomal protein L23, putative
PBANKA_0926700.1-p1	19	13	25	15	19	17	0,15	5,91E-01	19,0	17,0	PBANKA_0926700	exported protein 1
PBANKA_1317400.1-p1	19	14	25	22	20	18	-0,04	9,13E-01	19,3	20,0	PBANKA_1317400	HSP90 co-chaperone p23, putative
PBANKA_1112300.1-p1	15	21	14	24	17	19	-0,22	4,29E-01	16,7	20,0	PBANKA_1112300	ras-related protein Rab-1B, putative
PBANKA_0103300.1-p1	26	18	37	30	16	12	0,51	7,20E-02	27,0	19,3	PBANKA_0103300	GYF domain-containing protein, putative
PBANKA_1406700.1-p1	17	14	22	21	28	15	-0,27	3,46E-01	17,7	21,3	PBANKA_1406700	carbamoyl phosphate synthetase, putative
PBANKA_1003800.1-p1	13	8	16	22	23	14	-0,66	3,65E-02	12,3	19,7	PBANKA_1003800	V-type proton ATPase subunit B, putative
PBANKA_1416300.1-p1	22	15	24	25	18	13	0,15	5,91E-01	20,3	18,7	PBANKA_1416300	40S ribosomal protein S19, putative
PBANKA_0939600.1-p1	25	14	35	30	15	17	0,28	3,27E-01	24,7	20,7	PBANKA_0939600	polyadenylate-binding protein-interacting protein 1, putative
PBANKA_1453300.1-p1	22	12	13	28	22	11	-0,32	3,15E-01	15,7	20,3	PBANKA_1453300	acyl-CoA synthetase, putative

Table S3: LCMSMS analyses of “all blood stages” parasites (raw data). Legends are indicated as well as the overall variability between samples (WT-2, WT-3, WT-4, KO-1, KO-2 and KO-4) is visualized using MDS plot.

PBANKA_1000600.1-p1	17	13	23	18	19	16	0,00	9,92E-01	17,7	17,7	PBANKA_1000600	erythrocyte membrane antigen 1
PBANKA_1420600.1-p1	18	22	17	18	14	16	0,28	3,42E-01	19,0	16,0	PBANKA_1420600	histone H2B variant, putative
PBANKA_1103400.1-p1	18	16	22	19	17	19	0,04	8,95E-01	18,7	18,3	PBANKA_1103400	60S ribosomal protein L31, putative
PBANKA_0503600.1-p1	17	17	20	14	16	18	0,17	5,47E-01	18,0	16,0	PBANKA_0503600	60S ribosomal protein L30e, putative
PBANKA_1028400.1-p1	19	17	22	20	13	16	0,27	3,46E-01	19,3	16,3	PBANKA_1028400	60S ribosomal protein L10, putative
PBANKA_1359200.1-p1	22	19	25	19	16	21	0,25	3,55E-01	22,0	18,7	PBANKA_1359200	DNA/RNA-binding protein Alba 2, putative
PBANKA_1234500.1-p1	16	12	13	25	16	13	-0,35	2,53E-01	13,7	18,0	PBANKA_1234500	FoP domain-containing protein, putative
PBANKA_0617100.1-p1	19	14	19	15	17	18	0,06	8,27E-01	17,3	16,7	PBANKA_0617100	60S ribosomal protein L11a, putative
PBANKA_1359700.1-p1	22	14	4	21	17	19	-0,45	4,63E-01	13,3	19,0	PBANKA_1359700	6-cysteine protein P47
PBANKA_1411300.1-p1	25	16	26	23	14	15	0,39	1,55E-01	22,3	17,3	PBANKA_1411300	eukaryotic translation initation factor 4 gamma, putative
PBANKA_0804100.1-p1	16	6	19	27	19	8	-0,36	3,93E-01	13,7	18,0	PBANKA_0804100	conserved Plasmodium protein, unknown function
PBANKA_1008800.1-p1	15	10	18	25	16	15	-0,35	2,37E-01	14,3	18,7	PBANKA_1008800	glucose-6-phosphate isomerase, putative
PBANKA_0405400.1-p1	23	13	22	22	16	14	0,18	5,19E-01	19,3	17,3	PBANKA_0405400	40S ribosomal protein S12, putative
PBANKA_1351900.1-p1	26	20	24	24	14	12	0,53	5,91E-02	23,3	16,7	PBANKA_1351900	60S ribosomal protein L6, putative
PBANKA_1338300.1-p1	13	10	16	19	14	14	-0,25	4,30E-01	13,0	15,7	PBANKA_1338300	60S ribosomal protein L6, putative
PBANKA_1127700.1-p1	23	12	24	22	17	13	0,20	4,75E-01	19,7	17,3	PBANKA_1127700	nicotinate phosphoribosyltransferase, putative
PBANKA_1461800.1-p1	14	15	19	22	14	14	-0,03	9,16E-01	16,0	16,7	PBANKA_1461800	26S protease regulatory subunit 8, putative
PBANKA_1111400.1-p1	25	11	19	24	14	12	0,18	5,53E-01	18,3	16,7	PBANKA_1111400	inositol-3-phosphate synthase, putative
PBANKA_1423600.1-p1	18	21	26	18	15	13	0,51	6,48E-02	21,7	15,3	PBANKA_1423600	40S ribosomal protein S16, putative
PBANKA_1201900.1-p1	6	13	17	14	18	15	-0,39	2,52E-01	12,0	15,7	PBANKA_1201900	40S ribosomal protein S20e, putative
PBANKA_0619200.1-p1	26	24	1	13	9	23	0,24	8,36E-01	17,0	15,0	PBANKA_0619200	secreted ookinete protein, putative
PBANKA_0407600.1-p1	20	17	24	22	15	14	0,28	3,08E-01	20,3	17,0	PBANKA_0407600	asparagine synthetase [glutamine-hydrolyzing]
PBANKA_1452600.1-p1	15	10	16	23	14	13	-0,25	4,18E-01	13,7	16,7	PBANKA_1452600	calcyclin binding protein, putative
PBANKA_1301400.1-p1	18	13	16	16	13	11	0,26	4,15E-01	15,7	13,3	PBANKA_1301400	proteasome subunit alpha type-1, putative
PBANKA_1346700.1-p1	15	17	14	13	16	16	0,05	8,81E-01	15,3	15,0	PBANKA_1346700	60S ribosomal protein L23, putative
PBANKA_1010800.1-p1	14	10	17	22	16	13	-0,29	3,47E-01	13,7	17,0	PBANKA_1010800	CCR4-associated factor 16, putative
PBANKA_0302500.1-p1	16	16	14	14	17	14	0,05	8,69E-01	15,3	15,0	PBANKA_0302500	hexose transporter
PBANKA_0211500.1-p1	10	11	16	20	15	16	-0,45	1,55E-01	12,3	17,0	PBANKA_0211500	proteasome subunit alpha type-5, putative
PBANKA_1237900.1-p1	18	9	9	17	20	14	-0,47	1,63E-01	12,0	17,0	PBANKA_1237900	mitochondrial-processing peptidase subunit alpha, putative
PBANKA_1431050.1-p1	12	9	9	11	11	7	0,08	8,37E-01	10,0	9,7	PBANKA_1431050	10 kDa chaperonin, putative
PBANKA_0615400.1-p1	21	15	24	18	14	17	0,30	2,76E-01	20,0	16,3	PBANKA_0615400	serine--tRNA ligase, putative
PBANKA_0204500.1-p1	24	9	0	19	16	16	-0,55	6,54E-01	11,0	17,0	PBANKA_0204500	LCCL domain-containing protein, putative
PBANKA_1305000.1-p1	23	11	29	26	12	10	0,42	2,09E-01	21,0	16,0	PBANKA_1305000	conserved Plasmodium protein, unknown function
PBANKA_1406800.1-p1	15	16	15	16	16	14	0,02	9,47E-01	15,3	15,3	PBANKA_1406800	40S ribosomal protein S27, putative
PBANKA_0823000.1-p1	14	6	15	15	20	14	-0,48	1,56E-01	11,7	16,3	PBANKA_0823000	ubiquitin-like protein, putative
PBANKA_1418900.1-p1	10	5	13	17	16	13	-0,70	5,16E-02	9,3	15,3	PBANKA_1418900	ras-related protein Rab-11A
PBANKA_0943600.1-p1	16	14	16	23	12	13	-0,02	9,51E-01	15,3	16,0	PBANKA_0943600	60S acidic ribosomal protein P1, putative
PBANKA_0937700.1-p1	17	12	23	24	10	9	0,31	3,30E-01	17,3	14,3	PBANKA_0937700	60S ribosomal protein L36, putative
PBANKA_1217600.1-p1	19	10	20	22	11	7	0,34	3,27E-01	16,3	13,3	PBANKA_1217600	histone H2A.Z, putative
PBANKA_0709000.1-p1	16	13	17	13	12	12	0,33	3,06E-01	15,3	12,3	PBANKA_0709000	protein transport protein SEC61 subunit beta, putative
PBANKA_0207000.1-p1	13	6	9	17	15	10	-0,55	1,39E-01	9,3	14,0	PBANKA_0207000	calcium-transporting ATPase, putative
PBANKA_1450700.1-p1	17	12	15	19	12	15	-0,03	9,15E-01	14,7	15,3	PBANKA_1450700	clustered-asparagine-rich protein, putative
PBANKA_0721700.1-p1	12	10	17	23	12	10	-0,17	6,06E-01	13,0	15,0	PBANKA_0721700	ran-specific GTPase-activating protein 1, putative
PBANKA_1213600.1-p1	12	9	10	17	13	18	-0,60	7,52E-02	10,3	16,0	PBANKA_1213600	cysteine--tRNA ligase, putative
PBANKA_0414600.1-p1	11	3	18	21	13	10	-0,44	3,11E-01	10,7	14,7	PBANKA_0414600	40S ribosomal protein S15A, putative
PBANKA_1346600.1-p1	17	16	18	19	10	14	0,28	3,72E-01	17,0	14,3	PBANKA_1346600	glutamine--tRNA ligase, putative
PBANKA_0704700.1-p1	21	20	1	16	10	21	-0,09	9,28E-01	14,0	15,7	PBANKA_0704700	conserved Plasmodium protein, unknown function
PBANKA_1358600.1-p1	19	5	5	17	16	13	-0,61	2,28E-01	9,7	15,3	PBANKA_1358600	isocitrate dehydrogenase [NADP], mitochondrial, putative
PBANKA_1348900.1-p1	12	6	21	23	13	10	-0,22	5,39E-01	13,0	15,3	PBANKA_1348900	chaperone binding protein, putative
PBANKA_1234200.1-p1	13	9	24	24	12	9	0,06	8,69E-01	15,3	15,0	PBANKA_1234200	40S ribosomal protein S24, putative
PBANKA_0712900.1-p1	18	13	29	19	14	13	0,39	1,83E-01	20,0	15,3	PBANKA_0712900	high mobility group protein B2
PBANKA_0316800.1-p1	14	11	26	17	14	10	0,32	3,19E-01	17,0	13,7	PBANKA_0316800	erythrocyte membrane associated protein 2
PBANKA_1209000.1-p1	20	15	25	18	14	13	0,43	1,33E-01	20,0	15,0	PBANKA_1209000	eukaryotic translation initiation factor 2 subunit beta, putative
PBANKA_0404700.1-p1	11	14	16	18	12	15	-0,11	7,20E-01	13,7	15,0	PBANKA_0404700	glutaredoxin 1, putative
PBANKA_0932400.1-p1	9	9	12	17	14	10	-0,42	2,30E-01	10,0	13,7	PBANKA_0932400	berghepain-2
PBANKA_0403000.1-p1	17	12	26	20	10	13	0,37	2,27E-01	18,3	14,3	PBANKA_0403000	60S ribosomal protein L44, putative
PBANKA_1429600.1-p1	19	14	25	19	15	10	0,42	1,60E-01	19,3	14,7	PBANKA_1429600	proline--tRNA ligase
PBANKA_1143600.1-p1	9	8	12	16	18	11	-0,62	8,01E-02	9,7	15,0	PBANKA_1143600	alanine--tRNA ligase, putative
PBANKA_1226500.1-p1	15	10	12	23	10	11	-0,19	5,67E-01	12,3	14,7	PBANKA_1226500	proteasome subunit beta type-4, putative
PBANKA_1460400.1-p1	13	8	14	18	17	10	-0,34	3,15E-01	11,7	15,0	PBANKA_1460400	peptidyl-prolyl cis-trans isomerase FKBP35, putative
PBANKA_0906500.1-p1	14	15	20	14	15	11	0,30	3,33E-01	16,3	13,3	PBANKA_0906500	60S ribosomal protein L28, putative
PBANKA_0623300.1-p1	10	10	13	14	11	15	-0,26	4,47E-01	11,0	13,3	PBANKA_0623300	tryptophan-rich protein
PBANKA_1407600.1-p1	10	13	16	13	13	13	0,01	9,86E-01	13,0	13,0	PBANKA_1407600	60S ribosomal protein L24, putative
PBANKA_0905600.1-p1	13	11	19	17	14	13	-0,02	9,66E-01	14,3	14,7	PBANKA_0905600	translation initiation factor eIF-1A, putative
PBANKA_0618600.1-p1	7	9	6	15	14	12	-0,86	2,72E-02	7,3	13,7	PBANKA_0618600	conserved protein, unknown function
PBANKA_0108800.1-p1	12	8	14	12	14	8	0,01	9,77E-01	11,3	11,3	PBANKA_0108800	histone H3, putative
PBANKA_0410600.1-p1	13	8	22	22	14	8	-0,01	9,71E-01	14,3	14,7	PBANKA_0410600	60S ribosomal protein L26, putative
PBANKA_1362000.1-p1	8	13	14	11	17	12	-0,19	5,81E-01	11,7	13,3	PBANKA_1362000	glutamate--tRNA ligase, putative
PBANKA_1329700.1-p1	14	12	16	18	12	9	0,14	6,92E-01	14,0	13,0	PBANKA_1329700	26S proteasome regulatory subunit RPN2, putative
PBANKA_1232500.1-p1	11	8	10	15	14	8	-0,32	3,88E-01	9,7	12,3	PBANKA_1232500	eukaryotic translation initiation factor 3 subunit B, putative
PBANKA_0310000.1-p1	12	13	18	15	14	12	0,08	8,04E-01	14,3	13,7	PBANKA_0310000	protein SIS1, putative
PBANKA_0614500.1-p1	14	5	11	15	13	10	-0,31	4,02E-01	10,0	12,7	PBANKA_0614500	eukaryotic translation initiation factor 3 subunit I, putative
PBANKA_0709400.1-p1	15	9	18	10	8	8	0,70	5,99E-02	14,0	8,7	PBANKA_0709400	conserved Plasmodium protein, unknown function
PBANKA_0311000.1-p1	15	12	12	16	12	11	0,04	9,51E-01	13,0	13,0	PBANKA_0311000	protein transport protein SEC31, putative
PBANKA_1121700.1-p1	14	9	15	16	11	11	0,02	9,52E-01	12,7	12,7	PBANKA_1121700	leucine--tRNA ligase, putative
PBANKA_1440700.1-p1	13	9	9	19	7	14	-0,32	3,91E-01	10,3	13,3	PBANKA_1440700	ubiquitin-activating enzyme E1, putative
PBANKA_1320900.1-p1	10	3	8	22	9	6	-0,75	1,07E-01	7,0	12,3	PBANKA_1320900	thioredoxin 1, putative
PBANKA_1036600.1-p1	7	4	8	18	9	11	-0,95	2,18E-02	6,3	12,7	PBANKA_1036600	ribonucleoside-diphosphate reductase small chain, putative
PBANKA_1232100.1-p1	16	11	25	20	8	10	0,48	1,51E-01	17,3	12,7	PBANKA_1232100	serine/arginine-rich splicing factor 1, putative
PBANKA_0715600.1-p1	14	11	14	16	11	11	0,07	8,61E-01	13,0	12,7	PBANKA_0715600	26S protease regulatory subunit 6B, putative
PBANKA_0107400.1-p1	16	8	14	14	13	11	0,02	9,56E-01	12,7	12,7	PBANKA_0107400	ornithine aminotransferase, putative
PBANKA_0418200.1-p1	12	12	11	15	13	10	-0,09	8,03E-01	11,7	12,7	PBANKA_0418200	ras-related protein RAB7, putative

Table S3: LCMSMS analyses of “all blood stages” parasites (raw data). Legends are indicated as well as the overall variability between samples (WT-2, WT-3, WT-4, KO-1, KO-2 and KO-4) is visualized using MDS plot.

PBANKA_1334300.1-p1	12	6	12	11	17	4	-0,08	8,52E-01	10,0	10,7	PBANKA_1334300	exported protein 2
PBANKA_0307800.1-p1	19	11	15	16	13	9	0,28	4,05E-01	15,0	12,7	PBANKA_0307800	conserved Plasmodium protein, unknown function
PBANKA_1117100.1-p1	14	8	12	11	12	7	0,20	5,94E-01	11,3	10,0	PBANKA_1117100	histone H3 variant, putative
PBANKA_1214700.1-p1	16	13	2	10	8	18	-0,17	8,40E-01	10,3	12,0	PBANKA_1214700	conserved Plasmodium protein, unknown function
PBANKA_1206600.1-p1	15	8	13	16	9	10	0,08	8,33E-01	12,0	11,7	PBANKA_1206600	26S protease regulatory subunit 4, putative
PBANKA_0602700.1-p1	11	9	12	13	11	9	-0,02	9,53E-01	10,7	11,0	PBANKA_0602700	nucleosome assembly protein, putative
PBANKA_1364300.1-p1	13	7	9	14	13	10	-0,32	3,89E-01	9,7	12,3	PBANKA_1364300	glycerol kinase, putative
PBANKA_1365200.1-p1	12	11	8	13	11	12	-0,18	6,20E-01	10,3	12,0	PBANKA_1365200	thioredoxin-related protein, putative
PBANKA_1221200.1-p1	10	8	11	13	6	7	0,19	6,48E-01	9,7	8,7	PBANKA_1221200	60S ribosomal protein L34, putative
PBANKA_0105600.1-p1	10	11	12	14	12	10	-0,10	7,73E-01	11,0	12,0	PBANKA_0105600	translation initiation factor IF-2, putative
PBANKA_0938500.1-p1	13	12	5	13	12	11	-0,21	5,78E-01	10,0	12,0	PBANKA_0938500	succinyl-CoA synthetase alpha subunit, putative
PBANKA_1138200.1-p1	6	4	7	9	13	12	-0,99	2,35E-02	5,7	11,3	PBANKA_1138200	RuvB-like helicase 3, putative
PBANKA_1303700.1-p1	11	8	12	21	12	4	-0,20	6,21E-01	10,3	12,3	PBANKA_1303700	vesicle-associated membrane protein, putative
PBANKA_0708000.1-p1	12	8	10	17	10	7	-0,13	7,28E-01	10,0	11,3	PBANKA_0708000	protein transport protein SEC23, putative
PBANKA_1445400.1-p1	14	12	17	13	10	11	0,35	2,91E-01	14,3	11,3	PBANKA_1445400	protein transport protein SEC13
PBANKA_1023400.1-p1	9	4	6	16	12	8	-0,87	4,08E-02	6,3	12,0	PBANKA_1023400	glutathione reductase, putative
PBANKA_0403800.1-p1	7	8	18	11	14	9	-0,06	8,78E-01	11,0	11,3	PBANKA_0403800	transporter, putative
PBANKA_0715200.1-p1	15	11	13	13	10	9	0,31	3,74E-01	13,0	10,7	PBANKA_0715200	eukaryotic translation initiation factor 3 subunit G, putative
PBANKA_0938300.1-p1	10	7	9	12	11	11	-0,36	3,40E-01	8,7	11,3	PBANKA_0938300	heat shock protein J2, putative
PBANKA_1101300.1-p1	12	8	6	16	11	9	-0,41	2,89E-01	8,7	12,0	PBANKA_1101300	skeleton-binding protein 1
PBANKA_1130400.1-p1	13	12	9	12	11	11	0,03	9,30E-01	11,3	11,3	PBANKA_1130400	proteasome subunit alpha type-4, putative
PBANKA_0924900.1-p1	7	5	11	14	11	10	-0,59	1,38E-01	7,7	11,7	PBANKA_0924900	eukaryotic peptide chain release factor GTP-binding subunit, putative
PBANKA_1030100.1-p1	9	8	5	16	8	9	-0,52	2,10E-01	7,3	11,0	PBANKA_1030100	actin II
PBANKA_1030300.1-p1	12	6	10	14	9	9	-0,16	6,82E-01	9,3	10,7	PBANKA_1030300	nuclear transport factor 2, putative
PBANKA_0918100.1-p1	15	11	14	13	12	10	0,21	5,29E-01	13,3	11,7	PBANKA_0918100	60S ribosomal protein L38, putative
PBANKA_1038000.1-p1	12	6	10	12	9	9	-0,07	8,52E-01	9,3	10,0	PBANKA_1038000	cytochrome c, putative
PBANKA_0314500.1-p1	14	7	17	17	7	7	0,33	3,88E-01	12,7	10,3	PBANKA_0314500	40S ribosomal protein S26, putative
PBANKA_1452300.1-p1	8	5	9	11	11	8	-0,43	3,01E-01	7,3	10,0	PBANKA_1452300	conserved protein, unknown function
PBANKA_0817700.1-p1	18	9	18	15	9	7	0,57	1,13E-01	15,0	10,3	PBANKA_0817700	RNA-binding protein musashi, putative
PBANKA_1309500.1-p1	14	10	21	12	11	9	0,49	1,53E-01	15,0	10,7	PBANKA_1309500	conserved Plasmodium protein, unknown function
PBANKA_1120700.1-p1	8	5	15	11	12	8	-0,15	7,03E-01	9,3	10,3	PBANKA_1120700	nascent polypeptide-associated complex subunit alpha, putative
PBANKA_1126500.1-p1	15	8	17	16	9	7	0,35	3,34E-01	13,3	10,7	PBANKA_1126500	acetyl-CoA synthetase, putative
PBANKA_1340300.1-p1	13	11	10	11	11	8	0,21	5,79E-01	11,3	10,0	PBANKA_1340300	phosphoribosylpyrophosphate synthetase, putative
PBANKA_0917900.1-p1	11	11	13	13	9	9	0,20	5,83E-01	11,7	10,3	PBANKA_0917900	26S protease regulatory subunit 6A, putative
PBANKA_1210900.1-p1	11	6	6	12	9	11	-0,44	2,86E-01	7,7	10,7	PBANKA_1210900	phosphoglucomutase, putative
PBANKA_0934200.1-p1	11	6	12	14	10	9	-0,16	6,68E-01	9,7	11,0	PBANKA_0934200	ubiquitin domain-containing protein DSK2, putative
PBANKA_1130500.1-p1	13	6	7	17	8	6	-0,19	6,53E-01	8,7	10,3	PBANKA_1130500	proteasome subunit alpha type-7, putative
PBANKA_0505100.1-p1	13	6	10	13	11	9	-0,16	6,80E-01	9,7	11,0	PBANKA_0505100	ADP-ribosylation factor, putative
PBANKA_1417300.1-p1	11	6	7	12	10	9	-0,33	4,11E-01	8,0	10,3	PBANKA_1417300	translocation protein SEC63, putative
PBANKA_1039400.1-p1	13	9	22	20	6	7	0,45	2,47E-01	14,7	11,0	PBANKA_1039400	ribosomal protein S27a, putative
PBANKA_0919000.1-p1	6	7	8	12	8	11	-0,53	1,95E-01	7,0	10,3	PBANKA_0919000	26S proteasome regulatory subunit RPN7, putative
PBANKA_1456900.1-p1	11	9	13	8	13	11	0,04	9,16E-01	11,0	10,7	PBANKA_1456900	translation initiation factor SUI1, putative
PBANKA_0300600.1-p1	12	8	7	11	12	6	-0,06	8,73E-01	9,0	9,7	PBANKA_0300600	Plasmodium exported protein, unknown function
PBANKA_0501100.1-p1	8	11	8	8	9	11	-0,04	9,27E-01	9,0	9,3	PBANKA_0501100	early transcribed membrane protein
PBANKA_0803400.1-p1	8	9	14	8	9	10	0,19	6,23E-01	10,3	9,0	PBANKA_0803400	40S ribosomal protein S29, putative
PBANKA_1223800.1-p1	12	9	4	12	14	6	-0,30	4,84E-01	8,3	10,7	PBANKA_1223800	V-type proton ATPase subunit a, putative
PBANKA_1320500.1-p1	13	7	11	10	9	9	0,16	6,71E-01	10,3	9,3	PBANKA_1320500	V-type H(+)-translocating pyrophosphatase, putative
PBANKA_0707400.1-p1	10	2	14	14	9	8	-0,24	5,93E-01	8,7	10,3	PBANKA_0707400	RNA-binding protein, putative
PBANKA_0511400.1-p1	13	6	16	18	5	3	0,48	3,60E-01	11,7	8,7	PBANKA_0511400	peroxiredoxin, putative
PBANKA_0922500.1-p1	6	10	10	11	10	9	-0,19	6,35E-01	8,7	10,0	PBANKA_0922500	kelch domain-containing protein, putative
PBANKA_1452500.1-p1	8	7	7	11	9	10	-0,42	3,09E-01	7,3	10,0	PBANKA_1452500	conserved Plasmodium protein, unknown function
PBANKA_0928200.1-p1	10	10	20	13	7	10	0,42	2,50E-01	13,3	10,0	PBANKA_0928200	conserved protein, unknown function
PBANKA_1343300.1-p1	7	11	14	13	7	10	0,11	7,70E-01	10,7	10,0	PBANKA_1343300	proteasome subunit beta type-7, putative
PBANKA_0307000.1-p1	9	15	17	15	9	8	0,38	2,81E-01	13,7	10,7	PBANKA_0307000	60S ribosomal protein L37ae, putative
PBANKA_1008500.1-p1	8	5	20	13	10	7	0,13	7,47E-01	11,0	10,0	PBANKA_1008500	translocon component PTEX150
PBANKA_1142800.1-p1	13	8	20	14	8	7	0,51	1,67E-01	13,7	9,7	PBANKA_1142800	conserved protein, unknown function
PBANKA_1331400.1-p1	7	2	8	12	11	4	-0,64	1,88E-01	5,7	9,0	PBANKA_1331400	MORC family protein, putative
PBANKA_1126200.1-p1	12	6	13	13	8	9	0,07	8,58E-01	10,3	10,0	PBANKA_1126200	protein DJ-1, putative
PBANKA_0107100.1-p1	10	7	10	14	6	8	-0,01	9,76E-01	9,0	9,3	PBANKA_0107100	proteasome subunit alpha type-2, putative
PBANKA_0931200.1-p1	11	4	11	11	10	7	-0,09	8,29E-01	8,7	9,3	PBANKA_0931200	heat shock protein 101
PBANKA_1126400.1-p1	8	6	10	16	7	7	-0,28	5,01E-01	8,0	10,0	PBANKA_1126400	transportin, putative
PBANKA_1200800.1-p1	12	7	15	11	9	9	0,24	5,28E-01	11,3	9,7	PBANKA_1200800	transformer-2 protein homolog beta, putative
PBANKA_0405300.1-p1	8	9	17	11	9	7	0,33	3,86E-01	11,3	9,0	PBANKA_0405300	40S ribosomal protein S23, putative
PBANKA_1209900.1-p1	10	8	4	11	9	9	-0,35	4,17E-01	7,3	9,7	PBANKA_1209900	conserved protein, unknown function
PBANKA_1419100.1-p1	10	8	4	8	13	8	-0,36	4,05E-01	7,3	9,7	PBANKA_1419100	dihydrolipoyllysine-residue succinyltransferase component of 2-oxoglutarate dehydr
PBANKA_1228000.1-p1	12	5	16	12	7	10	0,19	6,24E-01	11,0	9,7	PBANKA_1228000	1-cys peroxiredoxin, putative
PBANKA_0834400.1-p1	8	4	3	9	10	10	-0,91	5,44E-02	5,0	9,7	PBANKA_0834400	mitochondrial-processing peptidase subunit beta, putative
PBANKA_0619900.1-p1	13	8	16	14	8	7	0,38	3,14E-01	12,3	9,7	PBANKA_0619900	Obg-like ATPase 1, putative
PBANKA_0212100.1-p1	9	8	8	13	7	8	-0,12	7,67E-01	8,3	9,3	PBANKA_0212100	eukaryotic translation initiation factor 2 subunit alpha
PBANKA_1144000.1-p1	6	7	6	11	9	9	-0,57	1,79E-01	6,3	9,7	PBANKA_1144000	26S proteasome regulatory subunit RPN11, putative
PBANKA_0905000.1-p1	7	6	10	8	7	7	0,07	8,67E-01	7,7	7,3	PBANKA_0905000	40S ribosomal protein S21, putative
PBANKA_0923400.1-p1	9	6	5	13	8	5	-0,32	4,78E-01	6,7	8,7	PBANKA_0923400	60S ribosomal protein L35, putative
PBANKA_1222800.1-p1	15	6	8	10	8	9	0,13	7,43E-01	9,7	9,0	PBANKA_1222800	tyrosine--tRNA ligase, putative
PBANKA_1223100.1-p1	9	5	9	13	9	6	-0,25	5,57E-01	7,7	9,3	PBANKA_1223100	proteasome subunit alpha type-6, putative
PBANKA_1438000.1-p1	7	4	5	10	12	5	-0,71	1,26E-01	5,3	9,0	PBANKA_1438000	cAMP-dependent protein kinase regulatory subunit, putative
PBANKA_1404900.1-p1	9	7	10	12	10	5	-0,02	9,53E-01	8,7	9,0	PBANKA_1404900	26S protease regulatory subunit 10B, putative
PBANKA_0518700.1-p1	9	2	6	13	6	9	-0,67	1,55E-01	5,7	9,3	PBANKA_0518700	methionine--tRNA ligase, putative
PBANKA_0617200.1-p1	10	7	13	12	7	7	0,23	5,67E-01	10,0	8,7	PBANKA_0617200	40S ribosomal protein S10, putative
PBANKA_1242800.1-p1	9	5	7	11	7	8	-0,27	5,29E-01	7,0	8,7	PBANKA_1242800	eukaryotic translation initiation factor 3 subunit E, putative
PBANKA_0505800.1-p1	13	4	7	11	9	7	-0,13	7,62E-01	8,0	9,0	PBANKA_0505800	deoxyribose-phosphate aldolase, putative
PBANKA_1127800.1-p1	6	5	5	10	8	7	-0,60	1,87E-01	5,3	8,3	PBANKA_1127800	DnaJ protein, putative
PBANKA_1012800.1-p1	10	1	6	14	8	4	-0,55	3,48E-01	5,7	8,7	PBANKA_1012800	voltage-dependent anion-selective channel protein, putative

Table S3: LCMSMS analyses of “all blood stages” parasites (raw data). Legends are indicated as well as the overall variability between samples (WT-2, WT-3, WT-4, KO-1, KO-2 and KO-4) is visualized using MDS plot.

PBANKA_1425100.1-p1	7	5	8	8	10	5	-0,19	6,80E-01	6,7	7,7	PBANKA_1425100	karyopherin alpha, putative
PBANKA_1457800.1-p1	8	8	6	6	7	12	-0,17	6,97E-01	7,3	8,3	PBANKA_1457800	ADP-ribosylation factor GTPase-activating protein 1, putative
PBANKA_0623100.1-p1	9	7	7	10	8	6	-0,03	9,53E-01	7,7	8,0	PBANKA_0623100	tryptophan-rich protein
PBANKA_1211000.1-p1	7	4	7	12	6	7	-0,43	3,39E-01	6,0	8,3	PBANKA_1211000	GMP synthase [glutamine-hydrolyzing], putative
PBANKA_1303300.1-p1	7	1	5	13	8	5	-0,94	7,13E-02	4,3	8,7	PBANKA_1303300	cytochrome b-c1 complex subunit Rieske, putative
PBANKA_0715500.1-p1	5	4	6	6	8	7	-0,47	3,37E-01	5,0	7,0	PBANKA_0715500	phosphoglucomutase-2
PBANKA_1117000.1-p1	7	6	3	3	6	7	0,02	9,76E-01	5,3	5,3	PBANKA_1117000	histone H2A, putative
PBANKA_0305100.1-p1	7	14	3	8	8	6	0,18	7,15E-01	8,0	7,3	PBANKA_0305100	serine repeat antigen 1
PBANKA_1137200.1-p1	8	4	7	9	6	8	-0,25	5,82E-01	6,3	7,7	PBANKA_1137200	protein transport protein Sec24A, putative
PBANKA_0303600.1-p1	8	6	9	7	8	6	0,14	7,49E-01	7,7	7,0	PBANKA_0303600	26S proteasome regulatory subunit RPN1, putative
PBANKA_1222900.1-p1	8	4	8	9	8	6	-0,18	6,88E-01	6,7	7,7	PBANKA_1222900	26S proteasome regulatory subunit RPN10, putative
PBANKA_1135000.1-p1	7	5	4	7	7	7	-0,36	4,53E-01	5,3	7,0	PBANKA_1135000	YOP1-like protein, putative
PBANKA_0913400.1-p1	9	1	15	15	5	3	0,15	8,65E-01	8,3	7,7	PBANKA_0913400	protein phosphatase PPM8
PBANKA_0316000.1-p1	4	4	6	7	12	4	-0,70	1,61E-01	4,7	7,7	PBANKA_0316000	replication factor C subunit 1, putative
PBANKA_1456200.1-p1	4	5	8	10	6	7	-0,41	3,72E-01	5,7	7,7	PBANKA_1456200	rab specific GDP dissociation inhibitor, putative
PBANKA_0833000.1-p1	10	7	10	8	4	8	0,45	3,03E-01	9,0	6,7	PBANKA_0833000	profilin
PBANKA_0412800.1-p1	10	1	6	12	7	4	-0,38	4,99E-01	5,7	7,7	PBANKA_0412800	eukaryotic translation initiation factor 4E, putative
PBANKA_1325000.1-p1	7	5	8	9	4	8	-0,05	9,19E-01	6,7	7,0	PBANKA_1325000	40S ribosomal protein S28e, putative
PBANKA_1359000.1-p1	6	4	4	7	8	9	-0,75	1,20E-01	4,7	8,0	PBANKA_1359000	protein transport protein SEC61 subunit alpha, putative
PBANKA_0315600.1-p1	6	4	8	7	7	8	-0,28	5,56E-01	6,0	7,3	PBANKA_0315600	40S ribosomal protein S30, putative
PBANKA_0619300.1-p1	4	6	10	9	9	6	-0,26	5,77E-01	6,7	8,0	PBANKA_0619300	conserved Plasmodium protein, unknown function
PBANKA_0910200.1-p1	6	4	14	11	5	7	0,07	8,83E-01	8,0	7,7	PBANKA_0910200	protein phosphatase PPM2
PBANKA_0103900.1-p1	5	3	7	10	8	5	-0,59	2,21E-01	5,0	7,7	PBANKA_0103900	RNA-binding protein, putative
PBANKA_1360100.1-p1	10	9	10	8	6	7	0,48	2,47E-01	9,7	7,0	PBANKA_1360100	nucleoside transporter 1
PBANKA_0824800.1-p1	7	5	10	10	6	5	0,09	8,43E-01	7,3	7,0	PBANKA_0824800	polyadenylate-binding protein 2, putative
PBANKA_0938600.1-p1	7	1	5	8	7	5	-0,59	2,69E-01	4,3	6,7	PBANKA_0938600	casein kinase 2, alpha subunit
PBANKA_0803600.1-p1	10	6	11	8	7	7	0,30	4,72E-01	9,0	7,3	PBANKA_0803600	importin-7, putative
PBANKA_0618900.1-p1	8	6	11	8	8	7	0,12	7,69E-01	8,3	7,7	PBANKA_0618900	rhoptry protein, putative
PBANKA_0820000.1-p1	8	6	4	6	10	5	-0,19	6,86E-01	6,0	7,0	PBANKA_0820000	DnaJ protein, putative
PBANKA_1444000.1-p1	8	4	11	11	6	6	0,02	9,62E-01	7,7	7,7	PBANKA_1444000	macrophage migration inhibitory factor
PBANKA_0801200.1-p1	11	3	8	8	8	5	0,09	8,50E-01	7,3	7,0	PBANKA_0801200	erythrocyte membrane-associated antigen, putative
PBANKA_1018500.1-p1	8	11	18	4	8	8	0,85	4,43E-02	12,3	6,7	PBANKA_1018500	transcription factor BTF3, putative
PBANKA_1315500.1-p1	6	5	2	7	6	8	-0,64	2,10E-01	4,3	7,0	PBANKA_1315500	sortilin, putative
PBANKA_1200600.1-p1	10	5	13	9	7	4	0,49	2,62E-01	9,3	6,7	PBANKA_1200600	Plasmodium exported protein, unknown function
PBANKA_0809100.1-p1	10	4	13	12	5	4	0,39	3,91E-01	9,0	7,0	PBANKA_0809100	proteasome activator 28, putative
PBANKA_1037300.1-p1	8	4	10	12	7	3	0,03	9,40E-01	7,3	7,3	PBANKA_1037300	conserved Plasmodium protein, unknown function
PBANKA_0517200.1-p1	4	4	5	9	6	5	-0,58	2,45E-01	4,3	6,7	PBANKA_0517200	haloacid dehalogenase-like hydrolase, putative
PBANKA_0919300.1-p1	5	3	7	8	8	5	-0,47	3,38E-01	5,0	7,0	PBANKA_0919300	spermidine synthase, putative
PBANKA_1241900.1-p1	5	7	11	11	5	5	0,16	7,29E-01	7,7	7,0	PBANKA_1241900	ubiquitin-conjugating enzyme E2 N, putative
PBANKA_0714200.1-p1	8	4	4	10	6	4	-0,26	5,93E-01	5,3	6,7	PBANKA_0714200	chaperone protein ClpB1, putative
PBANKA_0832600.1-p1	8	4	10	10	5	4	0,24	6,11E-01	7,3	6,3	PBANKA_0832600	proteasome subunit beta type-6, putative
PBANKA_1224200.1-p1	7	3	5	7	7	4	-0,23	6,46E-01	5,0	6,0	PBANKA_1224200	DnaJ protein, putative
PBANKA_1426700.1-p1	6	2	7	12	6	3	-0,44	3,93E-01	5,0	7,0	PBANKA_1426700	hydroxymethyldihydropterin pyrophosphokinase-dihydropteroate synthase, putative
PBANKA_0811300.1-p1	8	2	2	11	5	5	-0,73	1,87E-01	4,0	7,0	PBANKA_0811300	exportin-7, putative
PBANKA_1341500.1-p1	4	4	5	5	8	7	-0,61	2,37E-01	4,3	6,7	PBANKA_1341500	RNA-binding protein, putative
PBANKA_1123500.1-p1	8	2	4	11	7	2	-0,45	4,21E-01	4,7	6,7	PBANKA_1123500	SNF2 helicase, putative
PBANKA_0304900.1-p1	2	13	9	6	4	9	0,34	5,17E-01	8,0	6,3	PBANKA_0304900	serine repeat antigen 3
PBANKA_1110500.1-p1	7	5	7	8	6	6	-0,05	9,14E-01	6,3	6,7	PBANKA_1110500	translationally-controlled tumor protein homolog
PBANKA_1134200.1-p1	6	2	7	10	5	5	-0,38	4,50E-01	5,0	6,7	PBANKA_1134200	pyrroline-5-carboxylate reductase, putative
PBANKA_1415900.1-p1	8	5	17	11	5	3	0,67	1,52E-01	10,0	6,3	PBANKA_1415900	zinc finger protein, putative
PBANKA_1320700.1-p1	7	7	4	5	7	6	0,02	9,60E-01	6,0	6,0	PBANKA_1320700	signal peptide peptidase, putative
PBANKA_0904100.1-p1	8	7	6	5	6	5	0,41	3,90E-01	7,0	5,3	PBANKA_0904100	ras-related protein Rab-6
PBANKA_1113500.1-p1	5	7	5	7	6	5	-0,05	9,17E-01	5,7	6,0	PBANKA_1113500	ras-related protein Rab-1A, putative
PBANKA_1424200.1-p1	9	9	15	9	4	5	0,88	4,16E-02	11,0	6,0	PBANKA_1424200	conserved protein, unknown function
PBANKA_1345800.1-p1	8	4	17	10	4	4	0,69	1,46E-01	9,7	6,0	PBANKA_1345800	RNA-binding protein, putative
PBANKA_1302200.1-p1	6	4	6	8	5	3	0,04	9,69E-01	5,3	5,3	PBANKA_1302200	translocation protein SEC62, putative
PBANKA_0833100.1-p1	8	3	4	9	5	5	-0,29	5,67E-01	5,0	6,3	PBANKA_0833100	M18 aspartyl aminopeptidase, putative
PBANKA_0209200.1-p1	8	1	4	9	7	2	-0,41	4,89E-01	4,3	6,0	PBANKA_0209200	parasite-infected erythrocyte surface protein
PBANKA_1350600.1-p1	6	3	6	9	4	4	-0,14	7,83E-01	5,0	5,7	PBANKA_1350600	nuclear movement protein, putative
PBANKA_1446900.1-p1	4	2	4	6	9	4	-0,89	9,93E-02	3,3	6,3	PBANKA_1446900	dihydrolipoyl dehydrogenase, mitochondrial, putative
PBANKA_1023500.1-p1	4	4	5	7	6	5	-0,44	3,89E-01	4,3	6,0	PBANKA_1023500	eukaryotic translation initiation factor 3 subunit H, putative
PBANKA_0309100.1-p1	5	4	5	8	8	3	-0,40	4,26E-01	4,7	6,3	PBANKA_0309100	eukaryotic peptide chain release factor subunit 1, putative
PBANKA_0524300.1-p1	5	7	6	6	6	6	0,02	9,69E-01	6,0	6,0	PBANKA_0524300	tryptophan-rich protein
PBANKA_1422400.1-p1	2	2	6	9	5	5	-0,89	1,01E-01	3,3	6,3	PBANKA_1422400	importin subunit beta, putative
PBANKA_0401500.1-p1	5	5	6	8	5	4	-0,05	9,13E-01	5,3	5,7	PBANKA_0401500	exportin-1, putative
PBANKA_0101000.1-p1	1	2	9	6	5	4	-0,32	5,70E-01	4,0	5,0	PBANKA_0101000	MYND-type zinc finger protein, putative
PBANKA_0706800.1-p1	5	2	5	8	6	4	-0,55	2,95E-01	4,0	6,0	PBANKA_0706800	DnaJ protein, putative
PBANKA_1117700.1-p1	8	4	3	6	5	7	-0,23	6,59E-01	5,0	6,0	PBANKA_1117700	malate dehydrogenase, putative
PBANKA_1325600.1-p1	5	4	8	9	6	3	-0,06	9,11E-01	5,7	6,0	PBANKA_1325600	valine--tRNA ligase, putative
PBANKA_0720300.1-p1	3	2	4	8	4	6	-0,95	8,67E-02	3,0	6,0	PBANKA_0720300	eukaryotic translation initiation factor 3 subunit M, putative
PBANKA_0918300.1-p1	6	7	3	4	6	6	0,02	9,63E-01	5,3	5,3	PBANKA_0918300	major facilitator superfamily-related transporter, putative
PBANKA_0830000.1-p1	5	4	6	7	4	4	0,03	9,70E-01	5,0	5,0	PBANKA_0830000	RNA-binding protein, putative
PBANKA_0206300.1-p1	2	1	6	6	8	3	-0,89	1,22E-01	3,0	5,7	PBANKA_0206300	centrin-1, putative
PBANKA_1326300.1-p1	4	3	3	5	7	6	-0,81	1,37E-01	3,3	6,0	PBANKA_1326300	cytochrome c1, heme protein, mitochondrial, putative
PBANKA_0414400.1-p1	5	2	6	6	4	2	0,14	8,14E-01	4,3	4,0	PBANKA_0414400	formate-nitrite transporter, putative
PBANKA_0414500.1-p1	5	2	2	6	6	5	-0,86	1,22E-01	3,0	5,7	PBANKA_0414500	protein YOP1, putative
PBANKA_1322700.1-p1	10	7	14	11	4	2	0,90	5,67E-02	10,3	5,7	PBANKA_1322700	ATP-dependent RNA helicase DBP5, putative
PBANKA_1220200.1-p1	12	4	10	8	6	3	0,63	1,81E-01	8,7	5,7	PBANKA_1220200	lysophospholipase, putative
PBANKA_0715900.1-p1	7	2	5	8	5	4	-0,24	6,44E-01	4,7	5,7	PBANKA_0715900	ubiquitin carboxyl-terminal hydrolase 13, putative
PBANKA_0110400.1-p1	4	2	4	8	3	3	-0,43	4,37E-01	3,3	4,7	PBANKA_0110400	eukaryotic translation initiation factor 3 subunit L, putative
PBANKA_0920800.1-p1	3	5	7	7	6	3	-0,07	8,88E-01	5,0	5,3	PBANKA_0920800	CRAL/TRIO domain-containing protein, putative
PBANKA_0314600.1-p1	3	2	5	9	4	4	-0,72	1,87E-01	3,3	5,7	PBANKA_0314600	thioesterase/thiol ester dehydrase-isomerase, putative

Table S3: LCMSMS analyses of “all blood stages” parasites (raw data). Legends are indicated as well as the overall variability between samples (WT-2, WT-3, WT-4, KO-1, KO-2 and KO-4) is visualized using MDS plot.

PBANKA_0908800.1-p1	8	3	6	7	6	3	0,12	8,20E-01	5,7	5,3	PBANKA_0908800	conserved Plasmodium protein, unknown function
PBANKA_1211300.1-p1	4	2	4	8	7	2	-0,71	1,98E-01	3,3	5,7	PBANKA_1211300	autophagy-related protein 18, putative
PBANKA_0609900.1-p1	8	3	6	7	6	3	0,12	8,20E-01	5,7	5,3	PBANKA_0609900	heat shock protein DNAJ homologue Pfj4, putative
PBANKA_0314200.1-p1	4	2	4	6	7	4	-0,73	1,87E-01	3,3	5,7	PBANKA_0314200	calcium-dependent protein kinase 1
PBANKA_1127000.1-p1	3	3	4	3	4	2	0,16	7,95E-01	3,3	3,0	PBANKA_1127000	choline/ethanolaminephosphotransferase
PBANKA_0922300.1-p1	9	4	4	6	6	4	0,12	8,11E-01	5,7	5,3	PBANKA_0922300	threonine--tRNA ligase, putative
PBANKA_0704500.1-p1	2	2	4	8	6	2	-0,94	1,06E-01	2,7	5,3	PBANKA_0704500	HECT-like E3 ubiquitin ligase, putative
PBANKA_0711200.1-p1	9	4	8	8	5	2	0,51	3,07E-01	7,0	5,0	PBANKA_0711200	conserved protein, unknown function
PBANKA_1035100.1-p1	9	5	8	8	3	1	0,91	9,10E-02	7,3	4,0	PBANKA_1035100	rRNA 2'-O-methyltransferase fibrillarin, putative
PBANKA_1022800.1-p1	4	1	3	10	3	3	-0,92	1,20E-01	2,7	5,3	PBANKA_1022800	glycine--tRNA ligase, putative
PBANKA_1131900.1-p1	5	2	6	4	6	6	-0,30	6,03E-01	4,3	5,3	PBANKA_1131900	serine/threonine protein phosphatase 5
PBANKA_0617900.1-p1	6	4	3	8	5	3	-0,24	6,43E-01	4,3	5,3	PBANKA_0617900	apoptosis-inducing factor, putative
PBANKA_0404600.1-p1	4	3	6	7	6	2	-0,18	7,36E-01	4,3	5,0	PBANKA_0404600	activator of Hsp90 ATPase, putative
PBANKA_0808900.1-p1	3	2	2	8	4	2	-0,92	1,31E-01	2,3	4,7	PBANKA_0808900	ATP-dependent protease ATPase subunit ClpY, putative
PBANKA_0906200.1-p1	6	2	3	7	7	2	-0,49	3,80E-01	3,7	5,3	PBANKA_0906200	ATP synthase-associated protein, putative
PBANKA_1445800.1-p1	4	2	3	7	5	3	-0,68	2,31E-01	3,0	5,0	PBANKA_1445800	ras-related protein Rab-2, putative
PBANKA_1418300.1-p1	5	2	5	7	4	2	-0,08	8,85E-01	4,0	4,3	PBANKA_1418300	golgi protein 1, putative
PBANKA_0719300.1-p1	3	3	2	7	6	2	-0,84	1,50E-01	2,7	5,0	PBANKA_0719300	bifunctional dihydrofolate reductase-thymidylate synthase, putative
PBANKA_1231500.1-p1	5	3	3	8	4	1	-0,18	7,50E-01	3,7	4,3	PBANKA_1231500	ubiquitin carboxyl-terminal hydrolase 2, putative
PBANKA_1441400.1-p1	6	5	3	9	3	3	-0,03	9,47E-01	4,7	5,0	PBANKA_1441400	proliferating cell nuclear antigen 2
PBANKA_0605300.1-p1	4	2	5	7	5	3	-0,41	4,53E-01	3,7	5,0	PBANKA_0605300	eukaryotic translation initiation factor 5, putative
PBANKA_0813400.1-p1	4	5	2	8	2	4	-0,28	6,14E-01	3,7	4,7	PBANKA_0813400	alkaline phosphatase, putative
PBANKA_1310400.1-p1	4	4	3	5	7	3	-0,41	4,53E-01	3,7	5,0	PBANKA_1310400	centrin-2, putative
PBANKA_0913700.1-p1	6	2	8	7	5	3	0,11	8,37E-01	5,3	5,0	PBANKA_0913700	coatomer subunit delta, putative
PBANKA_1351800.1-p1	5	4	2	5	5	3	-0,20	7,19E-01	3,7	4,3	PBANKA_1351800	26S proteasome regulatory subunit RPN3, putative
PBANKA_1023900.1-p1	6	3	3	5	5	5	-0,29	5,88E-01	4,0	5,0	PBANKA_1023900	glutathione S-transferase, putative
PBANKA_1228400.1-p1	9	4	11	7	5	2	0,78	1,16E-01	8,0	4,7	PBANKA_1228400	mannose-6-phosphate isomerase, putative
PBANKA_0807000.1-p1	7	2	3	6	4	3	-0,07	8,94E-01	4,0	4,3	PBANKA_0807000	DNA-directed RNA polymerase II subunit RPB1, putative
PBANKA_1347800.1-p1	7	4	6	11	2	1	0,34	5,66E-01	5,7	4,7	PBANKA_1347800	20 kDa chaperonin, putative
PBANKA_0827500.1-p1	7	2	5	7	5	2	0,04	9,71E-01	4,7	4,7	PBANKA_0827500	glutamine-dependent NAD(+) synthetase, putative
PBANKA_1307800.1-p1	3	1	4	8	3	3	-0,75	2,09E-01	2,7	4,7	PBANKA_1307800	heat shock protein 90, putative
PBANKA_0924800.1-p1	4	3	4	4	5	4	-0,22	7,08E-01	3,7	4,3	PBANKA_0924800	golgi protein 2
PBANKA_0502200.1-p1	5	3	5	5	3	5	0,02	9,72E-01	4,3	4,3	PBANKA_0502200	26S proteasome regulatory subunit p55, putative
PBANKA_0921300.1-p1	6	2	5	8	4	2	-0,06	9,07E-01	4,3	4,7	PBANKA_0921300	deoxyuridine 5'-triphosphate nucleotidohydrolase, putative
PBANKA_1430800.1-p1	10	3	3	6	5	3	0,23	6,65E-01	5,3	4,7	PBANKA_1430800	thioredoxin peroxidase 2, putative
PBANKA_1202700.1-p1	3	3	6	8	3	3	-0,19	7,29E-01	4,0	4,7	PBANKA_1202700	RNA-binding protein, putative
PBANKA_0920000.1-p1	6	6	10	4	3	6	0,74	1,37E-01	7,3	4,3	PBANKA_0920000	multiprotein-bridging factor 1, putative
PBANKA_1103000.1-p1	4	3	7	6	4	4	0,01	9,81E-01	4,7	4,7	PBANKA_1103000	serine/arginine-rich splicing factor 12, putative
PBANKA_1218900.1-p1	4	2	5	8	3	2	-0,20	7,26E-01	3,7	4,3	PBANKA_1218900	elongation factor 1-delta, putative
PBANKA_1017900.1-p1	2	2	4	4	4	5	-0,67	2,87E-01	2,7	4,3	PBANKA_1017900	phosphoenolpyruvate carboxylase
PBANKA_1425000.1-p1	5	3	5	7	4	3	-0,07	8,91E-01	4,3	4,7	PBANKA_1425000	RNA-binding protein, putative
PBANKA_1008000.1-p1	5	2	4	5	4	3	-0,10	8,61E-01	3,7	4,0	PBANKA_1008000	armadillo-type repeat protein ATRP, putative
PBANKA_0315800.1-p1	3	3	3	3	5	3	-0,27	6,77E-01	3,0	3,7	PBANKA_0315800	ribosome associated membrane protein RAMP4, putative
PBANKA_0601100.1-p1	4	2	3	6	4	3	-0,48	4,11E-01	3,0	4,3	PBANKA_0601100	mitochondrial phosphate carrier protein, putative
PBANKA_1306000.1-p1	3	3	2	5	4	3	-0,53	3,86E-01	2,7	4,0	PBANKA_1306000	replication factor A protein 3, putative
PBANKA_0408600.1-p1	4	1	4	6	3	4	-0,49	4,11E-01	3,0	4,3	PBANKA_0408600	eukaryotic translation initiation factor 3 subunit K, putative
PBANKA_0823500.1-p1	8	4	8	5	5	3	0,62	2,17E-01	6,7	4,3	PBANKA_0823500	glutamine synthetase, putative
PBANKA_0833600.1-p1	3	2	4	6	4	3	-0,49	4,11E-01	3,0	4,3	PBANKA_0833600	importin alpha re-exporter, putative
PBANKA_1347700.1-p1	1	2	5	8	3	2	-0,65	2,87E-01	2,7	4,3	PBANKA_1347700	isoleucine--tRNA ligase, putative
PBANKA_0401600.1-p1	3	4	4	6	4	3	-0,21	7,08E-01	3,7	4,3	PBANKA_0401600	N-ethylmaleimide-sensitive fusion protein, putative
PBANKA_1004000.1-p1	5	5	9	8	2	3	0,57	2,76E-01	6,3	4,3	PBANKA_1004000	cytosolic glyoxalase II, putative
PBANKA_1210100.1-p1	3	1	5	7	2	3	-0,38	5,33E-01	3,0	4,0	PBANKA_1210100	DNA repair protein RAD23, putative
PBANKA_1426300.1-p1	5	1	1	5	6	2	-0,83	1,95E-01	2,3	4,3	PBANKA_1426300	ER membrane protein complex subunit 1, putative
PBANKA_1028700.1-p1	4	3	2	3	4	6	-0,50	4,11E-01	3,0	4,3	PBANKA_1028700	26S proteasome regulatory subunit RPN13, putative
PBANKA_0912100.1-p1	4	4	2	5	4	3	-0,22	6,95E-01	3,3	4,0	PBANKA_0912100	casein kinase 1, putative
PBANKA_1120800.1-p1	3	3	3	7	3	3	-0,48	4,11E-01	3,0	4,3	PBANKA_1120800	signal recognition particle subunit SRP68, putative
PBANKA_1116300.1-p1	4	1	2	6	5	2	-0,83	1,86E-01	2,3	4,3	PBANKA_1116300	malate:quinone oxidoreductase, putative
PBANKA_1223300.1-p1	3	2	3	5	5	1	-0,42	5,10E-01	2,7	3,7	PBANKA_1223300	ras-related protein Rab-18, putative
PBANKA_0718800.1-p1	2	1	4	5	4	4	-0,85	1,86E-01	2,3	4,3	PBANKA_0718800	small GTP-binding protein sar1, putative
PBANKA_1239500.1-p1	3	2	3	4	2	4	-0,29	6,58E-01	2,7	3,3	PBANKA_1239500	mitochondrial import receptor subunit TOM22, putative
PBANKA_0823100.1-p1	7	6	7	5	3	4	0,75	1,44E-01	6,7	4,0	PBANKA_0823100	S-adenosylmethionine synthetase, putative
PBANKA_1025200.1-p1	5	0	7	9	2	1	0,04	9,71E-01	4,0	4,0	PBANKA_1025200	H/ACA ribonucleoprotein complex subunit 4, putative
PBANKA_0909600.1-p1	1	1	4	4	5	3	-0,95	1,62E-01	2,0	4,0	PBANKA_0909600	AP2 domain transcription factor, putative
PBANKA_0514500.1-p1	6	2	4	6	4	2	0,03	9,73E-01	4,0	4,0	PBANKA_0514500	26S proteasome regulatory subunit RPN9, putative
PBANKA_0923700.1-p1	4	3	9	7	3	2	0,42	4,34E-01	5,3	4,0	PBANKA_0923700	ethanolamine kinase, putative
PBANKA_1321000.1-p1	5	3	3	6	3	3	-0,08	8,79E-01	3,7	4,0	PBANKA_1321000	MA3 domain-containing protein, putative
PBANKA_0916400.1-p1	3	3	2	5	4	2	-0,41	5,10E-01	2,7	3,7	PBANKA_0916400	ubiquitin-like protein, putative
PBANKA_0903900.1-p1	3	2	3	4	4	4	-0,55	3,86E-01	2,7	4,0	PBANKA_0903900	coatomer subunit gamma, putative
PBANKA_1338400.1-p1	6	3	6	5	3	4	0,33	5,39E-01	5,0	4,0	PBANKA_1338400	V-type proton ATPase subunit G, putative
PBANKA_1430200.1-p1	4	3	2	4	4	4	-0,38	5,33E-01	3,0	4,0	PBANKA_1430200	ER membrane protein complex subunit 6, putative
PBANKA_0800400.1-p1	2	3	2	3	3	2	-0,16	8,17E-01	2,3	2,7	PBANKA_0800400	conserved Plasmodium protein, unknown function
PBANKA_1309700.1-p1	5	4	5	3	2	4	0,63	2,80E-01	4,7	3,0	PBANKA_1309700	ATP-dependent RNA helicase DDX5, putative
PBANKA_1219500.1-p1	4	2	3	4	3	3	-0,12	8,42E-01	3,0	3,3	PBANKA_1219500	chloroquine resistance transporter, putative
PBANKA_1348100.1-p1	3	2	4	5	3	3	-0,26	6,77E-01	3,0	3,7	PBANKA_1348100	AMMECR1 domain-containing protein, putative
PBANKA_1221600.1-p1	5	3	3	4	4	3	0,03	9,74E-01	3,7	3,7	PBANKA_1221600	cell division cycle ATPase, putative
PBANKA_0813000.1-p1	5	3	4	8	2	1	0,17	8,09E-01	4,0	3,7	PBANKA_0813000	inhibitor of cysteine proteases
PBANKA_1358700.1-p1	4	2	3	4	3	4	-0,26	6,77E-01	3,0	3,7	PBANKA_1358700	conserved Plasmodium protein, unknown function
PBANKA_0506100.1-p1	7	2	3	6	3	2	0,17	8,09E-01	4,0	3,7	PBANKA_0506100	PHAX domain-containing protein, putative
PBANKA_0919100.1-p1	4	3	3	8	1	2	-0,08	8,90E-01	3,3	3,7	PBANKA_0919100	parasitophorous vacuolar protein 1
PBANKA_0942700.1-p1	5	2	6	4	4	2	0,38	5,10E-01	4,3	3,3	PBANKA_0942700	chromatin remodeling protein, putative
PBANKA_0704100.1-p1	3	4	3	5	2	4	-0,10	8,55E-01	3,3	3,7	PBANKA_0704100	ubiquitin conjugation factor E4 B, putative
PBANKA_0105500.1-p1	7	1	4	6	4	1	0,16	7,96E-01	4,0	3,7	PBANKA_0105500	glutaredoxin-like protein

Table S3: LCMSMS analyses of “all blood stages” parasites (raw data). Legends are indicated as well as the overall variability between samples (WT-2, WT-3, WT-4, KO-1, KO-2 and KO-4) is visualized using MDS plot.

PBANKA_0810500.1-p1	4	3	5	6	2	2	0,29	6,46E-01	4,0	3,3		PBANKA_0810500	apoptosis-related protein, putative
PBANKA_1323000.1-p1	2	1	4	4	4	3	-0,62	3,59E-01	2,3	3,7		PBANKA_1323000	conserved protein, unknown function
PBANKA_0928800.1-p1	5	1	7	4	4	3	0,24	6,75E-01	4,3	3,7		PBANKA_0928800	splicing factor U2AF small subunit, putative
PBANKA_0706700.1-p1	3	1	3	4	3	3	-0,47	4,83E-01	2,3	3,3		PBANKA_0706700	dicarboxylate/tricarboxylate carrier, putative
PBANKA_1103100.1-p1	4	3	3	3	3	3	0,17	7,95E-01	3,3	3,0		PBANKA_1103100	actin-depolymerizing factor 1
PBANKA_0816100.1-p1	2	1	4	4	4	3	-0,62	3,59E-01	2,3	3,7		PBANKA_0816100	SUMO-conjugating enzyme UBC9, putative
PBANKA_0517500.1-p1	5	2	8	5	2	2	0,73	2,06E-01	5,0	3,0		PBANKA_0517500	bromodomain protein 1, putative
PBANKA_1122000.1-p1	3	1	3	4	4	2	-0,47	4,83E-01	2,3	3,3		PBANKA_1122000	nuclear polyadenylated RNA-binding protein NAB2, putative
PBANKA_0508100.1-p1	3	0	7	5	2	2	0,16	8,26E-01	3,3	3,0		PBANKA_0508100	chromodomain-helicase-DNA-binding protein 1, putative
PBANKA_0316200.1-p1	1	1	4	5	3	2	-0,69	3,28E-01	2,0	3,3		PBANKA_0316200	Plasmodium exported protein, unknown function
PBANKA_0813900.1-p1	3	4	2	5	3	2	-0,11	8,54E-01	3,0	3,3		PBANKA_0813900	26S proteasome regulatory subunit RPN8, putative
PBANKA_1345600.1-p1	5	4	4	6	4	0	0,41	5,16E-01	4,3	3,3		PBANKA_1345600	elongation factor Tu, putative
PBANKA_0806400.1-p1	3	2	2	3	5	2	-0,47	4,83E-01	2,3	3,3		PBANKA_0806400	conserved protein, unknown function
PBANKA_1146000.1-p1	3	2	4	2	5	3	-0,14	8,42E-01	3,0	3,3		PBANKA_1146000	tryptophan-rich protein
PBANKA_1116500.1-p1	3	1	2	5	3	2	-0,67	3,28E-01	2,0	3,3		PBANKA_1116500	mitochondrial import receptor subunit TOM40, putative
PBANKA_1125500.1-p1	4	3	2	4	4	2	-0,12	8,45E-01	3,0	3,3		PBANKA_1125500	ATPase, putative
PBANKA_0943100.1-p1	3	1	2	5	2	2	-0,52	4,53E-01	2,0	3,0		PBANKA_0943100	CCR4-NOT transcription complex subunit 1, putative
PBANKA_1209800.1-p1	3	3	3	3	3	4	-0,13	8,42E-01	3,0	3,3		PBANKA_1209800	proteasome subunit beta type-5, putative
PBANKA_0819000.1-p1	6	4	4	3	4	2	0,64	2,80E-01	4,7	3,0		PBANKA_0819000	glideosome-associated protein 50, putative
PBANKA_1334100.1-p1	4	0	4	6	2	2	-0,28	6,84E-01	2,7	3,3		PBANKA_1334100	proteasome subunit beta type-2, putative
PBANKA_1400700.1-p1	3	2	2	3	4	3	-0,47	4,83E-01	2,3	3,3		PBANKA_1400700	Plasmodium exported protein, unknown function
PBANKA_0523100.1-p1	3	0	3	4	4	2	-0,69	3,28E-01	2,0	3,3		PBANKA_0523100	eukaryotic initiation factor 4A-III, putative
PBANKA_1025800.1-p1	3	3	3	7	1	2	-0,10	8,67E-01	3,0	3,3		PBANKA_1025800	prefoldin subunit 2, putative
PBANKA_1140600.1-p1	2	3	2	2	4	3	-0,33	6,36E-01	2,3	3,0		PBANKA_1140600	DNA-directed RNA polymerases I, II, and III subunit RPABC1, putative
PBANKA_1332100.1-p1	2	2	4	4	3	3	-0,29	6,58E-01	2,7	3,3		PBANKA_1332100	zinc finger protein, putative
PBANKA_1356700.1-p1	8	3	6	4	3	2	0,92	1,06E-01	5,7	3,0		PBANKA_1356700	kelch protein K13, putative
PBANKA_1446500.1-p1	2	3	8	3	2	3	0,68	2,59E-01	4,3	2,7		PBANKA_1446500	asparagine-rich protein, putative
PBANKA_1205900.1-p1	3	4	6	3	3	2	0,69	2,59E-01	4,3	2,7		PBANKA_1205900	AP2 domain transcription factor AP2-I, putative
PBANKA_0929800.1-p1	2	1	3	2	5	2	-0,55	4,53E-01	2,0	3,0		PBANKA_0929800	insulinase, putative
PBANKA_0927200.1-p1	1	0	8	4	3	2	-0,01	9,96E-01	3,0	3,0		PBANKA_0927200	conserved protein, unknown function
PBANKA_1225700.1-p1	2	3	3	4	2	3	-0,14	8,30E-01	2,7	3,0		PBANKA_1225700	GTPase-activating protein, putative
PBANKA_1120200.1-p1	3	2	6	5	4	0	0,30	6,51E-01	3,7	3,0		PBANKA_1120200	pyridoxine biosynthesis protein PDX1, putative
PBANKA_0401100.1-p1	4	3	4	4	2	3	0,30	6,32E-01	3,7	3,0		PBANKA_0401100	serine/threonine protein kinase, putative
PBANKA_1239200.1-p1	3	2	5	3	2	2	0,51	4,48E-01	3,3	2,3		PBANKA_1239200	ribosome-interacting GTPase 1, putative
PBANKA_1009300.1-p1	2	3	5	3	2	4	0,15	7,95E-01	3,3	3,0		PBANKA_1009300	clathrin light chain, putative
PBANKA_1458300.1-p1	3	3	1	2	4	3	-0,33	6,36E-01	2,3	3,0		PBANKA_1458300	kinesin-13, putative
PBANKA_0105300.1-p1	1	1	3	3	4	2	-0,79	2,93E-01	1,7	3,0		PBANKA_0105300	conserved Plasmodium protein, unknown function
PBANKA_0302000.1-p1	2	2	2	4	3	2	-0,53	4,53E-01	2,0	3,0		PBANKA_0302000	conserved Plasmodium protein, unknown function
PBANKA_0213100.1-p1	4	3	4	3	3	3	0,30	6,32E-01	3,7	3,0		PBANKA_0213100	signal recognition particle subunit SRP9, putative
PBANKA_0406700.1-p1	1	1	3	3	2	4	-0,79	2,93E-01	1,7	3,0		PBANKA_0406700	activator of Hsp90 ATPase, putative
PBANKA_0418000.1-p1	5	3	5	3	3	2	0,69	2,59E-01	4,3	2,7		PBANKA_0418000	ATP-dependent RNA helicase DDX60, putative
PBANKA_0406800.1-p1	5	0	2	4	3	1	-0,15	8,41E-01	2,3	2,7		PBANKA_0406800	pre-mRNA-processing factor 19, putative
PBANKA_1213000.1-p1	3	3	4	3	4	1	0,33	6,16E-01	3,3	2,7		PBANKA_1213000	transcriptional coactivator ADA2, putative
PBANKA_0210200.1-p1	4	2	4	4	3	1	0,33	6,16E-01	3,3	2,7		PBANKA_0210200	aspartate--tRNA ligase, putative
PBANKA_1132400.1-p1	4	2	2	3	1	4	0,02	9,78E-01	2,7	2,7		PBANKA_1132400	conserved Plasmodium protein, unknown function
PBANKA_1112400.1-p1	3	3	3	4	2	2	0,19	7,86E-01	3,0	2,7		PBANKA_1112400	orotate phosphoribosyltransferase, putative
PBANKA_0823900.1-p1	2	0	3	4	3	1	-0,62	4,40E-01	1,7	2,7		PBANKA_0823900	DNA-directed RNA polymerase II subunit RPB3, putative
PBANKA_1244000.1-p1	2	2	5	2	2	4	0,16	7,97E-01	3,0	2,7		PBANKA_1244000	cell cycle regulator protein, putative
PBANKA_1350700.1-p1	2	3	4	2	3	3	0,17	7,86E-01	3,0	2,7		PBANKA_1350700	tryptophan--tRNA ligase, putative
PBANKA_0605400.1-p1	2	1	3	3	3	2	-0,38	6,10E-01	2,0	2,7		PBANKA_0605400	conserved Plasmodium protein, unknown function
PBANKA_0834000.1-p1	1	1	5	4	4	0	-0,17	8,26E-01	2,3	2,7		PBANKA_0834000	calcyclin-binding protein, putative
PBANKA_1122500.1-p1	2	1	2	3	2	2	-0,44	5,87E-01	1,7	2,3		PBANKA_1122500	splicing factor-like protein 1, putative
PBANKA_1218500.1-p1	3	4	3	4	2	2	0,34	6,16E-01	3,3	2,7		PBANKA_1218500	protein phosphatase inhibitor 2, putative
PBANKA_0409800.1-p1	3	0	1	4	3	1	-0,91	2,98E-01	1,3	2,7		PBANKA_0409800	ATP synthase F0 subunit d-like protein, putative
PBANKA_1420300.1-p1	1	2	1	2	3	2	-0,74	4,01E-01	1,3	2,3		PBANKA_1420300	conserved Plasmodium protein, unknown function
PBANKA_1459800.1-p1	2	1	2	1	4	2	-0,45	5,82E-01	1,7	2,3		PBANKA_1459800	conserved Plasmodium protein, unknown function
PBANKA_1104200.1-p1	3	1	1	3	3	2	-0,61	4,24E-01	1,7	2,7		PBANKA_1104200	2-oxoisovalerate dehydrogenase subunit beta, mitochondrial, putative
PBANKA_1413200.1-p1	2	2	1	3	2	2	-0,43	5,95E-01	1,7	2,3		PBANKA_1413200	pinin/SDK/MemA domain-containing protein, putative
PBANKA_1014900.1-p1	5	3	3	2	3	2	0,65	3,29E-01	3,7	2,3		PBANKA_1014900	coatomer subunit beta, putative
PBANKA_0610800.1-p1	4	0	3	3	4	0	0,02	9,82E-01	2,3	2,3		PBANKA_0610800	eukaryotic translation initiation factor eIF2A, putative
PBANKA_1028300.1-p1	3	3	3	5	1	1	0,38	5,97E-01	3,0	2,3		PBANKA_1028300	serine/threonine protein phosphatase PP1
PBANKA_0922800.1-p1	2	1	4	3	2	1	0,23	7,68E-01	2,3	2,0		PBANKA_0922800	small nuclear ribonucleoprotein Sm D1, putative
PBANKA_1455300.1-p1	3	0	2	4	1	2	-0,43	6,15E-01	1,7	2,3		PBANKA_1455300	tetratricopeptide repeat protein, putative
PBANKA_1220300.1-p1	4	1	1	5	1	1	-0,16	8,36E-01	2,0	2,3		PBANKA_1220300	prodrug activation and resistance esterase, putative
PBANKA_1239800.1-p1	2	2	6	2	2	3	0,49	4,48E-01	3,3	2,3		PBANKA_1239800	zinc finger protein, putative
PBANKA_1144800.1-p1	1	3	3	2	3	2	0,01	9,87E-01	2,3	2,3		PBANKA_1144800	conserved protein, unknown function
PBANKA_0719100.1-p1	3	1	1	3	2	2	-0,43	5,99E-01	1,7	2,3		PBANKA_0719100	conserved Plasmodium protein, unknown function
PBANKA_1117400.1-p1	2	2	4	3	3	1	0,20	7,76E-01	2,7	2,3		PBANKA_1117400	conserved protein, unknown function
PBANKA_1462000.1-p1	4	0	5	2	3	1	0,56	4,55E-01	3,0	2,0		PBANKA_1462000	conserved protein, unknown function
PBANKA_0404200.1-p1	1	2	3	4	2	1	-0,19	8,08E-01	2,0	2,3		PBANKA_0404200	ubiquitin-conjugating enzyme E2, putative
PBANKA_1355500.1-p1	1	3	3	3	2	2	0,02	9,79E-01	2,3	2,3		PBANKA_1355500	casein kinase II beta chain, putative
PBANKA_0709100.1-p1	4	1	4	4	2	1	0,37	5,97E-01	3,0	2,3		PBANKA_0709100	60S ribosomal protein L22, putative
PBANKA_1457400.1-p1	1	0	3	5	1	1	-0,73	4,36E-01	1,3	2,3		PBANKA_1457400	N-alpha-acetyltransferase 15, NatA auxiliary subunit, putative
PBANKA_0701100.1-p1	0	1	3	3	2	2	-0,74	4,12E-01	1,3	2,3		PBANKA_0701100	CRA domain-containing protein, putative
PBANKA_0700700.1-p1	3	1	1	3	2	2	-0,43	5,99E-01	1,7	2,3		PBANKA_0700700	Plasmodium exported protein, unknown function
PBANKA_0305900.1-p1	2	1	3	4	2	1	-0,19	8,08E-01	2,0	2,3		PBANKA_0305900	conserved Plasmodium protein, unknown function
PBANKA_0706200.1-p1	1	1	3	2	2	2	-0,24	7,82E-01	1,7	2,0		PBANKA_0706200	nucleoside transporter 2, putative
PBANKA_0506700.1-p1	3	1	1	3	3	1	-0,43	6,03E-01	1,7	2,3		PBANKA_0506700	citrate synthase, mitochondrial, putative
PBANKA_1323700.1-p1	2	1	3	2	3	2	-0,20	8,01E-01	2,0	2,3		PBANKA_1323700	FYVE and coiled-coil domain-containing protein, putative
PBANKA_1202100.1-p1	1	3	1	3	4	3	-0,93	2,02E-01	1,7	3,3		PBANKA_1202100	MKT1 domain-containing protein, putative
PBANKA_0836200.1-p1	0	3	3	2	5	4	-0,84	2,33E-01	2,0	3,7		PBANKA_0836200	conserved Plasmodium protein, unknown function
PBANKA_1435200.1-p1	3	1	0	2	4	2	-0,91	2,92E-01	1,3	2,7		PBANKA_1435200	zinc finger protein, putative

Table S3: LCMSMS analyses of “all blood stages” parasites (raw data). Legends are indicated as well as the overall variability between samples (WT-2, WT-3, WT-4, KO-1, KO-2 and KO-4) is visualized using MDS plot.

PBANKA_0310600.1-p1	1	2	2	3	3	3	-0,79	2,93E-01	1,7	3,0	PBANKA_0310600	conserved protein, unknown function
PBANKA_1409600.1-p1	2	3	2	3	4	4	-0,61	3,59E-01	2,3	3,7	PBANKA_1409600	meiosis-specific nuclear structural protein 1, putative
PBANKA_1405400.1-p1	1	1	1	1	3	2	-0,91	3,74E-01	1,0	2,0	PBANKA_1405400	U1 small nuclear ribonucleoprotein A, putative
PBANKA_1429400.1-p1	1	2	0	2	2	2	-0,89	3,93E-01	1,0	2,0	PBANKA_1429400	dynein light chain 1, putative
PBANKA_0407300.1-p1	2	3	0	5	1	2	-0,59	4,69E-01	1,7	2,7	PBANKA_0407300	OMD protein
PBANKA_0523900.1-p1	1	1	0	1	2	1	-0,86	5,06E-01	0,7	1,3	PBANKA_0523900	glideosome associated protein with multiple membrane spans 2, putative
PBANKA_0522900.1-p1	0	1	1	2	2	0	-0,86	5,14E-01	0,7	1,3	PBANKA_0522900	pre-mRNA-splicing helicase BRR2, putative
PBANKA_1425400.1-p1	0	1	1	3	0	1	-0,85	5,21E-01	0,7	1,3	PBANKA_1425400	proteasome activator complex subunit 4, putative
PBANKA_0919900.1-p1	1	1	0	3	0	1	-0,84	5,27E-01	0,7	1,3	PBANKA_0919900	ATP-dependent 6-phosphofructokinase, putative
PBANKA_0415500.1-p1	1	1	1	4	1	0	-0,63	5,76E-01	1,0	1,7	PBANKA_0415500	coatomer subunit beta, putative
PBANKA_1105400.1-p1	1	4	1	4	2	2	-0,36	6,26E-01	2,0	2,7	PBANKA_1105400	small ubiquitin-related modifier, putative
PBANKA_1035500.1-p1	0	0	1	1	1	0	-0,78	6,55E-01	0,3	0,7	PBANKA_1035500	vacuolar protein sorting-associated protein 29, putative
PBANKA_1428500.1-p1	1	1	3	4	1	2	-0,44	5,97E-01	1,7	2,3	PBANKA_1428500	glycerol-3-phosphate 1-O-acyltransferase, putative
PBANKA_0933900.1-p1	1	0	3	4	1	2	-0,74	4,23E-01	1,3	2,3	PBANKA_0933900	glyoxalase I, putative
PBANKA_1302500.1-p1	3	0	2	4	2	1	-0,43	6,15E-01	1,7	2,3	PBANKA_1302500	conserved protein, unknown function
PBANKA_1235100.1-p1	0	2	3	1	2	2	0,00	9,99E-01	1,7	1,7	PBANKA_1235100	U6 snRNA-associated Sm-like protein LSm2, putative
PBANKA_1339900.1-p1	2	2	1	2	2	2	-0,22	7,95E-01	1,7	2,0	PBANKA_1339900	SNARE protein, putative
PBANKA_0826300.1-p1	1	1	2	3	2	2	-0,74	3,99E-01	1,3	2,3	PBANKA_0826300	thioredoxin-like protein 2, putative
PBANKA_0111200.1-p1	2	3	5	2	2	2	0,71	3,02E-01	3,3	2,0	PBANKA_0111200	nucleolar GTP-binding protein 1, putative
PBANKA_1003100.1-p1	2	1	1	3	3	0	-0,51	5,98E-01	1,3	2,0	PBANKA_1003100	pre-mRNA-processing-splicing factor 8, putative
PBANKA_1421100.1-p1	0	1	6	2	2	2	0,20	8,05E-01	2,3	2,0	PBANKA_1421100	transcription elongation factor s-II, putative
PBANKA_0205400.1-p1	3	1	2	2	1	3	0,02	9,82E-01	2,0	2,0	PBANKA_0205400	proteasome subunit beta type-3, putative
PBANKA_1025500.1-p1	1	0	2	5	1	0	-0,88	4,22E-01	1,0	2,0	PBANKA_1025500	NOT family protein, putative
PBANKA_1360500.1-p1	3	1	5	3	1	2	0,57	4,21E-01	3,0	2,0	PBANKA_1360500	ethanolamine-phosphate cytidylyltransferase
PBANKA_1426200.1-p1	3	0	2	3	3	0	-0,22	8,13E-01	1,7	2,0	PBANKA_1426200	CCR4-associated factor 1, putative
PBANKA_0941100.1-p1	2	1	1	4	1	1	-0,50	5,96E-01	1,3	2,0	PBANKA_0941100	conserved Apicomplexan protein, unknown function
PBANKA_1327300.1-p1	1	1	3	4	2	0	-0,22	8,08E-01	1,7	2,0	PBANKA_1327300	fam-a protein
PBANKA_1414400.1-p1	3	3	2	1	2	2	0,66	3,89E-01	2,7	1,7	PBANKA_1414400	exportin-T, putative
PBANKA_0802300.1-p1	3	1	2	4	1	1	0,04	9,66E-01	2,0	2,0	PBANKA_0802300	HECT-type E3 ubiquitin ligase UT, putative
PBANKA_0904500.1-p1	2	0	2	3	2	1	-0,52	5,88E-01	1,3	2,0	PBANKA_0904500	SUMO-activating enzyme subunit 1, putative
PBANKA_1010200.1-p1	2	0	2	3	2	1	-0,52	5,88E-01	1,3	2,0	PBANKA_1010200	methionine aminopeptidase 2, putative
PBANKA_0939900.1-p1	3	0	1	3	1	2	-0,51	5,97E-01	1,3	2,0	PBANKA_0939900	U6 snRNA-associated Sm-like protein LSm4, putative
PBANKA_0712100.1-p1	1	2	1	1	4	0	-0,28	7,88E-01	1,3	1,7	PBANKA_0712100	DNA helicase, putative
PBANKA_0506600.1-p1	1	1	2	2	3	1	-0,53	5,72E-01	1,3	2,0	PBANKA_0506600	serine/arginine-rich splicing factor 4, putative
PBANKA_0715700.1-p1	2	3	3	3	2	1	0,42	5,75E-01	2,7	2,0	PBANKA_0715700	lysine decarboxylase-like protein, putative
PBANKA_1235200.1-p1	2	1	2	3	1	1	0,03	9,76E-01	1,7	1,7	PBANKA_1235200	single-stranded DNA-binding protein, putative
PBANKA_0516300.1-p1	2	1	2	2	1	2	0,02	9,84E-01	1,7	1,7	PBANKA_0516300	DER1-like protein, putative
PBANKA_1107200.1-p1	3	1	1	3	1	1	0,04	9,69E-01	1,7	1,7	PBANKA_1107200	protein CAF40, putative
PBANKA_1445100.1-p1	1	1	1	0	3	3	-0,92	3,86E-01	1,0	2,0	PBANKA_1445100	ATP-dependent protease subunit ClpQ, putative
PBANKA_1449700.1-p1	2	1	1	2	1	3	-0,52	5,78E-01	1,3	2,0	PBANKA_1449700	conserved protein, unknown function
PBANKA_1215500.1-p1	3	3	2	3	2	1	0,42	5,75E-01	2,7	2,0	PBANKA_1215500	translation machinery-associated protein 7, putative
PBANKA_1036200.1-p1	2	1	2	2	2	2	-0,23	7,87E-01	1,7	2,0	PBANKA_1036200	RNA-binding protein 8A, putative
PBANKA_0815200.1-p1	2	1	1	2	2	2	-0,52	5,75E-01	1,3	2,0	PBANKA_0815200	phospholipid or glycerol acyltransferase, putative
PBANKA_1014000.1-p1	2	0	2	3	2	1	-0,52	5,88E-01	1,3	2,0	PBANKA_1014000	NADP-specific glutamate dehydrogenase, putative
PBANKA_1340200.1-p1	1	0	3	3	1	2	-0,53	5,84E-01	1,3	2,0	PBANKA_1340200	U6 snRNA-associated Sm-like protein LSm6, putative
PBANKA_1244400.1-p1	1	2	5	3	1	2	0,40	5,81E-01	2,7	2,0	PBANKA_1244400	conserved Plasmodium protein, unknown function
PBANKA_0402800.1-p1	4	0	3	2	1	2	0,47	5,78E-01	2,3	1,7	PBANKA_0402800	EH domain-containing protein, putative
PBANKA_1434100.1-p1	5	0	0	4	1	0	0,06	9,65E-01	1,7	1,7	PBANKA_1434100	dynamin-like protein, putative
PBANKA_0402300.1-p1	3	1	0	3	1	1	-0,25	8,07E-01	1,3	1,7	PBANKA_0402300	lipoamide acyltransferase component of branched-chain alpha-keto acid dehydrog
PBANKA_1433500.1-p1	3	1	2	3	1	1	0,28	7,51E-01	2,0	1,7	PBANKA_1433500	PPPDE peptidase domain-containing protein, putative
PBANKA_1428900.1-p1	3	0	4	1	2	2	0,46	5,91E-01	2,3	1,7	PBANKA_1428900	bromodomain protein 2, putative
PBANKA_1458000.1-p1	2	1	4	2	1	2	0,47	5,68E-01	2,3	1,7	PBANKA_1458000	translation machinery-associated protein 46, putative
PBANKA_0515900.1-p1	1	1	2	3	2	0	-0,27	7,92E-01	1,3	1,7	PBANKA_0515900	mRNA-decapping enzyme subunit 1, putative
PBANKA_1313800.1-p1	0	2	3	3	0	2	0,02	9,85E-01	1,7	1,7	PBANKA_1313800	signal recognition particle subunit SRP54, putative
PBANKA_1424400.1-p1	2	3	2	3	1	1	0,49	5,48E-01	2,3	1,7	PBANKA_1424400	CS domain protein, putative
PBANKA_1029800.1-p1	3	1	3	4	0	1	0,49	5,67E-01	2,3	1,7	PBANKA_1029800	glycylpeptide N-tetradecanoyltransferase, putative
PBANKA_1109000.1-p1	2	2	4	1	3	1	0,64	4,04E-01	2,7	1,7	PBANKA_1109000	RNA polymerase I, putative
PBANKA_0416500.1-p1	2	2	1	2	1	2	0,03	9,77E-01	1,7	1,7	PBANKA_0416500	copper-transporting ATPase
PBANKA_1211700.1-p1	1	1	2	2	1	2	-0,28	7,77E-01	1,3	1,7	PBANKA_1211700	conserved Plasmodium protein, unknown function
PBANKA_1354100.1-p1	1	1	1	2	1	1	-0,35	7,61E-01	1,0	1,3	PBANKA_1354100	ras-related protein Rab-11B, putative
PBANKA_0924400.1-p1	2	2	2	1	2	1	0,56	5,49E-01	2,0	1,3	PBANKA_0924400	13 kDa ribonucleoprotein-associated protein, putative
PBANKA_1032500.1-p1	2	2	1	2	2	1	0,03	9,77E-01	1,7	1,7	PBANKA_1032500	ER membrane protein complex subunit 2, putative
PBANKA_1024800.1-p1	3	1	1	1	3	1	0,02	9,85E-01	1,7	1,7	PBANKA_1024800	ATP synthase-associated protein, putative
PBANKA_0701500.1-p1	2	0	3	3	1	1	0,02	9,84E-01	1,7	1,7	PBANKA_0701500	prohibitin 1
PBANKA_1451600.1-p1	1	1	1	2	1	1	-0,35	7,61E-01	1,0	1,3	PBANKA_1451600	SUMO-activating enzyme subunit 2, putative
PBANKA_1124600.1-p1	2	0	1	3	1	1	-0,64	5,65E-01	1,0	1,7	PBANKA_1124600	conserved protein, unknown function
PBANKA_0808200.1-p1	2	1	1	3	1	1	-0,26	7,93E-01	1,3	1,7	PBANKA_0808200	proteasome subunit alpha type-3, putative
PBANKA_1105300.1-p1	3	2	0	1	1	3	0,03	9,79E-01	1,7	1,7	PBANKA_1105300	conserved Plasmodium protein, unknown function
PBANKA_0316941.1-p1	2	1	2	1	1	1	0,69	5,25E-01	1,7	1,0	PBANKA_0316941	PIR protein
PBANKA_0611800.1-p1	3	1	2	4	1	0	0,29	7,54E-01	2,0	1,7	PBANKA_0611800	N-acetyltransferase, GNAT family, putative
PBANKA_1431900.1-p1	2	2	3	3	1	1	0,48	5,53E-01	2,3	1,7	PBANKA_1431900	glycerol-3-phosphate dehydrogenase [NAD(+)], putative
PBANKA_0920900.1-p1	1	2	2	2	2	1	0,02	9,84E-01	1,7	1,7	PBANKA_0920900	protein disulfide-isomerase, putative
PBANKA_1347400.1-p1	1	1	2	3	1	1	-0,27	7,86E-01	1,3	1,7	PBANKA_1347400	DNA-(apurinic or apyrimidinic site) lyase 1, putative
PBANKA_0411700.1-p1	3	1	2	3	1	1	0,28	7,51E-01	2,0	1,7	PBANKA_0411700	HSP20-like chaperone, putative
PBANKA_1018400.1-p1	3	1	1	3	1	1	0,04	9,69E-01	1,7	1,7	PBANKA_1018400	protein arginine N-methyltransferase 1, putative
PBANKA_1432500.1-p1	2	0	2	2	1	1	0,02	9,86E-01	1,3	1,3	PBANKA_1432500	DNA-binding chaperone, putative
PBANKA_0829700.1-p1	2	2	2	1	2	2	0,26	7,63E-01	2,0	1,7	PBANKA_0829700	guanylate kinase, putative
PBANKA_1464200.1-p1	2	2	1	2	2	1	0,03	9,77E-01	1,7	1,7	PBANKA_1464200	thymidylate kinase, putative
PBANKA_1306300.1-p1	1	1	2	2	2	1	-0,28	7,77E-01	1,3	1,7	PBANKA_1306300	protein KIC9, putative
PBANKA_0907300.1-p1	0	1	2	2	1	1	-0,36	7,60E-01	1,0	1,3	PBANKA_0907300	OTU domain-containing protein, putative
PBANKA_0929600.1-p1	1	1	5	2	0	2	0,76	4,13E-01	2,3	1,3	PBANKA_0929600	nucleolar protein 56, putative
PBANKA_1308900.1-p1	3	0	1	1	1	2	0,02	9,88E-01	1,3	1,3	PBANKA_1308900	histidine--tRNA ligase, putative

Table S3: LCMSMS analyses of “all blood stages” parasites (raw data). Legends are indicated as well as the overall variability between samples (WT-2, WT-3, WT-4, KO-1, KO-2 and KO-4) is visualized using MDS plot.

PBANKA_0401800.1-p1	3	0	1	3	1	0	0,04	9,73E-01	1,3	1,3	PBANKA_0401800	HAD superfamily protein, putative
PBANKA_0942900.1-p1	2	1	0	3	1	0	-0,33	7,86E-01	1,0	1,3	PBANKA_0942900	phenylalanine--tRNA ligase beta subunit, putative
PBANKA_1032300.1-p1	1	2	2	4	0	0	0,34	7,51E-01	1,7	1,3	PBANKA_1032300	CTP synthase, putative
PBANKA_0717400.1-p1	2	0	0	3	0	1	-0,84	5,35E-01	0,7	1,3	PBANKA_0717400	coatomer subunit zeta, putative
PBANKA_0208600.1-p1	2	0	0	1	0	2	-0,48	7,36E-01	0,7	1,0	PBANKA_0208600	conserved protein, unknown function
PBANKA_1213100.1-p1	1	0	3	2	2	0	0,01	9,93E-01	1,3	1,3	PBANKA_1213100	prohibitin 2
PBANKA_1308200.1-p1	2	0	2	2	1	0	0,40	7,41E-01	1,3	1,0	PBANKA_1308200	1-acyl-sn-glycerol-3-phosphate acyltransferase, putative
PBANKA_1009500.1-p1	2	2	0	1	2	1	0,03	9,81E-01	1,3	1,3	PBANKA_1009500	glutamate synthase [NADH], putative
PBANKA_1448200.1-p1	1	1	2	2	1	1	0,02	9,86E-01	1,3	1,3	PBANKA_1448200	asparagine/aspartate rich protein, putative
PBANKA_0801900.1-p1	0	2	1	2	1	1	-0,35	7,67E-01	1,0	1,3	PBANKA_0801900	methyltransferase, putative
PBANKA_0616700.1-p1	2	1	0	1	0	2	0,03	9,84E-01	1,0	1,0	PBANKA_0616700	NIMA related kinase 4
PBANKA_1357700.1-p1	0	0	3	2	2	0	-0,37	7,66E-01	1,0	1,3	PBANKA_1357700	aspartate carbamoyltransferase, putative
PBANKA_0206000.1-p1	2	0	0	1	3	0	-0,86	5,26E-01	0,7	1,3	PBANKA_0206000	ATP synthase-associated protein, putative
PBANKA_1336300.1-p1	1	0	1	1	1	2	-0,87	5,00E-01	0,7	1,3	PBANKA_1336300	GTPase-activating protein, putative
PBANKA_1346200.1-p1	1	1	1	1	2	1	-0,36	7,55E-01	1,0	1,3	PBANKA_1346200	signal peptidase complex catalytic subunit SEC11, putative
PBANKA_1112700.1-p1	2	1	0	1	2	1	-0,35	7,67E-01	1,0	1,3	PBANKA_1112700	conserved protein, unknown function
PBANKA_0911400.1-p1	3	0	1	3	1	0	0,04	9,73E-01	1,3	1,3	PBANKA_0911400	CLPTM1 domain-containing protein, putative
PBANKA_0933800.1-p1	1	0	1	1	3	0	-0,87	5,12E-01	0,7	1,3	PBANKA_0933800	conserved Plasmodium protein, unknown function
PBANKA_0828100.1-p1	1	0	1	1	1	2	-0,87	5,00E-01	0,7	1,3	PBANKA_0828100	fumarate hydratase, putative
PBANKA_0107600.1-p1	1	0	1	2	1	1	-0,86	5,05E-01	0,7	1,3	PBANKA_0107600	nucleoporin NUP637, putative
PBANKA_0302300.1-p1	2	1	1	4	0	0	0,05	9,66E-01	1,3	1,3	PBANKA_0302300	aspartate aminotransferase, putative
PBANKA_1118700.1-p1	1	0	1	1	2	1	-0,87	5,00E-01	0,7	1,3	PBANKA_1118700	acyl-CoA synthetase, putative
PBANKA_1208500.1-p1	1	0	1	3	0	1	-0,85	5,21E-01	0,7	1,3	PBANKA_1208500	PI31 domain-containing protein, putative
PBANKA_1357800.1-p1	1	0	2	2	1	1	-0,36	7,60E-01	1,0	1,3	PBANKA_1357800	conserved Plasmodium protein, unknown function
PBANKA_1415100.1-p1	2	0	1	2	2	0	-0,35	7,72E-01	1,0	1,3	PBANKA_1415100	choline-phosphate cytidylyltransferase
PBANKA_1128200.1-p1	1	0	1	3	1	0	-0,85	5,21E-01	0,7	1,3	PBANKA_1128200	polyadenylate-binding protein 3, putative
PBANKA_1242700.1-p1	1	0	1	2	0	1	-0,48	7,31E-01	0,7	1,0	PBANKA_1242700	AP-1/2 complex subunit beta, putative
PBANKA_1107800.1-p1	1	1	1	1	1	1	0,02	9,89E-01	1,0	1,0	PBANKA_1107800	longevity-assurance (LAG1) protein, putative
PBANKA_1336400.1-p1	1	3	1	2	1	1	0,33	7,45E-01	1,7	1,3	PBANKA_1336400	DnaJ protein, putative
PBANKA_0801400.1-p1	2	1	1	2	0	1	0,41	7,31E-01	1,3	1,0	PBANKA_0801400	conserved protein, unknown function
PBANKA_0705200.1-p1	1	1	1	2	1	1	-0,35	7,61E-01	1,0	1,3	PBANKA_0705200	ATP synthase-associated protein, putative
PBANKA_1334600.1-p1	1	0	3	2	1	1	0,01	9,93E-01	1,3	1,3	PBANKA_1334600	diacylglycerol kinase, putative
PBANKA_1123900.1-p1	0	1	2	2	2	0	-0,36	7,66E-01	1,0	1,3	PBANKA_1123900	sphingomyelin synthase 1, putative
PBANKA_1423900.1-p1	0	2	1	0	2	2	-0,37	7,59E-01	1,0	1,3	PBANKA_1423900	translation initiation factor SUI1, putative
PBANKA_1235300.1-p1	2	0	2	1	1	2	0,01	9,94E-01	1,3	1,3	PBANKA_1235300	bis(5'-nucleosyl)-tetraphosphatase [asymmetrical], putative
PBANKA_0513400.1-p1	2	0	1	2	1	1	-0,35	7,67E-01	1,0	1,3	PBANKA_0513400	LEM3/CDC50 family protein, putative
PBANKA_1438600.1-p1	1	2	2	1	1	2	0,31	7,57E-01	1,7	1,3	PBANKA_1438600	vacuolar iron transporter
PBANKA_0604600.1-p1	1	0	1	0	2	2	-0,88	5,04E-01	0,7	1,3	PBANKA_0604600	conserved protein, unknown function
PBANKA_1245800.1-p1	2	0	0	1	2	1	-0,86	5,15E-01	0,7	1,3	PBANKA_1245800	conserved Plasmodium protein, unknown function
PBANKA_1434400.1-p1	2	0	0	2	1	1	-0,85	5,19E-01	0,7	1,3	PBANKA_1434400	secreted ookinete protein, putative
PBANKA_1139900.1-p1	1	1	2	2	1	1	0,02	9,86E-01	1,3	1,3	PBANKA_1139900	reticulon-like protein, putative
PBANKA_1417800.1-p1	2	1	3	2	1	0	0,94	3,69E-01	2,0	1,0	PBANKA_1417800	tRNA (guanine(26)-N(2))-dimethyltransferase, putative
PBANKA_0503200.1-p1	2	1	1	3	0	0	0,42	7,31E-01	1,3	1,0	PBANKA_0503200	eukaryotic translation initiation factor subunit eIF2A, putative
PBANKA_1426100.1-p1	1	1	2	0	1	1	0,88	4,93E-01	1,3	0,7	PBANKA_1426100	conserved protein, unknown function
PBANKA_1406200.1-p1	3	0	2	1	1	1	0,69	5,38E-01	1,7	1,0	PBANKA_1406200	TOM1-like protein, putative
PBANKA_1035900.1-p1	2	1	0	1	1	1	0,03	9,83E-01	1,0	1,0	PBANKA_1035900	glycerophosphodiester phosphodiesterase, putative
PBANKA_0717000.1-p1	2	0	1	3	0	0	0,04	9,76E-01	1,0	1,0	PBANKA_0717000	arsenical pump-driving ATPase, putative
PBANKA_1422700.1-p1	2	0	1	2	0	1	0,03	9,83E-01	1,0	1,0	PBANKA_1422700	superoxide dismutase [Fe], putative
PBANKA_0509200.1-p1	2	0	1	2	1	0	0,03	9,82E-01	1,0	1,0	PBANKA_0509200	Eps15-like protein, putative
PBANKA_1415000.1-p1	1	0	1	2	1	0	-0,48	7,32E-01	0,7	1,0	PBANKA_1415000	pre-mRNA-processing factor 40, putative
PBANKA_0804600.1-p1	2	0	1	2	1	0	0,03	9,82E-01	1,0	1,0	PBANKA_0804600	AAA family ATPase, putative
PBANKA_1038800.1-p1	1	2	1	2	1	0	0,41	7,31E-01	1,3	1,0	PBANKA_1038800	EGF domain-containing protein, putative
PBANKA_0832200.1-p1	0	1	3	3	0	0	0,40	7,49E-01	1,3	1,0	PBANKA_0832200	PUB domain-containing protein, putative
PBANKA_0108900.1-p1	2	2	2	2	1	0	0,95	3,62E-01	2,0	1,0	PBANKA_0108900	peptidyl-tRNA hydrolase PTRHD1, putative
PBANKA_1222400.1-p1	1	2	1	2	0	1	0,41	7,31E-01	1,3	1,0	PBANKA_1222400	ubiquitin regulatory protein, putative
PBANKA_1415500.1-p1	2	1	2	1	1	1	0,69	5,25E-01	1,7	1,0	PBANKA_1415500	U4/U6.U5 tri-snRNP-associated protein 2, putative
PBANKA_0937100.1-p1	1	1	1	0	2	1	0,01	9,96E-01	1,0	1,0	PBANKA_0937100	vacuolar protein sorting-associated protein 35, putative
PBANKA_1413900.1-p1	1	2	0	1	1	1	0,03	9,83E-01	1,0	1,0	PBANKA_1413900	zinc finger (CCCH type) protein, putative
PBANKA_0109600.1-p1	1	1	1	1	1	1	0,02	9,89E-01	1,0	1,0	PBANKA_0109600	ATP synthase-associated protein, putative
PBANKA_1231200.1-p1	2	1	1	1	1	1	0,40	7,32E-01	1,3	1,0	PBANKA_1231200	phosducin-like protein 1, putative
PBANKA_1303600.1-p1	1	0	1	1	1	1	-0,49	7,21E-01	0,7	1,0	PBANKA_1303600	leucine carboxyl methyltransferase, putative
PBANKA_0414800.1-p1	1	1	2	2	1	0	0,40	7,36E-01	1,3	1,0	PBANKA_0414800	arginase
PBANKA_1017700.1-p1	2	1	1	0	1	1	0,89	4,89E-01	1,3	0,7	PBANKA_1017700	cytochrome b-c1 complex subunit 6, putative
PBANKA_0100700.1-p1	0	0	2	2	1	0	-0,49	7,31E-01	0,7	1,0	PBANKA_0100700	Plasmodium exported protein, unknown function
PBANKA_1417500.1-p1	2	1	1	2	1	0	0,41	7,30E-01	1,3	1,0	PBANKA_1417500	conserved Plasmodium protein, unknown function
PBANKA_1234000.1-p1	2	1	1	0	2	1	0,38	7,45E-01	1,3	1,0	PBANKA_1234000	V-type proton ATPase 16 kDa proteolipid subunit, putative
PBANKA_1222000.1-p1	1	0	1	1	1	1	-0,49	7,21E-01	0,7	1,0	PBANKA_1222000	histone deacetylase complex subunit SAP18, putative
PBANKA_1018700.1-p1	1	0	1	1	1	1	-0,49	7,21E-01	0,7	1,0	PBANKA_1018700	conserved Plasmodium protein, unknown function
PBANKA_1463900.1-p1	2	1	0	2	0	1	0,04	9,77E-01	1,0	1,0	PBANKA_1463900	HSP20-like chaperone, putative
PBANKA_1142500.1-p1	0	1	0	0	1	1	-0,78	6,56E-01	0,3	0,7	PBANKA_1142500	signal recognition particle receptor subunit alpha, putative
PBANKA_1024700.1-p1	1	0	1	1	1	1	-0,49	7,21E-01	0,7	1,0	PBANKA_1024700	ubiquitin fusion degradation protein 1, putative
PBANKA_1449100.1-p1	1	0	1	1	1	1	-0,49	7,21E-01	0,7	1,0	PBANKA_1449100	conserved Plasmodium protein, unknown function
PBANKA_0507400.1-p1	1	2	1	1	1	1	0,40	7,32E-01	1,3	1,0	PBANKA_0507400	orotidine 5'-phosphate decarboxylase, putative
PBANKA_0210600.1-p1	1	0	0	2	0	0	-0,75	6,69E-01	0,3	0,7	PBANKA_0210600	ubiquitin carboxyl-terminal hydrolase, putative
PBANKA_1437200.1-p1	1	0	1	1	1	0	0,02	9,91E-01	0,7	0,7	PBANKA_1437200	conserved Plasmodium protein, unknown function
PBANKA_0942800.1-p1	1	0	1	2	0	0	0,03	9,85E-01	0,7	0,7	PBANKA_0942800	syntaxin, putative
PBANKA_1134400.1-p1	1	1	1	1	1	0	0,53	7,02E-01	1,0	0,7	PBANKA_1134400	Sas10 domain-containing protein, putative
PBANKA_1222100.1-p1	2	0	1	2	0	0	0,54	7,07E-01	1,0	0,7	PBANKA_1222100	regulator of chromosome condensation, putative
PBANKA_1421300.1-p1	1	0	0	1	1	0	-0,76	6,60E-01	0,3	0,7	PBANKA_1421300	phosphoglycolate phosphatase
PBANKA_1141500.1-p1	0	1	0	1	1	0	-0,76	6,60E-01	0,3	0,7	PBANKA_1141500	SNARE associated Golgi protein, putative
PBANKA_1120100.1-p1	1	1	0	0	1	2	-0,50	7,26E-01	0,7	1,0	PBANKA_1120100	conserved Plasmodium protein, unknown function
PBANKA_1449500.1-p1	1	1	0	1	1	1	-0,48	7,27E-01	0,7	1,0	PBANKA_1449500	CHCH domain-containing protein, putative

Table S3: LCMSMS analyses of “all blood stages” parasites (raw data). Legends are indicated as well as the overall variability between samples (WT-2, WT-3, WT-4, KO-1, KO-2 and KO-4) is visualized using MDS plot.

PBANKA_1218400.1-p1	1	1	0	2	1	0	-0,47	7,38E-01	0,7	1,0	PBANKA_1218400	protein transport protein SEC22, putative
PBANKA_1105100.1-p1	0	2	0	0	3	0	-0,49	7,39E-01	0,7	1,0	PBANKA_1105100	DNA mismatch repair protein MSH6, putative
PBANKA_1305700.1-p1	0	2	1	1	0	3	-0,36	7,67E-01	1,0	1,3	PBANKA_1305700	vacuolar protein sorting-associated protein 60, putative
PBANKA_0305000.1-p1	0	6	1	3	4	1	-0,15	8,60E-01	2,3	2,7	PBANKA_0305000	serine repeat antigen 2
PBANKA_0919800.1-p1	0	2	0	1	0	1	0,03	9,86E-01	0,7	0,7	PBANKA_0919800	bifunctional farnesyl/geranylgeranyl diphosphate synthase, putative
PBANKA_0314400.1-p1	0	1	0	1	0	0	0,03	9,90E-01	0,3	0,3	PBANKA_0314400	E2F-associated phosphoprotein, putative
PBANKA_1115300.1-p1	0	1	0	0	1	0	0,01	9,94E-01	0,3	0,3	PBANKA_1115300	glideosome-associated protein 40, putative
PBANKA_1358900.1-p1	0	1	0	0	0	1	0,01	9,94E-01	0,3	0,3	PBANKA_1358900	dynactin subunit 2, putative
PBANKA_1012100.1-p1	0	1	0	0	0	1	0,01	9,94E-01	0,3	0,3	PBANKA_1012100	HP12 protein homolog, putative
PBANKA_1429500.1-p1	0	1	0	0	0	1	0,01	9,94E-01	0,3	0,3	PBANKA_1429500	DNA-directed RNA polymerases I, II, and III subunit RPABC3, putative
PBANKA_0209900.1-p1	1	0	0	1	0	1	-0,77	6,59E-01	0,3	0,7	PBANKA_0209900	nucleoside transporter 4, putative
PBANKA_1321700.1-p1	2	0	0	2	0	0	0,04	9,81E-01	0,7	0,7	PBANKA_1321700	berghepain-1
PBANKA_1024000.1-p1	0	0	2	1	0	1	0,01	9,96E-01	0,7	0,7	PBANKA_1024000	thioredoxin-like protein, putative
PBANKA_0919600.1-p1	1	0	1	2	0	0	0,03	9,85E-01	0,7	0,7	PBANKA_0919600	CCR4-NOT transcription complex subunit 2, putative
PBANKA_0929100.1-p1	2	0	0	1	1	0	0,03	9,86E-01	0,7	0,7	PBANKA_0929100	acyl-CoA-binding protein, putative
PBANKA_1336700.1-p1	0	1	1	1	0	1	0,02	9,91E-01	0,7	0,7	PBANKA_1336700	conserved Plasmodium protein, unknown function
PBANKA_0804300.1-p1	1	1	0	0	2	0	0,02	9,92E-01	0,7	0,7	PBANKA_0804300	DNA mismatch repair protein MSH2
PBANKA_1365300.1-p1	0	0	1	1	1	0	-0,78	6,55E-01	0,3	0,7	PBANKA_1365300	intron-binding protein aquarius, putative
PBANKA_0203800.1-p1	0	0	3	2	0	0	0,52	7,22E-01	1,0	0,7	PBANKA_0203800	phenylalanine--tRNA ligase alpha subunit, putative
PBANKA_0100900.1-p1	0	0	1	0	2	0	-0,79	6,57E-01	0,3	0,7	PBANKA_0100900	ATP-dependent RNA helicase MTR4, putative
PBANKA_0214000.1-p1	2	0	0	1	0	1	0,03	9,86E-01	0,7	0,7	PBANKA_0214000	dynein heavy chain, putative
PBANKA_1336100.1-p1	1	1	2	2	0	0	0,91	4,90E-01	1,3	0,7	PBANKA_1336100	dihydroorotase, putative
PBANKA_1454100.1-p1	1	0	1	1	1	0	0,02	9,91E-01	0,7	0,7	PBANKA_1454100	ATP-dependent zinc metalloprotease FTSH 1, putative
PBANKA_0104900.1-p1	1	0	2	1	1	0	0,52	7,12E-01	1,0	0,7	PBANKA_0104900	RNA-binding protein, putative
PBANKA_0905800.1-p1	1	1	1	1	1	0	0,53	7,02E-01	1,0	0,7	PBANKA_0905800	DnaJ protein, putative
PBANKA_1108600.1-p1	1	0	1	1	1	0	0,02	9,91E-01	0,7	0,7	PBANKA_1108600	alpha-soluble NSF attachment protein, putative
PBANKA_1316400.1-p1	0	0	1	2	0	0	-0,76	6,65E-01	0,3	0,7	PBANKA_1316400	U1 snRNP-associated protein, putative
PBANKA_1441900.1-p1	1	0	2	2	0	0	0,53	7,11E-01	1,0	0,7	PBANKA_1441900	DNA helicase 60, putative
PBANKA_1027900.1-p1	0	1	2	2	0	0	0,53	7,11E-01	1,0	0,7	PBANKA_1027900	small nuclear ribonucleoprotein-associated protein B, putative
PBANKA_1332500.1-p1	1	0	2	0	1	1	0,51	7,19E-01	1,0	0,7	PBANKA_1332500	pre-rRNA-processing protein PNO1, putative
PBANKA_0931700.1-p1	2	0	1	1	1	0	0,53	7,08E-01	1,0	0,7	PBANKA_0931700	peptidyl-prolyl cis-trans isomerase, putative
PBANKA_1337400.1-p1	2	0	0	2	0	0	0,04	9,81E-01	0,7	0,7	PBANKA_1337400	nucleoside-diphosphatase, putative
PBANKA_1022100.1-p1	1	1	1	0	1	1	0,52	7,09E-01	1,0	0,7	PBANKA_1022100	conserved Plasmodium protein, unknown function
PBANKA_1409900.1-p1	2	0	0	2	0	0	0,04	9,81E-01	0,7	0,7	PBANKA_1409900	AP-1 complex subunit mu-1, putative
PBANKA_1002000.1-p1	1	0	1	1	0	1	0,02	9,91E-01	0,7	0,7	PBANKA_1002000	conserved Plasmodium protein, unknown function
PBANKA_1455700.1-p1	0	2	0	1	0	1	0,03	9,86E-01	0,7	0,7	PBANKA_1455700	conserved Plasmodium protein, unknown function
PBANKA_1234400.1-p1	1	0	1	1	1	0	0,02	9,91E-01	0,7	0,7	PBANKA_1234400	zinc finger protein, putative
PBANKA_1318900.1-p1	1	0	1	0	2	0	0,00	9,97E-01	0,7	0,7	PBANKA_1318900	methyltransferase, putative
PBANKA_1439800.1-p1	1	0	1	1	1	0	0,02	9,91E-01	0,7	0,7	PBANKA_1439800	splicing factor 3B subunit 6, putative
PBANKA_1126900.1-p1	1	0	1	1	1	0	0,02	9,91E-01	0,7	0,7	PBANKA_1126900	eukaryotic translation initiation factor 2-alpha kinase
PBANKA_1145700.1-p1	0	0	1	1	0	1	-0,78	6,55E-01	0,3	0,7	PBANKA_1145700	U2 small nuclear ribonucleoprotein A', putative
PBANKA_0408500.1-p1	2	1	0	1	1	0	0,54	7,03E-01	1,0	0,7	PBANKA_0408500	parasite-infected erythrocyte surface protein
PBANKA_0815700.1-p1	1	0	2	0	2	0	0,51	7,24E-01	1,0	0,7	PBANKA_0815700	major facilitator superfamily-related transporter, putative
PBANKA_0931100.1-p1	2	1	1	0	0	2	0,89	4,99E-01	1,3	0,7	PBANKA_0931100	conserved protein, unknown function
PBANKA_1356900.1-p1	1	0	1	1	1	0	0,02	9,91E-01	0,7	0,7	PBANKA_1356900	U4/U6 small nuclear ribonucleoprotein PRP4, putative
PBANKA_0716000.1-p1	0	0	1	0	1	1	-0,79	6,51E-01	0,3	0,7	PBANKA_0716000	structural maintenance of chromosomes protein 3, putative
PBANKA_0515500.1-p1	0	0	1	0	1	1	-0,79	6,51E-01	0,3	0,7	PBANKA_0515500	protein phosphatase inhibitor 3, putative
PBANKA_0418300.1-p1	0	1	0	0	1	1	-0,78	6,56E-01	0,3	0,7	PBANKA_0418300	protein RER1, putative
PBANKA_0410300.1-p1	2	0	1	1	1	0	0,53	7,08E-01	1,0	0,7	PBANKA_0410300	26S proteasome regulatory subunit RPN12, putative
PBANKA_1115600.1-p1	1	0	1	2	0	0	0,03	9,85E-01	0,7	0,7	PBANKA_1115600	conserved Plasmodium protein, unknown function
PBANKA_1310200.1-p1	1	0	1	1	1	0	0,02	9,91E-01	0,7	0,7	PBANKA_1310200	nucleoporin NUP313
PBANKA_1121500.1-p1	0	0	1	1	1	0	-0,78	6,55E-01	0,3	0,7	PBANKA_1121500	cytochrome b-c1 complex subunit 9, putative
PBANKA_0822500.1-p1	1	0	1	1	1	0	0,02	9,91E-01	0,7	0,7	PBANKA_0822500	tetratricopeptide repeat protein, putative
PBANKA_0620100.1-p1	1	0	0	1	1	0	-0,76	6,60E-01	0,3	0,7	PBANKA_0620100	U3 small nucleolar RNA-associated protein 7, putative
PBANKA_1450100.1-p1	1	0	1	1	1	0	0,02	9,91E-01	0,7	0,7	PBANKA_1450100	N6-adenosine-methyltransferase, putative
PBANKA_0417000.1-p1	1	1	0	1	0	1	0,03	9,86E-01	0,7	0,7	PBANKA_0417000	signal peptidase complex subunit 3, putative
PBANKA_0931800.1-p1	0	0	1	1	1	0	-0,78	6,55E-01	0,3	0,7	PBANKA_0931800	pyridoxine biosynthesis protein PDX2, putative
PBANKA_1039700.1-p1	1	0	1	1	1	0	0,02	9,91E-01	0,7	0,7	PBANKA_1039700	cytochrome c oxidase subunit ApiCOX19, putative
PBANKA_1355900.1-p1	0	1	1	1	0	1	0,02	9,91E-01	0,7	0,7	PBANKA_1355900	phosphoenolpyruvate carboxykinase, putative
PBANKA_0502700.1-p1	0	0	1	1	0	1	-0,78	6,55E-01	0,3	0,7	PBANKA_0502700	pre-mRNA-splicing factor RDS3, putative
PBANKA_0208100.1-p1	0	0	1	1	1	0	-0,78	6,55E-01	0,3	0,7	PBANKA_0208100	heptatricopeptide repeat and RAP domain-containing protein, putative
PBANKA_0303100.1-p1	0	0	1	0	1	1	-0,79	6,51E-01	0,3	0,7	PBANKA_0303100	PCI domain-containing protein, putative
PBANKA_1217000.1-p1	0	0	1	0	1	1	-0,79	6,51E-01	0,3	0,7	PBANKA_1217000	peptidase, putative
PBANKA_0315400.1-p1	0	0	1	1	1	0	-0,78	6,55E-01	0,3	0,7	PBANKA_0315400	pre-mRNA-processing protein 45, putative
PBANKA_0616500.1-p1	1	1	1	1	1	0	0,53	7,02E-01	1,0	0,7	PBANKA_0616500	conserved protein, unknown function
PBANKA_0718400.1-p1	1	0	0	0	1	1	-0,78	6,56E-01	0,3	0,7	PBANKA_0718400	histone acetyltransferase, putative
PBANKA_0827200.1-p1	1	0	0	1	1	0	-0,76	6,60E-01	0,3	0,7	PBANKA_0827200	monocarboxylate transporter, putative
PBANKA_1111800.1-p1	0	0	1	1	1	0	-0,78	6,55E-01	0,3	0,7	PBANKA_1111800	glutathione synthetase
PBANKA_1143500.1-p1	1	1	1	1	1	0	0,53	7,02E-01	1,0	0,7	PBANKA_1143500	ribosome biogenesis protein MRT4, putative
PBANKA_0621900.1-p1	0	0	1	1	1	0	-0,78	6,55E-01	0,3	0,7	PBANKA_0621900	mitochondrial import inner membrane translocase subunit TIM14, putative
PBANKA_0825500.1-p1	1	0	0	2	0	0	-0,75	6,69E-01	0,3	0,7	PBANKA_0825500	conserved Plasmodium protein, unknown function
PBANKA_0523000.1-p1	1	0	0	1	1	0	-0,76	6,60E-01	0,3	0,7	PBANKA_0523000	conserved Plasmodium protein, unknown function
PBANKA_1411200.1-p1	1	1	1	1	1	0	0,53	7,02E-01	1,0	0,7	PBANKA_1411200	conserved Plasmodium protein, unknown function
PBANKA_0927800.1-p1	1	1	0	1	0	1	0,03	9,86E-01	0,7	0,7	PBANKA_0927800	tRNA nucleotidyltransferase, putative
PBANKA_0708400.1-p1	0	0	1	2	0	0	-0,76	6,65E-01	0,3	0,7	PBANKA_0708400	small nuclear ribonucleoprotein G, putative
PBANKA_1429000.1-p1	0	0	1	1	1	0	-0,78	6,55E-01	0,3	0,7	PBANKA_1429000	mediator of RNA polymerase II transcription subunit 18, putative
PBANKA_0518200.1-p1	2	0	0	1	0	0	0,82	6,44E-01	0,7	0,3	PBANKA_0518200	flavoprotein subunit of succinate dehydrogenase, putative
PBANKA_0717500.1-p1	0	0	2	0	1	0	0,79	6,56E-01	0,7	0,3	PBANKA_0717500	nuclear cap-binding protein subunit 2, putative
PBANKA_0604200.1-p1	1	0	1	0	1	0	0,80	6,46E-01	0,7	0,3	PBANKA_0604200	zinc finger protein, putative
PBANKA_0911300.1-p1	1	0	1	0	1	0	0,80	6,46E-01	0,7	0,3	PBANKA_0911300	UVB-resistance protein UVR8 homologue, putative
PBANKA_0807900.1-p1	1	0	0	1	0	0	0,03	9,90E-01	0,3	0,3	PBANKA_0807900	conserved Plasmodium protein, unknown function
PBANKA_0411800.1-p1	1	0	1	1	0	0	0,81	6,41E-01	0,7	0,3	PBANKA_0411800	vesicle transport v-SNARE protein, putative

Table S3: LCMSMS analyses of “all blood stages” parasites (raw data). Legends are indicated as well as the overall variability between samples (WT-2, WT-3, WT-4, KO-1, KO-2 and KO-4) is visualized using MDS plot.

PBANKA_1202600.1-p1	0	0	2	0	1	0	0,79	6,56E-01	0,7	0,3	PBANKA_1202600	E3 ubiquitin-protein ligase, putative
PBANKA_0928900.1-p1	0	0	2	0	0	1	0,78	6,56E-01	0,7	0,3	PBANKA_0928900	conserved protein, unknown function
PBANKA_1237500.1-p1	0	0	1	0	1	0	0,00	9,98E-01	0,3	0,3	PBANKA_1237500	pre-mRNA-splicing factor BUD31, putative
PBANKA_1221300.1-p1	0	0	2	1	0	0	0,80	6,51E-01	0,7	0,3	PBANKA_1221300	conserved Plasmodium protein, unknown function
PBANKA_0311800.1-p1	0	1	1	1	0	0	0,81	6,42E-01	0,7	0,3	PBANKA_0311800	acyl-CoA synthetase, putative
PBANKA_1301600.1-p1	0	0	1	1	0	0	0,02	9,94E-01	0,3	0,3	PBANKA_1301600	vacuole membrane protein 1, putative
PBANKA_0804800.1-p1	0	0	1	0	1	0	0,00	9,98E-01	0,3	0,3	PBANKA_0804800	mediator of RNA polymerase II transcription subunit 10, putative
PBANKA_0601600.1-p1	0	0	2	1	0	0	0,80	6,51E-01	0,7	0,3	PBANKA_0601600	nuclear export mediator factor NEMF, putative
PBANKA_1033800.1-p1	1	0	0	1	0	0	0,03	9,90E-01	0,3	0,3	PBANKA_1033800	conserved protein, unknown function
PBANKA_0814000.1-p1	1	0	1	1	0	0	0,81	6,41E-01	0,7	0,3	PBANKA_0814000	conserved protein, unknown function
PBANKA_0401900.1-p1	0	0	1	0	1	0	0,00	9,98E-01	0,3	0,3	PBANKA_0401900	DNA-directed RNA polymerases I, II, and III subunit RPABC2, putative
PBANKA_1211500.1-p1	0	0	1	1	0	0	0,02	9,94E-01	0,3	0,3	PBANKA_1211500	U3 small nucleolar RNA-associated protein 13, putative
PBANKA_0414100.1-p1	1	0	0	1	0	0	0,03	9,90E-01	0,3	0,3	PBANKA_0414100	inorganic pyrophosphatase, putative
PBANKA_0524000.1-p1	0	0	1	1	0	0	0,02	9,94E-01	0,3	0,3	PBANKA_0524000	conserved Plasmodium protein, unknown function
PBANKA_1241700.1-p1	0	0	1	0	1	0	0,00	9,98E-01	0,3	0,3	PBANKA_1241700	transmembrane emp24 domain-containing protein, putative
PBANKA_0401400.1-p1	1	0	0	0	1	0	0,01	9,94E-01	0,3	0,3	PBANKA_0401400	RNA-binding protein, putative
PBANKA_1348300.1-p1	1	0	1	0	1	0	0,80	6,46E-01	0,7	0,3	PBANKA_1348300	U3 small nucleolar RNA-associated protein 4, putative
PBANKA_1033500.1-p1	0	0	1	0	0	1	0,00	9,98E-01	0,3	0,3	PBANKA_1033500	WD repeat-containing protein, putative
PBANKA_0713300.1-p1	1	0	0	0	1	0	0,01	9,94E-01	0,3	0,3	PBANKA_0713300	histidine triad nucleotide-binding protein 1, putative
PBANKA_1233100.1-p1	1	0	1	0	1	0	0,80	6,46E-01	0,7	0,3	PBANKA_1233100	proteasome subunit beta type-1, putative
PBANKA_0905100.1-p1	1	0	0	0	0	1	0,01	9,94E-01	0,3	0,3	PBANKA_0905100	ATP-dependent (S)-NAD(P)H-hydrate dehydratase, putative
PBANKA_0602800.1-p1	1	0	1	1	0	0	0,81	6,41E-01	0,7	0,3	PBANKA_0602800	ubiquitin-conjugating enzyme E2, putative
PBANKA_0932000.1-p1	0	1	0	0	0	1	0,01	9,94E-01	0,3	0,3	PBANKA_0932000	rhoptry neck protein 4
PBANKA_1127300.1-p1	0	0	1	1	0	0	0,02	9,94E-01	0,3	0,3	PBANKA_1127300	DNA methyltransferase 1-associated protein 1, putative
PBANKA_1464500.1-p1	1	0	0	1	0	0	0,03	9,90E-01	0,3	0,3	PBANKA_1464500	ATP-dependent RNA helicase DRS1, putative
PBANKA_1317700.1-p1	1	0	1	0	1	0	0,80	6,46E-01	0,7	0,3	PBANKA_1317700	RNA-binding protein, putative
PBANKA_1418800.1-p1	0	1	1	1	0	0	0,81	6,42E-01	0,7	0,3	PBANKA_1418800	SNARE protein, putative
PBANKA_0509000.1-p1	1	0	0	1	0	0	0,03	9,90E-01	0,3	0,3	PBANKA_0509000	exported protein 3, putative
PBANKA_0613700.1-p1	1	0	1	1	0	0	0,81	6,41E-01	0,7	0,3	PBANKA_0613700	RNA-binding protein, putative
PBANKA_0711700.1-p1	0	0	2	1	0	0	0,80	6,51E-01	0,7	0,3	PBANKA_0711700	BRIX domain, putative
PBANKA_1203400.1-p1	0	0	1	1	0	0	0,02	9,94E-01	0,3	0,3	PBANKA_1203400	U3 small nucleolar RNA-associated protein 25, putative
PBANKA_1408500.1-p1	1	1	0	1	0	0	0,82	6,38E-01	0,7	0,3	PBANKA_1408500	ATP synthase subunit O, mitochondrial, putative
PBANKA_0808800.1-p1	1	0	1	1	0	0	0,81	6,41E-01	0,7	0,3	PBANKA_0808800	prefoldin-like protein, putative
PBANKA_1233000.1-p1	0	0	1	1	0	0	0,02	9,94E-01	0,3	0,3	PBANKA_1233000	SWIB/MDM2 domain-containing protein, putative
PBANKA_0511500.1-p1	1	0	0	1	0	0	0,03	9,90E-01	0,3	0,3	PBANKA_0511500	DNA-directed RNA polymerase II subunit RPB7, putative
PBANKA_0316100.1-p1	0	1	1	0	0	1	0,80	6,47E-01	0,7	0,3	PBANKA_0316100	Plasmodium exported protein, unknown function
PBANKA_0926600.1-p1	1	1	0	0	0	1	0,81	6,43E-01	0,7	0,3	PBANKA_0926600	protein GCN20, putative
PBANKA_0202300.1-p1	1	0	1	1	0	0	0,81	6,41E-01	0,7	0,3	PBANKA_0202300	UMP-CMP kinase, putative
PBANKA_1027300.1-p1	0	0	1	0	0	1	0,00	9,98E-01	0,3	0,3	PBANKA_1027300	Btz domain-containing protein, putative
PBANKA_0600500.1-p1	0	0	1	1	0	0	0,02	9,94E-01	0,3	0,3	PBANKA_0600500	GPN-loop GTPase, putative
PBANKA_1427000.1-p1	0	0	1	1	0	0	0,02	9,94E-01	0,3	0,3	PBANKA_1427000	protein phosphatase PPM7
PBANKA_0407100.1-p1	0	0	1	1	0	0	0,02	9,94E-01	0,3	0,3	PBANKA_0407100	splicing factor 3B subunit 1, putative
PBANKA_1339500.1-p1	0	0	1	1	0	0	0,02	9,94E-01	0,3	0,3	PBANKA_1339500	conserved Plasmodium protein, unknown function
PBANKA_0406300.1-p1	1	1	0	0	0	1	0,81	6,43E-01	0,7	0,3	PBANKA_0406300	DNA polymerase delta small subunit, putative
PBANKA_0819800.1-p1	1	0	0	1	0	0	0,03	9,90E-01	0,3	0,3	PBANKA_0819800	gamma-glutamylcysteine synthetase
PBANKA_0213000.1-p1	1	0	0	1	0	0	0,03	9,90E-01	0,3	0,3	PBANKA_0213000	RNA-binding protein, putative
PBANKA_1334200.1-p1	0	0	1	0	1	0	0,00	9,98E-01	0,3	0,3	PBANKA_1334200	RNA 3'-terminal phosphate cyclase-like protein, putative
PBANKA_1212300.1-p1	0	0	1	1	0	0	0,02	9,94E-01	0,3	0,3	PBANKA_1212300	translation initiation factor eIF-2B subunit delta, putative
PBANKA_0918800.1-p1	1	0	1	1	0	0	0,81	6,41E-01	0,7	0,3	PBANKA_0918800	rRNA (cytosine-C(5))-methyltransferase, putative
PBANKA_1352800.1-p1	0	0	0	0	0	0			0,0	0,0	PBANKA_1352800	cytochrome c oxidase subunit ApiCOX14, putative
PBANKA_1408000.1-p1	0	0	0	0	0	0			0,0	0,0	PBANKA_1408000	H/ACA ribonucleoprotein complex subunit 1, putative
PBANKA_1353700.1-p1	0	0	0	0	0	0			0,0	0,0	PBANKA_1353700	nucleolar complex protein 2, putative
PBANKA_0105200.1-p1	0	0	0	0	0	0			0,0	0,0	PBANKA_0105200	polypyrimidine tract-binding protein, putative
PBANKA_1301700.1-p1	0	0	0	0	0	0			0,0	0,0	PBANKA_1301700	splicing factor 3A subunit 1, putative
PBANKA_0826500.1-p1	0	0	0	0	0	0			0,0	0,0	PBANKA_0826500	histone deacetylase 1, putative
PBANKA_0102100.1-p1	0	0	0	0	0	0			0,0	0,0	PBANKA_0102100	dihydroorotate dehydrogenase, putative
PBANKA_1227100.1-p1	0	0	0	0	0	0			0,0	0,0	PBANKA_1227100	U3 small nucleolar RNA-associated protein 14, putative
PBANKA_1007000.1-p1	0	0	0	0	0	0			0,0	0,0	PBANKA_1007000	chaperone protein DnaJ, putative
PBANKA_0811000.1-p1	0	0	0	0	0	0			0,0	0,0	PBANKA_0811000	small nuclear ribonucleoprotein Sm D3, putative
PBANKA_1119300.1-p1	0	0	0	0	0	0			0,0	0,0	PBANKA_1119300	ATP synthase-associated protein, putative
PBANKA_1141800.1-p1	0	0	0	0	0	0			0,0	0,0	PBANKA_1141800	conserved Plasmodium protein, unknown function
PBANKA_1413100.1-p1	0	0	0	0	0	0			0,0	0,0	PBANKA_1413100	lipoate-protein ligase 1
PBANKA_0208300.1-p1	0	0	0	0	0	0			0,0	0,0	PBANKA_0208300	novel putative transporter 1
PBANKA_1450400.1-p1	0	0	0	0	0	0			0,0	0,0	PBANKA_1450400	peptidase, putative
PBANKA_1102000.1-p1	0	0	0	0	0	0			0,0	0,0	PBANKA_1102000	protein Mpv17, putative
PBANKA_0714600.1-p1	0	0	0	0	0	0			0,0	0,0	PBANKA_0714600	vacuolar protein sorting-associated protein 2, putative
PBANKA_1145500.1-p1	0	0	0	0	0	0			0,0	0,0	PBANKA_1145500	conserved protein, unknown function

Table S4: QRT-PCR raw data. For each "all blood stages" samples, qRT-PCR data the primers as well as the quality control of the RNA samples are shown.

		Average Ct (triplicate)			ΔCt			Efficiency			Mean	RQ	Mean RQ	SD	SEM
Genotype	Sample	MCM7	Hsp70	EF1-α	MCM7	Hsp70	EF1-α	MCM7	Hsp70	EF1-α	Hsp70/EF1-α	MCM7	MCM7		
WT	2	19,82	19,77	17,86	-1,10	-0,59	0,88	2,14	1,50	0,54	0,90	2,37			
WT	3	20,73	21,54	16,21	-0,19	1,18	-0,77	1,14	0,44	1,71	0,87	1,32	**1,77**	0,49	**0,28**
WT	4	20,79	20,96	17,50	-0,13	0,60	0,52	1,09	0,66	0,70	0,68	1,62			
KO	1	21,87	19,99	16,73	0,95	-0,37	-0,25	0,52	1,29	1,19	1,24	0,42			
KO	2	21,27	19,75	16,30	0,35	-0,61	-0,68	0,78	1,52	1,60	1,56	0,50	**0,62**	0,25	**0,14**
KO	4	21,04	20,14	17,27	0,12	-0,22	0,29	0,92	1,16	0,82	0,97	0,94			
Mean		20,92	20,36	16,98									**p-value = 0,03**		

		Average Ct (triplicate)			ΔCt			Efficiency			Mean	RQ	Mean RQ	SD	SEM
Genotype	Sample	ChAF1C	Hsp70	EF1-α	ChAF1C	Hsp70	EF1-α	ChAF1C	Hsp70	EF1-α	Hsp70/EF1-α	ChAF1C	ChAF1C		
WT	2	17,89	19,37	15,75	-3,29	-2,68	-2,32	9,75	6,42	4,98	5,65	1,72			
WT	3	24,23	26,49	23,51	3,06	4,44	5,45	0,12	0,05	0,02	0,03	3,70	**2,70**	0,88	**0,51**
WT	4	21,34	23,53	19,75	0,16	1,48	1,69	0,89	0,36	0,31	0,33	2,67			
KO	1	23,80	23,57	16,11	2,63	1,52	-1,96	0,16	0,35	3,88	1,16	0,14			
KO	2	19,23	18,95	15,72	-1,95	-3,10	-2,35	3,85	8,59	5,08	6,61	0,58	**0,48**	0,27	**0,15**
KO	4	20,56	20,41	17,55	-0,62	-1,64	-0,52	1,53	3,12	1,43	2,11	0,72			
Mean		21,18	22,05	18,07									**p-value = 0,02**		

		Average Ct (triplicate)			ΔCt			Efficiency			Mean	RQ	Mean RQ	SD	SEM
Genotype	Sample	UF	Hsp70	EF1-α	UF	Hsp70	EF1-α	UF	Hsp70	EF1-α	Hsp70/EF1-α	UF	UF		
WT	2	19,91	19,78	16,19	-2,09	-0,61	-0,72	4,26	1,53	1,64	1,59	2,68			
WT	3	21,13	21,74	17,98	-0,87	1,35	1,07	1,83	0,39	0,48	0,43	4,23	**3,23**	0,77	**0,44**
WT	4	20,98	20,92	17,30	-1,02	0,53	0,39	2,03	0,69	0,76	0,73	2,79			
KO	1	24,04	19,92	16,70	2,04	-0,47	-0,21	0,24	1,39	1,15	1,27	0,19			
KO	2	22,68	19,47	16,01	0,68	-0,93	-0,90	0,62	1,90	1,86	1,88	0,33	**0,34**	0,14	**0,08**
KO	4	23,26	20,54	17,26	1,26	0,15	0,35	0,42	0,90	0,78	0,84	0,50			
Mean		22,00	20,40	16,91									**p-value = 0,0046**		

		Average Ct (triplicate)			ΔCt			Efficiency			Mean	RQ	Mean RQ	SD	SEM
Genotype	Sample	RON2	Hsp70	EF1-α	RON2	Hsp70	EF1-α	RON2	Hsp70	EF1-α	Hsp70/EF1-α	RON2	RON2		
WT	2	22,40	16,56	20,20	-1,57	-2,50	-1,25	2,96	5,67	2,38	3,67	0,81			
WT	3	25,74	21,36	24,69	1,78	2,29	3,24	0,29	0,20	0,11	0,15	1,98	**1,35**	0,53	**0,3**
WT	4	24,74	19,53	23,24	0,78	0,47	1,79	0,58	0,72	0,29	0,46	1,27			
KO	1	26,68	20,50	23,82	2,72	1,43	2,37	0,15	0,37	0,19	0,27	0,57			
KO	2	22,74	16,17	19,60	-1,22	-2,90	-1,85	2,33	7,45	3,60	5,18	0,45	**0,98**	0,74	**0,42**
KO	4	21,46	20,27	17,14	-2,50	1,21	-4,31	5,66	0,43	19,80	2,93	1,93			
Mean		23,96	19,06	21,45									**p-value = 0,56**		

		Average Ct (triplicate)			ΔCt			Efficiency			Mean	RQ	Mean RQ	SD	SEM
Genotype	Sample	RAP1	Hsp70	EF1-α	RAP1	Hsp70	EF1-α	RAP1	Hsp70	EF1-α	Hsp70/EF1-α	RAP1	RAP1		
WT	2	22,91	20,16	16,80	-0,65	-1,09	-1,25	1,57	2,13	2,38	2,25	0,70			
WT	3	24,82	23,06	19,81	1,26	1,81	1,76	0,42	0,29	0,30	0,29	1,44	**1,04**	0,34	**0,19**
WT	4	24,30	21,99	18,73	0,74	0,74	0,68	0,60	0,60	0,62	0,61	0,98			
KO	1	25,02	22,55	19,66	1,46	1,30	1,61	0,36	0,41	0,33	0,37	1,00			
KO	2	22,92	19,49	16,17	-0,65	-1,76	-1,88	1,57	3,39	3,69	3,54	0,44	**1,25**	0,86	**0,49**
KO	4	21,41	20,27	17,14	-2,15	-0,98	-0,91	4,45	1,98	1,88	1,93	2,31			
Mean		23,56	21,25	18,05									**p-value = 0,74**		

		Average Ct (triplicate)			ΔCt			Efficiency			Mean	RQ	Mean RQ	SD	SEM
Genotype	Sample	HMGB1	Hsp70	EF1-α	HMGB1	Hsp70	EF1-α	HMGB1	Hsp70	EF1-α	Hsp70/EF1-α	HMGB1	HMGB1		
WT	2	19,04	20,24	16,72	-2,80	-2,60	-2,69	6,98	6,07	6,47	6,27	1,11			
WT	3	24,84	27,13	23,63	2,99	4,29	4,22	0,13	0,05	0,05	0,05	2,40	**1,51**	0,69	**0,39**
WT	4	23,80	25,04	21,16	1,95	2,20	1,75	0,26	0,22	0,30	0,25	1,02			
KO	1	24,41	24,55	21,49	2,56	1,72	2,07	0,17	0,30	0,24	0,27	0,63			
KO	2	19,77	19,80	16,34	-2,08	-3,03	-3,07	4,21	8,20	8,41	8,30	0,51	**0,76**	0,31	**0,18**
KO	4	19,22	20,27	17,14	-2,63	-2,57	-2,27	6,17	5,93	4,84	5,36	1,15			
Mean		21,85	22,84	19,41									**p-value = 0,20**		

Gene ID and name (expression status in tRip-KO)	Primers		Primer efficiency	r^2
PBANKA_0803100				
DNA replication licensing factor MCM7	Forward	CAACCATTTCCCCTGAACTA	105.4 %	0.965
	Reverse	CACTATCTCTTACCCTTGCC		
(down regulated)	this study			
PBANKA_0203000				
chromatin assembly 1	Forward	GGACATTTTGCATCTGGAAG	99.8 %	0,98
	Reverse	GCATCTAACTCTTCACCGAT		
(down regulated)	this study			
PBANKA_1029400				
unknown function	Forward	TAGCTACTTGTTTACCGCAA	96.0%	0.990
	Reverse	TGAGGCCCCTTTAATTACTCTGT		
(down regulated)	this study			
PBANKA_1315700				
Rhoptry neck protein 2	Forward	CGTCTACATCGGCCTTTATTC	90.3%	0.992
	Reverse	GCGATAGCATGTGTTGTAAATTGG		
(up regulated)	Tokunaga et al., 2019			
PBANKA_1032100				
Rhoptry-associated protein 1	Forward	CAAGTGCCGATTTGCCAGATTA	106.2%	0.973
	Reverse	TTTGGTAGAATGCTGAAATACGC		
(up regulated)	Tokunaga et al., 2019			
PBANKA_0601900				
High mobility group protein B1	Forward	AAAATGGGTGGAAAGGAAGT	102.6%	0.99
	Reverse	TTTCCAACAGTTGCAACATC		
(up regulated)	this study			

Table S4: QRT-PCR raw data. For each “all blood stages” samples, qRT-PCR data the primers as well as the quality control of the RNA samples are shown.

RNA analyses

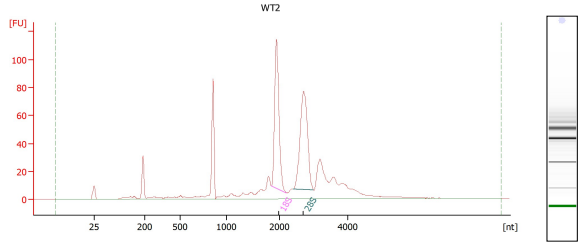

Overall Results for sample 4 : WT2

RNA Area:	696,1	RNA Integrity Number (RIN):	7 (B.02.08, Anomaly Threshold(s) manually adapted)
RNA Concentration:	3 079 pg/µl		
rRNA Ratio [28s / 18s]:	1,1	Result Flagging Color:	
		Result Flagging Label:	RIN:7

Fragment table for sample 4 : WT2

Name	Start Size [nt]	End Size [nt]	Area	% of total Area
18S	1 853	2 206	132,8	19,1
28S	2 399	2 985	142,1	20,4

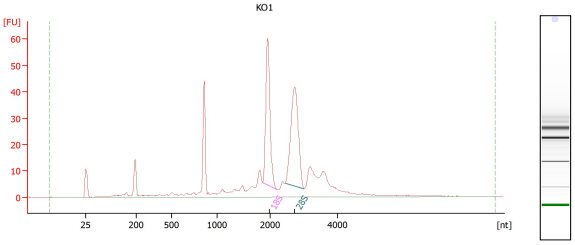

Overall Results for sample 3 : KO1

RNA Area:	383,0	RNA Integrity Number (RIN):	6.7 (B.02.08, Anomaly Threshold(s) manually adapted)
RNA Concentration:	1 694 pg/µl		
rRNA Ratio [28s / 18s]:	1,1	Result Flagging Color:	
		Result Flagging Label:	RIN: 6.70

Fragment table for sample 3 : KO1

Name	Start Size [nt]	End Size [nt]	Area	% of total Area
18S	1 865	2 214	68,6	17,9
28S	2 443	3 010	77,9	20,3

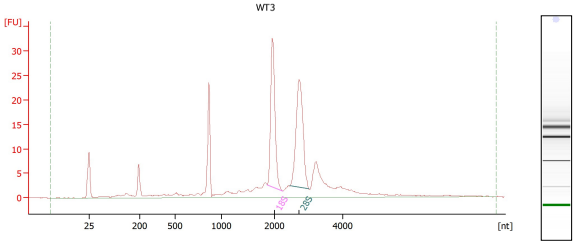

Overall Results for sample 6 : WT3

RNA Area:	197,8	RNA Integrity Number (RIN):	7.6 (B.02.08, Anomaly Threshold(s) manually adapted)
RNA Concentration:	875 pg/µl		
rRNA Ratio [28s / 18s]:	1,1	Result Flagging Color:	
		Result Flagging Label:	RIN: 7.60

Fragment table for sample 6 : WT3

Name	Start Size [nt]	End Size [nt]	Area	% of total Area
18S	1 865	2 259	37,4	18,9
28S	2 458	3 009	41,9	21,2

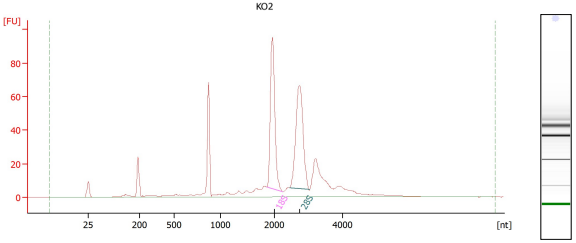

Overall Results for sample 5 : KO2

RNA Area:	533,8	RNA Integrity Number (RIN):	7.4 (B.02.08, Anomaly Threshold(s) manually adapted)
RNA Concentration:	2 361 pg/µl		
rRNA Ratio [28s / 18s]:	1,1	Result Flagging Color:	
		Result Flagging Label:	RIN: 7.40

Fragment table for sample 5 : KO2

Name	Start Size [nt]	End Size [nt]	Area	% of total Area
18S	1 863	2 260	115,6	21,7
28S	2 456	3 040	122,3	22,9

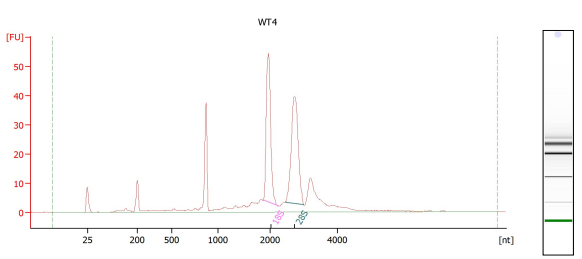

Overall Results for sample 8 : WT4

RNA Area:	299,3	RNA Integrity Number (RIN):	7.7 (B.02.08, Anomaly Threshold(s) manually adapted)
RNA Concentration:	1 324 pg/µl		
rRNA Ratio [28s / 18s]:	1,1	Result Flagging Color:	
		Result Flagging Label:	RIN: 7.70

Fragment table for sample 8 : WT4

Name	Start Size [nt]	End Size [nt]	Area	% of total Area
18S	1 875	2 277	63,9	21,4
28S	2 461	3 008	71,3	23,8

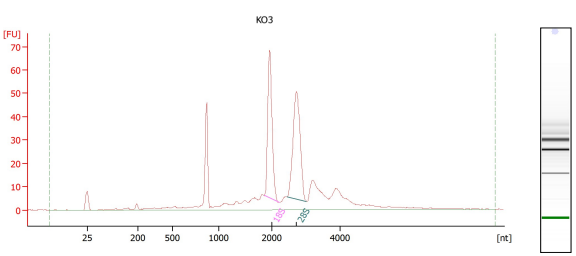

Overall Results for sample 7 : KO3

RNA Area:	419,7	RNA Integrity Number (RIN):	7.4 (B.02.08, Anomaly Threshold(s) manually adapted)
RNA Concentration:	1 857 pg/µl		
rRNA Ratio [28s / 18s]:	1,1	Result Flagging Color:	
		Result Flagging Label:	RIN: 7.40

Fragment table for sample 7 : KO3

Name	Start Size [nt]	End Size [nt]	Area	% of total Area
18S	1 866	2 217	80,2	19,1
28S	2 462	3 027	90,2	21,5

Reference genes

PBANKA_1133300				
EF1-α	Forward	TGGAACCACCCAAAAGACCA	100.7%	1
	Reverse	ACAACAGCAGATGGAGCGAA		
		Tokunaga et al., 2019		
PBANKA_0914400				
Hsp70	Forward	AGAGAAGCAGCTGAAACAGC	106.9%	0.999
	Reverse	TCCCTTTAATAAATCATGGC		
		Sanyal et al., 2013		

Table S5: Top 0.5% of the most asparagine-rich proteins in 6 Plasmodium strains. Color legends are indicated.

Conserved in all *Plasmodia*
other transcription factors
unknown function and no similarity to PDB

P. falciparum

Protein id	Prot length	Asn (%)	function
PF3D7_0923500	357	42,017	cyclin-dependent kinases regulatory subunit
PF3D7_1366900	685	34,891	conserved protein, unknown function
PF3D7_0218200	807	33,333	SUZ domain-containing protein, putative
PF3D7_1439500	1074	32,961	oocyst rupture protein 2, putative
PF3D7_0706500	1706	32,298	conserved Plasmodium protein, unknown function
PF3D7_0811300	1774	32,187	CCR4-associated factor 1
PF3D7_0611800	3248	31,989	conserved Plasmodium protein, unknown function
PF3D7_1249700	908	31,608	conserved Plasmodium protein, unknown function
PF3D7_0817300	2235	31,588	conserved Plasmodium protein, unknown function
PF3D7_1236100	445	31,236	clustered-asparagine-rich protein
PF3D7_0525300	481	31,185	conserved protein, unknown function
PF3D7_0323800	977	31,116	conserved Plasmodium protein, unknown function
PF3D7_0212100	1844	31,074	conserved Plasmodium protein, unknown function
PF3D7_1329600	301	30,897	conserved Plasmodium protein, unknown function
PF3D7_1473500	675	30,667	conserved Plasmodium protein, unknown function
PF3D7_0926100	3178	30,585	protein kinase, putative
PF3D7_0411000	1570	30,382	AP2 domain transcription factor AP2-Z
PF3D7_1146800	3188	30,332	conserved Plasmodium protein, unknown function
PF3D7_1337500	3334	30,324	conserved Plasmodium protein, unknown function
PF3D7_1317200	2672	30,202	AP2 domain transcription factor AP2-FG
PF3D7_0602000	1437	29,923	zinc finger protein, putative
PF3D7_1222600	2432	29,852	AP2 domain transcription factor AP2-G
PF3D7_0906600	843	29,775	zinc finger protein, putative
PF3D7_1205500	1785	29,636	zinc finger protein, putative
PF3D7_0629400	780	29,487	polyadenylate-binding protein 3, putative
PF3D7_0304600	397	29,471	circumsporozoite (CS) protein

P. yoelii

Protein id	Prot length	Asn (%)	function
PY17X_1428300	1807	30,825	CCR4-associated factor 1, putative
PY17X_1129700	535	30,654	polyadenylate-binding protein 3
PY17X_0111700	2872	28,482	conserved Plasmodium protein, unknown function
PY17X_1225100	169	28,402	conserved Plasmodium protein, unknown function
PY17X_1213800	261	27,969	rhoptry associated adhesin, putative
PY17X_1341400	610	27,869	conserved Plasmodium protein, unknown function
PY17X_1334500	967	27,611	AP2 domain transcription factor AP2-SP, putative
PY17X_0929400	122	27,049	heat shock factor-binding protein 1
PY17X_1453200	411	26,764	clustered-asparagine-rich protein, putative
PY17X_1356400	1912	26,569	conserved Plasmodium protein, unknown function
PY17X_0309500	987	26,444	conserved Plasmodium protein, unknown function
PY17X_1307200	960	26,354	oocyst rupture protein 2, putative
PY17X_1110800	1966	26,144	KH domain-containing protein, putative
PY17X_0614700	1230	25,528	apicomplexan kinetochore protein 3, putative
PY17X_1313200	552	25,362	RNA-binding protein, putative
PY17X_1334300	2085	25,324	conserved Plasmodium protein, unknown function
PY17X_0103500	483	25,259	RNA-binding protein, putative
PY17X_1440000	2341	25,16	AP2 domain transcription factor AP2-G
PY17X_0806800	1567	25,144	conserved Plasmodium protein, unknown function
PY17X_0315400	830	25,06	SUZ domain-containing protein, putative
PY17X_1417400	2502	25,02	AP2 domain transcription factor AP2-SP, putative
PY17X_1403500	312	25	LisH domain-containing protein, putative
PY17X_0930400	329	24,924	conserved Plasmodium protein, unknown function
PY17X_1426800	201	24,876	U1 small nuclear ribonucleoprotein C, putative
PY17X_1454600	1693	24,867	conserved Plasmodium protein, unknown function
PY17X_1205700	1022	24,853	E3 ubiquitin-protein ligase, putative
PY17X_0903500	3240	24,846	sporozoite and liver stage asparagine-rich protein
PY17X_1457300	1863	24,745	RNA-binding protein, putative
PY17X_1465200	746	24,665	conserved Plasmodium protein, unknown function
PY17X_0943000	142	24,648	conserved Plasmodium protein, unknown function

P. knowlesi

Protein id	Prot length	Asn (%)	function
PKNH_0515300	239	23,013	apical asparagine-rich protein AARP
PKNH_API05400	97	21,649	hypothetical protein
PKNH_0934400	741	20,783	conserved Plasmodium protein, unknown function
PKNH_1427000	689	20,174	conserved protein, unknown function
PKNH_1245200	334	20,06	trailer hitch homolog, putative
PKNH_1236600	775	19,613	RNA-binding protein, putative
PKNH_1429400	1971	19,533	CCR4-associated factor 1, putative
PKNH_API04400	125	19,2	apicoplast ribosomal protein L11, putative
PKNH_0826500	1208	19,123	zinc finger protein, putative
PKNH_1427400	615	19,024	protein KIC7, putative
PKNH_1007500	471	18,684	conserved protein, unknown function
PKNH_0301400	75	18,667	RNA-binding protein, putative
PKNH_0812000	281	18,505	rhoptry associated adhesin, putative
PKNH_1430100	908	18,392	ATP-dependent RNA helicase DBP1, putative
PKNH_1215100	1094	18,282	AP2 domain transcription factor AP2-EXP, putative
PKNH_1007800	880	18,182	zinc finger protein, putative
PKNH_0101500	143	18,182	conserved Plasmodium protein, unknown function
PKNH_1455800	474	18,143	clustered-asparagine-rich protein, putative
PKNH_API02500	89	17,978	apicoplast ribosomal protein S19, putative
PKNH_1348500	497	17,706	CUGBP Elav-like family member 2, putative
PKNH_1264600	147	17,687	parasitophorous vacuolar protein 3, putative
PKNH_0811000	119	17,647	BET1-like protein, putative
PKNH_0917400	721	17,614	conserved Plasmodium protein, unknown function
PKNH_1120100	644	17,547	polyadenylate-binding protein 3, putative
PKNH_API03300	80	17,5	hypothetical protein
PKNH_API04900	103	17,476	hypothetical chloroplast reading frame 93, putative
PKNH_0827400	1201	17,402	RING finger protein RNF1, putative
PKNH_API05300	1021	17,042	DNA-directed RNA polymerase subunit beta, putative
PKNH_0621400	1861	17,034	conserved Plasmodium protein, unknown function

P. berghei

Protein id	Prot length	Asn (%)	function
PBANKA_1426200	1801	30,372	CCR4-associated factor 1
PBANKA_0927400	122	28,689	heat shock factor-binding protein 1
PBANKA_0928400	358	28,492	conserved Plasmodium protein, unknown function
PBANKA_1128200	511	27,984	polyadenylate-binding protein 3,
PBANKA_1210600	256	27,734	rhoptry associated adhesin, putative
PBANKA_1303400	875	27,429	oocyst rupture protein 2
PBANKA_0612200	1251	27,338	apicomplexan kinetochore protein 3
PBANKA_0939600	3296	27,306	polyadenylate-binding protein-interacting protein 1
PBANKA_1336700	607	27,183	conserved Plasmodium protein, unknown function
PBANKA_1329600	2115	27,139	conserved Plasmodium protein, unknown function
PBANKA_1107200	677	27,031	protein CAF40, putative
PBANKA_1245900	412	26,942	Plasmodium exported protein, unknown function
PBANKA_0110100	2611	26,848	conserved Plasmodium protein, unknown function
PBANKA_1351300	1864	26,019	conserved Plasmodium protein, unknown function
PBANKA_0101900	478	25,941	RNA-binding protein, putative
PBANKA_1100600	54	25,926	PIR protein, pseudogene
PBANKA_1329800	943	25,875	AP2 domain transcription factor AP2-SP
PBANKA_0804100	1572	25,509	conserved Plasmodium protein, unknown function
PBANKA_0103300	2033	25,43	GYF domain-containing protein, putative
PBANKA_0308900	918	25,272	conserved Plasmodium protein, unknown function
PBANKA_1450700	397	25,189	clustered-asparagine-rich protein, putative
PBANKA_0604500	2264	25,044	high mobility group protein B3, putative
PBANKA_1415700	2487	24,568	AP2 domain transcription factor AP2-FG
PBANKA_1109700	1930	24,508	KH domain-containing protein, putative
PBANKA_0514300	947	24,498	conserved Plasmodium protein, unknown function

P. chabaudi

Protein id	Prot length	Asn (%)	function
PCHAS_1428000	1775	29,972	CCR4-associated factor 1
PCHAS_1341300	641	29,173	conserved Plasmodium protein, unknown function
PCHAS_0915900	329	28,875	conserved Plasmodium protein, unknown function
PCHAS_0916900	122	27,869	heat shock factor-binding protein 1, putative
PCHAS_1127700	510	27,647	polyadenylate-binding protein 3
PCHAS_1211300	246	26,423	rhoptry associated adhesin, putative
PCHAS_1306600	957	26,332	oocyst rupture protein 2, putative
PCHAS_0804400	1528	26,113	conserved Plasmodium protein, unknown function
PCHAS_0110700	2594	25,867	conserved Plasmodium protein
PCHAS_1426400	533	25,328	protein KIC7, putative
PCHAS_1453000	396	25,253	clustered-asparagine-rich protein, putative
PCHAS_0613900	1198	25,209	apicomplexan kinetochore protein 3, putative
PCHAS_1334400	984	24,695	AP2 domain transcription factor AP2-SP
PCHAS_1142300	556	24,46	conserved protein, unknown function
PCHAS_0311100	953	24,449	conserved Plasmodium protein, unknown function
PCHAS_0625600	336	24,405	fam-c protein
PCHAS_0514400	948	24,262	conserved Plasmodium protein, unknown function
PCHAS_1417500	2390	24,226	AP2 domain transcription factor AP2-FG
PCHAS_0703300	3131	24,082	sporozoite and liver stage asparagine-rich protein
PCHAS_1454400	1526	24,05	conserved Plasmodium protein, unknown function
PCHAS_0102600	488	23,975	RNA-binding protein, putative
PCHAS_1109400	1837	23,625	KH domain-containing protein
PCHAS_1464900	726	23,416	conserved Plasmodium protein, unknown function
PCHAS_0520100	1543	23,396	conserved Plasmodium protein
PCHAS_0413300	893	23,292	RING finger protein RNF1, putative
PCHAS_1457100	1728	23,09	RNA-binding protein, putative

P. vivax

Protein id	Prot length	Asn (%)	function
PVP01_0937100	779	24,904	conserved Plasmodium protein, unknown function
PVP01_1001950	86	22,093	PIR protein, pseudogene
PVP01_API04400	97	21,649	hypothetical protein
PVP01_0531900	297	20,539	apical asparagine-rich protein AARP
PVP01_1426900	699	19,886	conserved protein, unknown function
PVP01_API01500	89	19,101	apicoplast ribosomal protein S19, putative
PVP01_1269800	341	19,062	trailer hitch homolog, putative
PVP01_API02300	80	18,75	hypothetical protein
PVP01_0421700	91	18,681	conserved protein, unknown function
PVP01_0811300	118	18,644	BET1-like protein, putative
PVP01_API03400	125	18,4	apicoplast ribosomal protein L11, putative
PVP01_API01200	202	18,317	505 ribosomal protein L4, putative
PVP01_1401600	205	18,049	Plasmodium exported protein, unknown function
PVP01_1218000	139	17,986	parasitophorous vacuolar protein 3, putative
PVP01_1429000	2030	17,98	CCR4-associated factor 1, putative
PVP01_0705100	842	17,815	zinc finger protein, putative
PVP01_API04100	975	17,744	DNA-directed RNA polymerase subunit beta'', putative
PVP01_1429700	923	17,66	ATP-dependent RNA helicase DBP1, putative
PVP01_API03900	121	17,355	hypothetical chloroplast reading frame 93, putative
PVP01_API04300	1021	17,336	DNA-directed RNA polymerase subunit beta, putative
PVP01_1404300	1063	17,31	LisH domain-containing protein, putative
PVP01_1339100	503	17,296	CUGBP Elav-like family member 2, putative
PVP01_1120100	670	17,164	polyadenylate-binding protein 3, putative
PVP01_0010790	112	16,964	PIR protein
PVP01_1427300	661	16,944	protein KIC7, putative
PVP01_0103500	143	16,783	conserved Plasmodium protein, unknown function
PVP01_API02500	132	16,667	apicoplast ribosomal protein S11, putative
PVP01_1001850	42	16,667	PIR protein, pseudogene
PVP01_1008800	1006	16,501	zinc finger protein, putative
PVP01_1420400	75	16	conserved protein, unknown function

II. tRip as a target for new anti-malarial therapeutic approaches

In this second part of my work, I focused my attention on tRip as a potential therapeutic target. Given the ongoing challenges in finding effective medications, especially due to the emergence of resistance, and the difficulty in developing a successful vaccine, we explored tRip as a promising candidate for therapeutic approaches. By investigating the immunogenicity of the C-terminal domain of tRip and its interaction with aptamers, we aimed to identify novel strategies for combating *Plasmodium* infections.

1. Selection of RNA aptamers and characterization of their interaction with tRip

Understanding the specific interactions between tRip and aptamers could open the way for the development of innovative therapies, potentially blocking tRip mediated import or delivering toxic molecules into the parasite. Aptamers are nucleic acid molecules, such as DNA or RNA, that can selectively bind specific targets, such as proteins, small molecules or other compounds (Nimjee et al., 2017). We decided to work with RNA aptamers because tRip is an RNA binding protein (Bour et al., 2016).

1.2. Aptamers selection by SELEX

Marta Cela (former PhD student of the team) selected the RNA aptamers using the SELEX technique. To achieve this, 25 random nucleotides were introduced into a DNA library constructed through PCR and *in vitro* transcription. Five cycles of selection were carried out. The first cycle involved only positive selection. For positive selection, the C-terminal domain of tRip, used as a bait, was fused to the glutathione-S transferase protein (GST) and immobilized on a glutathione-agarose resin. In the other four selection cycles, negative selections were introduced: they were used to eliminate aptamers that bind non-specifically to the resin, the GST or outside the tRip binding site. The selected RNA molecules were reverse transcribed, cloned and then sequenced. But there was no sequence similarity between them and no similarity with the tRNA sequence.

However, using RNAfold for predicting secondary structures, the aptamers could be grouped into three families: (i) the group A presented the ACCUA motif in an apical loop, (ii) the group B contained variants with mutations at one of the five positions within the ACCUA motif, and (iii) the remaining aptamers, without motif, formed the group C.

1.3. Interaction between aptamers and tRip

Representative aptamers (Aptamer-15, Aptamer-17, Aptamer-24 and Aptamer-37) from the group A were radioactively transcribed *in vitro* and subjected to electrophoresis mobility shift assay (EMSA) in the presence of increasing concentrations of C-terminal domain of tRip. The results showed that these aptamers from group A interacted with tRip with an affinity comparable to that of tRNA transcripts. In fact, the aptamers and the $tRNA^{Phe}$ transcript (tr^{Phe}), that we used as control, exhibit the same interaction profile and comparable affinity. In addition, the size of the apical loop influenced the efficiency of the interaction.

In a second step, we focused our attention on Aptamer-15. The structure of the aptamer with a stem and an apical loop containing the motif was confirmed by *in vitro* structure probing experiments and the recognition of the ACCUA motif was tested by footprinting. To confirm whether effectively the ACCUA motif is involved in the interaction with tRip, different mutants were used. We made several point mutations of the ACCUA motif at the the first, second, third, fourth or fifth base of the motif, respectively as well as a global mutant where all bases were mutated (mutant 1). In other variants (mutant-7, -8, -9) we changed the stem: its size or its sequence. We found that (i) the ACCUA motif in the apical loop is essential for the aptamer to interact with tRip, (ii) each nucleotide of the motif contributes differently to the interaction, (iii) the motif is recognized only when it is in a loop and not in a stem. Finally, as expected, a mutated tRip protein that no longer interacted with tRNAs also failed interact with aptamers in EMSA experiments and to protect the nucleotides of the ACCUA motif in a footprint experiment.

Biochimie xxx (xxxx) xxx

Contents lists available at ScienceDirect

Biochimie

journal homepage: www.elsevier.com/locate/biochi

RNA aptamers developed against tRip: A preliminary approach targeting tRNA entry in *Plasmodium*

Martina Pitolli [1], Marta Cela [1], Caroline Paulus, Joëlle Rudinger-Thirion, Magali Frugier*

Université de Strasbourg, CNRS, Architecture et Réactivité de l'ARN, UPR 9002, F-67084, Strasbourg, France

ARTICLE INFO

Article history:
Received 25 April 2023
Received in revised form
26 May 2023
Accepted 24 June 2023
Available online xxx

Handling Editor: Dr B Friguet

Keywords:
RNA
Aptamers
tRNA
SELEX
Plasmodium
tRip

ABSTRACT

Malaria is caused by *Plasmodium* parasites that multiply inside host cells and can be lethal when *P. falciparum* is involved. We identified tRip as a membrane protein that facilitates the import of exogenous transfer RNA (tRNA) into the parasite. tRip encompasses a tRNA binding domain exposed on the parasite surface. We used the SELEX approach to isolate high-affinity and specific tRip-binding RNA motifs from a library of random 25 nucleotide-long sequences. In five rounds of combined negative and positive selections, an enriched pool of aptamers was obtained; sequencing revealed that they were all different in their primary sequence; only by comparing their structure predictions did most of the selected aptamers reveal a conserved 5-nucleotide motif sequence. We showed that the integral motif is essential for tRip-binding while the rest of the molecule can be significantly reduced or mutated as long as the motif is presented in a single-stranded region. Such RNA aptamers bind in place of the original tRNA substrate and act as an efficient competitor, suggesting that they can block tRip function and slow parasite development.

1. Introduction

Malaria is a parasitic disease caused by *Plasmodium* that affects millions of people, particularly in developing countries. The emergence of *Plasmodium* strains resistant to drugs represents a major threat to malaria control efforts [1]. There is therefore a need to discover new molecular targets and develop new therapeutic approaches against malaria. We have previously identified a conserved protein in *Plasmodium*, named tRip for transfer RNA import protein. This protein allows exogenous tRNAs to efficiently enter the parasite *in vitro* [2]. Although the role of tRNA trafficking is not yet clearly defined, it has been shown that in the absence of tRip the growth of blood stage parasites is significantly reduced compared to the wild-type parasite. Not only is tRip expressed at many stages of parasite development, but it is also an accessible surface protein (Fig. 1A); therefore, inhibition of tRip could potentially disrupt the ability of *Plasmodium* to replicate and survive in the host. One potential strategy for the development of new therapies is the use of aptamers, which are short, structured nucleic acids that can bind to specific molecular targets (reviewed in Ref. [3]). Aptamers have several advantages over traditional therapies, including low immunogenicity, low toxicity, and the ability to target a wide range of biomolecules [4]. Here, selection of tRip-specific RNA aptamers involved a process known as Systematic Evolution of Ligands by EXponential enrichment (SELEX) [5], a powerful technique that selects RNA sequences for their ability to bind to a molecular target (here, tRip). tRip contains a transmembrane helix [6] that anchors the protein to the parasite plasma membrane [2]. The internal N-terminal GST-like domain is involved in the association of the two *Plasmodium* multisynthetase complexes, the Q- (tRip, glutamyl- and glutaminyl-tRNA synthetase) and M – (tRip, glutamyl- and methionyl-tRNA synthetase) complexes [6,7], while the C-terminal domain is displayed outside of the parasite and is involved in tRNA recognition (Fig. 1A). This tRip tRNA-binding domain is an EMAPII-like domain that shares homology with *Aquifex aeolicus* Trbp111 [8]. Such domain is sufficient to efficiently bind and recognize tRNAs, especially the corner of their L-shaped structure formed by the coaxial stacking of D- and T-loops [9].

RNA aptamers, which bind specifically the C-terminal domain of tRip were isolated by SELEX, they correspond to unexpected sequences not related to tRNAs, yet competing with tRNAs for the same binding site on tRip. One of these molecules was further

* Corresponding author.
E-mail address: m.frugier@ibmc-cnrs.unistra.fr (M. Frugier).
[1] MP and MC contributed equally to this work.

https://doi.org/10.1016/j.biochi.2023.06.011
0300-9084/

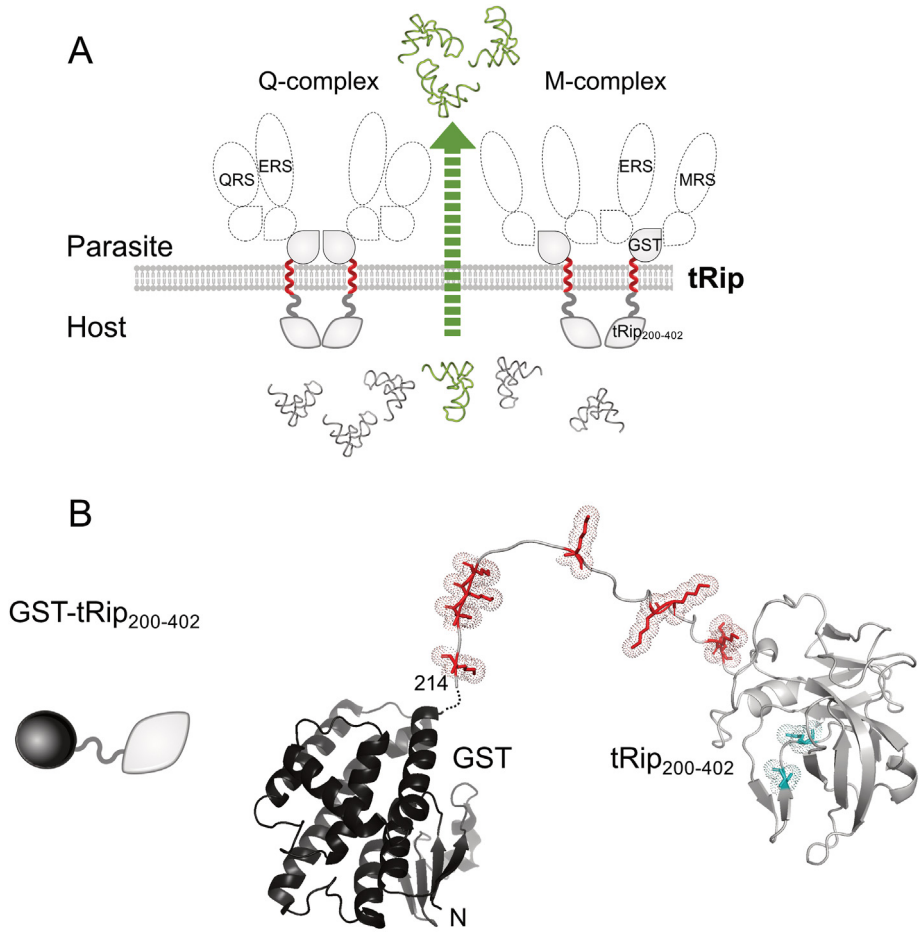

Fig. 1. Membrane-bound *Plasmodium* tRip and associated multi-synthetase complexes. (**A**) tRip, glutamyl- (ERS), glutaminyl- (QRS) and methionyl- (MRS) tRNA synthetases form two independent Q- (tRip:ERS:QRS) and M − (ERS:tRip:MRS) multi-synthetase complexes. GST-like interacting domains are shown with drop shape in tRip, ERS, QRS and MRS [6]. The tRip C-terminal EMAPII-like domains (grey diamond) is a tRNA-binding domain. The singular feature of the *Plasmodium* Q- and M − complexes is that tRip is bound to the plasma membrane and interact with parasite aaRSs inside and the tRNA-binding domain of tRip is exposed to external/host tRNAs. The tRip helix α8 has the capacity to associate with membranes and is shown here as a red transmembrane helix. The host tRNAs preferentially bound by tRip [9] are indicated in green and are supposed to enter the parasite better. (**B**) Target of the selection. The 3-dimensional folding of the fusion between GST (black, PDB 1R5A) and *P. falciparum* $tRip_{214-402}$ (light grey). The model was obtained by using AlphaFold2 based on the crystal structure of the C-terminal domain of *P. vivax* tRip (p43) (PDB 5ZKG [10]). The lysine residues present in the connection between both domains as well as the Ser_{312} and Met_{315} residues located in the OB-fold portion of the fusion protein are shown in red and cyan, respectively.

characterized to determine its folding, binding properties, and selectivity.

2. Materials and methods

2.1. Protein purification

The gene sequence of the C-terminal domain of the *P. falciparum* tRip ($tRip_{214-402}$) was cloned into the pGEX-2T plasmid (Sigma-Aldrich) between BamHI and EcoRI sites, to produce an N-terminal GST fusion protein: GST-$tRip_{214-402}$WT(using the following forward primer 5′-GCCGGATCCGAATTTTCATATATTTATAGATGG-3′ and reverse primer 5′-GCCGAATTCTTATGATATTGTTCCTTGATTTAAAA-CAC-3′). The S_{312}A and M_{315}A mutations were introduced by site-directed mutagenesis (QuickChange site-directed mutagenesis kit, Agilent) to get GST-$tRip_{214-402}$*. Proteins (GST-$tRip_{214-402}$WT, GST-$tRip_{214-402}$* and GST) were over-expressed in ER2566 bacteria together with plasmid pGro7 that encodes the GroEL and GroES chaperones (Takara Bio). Cultures were performed in LB medium, 2% glucose, 0.1 mg/mL ampicillin, 0.03 mg/mL chloramphenicol and 0.25 mg/mL arabinose (induction of chaperone proteins) at 37 °C with agitation until $OD_{600} = 2$. Cells were washed and expression of recombinant proteins was induced overnight at 18 °C in LB containing both antibiotics and 0.25 mM IPTG. Cells were recovered in 50 mM sodium phosphate buffer pH 8.0 and 300 mM NaCl, sonicated (7 min at 120 V, Ultrasons Annemasse, type 25OTS) and centrifuged 45 min at 35000 rpm at 4 °C. Fusion proteins were batch affinity purified on glutathione-agarose resin (Sigma-Aldrich), eluted in the same buffer containing 10 mM reduced glutathione (Sigma-Aldrich), dialyzed at 4 °C overnight against the preservation buffer (50 mM potassium phosphate pH 7.5, 150 mM KCl, 50% glycerol) and stored at −20 °C. The proteins' purity was verified on SDS-PAGE gel (Figs. S1A–C).

Equivalent sequences ($tRip_{200-402}$) were inserted into the plasmid pET15b to produce recombinant proteins fused to a 6-histidine (6-His) tag at the N-terminus: tRip $tRip_{200-402}$WT and $tRip_{200-402}$*. The clones were transformed into Top10 cells and proteins were purified by affinity (HIS-Select HF Nickel Affinity Gel, Sigma-Aldrich) according to the protocol detailed for $tRip_{1-402}$ in Ref. [9], the 6-His tag was cleaved with thrombin, and the proteins were kept in 25 mM HEPES-KOH pH7.0, 75 mM KCl, 5 mM ß-mercaptoethanol and 30% glycerol at −80 °C until use.

2.2. Construction of DNA and RNA libraries

The initial DNA library was constructed by PCR using the following template: 5′-GCCTGTTGTGAGCCTCCTGTCGAA($\mathbf{N_{25}}$)TTGAGCGTTTATTCTTGTCTCCC-3′ and two specific primers: 5′-*TAATACGACTCACTATAGGGAGA*CAAGAATAAACGCTCAA-3' (the T7 promoter sequence is shown in italic) and 5′-GCCTGTTGTGAGCCTCCTGTCGAA-3'. DNA library synthesis was performed using 2 ng of template, 3 ng of each primer in medium containing 75 mM Tris pH 8.8, 20 mM ammonium sulfate, 0.01% Tween 20, 2 mM $MgCl_2$, 60 μg Taq polymerase, and 1 mM of each dNTP. After 2 cycles (1 min at 95 °C, 1 min at 58 °C, 10 min at 72 °C) the PCR product was purified on a 12% acrylamide/bisacrylamide (37.5:1),1XTBE gel (Fig. S1D). The resulting double stranded DNA library contains the T7 RNA polymerase promoter followed by 25 random nucleotides (N_{25}) and a sequence of 23 nucleotides used for PCR amplification.

The DNA library was used as a template to transcribe the RNA aptamer library *in vitro*: 100 μg of purified PCR product was transcribed in 2 mL of 20 mM Tris-HCl pH 8, 11 mM $MgCl_2$, 2 mM of each nucleotide, 2.5 mM DTT, 0.5 mM spermidine in the presence of 10 μL of T7 polymerase, at 37 °C for 3 h. The transcription product was further purified on a 12% acrylamyde/bisacrylamyde (19:1), 8 M urea,1XTBE gel (Fig. S1D).

2.3. Selection procedure

Five successive selection rounds were performed (Fig. 2): the first step consisted of a positive selection to enrich the library with aptamers that bind to the immobilized fusion protein GST-tRip$_{214-402}$WT. The other 4 selection rounds encompassed both a negative and a positive selection. Negative selections were performed in the presence of different competitors to remove aptamers that bind to the resin (beads alone: selection #2), to the GST (beads-GST: selection #3) or outside the tRip tRNA binding site (beads-GST-tRip$_{214-402}$*: selections #4 and #5). 320 pmol of protein (none, GST or GST-tRip$_{214-402}$*) were immobilized on 200 μL of glutathione agarose and incubated with various concentrations of aptamer libraries in 1 mL of buffer A (50 mM HEPES-KOH pH 7.5, 150 mM KCl) under different temperature and time conditions (26 or 37 °C for 30 min down to 5 min). Aptamers of interest are those that do not bind to the column. These fractions were then directly used for the next positive selection in the presence of 320 pmol of immobilized GST-tRip$_{214-402}$WT (4, 26 or 37 °C for 7 h down to 5 min). In this case, aptamers of interest are those that remain bound to the affinity column. The resin was washed with 5 ml of buffer A and the bound RNAs were eluted with 400 μL of buffer A containing 10 mM reduced glutathione. Between each selection cycle, the selected RNAs were precipitated and reverse transcribed for 60 min at 42 °C in 75 μL of AMV-RT buffer, 75 mM dNTP, and 20 units of AMV-Reverse Transcriptase (Life Sciences). The reaction was stopped by phenolic extraction and precipitation and the resulting cDNA was

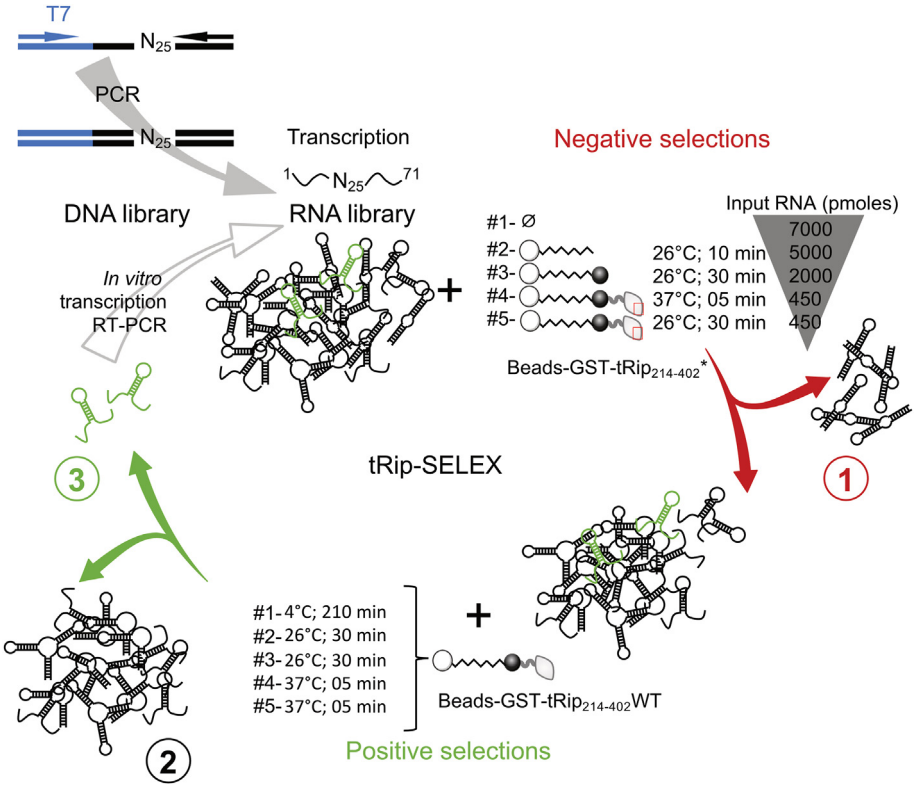

Fig. 2. Summary of the SELEX protocol and RNA selection. The initial oligonucleotide library, containing 25 random nucleotides (N_{25}), was amplified by PCR and transcribed *in vitro*, producing a random pool of candidate RNAs. The target proteins used in this study were constructed by fusing a GST domain to the N-terminus of the tRNA-binding domain (tRip$_{214-402}$, grey diamond) of wild-type (WT) or mutated (*), red cross) tRip. GST-tRip$_{214-402}$* was mutated at two positions essential for specific tRNA binding (Ser_{312} and Met_{315} mutated to alanine) [9]. Each round (except the first one) consists of a negative selection to eliminate RNAs binding either to the resin, to the GST domain or to the mutated GST-tRip$_{214-402}$*(**1**). RNA aptamers that do not bind to competitors are used as is in the following positive selection in the presence of the GST-tRip$_{214-402}$WT and unbound RNAs are washed out (**2**). At the end of the positive selection, the bound sequences are eluted (**3**), amplified by RT-PCR and *in vitro* transcribed. Along the 5 selection rounds, more and more stringent experimental conditions (time and temperature of incubation) were used to keep only RNA molecules with the highest specificity for tRip. At the end of the process, cDNAs are PCR amplified, cloned and sequenced to identify the selected sequences.

then amplified by PCR (25 cycles, 1 min at 95 °C, 1 min at 58 °C, 30 s at 72 °C) and transcribed again. The PCR product corresponding to the aptamers from the fifth round of selection was cloned into the pDrive plasmid (Qiagen PCR cloning kit) and 46 clones were sequenced.

2.4. Preparation of RNA molecules

Native yeast $tRNA^{Phe}$ was purified according to Ref. [11]. The corresponding unmodified transcript (tr^{Phe}) was produced by *in vitro* T7 transcription of linearized plasmid as described in Ref. [9], while all aptamers' transcripts were amplified by transcription of annealed oligonucleotides [12]. For Electrophoretic Mobility Shift Assays (EMSA), aptamers were radiolabeled during transcription by adding 20 μCi of [α^{32}P] ATP to 100 μl of transcription mix. All transcripts were purified on a 12% acrylamide/bisacrylamide (19:1), 8 M urea, 1XTBE gel and renatured in H_2O by heating for 2 min at 65 °C followed by 10 min cooling to room temperature before use.

2.5. Electrophoretic Mobility shift assay (EMSA)

RNA/protein complexes were formed by incubating 10000 cpm of ^{32}P labeled RNA with different concentrations of protein ($tRip_{200-402}$WT or $tRip_{200-402}$*) in a total volume of 20 μl for 20 min at 4 °C in 25 mM HEPES-NaOH pH 7.5, 75 mM KCl, 5 mM $MgCl_2$, 20 nM dT_{15} and 10% glycerol. The reaction was analyzed on a native gel (6% acrylamide/bisacrylamide 37.5:1, 1XTBE) for 1.5 h at 140 V at 4 °C. The *K*d was determined as the concentration of $tRip_{200-402}$WT shifting 50% of the labeled RNA. The *p-values* (paired T-test), less than 0.05, allow to conclude that the *K*ds determined for aptamers are significantly different from the *K*d determined for tr^{Phe}. A variant of EMSA consists of competitions between two RNAs. In this case, 100 nM $tRip_{200-402}$ was incubated with 10000 cpm of aptamer-15 and different concentrations of unlabeled aptamer-15, aptamer-15#1, tr^{Phe} or native yeast $tRNA^{Phe}$ (60–1000 nM) are added to displace aptamer-15 from $tRip_{200-402}$.

2.6. Structural mapping procedures and footprinting

Probing of aptamer-15 was performed using the $Pb(OAc)_2$ as chemical probe. The transcript was 5′-labeled with [γ^{32}P] ATP [13]. Probing (10 μL) was performed on 50000 cpm of labeled transcript and 20 pmol of unlabeled transcript for 8 min in 50 mM HEPES-KOH pH 7.5, 5 mM Mg acetate and 50 mM K acetate at 25 °C. A freshly prepared $Pb(OAc)_2$ solution in H_2O was added to reach a final concentration of 1, 2.5, 5 and 10 mM. Reactions were stopped by rapid cooling on ice and addition of 20 mM EDTA and ethanol precipitation; samples were washed twice and dried. Pellets were dissolved in formamide dye and heated 2 min at 90 °C before analysis on a 12% denaturing gel. A control without $Pb(OAc)_2$ was performed and bands were assigned by alkaline degradation and nuclease T1 digestion under denaturing conditions [14].

In footprinting experiments, aptamer-15 transcript (50000 cpm, 10 pmoles in 10 μL) was preincubated with $tRip_{200-402}$ or $tRip_{200-402}$* (2 and 4 μM) in 50 mM HEPES-KOH pH 7.5, 5 mM Mg acetate and 50 mM K acetate for 20 min at 4 °C. Then 5 mM $Pb(OAc)_2$ was added, and incubation was completed for 8 min at 25 °C. Reactions were stopped by adding EDTA and glycogen. Samples were submitted to phenol extraction and treated as described above.

3. Results

3.1. SELEX: selection strategy and results

The SELEX technology was used to isolate RNA sequences able to bind with high affinity and specificity to the tRNA binding site in the C-terminal domain of *P. falciparum* tRip ($tRip_{214-402}$). In this study we chose to use only the C-terminal domain of tRip, which is solely responsible for tRNA binding (Fig. 1B) [2]. The DNA library contains 25 random nucleotides (nt), thus its complexity is theoretically 4^{25} (1.12×10^{15}). *In vitro* transcription of the DNA library yielded 90 μg (7 nmol) of purified RNA aptamers, i.e. 4.2×10^{15} molecules, suggesting that most of the sequences are present at least once in the starting RNA library. Three proteins were used in the different rounds of selection (Figs. 2A and 3A). The GST-$tRip_{214-402}$WT was used for positive selections and retained all aptamers that bind to the C-terminal domain of tRip. The other two proteins (the GST domain alone and GST-$tRip_{214-402}$*, displaying a mutated tRNA binding site) were used in negative selections to increase the stringency and remove aptamers that bind non-specifically to the column, to the GST portion of the fusion protein or to a region other than the tRNA recognition site of the C-terminal domain of tRip.

Each selection was performed by varying the incubation conditions: time (between 5 and 30 min of incubation), temperature (between 26 and 37 °C) and initial RNA concentration (from 7 down to 0.45 μM). Each step was controlled by the analysis of the samples on denaturing gels (Fig. 3A). Monitoring aptamers enrichment over the 5 selection rounds revealed a low selection efficiency in the first two rounds, indicating that only a small proportion of aptamers can bind efficiently and specifically to the C-terminal domain of tRip. Yet, selection efficiency increases significantly for the last two rounds (up to 13%) suggesting that the most efficient and specific ligands have been selected (Fig. 3B). After the fifth selection round, selected aptamers were reverse transcribed and cloned. Of the 50 clones analyzed, 28 contained an insert and were sequenced. These sequences are pyrimidine-rich, but no alignment was possible, indicating no obvious similarities and suggesting that each sequence was unique (Fig. 3C). Further, *in silico* secondary structures prediction [15] showed (i) that the selected sequences base-pair with the regions imposed during the design of the library, but (ii) no structural features reminiscent to tRNA (*e.g.* to D- or T-loops known to interact with tRip) could be identified (Fig. S2). However, 10 of them (group A: aptamers 13, 15, 16, 24, 26, 17, 30, 33, 37 and 47) presented a single-stranded conserved 5-nucleotide motif: ACCUA, and 5 others (group B: aptamers 14, 32, 43, 45, 46) differ only by one nucleotide (Fig. 3C). For the rest (group C), no obvious consensus is detectable.

3.2. Characterization of selected aptamers for tRip binding

In previous experiments, we could show that, whether $tRip_{238-402}$ (a shorter version of tRip lacking the lysine-rich (K) N-terminal region) or $tRip_{200-402}$* (mutated at Ser_{312} and Met_{315}) are both characterized by very weak tRNA binding capacities, indicating that the K-rich sequence and conserved Ser_{312} and Met_{315} (Fig. 1B) act together to interact efficiently and specifically with tRNAs. In addition, the full-length tRip protein homodimerizes *via* its N-terminal domain [10] and results in the formation of a complex with a stoichiometry of 1 tRNA to 1 $tRip_{1-402}$ dimer [9]. Here, with the monomeric C-terminal domain [10] we observe two types of complexes that we interpret as the coexistence of complexes containing 1 tRNA bound to one $tRip_{200-402}$WT monomer or 1 tRNA bound to two $tRip_{200-402}$WT monomers depending on the protein concentration in the assay (Fig. 4A, tr^{Phe}). We focused on aptamers containing the ACCUA motif and tested aptamers 37, 17, 15 and 24

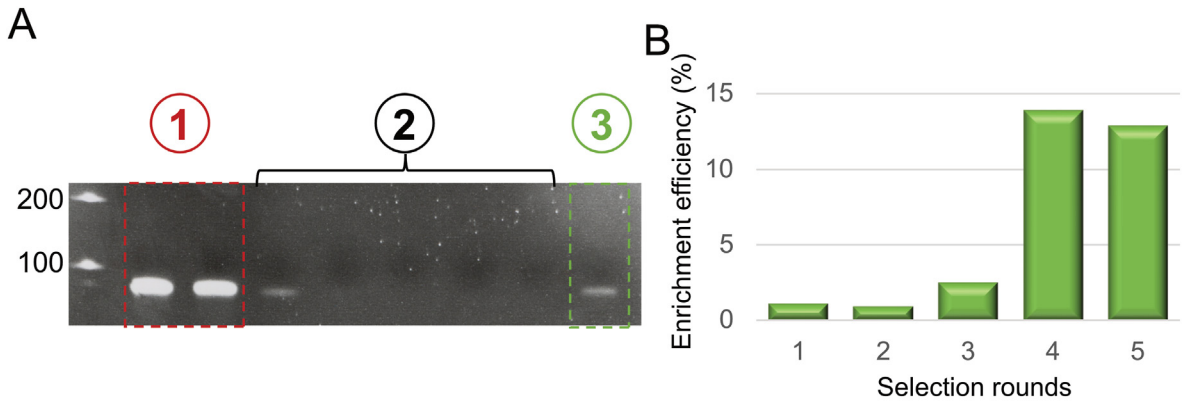

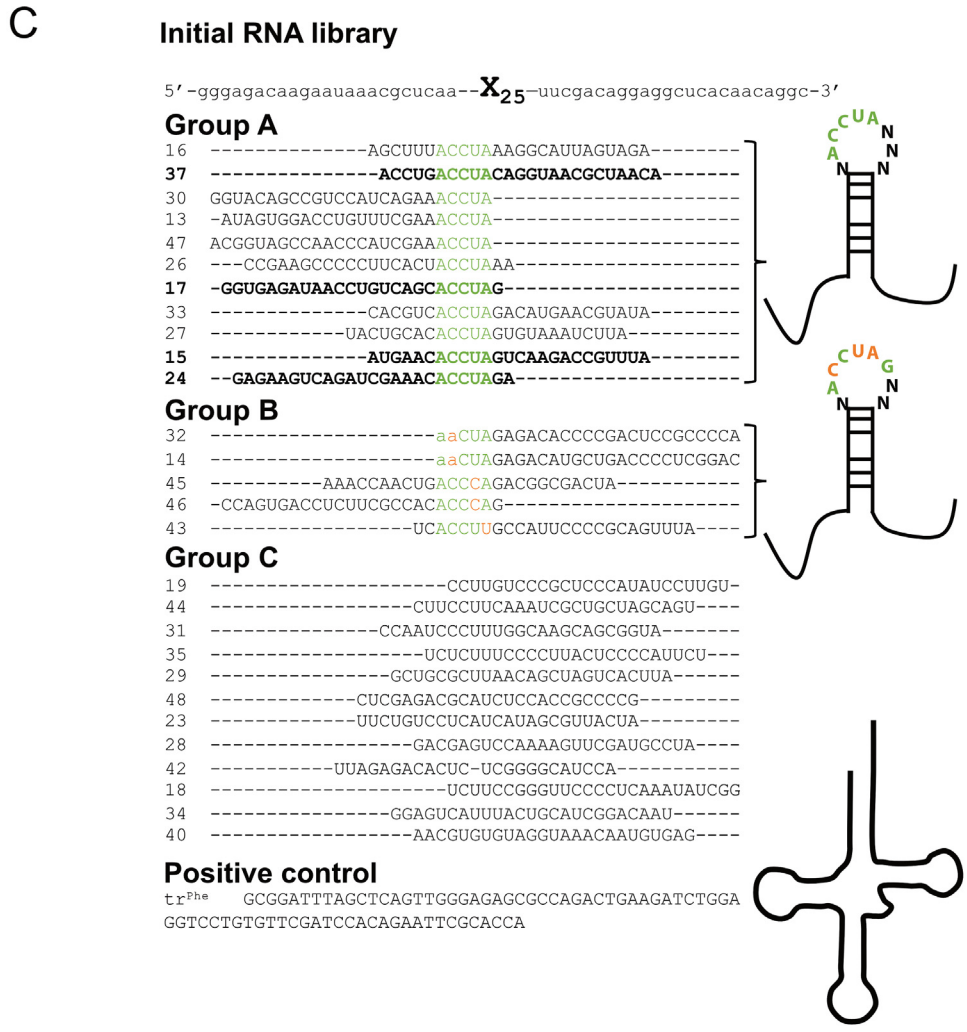

Fig. 3. Target of the selection and selected aptamers. (A) At each step of each selection round (here round #2) RNAs were controlled on denaturing analytical gel. The RNA present in the fraction that does not bind during the negative selection (1) is used in the positive selection. The resin is washed extensively (2) and the RNA/GST-tRip$_{214-402}$WT complexes are eluted (3). Refer to Fig. 2. (**B**) Enrichment efficiencies of GST-tRip$_{214-402}$WT-bound RNA were monitored during the 5 successive selection rounds as the ratio (%) between eluted RNA after the positive selection and initial RNA (before negative selection). (**C**) RNA library and selected aptamers. The entire sequence of the RNA library is shown while only the nucleotides corresponding to the selected sequences are given in the alignments. Aptamers were classified into three groups corresponding to the presence of (i) the ACCUA motif when present in an apical loop (group A), (ii) the same ACCUA motif mutated at one of the 5 positions (group B), and (iii) other sequences without obvious conserved motifs (group C). The ACCUA motif is shown in green, and the point mutations are in orange; the lower-case letters indicate that the nucleotides belong to the imposed sequences of the library. The four sequences highlighted in bold correspond to the sequences chosen to be tested by EMSA for their ability to bind tRip$_{200-402}$WT. The sequence of yeast tRNA^{Phe} is also shown; this sequence was transcribed *in vitro* (tr^{Phe}) and used as a positive control in all band shift experiments. For each aptamer, the corresponding two-dimensional fold obtained with RNAFold is shown in Fig. S2.

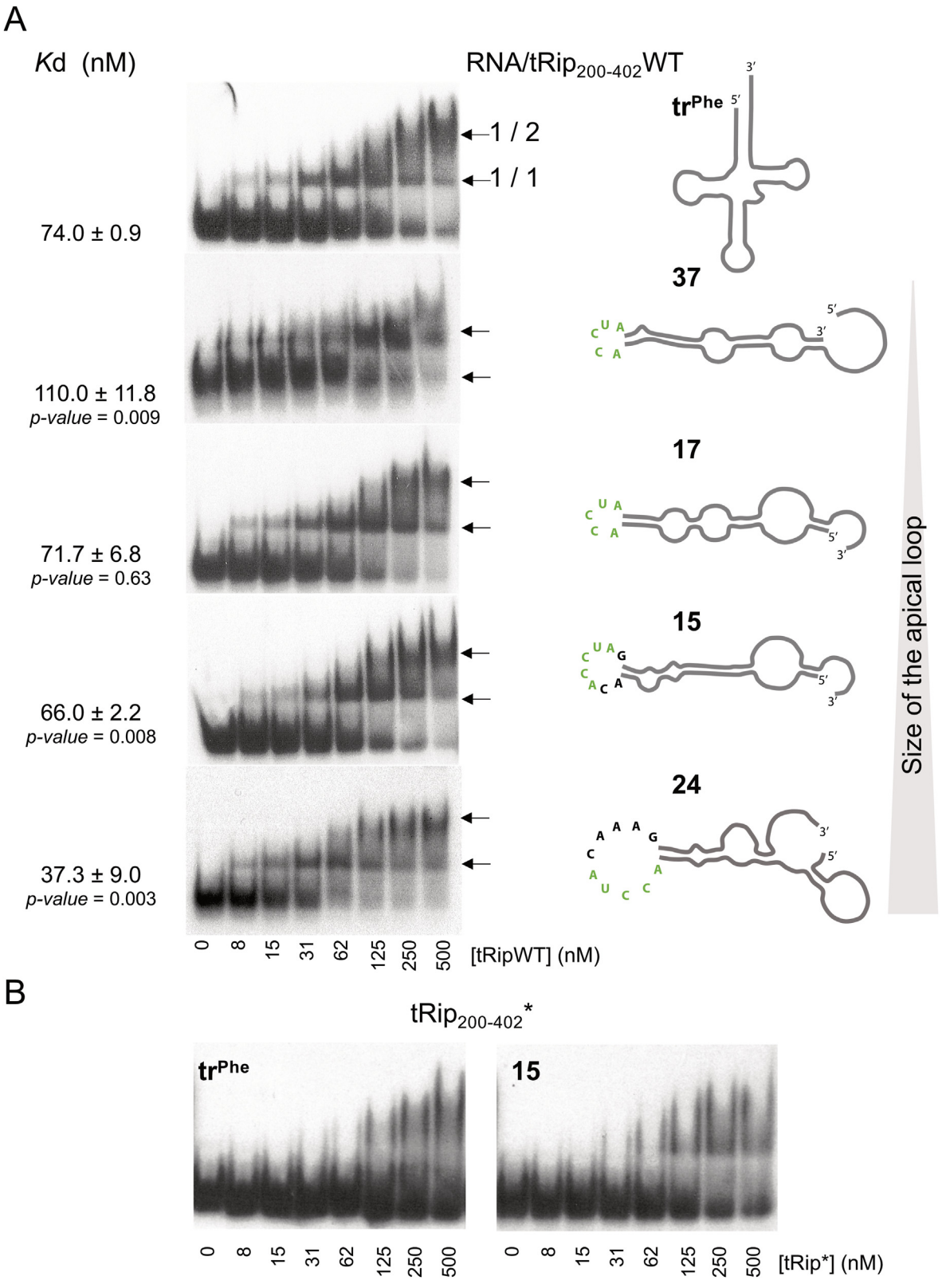

Fig. 4. Comparison of the binding capacities of aptamers 37, 17, 15 and 24 to tRip$_{200\text{-}402}$WT. (**A**) The affinities of each aptamer were determined by EMSA and compared to the positive control tr^{Phe}. RNAs were radioactively labeled, their concentration is fixed and limiting in the assay, while the concentration of tRip$_{200\text{-}402}$WT increases from 8 to 500 nM. All four aptamers are characterized by the presence of the ACCUA consensus motif (green) presented in apical loops of increasing sizes (schematic view based on RNAfold models). The *Kd* values as well as the corresponding *p-values* (n = 3) are indicated on the left side of each aptamer molecule. The two RNA:tRip$_{200\text{-}402}$WT complexes with stoichiometries of 1:1 and 1:2 are indicated with arrows. (**B**) Negative control experiments were performed in the presence of mutated tRip$_{200\text{-}402}$* with either aptamer-15 or tr^{Phe} in the same conditions. Such smeary profiles indicate non-specific binding and therefore cannot be quantified.

for their capacity to bind the C-terminal domain of tRip. These sequences are characterized by apical loops with increasing sizes (from 5 to 10 nucleotides). All bind efficiently to tRip$_{200\text{-}402}$WT, with the same profile, i.e., with 2 well-defined bands and *Kd* values in the same range as the tRNA^{Phe} transcript (tr^{Phe}) although significantly different (*p-values* < 0.05, except for aptamer-17), indicating that the selections were effective and provided very strong ligands (Fig. 4A, Fig. S3A). Furthermore, the binding efficiency of the ACCUA-containing aptamers increases with the size of the apical loop.

Aptamer-15 was chosen to experimentally investigate its overall folding and the involvement not only of the conserved motif but also of the rest of the molecule in its specific recognition by tRip$_{200\text{-}402}$WT. First, aptamer-15 was compared to tr^{Phe} for its ability to bind or not the mutated tRip$_{200\text{-}402}$* (Fig. 1B). In both cases, EMSAs show mainly smeary profiles, with a faint band in the case of aptamer-15 yet consistent with what was previously observed in Ref. [9], suggesting that the shifted RNAs interact nonspecifically with the K-rich sequence of tRip$_{200\text{-}402}$* (Fig. 4B).

3.3. Probing the secondary structure of aptamer-15

The secondary structure of aptamer-15 was probed with Pb(OAc)$_2$ (Fig. 5A), that maps preferentially single-stranded regions. The resulting 2D model is shown in Fig. 5B. It confirms the presence of a stem-loop structure with 9 base-pairs, an internal loop (nts 4 to 9 and nts 52 to 60) and an apical loop (nts 22 to 39). As expected, the ACCUA motif (nt 30 to 34) is fully accessible. However, this experimental model does not compare exactly to the model predicted *in silico*, especially with respect to the size of the apical loop. Yet, absence of cleavages at nt 34 to 39 as well as the presence of few cleavages in the stem-loop (residues 46 to 51) (Fig. 5A) indicate that the molecule is characterized by some flexibility within both domains and suggests that several conformers coexist in solution.

3.4. Search for key features driving tRip binding

Footprinting experiments were performed on aptamer-15 complexed to either tRip$_{200\text{-}402}$WT or tRip$_{200\text{-}402}$* using Pb(OAc)$_2$ to determine the regions of the RNA that are specifically protected by the wild-type protein. Fig. 5C shows that residues located in the apical loop, including the ACCUA motif, are protected by tRip$_{200\text{-}402}$WT and not by tRip$_{200\text{-}402}$*, indicating that this sequence interacts with tRip. Protections were also visible in the rest of the molecule, raising the question of which region of the aptamer is required for high-affinity and specific binding (Fig. 6A, Fig. S4). By replacing the ACCUA motif by the CAACC sequence in aptamer-15 (mutant #1), tRip$_{200\text{-}402}$WT does not longer bind, confirming that the motif is essential for complex formation (Fig. 6B). Point mutations were therefore introduced into the conserved motif to further define which residues predominantly contribute to the recognition of selected aptamers (Fig. 6A and Fig. S4). Of the 5 mutants, only mutant #2 still binds to the protein while mutation of positions 2 to 5 (mutants #3, #4, #5 and #6) significantly disrupt binding. However, only a complex corresponding to the 1:1 stoichiometry is detectable with mutant #2, suggesting that some interactions with the second monomer of tRip $_{200\text{-}402}$ have been lost. Next the

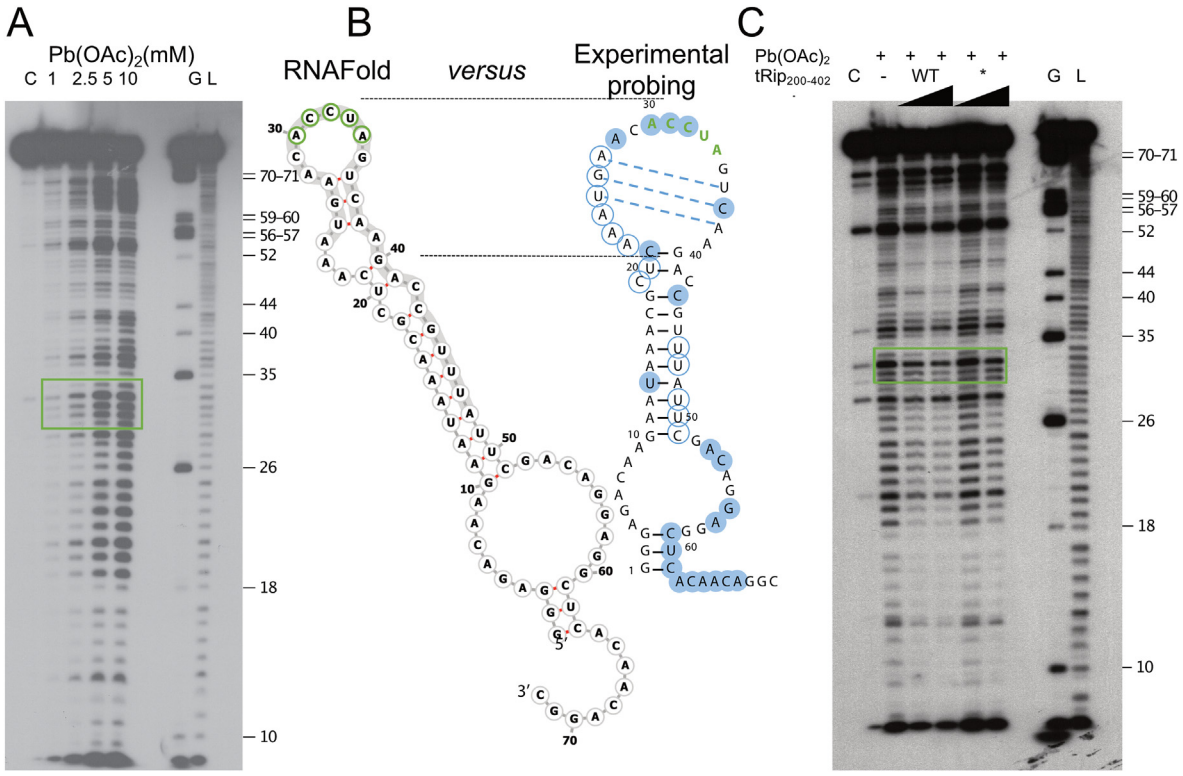

Fig. 5. Secondary structure of aptamer-15 and specific tRip$_{200\text{-}402}$WT footprint. (**A**) Autoradiograms of Pb(OAc)$_2$ probing experiments on 5′-labeled aptamer-15. Pb(OAc)$_2$ preferentially cuts unstructured areas. Each probing experiment is associated with a control (C, RNA incubated under the same conditions but without Pb(OAc)$_2$), a ladder achieved by alkaline hydrolysis (L) and a T1 ladder under denaturing conditions (G) that defines the positions of G residues and allows sequence numbering. The 5-nucleotides motif (ACCUA) is boxed in green. (**B**) Summary of Pb(OAc)$_2$ probing results on aptamer-15 sequence (right); nt cleaved by Pb(OAc)$_2$ are indicated by blue empty rings (weak cleavages) and solid rings (strong cleavages). The RNAFold model (left) is shown for comparison and the 3 base-pairs that are not visible in the probing experiments are indicated with blue dotted lines. (**C**) Autoradiogram of footprinting experiments performed on aptamer-15 in the absence and presence of either tRip$_{200\text{-}402}$WT or tRip$_{200\text{-}402}$* (2 and 4 μM). (**D**) Mutations (orange) introduced in aptamer-15.

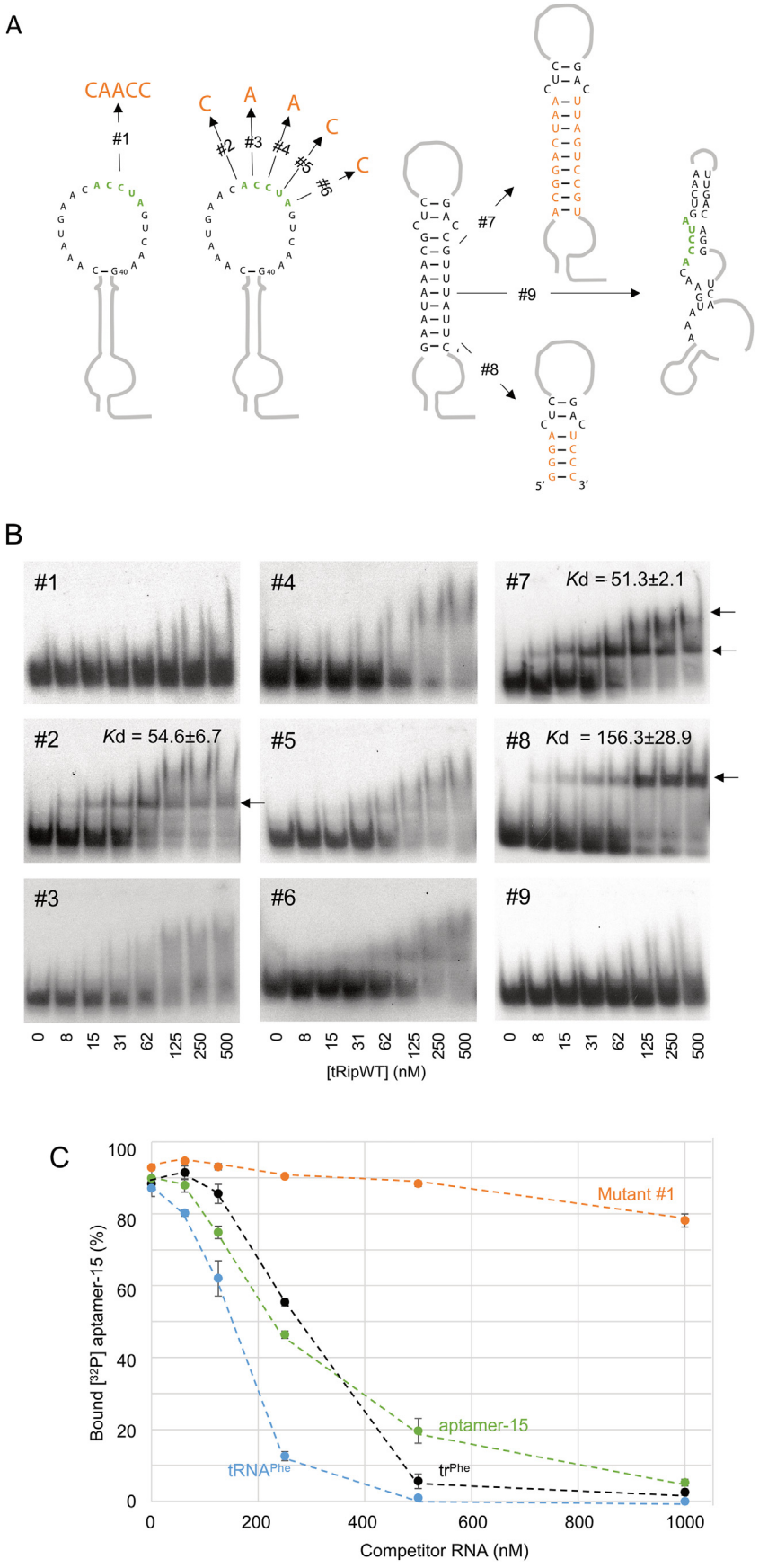

Fig. 6. Deciphering aptamer-15 specificity for tRip$_{200\text{-}402}$WT. (**A**) Mutations (orange) introduced in aptamer-15. In mutant #1, the consensus sequence has been completely replaced by the CAACC sequence. Mutants #2 through #6 present point mutations in the consensus motif sequence (green). The stems of mutated aptamers #7, #8 and #9 are

modified with 9 fully mutated base pairs, its reduction to retain only 4 base pairs, and a deletion that leads to a drastically different predicted fold, respectively.
(**B**) Mutants ~~of aptamer-15 described in~~ Fig. 5D were tested by EMSA for their affinity for $tRip_{200\text{-}402}$WT in the exact same conditions than in Fig. 4A. Each experiment was performed in parallel with the positive control (tr^{Phe}). (**C**) Ability of native yeast $tRNA^{Phe}$ and tr^{Phe} to dissociate the pre-established complex between aptamer-15 and $tRip_{200\text{-}402}$WT. The percentage of bound radiolabeled aptamer-15 is plotted as the function of the concentration of the different competing RNAs: concentrations of aptamers 15 (green, positive control), 15#1 (orange, negative control), natif yeast $tRNA^{Phe}$ (blue) or tr^{Phe} (black) ranged from 60 to 1000 nM.

contribution of the double-stranded region of aptamer-15 was tested, first by changing its sequence entirely (mutant # 7) and then by shortening it (mutant #8). Neither changing the sequence of the stem nor reducing its size hinders the binding of aptamer-15 (Fig. 6A,B and S3B). The mutated sequence in the stem-loop provides the exact same binding profile as tr^{Phe} and aptamer-15. However, only one copy of $tRip_{200\text{-}402}$ can bind the mutant #8, indicating that this mutant is too short to adapt two EMAPII-like domains. Finally, when the motif is predicted to be involved in a double-stranded structure (mutant #9), it is no longer recognized. Overall, these observations support that as long as the ACCUA motif is single stranded, an RNA as short as 35 nts can be efficiently and specifically recognized by the C-terminal domain of tRip.

3.5. Competitive binding assays

Aptamer-15 (positive control) and mutant #1 (negative control) as well as both the native yeast $tRNA^{Phe}$ (with post-transcriptional modifications) and the corresponding transcript (tr^{Phe}) were tested for their capacities to dissociate the complex formed between $tRip_{200\text{-}402}$WT and radiolabeled aptamer-15. A graph was plotted showing the percentage of [^{32}P]-aptamer-15 bound to $tRip_{200\text{-}402}$WT *versus* increasing concentrations of competing RNAs (Fig. 6C). Molecules requiring a larger molar excess to displace the [^{32}P]-aptamer-15 are those that bind loosely to $tRip_{200\text{-}402}$ and therefore have a lower relative IC50 (molar concentration required to displace 50% of the radiolabeled aptamer-15). On the one hand, mutant #1 does not dissociate the complex, on the other hand both tr^{Phe} and aptamer-15 behave similarly (with identical IC50s of 250 nM) while the native yeast $tRNA^{Phe}$ has an IC50 lower than 200 nM. The difference in dissociation strengths of tRNAPhe and its transcript (trPhe) is consistent with the fact that tRip binds and discriminates tRNAs based on their post-transcriptional modifications [9].

4. Discussion

EMAPII-like domains adopt an OB-fold, which has been shown to bind the corner of L-shaped tRNAs [8,16,17]. These domains are often fused to GST-like domains that are in turn involved in the formation of multi-synthetase complexes (MSC). Together, these GST-like and EMAPII-like fusions are essential in controlling MSC formation and also in improving aminoacylation efficiency of MSC-associated aaRSs towards their cognate tRNAs. Until now, such proteins (*e.g.* AIMP1/AIMP2 from *Homo sapiens*, Arc1p from *Saccharomyces cerevisiae*, Tg-p43 from *Toxoplasma gondii*) have been shown to be cytosolic [18–20]. However, *Plasmodium* tRip is an exception, since it is the only example to date of an EMAPII-like domain displayed on the parasite surface [2], thus in contact with the outside or contents of host cells. In this configuration, tRip can still associate aaRSs into MSCs [6,7] but its C-terminal EMAPII-like domain cannot participate in parasite aminoacylation (Fig. 1A). Nevertheless, tRip has been shown to be involved in tRNA import across the parasite plasma membrane [2]. These unique localization and function make the C-terminal domain of tRip a good target for developing either molecules that block tRNA entry into the parasite or specific transporters of toxic molecules for the parasite. tRip specificity was approached by selecting RNA molecules that bind to its C-terminal domain under increasingly stringent experimental conditions. To this end, the SELEX technique was used and yielded a group of 11 RNA aptamers that all possess a common ACCUA motif in their apical loop but do not share any sequence or structural similarity to tRNAs (Fig. 4 and S2). Based on the study of aptamer-15, it appears that the stem region can be shortened, or its sequence mutated without significantly destabilizing complex formation, suggesting that there are no specific restrictions on the size or structures that can participate in protein binding. The selected structures that display the recognition motif ACCUA are strikingly different from the elbow of the tRNA L-shaped structure. Thus, we isolated a single stranded 5-nt motif that can be recognized as efficiently by tRip as the intricate 3D structure of tRNAs. However, *in vivo*, the presence of post-transcriptional modifications on tRNAs would lead to stronger competitions, especially with the favorite tRip-binders ($tRNA^{Ser}_{AGA}$ or $tRNA_{Asn}$ in human [9]). The next step would therefore require the incorporation of modified nucleotides into selected aptamers, *e.g.* pseudouridines (which are more represented in tRip-preferentially bound tRNAs) in order to produce molecules capable of competing even more efficiently with host tRNAs.

Funding

This work was performed under the framework of the Interdisciplinary Thematic Institute IMCBio, as part of the ITI 2021–2028 program of the University of Strasbourg, CNRS and Inserm. It was supported by IdEx Unistra (ANR-10-IDEX-0002), by SFRI-STRAT'US project (ANR 20-SFRI-0012), and EUR IMCBio (IMCBio ANR-17-EURE-0023) under the framework of the French Investments for the Future Program », by previous Labex NetRNA (ANR-10-LABX-0036) and by the Fondation pour la Recherche Médicale (FRM) (grant number FDT201704337050) to Marta Cela.

Authors contributions

MP, MC, and CP performed the experiments, including cloning, protein purification, selections, characterization of aptamers, analysis, and interpretation of results. JRT and MF managed the conception, design, and interpretation of the data, and wrote, reviewed, and edited the manuscript. MF was responsible of fundings. All authors approved the final article.

Declaration of competing interest

Authors declare no conflict of interest.

Acknowledgements

We would like to thank Dr Anne Théobald-Dietrich for her insights.

Appendix A. Supplementary data

Supplementary data to this article can be found online at https://doi.org/10.1016/j.biochi.2023.06.011.

References

[1] World Health Organization, World Malaria Report 2022, 2022. https://www.who.int/teams/global-malaria-programme/reports/world-malaria-report-2022.

[2] T. Bour, N. Mahmoudi, D. Kapps, S. Thiberge, D. Bargieri, R. Ménard, M. Frugier, *Apicomplexa* -specific tRip facilitates import of exogenous tRNAs into malaria parasites, Proc. Natl. Acad. Sci. U.S.A. 113 (2016) 4717–4722, https://doi.org/10.1073/pnas.1600476113.

[3] Y. Zhang, B. Lai, M. Juhas, Recent advances in aptamer discovery and applications, Molecules 24 (2019) 941, https://doi.org/10.3390/molecules24050941.

[4] J. Zhou, J. Rossi, Aptamers as targeted therapeutics: current potential and challenges, Nat. Rev. Drug Discov. 16 (2017) 181–202, https://doi.org/10.1038/nrd.2016.199.

[5] M. Darmostuk, S. Rimpelova, H. Gbelcova, T. Ruml, Current approaches in SELEX: an update to aptamer selection technology, Biotechnol. Adv. 33 (2015) 1141–1161, https://doi.org/10.1016/j.biotechadv.2015.02.008.

[6] J.R. Jaramillo Ponce, A. Théobald-Dietrich, P. Bénas, C. Paulus, C. Sauter, M. Frugier, Solution X-ray scattering highlights discrepancies in *Plasmodium* multi-aminoacyl-tRNA-synthetase complexes, Protein Sci. 32 (2023), https://doi.org/10.1002/pro.4564.

[7] J.R. Jaramillo Ponce, D. Kapps, C. Paulus, J. Chicher, M. Frugier, Discovery of two distinct aminoacyl-tRNA synthetase complexes anchored to the *Plasmodium* surface tRNA import protein, J. Biol. Chem. 298 (2022) 101987, https://doi.org/10.1016/j.jbc.2022.101987.

[8] A.J. Morales, M.A. Swairjo, P. Schimmel, Structure-specific tRNA-binding protein from the extreme thermophile *Aquifex aeolicus*, EMBO J. 18 (1999) 3475–3483, https://doi.org/10.1093/emboj/18.12.3475.

[9] M. Cela, A. Théobald-Dietrich, J. Rudinger-Thirion, P. Wolff, R. Geslain, M. Frugier, Identification of host tRNAs preferentially recognized by the *Plasmodium* surface protein tRip, Nucleic Acids Res. (2021) 10618–10629, https://doi.org/10.1093/nar/gkab769.

[10] S. Gupta, J. Chhibber-Goel, M. Sharma, S. Parvez, K. Harlos, A. Sharma, M. Yogavel, Crystal structures of the two domains that constitute the *Plasmodium vivax* p43 protein, Acta Crystallogr. D Struct. Biol. 76 (2020) 135–146, https://doi.org/10.1107/S2059798319016413.

[11] R. Giegé, A.C. Dock, D. Kern, B. Lorber, J.C. Thierry, D. Moras, The role of purification in the crystallization of proteins and nucleic acids, J. Cryst. Growth 76 (1986) 554–561, https://doi.org/10.1016/0022-0248(86)90172-7.

[12] M. Frugier, C. Florentz, M.W. Hosseini, J.-M. Lehn, R. Giegé, Synthetic polyamines stimulate *in vitro* transcription by T7 RNA polymerase, Nucleic Acids Res. 22 (1994) 2784–2790, https://doi.org/10.1093/nar/22.14.2784.

[13] M. Silberklang, A.M. Gillum, U.L. Rajbhandary, The use of nuclease P1 in sequence analysis of end group labeled RNA, Nucleic Acids Res. 4 (1977) 4091–4108, https://doi.org/10.1093/nar/4.12.4091.

[14] A. Théobald-Dietrich, R. Giegé, J. Rudinger-Thirion, Evidence for the existence in mRNAs of a hairpin element responsible for ribosome dependent pyrrolysine insertion into proteins, Biochimie 87 (2005) 813–817, https://doi.org/10.1016/j.biochi.2005.03.006.

[15] R. Lorenz, S.H. Bernhart, C. Höner zu Siederdissen, H. Tafer, C. Flamm, P.F. Stadler, I.L. Hofacker, ViennaRNA package 2.0, Algorithm Mol. Biol. 6 (2011) 26, https://doi.org/10.1186/1748-7188-6-26.

[16] T. Nomanbhoy, A.J. Morales, A.T. Abraham, C.S. Vörtler, R. Giegé, P. Schimmel, Simultaneous binding of two proteins to opposite sides of a single transfer RNA, Nat. Struct. Biol. 8 (2001) 344–348, https://doi.org/10.1038/86228.

[17] D. Kapps, M. Cela, A. Théobald-Dietrich, T. Hendrickson, M. Frugier, OB or Not OB: idiosyncratic utilization of the tRNA-binding OB-fold domain in unicellular, pathogenic eukaryotes, FEBS Lett. 590 (2016) 4180–4191, https://doi.org/10.1002/1873-3468.12441.

[18] J.-C. Robinson, P. Kerjan, M. Mirande, Macromolecular assemblage of aminoacyl-tRNA synthetases: quantitative analysis of protein-protein interactions and mechanism of complex assembly, J. Mol. Biol. 304 (2000) 983–994, https://doi.org/10.1006/jmbi.2000.4242.

[19] E. Karanasios, G. Simos, Building arks for tRNA: structure and function of the Arc1p family of non-catalytic tRNA-binding proteins, FEBS Lett. 584 (2010) 3842–3849, https://doi.org/10.1016/j.febslet.2010.08.023.

[20] J.M. van Rooyen, J.-B. Murat, P.-M. Hammoudi, S. Kieffer-Jaquinod, Y. Coute, A. Sharma, H. Pelloux, H. Belrhali, M.-A. Hakimi, Assembly of the novel five-component apicomplexan multi-aminoacyl-tRNA synthetase complex is driven by the hybrid scaffold protein Tg-p43, PLoS One 9 (2014) e89487, https://doi.org/10.1371/journal.pone.0089487.

SUPPLEMENTARY MATERIAL

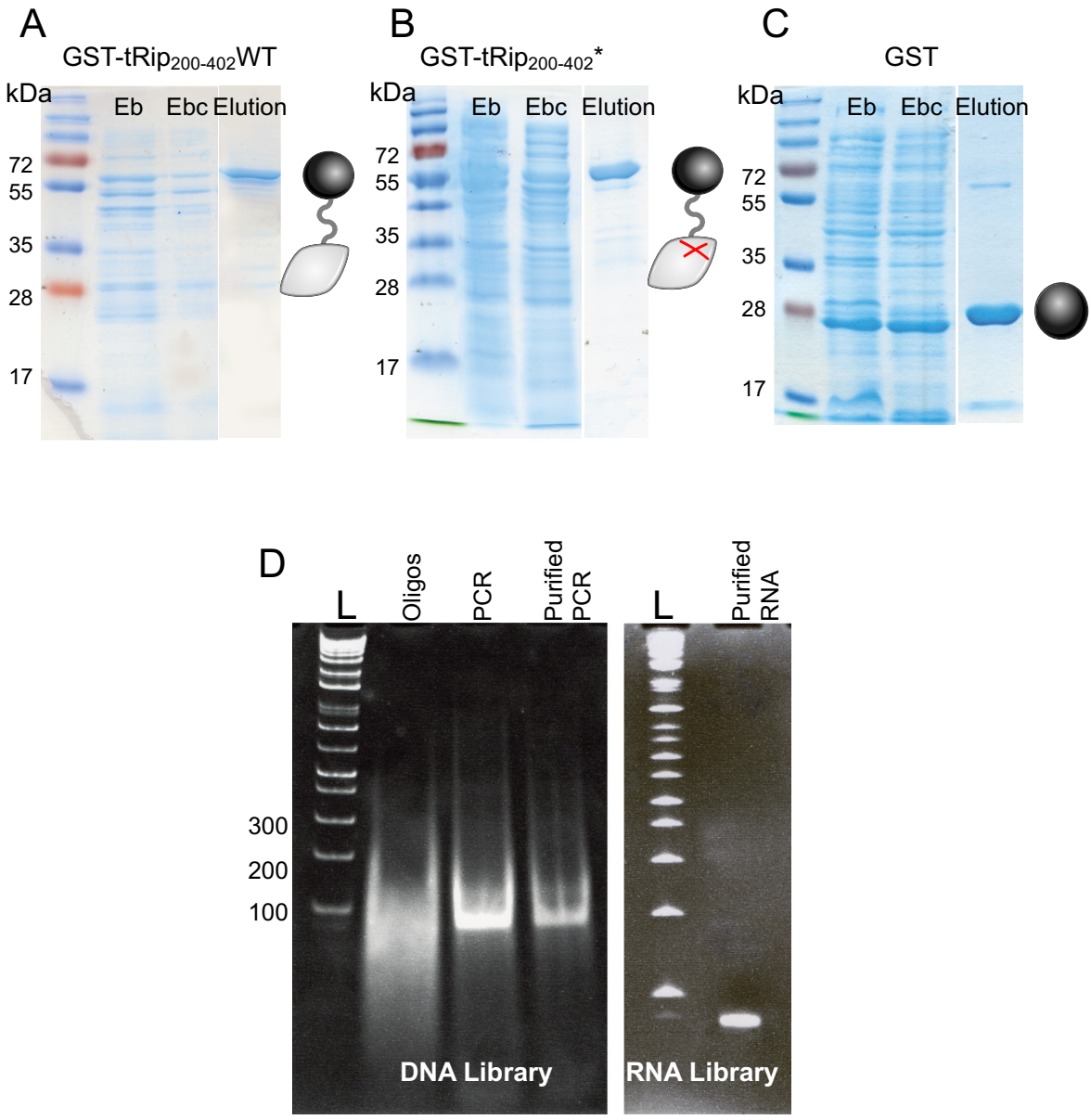

Figure S1. Production of fusion proteins used for SELEX experiments (A, B, C), and DNA and RNA libraries (D). (**A**, **B**) Purification of GST fusion proteins. (**C**) Purification of GST. Proteins were purified on glutathione-agarose columns; analyzed fractions correspond to the crude extract before (Eb), after (Ebc) centrifugation and Elution. Proteins migrate on gel at expected sizes (55 kDa for both fusion proteins and 25 kDa for GST). (**D**) The single-stranded randomized template was amplified by PCR using two specific primers and the resulting DNA library was purified on native gel (left) before being *in vitro* transcribed into RNA (right). L corresponds to the DNA size marker in base pairs.

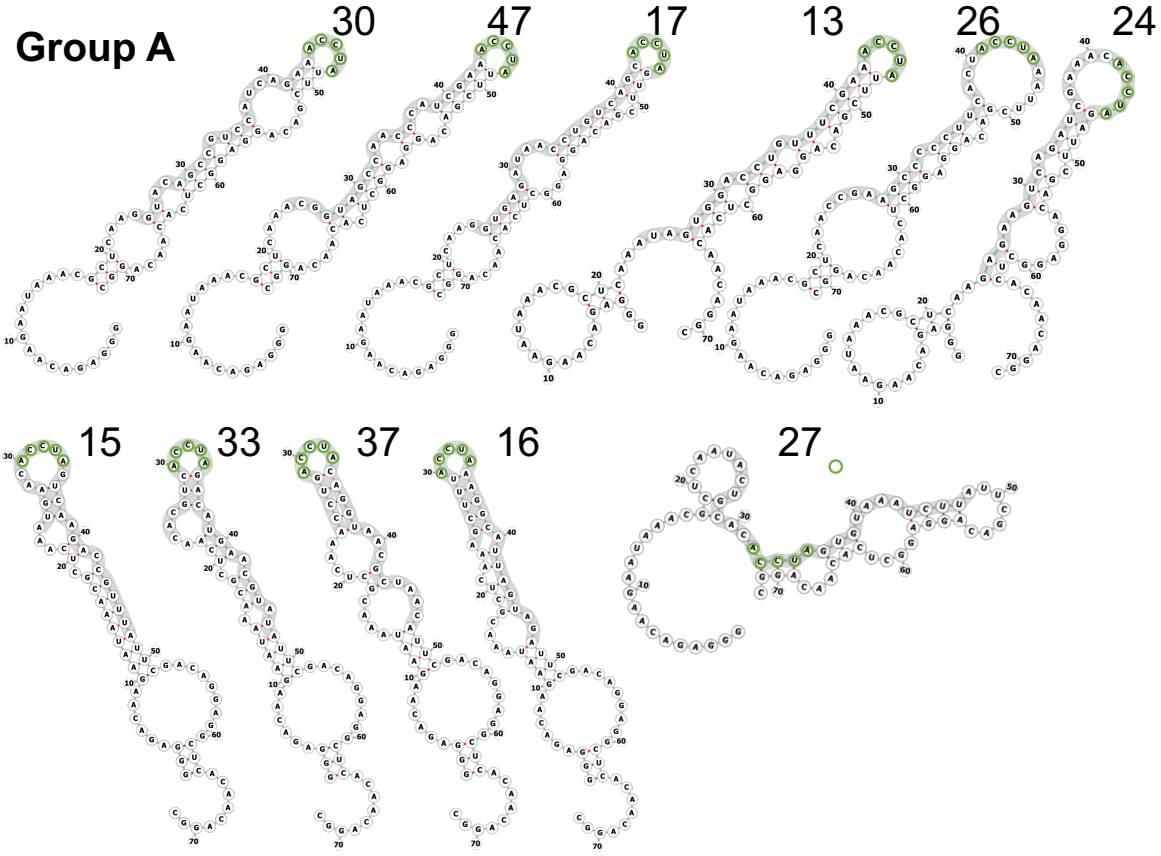
Group A
30
47
17
13
26
24
15
33
37
16
27

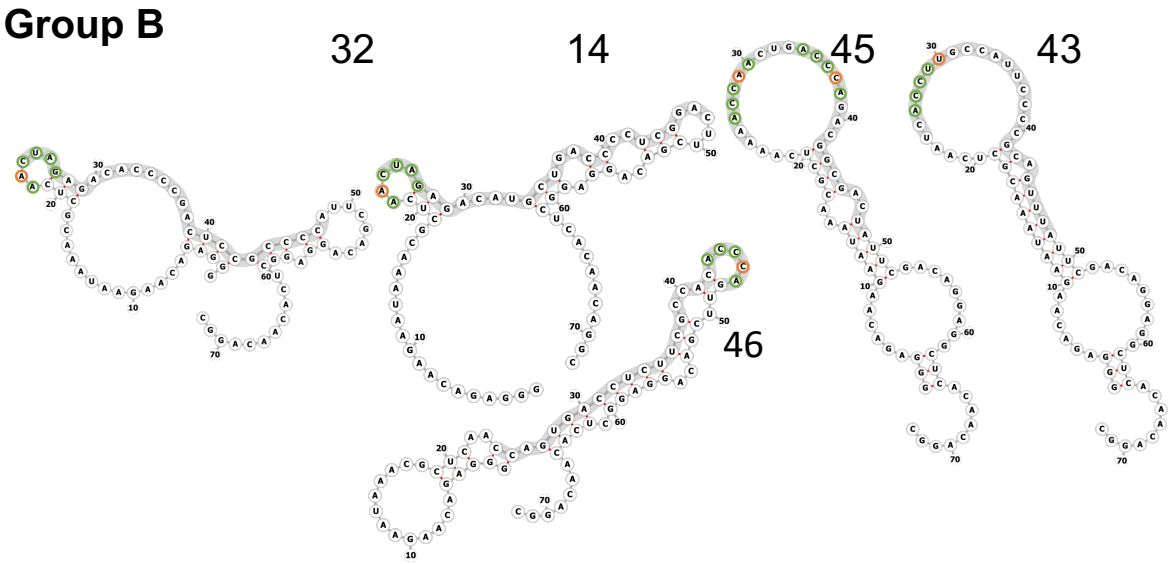
Group B
32
14
45
43
46

Group C

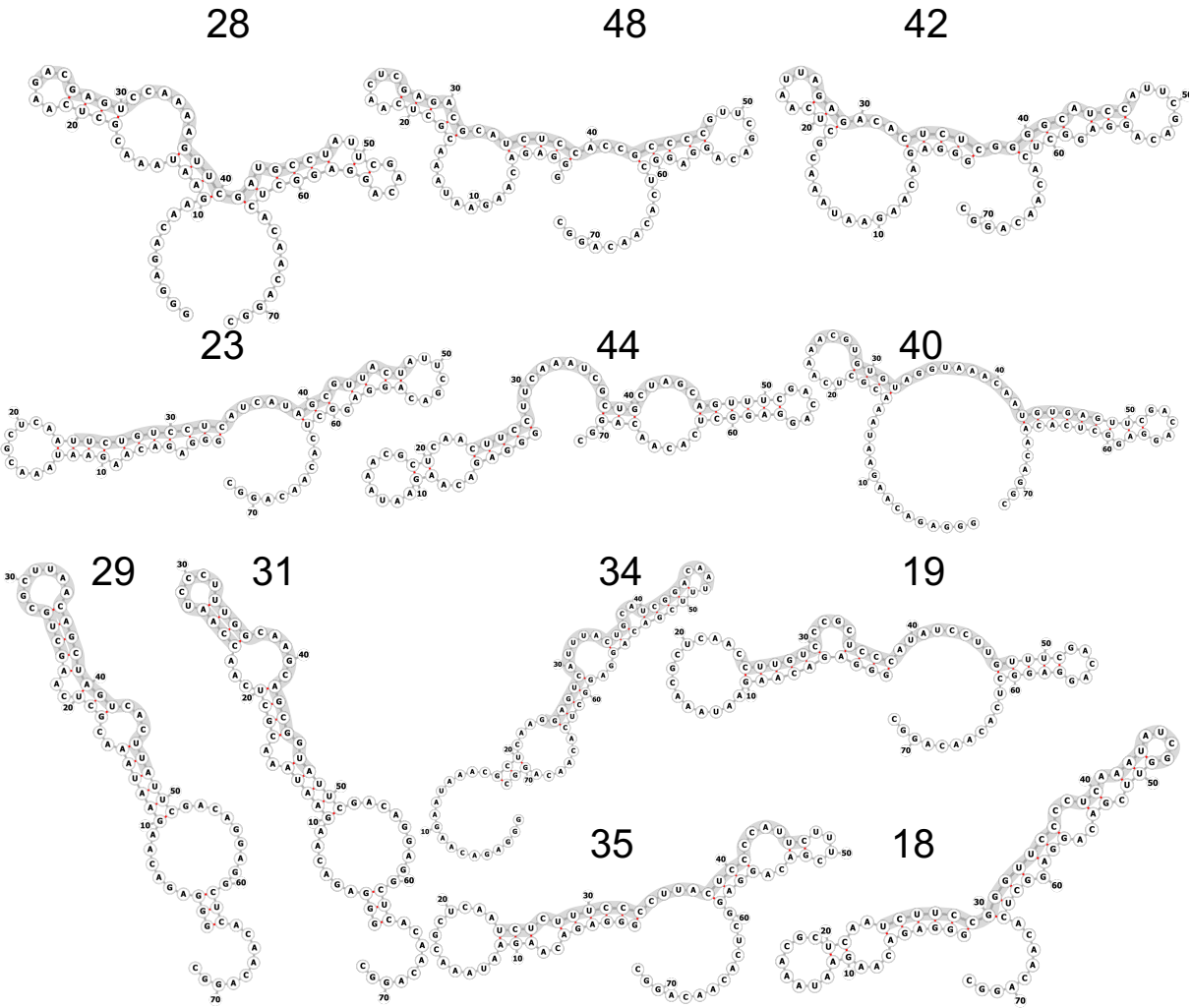

Figure S2. Prediction of secondary structures of selected aptamers. Folds were predicted using the RNAfold Webserver application (http://rna.tbi.univie.ac.at/cgi-bin/RNAWebSuite/RNAfold.cgi) and molecules were classified into three distinct groups (as in Figure 3) corresponding to the presence in of (i) the integral ACCUA motif (group A), (ii) this motif mutated at one position (group B), and (iii) the other sequences (group C). The selected regions are shaded in grey, the ACCUA motif is indicated in green, and the point mutations are in orange.

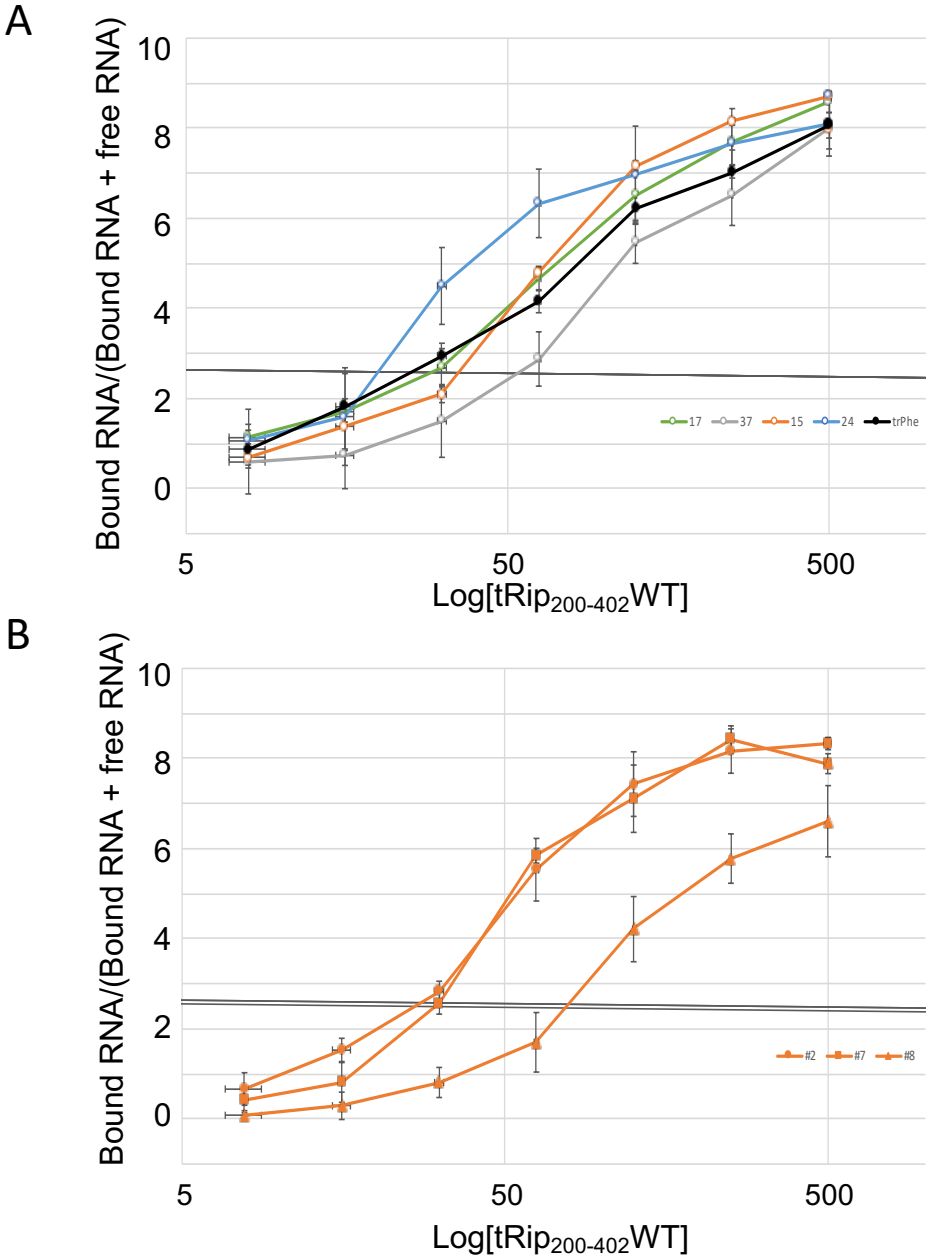

Figure S3. **Binding curves**. Curves are derived from EMSA experiments shown in Figure 4A (**A**) and 6A (**B**). The proportion of bound RNA is shown as a Log function of tRip concentration in the reaction (n=3).

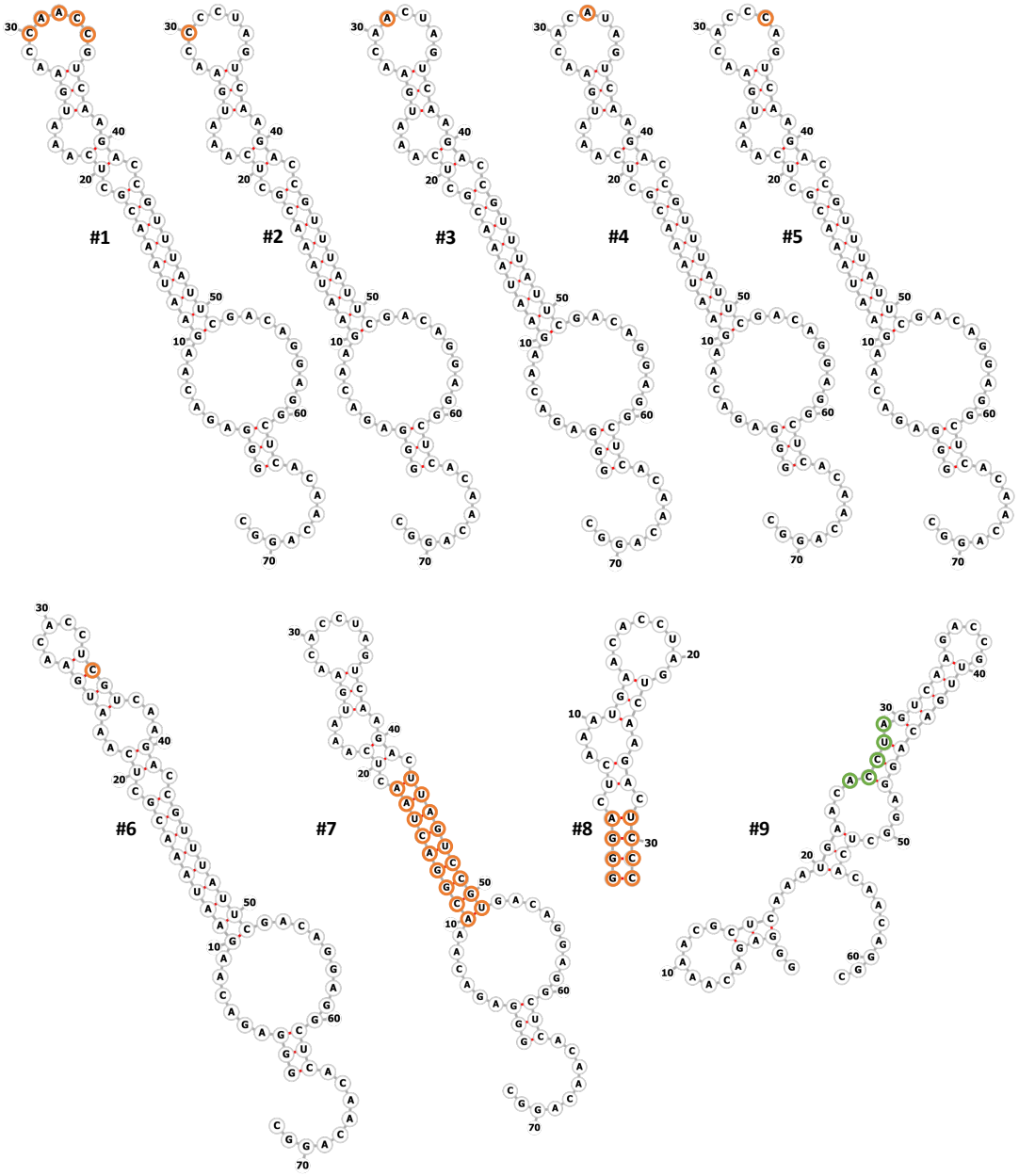

Figure S4. Prediction of secondary structures of mutated aptamers. The effect of each mutation (circled in orange) into aptamer-15 was tested on the prediction of their secondary structure with the RNAfold software.

III. tRip as a target for developing a malaria vaccine

The presence of tRip on the parasite surface and the conservation of the sequence of its external C-terminal domain in all *Plasmodium* strains make this protein an interesting target for immunizing vertebrate hosts against malaria. We chose as model for our experiment mice BALB/c. The C-terminal domain of tRip from *Plasmodium berghei* (the parasite responsible for rodent malaria) corresponding to amino acids 200-402 was expressed in bacterial cells and purified by affinity chromatography. To study the immunogenicity of tRip, we used 4-week-old BALB/c mice. They were divided into an 'experimental' group and a 'control' group. Immunization was carried out by intraperitoneal injection of 25 µg of $tRip_{200-402}$ in PBS in the presence of an adjuvant for the first group or with PBS and the adjuvant only for the second group. After 2 booster doses (at 3-week intervals) all mice were then infected with *P. berghei* (expressing GFP) either (i) by intravenous injection of 10^6, 1000 or 500 infected red blood cells, (ii) or by natural bites by exposing anaesthetized mice to hungry infected mosquitoes. At each immunization, antibody production was determined by ELISA tests and, at the final stage, the evolution of parasitemia was monitored by FACS. The results obtained indicated that the C-terminal domain of tRip is immunogenic since it induces the production of specific antibodies. On the other hand, under the conditions we tested, immunization does not confer effective protection of the mice against infection by *P. berghei*. Parasitemia increased in a similar way in the 2 groups of mice and they all died within 2 weeks of infection.

1. tRip as a target for malaria vaccine development

In this part, we examined the ability of tRip to induce an immune response in order to use tRip as a malaria vaccine candidate. The presence of tRip on the parasite surface throughout its development cycle (ookinete, sporozoites, hepatic stage and blood stage) and its sequence conservation accross all *Plasmodium* strains (Bour et al., 2016) make this protein an attractive target for immunization of vertebrate hosts (Figure 28). To this end, we expressed and purified the C-terminal domain of *P. berghei* tRip corresponding to amino acids 201 to 400, which has been shown to be responsible for specific tRNA binding (Bour et al., 2016). We chose to work with the *P. berghei* strain that specifically infects rodents, and Balb/c mice to test the immuneresponse.

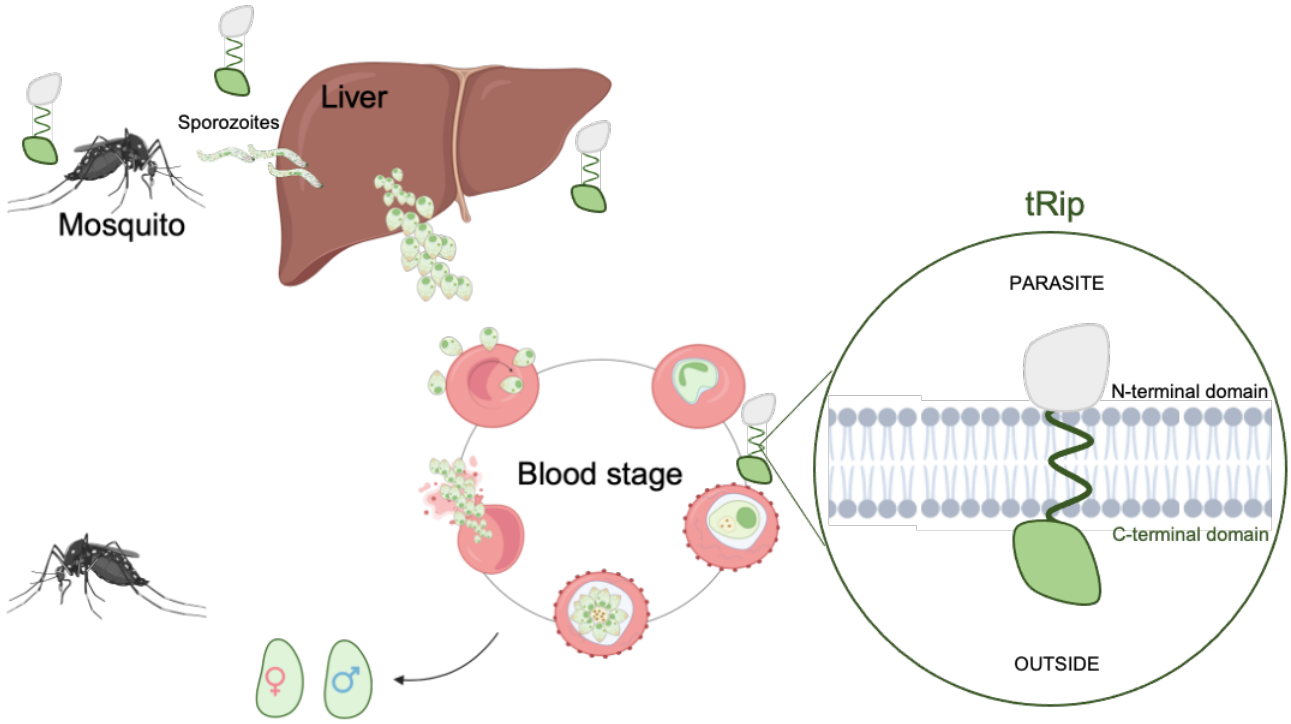

Figure 28: tRip expression during Plasmodium life cycle.
tRip is expressed at all stages of the parasite's life cycle: at the ookinete stage (in the mosquito) as well as at the sporozoite, liver and blood stages (in the vertebrate). A focus on schematized tRip anchored in the plasma membrane with its C-terminal tRNA binding domain (in green) exposed outside the parasite (Bour et al., 2016).

1.1. Measurement of the titers of antibodies developed against the C-terminal domain of tRip in immunized Balb/c mice

Purified C-terminal domain (25 µg) of tRip was injected into Balb/c mice on 3 attempts at 3-week intervals (Figure 29A). Details of these injections are given in the Method section of this manuscript. During this immunization period, we measured the titers antibodies developed by mice specifically against tRip. For this purpose, blood samples were collected before each injection (weeks 3, 6 and 8) and anti-tRip antibodies were detected by ELISA immunoassays (Figure 29A). The results presented in Figures 29B-E correspond to four independent immunization assays, each performed on 4 groups of 12 (B, C, D) or 22 (E) mice. Of the serial dilutions of the plasma used for these tests, only the 1/3200 dilution is reported here.

Experiments were analyzed using One-way ANOVA followed by Turkey's multiple comparision Test. The One-way Analysis of Variance (ANOVA) test is frequently used to compare a treated group to a control group by evaluating individual performance within each group. This method is more precise because it considers each individual's performance rather than averaging across the entire group. The major goal of the test is to discover whether the performance of one group differs significantly from that of the control group. Following the One-way ANOVA, a post-hoc test, such as the Tukey test, is commonly used to assess significance at specific time points.

We consistently observed a robust increase in the production of tRip-specific antibodies in immunized mice over time. In contrast, no antibodies were observed in the control goup injected with PBS, indicating the immunogenicity of the C-terminal domain of tRip. Experiments B, C and E led to a similar antibody production (between 1.5 and 2 absorbance units at 450 nm), while experiment D is characterized by a slightly higher value (greater than 3). These 4 independent immunization experiments of mice were performed to achieve 4 different challenges: either by injection of different concentrations of iRBCs or by bites from infected mosquitoes.

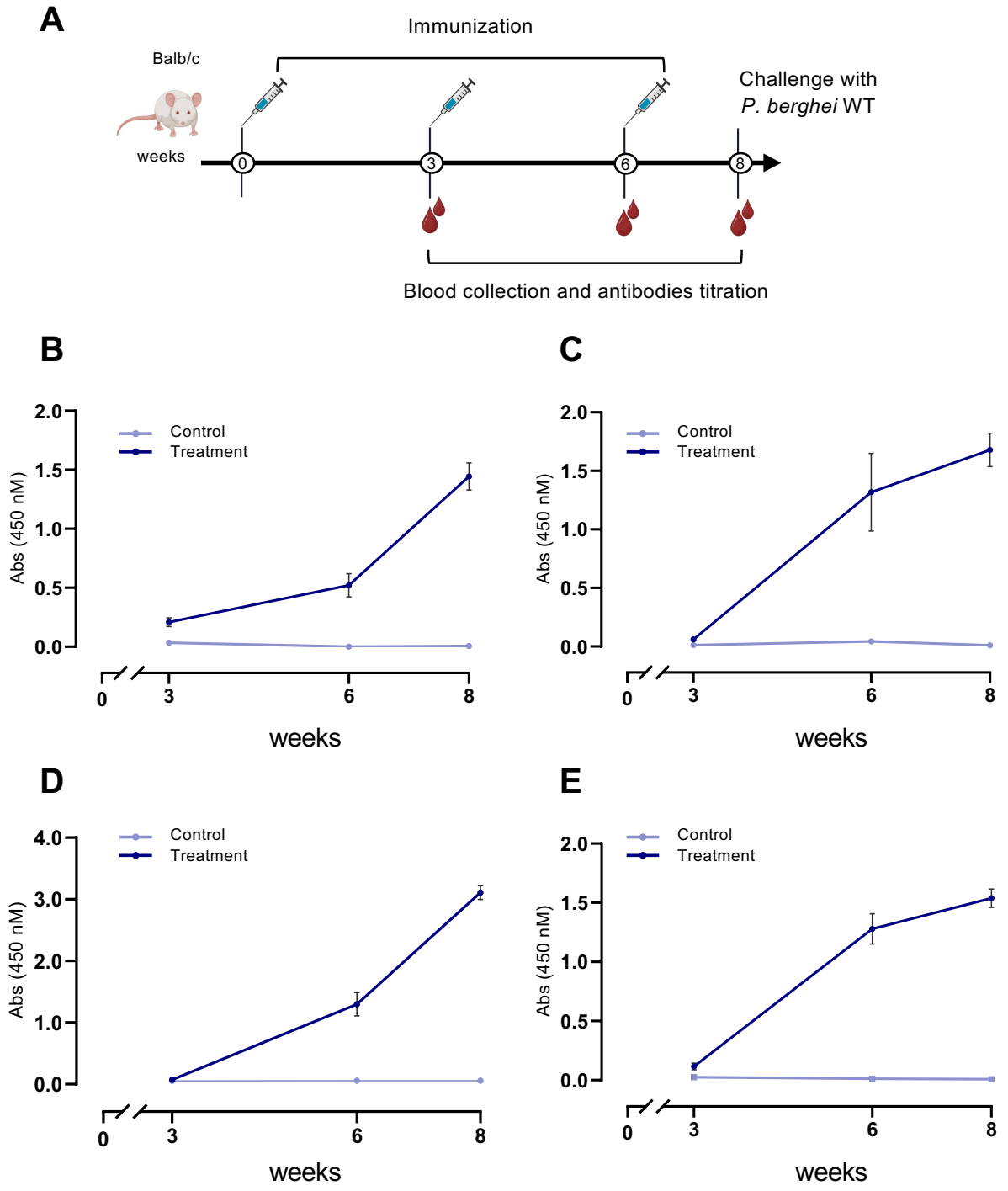

Figure 29: Monitoring of antibodiy synthesis during immunization of mice with tRip. **(A)** Schematic diagram of immunization protocol. Plasma was recovered at weeks 3, 6 and 8 and diluted 3200-fold to perform ELISA tests. **(B, C, D, E)** Comparison of the antibody production (ELISA test, absorbance at 450 nm) in 4 independent experiments: immunized groups are in dark blue and control groups in light blue. For assays B, C and D: n = 12 (6 control and 6 treated mice); in E: n = 22 (11 control and 11 and treated mice). Error bars represent the standard deviation (SEM).

1.2. Monitoring the parasitamia in immunized and control mice

1.2.1. Mice challenged with injections of infected red blood cells (iRBCs)

Infection of immunized and control mice was achieved by injection of 10^6, 10^3 or 500 iRBCs. Parasitemia was monitored daily by FACS analysis of red blood cells infected with the *P. berghei* WT/GFP parasite. Results are summarized in Figure 30.

Injection of 10^6 iRBCs led to an extremely rapid increase in parasitemia in the mice blood and to the sacrifice of all mice on day 8 (Figure 30A). In this case, there is a slight advantage for non-immunized mice, where the parasite appears to develop slightly less rapidly. We interpreted this difference as the result of immunized mice being more sensitive to extreme infection due to fatigue following antigen injections. This observation led us to repeat the same experiment, but with a reduced number of iRBCs injected.

By injecting 10^3 iRBCs, the survival of the mice was prolonged, between days 10 and 15 post-infection. In the treated group, two immunized mice did not develop parasitemia. It is difficult to determine whether this absence of parasitemia is the consequence of an efficient immunization or of a technical problem during intraperitoneal (IP) injection of iRBCs; so these mice were not taken into account for data processing. The evolution of parasitemia in the control (n=6) and treated (n=4) groups (Figure 30B) showed no significant differences in the percentage of infected red cells overall, although there was a slight time lag in the onset of parasitemia.

In the third experiment (Figure 30C), we further reduced the amount of iRBCs injected into the mice, using only 500 iRBCs. In this experiment, the control group contains only 4 mice, as one of them died directely following the injection and one did not develop parasitemia; the treated group contains 5 mice, as one of them was hyperactive, impossible to handle and was therefore withdrawn from the experiment. As observed previously (Figure 30B), the two groups developed comparable parasitemia overall, but with a time lag which this time was observed from the start of infection (Figure 30C).

Overall, these results show that the production of tRip-specific antibodies does not confer effective protection to mice against infection by the *P. berghei* parasite under the conditions tested. However, when these mice are infected with a reasonable number of iRBCs, there is a difference in the delay in the onset of infection in immunized mice, and hence in their death (Figure 30D). Indeed, the average survival time of the control mice was 9 days, while that of the immunized group was 12 days ($p \leq 0.5$).

This approach using direct injection of blood stage parasites into the mice bloodstream is in some way artificial. In nature, when an infected mosquito bites a vertebrate host, it injects at most a hundred sporozoites and many of them do not reach the blood stage (Frischknecht and Matuschewski, 2017).

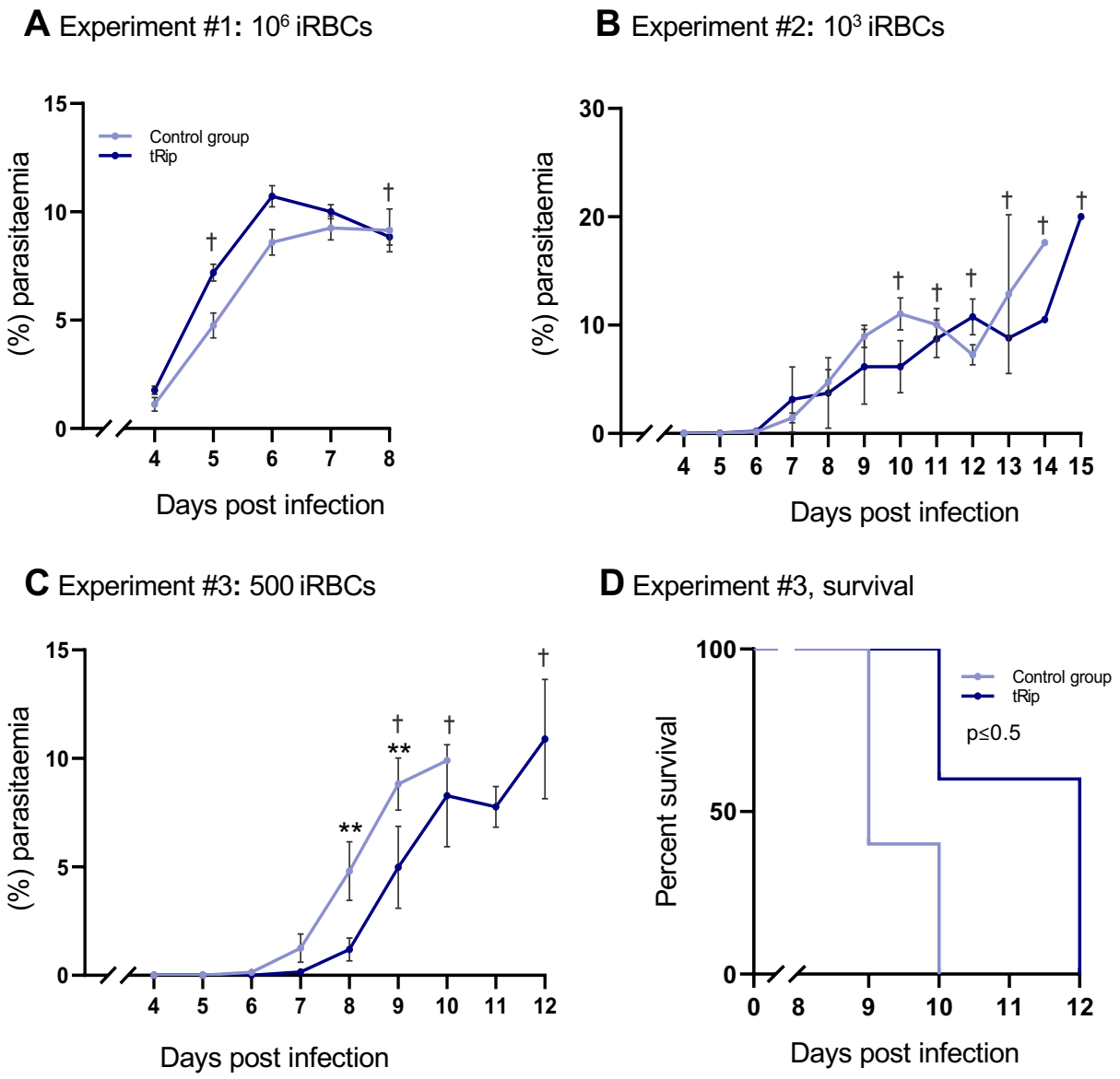

Figure 30: Monitoring parasitaemia in mice with and without immunization.
In all experiments, results for the control and treated groups are shown in light and dark blue, respectively. Mice were infected on day 0 and parasitaemia was monitored daily from day 4 after challenge. Mice were pre-immunized according to experiments 1 to 4 described in Figure 29 and only mice developing parasitemia were included in the analysis. **(A)** Immunized mice n=6 and controls n=6 were infected with 10^6 iRBC ($p > 0.5$). **(B)** Immunized n=4 and control n=6 mice were exposed to 10^3 iRBCs ($p > 0.5$). **(C)** Immunized n=5 mice and n=4 controls were exposed to 500 iRBCs ($p \leq 0.5$). **(D)** Kaplan-Meier survival analysis illustrating infection of mice with 500 RBC infected with *P. berghei* ($p \leq 0.5$). Experiments were analyzed using one-way ANOVA followed by Turkey's multiple comparison test. Error bars represent standard deviation (SEM), (*) $p \leq 0.5$, (**) $p \leq 0.001$, (***) $p \leq 0.0001$. (†) indicates animal death.

1.2.2. Mice challenged with infected mosquitoes' bites

The last group of mice was infected by bites from infected mosquitoes; this group comprised 11 control and 11 treated mice (one mouse died in each group before infection). As the mosquitoes were infected with *P. berghei*-GFP, only those showing fluorescence in the trunk, wings, intestines and salivary glands were selected to infect the mice (Figure 31 and Figure 32A). Although all mice were bitten, only 5 immunized mice and 7 control mice were effectively infected and developed parasitemia. These data are summarized in Table 3.

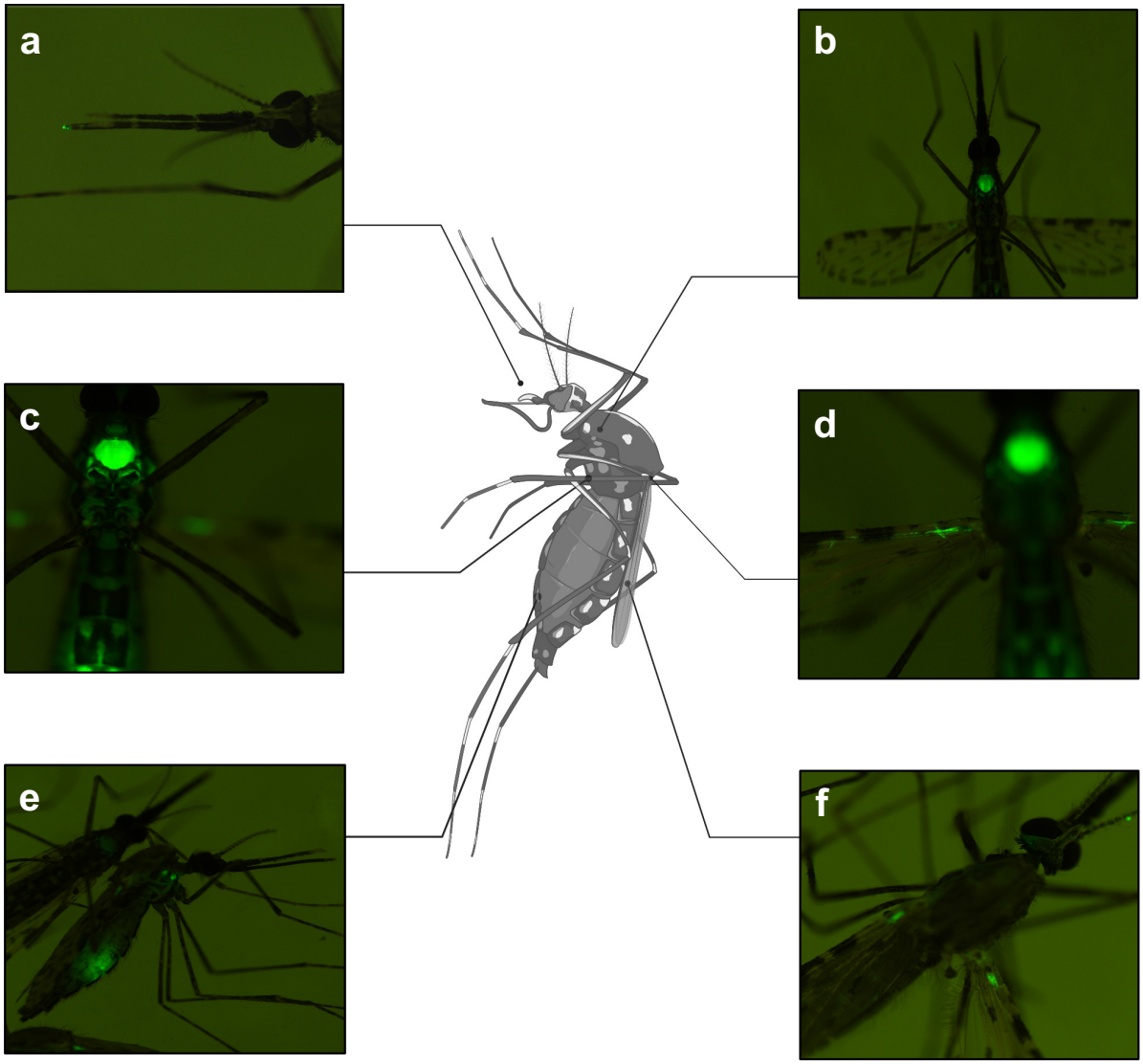

Figure 31: Fluorescence microscopy visualization of mosquitoes infected with *P. berghei*-GFP.
The *P. berghei* parasite constitutively expresses the green fluorescent protein GFP, which can be detected in various parts of the mosquito: proboscis (a), salivary glands (b), intestine (c, d) and wings (e, f).

Figure 32B summarizes the evolution of parasitemia in infected mice corresponding to the control group (n=7) and the immunized group (n=5). The trend observed in this single experiment differs from that observed in experiments with iRBCs. In this case, there was no visible delay in the rate of parasite development during infection. On the contrary, during the exponential phase of parasite development (days 12 and 13), parasitemia in immunized mice progresses more rapidly and reaches higher values than in control mice.

These exploratory experiments do not allow us to draw any definitive conclusions as to the protective effect of anti-tRip antibodies against the development of malaria in infected rodents. However, it is clear that the experimental conditions used in this study need to be greatly modified to obtain more convincing results.

Table 3: Efficacy of mosquito bite infections in mice.

Immunized	N	n	INFECTED?
Mouse 1	8	3	NO
Mouse 2	7	3	NO
Mouse 3	8	3	YES
Mouse 4	9	3	NO
Mouse 5	7	4	YES
Mouse 6	9	8	YES
Mouse 7	9	8	YES
Mouse 8	9	6	YES
Mouse 9	8	4	YES
Mouse 10	8	2	NO
Mouse 11	10	5	YES
Mouse 12	Dead		

Controls	N	n	INFECTED?
Mouse 13	8	3	YES
Mouse 14	9	7	YES
Mouse 15	8	8	NO
Mouse 16	9	5	YES
Mouse 17	9	6	NO
Mouse 18	8	3	YES
Mouse 19	9	5	NO
Mouse 20	Dead		
Mouse 21	8	4	YES
Mouse 22	9	3	NO
Mouse 23	8	5	NO
Mouse 24	9	3	NO

The Table summarizes, for each mouse, the total number of mosquitoes used to bite (N), and the number of mosquitoes that actually bit the mouse (n). The infectious status of the mouse is also indicated in the last column.

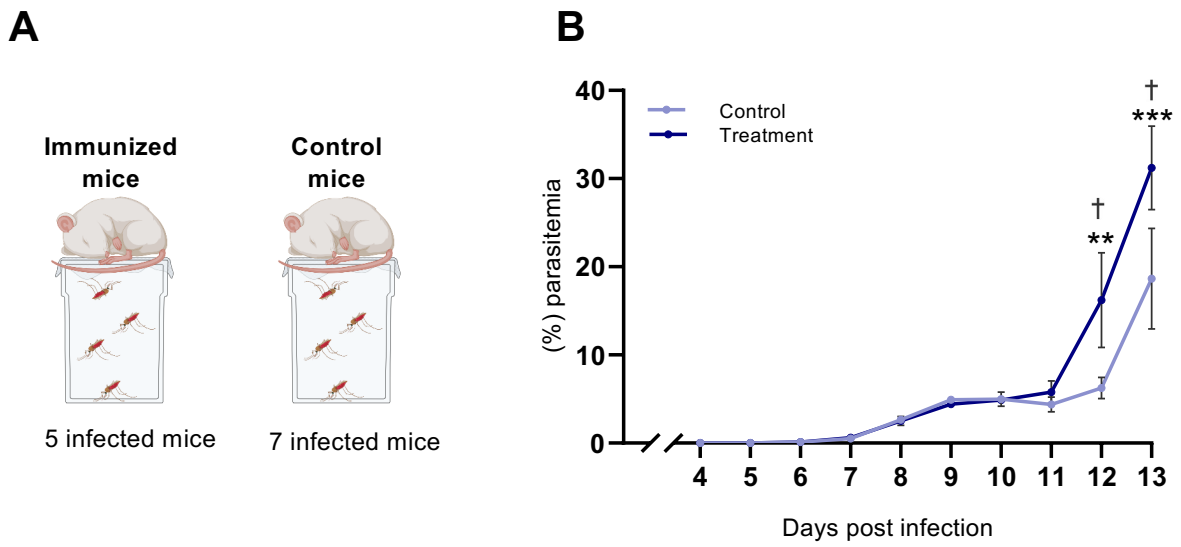

Figure 32: Mosquito bite infection and parasitaemia monitoring.
(A) Immunized n=11 and control n=11 mice were infected directly by infected mosquito bites on day 0. **(B)** Parasitaemia levels (%) were determined daily from day 4 post-infection. The control and immunized groups are shown in light and dark blue, respectively. The experiment was analyzed with the repeated measures ANOVA post-hoc test. Error bars represent standard deviation (SEM) and (†) death of mice.

DISCUSSION & PERSPECTIVES

1. Comparative proteomic analysis between wild-type and tRip-KO parasite

1.1. Disregulated proteins in tRip-KO parasite

In this part of my thesis, we conducted a comparative analysis of the proteomes between the wild-type and tRip-KO parasites. The comparison was performed in two distinct experiments: (a) at the schizont stage of the parasite, and (b) after purifying the parasite from the whole blood stage, containing the ring, trophozoite, and schizont phases.

The disregulated proteins differed between the two independent experiments. In experiment (a), we primarily identified proteins involved in the translation process, while in experiment (b), we observed a predominance of proteins related to DNA synthesis. These findings are expected since different stages of the parasite's life cycle necessitate distinct biological processes and functions, which are mediated by specific sets of proteins. During the all blood stage, comprising approximately 80% trophozoites, which corresponds to the stage of daughter cell division, we noted improved expression of genes associated with DNA replication. In the mature schizont stage, there was an upregulation of proteins involved in translation, especially ribosomal proteins (Bunnik et al., 2013).

1.2. tRip-KO pasasite has a problem synthetizing asparagine-rich proteins

In the two independent experiments, we observed that the down-regulated proteins in tRip-KO parasite are rich in asparagine. Asparagine is one of the most frequently utilized codons by *P. berghei* parasite, likely due to the presence of LCR (Chaudhry et al., 2018). This suggests that the tRip-KO parasite, unable to import tRNAs, has problems with protein synthesis in general, but especially with asparagine-rich proteins. Given that efficient translation relies on a balance between codon usage and the availability of tRNAs, and that *Plasmodium* possesses a minimal set of tRNAs (a single gene per tRNA isoacceptor), human tRNAs imported into the parasite could compensate for this deficiency. Therefore the exogenous tRNA import might restore a balance essential for optimal parasite gene expression. This hypothesis is supported by the following evidences:

(i) In the schizont stage experiment, we observed overexpression of asparaginyl-tRNA synthetase (NRS) and lysyl-tRNA synthetase (KRS) in the tRip-KO parasite. Normally, there is a balance between the amounts of aaRSs and the cognate aminoacyl-tRNAs. An increase in an aaRS expression suggests that the cognate aminoacyl-tRNA is in limiting concentration, and that the mechanisms regulating aaRS expression have been triggered to increase the aminoacylation efficiency of the available uncharged cognate tRNAs or maybe

misaminoacylate other tRNAs (Mohler and Ibba, 2017; Ryckelynck et al., 2005). The other aaRSs in the experiment are not as abundant to be considered, but an overall increase in aaRSs in tRip-KO parasite seems to occur (see Figure 2A and S1 in Article #1).
(ii) At least for the few systems tested, the parasite's aaRSs are capable of aminoacylating human tRNAs (Figure 4B in Article #1).
(iii) tRip exhibits a better affinity for $tRNA^{Asn}$ than most other tRNAs, strengthening its role in facilitating $tRNA^{Asn}$ import into the parasite (Cela et al., 2021).

1.3. Model of protein synthesis inhibition

Identification of the most asparagine-rich proteins revealed that two asparagine-rich proteins are conserved in all 6 *Plasmodium* species tested *(P. falciparum, P. yoelii, P. knowlesi, P. berghei, P. chabaudi* and *P. vivax*). These are Ccr4-associated factor 1 (CAF-1), involved in mRNA degradation, and Poly-(A) binding protein (PABP3), not yet well-characterized in *Plasmodium*. Both proteins are involved in recognizing the Poly-(A) mRNA tail, but they also share a specific organization with a well-conserved N-terminal sequence and a C-terminal sequence found only in *Plasmodium* with a high asparagine content. CAF-1 is a well-characterized protein. Its N-terminal domain has an exonuclease activity involved in the degradation of mRNAs rich in non-optimal codons. Indeed, CAF-1 is part of the CCr4-Not complex that binds to the empty E site of ribosomes when A site lacks tRNA. It thus positions CAF-1 in the right place to initiate degradation from the Poly-(A) tail of the mRNA (Collart, 2016; Nasertorabi et al., 2011). While CAF-1 is an essential protein, its C-terminal domain is not, and its deletion leads to reduced infection of the parasite, resulting in premature release of immature merozoites *in vitro* and inappropriate gametocytes development (Balu et al., 2011). Interestingly, the phenotype of the tRip-KO parasite (Bour et al., 2016) and the deletion of the C-terminal domain of CAF-1 are quite comparable since a reduced infectivity is observed in both cases. They also show over-expression of the same proteins involved in cell invasion (Figure 2C and S3 in Article #1). We propose that the tRip-KO parasite, defective in $tRNA^{Asn}$ import, is unable to translate asparagine-rich proteins, presumably including the C-terminal domain of CAF-1. The absence of CAF-1 C-terminal domain would result in the non-degradation of mRNAs encoding proteins involved in the premature egress of merozoites, leading to low infectivity of the produced parasites.

1.4. Can the blood stage serve as a tRNA source?

Red blood cells are highly specialized cells, which during their differentiation have eliminated their nucleus and all transcription and translation machineries. Hence our question: do blood cells contain enough tRNA to be an effective source of import for the parasite? The amount of

tRNA is low in RBCs but still sufficient to be imported into the parasite (Figure 4A in Article #1). Also in the blood there are reticulocytes, precursors of RBCs, shown to be rich in translation and in tRNA content (Smith and McNamara, 1972). Despite being present at only 2% in the blood, it has been shown that *P. berghei, P. chabaudi*, *P. yoelii* and *P. vivax* have a preference for infecting reticulocytes rather than RBCs (Antia et al., 2008; Cromer et al., 2006; Mons, 1990; Thawani et al., 2014).

1.5. Future perspectives

The identification of CAF-1 by mass spectrometry analysis was insufficient in our mass spectrometry experiments, due to the limited number of spectra obtained. Consequently, further work should enable us to test our hypothesis by looking either for a reduction in the amount of CAF-1 within the tRip-KO parasite, or by detecting a change in the size of the protein as a result of translation arrest linked to the lack of $tRNA^{Asn}$ in the mutant parasite. To this end, we could repeat mass spectrometry experiments either on total parasite protein samples (wild-type and tRip-KO) or on samples obtained from immunoprecipitation experiments to increase our chances of detecting CAF-1. For this, we lack an essential tool: an anti-*P. berghei* CAF-1 antibody. Indeed, despite very high sequence homologies between *Plasmodium* and human CAF-1 N-terminal domains, we were unable to detect the plasmodial protein with the antibody raised against the human protein by Western-Blot performed on infected blood samples.

Furthermore, given the similarity between the phenotypes of the tRip-KO and CAF-1-C-terminal-KO parasites -in which proteins involved in the parasite's exit from the RBC are deregulated-, it would be interesting to check whether merozoite egress of the tRip-KO merozoites also occurs prematurely from RBC *in vitro*.

Considering *Plasmodium*'s predilection for infecting reticulocytes, we could explore the concept of increasing the population of reticulocytes in the mouse bloodstream to observe potential variations in infectivity. This approach is based on the idea that an increased presence of reticulocytes, enriched in tRNA resources, might increase the differences in development speed between wild-type and tRip-KO parasites, with the wild-type parasite having an advantage in the presence of more reticulocytes, while the development of the tRip-KO parasite would not be affected by more tRNAs at its disposition.

2. Use of tRip in therapeutic approaches

In this part of my thesis work, I focused on the potential role of tRip in developing possible therapeutic approaches, adopting mainly two strategies: the selection of inhibitory RNA aptamers and the use of tRip as a target for a vaccine.

2.1. Using aptamers as therapeutic approach

We have explored potential therapeutic approaches against malaria using a promising technology involving aptamers. Aptamers are single-stranded DNA or RNA sequences with a unique three-dimensional structure, which gives them a high level of specificity and affinity for a particular target (Nimjee et al., 2017). Additionally, they exhibit low immunogenicity, meaning they are less likely to trigger adverse immune responses in patients (Nimjee et al., 2017). By doing so, they offer a promising avenue for the development of safer and more effective treatments. The inspiration behind utilizing small nucleic acid molecules, such as aptamers, comes from studying viruses like the Human Immunodeficiency Virus (HIV) and Adenovirus. These viruses encode small RNA molecules known as ligands, which have the ability to bind to endogenous proteins. Depending on their function, these RNA ligands can either facilitate viral replication or mitigate the host's antiviral response (Cullen and Greene, 1989; Marciniak et al., 1990). Thus far, MACUGEN (Pegaptanib sodium injection), an antivascular endothelial growth factor (VEGF) aptamer, has successfully obtained approval from the United State Food and Drug Administration (FDA) for the treatment of macular degeneration in the eye in 2004 (Ng and Adamis, 2006). Since then, numerous pre-clinical and clinical trials have been conducted on various therapeutic aptamers. This approach opens new possibilities for innovative therapeutic interventions against malaria.

2.1.1. Selected aptamers for targeted tRip

We have chosen tRip as the target for the selection of aptamers capable of binding it specifically. tRip contains an extracellular C-terminal domain, OB-fold EMAPII-like domain, capable of recognizing the elbow of the L-structure of tRNAs (Morales, 1999), and an intracellular N-terminal domain, GST-like, involved in the formation of two multi-aminoacyl-tRNA synthetase complexes (Jaramillo Ponce et al., 2022). The localization of tRip in the membrane and its unique function in importing tRNAs into the parasite *in vitro* (Bour et al., 2016), makes it an ideal candidate for aptamer targeting.

The therapeutic approach could be based on the following two hypotheses:

(i) Blocking tRNA import (Figure 33A): Aptamers can be specifically engineered to block the interaction between tRip and host tRNAs. By interfering with this interaction, the import of

tRNAs into the parasite can be blocked and/or reduced. As tRNA is important for protein synthesis, inhibiting its import can result in decreased protein production, leading to impaired parasite development. This approach is supported by evidence from tRip-KO parasites, which exhibit reduced development in the bloodstream and decreased protein synthesis (Figure 33B) (Bour et al., 2016). Although tRip itself may not be essential for the parasite's survival, blocking its function confers a significant disadvantage to the parasite, hindering its growth and proliferation.

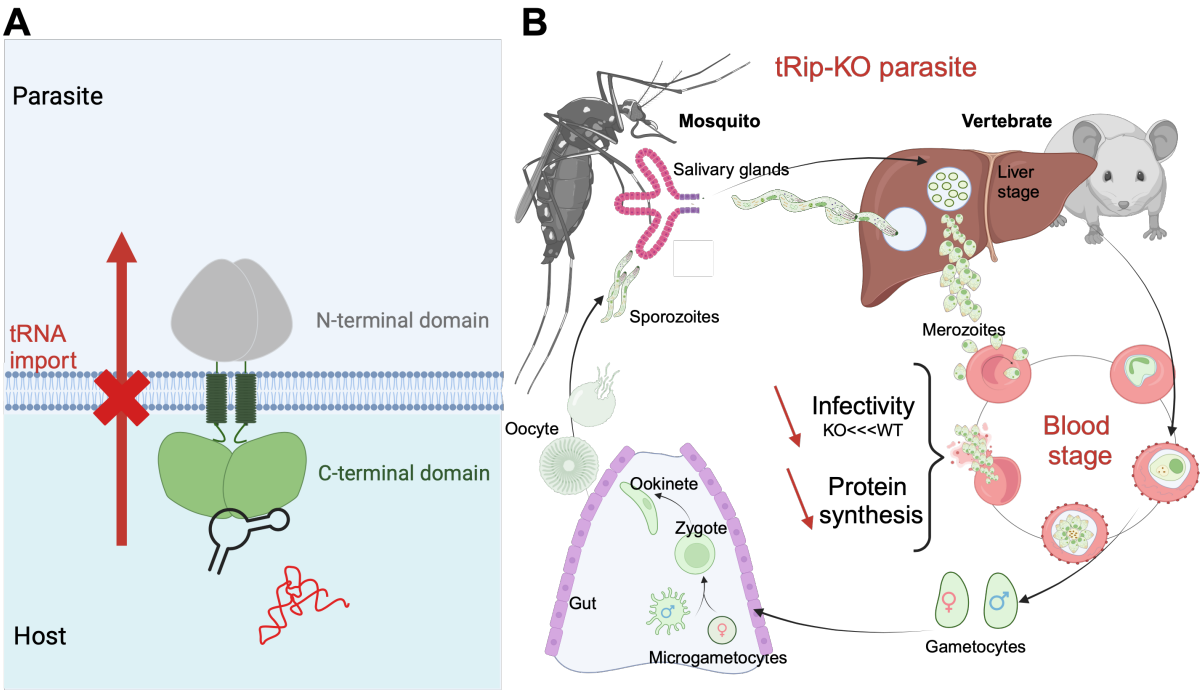

Figure 33: Using of therapeutic aptamer to block tRNA import.
(A) Aptamer (in black) bind to the C-terminal domain of tRip (in green) and thus blocks tRNA import (schematized by a red arrow) into the parasite *via* tRip. **(B)** Phenotype of the tRip-KO parasite: reduced infectivity and low protein synthesis in the blood stage (Bour et al., 2016).

(ii) Targeted delivery of toxic molecules *via* tRip (Figure 34): Another promising strategy involves engineering aptamers to carry toxic molecules that are released specifically within the parasite (Figure 34A). This targeted delivery of toxic compounds allows for precise disruption of essential biological processes within the parasite (Figure 34B). The advantage of this approach lies in minimizing off-target effects and reducing toxicity to the host since the toxic compounds are directed into the parasite.

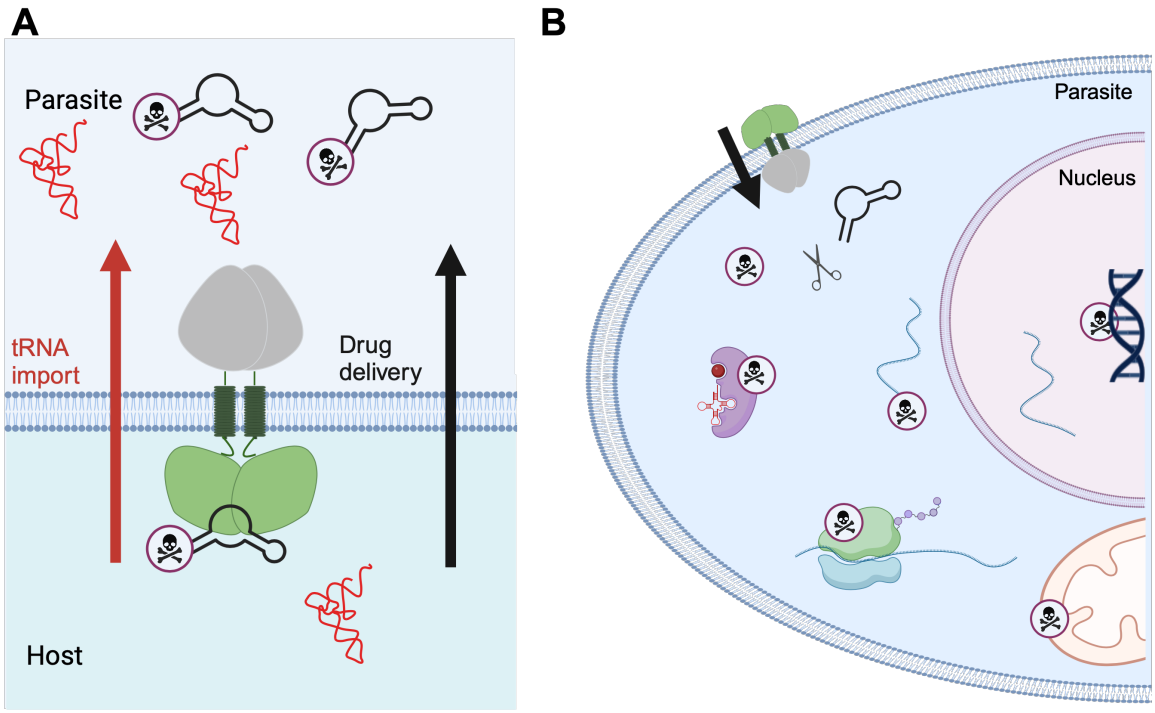

Figure 34: Using of delivery aptamer.
(A) Import by tRip of an aptamer bound to a toxic molecule (black arrow) without disturbing the tRNA import (red arrow). **(B)** Hypothetical function of the toxic molecule, which alters cellular functions such as enzyme function, RNA or DNA stability and protein translation.

For this study, we employed the SELEX (Systematic Evolution of Ligands by Exponential Enrichment) technique, which led to the identification of a group of 11 RNA aptamers, able to bind tRip, that share a common ACCUA motif in their apical loop. In the subsequent investigations, we focused our attention on Aptamer-15. This aptamer shows competitive binding with both tRNAs and tRNA transcripts, indicating that it likely targets the same binding site on tRip. Further, the 5-nucleotide motif ACCUA allows the aptamer to recognize tRip with an affinity (K_d=74 nM ± 0.9) comparable to that of a tRNA transcript (*tr*tRNA^{Phe}, K_d=66 nM ± 2.2). However, its binding affinity is lower than modified tRNAs (5-10 nM) (Cela et al., 2021). Notably, our analysis revealed that the stem region of Aptamer-15 could be shortened or mutated without significantly affecting complex formation, suggesting no involvement of the length or structure for protein binding. Interestingly, we observed that only the ACCUA motif is responsible for the interaction with tRip. Subsequent base-wise mutations on the ACCUA motif shows different contributions of the bases to the interaction. It appeared that only mutation of the first nucleotide permit to maintain a similar affinity to tRip (K_d=54.6 nM ± 6.7) while mutations at other positions or when the entire motif is mutated, there is no interaction at all (or it is no longer quantifiable). This suggests that the first base has the least involvement in the interaction with tRip compared to the rest of the CCUA motif.

Based on this observation, the affinity of the aptamer could then perhaps be increased by incorporating a specific modification such as the TΨ sequence always present in the T arm of tRNAs.

2.1.2. The next steps in the development of tRip-targeting aptamers strategy

We have discovered a motif, ACCUA, that has the ability to bind the tRip protein effficiently. However, several questions still need answers:
- How can the aptamer be administered *in vivo* to avoid degradation or toxicity?
- How can we improve its specificity for tRip?
- Can the aptamer enter into the parasite, or does it block its import?

Based on the obtained results, it is essential to further investigate these aspects to fully understand the potential of aptamer and its applications in targeting the tRip protein in parasites.

2.1.3. Aptamer stabilization and modification

A crucial step is the modification of the selected aptamer to enhance its stability and its binding affinity. The half-life of an unmodified nucleotide is approximately 5 min in serum and less than 1 h in cells (Healy et al., 2004). To overcome this limitation, we can draw on various post-transcriptional modifications known to stabilize RNA, such as pseudouridine (Ψ) (Schwartz et al., 2014), N4-acetylcytidine (ac4C) (Dominissini and Rechavi, 2018), N6-methyladenosine, N6,2′-O-dimethyladenosine (Boo and Kim, 2020). Modifications like Ψ and ac4C are most likely involved in the binding between tRip and tRNAs (Cela et al., 2021). They have the potential to stabilize the aptamer and to significantly enhance its binding affinity (Figure 35A). In Figure 35, different strategies commonly used in aptamers to increase their stability are summarized. For example, carriers like polyethylene glycol (PEG) or cholesterol can be attached to the aptamer's 5’-end, which can extend its half-life to several hours (Figure 35B) (Tucker et al., 2001). The approved aptamer developed against VEGF, for instance, is conjugated with 40 kD-PEG at its 5' end (Ruckman et al., 1998).

Circularization of the aptamer is another effective strategy (Figure 35B-C). A circular construct provides complete resistance to exonucleases and improves the thermal stability of the linear aptamer. Moreover, this process allows the use of natural nucleotides, potentially reducing the toxicity associated with chemical modifications (Mao et al., 2020). For instance, two double-strand circular aptamers were designed to target circulating tumor cells (CTCs), resulting in an enhanced stability to capture CTCs *in vivo* (Dong et al., 2017). In our specific case, the most

efficient strategy might involve the addition of Ψ to improve the aptamer's binding affinity, along with circularization to enhance its stability.

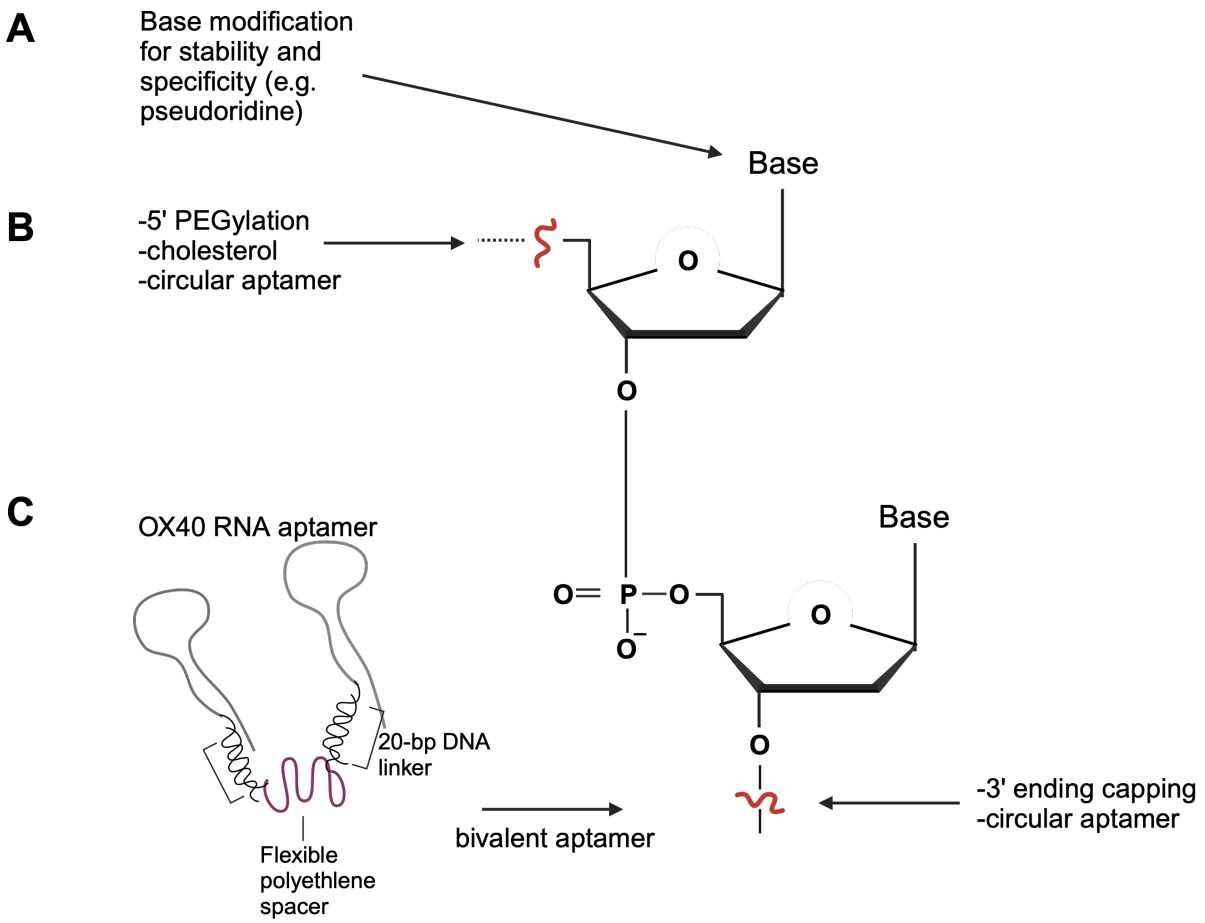

Figure 35: Strategies used to increase the stability and/or specificity of an aptamer. **(A)** Base modifications can be used to enhance stability and improve binding specificity. **(B)** The most commonly used modification currently to increase renal clearance is PEGylation at the 5' end of aptamers, while more recently, also conjugation with cholesterol has been tested to extend the half-life (Nimjee et al., 2017). Alternatively, circularization can be employed for protection against nucleases. **(C)** The 3'-end can be involved in circularization, capping strategy and formation of bivalent aptamers are other approaches. For instance, the bivalent OX40 aptamer directed against T-cells consists of a 20-nucleotide double-stranded DNA sequence at the 3'-end of the aptamer that binds, through a flexible polyethylene spacer, to 20-nucleotide DNA sequence present on another identical aptamer (Shurtz et al., 1979).

2.1.4. Identifying the optimal strategy: aptamer-mediated inhibition of tRNA import or aptamer-based delivery?

The next step is to determine whether the aptamer blocks tRNA import or if it is imported inside the cell *in vitro*. The FISH (Fluorescence In Situ Hybridization) experiment can be conducted using a probe specific to the aptamer sequence in order to observe (i) whether sporozoites import the aptamer inside, or (ii) whether tRNA import still occurs in the presence of the aptamer. This would help clarify the strategy to be followed.

If the aptamer can successfully enter the parasite, the issue of import would be bypassed. In such a scenario, the aptamer could be conjugated with a therapeutic drug that, once delivered directly into the parasite, could inhibit its development through various mechanisms. The designed molecule could be a small molecule, or a protein that disrupt essential cellular functions, such as translation, transcription, or DNA stability. For instance, it may target crucial proteins like aaRSs, thereby altering the translational machinery. Indeed aaRs are good targets for antimalarial development (Xie et al., 2023). Alternatively, the molecule could directly target the parasite's DNA. An example of a DNA-targeting aptamer is Sgc8c, which targets T-Acute Lymphoblastic Leukemia cells by binding to a transmembrane tyrosine kinase protein (PTK7) expressed in leukemic and tumor cells (Leitner et al., 2017). Sgc8c has demonstrated the potential for drug delivery by incorporating a metal complex called PHENEN ((1,10-phenanthroline)(ethylenediamine) platinum (II)) within the stem of the aptamer. Once transported into the nucleus, this complex acts as a DNA intercalator, exerting toxic effects on the cells (Ghasemii et al., 2022). Considering the similar stem structure with our Aptamer-15, such DNA intercalator could also be introduced in our aptamer. This approach would potentially allow Aptamer-15 to bring in the parasite's nucleus a DNA intercalator, causing damage to the parasite's cells and inhibiting its development. Moreover, such delivery aptamer could be employed in combinatorial therapy, where it facilitates the introduction of a molecule in combination with existing treatments. For example, it is known that mutations in K13 protein can lead to artemisinin resistance, and reduces iron availability (see Introduction, chapter II, paragraph 1.2.) and induces artemisinin resistance. Thus one can consider introducing a molecule that acts on this pathway, making iron more available to activate artemisinin.

3. tRip as a target for vaccine development

The development of an effective malaria vaccine remains a challenge. Despite the World Health Organization's approval of a vaccine targeting the circumsporozoite protein (CSP) in 2021 (WHO, 2021), its efficacy has been observed to be relatively low and decline over time.
tRip could be an excellent target. The extracellular location of tRip's C-terminal domain makes it accessible to the immune system, as it is the case for CSP, but in addition its expression pattern extends throughout the entire life cycle of the malaria parasite, whereas CSP is only expressed during the sporozoite stage. Our immunization experiments of Balb/c mice has confirmed the immunogenicity of tRip. However, this immunization did not lead to protection against parasite infection. In three independent experiments, mice were immunized with tRip and subsequently infected with different quantities (10^6, 10^3, 500) of *P. berghei* iRBCs. Only with the minimum quantity, there was a slight delay observed in the onset of parasitemia, which is encouraging, but full protection was not achieved. We should repeat the immunization experiment using lower quantities of iRBC to confirm this observation.
Several reasons may cause the failure of immunization. Firstly, it remains uncertain whether the stimulation of the immune response is sufficiently robust to confer protection. Factors such as the use of adjuvants, dosage, or administration method could influence the vaccine's efficacy (Zimmermann and Curtis, 2019).
An alternate natural infection approach was attempted using infected mosquitoes. Surprisingly, in this case, not only no protection was observed, but the treated mice appeared to develop the infection more rapidly than the control group treated with only PBS, leading to significantly higher parasitemia levels. It was confusing, perhaps by reconstituting the complete parasite cycle and thus exposing the immune system to the pre-erythrocytic stage, this approach may be counter-productive. It may be that the immune system already stimulated (by multiple injections of tRip) in the immunized mice cannot respond effectively to produce further antibodies against sporozoite surface proteins other than tRip, which somewhat protects control mice. Especially, we know that the sporozoite tRip is not well accessible to antibodies *in vitro* (immunolocalization experiments) due to the presence of CSP. Indeed, co-immunolocalization experiment conducted in our laboratory showed that the CSP protein completely coats the sporozoite's surface, partially obscuring the recognition of tRip. In fact, to co-localize the two proteins, sporozoites had to be treated first with anti-tRip antibodies and then with anti-CSP antibodies and not *vice versa* or together, otherwise tRip would not be detected efficiently.

Given the inconclusive nature of the current results, there are several possibilities for further exploration. Firstly, what could be done is to understand if the type of immune response induced by tRip in mice is sufficiently strong to confer protection. It is important to investigate whether the immune response persists over time, even during parasite infection. Additionally, different types of adjuvants could also be tested. Adjuvants are substances added to vaccines to enhance the immune response and improve the vaccine's effectiveness. Since different adjuvants can stimulate different aspects of the immune system, it's essential to identify the most effective adjuvant for each specific vaccine candidate. Another approach could use a recombinant protein to enhance the stimulation of the immune response. Indeed, it is possible that the protein alone may not be able to cause an adequate immune response. In the RTS,S vaccine, the CSP protein is conjugated to a highly immunogenic Hepatitis B virus surface antigen to improve its efficacy (Cohen et al., 2010).

MATERIALS & METHODES

I. Material

1. Chemical products

Ammonium acetate	Fluka
Ammonium persulfate	Sigma-Aldrich
Ampicilline	Euromedex
β-mercaptoethanol	Carl Roth
Bovine Serum Albumine Standard	Euromedex
Chloroform	Carl Roth
DTE	Euromedex
EDTA	Euromedex
Ethanol	VWR
Glycerol	Carl Roth
Glycogen	QBiogene
Heparin	SIGMA
HEPES	Fisher Bioreagents
His-Select® HF Nickel Affinity Gel	Sigma-Aldrich
Hydrochloric acid	VWR
Imidazole	Sigma-Aldrich
Imject Alum	Thermo Scientific
Isopropyl β-D-1-thiogalactopyranoside	Euromedex
Isoamyl alcohol	Fisher Scientific
Ispropanol	VWR
Magnesium acetate	Carl Roth
Magnesiun chloride	Carl Roth
p-Aminobenzamidine	Thermo Scientific
Phosphate buffered saline	Euromedex
Percoll	Cytiva
Phenol	Sigma-Aldrich
QuickBlue protein Stain	Lubio Science
Rotiphorese gel 30	Carl Roth
Rotiphorese Sequenziergel-Verdunner	Carl Roth
Rotiphorese Sequenziergel-Konzentrat	Carl Roth
Rotiphorese Sequenziergel Puffer-Kon.	Carl Roth
RPMI	Gibco
Saponin	Sigma-Aldrich
SDS	Sigma-Aldrich
Sodium acetate	Carl Roth
Sodium bicarbonate ($NaHCO_3$)	Merck
Sodium carbonate (Na_2CO_3)	TBE
Sodium chloride (NaCl)	TG-SDS
Spermidine	TMB
Merck	TEMED
Carl Roth	Tris-base
Sigma-Aldrich	Triton X-100

Euromedex	VWR
Euromedex	Euromedex
Sigma-Aldrich	Carl Roth
Tween 20	Fisher Bioreagents

2. Nucleotides and oligonucleotides

[α^{32}P]-ATP (SRP-207)	Hartmann Analytic
ATP, CTP, UTP, GTP	Jena Bioscience
GMP	Bio Basic
Oligonucleotides/primers	IDT
Poly-dT	IDT

3. Enzymes

Ambion RNase H, *E.coli*	Invitrogen
BamHI	Biolabs
HindIII	Biolabs
RNasin Ribonuclease Inhibitor	Promega
T7 RNA polymerase	Homemade
Thrombin	Cytiva

4. Antibody

Goat, anti-mouse HRP	Invitrogen

5. Kits

Individual PCR tubes, 8-tube strip	BIO-RAD
Optical Flat 8-Cap Strips for 0.2 ml	BIO-RAD
Plasmodipur Filters	EuroProxima
RapidOut DNA Removal Kit	Thermo Fischier Scientific
RNeasy Mini Kit	Qiagen
Syber Green qPCR Master Mix	Thermo Fisher Scientific
Plate ELISA	SARSTEDT

2. Animals and parasites

The parasite requires two hosts to develop: *Anopheles* mosquitoes and mice. All experiments with living animals were carried out in the institute's Insectarium and animal facility.

2.1. *Plasmodium* strains

1. *Plasmodium berghei* GOMO14. This strain expresses the GFP protein under the control of the promoter HSP70.
2. *Plasmodium berghei* tRip-KO. The gene encoding tRip was deleted and replaced by the mCherry gene in the genome of the WT strain of *P. berghei* ANKA (Bour et al., 2016).

2.2. Mice strains

All experiments with mice were performed in accordance with ethical protocols and regulations under the project license for animal experimentation #11124-2018010312571506, following the 3R rules to minimise animal suffering. The mice were divided into cages of four mice each, with a constant supply of food and water and changing the litter once a week. The animal facility where we worked has a SOPF health statute.

Two strains of mice were used:

1. Swiss CD1 mice provided by the animal facility of our institute were used for the parasite amplification and purification. We worked with four-week-old mice. Indeed, while *P. berghei* wild-type develops normally under any condition, *P. berghei* tRip-KO has a reduced infectivity and it develops slowly in the adult mice (Bour et al., 2016). For this reason, we chose to work with young mice, in which the immune system is not yet completely developed.
2. Balb/cJrj mice bought from JanvierLab were used for the vaccination experiments, after a week of acclimatization in the Insectarium's institute. Balb/c mice are often used in immunology experiments because they exhibit unique immune characteristics that make them a good model for studying immune responses. They can develop a strong immune response against infections and they can produce monoclonal antibodies with high affinity and specificity for a wide range of antigens.

2.3. Mosquito strains

The two mosquito strains used in our experiment are: *Anopheles coluzzii Ngousso* and *Anopheles stephensi,* Indian malaria mosquito. Mosquitoes were bred in the Insectarium by

Dr. Eric Marois, under standard conditions: 26-28°C, 60-80% humidity, day/night cycle of 12h/12h.

II. Methods

1. Preparation of molecules

1.1. Protein purification

- $tRip_{200-402}WT$

The gene encoding the C-terminal domain of *P. falciparum* tRip ($tRip_{200-402}WT$) corresponds to the tRNA binding domain (tRip sequence will be given below). It was cloned into the expression vector pET15b (Cela et al., 2021) and transformed into BL21 bacterial cells to produce the recombinant protein fused to a 6-histidine (6-His) tag at its N-terminus. Cultures were performed in LB medium containing 0.1 mg/ml ampicillin, at 30ºC under agitation (180 rpm) until an OD_{600} of 0.5-0.6 was reached. Expression of $tRip_{200-402}WT$ was induced in the presence of 0.5 mM IPTG overnight at 16ºC. Cells were harvested by centrifugation at 4000 rpm for 20 min and washed in PBS. The cell pellet was recovered in 25 ml of buffer A_2A_3, sonicated during 7 min at 120 V and ultracentrifuged 45 min at 45000 rpm at 4ºC. The supernatant was loaded on a Ni-NTA resin column (Sigma-Aldrich) previously equilibrated with buffer A_2A_3. The different chromatographic steps are depicted in Table 4 and the buffers composition is given in Table 5.

Table 4: Steps performed on Ni-NTA column for $tRip_{200-402}WT$ purification.

Number step	Volume	Purification step NiNTA
1	25 ml	Sample inject at 0,80 ml/min for 30 min
2	10 ml	Isocratic flow with buffer A_2A_3 at 1 ml/min
3	6 ml	Linear gradient with 100% A_2A_3 to 0 % B_1 at 1 ml/min
4	6 ml	Linear gradient with 0% A_2A_3 to 100 % B_1 at 1 ml/min
5	20 ml	Isocratic flow with buffer A_1 at 1 ml/min
6	20 ml	Linear gradient with 100% buffer B_2 at 1 ml/min
7	6 ml	Isocratic flow with buffer B_2 at 1 ml/min
8	6 ml	Isocratic flow with buffer A_1 at 1 ml/min

Table 5: Composition of buffers for tRip purification on Ni-NTA column.

Buffer Name	Component	Concentration stock	Volume	Final concentration
Buffer A_1 Ni-NTA	HEPES-Na pH 8 Imidazole Glycerol β-mercapoethanol H_20 qsp	1 M 2 M 100% 14 M	5 ml 500 µl 10 ml 36 µl 100 ml	50 mM 10 mM 10% 5 mM
Buffer A_2A_3 Ni-NTA	HEPES-Na pH 8 NaCl Glycerol β-mercapoethanol H_20 qsp	1 M 4 M 100% 14 M	12.5 ml 18.75 ml 25 ml 90 µl 250 ml	50 mM 300 mM 10% 5 mM
Buffer B_1 Ni-NTA	HEPES-Na pH 8 NaCl Glycerol β-mercapoethanol H_20 qsp	1 M 4 M 100% 14 M	5 ml 50 ml 10 ml 36 µl 100 ml	50 mM 2 M 10% 5 mM
Buffer B_2 Ni-NTA	HEPES-Na pH 8 Imidazole Glycerol β-mercapoethanol H_20 qsp	1 M 2 M 100% 14 M	5 ml 15 ml 10 ml 36 µl 100 ml	50 mM 300 mM 10% 5 mM
Dialysis buffer	HEPES-Na pH 7 NaCl $MgCl_2$ Glycerol β-mercapoethanol H_20 qsp	1 M 4 M 2 M 100% 14 M	25 ml 18.8 ml 2.5 ml 150 ml 180 µl 500 ml	50 mM 150 mM 10 mM 30% 5 mM
Buffer 500 nM NaCl HiTrap™ Benzamidine	HEPES-Na pH 8 NaCl Glycerol β-mercapoethanol H_20 qsp	1 M 4 M 100% 14 M	2.5 ml 6.25 ml 5 ml 18 µl 50 ml	50 mM 500 mM 10% 5 mM
Buffer 4-aminobenzamide HiTrap™ Benzamidine	Buffer A_2A_3 4-aminobenzamide	200 mM	22.5 ml 2.5 ml	20 mM

Importantly, after loading the sample on the column, a NaCl gradient (100% A_2A_3 to 100% B_1) is systematically applied to remove nucleic acids that associate non-specifically with tRip (Cela et al., 2021). Recombinant $tRip_{200-402}$WT protein is eluted during the imidazole gradient. The presence of the proteins is detected by monitoring absorbace at 280 nm (Figure 36A) and by

SDS-PAGE analysis (Figure 36B). Fractions containing $tRip_{200-402}WT$ were pooled and the 6-His tag was removed by adding 50 U of thrombin during the dialysis step performed in A_2A_3 buffer for 12 hours at 4°C. Tag cleavage was verified by migration of samples on a 10% SDS-PAGE gel before and after thrombin cleavage (Figure 36C). After cleavage, the dialysate was loaded on a 1 ml HiTrap Benzamidine FF (HS) column (Cytiva) equilibrated with 10 ml buffer A_2A_3 to remove thrombin. In a second step, the mixture was incubated for 10 min at 4°C with a resin HIS-Select® Nickel Affinity Gel (Sigma), equilibrated with the buffer A_2A_3 to remove uncleaved proteins. Tag free $tRip_{200-402}WT$ was recovered from the supernatant after 5 min centrifugation at 4000 rpm. Finally, the protein was dialysed in either 50 mM HEPES-NaOH pH 7.0, 150 mM NaCl, 10 mM $MgCl_2$, 5 mM ß-mercaptoethanol, 30% glycerol and stored at -80°C until use for EMSA experiments, or in PBS for immunization experiments.

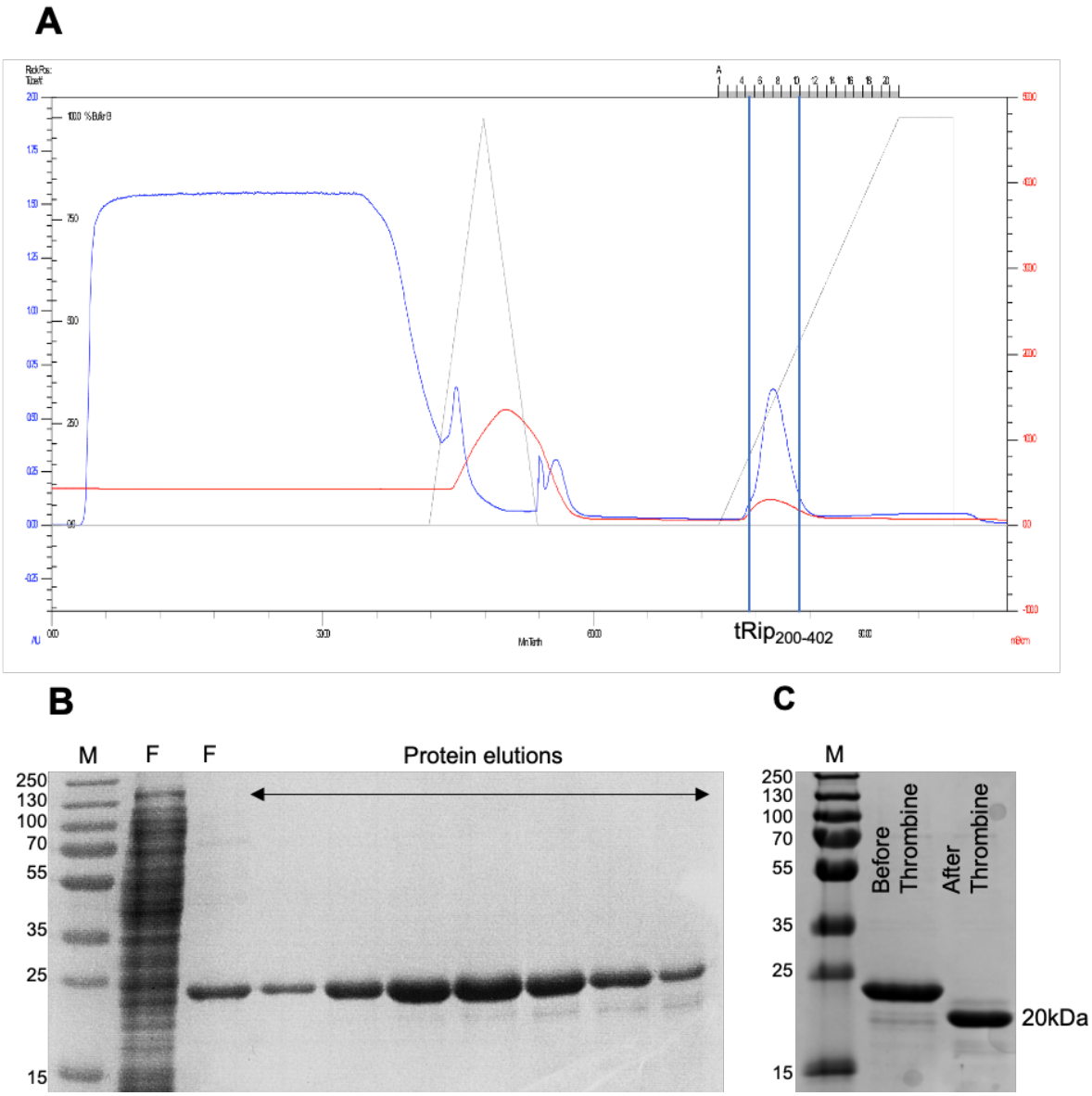

Figure 36: ***P. falciparum*** **$tRip_{200-402}WT$ purification.**
Legend continues next page.

(A) Chromatogram of Ni-NTA column. The red, blue and black profiles indicate conductivity, UV and theoretical percentage of buffer B, respectively. The peak observed in tubes 4 to 10 corresponds to the protein eluted during the imidazole gradient. **(B)** The presence of $tRip_{200-402}$WT was verified by migration of samples (tubes 4 to 10) on a 10% SDS-PAGE followed by staining in QuickBlue Protein Stain (Lubio Science). M: Molecular weight markers, F: flow-through. (**C**) 10% SDS-PAGE analysis after removal of the 6-His Tag from $tRip_{200-402}$WT by thrombin cleavage. $tRip_{200-402}$WT is a 20 kDa protein.

- $tRip_{200-402}$*

The same protocol was used to purify the $tRip_{200-402}$* double mutant whose Ser312 and Met315 were substituted by alanine (Figure 37). Both amino acids belong to the EMAPII-like domain of tRip and have previously been shown to be involved in tRNA recognition (Morales, 1999).

Both, WT and mutated proteins are estimated to be over 95 % pure by SDS-PAGE and about 3-5 mg of pure proteins were recovered from 250 ml of cell culture.

```
  1 MCVLTLVKDD IKSDILKLVL DYIKVTVVQD NENVKLPEIC YDKKITLQYK
 51 NKTYKDLFCT LYALIDIYDC YSELFNEDEG KVSENEEFIF HLASDKYILK
101 QSDMKHLNDL LCEKSYIISN KHASIVDIFY FCAIHKLLDE MAVKERIEFS
151 YIYRWYLHIQ ETLLANFSTL KKLIVKDSLE NLLNNKTTNN APEHKNNFVS
201 KESKENKSQN NESPKNKKKD VQNKNNAPNK KVEETKKLDD ISRLNVLVGY
251 VEQVEIHPDA DTLYCLKINL GEDKPRDICS GLRNKKNAED LLNKYVLVLA
301 NLKEKSLRGK KSHGMVLCGS FDEKVELLVP PNGVKIGERI LFHNMDPNVI
351 PDKNLSSDKE KNPFFHIQPH LILKDGVAHY KDTKWISSQG DITCVLNQGT
401 IS*
```

Figure 37: Sequence of P. falciparum tRip.
The N-terminal GST-like, the K-rich and the EMAPII-like domains are shown in grey, black and blue, respectively. $tRip_{200-402}$WT corresponds to the last 202 amino acids recapitulating the C-terminal domain responsible for tRNA binding (EMAPII-like). Residues S_{312} and M_{315} mutated to alanine in $tRip_{200-402}$* are shown in red.

1.2. Preparation of RNA molecules

S. cerevisiae native $tRNA^{Phe}$ was prepared according to (Giegé et al., 1986).

DNA sequences encoding Aptamers were either cloned into pUC119 under the control of the T7 RNA polymerase promoter (Aptamer 15, and yeast $tRNA^{Phe}$ transcript (tr^{Phe}) Figure 38A), or obtained by annealing two oligonucleotides recapitulating the T7 RNA polymerase promoter

in double-stranded form, followed by the complement of the aptamer sequence in sigle-stranded form (Aptamers 17, 24, 37 and all Aptamer 15 mutants) (Frugier et al., 1992) (Figure 38B).

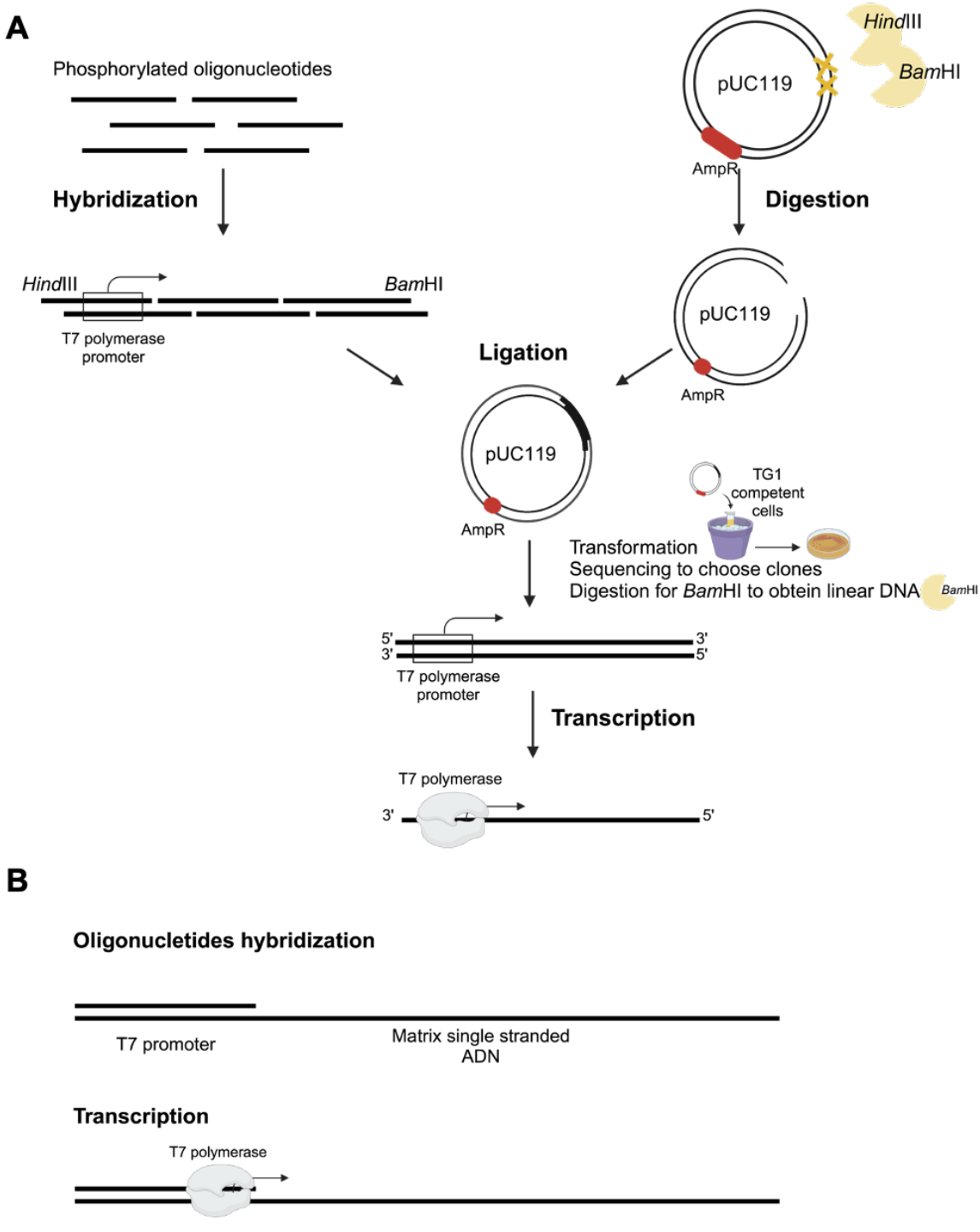

Figure 38: In vitro production of RNA aptamers either by the classical method (A) or by oligonucleotide hybridization (B).
The sequences are always combined to the T7 RNA polymerase promoter sequence to permit transcription after linearization of the plasmid (**A**) or annealing of the oligonucleotides (**B**).

Hybridization was performed by incubating 2.5 µM each oligonucleotide in a volume of 50 µl for 3 min at 90°C followed by a rapid cooling (0°C). Transcriptions (100 µl) were performed either with 10 µg of linearized DNA (Aptamer 15) or with 400 nM of hybridized oligonucleotides (other aptamers) in 40 mM Tris−HCl pH 8.1, 10 mM DTE, 2 mM spermidine, 11 mM $MgCl_2$ and 4 mM CTP, 4 mM GTP, 4 mM UTP, 4 mM ATP and 8 mM GMP and T7 RNA polymerase for 3 h at 37°C. Transcripts were purified on a preparative 12 % denaturing gel (19:1, 8 M urea, TBE 1X), bands were cut under UV shadowing and RNAs were extracted by 2 successive 1 hour electroelutions at 150 Volts. The electroeluted RNAs were precipitated, the pellets recovered in milliQ water and their concentrations determined by absorbance at 260 nm.

2. Caracterization of RNA-tRip complex by electrophoreisis mobility shift assays (EMSA)

To monitor the interaction between aptamers and tRip, RNAs were radioactively labeled during transcription by adding 20 µCi [α^{32}P]-ATP to 100 µl transcription mixture and reducing the cold ATP concentration to 0.5 mM. Radioactive transcripts were first purified on a 12% denaturing polyacrylamide gel and extracted from the gel by passive elution in 1 ml Maxam-Gilbert buffer (0.2 M $AcNH_4$, 10 mM AcMg, 20 mM Tris-HCl pH 7.4, 0.1% SDS) for 2 h at 20°C under medium agitation (300 rpm). After precipitation in the presence of 2 µg glycogen, transcript pellets were washed twice and dried. The radioactivity contained in the dry pellet was determined by Cerenkov counting. MilliQ water was added to the pellet to reach a final concentration of around 10000 cpm/µl.

Radiolabeled aptamers were renatured in water for 2 min at 65°C followed by 10 min at room temprature before adding 10 mM $MgCl_2$ and 40 nM dT_{15}. RNA/protein complexes were formed by incubating for 20 min at 4ºC, 10000 cpm of renatured radioactive RNA with different protein concentrations (from 0 to 500 nM $tRip_{200-402}$WT or $tRip_{200-402}$*) in a total volume of 20 µl of 25 mM HEPES-NaOH pH 7.5, 75 mM NaCl, 10 mM $MgCl_2$ and 10% glycerol. The formation of the RNA/protein complex was analyzed on a 6% native gel (37.5 :1, TBE 1X) for 1.5 h at 140 V at 4ºC. The gel was dried (Gel Dryer, Bio Rad) for 1h30 and radioactivity was visualized using the Typhoon FLA 7000 scanner (GE Life Science). Quantification was performed using ImageQ and Kd-values were determined as the concentrations of $tRip_{200-402}$WT capable of shifting 50% of the labeled RNAs.

To test the competitions between two RNAs, a variation of EMSA was performed. First a complex between $tRip_{200-402}$WT (100 nM) and Aptamer 15 (10000 cpm) was preformed and increasing concentrations (60 nM to 1 µM) of unlabeled tr^{Phe}, native $tRNA^{Phe}$ or the various mutated aptamers were added. Ki-values correspond to the concentration of competitor RNA required to dissociate half of the radiolabeled Aptamer 15 bound to tRip. Each experiment was repeated independently at least 3 times.

3. Parasite purification from infected mice

3.1. Parasite inoculation

Four-week-old male mice (Swiss CD1), weighing approximately 25 g, were injected intraperitoneally (IP) with red blood cells (RBC) from frozen stocks infected with either wild-type *P. berghei* ANKA parasites (100 µl of *Pb* GFP-GOMO14 iRBCs) or by tRip-KO parasites (200 µl of *Pb* tRip-KO mCherry iRBCs).

The end of each experiment was decided based on the animal's health status. As a rule, we set a parasitemia of 10-15% as the threshold before ending the life of the mice. However, some mice are very sick even though their parasitemia is still low and were put to death earlier, whereas sometimes "healthy" mice could be put to death with a higher parasitemia. Symptoms of a sick mouse include shaggy hair, whitish discoloration of ears and limbs, cloudy eyes, and weight loss.

3.2. Parasitemia monitoring

Parasitemia in mice infected with the wild-type parasite was monitored daily using a Flow Cytometer (BD Accuri C6). For this purpose, 5 µl of blood was collected from the mouse tail and mixed with heparin (v/v=1/1). The sample was then diluted 600-fold in PBS and green parasites (expressing GFP) were automatically counted. However, parasitemia in mice infected by the KO parasite (red fluorescent parasites, mCherry) was monitored by counting a 100-fold diluted sample under the microscope. In this case, parasitemia was determined from 3 different microscope fields and corresponds to the number of fluorescent cells versus the total number of RBC x100. To validate the parasitemia of KO parasite-infected mice, wild-type parasites were also counted under the microscope to compare the two approaches. Both methods were found to be equivalent.

3.3. Blood collection *via* cardiac puncture

When parasitemia in infected mice reached 5-10%, they were put to sleep with 100 µl of anaesthesia (85% of NaCl 0.9%, 10% of Zoletil 50% and 5% of Rompun 2%) per 10 g of body weight. Blood puncture was made on an anesthetized but alive mouse with a 1 ml heparin-soaked syringe. The needle was placed at 45° angle between the two ribs, and when the first drop of blood reaches the syringe, it indicates that the needle has entered the heart. The blood (about 1.5 ml) was aspirated and parasites were immediately purified.

3.4. Parasite purification

First, red blood cells (RBC) from infected blood (Figure 39A) are separated from serum by centrifugation for 5 min at 600 g (Figure 39B). The RBC pellet was washed 1-fold in 1 ml RPMI and finally recovered in 4 ml RPMI. The RBCs are subsequently filtered through a Plasmodipur filter (Europroxima) (Figure 39C) to remove mouse leukocytes and platelets. A cushion of 60% isotonic Percoll (7.5 ml) is gently pipetted under the RBCs (Figure 39D), the tube was centrifuged for 20 min at 1450 g in a swing-bucket rotor to separate iRBC present at the Percoll/RPMI interface from non-infected RBCs found at the bottom of the tube (Figure 39E). The iRBC are recovered and centrifuged for 10 min at 450 g (Figure 39F); the pellet is washed 3 times with 1 ml PBS, resuspended in 400 µl PBS and split in 2 equivalent tubes (one tube for proteomic experiments and one tube for qRT-PCR) (Figure 39G).

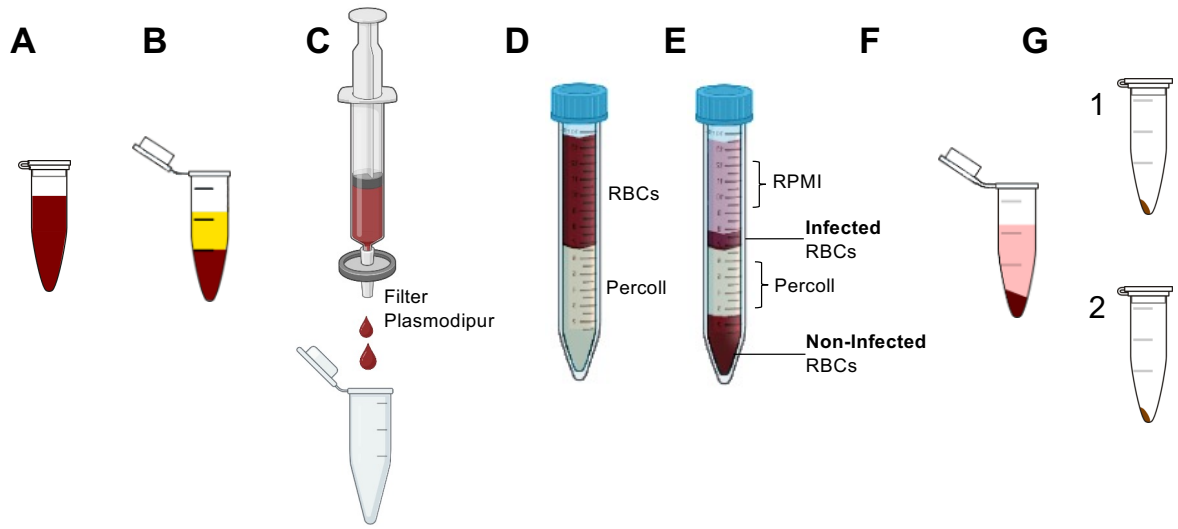

Figure 39: The different stages in the purification of P. berghei from the blood of infected mice.

(A) Parasitized blood recovered by cardiac puncture from mice. **(B)** Separation of red blood cells from blood plasma. **(C)** Filtration of iRBCs on Plasmodipur filter to eliminate leukocytes and platelets. Cushions of 60% percoll **(D)** before centrifugation and **(E)** after centrifugation: at this percentage, the percoll separates infected from non-infected RBCs. **(F)** iRBCs were lysed with saponin and **(G)** the parasites are divided into two equivalent pellets : (1) for proteomic analysis by mass spectrometry and (2) for qRT-PCR analysis.

4. Sample preparation for proteomics experiments (All blood stages)

4.1. Parasite purification

To lyse infected RBCs, 200 µl of 0.04% saponin (diluted in PBS) is added to 200 µl of iRBC and the mixture is incubated for 5 min on ice. The reaction is stopped by dilution with 500 µl PBS and the parasites are recovered by centrifugation for 5 min at 450 g. The pellet is resuspended in 50 µl of protein loading buffer (100 mM Tris-HCl pH 6.8, 20% glycerol, 0.2% bromophenol blue, 4% SDS, 200 mM DTT) and the sample is stored at -80°C prior to mass spectrometry analysis.

4.2. Protein quantification

Two tubes (Tube 1 and Tube 2) containing equivalent numbers of parasites were treated as follows:

- **Step 1 (Figures 40A to 40F)**

Tube 1 was resuspended in 110 µl of 50 mM HEPES-NaOH pH 8.0, 300 mM NaCl, 10% glycerol, 5 mM β-mercaptoethanol, 20 mM imidazole, 0,0005 % DDM, then sonicated twice for 2 sec and centrifuged 5 min at 15000 g. The protein concentration in Tube 1 was determined using the Bradford assay (BioRad). A serial dilution of sample 1 in PBS (A_2 to H_2, Figure 40D, E) was compared to a BSA standard curve (Figure 40A, B) and resulted in an estimated protein concentration in Tube 1 of 0.24 µg/µl, corresponding to a total of 25 µg (in 110 µl) as shown in Figure 40F.

- **Step 2 (Figure 40G)**

Tube 2 was resuspended in 50 µl of protein loading buffer to obtain a concentration of 0.5 µg/µl, based on the estimate made in step 1. Different volumes (5, 10 and 20 µl corresponding to 2.5, 5 and 10 µg, respectively) were loaded onto a 10% SDS-gel. After 10 min staining with QuickBlue Protein Stain (Lubio Science), this gel containing known quantities of proteins will be considered as a reference to estimate the amount of proteins present in other samples sent for analysis by mass spectrometry.

- **Step 3 (Figure 40H)**

The reference gel is used to estimate the quantifies the proteins present in 20 µl of samples WT1, WT2, WT3, WT4, KO1, KO2, KO3, KO4 deposited on gel shown Figure 40H using Image J software.

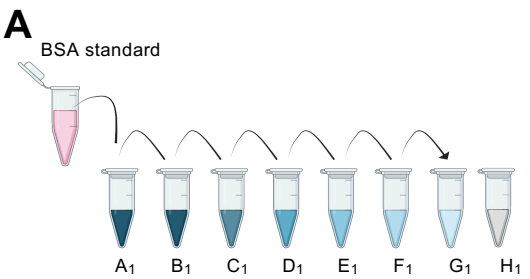

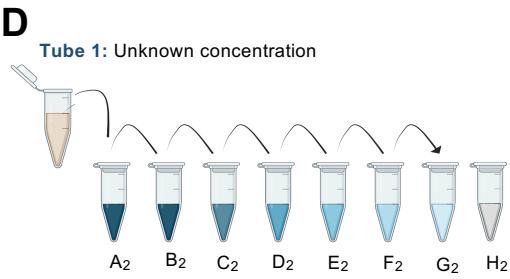

B

Dilution	Abs (y)	µg (x)
A_1	0.333	4
B_1	0.181	2
C_1	0.085	1
D_1	0.039	0.5
E_1	0.024	0.25
F_1	0.015	0.12
G_1	0.007	0.06

E

Dilution	Abs (y)	µg (x)
A_2	0.829	?
B_2	0.517	?
C_2	0.365	?
D_2	0.226	?
E_2	0.127	?
F_2	0.059	?
G_2	0.036	?

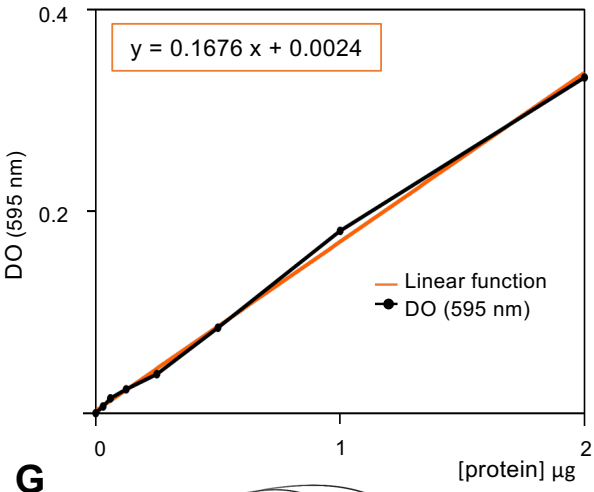

F

Dil	Abs (y)	µg (x)	V_{sample} µl	C_f µg/µl
A_2	0.829	4.94	50	0,09
B_2	0.517	3	25	0,12
C_2	0.365	2.2	12.5	0,17
D_2	0.226	1.35	6.25	0.22
E_2	0.127	0.75	3.12	0.24
F_2	0.059	0.35	1.56	0.23
G_2	0.036	0.21	0.75	0.28

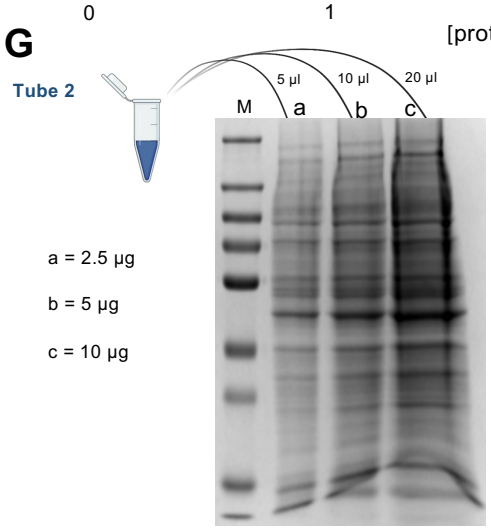

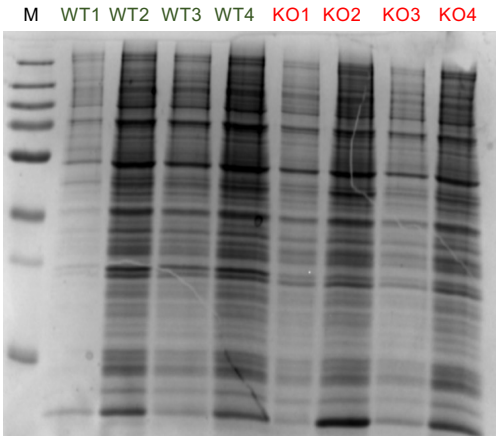

Figure 40: Protein quantification for Mass Spectrometry experiments.
Legend continues on the next page.

(A) Cascade dilution of BSA to establish the standard range for the Bradford assay. **(B)** Table summarizing the BSA amounts and the corresponding absorbance values at 595 nm. **(C)** Standard curve and corresponding equation. **(D)** Serial dilutions of sample 1 (Tube 1). **(E)** Table summarizing the absorbance values obtained for the content of Tube 1. **(F)** Determination of the amount of proteins in Tube 1. Only concentrations highlighted in blue were taken into account for the final calculation. **(G)** Reference gel with different amounts of sample 2 (Tube 2, 2.5 µg - 5 µg -10 µg); **(H)** 10% SDS-PAGE with samples for mass spectrometry analysis (WT1, WT2, WT3, WT4, KO1, KO2, KO3, KO4). M corresponds to the molecular weight marker.

The parasitaemia percentages and protein yields for the 8 infected blood samples are shown in Table 6.

Table 6: Quantification of proteins contained in blood samples arising from 8 infected mice (4 wild-type and 4 tRip-KO).

Mouse ID	% parasitemia	[proteins] µg
Wild-type 1	6,4	1,5
Wild-type 2	10,1	4,2
Wild-type 3	11	3,7
Wild-type 4	13,6	5
tRip-KO 1	7	2,8
tRip-KO 2	7,7	4,4
tRip-KO 3	9,1	2,5
tRip-KO 4	10,9	3,7

5. Mass Spectrometry analysis

Mass spectrometry analyses of protein samples from mice infected with the wild-type parasite (n=4; WT1-4) or the tRip-KO parasite (n=4; KO1-4) were performed and the data were processed by the IBMC proteomic platform. It appeared that the use of the Plasmodipur filter significantly reduces mouse protein contaminations of the parasite samples from 63% to 20% (test carried out on a single sample, not shown). For the analyses, the results from the WT1 and KO3 samples were not considered further as they differed too much from the other

samples. Therefore samples WT2, WT3, WT4, KO1, KO2, and KO4 were retained to study the impact of tRip deletion on protein synthesis in *P. berghei*.

Details of the mass spectrometry analyses and other proteomics experiments carried out by Dr Delphine Kapps on blood schizont samples are given in article #1 in the results section of this manuscript.

6. RNA analysis

6.1. RNA purification from parasites

Total RNA was extracted from the parasites using the RNeasy Mini Kit (Qiagen) according to the manufacturer's protocol, followed by DNAse treatment with the Rapid OUT DNA removal kit (Thermo Scientific). The quality of plasmodial total RNA produced and its quantification were determined on Bioanalyser (puce PICO).

6.2. Reverse transcription of plasmodial RNA, synthesis of cDNA

RNA samples were reverse transcribed in a mix containing 0.16 to 0.5 µg of purified RNA, 200 ng of Random Hexamer Primers (0.2 µg/µl) (Thermo Scientific), 10 mM dNTP in a final volume of 10 µl. After a 5 min hybridization step at 65°C followed by a rapid cooling on ice, 4 µl of 5x First-Strand buffer (Invitrogen), 2 µl of 0.1 M DTE and 1 µl of Recombinant RNasin® Ribonuclease Inhibitor (40 U/µl) were added. After 2 min pre-incubation at 25°C, 1 µl SuperScript II reverse transcriptase (200 U/µl) was added, and the volume ajusted to 20 µl. Incubation was pursued for 10 min at 25°C and followed by 50 min at 42°C. The reverse transcriptase was inactivated by heating at 70°C for 15 min and 0.2 µl of Ambion™ RNase H (10 U/µl) (Invitrogen) was added for 20 min at 37°C to hydrolyze the RNA in an RNA/DNA substrate.

6.3. qPCR

The cDNAs obtained from samples WT2, WT3, WT4 and tRip-KO1, tRip-KO2 tRip-KO4 were quantified by qPCR in 25 µl containing 4 µl of cDNA, 4 µM Sense PCR primers, 4 µM Antisense PCR primers on a CFx94 (Bio-Rad), using Maxima SYBER Green qPCR Master Mix 2X (Thermo Scientific), according to the following protocol: 10 min at 95°C followed by 40 cycles (30 sec at 95°C, 30 sec at 50°C and 1 min at 60°C). The oligonucleotides used for qPCR are listed in Table 7. The protein Hsp70 and eIF1-α were used as housekeeping genes (Sanyal et al., 2012; Tokunaga et al., 2019). For Rhoptry neck protein 2 (RON2) and Rhoptry-associated protein 1 (RAP1), oligonucleotide sequences were taken from the study of (Tokunaga et al., 2019). For the other genes (High Mobility Group Protein B1 (HMGB-1), Unknown Function Protein, DNA Replication Licensing Factor 7 (MCM7), Chromatin Assembly 1 (ChAF-1)), the

sequences were determined using Primer3 software (https://primer3.ut.ee/) (Rozen and Skaletsky, 2000) that allows to design of 20-25 bp primers with a T_m of 50°C to amplify a PCR product size of approximatively 150-200 bp. The specificity of each oligonucleotide was validated after dilutions of the cDNA (between 1/10 -1/100,000) with dissociation curves exhibiting a single peak (melting curve 65 °C to 95 °C, increment 0,5°C 0:05). Amplification efficiencies of the primer sets are all between 90 and 110 % and r^2 values greater than 0.96, individual values are given in Table 7. mRNAs levels were calculated according to the ΔCq method and normalized by the mRNA level of both eIF1-α and Hsp70 in each sample. Raw data are indicated as the mean of 3 technical replicates and results were expressed as the mean of 3 biological samples ± standard error of the mean (SEM). For each oligonucletide pair, a negative control was carried out (in triplicate) with water, and for each sample, an NRT control (no reverse transcription) was performed (in triplicate).

Table 7: Table of RT-PCR primer sequences and efficiency.

Primer name	ID	Primer sequence 5'-3'	Reference	E	r^2
eIF-1 RT-F	PBANKA_1133300	TGGAACCACCCAAAAGACCA	Tokunaga et al., 2019	100.7%	1
eIF-1 RT-R		ACAACAGCAGATGGAGCGAA			
HSP70 RT-F	PBANKA_0914400	AGAGAAGCAGCTGAAACAGC	Sanyal et al., 2013	106.9%	0.999
HSP70 RT-R		TCCCTTTAATAAATCATGGC			
RON2 RT-F	PBANKA_1315700	CGTCTACATCGGCCTTTATTC	Tokunaga et al., 2019	90.3%	0.992
RON2 RT-R		GCGATAGCATGTGTTGTAAATTGG			
RAP1 RT-F	PBANKA_1032100	CAAGTGCCGATTTGCCAGATTA	Tokunaga et al.,2019	106.2%	0.973
RAP1 RT-R		TTTGGTAGAATGCTGAAATACGC			
HM RT-F	PBANKA_0601900	AAAATGGGTGGAAAGGAAGT	Primer3	102.6%	0.990
HM RT-R		TTTCCAACAGTTGCAACATC			
UF RT-F	PBANKA_0601900	TAGCTACTTGTTTACCGCAA	Primer3	96.0%	0.990
UF RT-R		TGAGGCCCCTTTAATTACTCTGT			
MCM7 RT-F	PBANKA_0803100	CAACCATTTCCCCTGAACTA	Primer3	105.4%	0.965
MCM7 RT-R		CACTATCTCTTACCCTTGCC			
ChAF RT-F	PBANKA_0203000	GGACATTTTGCATCTGGAAG	Primer3	99.8%	0.98
ChAF RT-R		GCATCTAACTCTTCACCGAT			

r^2, correlation coefficient; E, primer efficiency.

7. Immunization assays with tRip

7.1. Globale immunization procedure

Four-week-old female mice (Balb/c), weighing approximately 20 g received 3 intraperitoneal injections (IP) of 200 µl containing 25 µg of pure recombinant *P. falciparum* $tRip_{200-402}$WT diluted in PBS and supplemented with 1 volume of Imject™ Alum adjuvant (Thermo Scientific) at 3-weeks intervals. As a control, a group of mice were injected with only PBS and adjuvant (v/v=1/1). Sera from immunized and control mice were collected prior to immunization and infection/challenge. Finally to follow the "potential" efficacy of mice immunization, 2 types of infection (challenge) were tested: either by direct injection of the parasite blood stages (IV) or *via* infected mosquitoes bites. This procedure is summarized in Figure 41.

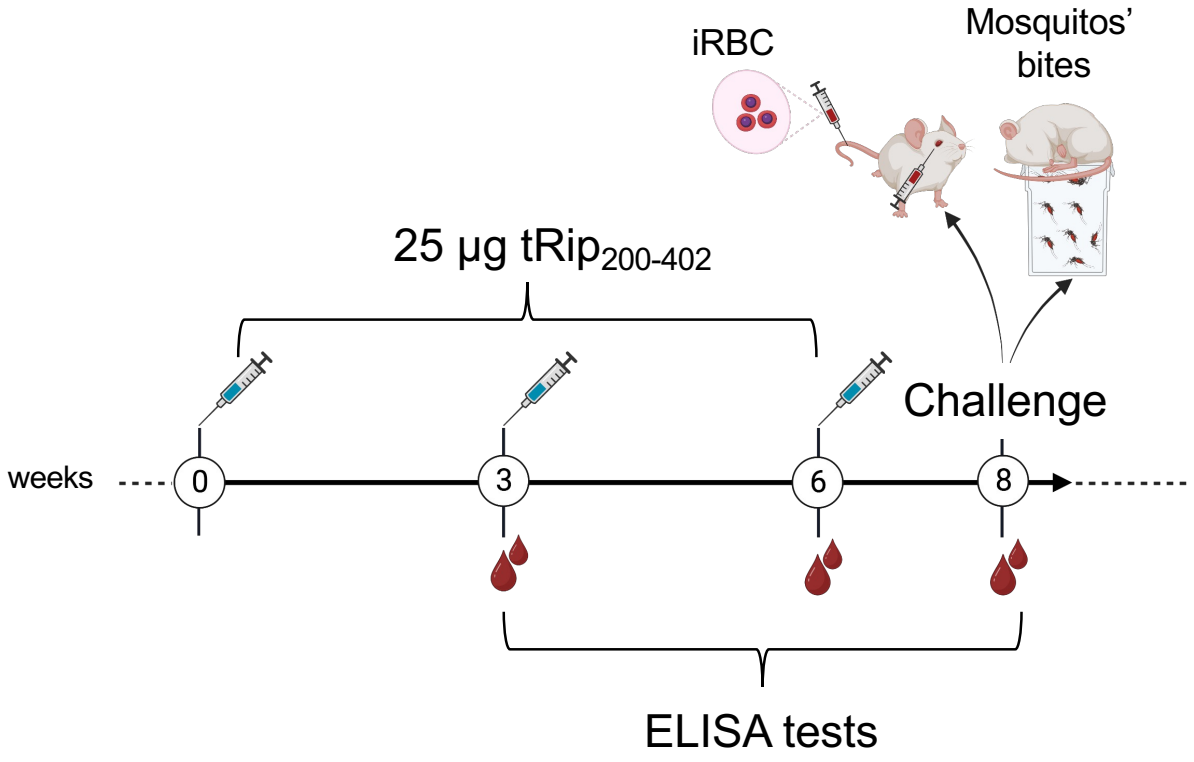

Figure 41: Immunization experiments.
Mice were immunized at three-week intervals (week 0, 3, and 6) with 25 µg purified $tRip_{200-402}$. Two weeks after the final immunization (week 8), the challenge was performed either by (i) infecting the mice with infected red blood cells or (ii) through bites of infected mosquitoes. After challenge, the parasitemia progression was monitored. During the experiment, blood samples were periodically collected (weeks 3, 6, and 8) to measure the antibody levels using ELISA test.

7.2. Antibodies detection by ELISA test

Approximately 200 µl of blood were collected by cutting the mice cheek vein. The blood is centrifuged for 5 min at 600 g to separate RBCs from plasma, and the presence of antibodies against $tRip_{200-402}$WT was checked in the plasma fraction.

ELISA plate preparation: 100 ng/ml of recombinant $tRip_{200-402}WT$ was diluted in 0.05 M citrate/carbonate pH 9.6 and coated onto multi-well ELISA binding plates overnigth at 4°C. Wells were blocked to reduce non-specific binding by adding 100 µl PBS-Tween/1% BSA for 1 hour at 37°C. Plasma, serially diluted in PBS-Tween/0,25% BSA (dliutions sera between 1/200 and 1/25,000), was added and incubated for 90 min at 37°C.

The presence of anti-tRip antibodies was detected using HRP-conjugated goat anti-mouse IgG, diluted 1:20000 and incubated for 90 min at 37°C. After each step, 5 washes were performed with 200 µl PBS/0.05% Tween. One volume (100 µl/well) HRP substrate, Tetramethilbenzamine (TMB), is added and incubated for 10 min in the dark and the reaction stopped by adding one volume of 1N HCl. Absorbance at 450 nm is then measured to determine the concentration of anti-tRip antibodies in blood.

7.3. Parasite injection *via* intraperioneal puncture (IP)

Intraperineal puncture is performed on awake animals. The mouse is taken from the cage, immobilized and placed in a supine position. The injection site is located in the lower right quadrant of the animal's abdomen. The syringe is inserted at an angle of 30-40°, towards the head.

7.4. Parasite injection *via* intravenous puncture (IV)

Two weeks after the last immunization, mice were challenged by intravenous injection of infected red blood cells. Upstream, a Swiss CD1 was infected with *P. berghei*-GFP WT parasites until a parasitemia of about 5% was obtained. Blood was collected by intracardiac puncture. Given that Balb/c mice have 10^7 RBC/ml and parasitemia is 5%, the blood sample theoretically contains 500000 iRBCs. After dilution in PBS, 10^6, 1000 or 100 iRBCs were injected into treated and control mice by intravenous puncture using 2 different techniques:

- (1) Tail vein puncture; mice were placed in a tube rodent holder under a heating lamp to allow the vein to dilate.
- (2) Retro-orbital sinus puncture in the eye of mice previously anaesthetized with isofluorane.

The course of parasitemia is monitored daily by flow cytometry of blood collected from the mice's tails. Mice were carefully watched and sacrificed before parasitemia levels induced suffering.

7.5. Parasite injection via mosquito bite

The first step consists in recovering infected mosquitos: two Swiss CD1 mice are injected with RBC infected with wild-type *P. berghei*-GFP parasites (ANKA strain from a frozen stock). When

the parasitemia reaches about 3-4%, mice are put to sleep and exposed to bites of starving female mosquitoes. After 17 days, the time period required for the parasite to develop into the salivery glands of *Anopheles*, the mosquitos are anesthetized and analyzed by fluorescent microscopy. The fluorescent, and therefore infected, mosquitoes were sorted and used to bite sleeping mice. Each mouse is placed on top of a beaker containing 7 to 10 mosquitoes and sealed with a mosquitoe net. After the blood meal, mosquitos were killed by placing them for a few minutes at 4°C and those with swollen bellies, full of blood, are counted to estimate the number of bites for each mouse.

REFERENCES

A

Alam A, Goyal M, Iqbal MS, Pal C, Dey S, Bindu S, Maity P, Bandyopadhyay U. 2009. Novel antimalarial drug targets: hope for new antimalarial drugs. *Expert Rev Clin Pharmacol* **2**:469–489. doi:10.1586/ecp.09.28

Alings F, Sarin LP, Fufezan C, Drexler HCA, Leidel SA. 2015. An evolutionary approach uncovers a diverse response of tRNA 2-thiolation to elevated temperatures in yeast. *RNA* **21**:202–212. doi:10.1261/rna.048199.114

Almeida MEMD, Vasconcelos MGSD, Tarragô AM, Mariúba LAM. 2021. Circumsporozoite Surface Protein-based malaria vaccines: a review. *Rev Inst Med trop S Paulo* **63**:e11. doi:10.1590/s1678-9946202163011

Amino R, Thiberge S, Blazquez S, Baldacci P, Renaud O, Shorte S, Ménard R. 2007. Imaging malaria sporozoites in the dermis of the mammalian host. *Nat Protoc* **2**:1705–1712. doi:10.1038/nprot.2007.120

Amino R, Thiberge S, Martin B, Celli S, Shorte S, Frischknecht F, Ménard R. 2006. Quantitative imaging of *Plasmodium* transmission from mosquito to mammal. *Nat Med* **12**:220–224. doi:10.1038/nm1350

Antia R, Yates A, De Roode JC. 2008. The dynamics of acute malaria infections. I. Effect of the parasite's red blood cell preference. *Proc Biol Sci* **275**:1449–1458. doi:10.1098/rspb.2008.0198

Aravind L, Iyer LM, Wellems TE, Miller LH. 2003. *Plasmodium* Biology. *Cell* **115**:771–785. doi:10.1016/S0092-8674(03)01023-7

Arora N, Anbalagan LC, Pannu AK. 2021. Towards Eradication of Malaria: Is the WHO's RTS,S/AS01 Vaccination Effective Enough? *Risk Manag Healthc Policy* **14**:1033–1039. doi:10.2147/RMHP.S219294

Azmi WA, Rizki AFM, Djuardi Y, Artika IM, Siregar JE. 2023. Molecular insights into artemisinin resistance in *Plasmodium falciparum*: An updated review. *Infect Genet Evol* **112**:105460. doi:10.1016/j.meegid.2023.105460

B

Badarinarayana V, Chiang Y-C, Denis CL. 2000. Functional Interaction of CCR4-NOT proteins with TATAA-binding protein (TBP) and its associated factors in yeast. *Genetics* **155**:1045–1054. doi:10.1093/genetics/155.3.1045

Baeza Garcia A, Siu E, Sun T, Exler V, Brito L, Hekele A, Otten G, Augustijn K, Janse CJ, Ulmer JB, Bernhagen J, Fikrig E, Geall A, Bucala R. 2018. Neutralization of the *Plasmodium*-encoded MIF ortholog confers protective immunity against malaria infection.

Nat Commun **9**:2714. doi:10.1038/s41467-018-05041-7

Balikagala B, Fukuda N, Ikeda M, Katuro O, Tachibana SI, Yamauchi M, Opio W, Emoto S, Anywar DA, Kimura E, Palacpac NMQ, Odongo-Aginya EI, Ogwang M, Horii T, Mita T. 2021. Evidence of Artemisinin-Resistant Malaria in Africa. *N Engl J Med.* **13**:1163-1171. doi: 10.1056/NEJMoa2101746

Balu B, Maher SP, Pance A, Chauhan C, Naumov AV, Andrews RM, Ellis PD, Khan SM, Lin J, Janse CJ, Rayner JC, Adams JH. 2011. CCR4-associated factor 1 coordinates the expression of *Plasmodium falciparum* egress and invasion proteins. *Eukaryot Cell* **10**:1257–1263. doi:10.1128/EC.05099-11

Bannister LH, Hopkins JM, Fowler RE, Krishna S, Mitchell GH. 2000. A brief illustrated guide to the ultrastructure of *Plasmodium falciparum* asexual blood stages. *Parasitol Today* **16**:427–433. doi:10.1016/S0169-4758(00)01755-5

Barr PJ, Green KM, Gibson HL, Bathurst IC, Quakyi IA, Kaslow DC. 1991. Recombinant Pfs25 protein of *Plasmodium falciparum* elicits malaria transmission-blocking immunity in experimental animals. *J Exp Med* **174**:1203–1208. doi:10.1084/jem.174.5.1203

Bastien O, Lespinats S, Roy S, Métayer K, Fertil B, Codani J-J, Maréchal E. 2004. Analysis of the compositional biases in *Plasmodium falciparum* genome and proteome using *Arabidopsis thaliana* as a reference. *Gene* **336**:163–173. doi:10.1016/j.gene.2004.04.029

Bennink S, Gabriele Pradel. 2019. The molecular machinery of translational control in malaria parasites. *Mol Microbiol* **112**:1658–1673. doi:10.1111/mmi.14388

Beri D, Balan B, Tatu U. 2018. Commit, hide and escape: the story of *Plasmodium* gametocytes. *Parasitology* **145**:1772–1782. doi:10.1017/S0031182018000926

Boo SH, Kim YK. 2020. The emerging role of RNA modifications in the regulation of mRNA stability. *Exp Mol Med* **52**:400–408. doi:10.1038/s12276-020-0407-z

Bour T, Mahmoudi N, Kapps D, Thiberge S, Bargieri D, Ménard R, Frugier M. 2016. *Apicomplexa* -specific tRip facilitates import of exogenous tRNAs into malaria parasites. *Proc Natl Acad Sci USA* **113**:4717–4722. doi:10.1073/pnas.1600476113

Bridgford JL, Xie SC, Cobbold SA, Pasaje CFA, Herrmann S, Yang T, Gillett DL, Dick LR, Ralph SA, Dogovski C, Spillman NJ, Tilley L. 2018. Artemisinin kills malaria parasites by damaging proteins and inhibiting the proteasome. *Nat Commun* **9**:3801. doi:10.1038/s41467-018-06221-1

Briquet S, Marinach C, Silvie O, Vaquero C. 2021. Preparing for transmission: Gene regulation in *Plasmodium* sporozoites. *Front Cell Infect Microbiol* **10**:618430. doi:10.3389/fcimb.2020.618430

Bruce MC, Alano P, Duthie S, Carter R. 1990. Commitment of the malaria parasite *Plasmodium falciparum* to sexual and asexual development. *Parasitology* **100**:191–200. doi:10.1017/S0031182000061199

Bunnik EM, Chung D-W, Hamilton M, Ponts N, Saraf A, Prudhomme J, Florens L, Le Roch KG. 2013. Polysome profiling reveals translational control of gene expression in the human malaria parasite *Plasmodium falciparum*. *Genome Biol* **14**:R128. doi:10.1186/gb-2013-14-11-r128

Burkhard P, Lanar DE. 2015. Malaria vaccine based on self-assembling protein nanoparticles. *Expert Rev Vaccines* **14**:1525–1527. doi:10.1586/14760584.2015.1096781

Buschauer R, Matsuo Y, Sugiyama T, Chen Y-H, Alhusaini N, Sweet T, Ikeuchi K, Cheng J, Matsuki Y, Nobuta R, Gilmozzi A, Berninghausen O, Tesina P, Becker T, Coller J, Inada T, Beckmann R. 2020. The Ccr4-Not complex monitors the translating ribosome for codon optimality. *Science* **368**:eaay6912. doi:10.1126/science.aay6912

C

Caro F, Ahyong V, Betegon M, DeRisi JL. 2014. Genome-wide regulatory dynamics of translation in the *Plasmodium falciparum* asexual blood stages. *eLife* **3**:e04106. doi:10.7554/eLife.04106

Cela M, Théobald-Dietrich A, Rudinger-Thirion J, Wolff P, Geslain R, Frugier M. 2021. Identification of host tRNAs preferentially recognized by the *Plasmodium* surface protein tRip. *Nucleic Acids Res* **49**:10618–10629. doi:10.1093/nar/gkab769

Cestari I, Kalidas S, Monnerat S, Anupama A, Phillips MA, Stuart K. 2013. A multiple aminoacyl-tRNA synthetase complex that enhances tRNA-aminoacylation in african trypanosomes. *Mol Cell Biol* **33**:4872–4888. doi:10.1128/MCB.00711-13

Chan PP, Lowe TM. 2016. GtRNAdb 2.0: an expanded database of transfer RNA genes identified in complete and draft genomes. *Nucleic Acids Res* **44**:D184–D189. doi:10.1093/nar/gkv1309

Chatterjee S, Bhardwaj N, Saxena RK. 2016. Identification of stages of erythroid differentiation in bone marrow and erythrocyte subpopulations in blood circulation that are preferentially lost in autoimmune hemolytic anemia in mouse. *PLoS One* **11**:e0166878. doi:10.1371/journal.pone.0166878

Chaubey S, Kumar A, Singh D, Habib S. 2005. The apicoplast of *Plasmodium falciparum* is translationally active: EF-Tu translation in malaria plastid. *Mol Microbiol* **56**:81–89. doi:10.1111/j.1365-2958.2005.04538.x

Chaudhry SR, Lwin N, Phelan D, Escalante AA, Battistuzzi FU. 2018. Comparative analysis of low complexity regions in *Plasmodia*. *Sci Rep* **8**:335. doi:10.1038/s41598-017-18695-y

Chêne A, Vembar SS, Rivière L, Lopez-Rubio JJ, Claes A, Siegel TN, Sakamoto H, Scheidig-Benatar C, Hernandez-Rivas R, Scherf A. 2012. PfAlbas constitute a new eukaryotic DNA/RNA-binding protein family in malaria parasites. *Nucleic Acids Res* **40**:3066–3077.

doi:10.1093/nar/gkr1215

Chitnis CE, Blackman MJ. 2000. Host cell invasion by malaria parasites. *Parasitol Today* **16**:411–415. doi:10.1016/S0169-4758(00)01756-7

Cid R, Bolívar J. 2021. Platforms for production of protein-based vaccines: from classical to next-generation strategies. *Biomolecules* **11**:1072. doi:10.3390/biom11081072

Cohen J, Nussenzweig V, Vekemans J, Leach A. 2010. From the circumsporozoite protein to the RTS,S/AS candidate vaccine. *Hum Vaccin* **6**:90–96. doi:10.4161/hv.6.1.9677

Collart MA. 2016. The Ccr4-Not complex is a key regulator of eukaryotic gene expression. *WIREs RNA* **7**:438–454. doi:10.1002/wrna.1332

Cooke BM, Lingelbach K, Bannister LH, Tilley L. 2004. Protein trafficking in *Plasmodium falciparum*-infected red blood cells. *Trends in Parasitol* **20**:581–589. doi:10.1016/j.pt.2004.09.008

Coppée R, Jeffares DC, Miteva MA, Sabbagh A, Clain J. 2019. Comparative structural and evolutionary analyses predict functional sites in the artemisinin resistance malaria protein K13. *Sci Rep* **9**:10675. doi:10.1038/s41598-019-47034-6

Coppi A, Pinzon-Ortiz C, Hutter C, Sinnis P. 2005. The *Plasmodium* circumsporozoite protein is proteolytically processed during cell invasion. *J Exp Med* **201**:27–33. doi:10.1084/jem.20040989

Coulson RMR, Hall N, Ouzounis CA. 2004. Comparative genomics of transcriptional control in the human malaria parasite *Plasmodium falciparum*. *Genome Res* **14**:1548–1554. doi:10.1101/gr.2218604

Cowman AF, Tonkin CJ, Tham W-H, Duraisingh MT. 2017. The Molecular basis of erythrocyte invasion by malaria parasites. *Cell Host Microbe* **22**:232–245. doi:10.1016/j.chom.2017.07.003

Cromer D, Evans KJ, Schofield L, Davenport MP. 2006. Preferential invasion of reticulocytes during late-stage *Plasmodium berghei* infection accounts for reduced circulating reticulocyte levels. *Int J Parasitol* **36**:1389–1397. doi:10.1016/j.ijpara.2006.07.009

Cui L. 2002. The malaria parasite *Plasmodium falciparum* encodes members of the Puf RNA-binding protein family with conserved RNA binding activity. *Nucleic Acids Res* **30**:4607–4617. doi:10.1093/nar/gkf600

Cui L, Lindner S, Miao J. 2015. Translational regulation during stage transitions in malaria parasites: translational regulation in *Plasmodium*. *Ann NY Acad Sci* **1342**:1–9. doi:10.1111/nyas.12573

Cullen BR, Greene WC. 1989. Regulatory pathways governing HIV-1 replication. *Cell* **58**:423–426. doi:10.1016/0092-8674(89)90420-0

Culvenor JG, Day KP, Anders RF. 1991. *Plasmodium falciparum* ring-infected erythrocyte surface antigen is released from merozoite dense granules after erythrocyte invasion. *Infect*

Immun **59**:1183–1187. doi:10.1128/iai.59.3.1183-1187.1991

D

Dalby AR. 2009. A comparative proteomic analysis of the simple amino acid repeat distributions in Plasmodia reveals lineage specific amino acid selection. *PLoS One* **4**:e6231. doi:10.1371/journal.pone.0006231

Das S, Hertrich N, Perrin AJ, Withers-Martinez C, Collins CR, Jones ML, Watermeyer JM, Fobes ET, Martin SR, Saibil HR, Wright GJ, Treeck M, Epp C, Blackman MJ. 2015. Processing of *Plasmodium falciparum* merozoite surface protein MSP1 activates a spectrin-binding function enabling parasite egress from RBCs. *Cell Host Microbe* **18**:433–444. doi:10.1016/j.chom.2015.09.007

Datoo MS, Natama HM, Somé A, Bellamy D, Traoré O, Rouamba T, Tahita MC, Ido NFA, Yameogo P, Valia D, Millogo A, Ouedraogo F, Soma R, Sawadogo S, Sorgho F, Derra K, Rouamba E, Ramos-Lopez F, Cairns M, Provstgaard-Morys S, Aboagye J, Lawrie A, Roberts R, Valéa I, Sorgho H, Williams N, Glenn G, Fries L, Reimer J, Ewer KJ, Shaligram U, Hill AVS, Tinto H. 2022. Efficacy and immunogenicity of R21/Matrix-M vaccine against clinical malaria after 2 years' follow-up in children in Burkina Faso: a phase 1/2b randomised controlled trial. *Lancet Infect Dis* **22**:1728–1736. doi:10.1016/S1473-3099(22)00442-X

Datoo MS, Natama MH, Somé A, Traoré O, Rouamba T, Bellamy D, Yameogo P, Valia D, Tegneri M, Ouedraogo F, Soma R, Sawadogo S, Sorgho F, Derra K, Rouamba E, Orindi B, Ramos Lopez F, Flaxman A, Cappuccini F, Kailath R, Elias S, Mukhopadhyay E, Noe A, Cairns M, Lawrie A, Roberts R, Valéa I, Sorgho H, Williams N, Glenn G, Fries L, Reimer J, Ewer KJ, Shaligram U, Hill AVS, Tinto H. 2021. Efficacy of a low-dose candidate malaria vaccine, R21 in adjuvant Matrix-M, with seasonal administration to children in Burkina Faso: a randomised controlled trial. *Lancet* **397**:1809–1818. doi:10.1016/S0140-6736(21)00943-0

Dias BKM, Nakabashi M, Alves MRR, Portella DP, Santos BM, Costa Da Silva Almeida F, Ribeiro RY, Schuck DC, Jordão AK, Garcia CRS. 2020. The *Plasmodium falciparum* eIK1 kinase (PfeIK1) is central for melatonin synchronization in the human malaria parasite. Melatotosil blocks melatonin action on parasite cell cycle. *J Pineal Res* **69**. doi:10.1111/jpi.12685

Dickson ZW, Golding GB. 2022. Low complexity regions in mammalian proteins are associated with low protein abundance and high transcript abundance. *Mol Biol Evol* **39**:msac087. doi:10.1093/molbev/msac087

Dittmar KA, Goodenbour JM, Pan T. 2006. Tissue-specific differences in human transfer RNA expression. *PLoS Genet* **2**:e221. doi:10.1371/journal.pgen.0020221

Dobson MJ. 1999. The malariology centenary. *Parassitologia* **41**:21–32.

Dominissini D, Rechavi G. 2018. N4-acetylation of cytidine in mRNA by NAT10 regulates stability and translation. *Cell* **175**:1725–1727. doi:10.1016/j.cell.2018.11.037

Dong H, Han L, Wu Z-S, Zhang T, Xie J, Ma J, Wang J, Li T, Gao Y, Shao J, Sinko PJ, Jia L. 2017. Biostable aptamer rings conjugated for targeting two biomarkers on circulating tumor cells *in vivo* with great precision. *Chem Mater* **29**:10312–10325. doi:10.1021/acs.chemmater.7b03044

Doolan DL, Hoffman SL, Southwood S, Wentworth PA, Sidney J, Chesnut RW, Keogh E, Appella E, Nutman TB, Lal AA, Gordon DM, Oloo A, Sette A. 1997. Degenerate cytotoxic T cell epitopes from *P. falciparum* rRestricted by multiple HLA-A and HLA-B supertype Alleles. *Immunity* **7**:97–112. doi:10.1016/S1074-7613(00)80513-0

Duffy PE, Patrick Gorres J. 2020. Malaria vaccines since 2000: progress, priorities, products. *NPJ Vaccines* **5**:48. doi:10.1038/s41541-020-0196-3

Dugbartey AT, Dugbartey MT, Spellacy FJ. 1998. Somatosensory discrimination deficits following pediatric cerebral malaria. *Amn J Trop Med Hyg* **59**:393–396. doi:10.4269/ajtmh.1998.59.393

Dupé A, Dumas C, Papadopoulou B. 2014. An Alba-domain protein contributes to the stage-regulated stability of amastin transcripts in *Leishmania*: Amastin gene regulation by Alba proteins. *Mol Microbiol* **91**:548–561. doi:10.1111/mmi.12478

Dyer M, Day KP. 2000. Commitment to gametocytogenesis in *Plasmodium falciparum*. *Parasitol Today* **16**:102–107. doi:10.1016/S0169-4758(99)01608-7

E

Eichner M, Diebner HH, Molineaux L, Collins WE, Jeffery GM, Dietz K. 2001. Genesis, sequestration and survival of *Plasmodium falciparum* gametocytes: parameter estimates from fitting a model to malariatherapy data. *Trans R Soc of Trop Med Hyg* **95**:497–501. doi:10.1016/S0035-9203(01)90016-1

Elias SC, Choudhary P, Cassan SC, Biswas S, Collins KA, Halstead FD, Bliss CM, Ewer KJ, Hodgson SH, Duncan CJA, Hill AVS, Draper SJ. 2014. Analysis of human B -cell responses following C h A d63- MVA MSP 1 and AMA 1 immunization and controlled malaria infection. *Immunology* **141**:628–644. doi:10.1111/imm.12226

Epstein JE, Paolino KM, Richie TL, Sedegah M, Singer A, Ruben AJ, Chakravarty S, Stafford A, Ruck RC, Eappen AG, Li T, Billingsley PF, Manoj A, Silva JC, Moser K, Nielsen R, Tosh D, Cicatelli S, Ganeshan H, Case J, Padilla D, Davidson S, Garver L, Saverino E, Murshedkar T, Gunasekera A, Twomey PS, Reyes S, Moon JE, James ER, Kc N, Li M, Abot E, Belmonte A, Hauns K, Belmonte M, Huang J, Vasquez C, Remich S, Carrington M,

Abebe Y, Tillman A, Hickey B, Regules J, Villasante E, Sim BKL, Hoffman SL. 2017. Protection against *Plasmodium falciparum* malaria by PfSPZ Vaccine. *JCI Insight* **2**. doi:10.1172/jci.insight.89154

Eriani G, Delarue M, Poch O, Gangloff J, Moras D. 1990. Partition of tRNA synthetases into two classes based on mutually exclusive sets of sequence motifs. *Nature* **347**:203–206. doi:10.1038/347203a0

Evans ME, Clark WC, Zheng G, Pan T. 2017. Determination of tRNA aminoacylation levels by high-throughput sequencing. *Nucleic Acids Res* **45**:e133–e133. doi:10.1093/nar/gkx514

F

Fan Q, Li J, Kariuki M, Cui L. 2004. Characterization of PfPuf2, member of the Puf family RNA-binding proteins from the malaria parasite *Plasmodium falciparum*. *DNA Cell Biol* **23**:753–760. doi:10.1089/dna.2004.23.753

Fantini B. 1999. The concept of specificity and the Italian contribution to the discovery of the malaria transmission cycle. *Parassitologia* **41**:39–47.

Fennell C, Babbitt S, Russo I, Wilkes J, Ranford-Cartwright L, Goldberg DE, Doerig C. 2009. PfeIK1, a eukaryotic initiation factor 2α kinase of the human malaria parasite *Plasmodium falciparum*, regulates stress-response to amino-acid starvation. *Malar J* **8**:99. doi:10.1186/1475-2875-8-99

Ferraro B, Talbott KT, Balakrishnan A, Cisper N, Morrow MP, Hutnick NA, Myles DJ, Shedlock DJ, Obeng-Adjei N, Yan J, Kayatani AKK, Richie N, Cabrera W, Shiver R, Khan AS, Brown AS, Yang M, Wille-Reece U, Birkett AJ, Sardesai NY, Weiner DB. 2013. Inducing humoral and cellular responses to multiple sporozoite and liver-stage malaria antigens using exogenous plasmid DNA. *Infect Immun* **81**:3709–3720. doi:10.1128/IAI.00180-13

Filisetti D, Théobald-Dietrich A, Mahmoudi N, Rudinger-Thirion J, Candolfi E, Frugier M. 2013. Aminoacylation of *Plasmodium falciparum* $tRNA^{Asn}$ and Insights in the synthesis of asparagine repeats. *J Biol Chem* **288**:36361–36371. doi:10.1074/jbc.M113.522896

Florens L, Washburn MP, Raine JD, Anthony RM, Grainger M, Haynes JD, Moch JK, Muster N, Sacci JB, Tabb DL, Witney AA, Wolters D, Wu Y, Gardner MJ, Holder AA, Sinden RE, Yates JR, Carucci DJ. 2002. A proteomic view of the *Plasmodium falciparum* life cycle. *Nature* **419**:520–526. doi:10.1038/nature01107

Foster PG, Jermiin LS, Hickey DA. 1997. Nucleotide Composition Bias Affects Amino Acid Content in Proteins Coded by Animal Mitochondria. *J Mol Evol* **44**:282–288. doi:10.1007/PL00006145

Foth BJ, Zhang N, Chaal BK, Sze SK, Preiser PR, Bozdech Z. 2011. Quantitative time-course profiling of parasite and host cell proteins in the human malaria parasite *Plasmodium*

falciparum. *Mol Cell Proteomics* **10**:M110.006411. doi:10.1074/mcp.M110.006411

Frevert U. 2004. Sneaking in through the back entrance: the biology of malaria liver stages. *Trends Parasitol* **20**:417–424. doi:10.1016/j.pt.2004.07.007

Frischknecht F, Baldacci P, Martin B, Zimmer C, Thiberge S, Olivo-Marin J-C, Shorte SL, Ménard R. 2004. Imaging movement of malaria parasites during transmission by *Anopheles* mosquitoes: Imaging *Plasmodium* sporozoites in mosquito salivary glands. *Cell Microbiol* **6**:687–694. doi:10.1111/j.1462-5822.2004.00395.x

Frugier M, Bour T, Ayach M, Santos MAS, Rudinger-Thirion J, Théobald-Dietrich A, Pizzi E. 2010. Low Complexity Regions behave as tRNA sponges to help co-translational folding of plasmodial proteins. *FEBS Lett* **584**:448–454. doi:10.1016/j.febslet.2009.11.004

Frugier M, Florentz C, Giegé R. 1992. Anticodon-independent aminoacylation of an RNA minihelix with valine. *Proc Natl Acad Sci USA* **89**:3990–3994. doi:10.1073/pnas.89.9.3990

G

Gajbhiye S, Patra PK, Yadav MK. 2017. New insights into the factors affecting synonymous codon usage in human infecting *Plasmodium* species. *Acta Trop* **176**:29–33. doi:10.1016/j.actatropica.2017.07.025

Gardner MJ, Hall N, Fung E, White O, Berriman M, Hyman RW, Carlton JM, Pain A, Nelson KE, Bowman S, Paulsen IT, James K, Eisen JA, Rutherford K, Salzberg SL, Craig A, Kyes S, Chan M-S, Nene V, Shallom SJ, Suh B, Peterson J, Angiuoli S, Pertea M, Allen J, Selengut J, Haft D, Mather MW, Vaidya AB, Martin DMA, Fairlamb AH, Fraunholz MJ, Roos DS, Ralph SA, McFadden GI, Cummings LM, Subramanian GM, Mungall C, Venter JC, Carucci DJ, Hoffman SL, Newbold C, Davis RW, Fraser CM, Barrell B. 2002. Genome sequence of the human malaria parasite *Plasmodium falciparum*. *Nature* **419**:498–511. doi:10.1038/nature01097

Garneau NL, Wilusz J, Wilusz CJ. 2007. The highways and byways of mRNA decay. *Nat Rev Mol Cell Biol* **8**:113–126. doi:10.1038/nrm2104

Gebauer F, Hentze MW. 2004. Molecular mechanisms of translational control. *Nat Rev Mol Cell Biol* **5**:827–835. doi:10.1038/nrm1488

Ghasemii K, Darroudi M, Rahimmanesh I, Ghomi M, Hassanpour M, Sharifi E, Yousefiasl S, Ahmadi S, Zarrabi A, Borzacchiello A, Rabiee M, Paiva-Santos AC, Rabiee N. 2022. Advances in aptamer-based drug delivery vehicles for cancer therapy. *Biomater Adv* **140**:213077. doi:10.1016/j.bioadv.2022.213077

Giegé R, Dock AC, Kern D, Lorber B, Thierry JC, Moras D. 1986. The role of purification in the crystallization of proteins and nucleic acids. *J Cryst Growth* **76**:554–561. doi:10.1016/0022-0248(86)90172-7

Giegé R, Eriani G. 2023. The tRNA identity landscape for aminoacylation and beyond. *Nucleic Acids Res* **51**:1528–1570. doi:10.1093/nar/gkad007

Giegé R, Jühling F, Pütz J, Stadler P, Sauter C, Florentz C. 2012. Structure of transfer RNAs: similarity and variability: Structure of transfer RNAs. *WIREs RNA* **3**:37–61. doi:10.1002/wrna.103

Gissot M, Walker R, Delhaye S, Alayi TD, Huot L, Hot D, Callebaut I, Schaeffer-Reiss C, Dorsselaer AV, Tomavo S. 2013. *Toxoplasma gondii* Alba proteins are involved in translational control of gene expression. *J Mol Biol* **425**:1287–1301. doi:10.1016/j.jmb.2013.01.039

Gomes-Santos CSS, Braks J, Prudêncio M, Carret C, Gomes AR, Pain A, Feltwell T, Khan S, Waters A, Janse C, Mair GR, Mota MM. 2011. Transition of *Plasmodium* sporozoites into liver stage-like forms is regulated by the RNA binding protein Pumilio. *PLoS Pathog* **7**:e1002046. doi:10.1371/journal.ppat.1002046

Gopalakrishnan AM, Kumar N. 2015. Antimalarial Action of Artesunate Involves DNA Damage Mediated by Reactive Oxygen Species. *Antimicrob Agents Chemother* **59**:317–325. doi:10.1128/AAC.03663-14

Gordon DM, McGovern TW, Krzych U, Cohen JC, Schneider I, LaChance R, Heppner DG, Yuan G, Hollingdale M, Slaoui M, Hauser P, Voet P, Sadoff JC, Ballou WR. 1995. Safety, immunogenicity, and efficacy of a recombinantly produced *Plasmodium falciparum* circumsporozoite protein-hepatitis B surface antigen subunit vaccine. *J Infect Dis* **171**:1576–1585. doi:10.1093/infdis/171.6.1576

Goundis D, Reid KBM. 1988. Properdin, the terminal complement components, thrombospondin and the circumsporozoite protein of malaria parasites contain similar sequence motifs. *Nature* **335**:82–85. doi:10.1038/335082a0

Goyal M, Banerjee C, Nag S, Bandyopadhyay U. 2016. The Alba protein family: Structure and function. *Biochim Biophys Acta* **1864**:570–583. doi:10.1016/j.bbapap.2016.02.015

Guan S, Rosenecker J. 2017. Nanotechnologies in delivery of mRNA therapeutics using nonviral vector-based delivery systems. *Gene Ther* **24**:133–143. doi:10.1038/gt.2017.5

Gunderson JH, Sogin ML, Wollett G, Hollingdale M, De La Cruz VF, Waters AP, McCutchan TF. 1987. Structurally distinct, stage-specific ribosomes occur in *Plasmodium*. *Science* **238**:933–937. doi:10.1126/science.3672135

Guo M, Schimmel P. 2013. Essential nontranslational functions of tRNA synthetases. *Nat Chem Biol* **9**:145–153. doi:10.1038/nchembio.1158

Gwadz RW. 1976. Malaria: Successful immunization against the sexual stages of *Plasmodium gallinaceum*. *Science* **193**:1150–1151. doi:10.1126/science.959832

H

Haldar K. 1998. Intracellular trafficking in *Plasmodium*-infected erythrocytes. *Curr Opin Microbiol* **1**:466–471. doi:10.1016/S1369-5274(98)80067-2

Haldar K, Mohandas N. 2009. Malaria, erythrocytic infection, and anemia. *Hematology* **2009**:87–93. doi:10.1182/asheducation-2009.1.87

Halfmann R, Alberti S, Krishnan R, Lyle N, O'Donnell CW, King OD, Berger B, Pappu RV, Lindquist S. 2011. Opposing effects of glutamine and asparagine govern prion formation by intrinsically disordered proteins. *Mol Cell* **43**:72–84. doi:10.1016/j.molcel.2011.05.013

Hall N, Karras M, Raine JD, Carlton JM, Kooij TWA, Berriman M, Florens L, Janssen CS, Pain A, Christophides GK, James K, Rutherford K, Harris B, Harris D, Churcher C, Quail MA, Ormond D, Doggett J, Trueman HE, Mendoza J, Bidwell SL, Rajandream M-A, Carucci DJ, Yates JR, Kafatos FC, Janse CJ, Barrell B, Turner CMR, Waters AP, Sinden RE. 2005. A comprehensive survey of the *Plasmodium* life cycle by genomic, transcriptomic, and proteomic analyses. *Science* **307**:82–86. doi:10.1126/science.1103717

Hamilton WL, Claessens A, Otto TD, Kekre M, Fairhurst RM, Rayner JC, Kwiatkowski D. 2016. Extreme mutation bias and high AT content in *Plasmodium falciparum*. *Nucleic Acids Res* gkw1259. doi:10.1093/nar/gkw1259

Hanson G, Coller J. 2018. Codon optimality, bias and usage in translation and mRNA decay. *Nat Rev Mol Cell Biol* **19**:20–30. doi:10.1038/nrm.2017.91

Hart KJ, Oberstaller J, Walker MP, Minns AM, Kennedy MF, Padykula I, Adams JH, Lindner SE. 2019. *Plasmodium* male gametocyte development and transmission are critically regulated by the two putative deadenylases of the CAF1/CCR4/NOT complex. *PLoS Pathog* **15**:e1007164. doi:10.1371/journal.ppat.1007164

Hayashi CTH, Cao Y, Clark LC, Tripathi AK, Zavala F, Dwivedi G, Knox J, Alameh M-G, Lin PJC, Tam YK, Weissman D, Kumar N. 2022. mRNA-LNP expressing PfCSP and Pfs25 vaccine candidates targeting infection and transmission of *Plasmodium falciparum*. *npj Vaccines* **7**:155. doi:10.1038/s41541-022-00577-8

Healy JM, Lewis SD, Kurz M, Boomer RM, Thompson KM, Wilson C, McCauley TG. 2004. Pharmacokinetics and biodistribution of novel aptamer compositions. *Pharm Res* **21**:2234–2246. doi:10.1007/s11095-004-7676-4

Hia F, Yang SF, Shichino Y, Yoshinaga M, Murakawa Y, Vandenbon A, Fukao A, Fujiwara T, Landthaler M, Natsume T, Adachi S, Iwasaki S, Takeuchi O. 2019. Codon bias confers stability to human mRNA s. *EMBO Rep* **20**:e48220. doi:10.15252/embr.201948220

Hollin T, Le Roch KG. 2020. From genes to transcripts, a tightly regulated journey in *Plasmodium*. *Front Cell Infect Microbiol* **10**:618454. doi:10.3389/fcimb.2020.618454

J

Jackson KE, Habib S, Frugier M, Hoen R, Khan S, Pham JS, Pouplana LRD, Royo M, Santos MAS, Sharma A, Ralph SA. 2011. Protein translation in *Plasmodium* parasites. *Trends in Parasitol* **27**:467–476. doi:10.1016/j.pt.2011.05.005

Jaramillo Ponce JR, Kapps D, Paulus C, Chicher J, Frugier M. 2022. Discovery of two distinct aminoacyl-tRNA synthetase complexes anchored to the *Plasmodium* surface tRNA import protein. *J Biol Chem* **298**:101987. doi:10.1016/j.jbc.2022.101987

Jaramillo Ponce JR, Théobald-Dietrich A, Bénas P, Paulus C, Sauter C, Frugier M. 2023. Solution X-ray scattering highlights discrepancies in *Plasmodium* multi-aminoacyl-tRNA synthetase complexes. *Protein Sci* **32**:e4564. doi:10.1002/pro.4564

K

Kapps D, Cela M, Théobald-Dietrich A, Hendrickson T, Frugier M. 2016. OB or Not OB: Idiosyncratic utilization of the tRNA-binding OB-fold domain in unicellular, pathogenic eukaryotes. *FEBS Lett* **590**:4180–4191. doi:10.1002/1873-3468.12441

Karanasios E, Simos G. 2010. Building arks for tRNA: Structure and function of the Arc1p family of non-catalytic tRNA-binding proteins. *FEBS Letters* **584**:3842–3849. doi:10.1016/j.febslet.2010.08.023

Kauffman KJ, Webber MJ, Anderson DG. 2016. Materials for non-viral intracellular delivery of messenger RNA therapeutics. *J Control Release* **240**:227–234. doi:10.1016/j.jconrel.2015.12.032

Ke H, Mather MW. 2017. +Targeting mitochondrial functions as antimalarial regime, what is next? *Curr Clin Micro Rpt* **4**:175–191. doi:10.1007/s40588-017-0075-5

Khan K, Baleanu-Gogonea C, Willard B, Gogonea V, Fox PL. 2020. 3-Dimensional architecture of the human multi-tRNA synthetase complex. *Nucleic Acids Res* **48**:8740–8754. doi:10.1093/nar/gkaa569

Kim SH, Suddath FL, Quigley GJ, McPherson A, Sussman JL, Wang AHJ, Seeman NC, Rich A. 1974. Three-Dimensional Tertiary Structure of Yeast Phenylalanine Transfer RNA. *Science* **185**:435–440. doi:10.1126/science.185.4149.435

Kim JH, Han JM, Kim S. 2013. Protein–protein interactions and multi-component complexes of aminoacyl-tRNA synthetases In: Kim S, editor. Aminoacyl-tRNA synthetases in biology and medicine, Top Curr Chem. Dordrecht: Springer Netherlands. pp. 119–144. doi:10.1007/128_2013_479

Kim SJ, Yoon JS, Shishido H, Yang Z, Rooney LA, Barral JM, Skach WR. 2015. Translational tuning optimizes nascent protein folding in cells. *Science* **348**:444–448. doi:10.1126/science.aaa3974

Kirchner S, Ignatova Z. 2015. Emerging roles of tRNA in adaptive translation, signalling dynamics and disease. *Nat Rev Genet* **16**:98–112. doi:10.1038/nrg3861

Kyriacou SV, Deutscher MP. 2008. An important role for the multienzyme aminoacyl-tRNA synthetase complex in mammalian translation and cell growth. *Mol Cell* **29**:419–427. doi:10.1016/j.molcel.2007.11.038

L

Lazarus MD, Schneider TG, Taraschi TF. 2008. A new model for hemoglobin ingestion and transport by the human malaria parasite *Plasmodium falciparum*. *J Cell Sci* **121**:1937–1949. doi:10.1242/jcs.023150

Le Roch KG, Johnson JR, Florens L, Zhou Y, Santrosyan A, Grainger M, Yan SF, Williamson KC, Holder AA, Carucci DJ, Yates JR, Winzeler EA. 2004. Global analysis of transcript and protein levels across the *Plasmodium falciparum* life cycle. *Genome Res* **14**:2308–2318. doi:10.1101/gr.2523904

Leitner M, Poturnayova A, Lamprecht C, Weich S, Snejdarkova M, Karpisova I, Hianik T, Ebner A. 2017. Characterization of the specific interaction between the DNA aptamer sgc8c and protein tyrosine kinase-7 receptors at the surface of T-cells by biosensing AFM. *Anal Bioanal Chem* **409**:2767–2776. doi:10.1007/s00216-017-0238-5

Lindner SE, Mikolajczak SA, Vaughan AM, Moon W, Joyce BR, Sullivan WJ, Kappe SHI. 2013a. Perturbations of *Plasmodium* Puf2 expression and RNA-seq of Puf2-deficient sporozoites reveal a critical role in maintaining RNA homeostasis and parasite transmissibility: Puf2 regulate sporozoite infectivity. *Cell Microbiol* **15**:1266–1283. doi:10.1111/cmi.12116

Lindner SE, Swearingen KE, Harupa A, Vaughan AM, Sinnis P, Moritz RL, Kappe SHI. 2013. Total and putative surface proteomics of malaria parasite salivary gland sporozoites. *Mol Cell Proteomics* **12**:1127–1143. doi:10.1074/mcp.M112.024505

Lindner SE, Swearingen KE, Shears MJ, Walker MP, Vrana EN, Hart KJ, Minns AM, Sinnis P, Moritz RL, Kappe SHI. 2019. Transcriptomics and proteomics reveal two waves of translational repression during the maturation of malaria parasite sporozoites. *Nat Commun* **10**:4964. doi:10.1038/s41467-019-12936-6

Liu Y. 2020. A code within the genetic code: codon usage regulates co-translational protein folding. *Cell Commun Signal* **18**:145. doi:10.1186/s12964-020-00642-6

Lopaticki S, Maier AG, Thompson J, Wilson DW, Tham W-H, Triglia T, Gout A, Speed TP, Beeson JG, Healer J, Cowman AF. 2011. Reticulocyte and erythrocyte binding-like proteins function cooperatively in invasion of human erythrocytes by malaria parasites. *Infect Immun*

79:1107–1117. doi:10.1128/IAI.01021-10

M

Ma N, Zhang Z, Liao F, Jiang T, Tu Y. 2020. The birth of artemisinin. *Pharmacol Ther* **216**:107658. doi:10.1016/j.pharmthera.2020.107658

Ma QP, Li C, Wang J, Wang Y, Ding ZT. 2015. Analysis of synonymous codon usage in FAD7 genes from different plant species. *Genet Mol Res* **14**:1414–1422. doi:10.4238/2015.February.13.20

Ma W, Balta VA, West R, Newlin KN, Miljanić OŠ, Sullivan DJ, Vekilov PG, Rimer JD. 2021. A second mechanism employed by artemisinins to suppress *Plasmodium falciparum* hinges on inhibition of hematin crystallization. *J Biol Chem* **296**:100123. doi:10.1074/jbc.RA120.016115

MacRaild CA, Richards JS, Anders RF, Norton RS. 2016. Antibody recognition of disordered antigens. *Structure* **24**:148–157. doi:10.1016/j.str.2015.10.028

Mair GR, Lasonder E, Garver LS, Franke-Fayard BMD, Carret CK, Wiegant JCAG, Dirks RW, Dimopoulos G, Janse CJ, Waters AP. 2010. Universal features of post-transcriptional gene regulation are critical for *Plasmodium* zygote development. *PLoS Pathog* **6**:e1000767. doi:10.1371/journal.ppat.1000767

Mani J, Güttinger A, Schimanski B, Heller M, Acosta-Serrano A, Pescher P, Späth G, Roditi I. 2011. Alba-domain proteins of *Trypanosoma brucei* are cytoplasmic RNA-binding proteins that interact with the translation machinery. *PLoS One* **6**:e22463. doi:10.1371/journal.pone.0022463

Mao Y, Gu J, Chang D, Wang L, Yao L, Ma Q, Luo Z, Qu H, Li Y, Zheng L. 2020. Evolution of a highly functional circular DNA aptamer in serum. *Nucleic Acids Res* **48**:10680–10690. doi:10.1093/nar/gkaa800

Marciniak RA, Garcia-Blanco MA, Sharp PA. 1990. Identification and characterization of a HeLa nuclear protein that specifically binds to the trans-activation-response (TAR) element of human immunodeficiency virus. *Proc Natl Acad Sci USA* **87**:3624–3628. doi:10.1073/pnas.87.9.3624

Markus MB. 2020. Transition from plasmodial hypnozoite to schizont demonstrated. *Trends Parasitol* **36**:407–408. doi:10.1016/j.pt.2020.01.011

Martin RE, Henry RI, Abbey JL, Clements JD, Kirk K. 2005. The 'permeome' of the malaria parasite: an overview of the membrane transport proteins of *Plasmodium falciparum*. *Genome Biol* **6**:R26. doi:10.1186/gb-2005-6-3-r26

Mathur S, Hoskins C. 2017. Drug development: Lessons from nature. *Biomed Rep* **6**:612–614. doi:10.3892/br.2017.909

Matuschewski K, Ross J, Brown SM, Kaiser K, Nussenzweig V, Kappe SHI. 2002. Infectivity-associated changes in the transcriptional repertoire of the malaria parasite sporozoite stage. *J Biol Chem* **277**:41948–41953. doi:10.1074/jbc.M207315200

Mbengue A, Bhattacharjee S, Pandharkar T, Liu H, Estiu G, Stahelin RV, Rizk SS, Njimoh DL, Ryan Y, Chotivanich K, Nguon C, Ghorbal M, Lopez-Rubio J-J, Pfrender M, Emrich S, Mohandas N, Dondorp AM, Wiest O, Haldar K. 2015. A molecular mechanism of artemisinin resistance in *Plasmodium falciparum* malaria. *Nature* **520**:683–687. doi:10.1038/nature14412

Mehrizi A, Bagheri Verjani S, Zakeri S. 2021. Advax, as a Co-adjuvant, in combination with Poly(I:C) elicits enhanced Th1 immune responses and parasite growth-inhibitory antibodies against *Plasmodium falciparum* merozoite surface protein-1 (PfMSP-142) in BALB/c mice. *Iran J Immunol* **18**. doi:10.22034/iji.2021.85629.1720

Ménard R, Heussler V, Yuda M, Nussenzweig V. 2008. *Plasmodium* pre-erythrocytic stages: what's new? *Trends in Parasitol* **24**:564–569. doi:10.1016/j.pt.2008.08.009

Miao J, Fan Q, Parker D, Li X, Li J, Cui L. 2013. Puf mediates translation repression of transmission-blocking vaccine candidates in malaria parasites. *PLoS Pathog* **9**:e1003268. doi:10.1371/journal.ppat.1003268

Miao J, Li J, Fan Q, Li Xiaolian, Li Xinyi, Cui L. 2010. The Puf-family RNA-binding protein PfPuf2 regulates sexual development and sex differentiation in the malaria parasite *Plasmodium falciparum*. *J Cell Sci* **123**:1039–1049. doi:10.1242/jcs.059824

Mirande M. 2017. The aminoacyl-tRNA synthetase complex In: Harris JR, Marles-Wright J, editors. Macromolecular protein complexes, subcellular biochemistry. Cham: Springer International Publishing. pp. 505–522. doi:10.1007/978-3-319-46503-6_18

Miura K. 2016. Progress and prospects for blood-stage malaria vaccines. *Expert Rev Vaccines* **15**:765–781. doi:10.1586/14760584.2016.1141680

Miura K, Zhou H, Diouf A, Moretz SE, Fay MP, Miller LH, Martin LB, Pierce MA, Ellis RD, Mullen GED, Long CA. 2009. Anti-apical-membrane-antigen-1 antibody is more effective than anti-42-kilodalton-merozoite-surface-protein-1 antibody in inhibiting *Plasmodium falciparum* growth, as determined by the *in vitro* growth inhibition assay. *Clin Vaccine Immunol* **16**:963–968. doi:10.1128/CVI.00042-09

Mohler K, Ibba M. 2017. Translational fidelity and mistranslation in the cellular response to stress. *Nat Microbiol* **2**:17117. doi:10.1038/nmicrobiol.2017.117

Molina-Franky J, Cuy-Chaparro L, Camargo A, Reyes C, Gómez M, Salamanca DR, Patarroyo MA, Patarroyo ME. 2020. *Plasmodium falciparum* pre-erythrocytic stage vaccine development. *Malar J* **19**:56. doi:10.1186/s12936-020-3141-z

Mondal SK, Kundu S, Das R, Roy S. 2016. Analysis of phylogeny and codon usage bias and relationship of GC content, amino acid composition with expression of the structural *nif*

genes. *J Biomol Struct Dyn* **34**:1649–1666. doi:10.1080/07391102.2015.1087334

Mons B. 1990. Preferential invasion of malarial merozoites into young red blood cells. *Blood Cells* **16**:299–312.

Morales AJ. 1999. Structure-specific tRNA-binding protein from the extreme thermophile *Aquifex aeolicus*. *The EMBO J* **18**:3475–3483. doi:10.1093/emboj/18.12.3475

Mordmüller B, Sulyok Z, Sulyok M, Molnar Z, Lalremruata A, Calle CL, Bayon PG, Esen M, Gmeiner M, Held J, Heimann H-L, Woldearegai TG, Ibáñez J, Flügge J, Fendel R, Kreidenweiss A, Kc N, Murshedkar T, Chakravarty S, Riyahi P, Billingsley PF, Church LWP, Richie TL, Sim BKL, Hoffman SL, Kremsner PG. 2022. A PfSPZ vaccine immunization regimen equally protective against homologous and heterologous controlled human malaria infection. *NPJ Vaccines* **7**:100. doi:10.1038/s41541-022-00510-z

Mota MM, Pradel G, Vanderberg JP, Hafalla JCR, Frevert U, Nussenzweig RS, Nussenzweig V, Rodríguez A. 2001. Migration of *Plasmodium* sporozoites through cells before infection. *Science* **291**:141–144. doi:10.1126/science.291.5501.141

Müller K, Matuschewski K, Silvie O. 2011a. The Puf-family RNA-binding protein Puf2 controls sporozoite conversion to liver stages in the malaria parasite. *PLoS One* **6**:e19860. doi:10.1371/journal.pone.0019860

Muñoz EE, Hart KJ, Walker MP, Kennedy MF, Shipley MM, Lindner SE. 2017. ALBA4 modulates its stage-specific interactions and specific mRNA fates during *Plasmodium yoelii* growth and transmission: ALBA4 affects mRNA fates differently across stages. *Mol Microbiol* **106**:266–284. doi:10.1111/mmi.13762

Muralidharan V, Oksman A, Pal P, Lindquist S, Goldberg DE. 2012. *Plasmodium falciparum* heat shock protein 110 stabilizes the asparagine repeat-rich parasite proteome during malarial fevers. *Nat Commun* **3**:1310. doi:10.1038/ncomms2306

N

Nasertorabi F, Batisse C, Diepholz M, Suck D, Böttcher B. 2011. Insights into the structure of the CCR4-NOT complex by electron microscopy. *FEBS Lett* **585**:2182–2186. doi:10.1016/j.febslet.2011.05.071

Ng EWM, Adamis AP. 2006. Anti-VEGF aptamer (pegaptanib) Therapy for ocular vascular diseases. *Ann N Y Acad Sci* **1082**:151–171. doi:10.1196/annals.1348.062

Nimjee SM, White RR, Becker RC, Sullenger BA. 2017. Aptamers as therapeutics. *Annu Rev Pharmacol Toxicol* **57**:61–79. doi:10.1146/annurev-pharmtox-010716-104558

Nqoro X, Tobeka N, Aderibigbe B. 2017. Quinoline-based hybrid compounds with antimalarial activity. *Molecules* **22**:2268. doi:10.3390/molecules22122268

Nussenzweig RS, Vanderberg J, Most H, Orton C. 1967. Protective immunity produced by the

injection of X-irradiated sporozoites of *Plasmodium berghei*. *Nature* **216**:160–162. doi:10.1038/216160a0

P

Painter HJ, Campbell TL, Llinás M. 2011. The Apicomplexan AP2 family: integral factors regulating *Plasmodium* development. *Mol Biochem Parasitoly* **176**:1–7. doi:10.1016/j.molbiopara.2010.11.014

Pandey AV, Tekwani BL. 1996. Formation of haemozoin/β-haematin under physiological conditions is not spontaneous. *FEBS Lett* **393**:189–192. doi:10.1016/0014-5793(96)00881-2

Pardi N, Hogan MJ, Porter FW, Weissman D. 2018. mRNA vaccines - a new era in vaccinology. *Nat Rev Drug Discov* **17**:261–279. doi:10.1038/nrd.2017.243

Parhizgar AR, Tahghighi A. 2017. Introducing new antimalarial analogues of chloroquine and amodiaquine: a narrative review. *Iran J Med Sci* **42**:115–128.

Paton MG, Barker GC, Matsuoka H, Ramesar J, Janse CJ, Waters AP, Sinden RE. 1993. Structure and expression of a post-transcriptionally regulated malaria gene encoding a surface protein from the sexual stages of *Plasmodium berghei*. *Mol Biochem Parasitol* **59**:263–275. doi:10.1016/0166-6851(93)90224-L

Perraut R, Varela M-L, Joos C, Diouf B, Sokhna C, Mbengue B, Tall A, Loucoubar C, Touré A, Mercereau-Puijalon O. 2017. Association of antibodies to Plasmodium falciparum merozoite surface protein-4 with protection against clinical malaria. *Vaccine* **35**:6720–6726. doi:10.1016/j.vaccine.2017.10.012

Pizzi E., Frontali C. 2001. Low-complexity regions in *Plasmodium falciparum* proteins. *Genome Res* **11**:218–229. doi:10.1101/gr.GR-1522R

Prudêncio M, Rodriguez A, Mota MM. 2006. The silent path to thousands of merozoites: the *Plasmodium* liver stage. *Nat Rev Microbiol* **4**:849–856. doi:10.1038/nrmicro1529

Pütz J, Giegé R, Florentz C. 2010. Diversity and similarity in the tRNA world: overall view and case study on malaria-related tRNAs. *FEBS Lett* **584**:350–358. doi:10.1016/j.febslet.2009.11.050

Q

Quax TEF, Claassens NJ, Söll D, van der Oost J. 2015. Codon bias as a means to fine-Tune gene expression. *Mol Cell* **59**:149–161. doi:10.1016/j.molcel.2015.05.035

Quenault T, Lithgow T, Traven A. 2011. PUF proteins: repression, activation and mRNA localization. *Trends Cell Biol* **21**:104–112. doi:10.1016/j.tcb.2010.09.013

R

Radtke AJ, Anderson CF, Riteau N, Rausch K, Scaria P, Kelnhofer ER, Howard RF, Sher A, Germain RN, Duffy P. 2017. Adjuvant and carrier protein-dependent T-cell priming promotes a robust antibody response against the *Plasmodium falciparum* Pfs25 vaccine candidate. *Sci Rep* **7**:40312. doi:10.1038/srep40312

Radványi Á, Kun Á. 2021. The mutational robustness of the genetic code and codon usage in environmental context: a non-extremophilic preference? *Life* **11**:773. doi:10.3390/life11080773

Rajendran V, Kalita P, Shukla H, Kumar A, Tripathi T. 2018. Aminoacyl-tRNA synthetases: structure, function, and drug discovery. *Int J Biol Macromol* **111**:400–414. doi:10.1016/j.ijbiomac.2017.12.157

Rak R, Dahan O, Pilpel Y. 2018. Repertoires of tRNAs: The couplers of genomics and proteomics. *Annu Rev Cell Dev Biol* **34**:239–264. doi:10.1146/annurev-cellbio-100617-062754

Ranjan N, Rodnina MV. 2016. tRNA wobble modifications and protein homeostasis. *Translation* **4**:e1143076. doi:10.1080/21690731.2016.1143076

Rao Y, Wu G, Wang Z, Chai X, Nie Q, Zhang X. 2011. Mutation bias is the driving force of codon usage in the *Gallus gallus* genome. *DNA Res* **18**:499–512. doi:10.1093/dnares/dsr035

Read D, Lensen AHW, Begarnie S, Haley S, Raza A, Carter R. 1994. Transmission-blocking antibodies against multiple, non-variant target epitopes of the *Plasmodium falciparum* gamete surface antigen Pfs230 are all complement-fixing. *Parasite Immunol* **16**:511–519. doi:10.1111/j.1365-3024.1994.tb00305.x

Restifo NP, Ying H, Hwang L, Leitner WW. 2000. The promise of nucleic acid vaccines. *Gene Ther* **7**:89–92. doi:10.1038/sj.gt.3301117

Rezgui VAN, Tyagi K, Ranjan N, Konevega AL, Mittelstaet J, Rodnina MV, Peter M, Pedrioli PGA. 2013. tRNA tK^{UUU}, tQ^{UUG}, and tE^{UUC} wobble position modifications fine-tune protein translation by promoting ribosome A-site binding. *Proc Natl Acad Sci USA* **110**:12289–12294. doi:10.1073/pnas.1300781110

Risco-Castillo V, Topçu S, Marinach C, Manzoni G, Bigorgne AE, Briquet S, Baudin X, Lebrun M, Dubremetz J-F, Silvie O. 2015. Malaria sporozoites traverse host cells within transient vacuoles. *Cell Host Microbe* **18**:593–603. doi:10.1016/j.chom.2015.10.006

Robertus JD, Ladner JE, Finch JT, Rhodes D, Brown RS, Clark BFC, Klug A. 1974. Structure of yeast phenylalanine tRNA at 3 Å resolution. *Nature* **250**:546–551. doi:10.1038/250546a0

Roestenberg M, Walk J, Van Der Boor SC, Langenberg MCC, Hoogerwerf M-A, Janse JJ, Manurung M, Yap XZ, García AF, Koopman JPR, Meij P, Wessels E, Teelen K, Van

Waardenburg YM, Van De Vegte-Bolmer M, Van Gemert GJ, Visser LG, Van Der Ven AJAM, De Mast Q, Natasha KC, Abebe Y, Murshedkar T, Billingsley PF, Richie TL, Sim BKL, Janse CJ, Hoffman SL, Khan SM, Sauerwein RW. 2020. A double-blind, placebo-controlled phase 1/2a trial of the genetically attenuated malaria vaccine PfSPZ-GA1. *Sci Transl Med* **12**:eaaz5629. doi:10.1126/scitranslmed.aaz5629

Rosenthal MR, Ng CL. 2020. *Plasmodium falciparum* artemisinin resistance: the effect of heme, protein damage, and parasite cell stress response. *ACS Infect Dis* **6**:1599–1614. doi:10.1021/acsinfecdis.9b00527

Rozen S, Skaletsky H. 2000. Primer3 on the WWW for general users and for biologist programmers. *Methods Mol Biol*. **132**:365–386. doi:10.1385/1-59259-192-2:365

Ruckman J, Green LS, Beeson J, Waugh S, Gillette WL, Henninger DD, Claesson-Welsh L, Janjic N. 1998. 2′-fluoropyrimidine RNA-based aptamers to the 165-amino acid form of vascular endothelial growth factor (VEGF165). *J Biol Chem* **273**:20556–20567. doi:10.1074/jbc.273.32.20556

Ryckelynck M, Giegé R, Frugier M. 2005. tRNAs and tRNA mimics as cornerstones of aminoacyl-tRNA synthetase regulations. *Biochimie* **87**:835–845. doi:10.1016/j.biochi.2005.02.014

S

Sallares R, Bouwman A, Anderung C. 2004. The spread of malaria to southern Europe in antiquity: new approaches to old problems. *Med Hist* **48**:311–328. doi:10.1017/S0025727300007651

Sanyal S, Templeton TJ, Moreira CK. 2012. Analysis of variant gene family expression by quantitative PCR In: Ménard R, editor. Malaria, Methods in Molecular Biology. Totowa, NJ: Humana Press. pp. 179–188. doi:10.1007/978-1-62703-026-7_12

Sato S. 2011. The apicomplexan plastid and its evolution. *Cell Mol Life Sci* **68**:1285–1296. doi:10.1007/s00018-011-0646-1

Sauerwein RW, Bousema T. 2015. Transmission blocking malaria vaccines: Assays and candidates in clinical development. *Vaccine* **33**:7476–7482. doi:10.1016/j.vaccine.2015.08.073

Schimmel P. 2018. The emerging complexity of the tRNA world: mammalian tRNAs beyond protein synthesis. *Nat Rev Mol Cell Biol* **19**:45–58. doi:10.1038/nrm.2017.77

Schorderet-Weber S, Noack S, Selzer PM, Kaminsky R. 2017. Blocking transmission of vector-borne diseases. *Int J Parasitol: Drugs Drug Resist* **7**:90–109. doi:10.1016/j.ijpddr.2017.01.004

Schwartz S, Bernstein DA, Mumbach MR, Jovanovic M, Herbst RH, León-Ricardo BX, Engreitz

JM, Guttman M, Satija R, Lander ES, Fink G, Regev A. 2014. Transcriptome-wide mapping reveals widespread dynamic-regulated pseudouridylation of ncRNA and mRNA. *Cell* **159**:148–162. doi:10.1016/j.cell.2014.08.028

Serfontein J, Nisbet RER, Howe CJ, De Vries PJ. 2010. Evolution of the TSC1/TSC2-TOR Signaling Pathway. *Sci Signal* **3**. doi:10.1126/scisignal.2000803

Seth L, Bingham Ferlez KM, Kaba SA, Musser DM, Emadi S, Matyas GR, Beck Z, Alving CR, Burkhard P, Lanar DE. 2017. Development of a self-assembling protein nanoparticle vaccine targeting *Plasmodium falciparum* circumsporozoite protein delivered in three army liposome formulation adjuvants. *Vaccine* **35**:5448–5454. doi:10.1016/j.vaccine.2017.02.040

Shalak V, Kaminska M, Mitnacht-Kraus R, Vandenabeele P, Clauss M, Mirande M. 2001. The EMAPII cytokine is released from the mammalian multisynthetase complex after cleavage of its p43/proEMAPII component. *J Biol Chem* **276**:23769–23776. doi:10.1074/jbc.M100489200

Sharp PM, Cowe E, Higgins DG, Shields DC, Wolfe KH, Wright F. 1988. Codon usage patterns in *Escherichia coli, Bacillus subtilis, Saccharomyces cerevisiae, Schizosaccharomyces pombe, Drosophila melanogaster* and *Homo sapiens* ; a review of the considerable within-species diversity. *Nucleic Acids Res* **16**:8207–8211. doi:10.1093/nar/16.17.8207

Shen F, Ong JJY, Sun Y, Lei Y, Chu R, Kassegne K, Fu H, Jin C, Han E-T, Russell B, Han J-H, Cheng Y. 2021. A chimeric *Plasmodium vivax* merozoite surface protein antibody recognizes and blocks erythrocytic *P. cynomolgi* Berok Merozoites *in vitro*. *Infect Immun* **89**:e00645-20. doi:10.1128/IAI.00645-20

Shock JL, Fischer KF, DeRisi JL. 2007. Whole-genome analysis of mRNA decay in *Plasmodium falciparum* reveals a global lengthening of mRNA half-life during the intra-erythrocytic development cycle. *Genome Biol* **8**:R134. doi:10.1186/gb-2007-8-7-r134

Shrestha S, Li X, Ning G, Miao J, Cui L. 2016. The RNA-binding protein PfPuf1 functions in the maintenance of gametocytes in *Plasmodium falciparum*. *J Cell Sci* jcs.186908. doi:10.1242/jcs.186908

Shurtz R, Dolev S, Aboud M, Salzberg S. 1979. Viral genome RNA serves as messenger early in the infectious cycle of murine leukemia virus. *J Virol* **31**:668–676. doi:10.1128/JVI.31.3.668-676.1979

Silva PAGC, Guerreiro A, Santos JM, Braks JAM, Janse CJ, Mair GR. 2016. Translational control of UIS4 protein of the host-parasite interface is mediated by the RNA Binding protein Puf2 in *Plasmodium berghei* sporozoites. *PLoS One* **11**:e0147940. doi:10.1371/journal.pone.0147940

Silvestrini F, Alano P, Williams JL. 2000. Commitment to the production of male and female gametocytes in the human malaria parasite *Plasmodium falciparum*. *Parasitology* **121**:465–

471. doi:10.1017/S0031182099006691

Silvie O, Briquet S, Müller K, Manzoni G, Matuschewski K. 2014. Post-transcriptional silencing of *UIS4* in *Plasmodium berghei* sporozoites is important for host switch: Post-transcriptional control in *Plasmodium* sporozoites. *Mol Microbiol* **91**:1200–1213. doi:10.1111/mmi.12528

Simos G, Sauer A, Fasiolo F, Hurt EC. 1998. A conserved domain within Arc1p delivers tRNA to aminoacyl-tRNA synthetases. *Mol Cell* **1**:235–242. doi:10.1016/S1097-2765(00)80024-6

Simos G, Segref A, Fasiolo F, Hellmuth K, Shevchenko A, Mann M, Hurt EC. 1996. The yeast protein Arc1p binds to tRNA and functions as a cofactor for the methionyl- and glutamyl-tRNA synthetases. *EMBO J* **15**:5437–5448.

Smith DWE, McNamara AL. 1972. The transfer RNA content of rabbit reticulocytes. *Biochim Biophys Acta* **269**:67–77. doi:10.1016/0005-2787(72)90075-5

Spencer PS, Siller E, Anderson JF, Barral JM. 2012. Silent substitutions predictably alter translation elongation rates and protein folding efficiencies. *J Mol Biol* **422**:328–335. doi:10.1016/j.jmb.2012.06.010

Sullivan DJ, Gluzman IY, Goldberg DE. 1996. *Plasmodium* hemozoin formation mediated by histidine-rich proteins. *Science* **271**:219–222. doi:10.1126/science.271.5246.219

T

Talaat KR, Ellis RD, Hurd J, Hentrich A, Gabriel E, Hynes NA, Rausch KM, Zhu D, Muratova O, Herrera R, Anderson C, Jones D, Aebig J, Brockley S, MacDonald NJ, Wang X, Fay MP, Healy SA, Durbin AP, Narum DL, Wu Y, Duffy PE. 2016. Safety and Immunogenicity of Pfs25-EPA/Alhydrogel®, a transmission blocking vaccine against *Plasmodium falciparum*: an open Label study in malaria naïve adults. *PLoS One* **11**:e0163144. doi:10.1371/journal.pone.0163144

Talman AM, Clain J, Duval R, Ménard R, Ariey F. 2019. Artemisinin bioactivity and resistance in malaria parasites. *Trends in Parasitol* **35**:953–963. doi:10.1016/j.pt.2019.09.005

Tandoh KZ, Wilson MD, Quashie NB, Duah-Quashie NO. 2021. Implicating extracellular vesicles in *Plasmodium falciparum* artemisinin resistance development. *Traffic* **22**:194–200. doi:10.1111/tra.12787

Tarique M, Ahmad M, Ansari A, Tuteja R. 2013. *Plasmodium falciparum* DOZI, an RNA helicase interacts with eIF4E. *Gene* **522**:46–59. doi:10.1016/j.gene.2013.03.063

Tawk L, Chicanne G, Dubremetz J-F, Richard V, Payrastre B, Vial HJ, Roy C, Wengelnik K. 2010. Phosphatidylinositol 3-phosphate, an essential lipid in *Plasmodium*, localizes to the food vacuole membrane and the apicoplast. *Eukaryot Cell* **9**:1519–1530. doi:10.1128/EC.00124-10

Thawani N, Tam M, Bellemare M-J, Bohle DS, Olivier M, De Souza JB, Stevenson MM. 2014.

Plasmodium products contribute to severe malarial anemia by inhibiting erythropoietin-induced proliferation of erythroid precursors. *J Infect Dis* **209**:140–149. doi:10.1093/infdis/jit417

Tilley L, Straimer J, Gnädig NF, Ralph SA, Fidock DA. 2016. Artemisinin action and resistance in *Plasmodium falciparum*. *Trends Parasitol* **32**:682–696. doi:10.1016/j.pt.2016.05.010

Tokunaga N, Nozaki M, Tachibana M, Baba M, Matsuoka K, Tsuboi T, Torii M, Ishino T. 2019. Expression and localization profiles of rhoptry proteins in *Plasmodium berghei* sporozoites. *Front Cell Infect Microbiol* **9**:316. doi:10.3389/fcimb.2019.00316

Tripathi H, Bhalerao P, Singh S, Arya H, Alotaibi BS, Rashid S, Hasan MR, Bhatt TK. 2023. Malaria therapeutics: are we close enough? *Parasit Vectors* **16**:130. doi:10.1186/s13071-023-05755-8

Tu Y. 2011. The discovery of artemisinin (qinghaosu) and gifts from Chinese medicine. *Nat Med* **17**:1217–1220. doi:10.1038/nm.2471

Tucker M, Valencia-Sanchez MA, Staples RR, Chen J, Denis CL, Parker R. 2001. The transcription factor associated Ccr4 and Caf1 proteins are components of the major cytoplasmic mRNA deadenylase in *Saccharomyces cerevisiae*. *Cell* **104**:377–386. doi:10.1016/S0092-8674(01)00225-2

Tuller T, Waldman YY, Kupiec M, Ruppin E. 2010. Translation efficiency is determined by both codon bias and folding energy. *Proc Natl Acad Sci USA* **107**:3645–3650. doi:10.1073/pnas.0909910107

V

Van Rooyen JM, Murat J-B, Hammoudi P-M, Kieffer-Jaquinod S, Coute Y, Sharma A, Pelloux H, Belrhali H, Hakimi M-A. 2014. Assembly of the novel five-component apicomplexan multi-aminoacyl-tRNA synthetase complex is driven by the hybrid scaffold protein Tg-p43. *PLoS One* **9**:e89487. doi:10.1371/journal.pone.0089487

Vembar SS, Droll D, Scherf A. 2016. Translational regulation in blood stages of the malaria parasite *Plasmodium spp.*: systems-wide studies pave the way. *RNA* **7**:772–792. doi:10.1002/wrna.1365

Vembar SS, Macpherson CR, Sismeiro O, Coppée J-Y, Scherf A. 2015. The PfAlba1 RNA-binding protein is an important regulator of translational timing in Plasmodium falciparum blood stages. *Genome Biol* **16**:212. doi:10.1186/s13059-015-0771-5

Voß Y, Klaus S, Guizetti J, Ganter M. 2023. Plasmodium schizogony, a chronology of the parasite's cell cycle in the blood stage. *PLoS Pathog* **19**:e1011157. doi:10.1371/journal.ppat.1011157

W

Wagh K, Ishikawa M, Garcia DA, Stavreva DA, Upadhyaya A, Hager GL. 2021. Mechanical regulation of transcription: recent advances. *Trends Cell Biol* **31**:457–472. doi:10.1016/j.tcb.2021.02.008

Wahle E, Winkler GS. 2013. RNA decay machines: deadenylation by the Ccr4–Not and Pan2–Pan3 complexes. *Biochim Biophys Acta* **1829**:561–570. doi:10.1016/j.bbagrm.2013.01.003

Waller RF, Keeling PJ, Donald RGK, Striepen B, Handman E, Lang-Unnasch N, Cowman AF, Besra GS, Roos DS, McFadden GI. 1998. Nuclear-encoded proteins target to the plastid in *Toxoplasma gondii* and *Plasmodium falciparum*. *Proc Natl Acad Sci USA* **95**:12352–12357. doi:10.1073/pnas.95.21.12352

Waters AP, Syin C, McCutchan TF. 1989. Developmental regulation of stage-specific ribosome populations in *Plasmodium*. *Nature* **342**:438–440. doi:10.1038/342438a0

Wek RC. 2018. Role of eIF2α kinases in translational control and adaptation to cellular stress. *Cold Spring Harb Perspect Biol* **10**:a032870. doi:10.1101/cshperspect.a032870

White NJ. 1996. The treatment of malaria. *N Engl J Med* **335**:800–806. doi:10.1056/NEJM199609123351107

World Health Organization. (2018). World Malaria Report 2018.

World Health Organization. (2020). World Malaria Report 2020.

World Health Organization. (2021). World Malaria Report 2021.

Wickens M, Bernstein DS, Kimble J, Parker R. 2002. A PUF family portrait: 3′UTR regulation as a way of life. *Trends Genet* **18**:150–157. doi:10.1016/S0168-9525(01)02616-6

Wickham ME, Culvenor JG, Cowman AF. 2003. Selective inhibition of a two-step egress of malaria parasites from the host erythrocyte. *J Biol Chem* **278**:37658–37663. doi:10.1074/jbc.M305252200

Wiser MF. 2023. Knobs, adhesion, and severe *falciparum* Malaria. *Trop Med Infect Dis* **8**:353. doi:10.3390/tropicalmed8070353

X

Xie S, Griffin MDW, Winzeler EA, Ribas De Pouplana L, Tilley L. 2023. Targeting aminoacyl tRNA synthetases for antimalarial drug development. *Annu Rev Microbiol* **77**:annurev-micro-032421-121210. doi:10.1146/annurev-micro-032421-121210

Xie SC, Ralph SA, Tilley L. 2020. K13, the cytostome, and artemisinin resistance. *Trends Parasitol* **36**:533–544. doi:10.1016/j.pt.2020.03.006

Y

Yadav MK, Swati D. 2012. Comparative genome analysis of six malarial parasites using codon usage bias based tools. *Bioinformation* **24**:1230-9. doi: 10.6026/97320630081230

Yang J, He Y, Li Y, Zhang X, Wong Y-K, Shen S, Zhong T, Zhang J, Liu Q, Wang J. 2020. Advances in the research on the targets of anti-malaria actions of artemisinin. *Pharmacol Ther* **216**:107697. doi:10.1016/j.pharmthera.2020.107697

Young JF, Hockmeyer WT, Gross M, Ballou WR, Wirtz RA, Trosper JH, Beaudoin RL, Hollingdale MR, Miller LH, Diggs CL, Rosenberg M. 1985. Expression of *Plasmodium falciparum* circumsporozoite proteins in *Escherichia coli* for potential use in a human malaria vaccine. *Science* **228**:958–962. doi:10.1126/science.2988125

Yu H, Li Q. 2011. Mutation and selection on the wobble nucleotide in tRNA anticodons in marine bivalve mitochondrial genomes. *PLoS One* **6**:e16147. doi:10.1371/journal.pone.0016147

Yusuf Y, Yoshii T, Iyori M, Mizukami H, Fukumoto S, Yamamoto DS, Emran TB, Amelia F, Islam A, Syafira I, Yoshida S. 2019. A viral-vectored multi-stage Malaria vaccine regimen with protective and transmission-blocking efficacies. *Front Immunol* **10**:2412. doi:10.3389/fimmu.2019.02412

Z

Zavala F, Tam JP, Hollingdale MR, Cochrane AH, Quakyi I, Nussenzweig RS, Nussenzweig V. 1985. Rationale for development of a synthetic vaccine against *Plasmodium falciparum* malaria. *Science* **228**:1436–1440. doi:10.1126/science.2409595

Zhang M, Fennell C, Ranford-Cartwright L, Sakthivel R, Gueirard P, Meister S, Caspi A, Doerig C, Nussenzweig RS, Tuteja R, Sullivan WJ, Roos DS, Fontoura BMA, Ménard R, Winzeler EA, Nussenzweig V. 2010. The *Plasmodium* eukaryotic initiation factor-2α kinase IK2 controls the latency of sporozoites in the mosquito salivary glands. *J Exp Med* **207**:1465–1474. doi:10.1084/jem.20091975

Zhang M, Joyce BR, Sullivan WJ, Nussenzweig V. 2013. Translational control in *Plasmodium* and *Toxoplasma* parasites. *Eukaryot Cell* **12**:161–167. doi:10.1128/EC.00296-12

Zhang M, Mishra S, Sakthivel R, Fontoura BMA, Nussenzweig V. 2016. UIS2: a unique phosphatase required for the development of *Plasmodium* liver stages. *PLoS Pathog* **12**:e1005370. doi:10.1371/journal.ppat.1005370

Zhang M, Mishra S, Sakthivel R, Rojas M, Ranjan R, Sullivan WJ, Fontoura BMA, Ménard R, Dever TE, Nussenzweig V. 2012. PK4, a eukaryotic initiation factor 2α(eIF2α) kinase, is essential for the development of the erythrocytic cycle of *Plasmodium*. *Proc Natl Acad Sci USA* **109**:3956–3961. doi:10.1073/pnas.1121567109

Zimmermann P, Curtis N. 2019. Factors that influence the immune response to vaccination. *Clin Microbiol Rev* **32**:e00084-18. doi:10.1128/CMR.00084-18

Martina Pitolli

Exploration fonctionnelle de la machinerie d'import des ARNt dans *Plasmodium*

Résumé Ma thèse s'articule autour de la caractérisation fonctionnelle de la protéine tRip (tRNA import protein), une protéine membranaire, présente à la surface de *Plasmodium,* le parasite responsable de la malaria. tRip comporte 2 domaines : (i) le domaine N-terminal de type "GST-like" qui en liant des aaRSs permet la formation de deux complexes multisynthétasiques et (ii) le domaine C-terminal de type "EMAPII-like" qui reconnaît spécifiquement les ARNt exogènes et permet leur import dans le parasite. Un parasite tRip-KO n'importe plus les ARNt, il est caractérisé par une synthèse protéique réduite et une multiplication ralentie lors du stade érythrocytaire. Pendant ma thèse, j'ai comparé les protéomes des parasites tRip-KO et sauvage afin de déterminer les conséquences de l'absence de cet import. Cette étude a montré que les protéines dérégulées dans le parasite tRip-KO sont impliquées dans des fonctions diverses. Néanmoins, l'analyse de l'usage des acides aminés montre que les protéines sous-exprimées dans le parasite tRip-KO sont riches en asparagine. Ces observations nous ont conduits à proposer un mécanisme de régulation post-transcriptionnelle de l'expression de gènes impliqués dans la maturation et l'infectivité de *Plasmodium*. Ce mécanisme serait dépendant de l'import des ARNt hôtes et en particulier de l'ARNtAsn et impliquerait le complexe Ccr4-Not. Comme tRip est présent à la surface du parasite, cette protéine est donc une cible intéressante pour le développement de molécules inhibitrices ou d'un vaccin. Nous avons donc utilisé le domaine C-terminal de tRip comme cible pour sélectionner des aptamères d'ARN capables d'interagir spécifiquement avec tRip et qui pourraient potentiellement soit bloquer l'import des ARNt dans le parasite soit servir de transporteur pour des molécules toxiques. Nous avons également testé la capacité de ce domaine à induire une réponse immunitaire chez la souris et à potentiellement la protéger contre une infection. Ce travail de thèse ouvre ainsi des perspectives ambitieuses tant au niveau de la biologie de ce parasite destructeur qu'à la proposition de solutions thérapeutiques.
Mots clés : ARNt, protéomique, contrôle de la traduction, aptamères, tRip

Summary My thesis project focuses on the functional characterization of tRip (tRNA import protein), a membrane protein located on the surface of *Plasmodium*, the parasite responsible for malaria. tRip comprises 2 domains: (i) the N-terminal "GST-like" domain which, by binding aaRSs, enables the formation of two multisynthetase complexes, and (ii) the C-terminal "EMAPII-like" domain which specifically recognizes exogenous tRNAs and enables their import into the parasite. A tRip-KO parasite no longer imports tRNAs, and is characterized by reduced protein synthesis and slower multiplication during the erythrocytic stage. During my thesis, I compared the proteomes of tRip-KO and wild-type parasites to determine the consequences of the absence of this import. This study showed that the proteins deregulated in the tRip-KO parasite are involved in diverse functions. Nevertheless, analysis of amino acid usage shows that proteins underexpressed in the tRip-KO parasite are rich in asparagine. These observations led us to propose a mechanism for post-transcriptional regulation of the expression of genes involved in *Plasmodium* maturation and infectivity. This mechanism would depend on the import of host tRNAs, particularly tRNAAsn, and would involve the Ccr4-Not complex. Since tRip is present on the parasite surface, this protein is an interesting target for the development of inhibitory molecules or a vaccine. We therefore used the C-terminal domain of tRip as a target to select RNA aptamers capable of interacting specifically with tRip and which could potentially either block the import of tRNAs into the parasite or act as a transporter for toxic molecules. We also tested the ability of this domain to induce an immune response in mice and potentially protect them against infection. This thesis work thus opens up ambitious perspectives both in terms of the biology of this destructive parasite and of proposing therapeutic solutions.
Keywords: tRNA, proteomics, translational control, aptamers, tRip